



# ISSW

**11<sup>th</sup> International Ship Stability Workshop**  
**hosted by MARIN, Wageningen, The Netherlands**  
**June 21<sup>st</sup> - 23<sup>rd</sup>, 2010**



**PROCEEDINGS**



## International Standing Committee Members

Dr. V. Belenky	Prof. M. Pawlowski
Mr. H. Bruhns	Prof. L. Perez-Rojas
Prof. A. Degtyarev	Prof. M. Neves
Prof. A. Francescutto	Prof. M. Renilson
Prof. Y. Ikeda	Prof. K. Spyrou
Dr. J.O. de Kat (Chairman)	Prof. N. Umeda
Prof. A. Papanikolaou	Prof. D. Vassalos

## Local Organising Committee

Dr. F. van Walree, Ms. P. Roseboom and Ms. E.A. te Winkel

## Sponsor

Maritime Research Institute Netherlands

## Previous Workshops

- 1995 Glasgow, UK
- 1996 Osaka, Japan
- 1997 Hersonissos, Greece
- 1998 St. John's, New Foundland, Canada
- 2001 Trieste, Italy
- 2002 Glen Cove, New York, USA
- 2004 Shanghai, China
- 2005 Istanbul, Turkey
- 2007 Hamburg, Germany
- 2008 Daejeon, Republic of Korea



## Contents

<b>Session 1 Goal-Based Stability Standards (Intact)</b>	<b>Page</b>
<b>Paper 1</b> Current Status of New Generation Intact Stability Criteria Development	A. Francescutto and N. Umeda 1 - 5
<b>Paper 2</b> On Vulnerability Criteria for Righting Lever Variations in Waves	W.S. Peters, V. Belenky and C.C. Bassler 6 - 16
<b>Paper 3</b> Designing New Generation Intact Stability Criteria on Broaching Associated with Surf-Riding	N. Umeda and S. Yamamura 17 - 25
<b>Paper 4</b> Research towards Goal Based Standards for Container Shipping	V. Shigunov, H. Rathje and O. El Moctar 26 - 31
<b>Session 2 Goal-Based Stability Standards (Damage)</b>	
<b>Paper 1</b> Going Forward with Safe Return to Port	J. Dodman 32 - 37
<b>Paper 2</b> Damage Stability of Ro-Pax Ships with Water-on-Deck	A.L. Scott 38 - 45
<b>Paper 3</b> GOALDS - Goal Based Damaged Stability	A. Papanikolaou et al 46 - 57
<b>Paper 4</b> Damage Stability Making Sense	D. Vassalos .....
<b>Session 3 Special problems</b>	
<b>Paper 1</b> Application of Wave Groups to Assess Ship Response in Irregular Seas	C.C. Bassler, V. Belenky and M.J. Dipper 58 - 66
<b>Paper 2</b> Risk Based Analysis of Inland Vessel Stability	M. Hoffman and I. Bačkalov 67 - 72
<b>Paper 3</b> Melnikov's Method Applied to a Multi-DOF Ship Model	W.Wu and L. McCue 73 - 78
<b>Paper 4</b> Freak waves and capsizing accidents	T.Waseda and T.Kinoshita 79 - 84

## Session 4 Risk-based analysis methods

**Page**

<b>Paper 1</b>	Assessment of Short-Term Risk with Monte-Carlo Method	B. Campbell and V. Belenky	85 - 92
<b>Paper 2</b>	Tolerable Capsize Risk of a Naval Vessel	A. Peters	93 - 107
<b>Paper 3</b>	Climatic Spectra and Long-Term Risk Assessment	A.B. Degtyarev and V.V. Mareev	108 - 114
<b>Paper 4</b>	Integrated Approach Towards Intact and Damage Stability	K. Spyrou	-

## Session 5 Naval Ship Stability

<b>Paper 1</b>	Developing a Shared Vision for Naval Stability Assessment	D. Perrault, T. Hughes and S. Marshall	115 - 120
<b>Paper 2</b>	Approaches for Evaluating Dynamic Stability in Design	P.R. Alman	121 - 128
<b>Paper 3</b>	Operator Guidance for French Mine Hunters	J.F. LeGuen	129 - 133
<b>Paper 4</b>	Landing Craft Stability Standard	J. Atkins, S. Marshall and N. Noel-Johnson	134 - 142

## Session 6 Safety of Damaged Vessels

<b>Paper 1</b>	On the Time Dependent Survivability of RoPax Ships	D.A. Spanos and A. Papanikolaou	143 - 147
<b>Paper 2</b>	Comparison of s-factor according to SOLAS and SEM for Ro-Pax vessels	M. Pawlowski	148 - 152
<b>Paper 3</b>	A study on the damage stability requirements for Ro-Ro passenger ships	Y. Ogawa and S. Takeda	153 - 158
<b>Paper 4</b>	FLOODSTAND: Integrated Flooding Control and Standard for Stability and Crisis Management	R. Jalonen et al	159 - 165

<b>Session 7</b>	<b>Developments in Intact and Damage Stability Modeling</b>		<b>Page</b>
<b>Paper 1</b>	Calculation method to include water on deck effects	N. Carette and F. van Walree	166 - 172
<b>Paper 2</b>	An Approach to the Validation of Ship Flooding Simulation Models	E. Ypma and T. Turner	173 - 184
<b>Paper 3</b>	CFD Applications to Damage Stability Modeling	Z. Gao	-
<b>Paper 4</b>	TEMPEST: A New Computationally Efficient Dynamic Stability Prediction Tool	W.F. Bellknap and A.M. Reed	185 - 197
<b>Session 8 Operational safety</b>			
<b>Paper 1</b>	Heavy Weather Ship-Handling Bridge Simulation	S. Marshall	198 - 201
<b>Paper 2</b>	Further Perspectives on Operator Guidance and Training for Heavy Weather Ship Handling	L.J. Van Buskirk, J. McTigue and P.A. Alman	202 - 208
<b>Paper 3</b>	Structural Failure & Progressive Flooding due to Collision/Grounding in Extreme Environments	S. Kwon and D. Vassalos	-
<b>Paper 4</b>	Decision Support for Crisis Management and Emergency Response	A. Jasionowski	209 - 216
<b>Session 9 Roll Damping</b>			
<b>Paper 1</b>	A Method to Model Large Amplitude Ship Roll Damping	C.C. Bassler, A.M. Reed and A.J. Brown	217 - 224
<b>Paper 2</b>	Some Topics for Estimation of Bilge Keel Component of Roll Damping	T. Katayama et al	225 - 230
<b>Paper 3</b>	Approximation of the Non-Linear Roll Damping	M. Pawlowski	231 - 237
<b>Paper 4</b>	Uncertainty Assessment in Experiments on a Floating Body in Forced Roll Motion in Calm Water	J. Chichowicz et al	238 - 244

## Session 10 Flooding of damaged ships

**Page**

<b>Paper 1</b>	Flooding Simulations of ITTC and Safedor Benchmark test cases using CRS Shipsurv Software	P. Corrigan and A. Arias	238 - 245
<b>Paper 2</b>	Study on the motions and flooding process of a damaged ship in waves	S.K. Cho et al	246 - 254
<b>Paper 3</b>	An Application of the DOE Methodology in Damage Survivability	C. Khaddaj-Mallat et al	255 - 261
<b>Paper 4</b>	The Capsize Band Concept Revisited	N. Tsakalakis, J. Cichowisz and D. Vassalos	262 - 271

## Session 11 Parametric roll

<b>Paper 1</b>	A Critical Assessment of Ship Parametric Roll Analysis	H. Moideen and J. Falzarano	272 - 279
<b>Paper 2</b>	On the prediction of parametric roll	M. Gusing and R.P. Dallinga	280 - 287
<b>Paper 3</b>	Integrity Diagrams of the Ship/U-Tank System Undergoing Parametric Rolling	M.A.S. Neves et al	288 - 294
<b>Paper 4</b>	A study on Quantitative Prediction of Parametric Roll in Regular Waves	H. Hashimoto and N. Umeda	295 - 301

# Current Status of New Generation Intact Stability Criteria Development

Alberto FRANCESCUTTO  
University of Trieste  
Naoya UMEDA  
Osaka University

## ABSTRACT

At the International Maritime Organization (IMO) the new generation intact stability criteria is now under development. This paper describes a current status of this development for facilitating discussion among experts in stability research. It was already agreed to consist of 3 levelled criteria and onboard operational guidances for four different stability failure modes, which include pure loss of stability, parametric rolling, broaching and stability under dead ship condition. Member states submitted available methodologies with sample calculation results so far but the first level criteria for pure loss of stability and parametric rolling are still missing and the first level criterion for broaching is required to be further upgraded. More verification and validation are essential for finalising this criterion set.

## KEYWORDS

Vulnerability criteria, direct stability assessment, stability failure, IMO, SLF, 2008 IS Code

## 1 INTRODUCTION

The first part of the long work undertaken in the revision of the IMO Intact Stability Code in 2001 with the establishment of an ad-hoc Working Group (ISWG) operating during the Sessions of the Sub-Committee on Stability, Load Lines and on Fishing Vessel Stability (SLF) and intersessionally between them, has been completed in 2008 (Bulian et al., 2009)

This part of the ISWG activity was mostly devoted to restructuring the previous Intact Stability Code (IMO Res. A.749(18)) in several parts and making Part A of the new "International Code on Intact Stability, 2008 (2008 IS Code) " (IMO, 2009) mandatory under the provisions of both SOLAS and ILLC Conventions. The new Part A contains mandatory instruments for passenger and cargo ships since 1 July 2010, while Part B contains recommendations for other ship typologies. An originally planned "Part C" containing nomenclature, an historical part

describing the origins and the developments of intact stability criteria and explanatory notes to the new International Intact Stability Code 2008, has been finalized as an MSC Circular (IMO, 2008).

Notwithstanding the importance of this work, the most important part of the initial scope of the revision, i.e. the formulation and implementation of a new generation intact stability criteria performance-based (Bulian et al, 2006; Umeda and Francescutto, 2008) is still to a large extent lying on the carpet. The time flown was in any case important for proving the potential cost-effectiveness implied in the new criteria and for the maturation of some important concepts connected with the dangerous phenomena to be covered, the basic structure and dictionary, and the philosophy of application of the new criteria (Chairman of ISWG, 2008).

It was subsequently decided that the following four dangerous situations should be individually addressed:

- stability failures under dead ship conditions;
- stability failures in following/stern quartering seas associated with matters related to stability variation in waves, in particular reduced righting levers of a ship situated on a wave crest;
- stability failures caused by parametric resonance, including consideration of matters related to large accelerations and loads on cargo and stability variation in waves;
- stability failures caused by broaching including consideration of matters related to manoeuvrability and course keeping ability as they affect stability.

Moreover the new generation intact stability criteria should be structured in three levels:

- Vulnerability 1<sup>st</sup> level;
- Vulnerability 2<sup>nd</sup> level;
- Direct stability assessment.

Specific Operational Guidelines should be added as a sort of "fourth level", in the acknowledgement that not all dangerous situations can be avoided only by design prescriptions.

In the following of this paper, the situation synthetically described in this Introduction is presented and discussed in some detail together with the potential methodologies identified up to now for the implementation in the 3x4 matrix of dangerous situation/level of criteria. Finally, some comments concerning the voids on the matrix are presented.

## **2 THE SCOPE AND APPLICATION OF THE NEW GENERATION INTACT STABILITY CRITERIA**

The scope of new generation intact stability criteria is to provide methods to assess ships which may be vulnerable to particular stability failure modes not adequately assessed by the existing criteria. These ships have typologies or sizes outside

the ships for which existing regulations were developed.

The new generation intact stability criteria is based on a multi-tiered assessment approach, which is considered for the time being, as a supplement or as part of an alternative to the existing criteria contained in part A of the 2008 IS Code. Since new generation intact stability criteria are focused on the assessment of ships that are vulnerable to stability failures, neither explicitly nor properly covered by the existing stability regulations (defined as "unconventional ships"), a particular ship under consideration must first be determined to be conventional or unconventional, for each specified stability failure mode. The first tier of the new generation intact stability criteria is therefore intended to serve this purpose.

If the first tier of the criteria (vulnerability criteria level 1) is passed, a ship is conventional for a particular failure mode and the 2008 IS Code on its own should be applied, if appropriate. If it is not passed, this indicates that the ship is unconventional, and therefore may be vulnerable to that particular dynamic stability failure, then direct stability assessment of this mode may be needed. However, in view of the additional complexity of direct stability assessment, an intermediate assessment is provided to confirm vulnerability, before requiring direct stability assessment. The objective of the second tier of the new generation stability criteria (vulnerability criteria level 2) is to provide justification for application of the direct stability assessment. If the vulnerability level 2 criteria does not confirm vulnerability for a particular dynamic stability failure, the 2008 IS Code is applied, if appropriate.

If a ship is confirmed to be vulnerable by the second tier of new generation stability criteria, for a particular failure mode, direct stability assessment with performance-based criteria will then be applied (as a supplement to 2008 IS Code on its own, if appropriate). The results of direct stability assessment are then used to reduce vulnerability, by either revision of the design, or development of

ship-specific operational guidance to assist the crew in operating the ship in as safe as possible manner. The results of direct stability assessment are also expected to provide indications on the safety level. The overall procedure scheme is shown in Fig. 1 (Bassler et al, 2009).

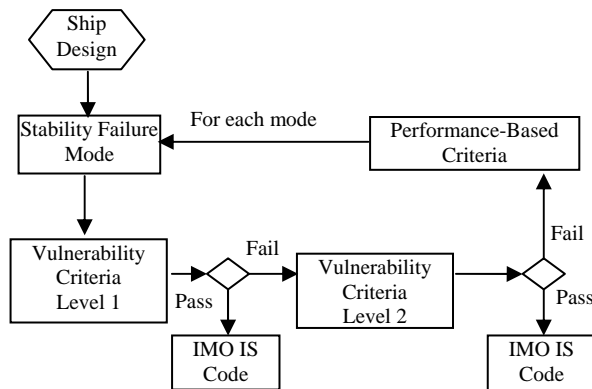


Figure 1 The proposed assessment process for next generation intact stability criteria

### 3 THE STRUCTURE AND PRELIMINARY SPECIFICATIONS OF THE NEW GENERATION INTACT STABILITY CRITERIA AFTER SLF52

During the 52<sup>nd</sup> Session of the SLF Sub-Committee held at IMO headquarters in London in January 2010 (Chairman of ISWG, 2010), the Ad Hoc Working Group for the Development of New Generation Intact Stability Criteria examined the proposal submitted from the member state delegations participating to the call issued at the end of previous session. It was agreed on the following specifications for the new criteria:

- Vulnerability Level 1 should consist in formulae or simple procedure based on geometry / hydrostatics, load condition and basic operational parameters, with low complexity and high safety margins;

- Vulnerability Level 2 should consist in simplified physics-based calculations with reduced computational efforts and straight forward application following suitable guidelines, with moderate complexity and safety margins;
- Direct assessment (third level) should be based on the best “state-of-the-art” concepts available. Time-domain numerical simulation with “hybrid” method and probability theory, as appropriate, should be used for the failure mode considered. The “hybrid” method includes potential flow + empirical viscous models. Specifically, rigid body-nonlinear dynamics model with undisturbed wave pressure (Froude-Krylov assumption). Specified formulation for added mass / wave damping / diffraction, externally specified coefficients for viscous / hydrodynamic lift components of roll damping and manoeuvring, and propulsion force, external environmental actions should be included, as appropriate. Suitable guidelines and procedures (e.g., wave scatter diagram, ship operation conditions, etc.) should be clearly stated. Assessment is expected to be made using a probabilistic measure to evaluate safety level. High complexity and low safety margins are expected.

Along the same lines, taking into account that the dangerous phenomena cannot in general be avoided only by design requirements, ship specific operational guidelines should be developed. This is an expected outcome of the direct assessment methodologies.

### 4 THE AVAILABLE ASSESSMENT METHODOLOGIES FOR THE DIFFERENT LEVELS

Hard work was done intersessionally between SLF51 and SLF52 with the active

participation of many delegations. As a result, several methodologies have been submitted. The developed methodologies cover most of

the cells of the matrix, as appears from the following Table 1.

Table 1 Submitted methodologies for four stability failure modes

Stability failure mode	Level 1	Level 2	Direct assessment	Operational guidance
Pure loss of stability		X	X	X
Parametric roll		X	X	X
Surf-riding/Broaching	X	X	X	
Dead ship condition	X	X	X	

This does not mean that these methodologies will be taken as they are for the foundations of the new generation intact stability criteria. There has been a lively discussion on the quality and validity of the presented methodologies and it was decided to move forward very cautiously, after through verification and validation. To this end, the terms for submission have been reopened until June 2010. Following the preliminary specifications stated, as reported in previous paragraph, it would have probably been better a reversal of the timeline, starting from the direct assessment to develop level 2 and from this level 1. This to some extent would ensure a low ratio of false positive and false negative by passing from a level to the higher one.

The different dangerous situations, on the other hand, are not equal in respect of the structure in levels. The scope of the first level vulnerability is to check the possible vulnerability of the subject ship to the considered phenomenon, so classifying her as an *unconventional* ship with respect to that phenomenon (but not necessarily vulnerable). Now, it is known since long time that *every ship* is vulnerable to the beam sea condition, which is a condition very close to the so-called dead-ship condition. This is, on the other hand, the only point where there was full agreement on a 1st level vulnerability based on present Weather Criterion but with extended wave steepness table.

Not very easy is the situation of the other cells of the first column. The proposal for 1st level vulnerability for the surf-riding and broaching is indeed based on the pure checking of the maximum service speed exceeding a critical speed defined through a critical Froude number. From a practical point of view, this means that a significant part of present ships having high Froude numbers could be categorised as "unconventional", irrespective of their actual dimensions, and would need to pass the 2nd level with the consequence of the need for applying more complex calculation methodologies. In this case, as well as the cases connected with stability variation in waves, it appears that design criteria should be supplemented by the development of ship-specific (and/or non ship-specific) operational guidelines.

The lack of first tier criteria for the phenomena connected with stability variation in waves, in particular, creates some difficulty inasmuch as it could entail that all ships are in principle vulnerable and have to pass at least through the second tier. Therefore, the development of the first tier criteria for pure loss of stability and parametric rolling is a top priority at this stage.

## 5 CONCLUSIONS

The deadline for proposing new methodologies with sample ship calculation is the end of June 2010 so that their development is urgent. Then verification, validation and refinement of the proposed methodologies will be required under collaboration of member states via their own or international research projects among experts in this research area for finalising the new generation intact stability criteria by 2012, which is the target date agreed at the IMO.

## REFERENCES

- Bassler, C., Belenky, V., Bulian, G., Francescutto, A., Spyrou, K., Umeda, N., 2009, "A Review of Available Methods for Application to Second Level Vulnerability Criteria", Proceedings 10<sup>th</sup> International Conference on Stability of Ships and Ocean Vehicles", A. B. Degtyarev Ed., Saint-Petersburg, pp. 111-128,.
- Bulian, G., Francescutto, A., Zotti, I., 2009, "The New International Regulations for Intact Stability, Subdivision and Damage Stability of Ships", CD Proceedings 12th International Conference on Transport Science – ICTS'2009 - Transport Science, Profession and Practice, Portorož, pp. 1-8.
- Bulian, G., Francescutto, A., Umeda, N., 2006, "The Development of Performance Oriented Intact Stability Criteria: Basic Aspects that should be Addressed", Proceedings International Conference on Ship and Shipping Research NAV2006, Genova, Vol. I, pp. 4.5.1-4.5.12.
- Chairman of the ISWG, 2008, "Revision of the Intact Stability Code - Report of the Working Group (part I)", SLF 51/WP.2, IMO (London).
- Chairman of the ISWG, 2010, "Development of New Generation Intact Stability Criteria – Report of the working group (Part 1)", SLF52/WP.1, IMO (London).
- IMO, 2008, "Explanatory Notes to the International Code on Intact Stability, 2008", MSC.1/Circ.1281, IMO (London).
- IMO, 2009, "International Code on Intact Stability, 2008 Third Edition", IMO (London).
- Umeda, N., Francescutto, A., 2008, "Performance-Based Ship Operation", Proc. 2nd International Workshop on Risk-Based Approaches in Maritime Industry, Glasgow, pp. 1-9.



## On Vulnerability Criteria for Righting Lever Variations in Waves

William S. Peters

Naval Architecture Division, Office of Design and Engineering Standards, U.S. Coast Guard

Vadim Belenky, Christopher C. Bassler

David Taylor Model Basin (DTMB), Naval Surface Warfare Center, Carderock Division

### ABSTRACT

This paper proposes assessment methods for use in evaluating level 1 and level 2 vulnerability, as outlined in the IMO preliminary specification for the new generation intact stability criteria under development in the Subcommittee on Stability and Load Lines and on Fishing Vessels Safety (SLF) of IMO. Particularly, these methods are developed for the identification of problems related to righting lever variations in waves— pure-loss of stability and parametric roll. Using these methods, the assessment results for a population of sample ships are presented and discussed.

### KEYWORDS

dynamic stability, pure-loss of stability, parametric roll, righting lever

### A REGULATORY PERSPECTIVE<sup>1</sup>

The international effort to not only develop, but also establish, new generation intact stability criteria in a community in which there is a general perception that adequate criteria already exists is a big challenge. History is replete with examples of efforts to replace something old with something new that have been dashed upon the rocks of prevailing contrary opinion.

In the international stability community, the example of how the 1973 IMO resolution A.265 on probabilistic damage stability for passenger ships was not incorporated into the 1974 SOLAS Convention but retained as an “equivalent” to existing criteria is a reminder

that substantial effort to develop a criterion can be met with disappointment, if the requirement for the criterion is sidelined (Robertson *et al.*, 1974). This problem was described five centuries ago in Machiavelli’s famous work *The Prince* (1532):

“There is nothing more difficult to take in hand, more perilous to conduct, or more uncertain in its success, than to take the lead in the introduction of a new order of things, because the innovator has for enemies all those who have done well under the old conditions, and lukewarm defenders in those who may do well under the new. This coolness arises partly from fear of the opponents, who have the laws on their side, and partly from the incredulity of men, who do not readily believe in new things until they have had a long experience of them.”

Recognizing this challenge, the case of the new generation intact stability criteria development may benefit from being considered as a companion or addition to the existing criteria rather than a replacement. In every respect, however, the need exists to demonstrate many times that the benefits of the new criteria outweigh the cost and in several

---

<sup>1</sup> This paper expresses the personal views of the authors, which are not necessarily the official views of the U.S. Coast Guard or the Department of the Navy.

forums, so that the new criteria may enjoy the best chance of acceptance. To assist this objective, the new criteria must be shown to be robust, which is a need that requires substantial verification.

The framework for new generation intact stability criteria (Annex 1, SLF 51/WP.2) covers dynamic stability failures related to righting lever variations in waves (pure-loss of stability and parametric roll), broaching, and dead ship conditions (see also Belenky, *et al.*, 2008). A multi-tiered approach is included in the preliminary specification for the new criteria, where initial analysis is done using vulnerability criteria that progresses from a simple assessment (level 1) to a more performance-based assessment (level 2) (Annex 2, SLF 52/WP.1). If the likelihood of one or more dynamic stability failure modes is indicated by the vulnerability criteria, then direct assessment methods are applied. The identification of hull forms that may have increased risk of these stability failures early in the design process allows ship design managers to justify hull form modifications or to undertake the necessary planning and budgeting for direct assessments using advanced hydrodynamic codes, numerical simulations and/or model experiments.

These vulnerability criteria are currently under development by the Correspondence Group on Intact Stability, established by IMO's SLF Subcommittee and its latest report contains the status of this development (SLF 52/3/1; SLF 52/INF.2).

In the case of righting lever variations in waves, several methods have been proposed to assess vulnerability for pure-loss of stability and parametric roll (levels 1 and 2). In order to provide a practical tool for the designer and regulator, several considerations must be examined. These include the ability to distinguish vulnerable ships from ships that are not vulnerable to these modes of stability failure, the ease of use of the methods (including input data requirements, calculation time, and interpretation and allowable error of

the results), and development of the standard (or safety level) using the criteria.

A useful standard for level 1 vulnerability assessment must be conservative, so that all ships which may be vulnerable to this mode of stability failure fail to meet the standard and therefore, must be assessed using a higher-fidelity approach (level 2 and possible direct assessment). If the standard is set at a threshold where some ships are able to pass, despite the possibility of vulnerability to the failure mode, then it fails to meet its objectives of usefulness to the designer and regulator. However, at the same time, the standard should not be overly conservative, such that nearly all ships fail, and require further assessment, which would negate the usefulness of the method.

#### TESTED SAMPLE SHIP TYPES

Twelve diverse ship types were examined to test the applicability of the proposed vulnerability criteria for righting lever variation modes of stability failure (pure-loss and parametric roll). The ship types considered included: a bulk carrier, a tanker (VLCC), five containerships, two general cargo ships, a RoPax, and a pair of notional naval combatants, specifically designed for research purposes (Table 1). The critical loading condition, limiting *GM*, is given based on the 2008 Intact Stability (IS) Code. This was used for the assessment of pure-loss of stability. For the assessment of parametric roll, a typical operational loading condition was used. The range of characteristics for the sample ship population is shown in Fig. 1.

**Table 1: Ship types and general characteristics**

Type	L/B	B/T	C <sub>B</sub>	Critical GM (m)
Bulk Carrier	5.85	2.24	0.85	4.192
Containership 1	7.07	3.05	0.62	0.1506
Containership 2	6.53	3.62	0.61	0.1507
Containership 3	7.24	3.14	0.64	0.1507
Containership 4	8.80	2.51	0.65	0.1509
Containership 5	6.55	3.12	0.55	0.1505
General Cargo 1	7.01	2.50	0.70	0.1504
General Cargo 2	7.05	2.73	0.57	0.1507

RoPax	6.76	3.64	0.60	0.3625
Tanker	5.52	2.76	0.80	1.723
Naval Combatant 1	8.19	3.42	0.54	0.20
Naval Combatant 2	8.19	3.42	0.54	1.161

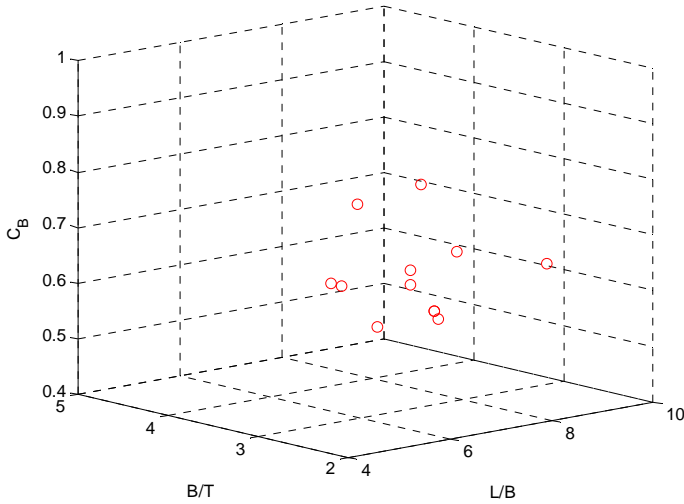


Fig. 1: Sample ship population characteristics:  $L/B$ ,  $B/T$ , and  $C_B$ .

Containership 5 is the C11-class containership. General cargo ship 1 is Series 60 hull form,  $C_B=0.7$  variant (Todd, 1953). General cargo ship 2 is the C4 type, similar to the one used in Paulling, *et al.* (1972). Naval combatants 1 and 2 are the ONR Topsides Series, flared and tumblehome configurations, respectively (Bishop, *et al.*, 2005). The RoPax is a notional vessel similar to the one from a reported stability accident (MNZ, 2007).

### LEVEL 1 VULNERABILITY CRITERIA FOR PURE-LOSS OF STABILITY AND PARAMETRIC ROLL

Because both of the modes of intact stability failure considered here, pure-loss and parametric roll, are fundamentally a result of the relation between changes in the area of the waterplane and the location of the wave crest along the hull, a common criterion to assess level 1 vulnerability is proposed. Four prospective criteria are discussed, along with the results for the sample ships.

### Method

A method to assess level 1 vulnerability to pure-loss of stability and parametric roll, based on static characteristics of the hull form, is proposed and four criteria were examined. The first criterion considered the value of the total coefficient for vertical “wall-sidedness,”  $C_{VWS}$ , or the variability of hull shape from the maximum dimensions over the range of draft,  $\max(A_{WP}(z))$ ,  $z \in [d - \Delta d; d + \Delta d]$ , which is similar to the more traditional vertical prismatic coefficient,  $C_{VP}$ , taken from the calm waterplane. This provides an indication of the change of the shape of the hull from the volume projected using the maximum waterplane dimensions over the vertical height of the ship.

$$C_{VWS} = \frac{\int_{d-\Delta d}^{d+\Delta d} A_{WP}(z) dz}{\max(A_{WP}(z)) \cdot 2\Delta d} \quad (1)$$

$$\Delta d = \max\left(\frac{d}{2}, \frac{L}{20}, D - d\right)$$

The second criterion considered the average of the vertical wall-sidedness coefficients for the fore and aft quarter portions of the hull, both above and below the waterline (Fig. 2). For each of the four sections (fore, aft, above, and below), the  $C_{VWS}$  was computed as the fraction of the volume from the maximum waterplane projection for the given section. Then the average value for the four sections was used to provide an indication of the total relative changes for the bow and stern shapes, both above and below the waterline.

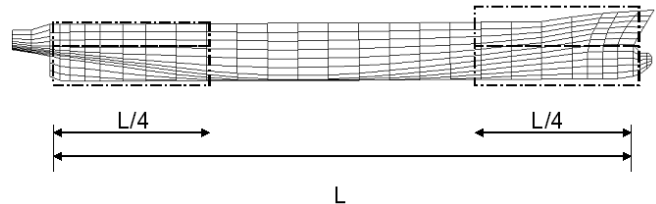


Fig. 2: Notional ship profile with the four portions of the  $C_{VWS}$  considered for the level 1 vulnerability assessment.

The third criterion considered the ratio of the transverse metacentric radius to the height of the transverse metacenter above the keel.

$$C1_3 = \frac{BM}{KM} \quad (2)$$

The fourth criterion considered the ratio of the transverse metacentric radius to the beam.

$$C1_4 = \frac{BM}{B} \quad (3)$$

**Results**

The first criterion does not show any clear separation between the ships which are known to be vulnerable and the ships which are not (Fig. 3). However, the second criterion, the average of the vertical wall-sidedness coefficient for the fore and aft quarters of the ship, seems to provide useful separation between the ships (Fig. 4) for this sample population.

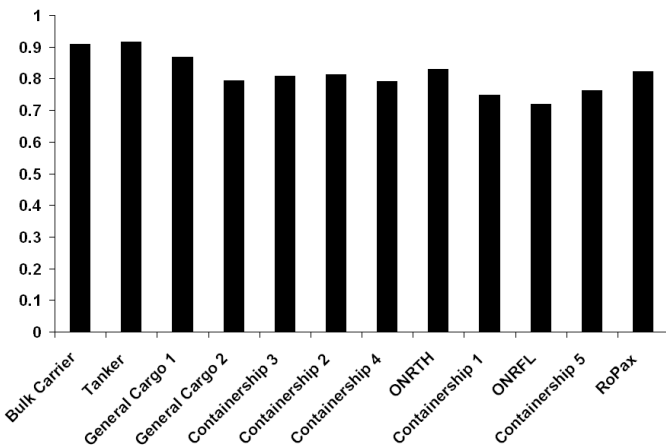


Fig. 3: Total Cws, both above and below the waterline, for the sample ship population.

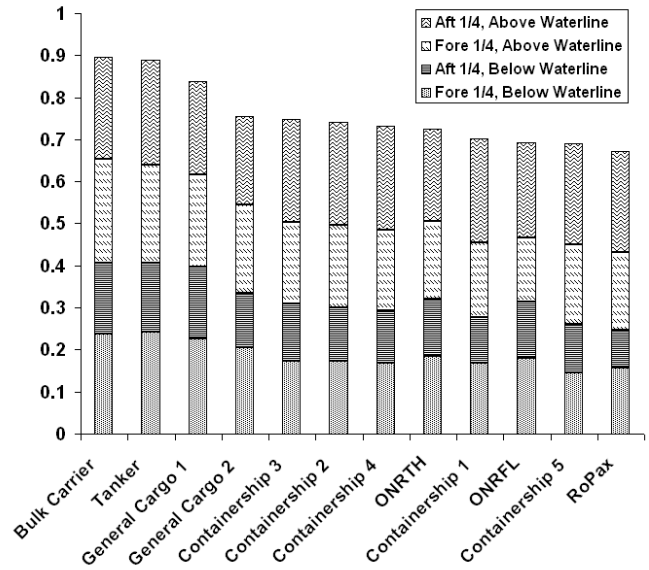


Fig. 4: Total average Cvws for the fore and aft quarters of the ship, both above and below the waterline, for the sample ship population. The contributions from each component of the average Cvws are identified.

Based on this sample population of ships, an initial estimate of the threshold for the standard could be proposed around 0.75-0.80. Ships above this value, the bulk carrier, tanker, and Series 60 are considered to be conventional vessels, not at risk for failures related to righting lever variations in waves. However, all of the other nine ships fall below this value, the highest being the general cargo ship 2, or C4, with a value of 0.75. The ships with the lowest values are containership 5 (the C-11 containership) and the RoPax, which have values of 0.69 and 0.67, respectively.

Of the four vertical wall-sidedness coefficients, fore and aft quarter, above and below the waterline, the aft coefficient above the waterline has the least variation for the ship population examined. However, in order to account for ships outside this population, with unconventional topside stern shapes, this effect should still be included.

The third and the fourth criteria, using ratios with the transverse metacentric radius, did not show any clear separation between the ships which are known to be vulnerable and the ships which are not.

The proposed method for level 1 vulnerability assessment does not consider the relative size of the ship and the waves. Typically it is assumed that higher sea states are more likely to result in stability failure. However, waves of large height are more likely to have larger length and waves of large length may not greatly affect stability, depending on their comparison with ship length. This important consideration is included in the proposed level 2 assessment methods.

## LEVEL 2 VULNERABILITY CRITERIA FOR PURE-LOSS OF STABILITY

The procedure described for vulnerability level 2 criteria for pure-loss of stability is based on SLF 52/INF.2, Annex 6. Further refinements and improvement to the method are discussed in Belenky & Bassler (2010), including application of the method to naval-type vessels.

### Methods

Pure loss of stability may be considered as a single wave event because of instantaneous changes in waterplane area. Typically, the worst-case wavelength is close to the length of the ship,  $\lambda/L \approx 1.0$ . However, in order to account for the effect of ship size relative to the wave conditions, righting lever variations should be evaluated in irregular waves. To characterize an event of pure-loss of stability, the distribution of random wave numbers and wave amplitudes,  $f(A,k)$ , is used to evaluate statistical weight of a wave encounter:

$$W_{ij} = \int_{A_j - \Delta A}^{A_j + \Delta A} \int_{k_j - \Delta k}^{k_j + \Delta k} f(A,k) dk dA \quad (4)$$

The  $GM$  value is calculated for each sinusoidal wave, with characteristics as defined above. These calculations are repeated for different positions of the wave crest along the ship length, so a complete wave pass is presented.

Calculation of the time while the stability is decreased can be easily performed when the  $GM$  is considered as a function of the wave

crest. The critical  $GM$  was calculated with the 2008 IS Code (Fig. 5).

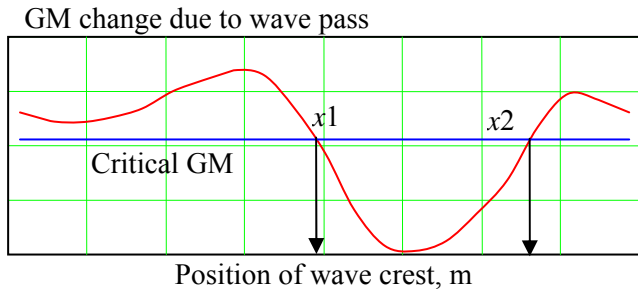


Fig. 5: Calculation of “time-below-critical-GM”

Points  $x1$  and  $x2$  (Fig. 5) show the distance when the  $GM$  remains below the critical level (based on 2008 IS Code), while the wave passes the ship. The “time-duration-below-critical  $GM$ ”,  $tbc$ , can be calculated as:

$$tbc = \frac{x2 - x1}{c - V_s} \quad (5)$$

where  $c$  is wave celerity and  $V_s$  is ship speed. The time-below-critical  $GM$  is a random number in irregular waves. Its mean value is estimated as:

$$m(tbc) = \sum_i \sum_j tbc_{ij} W_{ij} \quad (6)$$

The criterion value,  $Cr1$ , is proposed as the following ratio:

$$Cr1 = \frac{m(tbc)}{T_\phi} ; \quad (7)$$

where  $T_\phi$  is natural period of roll corresponding to critical  $GM$ .

This criterion assesses the significance of stability change in waves. If stability is degraded only for a short duration, this degradation may not be significant. However, for longer durations of decreased stability below the critical level, the restoring moment may be degraded enough to result in a dangerously large roll angle.

The second criterion is set to detect if there were significant durations of negative  $GM$ . Appearance of an angle of loll may lead to the development of partial stability failure faster, as the upright equilibrium is no longer stable. It is quite possible that some ships may be more vulnerable for these types of failure than others (see the example for a notional RoPax vessel in Fig. 6).

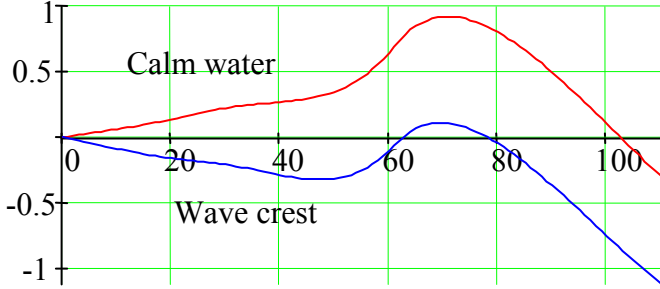


Fig. 6: Deterioration of GZ curve near wave crest

The second criterion,  $Cr2$ , is based on characteristics of time when the angle of loll is above a certain limit angle,  $\phi_{lim}$  (30 degrees was used in this example). For each position of the wave crest along the hull, the indicator value,  $z$ , is calculated:

$$z = \begin{cases} 0 & \text{if } \phi_{loll} < \phi_{lim} \\ 1 & \text{if } \phi_{loll} \geq \phi_{lim} \end{cases} \quad (8)$$

The angle of loll,  $\phi_{loll}$ , can be obtained from the “true” instantaneous  $GZ$  curve in waves, or from its approximation using a calm water  $GZ$  curve and the instantaneous  $GM$  in waves:

$$GZ_w(\phi, t) = \frac{GM_w(t)}{GM_0} GZ_0(\phi) \quad (9)$$

Here the index “0” refers to calm water conditions. The time while the angle of loll is too large during the wave pass is expressed as:

$$tbz = \sum_k z_k \Delta t \quad (10)$$

where  $\Delta t$  is the time-step and index  $k$  corresponds to a particular time instant during the wave pass.

Formulation of the second criteria is similar to the first one:

$$Cr2 = \frac{m(tbz)}{T_\phi} \quad (11)$$

where  $m(tbz)$  is the weighted average over the wave encounters:

$$m(tbz) = \sum_i \sum_j tbz_{ij} W_{ij} \quad (12)$$

## Results

Results are shown for calculations using the two criteria ( $Cr1$  and  $Cr2$ ) for the sample ships. The results (Fig. 7) are given for Sea State 7 and an operational speed of 15 knots, with the critical  $KG$  based on the conditions from compliance with the 2008 IS Code.

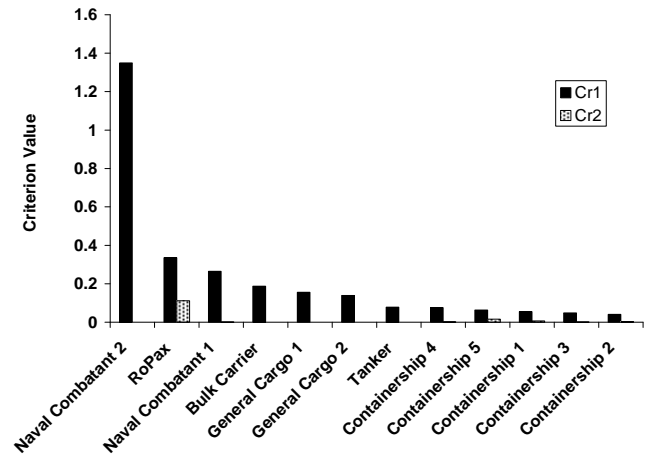


Fig. 7: Calculation results for the two level 2 vulnerability criteria for pure-loss of stability for the sample ships, ship speed of 15 kts, in Sea State 7.

Comparing the sample calculations for the level 2 probabilistic criterion,  $Cr1$ , it can be observed that there is a great distinction between the Naval Combatant 2 (ONR tumblehome topside hull), which is known to be vulnerable to pure-loss of stability (Bishop,

*et al.*, 2005; Bassler, *et al.*, 2007; Hashimoto, 2009), compared to other ships, which are not known to be vulnerable to this type of stability failure, except for the notional RoPax. Given these results, and the sample calculations with a notional naval fleet (Belenky & Bassler, 2010), a standard using this criterion could be set around 1.0.

The second criterion indicates possible vulnerability for the notional RoPax vessel that is similar to one that attained large roll angles in stern waves (MNZ, 2007).

## LEVEL 2 VULNERABILITY CRITERIA FOR PARAMETRIC ROLL

### Method

Vulnerability to parametric roll is determined by the maximum angle of roll response on a “typical” wave group, related to a given sea state, see SLF 52/INF.2, Annex 7.

The “typical” wave group (Fig. 8) is assumed to consist of a number of waves of the same length, and a wave period corresponding to the spectral mean period. The amplitude of the group is considered as a function of time only; its spatial change is not modeled. A more detailed method to determine the characteristics of a “typical” group for a given sea state is currently under development. Recently, a method to identify wave groups, based on ship-specific considerations for the amplitude and duration has been proposed (Bassler, *et al.*, 2010).

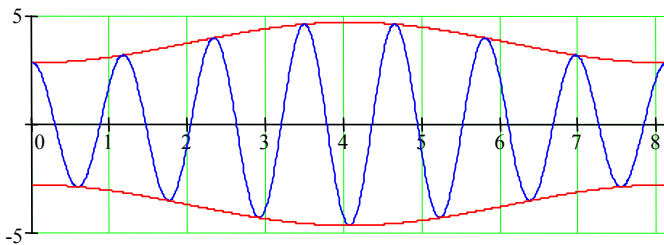


Fig. 8: Model of “typical” wave group

As parametric resonance may occur both in following and head waves, the attitude of a ship is calculated based on heave and pitch response on a wave group:

$$\begin{cases} (M + A_{33})\ddot{\zeta}_G + B_{33}\dot{\zeta}_G + F_\zeta(\zeta_G, \theta, t) = 0 \\ (I_Y + A_{55})\ddot{\theta} + B_{55}\dot{\theta} + M_\theta(\zeta_G, \theta, t) = 0 \end{cases} \quad (13)$$

where  $M$  is mass of the ship,  $I_Y$  is mass moment of inertia relative to the transversal axes,  $A_{33}$  and  $A_{55}$  are heave added mass and pitch moment of inertia (assumed to be equal to the corresponding mass and moment of inertia), respectively; and  $B_{33}$  and  $B_{55}$  are damping coefficients for heave and pitch. Functions  $F_\zeta$  and  $M_\theta$  are the difference between Froude-Krylov and hydrostatic forces and moments at the instant of time,  $t$ . These values are expressed as follows:

$$F_\zeta(\zeta_G, \theta, t) = \rho g \left( V_0 - \int_{-0.5L}^{0.5L} \Omega(x, z(\zeta_G, \theta, t)) dx \right) \quad (14)$$

$$M_\theta(\zeta_G, \theta, t) = \rho g \left( V_0 \cdot LCB_0 - \int_{-0.5L}^{0.5L} M_\Omega(x, z(\zeta_G, \theta, t)) dx \right) \quad (15)$$

where  $\rho$  is mass density of water,  $V_0$  volumetric displacement in calm water,  $LCB_0$  is the longitudinal position of center of buoyancy in calm water. Functions  $\Omega$  and  $M_\Omega$  calculate an area and a static moment relative to the  $y$ -axis of a station located at abscissa  $x$ . The second argument of this function shows submergence of this station, as expressed by the function of instantaneous waterline  $z(\zeta_G, \theta, t)$ , see Fig. 9. These waterlines allow for the evaluation of the  $GM$  response to the wave group (Fig. 10).

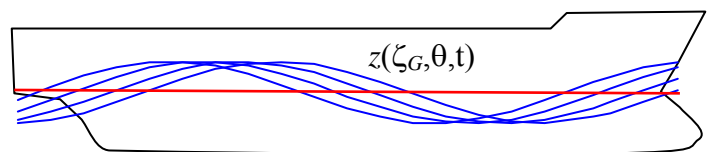


Fig. 9: Sample instantaneous waterlines evaluated from

heave and pitch response on a group

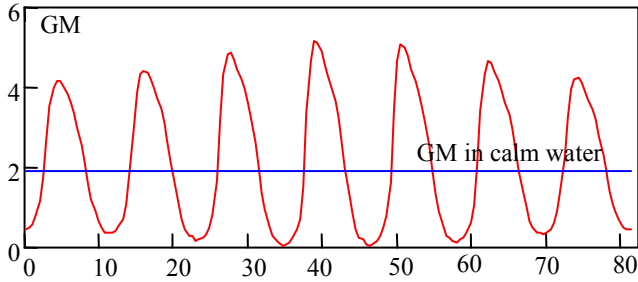


Fig. 10: GM response on “typical” wave group, with the GM value in calm water shown in blue.

The  $GM$  response to a “typical” wave group then can be approximated using a sine function with time-dependent amplitude:

$$f_L(\phi, t) = \frac{GM_m + GM_a(t) \cos(\omega_e t + \phi)}{GM} \quad (16)$$

where  $\omega_e$  is the encounter frequency,

$$\omega_e = \omega_1 + k_1 V_S \quad (17)$$

and where  $\omega_1$  and  $k_1$  are the wave frequency and wave number corresponding to the mean spectral period,  $V_S$  is forward speed, chosen to satisfy the frequency condition for principal parametric resonance, while keeping the value within the achievable range for the given vessel in the considered sea state. Roll response is evaluated by the numerical solution of the roll equation with stiffness (16) and assumed roll damping. The initial conditions for the numerical solution of roll motion can be chosen as 5-10 degrees for the initial roll angle and zero roll rate.

$$\ddot{\phi} + 2\delta_\phi \dot{\phi} + \omega_0^2 f_L(\phi, t) = 0 \quad (18)$$

Equation (18) is essentially the Mathieu equation. If the amplification of roll

oscillations is observed, then parametric excitation is large enough, taking into account speed limitations. The largest absolute value of the roll angle observed during the wave group pass can be used as a criterion:

$$CrL = \max(|\phi|) \quad \text{for } f = f_L \quad (19)$$

Due to significant nonlinearity of the GZ curve, the development of parametric resonance may be reversed as the change in instantaneous  $GM$  with roll angle may take the system out of the Mathieu instability region (Spyrou, 2004).

To model this nonlinearity, formula (9) can be used in the roll equation with nonlinear stiffness. Equation (20) is a variation of Hill's equation:

$$f_N(\phi, t) = \frac{GZ_w(\phi, t)}{GM} \quad (20)$$

$$\ddot{\phi} + 2\delta_\phi \dot{\phi} + \omega_0^2 f_N(\phi, t) = 0 \quad (21)$$

However, it may be necessary to extend (20) up to 180 degrees to avoid numerical issues while solving equation (21), see Fig.11.

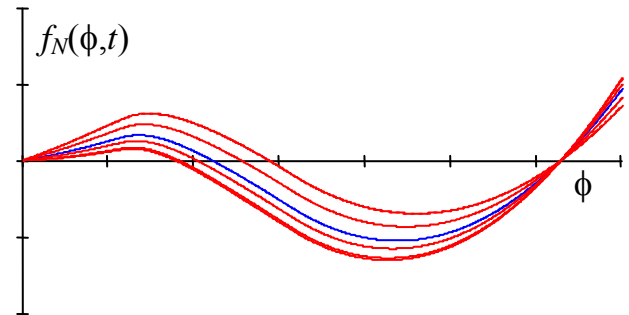


Fig. 11: GZ curve modeled for response on “typical” wave group

Instead of the approximation (9), the actual GZ curve in waves can be used as well. Based on the solution of (21), the second criterion,  $CrN$ , is formulated:

$$CrN = \max(|\phi|) \quad \text{for } f = f_N \quad (22)$$

Due to nonlinearity of the time-dependent stiffness, it is not known in advance what frequency region may lead to parametric resonance, so several speeds with the achievable range must be used.

**Results**

Results are shown for the two criteria ( $CrL$  and  $CrN$ ) for the sample ships (Fig. 12). The values used for the evaluation for each ship are given in Table 2. For the ships considered, a common damping ratio was chosen, typical for these types of ships. For the two naval combatants, which typically have larger bilge keels and therefore, a larger damping ratio was specified. The  $GM$  condition used was a typical operational load condition for each of the sample ships,  $GM_{OP}$ . Sea States 5-8 were evaluated, but only the particular sea state where parametric roll was observed and the given speed condition to satisfy the frequency ratio conditions are presented.

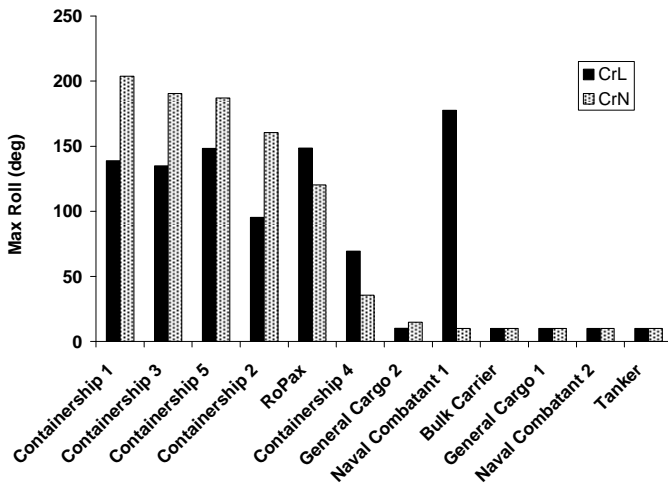


Fig. 12: Calculation results for the two level 2 vulnerability criteria for parametric roll for the sample ships in Sea State 7.

**Table 2: Ship types and general characteristics**

Type	Sea state	$GM_{OP}$ (m)	Roll damp.	Speed (kts)
Bulk Carrier	7	9.41	0.05	10
Containership 1	7	1.12	0.05	10
Containership 2	7	1.84	0.05	2

Containership 3	8	1.64	0.05	1
Containership 4	7	1.06	0.05	10
Containership 5	7	1.91	0.05	0
General Cargo 1	6	0.25	0.05	9.3
General Cargo 2	6	1.10	0.05	5.1
RoPax	6	1.77	0.05	25
Tanker	7	9.76	0.05	10
Naval Combatant 1	6	1.03	0.15	15
Naval Combatant 2	6	3.01	0.15	25

Modern containerships, particularly the C11-class containership, are known for their vulnerability to parametric roll (France, *et al* 2003). The proposed criteria shows large roll angles for all five containerships, as well as the notional RoPax vessel, encountering representative wave groups in Sea State 6, 7, and 8. As expected, Series 60, which is representative of a conventional ship type, the tanker, and bulk carrier did not show any vulnerability for the considered loading and operational conditions.

Both ONR Topside configurations (flared and tumblehome) have relatively large bilge keels. The damping ratio used was meant to model the fully appended hulls. While the ONR Tumblehome Topside did not show any parametric roll for the analyzed loading condition, parametric roll was observed for ONR Flared Topside, using the linear formulation. However, parametric roll was not observed from earlier numerical and experimental investigations for these hull forms (Bassler, 2008; Olivieri, *et al.*, 2008; Hashimoto and Matsuda, 2009), including for the flared topside configuration with roll damping coefficients, corresponding to the fully appended hull. However, when the instantaneous  $GZ$  curve is used instead of the approximation, parametric roll was not indicated, which corresponded to previous findings.

**CONCLUSIONS**

Several methods were proposed to assess vulnerability to righting lever variations in

waves (pure-loss of stability and parametric roll). Calculation results for a sample population of 12 ships were examined for both simple, geometry-based (level 1) and more complex (level 2) analysis methods. Of the proposed criteria, one for level 1 vulnerability to pure-loss and parametric roll, and two for level 2 pure-loss of stability and one for level 2 parametric roll show promise for possible criteria to assess these modes of stability failure in early-stage ship design. However, additional work remains to determine results for the methods with a larger population of sample ships and then determine possible standards for the criteria.

## ACKNOWLEDGEMENTS

The authors appreciate support of this work from the Office of Design and Engineering Standards, U.S. Coast Guard Headquarters. Earlier contributions related to this work have been supported by Mr. James Webster (NAVSEA) and Dr. Patrick Purtell (ONR). The authors are grateful to Mr. Martin J. Dipper, Jr. (NSWCCD), Prof. Naoya Umeda (Osaka University), Prof. Alberto Francescutto and Dr. Gabriele Bulian (University of Trieste), and Prof. Kostas Spyrou (NTUA) for fruitful discussions which helped to shape the ideas discussed in this paper. The authors also appreciate Dr. Arthur Reed and Mr. Terrence Applebee (NSWCCD) for their support.

## REFERENCES

- Bassler, C, B. Campbell, W. Belknap, and L. McCue (2007), "Dynamic Stability of Flared and Tumblehome Hull Forms in Waves," *Proc. 9th Intl. Ship Stability Workshop*, Hamburg, Germany.
- Bassler, C. (2008), "Application of Parametric Roll Criteria to Naval Vessels," *Proc. 10th Int. Ship Stability Workshop*, Daejeon, South Korea.
- Bassler, C. C. V. Belenky, and M. J. Dipper, Jr. (2010), "Application of Wave Groups to Assess Ship Response in Irregular Seas," *Proc. 11<sup>th</sup> Intl. Ship Stability Workshop*, Wageningen, The Netherlands.
- Belenky, V., J. O. de Kat, and N. Umeda (2008), "Toward Performance-Based Criteria for Intact Stability," *Marine Technology*, 45(2).
- Belenky, V. and C. Bassler (2010), "Procedures for Early-Stage Naval Ship Design Evaluation of Dynamic Stability: Influence of the Wave Crest," *Proc. American Society of Naval Engineers (ASNE) Day 2010*, Arlington, VA.
- Bishop, R. C., W. Belknap, C. Turner, B. Simon & J. H. Kim (2005), "Parametric Investigation on the Influence of GM, Roll Damping, and Above-Water Form on the Roll Response of Model 5613," Hydromechanics Dept. Technical Report, NSWCCD-50-TR-2005/027.
- France, W.M, Levadou, M, Treacle, T.W., Paulling, J. R., Michel, K. and Moore, C. 2003. "An Investigation of Head-Sea Parametric Rolling and its Influence on Container Lashing Systems," *Marine Technology*, Vol. 40, No. 1, pp. 1-19.
- Hashimoto, H. (2009), "Pure Loss of Stability of a Tumblehome Hull in Following Seas," *Proc. of the 19th Intl. Offshore and Polar Engineering Conf.*, Osaka, Japan.
- Hashimoto, H. and A. Matsuda (2009), "Parametric Roll of a Tumblehome Hull in Head Seas," *Proc. 19th Intl. Offshore and Polar Engineering Conf.*, Osaka, Japan.
- IMO SLF 51/WP.2 (2008) Revision of the intact stability code, Report of the working group (part 1), London.
- IMO SLF 52/3/1 (2009), Report of the Intersessional Correspondence Group on Intact Stability. Submitted by Japan, London.
- IMO SLF 52/INF.2 (2009), Information collected by the Intersessional Correspondence Group on Intact Stability. Submitted by Japan, London.
- IMO SLF 52/WP.1 (2010) Development of new generation intact stability criteria, Report of the working group (part 1), London.
- Machiavelli, N. (1532), *The Prince*.
- Maritime New Zealand (2007), "Incident Report Heavy Weather/Cargo Shift *Aratere* 3 March 2006," Maritime

New Zealand Investigation Report, 23 August.

Olivieri, A, A. Francescutto, E. F. Campana, and F. and Stern (2008), "Parametric Roll: Highly Controlled Experiments for an Innovative Ship Design," *Proc 27th Int. Conf on Offshore Mechanics and Arctic Engineering*, Estoril, Portugal.

Paulling, J. R., S. Kastner, and S. Schaffran (1972), "Experimental Studies of Capsizing of Intact Ships in Heavy Seas," U.S. Coast Guard Technical Report (also IMO Doc. STAB/7, 1973).

Robertson, J., G. Nickum, R. Price, and E. Middleton (1974), "The New Equivalent Regulations on Subdivision and Stability of Passenger Ships," *Trans. SNAME*, 344.

Spyrou, K.J. 2004, "Criteria for Parametric Rolling?," *Proceedings of 7<sup>th</sup> International Ship Stability Workshop*, Shanghai, China, 1-3 Nov. 2004

Todd, F. H. (1953), "Some Further Experiments on Single-Screw Merchant Ship Forms," *Trans. SNAME*, Vol. 61, pp. 516-589.



## Designing New Generation Intact Stability Criteria on Broaching Associated with Surf-Riding

Naoya Umeda and Shinya Yamamura

Osaka University, Japan

### ABSTRACT

This paper describes a proposal of new generation intact stability criteria on broaching associated with surf-riding for contributing to discussion at the IMO (International Maritime Organization). It consists of two-layered vulnerability criterion and direct assessment procedures. The first layer vulnerability criterion indicates critical ship speed for avoiding surf-riding in following regular waves, which is determined with sample calculation results of several ships using numerical global bifurcation analyses. Under certain wave conditions, a ship is required to reduce her speed below this critical speed. Alternatively, the ship may use the result of numerical or analytical bifurcation analysis with her own geometric and hydrodynamic data as the critical speed in the use of operational guidance. This is the second layer vulnerability criterion. If the ship fails to comply with both the vulnerability criteria, the direct assessment procedure is applied to her. It requires the failure probability due to broaching associated with surf-riding in the North Atlantic is smaller than the acceptable level. Here the probability is calculated using the combination of deterministic ship dynamics and probabilistic wave theory. If the ship fails it, the failure probabilities for stationary sea states are required to be noted in her ship stability booklet as an onboard operational guidance. For demonstrating feasibility of these criteria, sample calculation results with a fishing vessel and a RoPax ship are shown and impact on design aspects are also investigated.

### KEYWORDS

Surf-riding threshold; global bifurcation; broaching probability; operational guidance; rudder size.

### INTRODUCTION

At the IMO, new generation intact stability criteria on major capsizing modes are now under development. Broaching associated with surf-riding is one of these major capsizing modes. It was already agreed that the new criteria should be physics-based, consist of vulnerability criteria and direct stability assessment and be supplemented with operational guidance (IMO, 2008). Here the vulnerability criteria could consist of two levels: one shall be simpler but with larger

margin and the other shall be more complex but with less conservative (IMO, 2010). The delegation of Japan (2009) submitted the draft criteria on broaching to the 52<sup>nd</sup> session of the Sub-Committee on Stability, Load lines and on Fishing Vessel Safety (SLF) of the IMO via the ISCG (Intersessional Correspondence Group on Intact Stability) with sample calculation results last year. In the draft vulnerability criteria here, the calm-water Froude number is requested to be smaller than the threshold of surf-riding in regular following waves, which

can be regarded as a heteroclinic bifurcation of uncoupled surge model. For the level 1 vulnerability criterion, the surf-riding threshold is empirically determined to be 0.3 as the current operational guidance known as MSC.1/Circ. 1228 (Japan, 1991). For the level 2 vulnerability criterion, it is required to be directly calculated by a numerical or analytical bifurcation analysis (Umeda et al., 2007b) (Maki et al., 2010) together with a comparison of wave-induced and rudder-induced yaw moment. (Yamamura et al., 2009) For the direct stability assessment, a method based on combination of deterministic simulation and probabilistic wave theory is recommended (Umeda et al., 2007a). If the ship can comply with one of the above-mentioned three criteria, it can be regarded as safe within the scheme of the draft proposal in Japan.

At the SLF 52 this January, some delegations expressed their concern that the draft level 1 criterion could penalise all ships having the calm-water Froude number of 0.3 or over and then recommended to consider the ship size. The delegation of IACS (International Association of Classification Societies) is of the opinion that the use of direct stability assessment should be exceptional so that feasibility of vulnerability criteria is essential. And the deadline for proposing new criteria is set to be June 2010 at the IMO. Therefore, drafting a new generation intact stability criteria on broaching associated with surf-riding is an urgent task for member states of the IMO.

Recognising these situations, the authors attempt to contribute to this further

development of new generation intact stability criteria on broaching associated with surf-riding. As a whole, it is recommended that new criteria shall be supplemented with ship-dependent operational guidance at each level. Firstly, a new draft level 1 criterion is proposed with hull form effect taken into account. Secondly, a new draft level 2 criterion is developed with effect of ship size taken into account. Here the mutual relationship between the level 2 and the direct stability assessment is carefully adjusted. Finally, a design impact of the direct stability assessment based on the combination of deterministic ship dynamics and probabilistic wave theory is remarked with a sample calculation.

## **LEVEL 1 VULNERABILITY CRITERION**

### *Background*

For broaching, estimation of surf-riding threshold in regular following waves could be used as a vulnerability criterion. This is because the surf-riding is a prerequisite for broaching. In addition, broaching without surf-riding can be generally avoided with appropriate operational efforts such as a differential control (Spyrou, 1997) and an optimal control (Maki & Umeda, 2009).

In the operational guidance, MSC.1/Circ. 1228, surf-riding threshold is assumed to be the calm-water Froude number of 0.3 for all ships. This is based on phase plane analyses of uncoupled surge model in regular following waves with the wave steepness of 0.1 for conventional ships. Theoretically this surf-riding threshold depends on mainly calm-water resistance and the Froude-Krylov surge force.

It was recently reported, however, the surf-riding threshold could be smaller than the calm-water Froude number of 0.3 for finer ships. Thus it is important to develop a simple formula to empirically estimate surf-riding threshold as a function of hull form.

**Proposal Based on Sample Calculations**

For determining the surf-riding threshold, a numerical global bifurcation analysis is applied to several ships. Since surf-riding can be regarded as an equilibrium of the uncoupled surge model defined with a wave-fixed inertia system, a heteroclinic orbit represents a periodic orbit having infinite period. Here the heteroclinic bifurcation point, in which the unstable invariant manifold of a saddle-type equilibrium coincides with the stable invariant manifold of a different saddle-type equilibrium, is identified by the Newton method. (Umeda et al., 2007) The subject ships used here include a RoRo ship, a post Panamax containership, two high-speed slender ships and three fishing vessels. Here their calm-water resistance curves are estimated with conventional model tests and the wave-induced surge force is calculated with the Froude-Krylov assumption. The wave steepness is set to be 1/10 as the current operational guidance and the wavelength is the worst cases in the range of the wavelength to ship length ratio from 1.0 to 2.0. The calculated results are plotted in Fig. 1 as a function of the prismatic coefficient. When the ship becomes finer, the critical speed for surf-riding becomes smaller. This is because the clam-water resistance depends on the prismatic coefficient as shown in Fig. 2. If the prismatic coefficient is small, the calm-water

resistance does not increase very much even at higher forward speed. As a result, surf-riding can be more easily realised. Based on these results, an empirical formula is obtained as follows:

$$Fn = 0.28C_p + 0.096 \quad (1)$$

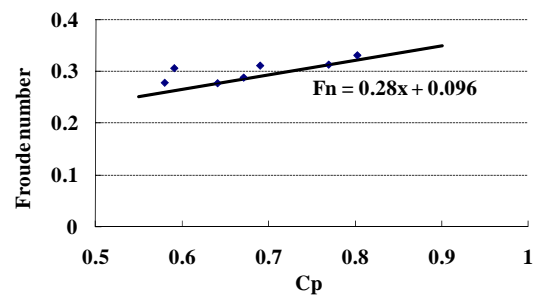


Fig. 1 Surf-riding threshold for the sample ships as a function of the prismatic coefficient ( $C_p$ ) with the wave steepness of 0.1 and the worst wavelength.

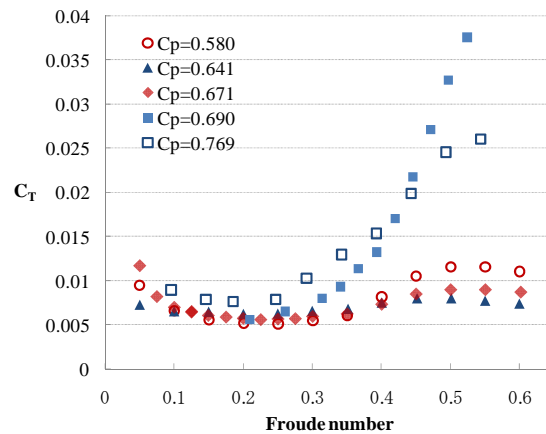


Fig. 2 Calm-water total resistance coefficient ( $C_T$ ) curves for the sample ships.

This formula can be recommended as the level 1 vulnerability criterion in place of the calm-water Froude number of 0.3. This means that if

the operational calm-water Froude number is larger than the value specified by Eq. (1), the ship has a potential danger of surf-riding. In other words, if the nominal speed is reduced to that below this critical value, no danger exists. Thus, it is also recommended to use the Eq. (1) in the operational guidance.

## **LEVEL 2 VULNERABILITY CRITERION**

The level 1 vulnerability criterion is sufficiently simple so that its use for all SOLAS and LL ships seems to be feasible. For unconventional ships, however, this empirical estimation could be conservative because application of wave resistance theory could realise the smaller resistance only at the design speed so that the calm-water resistance could be larger outside the design point. Thus it is useful to allow direct use of global bifurcation analysis as the level 2 criterion. Currently other than the numerical global bifurcation analysis, analytical bifurcation analyses based on the Melnikov approach and piece-wise linear approach are available and well validated with numerical and experimental methods (Maki et al., 2010). These methods can be easily applied to any ships if the calm-water resistance and the propeller thrust can be estimated in advance. At this stage it is important to specify the wave steepness for this calculation. This issue will be revisited with the calculation results of the direct stability assessment later.

## **DIRECT STABILITY ASSESSMENT (LEVEL 3)**

For the direct stability assessment, the combination of deterministic ship dynamics and the probabilistic wave theory can be recommended because the Monte Carlo simulation of ship behaviours in irregular waves requires prohibitively large amount of computations because of very small failure probability and so many operational cases. Umeda et al. (2007a) already proposed a method and well validated it with the Monte Carlo simulation. Firstly, using a numerical simulation code of the surge-sway-yaw-roll model in the time domain with a PD autopilot, the deterministic dangerous zone of stability failure due to broaching is obtained in various regular waves with a wide range of wave steepness and length. Secondly, failure probability due to broaching in irregular waves is calculated using the deterministic dangerous zone together with Longuet-Higgins' probabilistic wave theory (Longuet-Higgins, 1983). Finally if the calculated failure probability per hour in the North Atlantic is smaller than the acceptable value, e.g.  $10^{-6}$ , the ship is judged as safe. Here the wave statistics, as a joint probability density of the significant wave height and mean wave period, in the North Atlantic is required. One of the examples is shown in Fig. 3 for a RoRo ship of 187.7 metres in length. In the current proposal, if the ship fails to comply with this level 3 criterion, it is required to provide the failure probability presented as a function of the significant wave height and mean wave period as shown in Fig. 4 for the ship master in the stability booklet. If



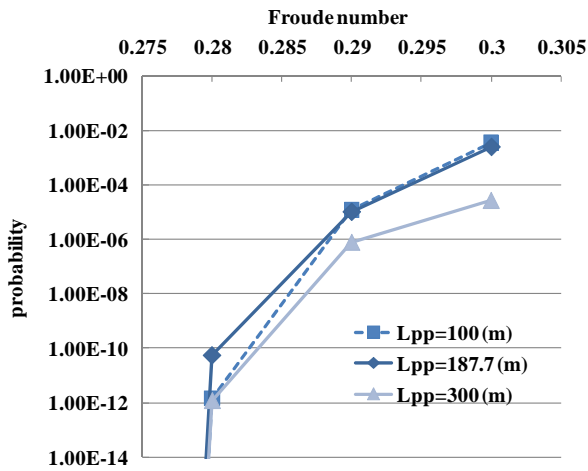


Fig. 6 Calculated stability failure probabilities per hour for the RoRo ships having different lengths in the North Atlantic with operational limitation.

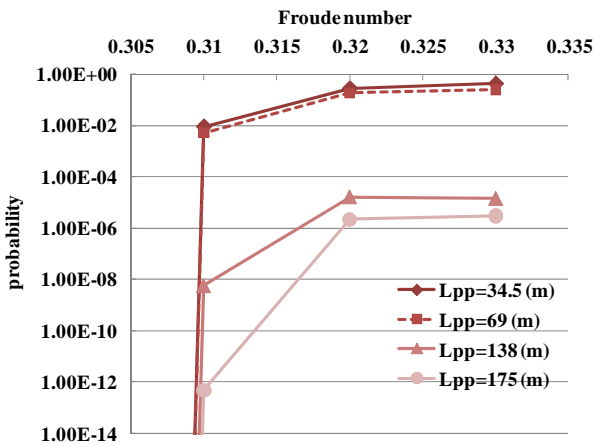


Fig. 7 Calculated stability failure probabilities per hour for the ITTC A2 ships having different lengths in the North Atlantic with operational limitation.

Then the lengths of these ships are systematically changed keeping their geometry for the failure probability calculation. The

results shown in Figs. 6-7 indicate that failure probability increases with the calm-water Froude number and longer ships are generally safer. However, it is noteworthy here that the probability of stability failure due to broaching is not negligibly small even for a ship having her length of 300 metres.

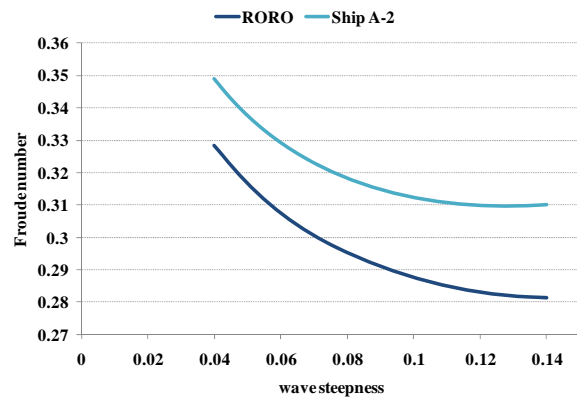


Fig. 8 Deterministic surf-riding threshold for the RoRo ship and the ITTC A2 Ship.

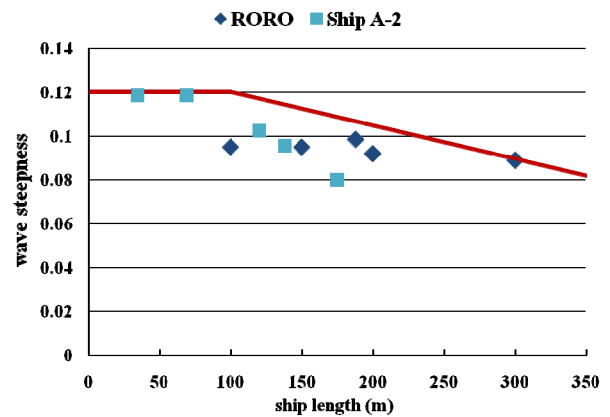


Fig. 9 Equivalent wave steepness for the level 2 vulnerability criterion

The global bifurcation analysis proposed for the level 2 is applied to these two hull forms so that their deterministic surf-riding thresholds, which are normalised with the ship lengths, are

obtained as Fig. 8. Here the wavelengths are set to be the worst cases. If the acceptable probability is  $10^{-6}$ , Fig. 6 suggests the critical Froude number for the 300 metres-long RoRo ship is 0.29 so that Fig. 8 indicates the equivalent wave steepness is about 0.09. Repeating this procedure for various ships, the relationship between the equivalent wave steepness and the ship length is obtained in Fig. 9. This result suggests that effect of ship length on the equivalent wave steepness is significant but effect of hull form is not so. Thus, the following formula for determining the equivalent wave steepness can be recommended:

$$\begin{aligned}
 H / \lambda = 0.12 & & L_{pp} < 100m \\
 = -0.000152L_{pp} + 0.1352 & & L_{pp} > 100m
 \end{aligned}
 \tag{2}$$

In conclusion, if the equivalent wave steepness is determined with Eq. (2), the safety level of the level 2 criterion is comparable to that of the level 3.

### DESIGN IMPACT OF DIRECT STABILITY ASSESSMENT

It was already demonstrated that the direct stability assessment is useful for a ship-dependent operational guidance. Obviously this assessment is useful also for ship design. This is because this assessment provides an opportunity for the ship owners to distinguish a safer design. For example, it is possible to evaluate the effect of rudder size on safety against broaching. The direct stability assessment technique is applied to both the

RoRo ship having original rudder and that with double sized rudder. The results shown in Figs. 10-11 demonstrated that double sized rudder can exempt the use of operational guidance so that the increase of rudder size is highly recommended in this case.

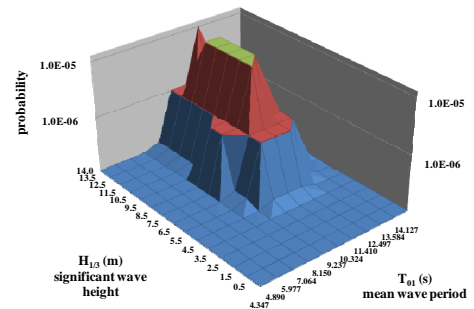


Fig. 10 Probability of stability failure for various sea states for the RoRo ship in the Northern Atlantic with the designed rudder.

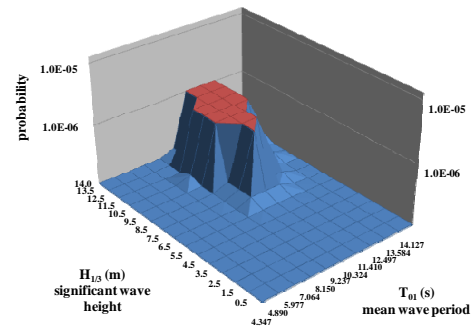


Fig. 11 Probability of stability failure for various sea states for the RoRo ship in the Northern Atlantic with the double-sized rudder.

### CONCLUDING REMARKS

The proposed new generation intact stability criteria on broaching associated with surf-riding is summarised below (See also Fig. 12):

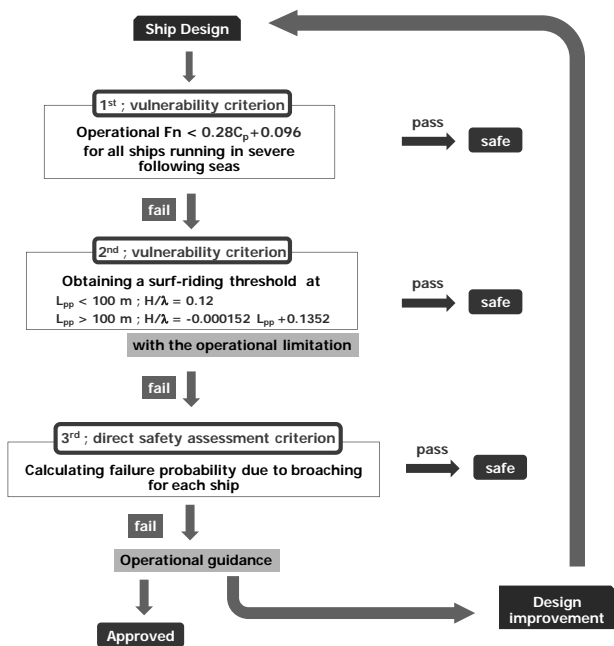


Fig. 12 Structure of newly proposed criteria

- The ship is requested to be operated with the operational speed below the empirical surf-riding threshold as a function of the prismatic coefficient. (Level 1 vulnerability criterion)
- If the ship fails to comply with the above, the ship is requested to be operated with the operational speed below the deterministic surf-riding threshold directly calculated by a numerical or analytical global bifurcation for the specified wave steepness which is a function of the ship length. (Level 2 vulnerability criterion)
- If the ship fails to both the above, stability failure probability in the North Atlantic is required to be calculated by the combination of deterministic ship dynamics and probabilistic wave theory. These results are requested to be supplied to the ship master for identifying the dangerous operational sea states.

## ACKNOWLEDGEMENTS

This work was supported by a Grant-in Aid for Scientific Research of the Japan Society for Promotion of Science (No. 21360427). It was partly carried out as a research activity of Stability Project of Japan Ship Technology Research Association in the fiscal year of 2009, funded by the Nippon Foundation. The authors thank Dr. Atsuo Maki from Kobe University for his excellent assistance on this work.

## REFERENCES

- IMO, 2008, "Revision of the Intact Stability Code - Report of the Working Group (part I)", SLF 51/WP.2.
- IMO, 2010, "Development of New Generation Intact Stability Criteria - Report of the Working Group (part I)", SLF 52/WP.1.
- Japan, 1991, "Intact Stability - Danger of Capsizing of Ships Navigating in Following and Quartering Seas", SLF 36/INF.4
- Japan, 2009, "Development of New Generation Intact Stability Criteria - Explanation of a Proposal on New Generation Intact Stability Criteria", SLF 52/3/6.
- Longuet-Higgins, M. S, 1983, "On the Joint Distribution of Wave Periods and Amplitudes in a Random Wave Field", Proceedings of Royal Society London, A389, pp.241-258.
- Maki, A. and Umeda, N., 2009, "Bifurcation and Chaos in Yaw Motion of a Ship at Lower Speed in Waves and Its Prevention Using Optimal Control", Proceedings of the 10th International Conference on Stability of Ships and Ocean Vehicles, St. Petersburg, pp. 429-440.
- Maki, A., Umeda, N., Renilson, M.R. and Ueta, T., 2010, "Analytical Formulae for Predicting the Surf-Riding Threshold for a Ship in Following Seas", Journal of Marine Science and Technology, DOI: 10.1007/s00773-010-0085-y.
- Spyrou, K.J., 1997, "Dynamical Instability in Quartering Seas- Part III: Nonlinear Effects on Periodic Motions", Journal

of Ship Research, Vol. 41, No.3, pp. 210-223.

Umeda, N., Shuto, M. and Maki, A., 2007a, "Theoretical Prediction of Broaching Probability for a Ship in Irregular Astern Seas", Proceedings of the 9th International Ship Stability Workshop, Hamburg, pp. 1.5.1-1.5.7.

Umeda, N., Hori, M. and Hashimoto, H., 2007b, "Theoretical Prediction of Broaching in the Light of Local and Global

Bifurcation Analysis", International Shipbuilding Progress, Vol. 54, No.4, pp. 269-281.

Yamamura, S. , Umeda, N., Maki, A. and Sano, H., 2009, "Numerical Study Towards Physics-Based Criteria for Avoiding Broaching and Capsizing in Following/Quartering Waves", Conference Proceedings of the Japan Society of Naval Architects and Ocean Engineers, Vol. 9k, pp. 109-112.



## Research towards Goal-Based Standards for Container Shipping

Vladimir Shigunov, Helge Rathje, Ould El Moctar

Germanischer Lloyd, Hamburg, Germany

### ABSTRACT

Commitment to analyse and verify rule-related technical aspects of safe and efficient container shipping initiated broad R&D activities at Germanischer Lloyd. Casualty statistics show that container loss in heavy weather is an important issue for innovative container ship designs. The paper demonstrates two examples of research activities at Germanischer Lloyd aiming at the reduction of cargo losses. One example is ship-specific operational guidance, assisting the ship master to avoid excessive motions and accelerations in heavy weather. The design accelerations underlying the operational guidance are part of classification rules, requiring understanding of the physics of dynamic loads on containers and lashing. The status of the ongoing research in this area is shown, in particular, the study of the effects of container flexibility and dynamic load amplification, not addressed explicitly in the present classification rules.

### KEYWORDS

container ships; dynamic stability; cargo loss

### INTRODUCTION

As a classification society, Germanischer Lloyd is committed to maintain technical aspects of existing and new regulations related to safe and efficient container shipping. When new regulations are developed, they should be relevant (i.e. address real problems), feasible (not too restrictive to outweigh the expected benefits), consistent with the safety level provided by other measures and efficient (i.e. aiming at the issues where maximum gains can be achieved by ship owners).

In the EU-funded research project SAFEDOR, FSA study for container vessels has been carried out in order to estimate current risk levels for major risk scenarios, develop generic risk-benefit models for future use and identify cost-effective risk-control options.

Historical data *LMI (2004)* were used to determine the frequency of occurrence for different risk categories, based on the casualty

data for modern fully cellular container ships for the period 1993-2004.

The world container fleet is relatively young: 71% of ships by number and 81% by the capacity are built less than 16 years ago. Larger container carriers (post-panamax and panamax) comprise 29.1% by number and 60.6% by capacity, while smaller vessels (sub-panamax, handysize and feeder) 70.9 and 39.4%, respectively. The results of the study show that incidents occur for all sizes similarly: while smaller container vessels are known to suffer substantial losses and damages, larger are suspected to be even more vulnerable because of immature technical standards and the associated lack of experience. Because of high rate of innovation in both design and operation of container ships, designers, operators and regulators alike have limited experience regarding cost-effective safety of newly built container ships.

The results show that container carriers are a relatively safe ship type in heavy weather.

The societal risk (F-N diagram) for container ship crew fits into the ALARP range, thus justifying further exploration of cost-efficient risk-control options. However, this risk is dominated by collision and grounding; heavy weather produces the lowest contribution. The individual risk to crew members is also in the ALARP region, dominated by collision (with the contribution 67.9%), fire and explosion (16.7%) and grounding (13.7%); heavy weather contribution (0.3%) is again insignificant.

Environmental risk (the expected quantity of released dangerous cargo from damaged containers) comprises in total about 1.0 t per ship per year, with the largest contributions from collision (53.3%), grounding (26.6%) and fire and explosion (10.3%); heavy weather contribution is 6.4%.

The consequences of heavy weather accidents are dominated by miscellaneous reasons (78% of all accidents in heavy weather, mostly loss of cargo), hull damage (15%) and machinery damage (6%); only 1% of accidents lead to foundering.

This assessment shows that cargo loss and damage due to ship motions in waves is the most significant intact stability problem for container ships, while capsize and hull damage are much less relevant. The situation could change if container ships would sail not on the damage stability boundary, as it is usually now, but on the intact stability boundary due to different subdivision.

Both the SAFEDOR study and data from insurance companies suggest that containers are lost mostly due to excessive ship motions and accelerations in heavy weather (60% of all lost containers according to SAFEDOR results); however, there is large discrepancy regarding the total number of lost containers. According to SAFEDOR results, 100 containers are lost due to heavy weather per year, while according to insurance clubs, this number is at least one order of magnitude higher, comprising 2000 to 10000 containers per year.

This leads to different estimations of long-term safety level provided by container vessels: 0.039 lost containers per ship per year and  $1.5 \cdot 10^{-3}$  container loss events per ship per year according to SAFEDOR compared to 0.4 lost containers per ship per year and 0.1 container loss events per ship per year according to insurance companies. As a possible explanation, the authors of SAFEDOR results assume significant underreporting in the used data, because container losses are not safety related. This explanation agrees with the estimation of the number of lost containers per accident: 26.7 according to SAFEDOR data vs. 4 according to insurance companies, which implies that *LMI (2004)* database contains only the largest accidents, while smaller loss events are not always reported, because this leads to delays due to loss claims.

Consistently with the identified risk levels due to heavy weather, the corresponding risk-control options were prioritised in the SAFEDOR FSA study as medium (exact weight distribution, constructive roll-damping devices, shipboard routing assistance and enhanced weather routing) to low (modified hull shape); none of these options were selected for a more detailed assessment with respect to their cost-effectiveness.

## COUNTER-MEASURES

Container losses in heavy weather may occur due to accidental combination of several factors, including large accelerations, wave impacts and green water, dynamic deformations of containers and lashing, pre-damaged containers, twistlocks and lashing and improper loading (e.g. container overweight or heavy containers on top of a stack). The risk of such accidents may increase due to innovative ship designs (e.g. higher container stacks), tighter operating and loading schedules, as well as crew with insufficient experience on modern vessels.

Experience from the investigations of container damage accidents highlights the need for prompt pro-active measures in regulatory framework, including stricter control of

container strength, weight and stowage, ship loading and operational performance standards. Presently, cargo safety is addressed by the following regulations:

- containers are designed and built according to ISO standards, thus their structural strength is pre-defined
- the *Container stowage and lashing plan* (subject to class approval) specifies allowable weights of container stack and properties of lashing system
- twistlocks and fully automatic locks are subject to class-specific standards
- ship-specific accelerations are maintained by and updated in classification rules

According to GL rules, either rule-based or calculated design accelerations can be specified; the former represent a 'safety envelope' over calculated accelerations for a large number of modern container ships, while the latter follow from hydrodynamic analysis in design wave conditions with an appropriate frequency of occurrence, not covering the most extreme scenarios. The level of safety implied by design accelerations is consistent with the ISO standards for container strength and the class regulations for stowage, lashing and locks. Therefore it would not be efficient to simply increase class-controlled safety level without controlling ISO container standards.

Moreover, the control of the entire system of regulations will not be efficient without the supervision of its implementation. Presently, the implementation of standards regarding container cargo safety is not sufficiently controlled. Although classification societies have competence and infrastructure to do this, authorisation by flag or port authorities is required.

Further, design accelerations as well as other relevant design rules are based on the assumption of prudent seamanship, which may imply increased risks for those modern hull forms where crew experience is insufficient; this issue is also not controlled. Thus, one of important missing parts in the current

regulatory framework is the ship-specific operational guidance.

Such operational guidance should be consistent with the other regulations, e.g. with rule-based design accelerations, and is expected to increase the safety level in operation up to the other risks. In other words, the operational guidance supports the achievement of 'prudent seamanship' implied by other regulations, up to standard service performance, which is particularly urgent for innovative designs.

In addition, such an operational guidance provides a very flexible measure for prompt support of future innovative designs and innovative operational solutions, and can also be used to address issues not related to cargo safety, e.g. wave loads and crew safety in heavy weather and people comfort onboard. Broadly speaking, ship master should not be left alone in heavy weather: regulators should take care of operations as strictly as it is done in design. Although increasing number of ships are employing onboard weather routing (*Rathje and Beiersdorf, 2005*) or similar decision-support systems, the quality and safety standards of such systems should be controlled. Development of the requirements to ship-specific operational guidance is presently on the IMO agenda.

## OPERATIONAL GUIDANCE

Operational guidance addresses excessive motions and accelerations in waves, which can occur due to rigid-body motions, particularly heave and pitch, due to slamming impacts and whipping responses, as well as due to green water on deck and wave impacts.

The purpose of the operational guidance is to indicate the combinations of operational parameters (ship speed and course) that should be avoided for given loading and seaway conditions. In order to do this, operational guidance requires some short-term performance measure (criterion) and the boundary between acceptable and unacceptable values of this criterion (standard).

Because this standard specifies short-term safety, a way is required of relating it to the

long-term performance. Two possibilities were proposed in *Shiginov et al. (2010)*:

- to determine the value of the short-term standard leading to the required long-term (i.e. average over operational life) safety level
- to set standard minimising the difference between additional benefits per time (due to reduced rate of cargo loss) and additional cost per time (due to increased time on route), incurred due to the use of operational guidance.

As an illustration of the first way, the long-term exceedance rate of the maximum (over ship) lateral acceleration  $g/2$  was computed as a function of short-term standard  $R_2$  using numerical Monte-Carlo simulations for an 8400 TEU container ship. The resulting dependency is shown in Fig. 1.

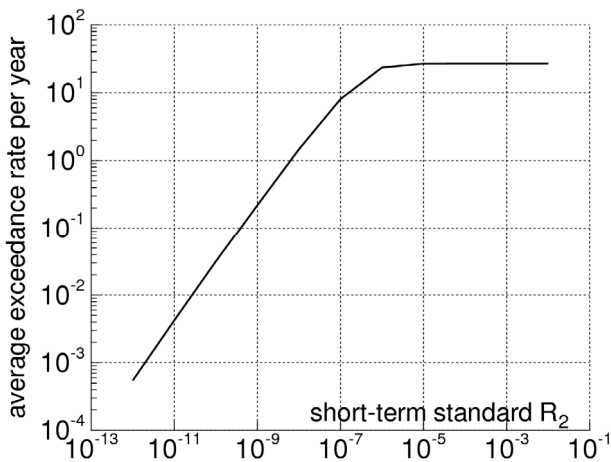


Fig. 1: Average annual exceedance rate vs. short-term standard

Assuming the required long-term safety level as 0.02 container loss events per ship per year the short-term standard  $R_2$  can be set to  $10^{-10} 1/(m \cdot s^2)$ . Fig. 2 shows examples of unacceptable combinations of operational parameters (grey areas) for the load case with  $GM=2.3m$  in two seaways.

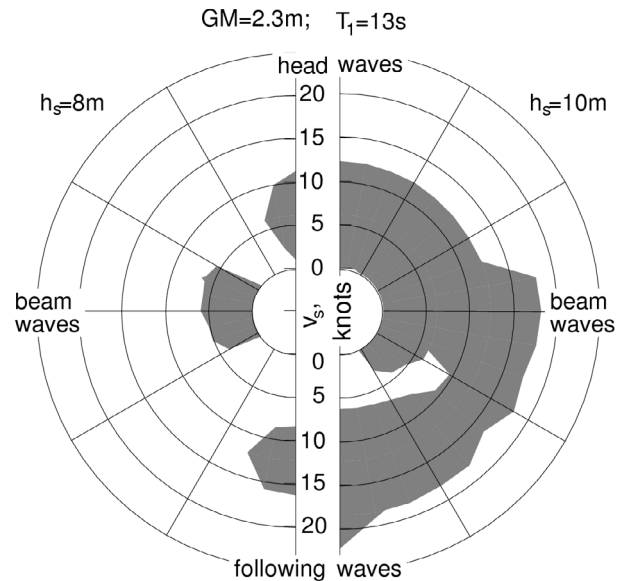


Fig. 2: Areas of unacceptable operational parameters for a 8400 TEU container ship with  $GM=2.3m$  in a seaway with the mean period 13 s and significant wave height 8.0 (left) and 10.0 (right) m

### SIMPLIFIED DESIGN ASSESSMENT PROCEDURE

In order to distinguish between ships requiring and not requiring operational guidance, a simplified design assessment procedure is proposed in *SLF51/INF.2 (2009)*: numerical Monte-Carlo simulations are performed for ‘design’ wave height prescribed as a function of the characteristic wave period  $T_1$ , and ‘design’ forward speed, depending on this wave height as well as wave direction  $\mu$ , in short-crested irregular waves for a wide range of seaway parameters  $T_1$  and  $\mu$ .

### FURTHER FACTORS

Besides rigid-body motions, further factors are becoming increasingly important for container ships: hull girder flexibility and flexibility of container stacks. An example in Fig. 3 shows time history of measured vertical acceleration at the forward perpendicular for a segmented flexible model of an 8400 TEU container ship, indicating significant dynamic amplification of vertical accelerations due to slamming impact

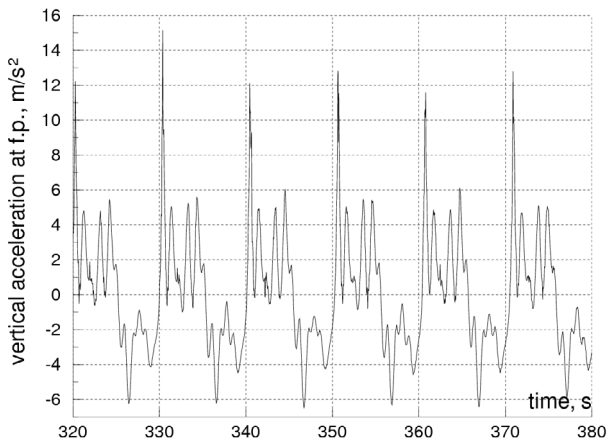


Fig. 3: Measured vertical acceleration at the forward perpendicular of a model of an 8400 TEU container ship (time scaled to full scale)

and the resulting whipping response, *Oberhagemann et al. (2009)*.

*Wolf and Rathje (2009)* studied the influence of container flexibility on container stack dynamics and loads on containers and showed that the consideration of prevailing dynamic effects due to flexible container stacks on the weather deck is essential for the assessment of stack loading.

The dynamic response of a container stack is highly nonlinear due to clearance in lashing, interaction with adjacent stacks, friction effects etc. Therefore, time-domain simulations were performed using a FE model of container stacks. Containers were modelled as super-elements with interfaces to other elements and with contact and friction effects between stacks; stiffness and mass inertia of the super-elements were condensed from a detailed FE-model of a container. Twistlocks were modelled as spring-damper elements with gap and contact capability; their stiffness was derived from a detailed FE-model. Lashing was not considered and is addressed in the ongoing work. Friction and damping parameters for high-frequency responses were derived from full-scale measurements of the dynamics of stowed containers.

An example study is shown for a container stack carried on the weather deck of a 9200 TEU container ship. Roll motion

characteristics are derived from hydrodynamic analysis, leading to design conditions with roll period 18 s and amplitude 26°.

Parametric studies were carried out in order to quantify the effects of the cargo distribution over the stack, twistlock stiffness, structural damping and adjacent stack interaction.

The study has revealed that flexibility effects lead to distinctive dynamic amplification of transverse racking forces and, particularly, vertical forces due to successive uplifting and crashing down of the upper containers while rolling to port or starboard, respectively. Due to this effect, the influence of the vertical cargo distribution is especially significant: container and twistlock loads are higher for stacks with higher centre of gravity.

Stack interaction has shown to also have a significant influence: both vertical and transverse loads are amplified due to the interaction of the upper containers in the adjacent stacks, Fig. 4.

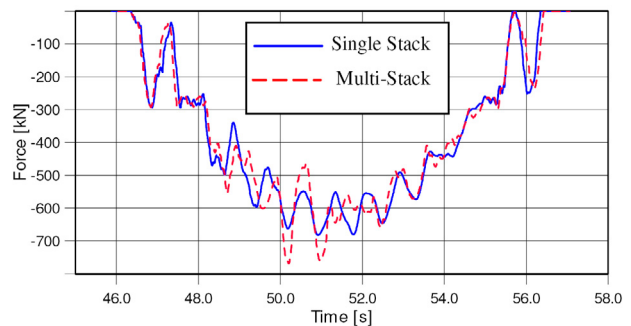


Fig. 4: Effect of stack interaction: vertical forces on container corner for a single stack and multiple stacks

The results of the simulations were compared with loads based on classification rules for a single unlash eight-tier rigid container stack with proper cargo distribution and standard accelerations.

Simulations (Fig. 5) show asymmetrical front-to rear-end distribution of container loads: the front end carries higher transverse and, particularly, vertical loads because of the higher flexibility of the door end.

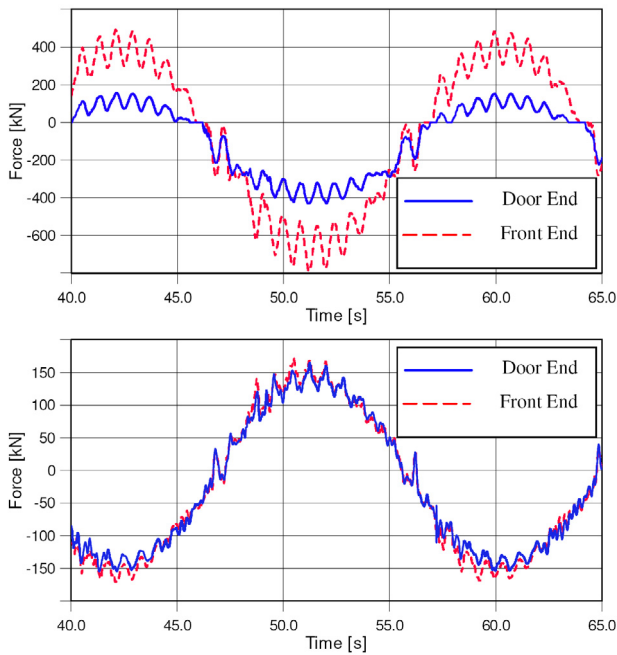


Fig. 5: Front-to-rear asymmetry of container loads: vertical (top) and transverse (bottom) forces on the top of the lower container

This effect is not considered in GL rules for unlash configurations: for unlash case, the loads at both ends are assumed identical and, effectively, equal to the average load between the front and rear ends. Therefore, the simulated vertical loads and corner post forces at the door end are lower (respectively, at the front end higher) than those from the rules. On the other hand, the average between the front and rear end lifting force in simulations is about 25% higher than the rule-based value due to dynamic load amplification (container uplifting and bouncing).

## CONCLUSIONS

Commitment to analyse and verify rule-related technical aspects of safe and efficient container shipping initiated broad R&D activities at Germanischer Lloyd. The presented results show that cargo loss and damage may be of especial concern for modern container carriers. Mitigation measures are proposed, such as ship-specific operational guidance. Example is shown of a possible approach to operational guidance reducing lateral accelerations to the

prescribed long-term rate. Further factors are identified which may be responsible for cargo losses, particularly flexibility of ship hull girder and container stacks.

Ongoing R&D activities concern further factors responsible for cargo loss and their design limits (e.g. vertical accelerations), cost-benefit analysis over operational life for setting economically sound short-term performance standards, incorporation of further factors into operational guidance (slamming and whipping, vertical accelerations, dynamic response of container stacks and lashing, crew safety and comfort) and roll-damping devices.

## REFERENCES

- MSC 83/INF.8 (2007) FSA – container vessels. Details of the Formal Safety Assessment, submitted by Denmark
- LMI (2004) Casualty database, Lloyd Maritime Information, December
- Rathje, H. and Beiersdorf, C. (2005) Decision support for container ship operation in heavy seas -- Shipboard Routing Assistance, 4-th Conf. Comp. and IT Applications in the Maritime Industries COMPIT, pp. 455-467
- Germanischer Lloyd (2007) Rules for classification and construction, I – Ship Technology, Part 1 – Seagoing Ships, Chapter 20– Stowage and Lashing of Containers. Hamburg
- Shigunov, V. El Moctar, O. and Rathje, H. (2010) Operational guidance for prevention of cargo loss and damage on container ships, Ship Technology Research 57(1) 6-23
- SLF 51/INF.3 (2008) New generation intact stability criteria, submitted by Germany
- Oberhagemann, J., El Moctar, O. and Schellin, T. E. (2008) Fluid-structure coupling to assess whipping effects on global loads of a large containership, Proc. 27-th Symp. on Naval Hydrodynamics, 296-311
- Wolf, V. and Rathje, H. (2009) Motion simulation of container stacks on deck, SNAME Annual Meeting and Ship Production Symp. 1, 277-285

## Going Forward with Safe Return to Port

Jane Dodman,

Lloyd's register EMEA

### ABSTRACT

In 2000 the IMO agreed that future large passenger ships should be designed based on the principle that a ship is its own best lifeboat. It was recognised that with vessels carrying ever increasing numbers of passengers the task of retrieving people in lifeboats from the ocean is a significant problem. The instruction from the IMO was that vessels should either be capable of returning to port or able to survive for three hours to allow for a timely evacuation.

The new SOLAS requirements will be applicable to all passenger ships built on or after July 1, 2010, having a length of 120 metres or having three or more Main Vertical Zones. A substantial part of these regulations deals with the complexities of system requirements for retaining people on board a distressed ship with the additional capacity to return to port. There are two casualty categories; namely, fire and flooding

Discussions concerning the fire casualty are virtually complete. However, work is ongoing at the IMO to provide guidance information to support the Master in the event of a flooding casualty and on time to flood. The adoption of the harmonised methodology for assessing ship survivability from flooding following damage does not provide information relevant to the Master in a real casualty situation. It is the intention that the guidance will provide support in ascertaining the immediate condition of the vessel for a possible safe voyage back to port. This is a step away from the original discussions which included a design concept. There are several reasons for not having moved forward with this. Most notably, the agreed view, that any new requirement should not impact the level of safety imposed by the harmonised damage stability requirements. Further, there is limited available data on how damaged ships operate in a real sea way.

This introduction paper is presented to open up discussions on what information should be presented on board to effectively support the Master in the uncharacteristic and possibly distressing situation of a damage casualty. Also, should ships be designed with a 'safe return to port' concept in mind and if so, how is this achieved?

### KEYWORDS

Safe return to port; Stability; Passenger ship

### INTRODUCTION

The purpose of this inaugural paper is to open up the debate on the 'Large Passenger Ship' initiative taken by the International Maritime Organisation (IMO) in 2000 to address concerns that increasing ship sizes and

passenger numbers might increase risk to above acceptable levels.

It is a resume of what has transpired based on familiarity gained at IMO from investigations into a safe return to port index and explains

certain practical aspects of the systems in order to maintain a certain holistic focus.

## HISTORY

The original instruction from IMO was that vessels should either be capable of returning to port or able to survive for three hours to allow for timely evacuation.

During this period there were also significant developments in stability regulations with the introduction of probabilistic damage stability for passenger ships.

The basic theme of the initiative was that future passenger ships should be designed for improved survivability so that in the event of a casualty persons can stay onboard as the ship proceeds to port.

In 2004 it was decided at IMO to drop ‘large’ from the title in order to extend the benefits to a larger number of passenger ships. Clearly many smaller ships operate in remote arctic and tropical areas which are equally susceptible to the difficulties of passenger retrieval in the event of a casualty. Ships of less than 120metres or three main fire zones are considered to have insufficient subdivision to implement system redundancy in flooding cases.

Amendments to SOLAS Chapters II-1 and II-2 were subsequently finalised and adopted at the 82<sup>nd</sup> session of the IMO’s Maritime Safety Committee (MSC) in December 2006, with requirements applicable to passenger ships built on or after the 1<sup>st</sup> July 2010.

## CASUALTY THRESHOLD

As it would be unreasonable to require that a passenger ship should be able to return to port following any possible casualty, the concept of casualty threshold was introduced.

There are two casualty thresholds defined for each of the two accident categories, fire and flooding; the threshold for safe return to port and the threshold for safe evacuation.

The casualty threshold for safe return to port is the envelope of the accident scenarios that the ship is expected to survive and be able to return

to port afterwards. The threshold for safe evacuation is similarly the envelope of the accident scenarios following which the ship is expected to provide a safe platform for evacuation for at least three hours.

The above casualty thresholds have been clearly defined in the regulations only for fire. In the flooding case a casualty threshold has yet to be defined and is only implicitly included in Regulation II-1/8-1 to facilitate designers but does not correspond to a specific accident scenario.

As the debate on time to flood has not yet been resolved at the IMO there is currently no casualty threshold for orderly evacuation in the flooding case.

## FLOODING CASUALTY THRESHOLD

In case of flooding it has been specified that the systems required for return to port shall remain operational following the loss of any one watertight compartment. As mentioned previously this is not related to a specific damage scenario or associated with stability requirements. It has been put in place only to ensure a reasonable degree of equipment redundancy. Figure 1 shows the application according to the extent of a flooding casualty.

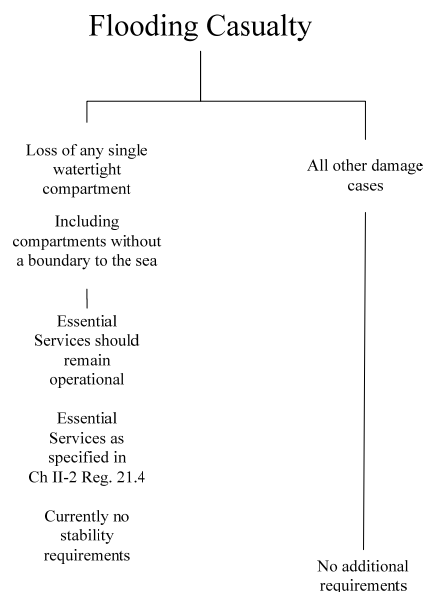


Fig. 1 Flooding casualty

## ESSENTIAL SYSTEMS

For a ship to be considered to have the capability to return to port, new SOLAS Regulation II-2/21 contains a list of systems considered essential. The list only describes the systems; both the Regulation and the corresponding performance standards contained in MSC.1/Circ.1214 are intentionally vague and lacking any reference to specific values or other determinants of performance. The essential systems for return to port are:

- Propulsion
- Steering
- Navigational systems
- Fuel transfer systems
- Internal and external communications
- Fire main system
- Fixed fire extinguishing systems
- Fire detection systems
- Bilge and ballast systems
- Basic services to support safe areas
- Flooding detection systems and
- Other systems determined by the Administration to be vital to the damage control efforts.

The basic services to be provided to support safe areas, as mentioned above, are the following:

- Sanitation
- Water and food
- Space for medical care
- Shelter from the weather
- Means of preventing heat stress and hypothermia
- Light and ventilation.

## RETURN TO PORT PERFORMANCE REQUIREMENTS

The new rules for return to port briefly described above are not prescriptive but are essentially performance requirements. There is

an element of intentional ambiguity in their formulation necessary to cater for the many different types of passenger ship operating in very different circumstances.

A cruise ship in a remote area days from the nearest ship and a cross channel ferry that is always within easy reach of Search and Rescue services should be treated differently. Requiring the cross-channel ferry to carry fuel, food and water to survive days does not make sense.

This has created some problems for designers as well as for the Flag Administrations and Classification Societies that have to verify compliance with the new requirements.

This is why it was decided at the IMO not to have an explicit reference for example to required speed, range, available power or capacities in either the regulations or the related MSC circular.

It is for the same reason that there is a consensus forming to restrict the appraisal to the measurement of the ship's capabilities to return to port and have specific and possibly area of operation related information contained in the ship's safety documentation.

## REGULATIONS

SOLAS2009 Chapter II-1, Regulation 8-1 'System capabilities after a flooding casualty on passenger ships' is placed in Part B-1 'Stability' and has sat as a placement for future developments on the stability aspects of safe return to port.

At IMO SLF 52 in March this year, the Sub-Committee reiterated its support of the United States' proposal (SLF 51/11/3) that only operational guidance should be developed; and that the draft amendments to SOLAS regulation II-1/8-1 should be finalized when the above guidance is developed, together with amendments on mandatory requirements for onboard computers.

This is move away from the initial intent of adopting design criteria but this may be re-introduced in the future if there are practical, robust solutions. Also, completion of the work

done on ‘time to flood’ carried out at IMO is awaited with interest as it may also have some bearing.

However, the question remains as to what is considered a suitable threshold of stability when considering a return journey to port, whether that be under power or under tow.

The complexity increases when considering the variety of ship types such as large cruise ships, mega yachts, ro-ro passenger ships and interesting multi hulls.

### DESIGN CRITERIA PROPOSAL

Discussions on benchmarking stability criteria for safe return to port tend to result in ‘something’ between the s-value and the intact stability requirement. Clearly the s-value parameters are insufficient since it is designed on the assumption of a damaged ship remaining in a location static position.

In 2008 a paper was presented at IMO Sub-Committee on Stability load Lines and on Fishing Vessel Safety (SLF) titled ‘Results of an investigation into the casualty threshold methodology by Lloyd’s Register’. This was completed in co-operation with several of the major passenger ship building yards in Europe.

The aim of the study is to define an acceptable level of residual stability for safe return to port after damage and to provide an indication of the ability of the vessel to do this by design.

The proposal is based on the same results as the damage calculations for compliance with SOLAS II-1, Regulations 4 to 7-2. It considers a measure of the ability of a vessel to return to port safely is the sum of the p factors associated with the damages that comply with adequate stability criteria for safe return to port. This is represented by a safe return to port required and attained index as shown in Figure 2.

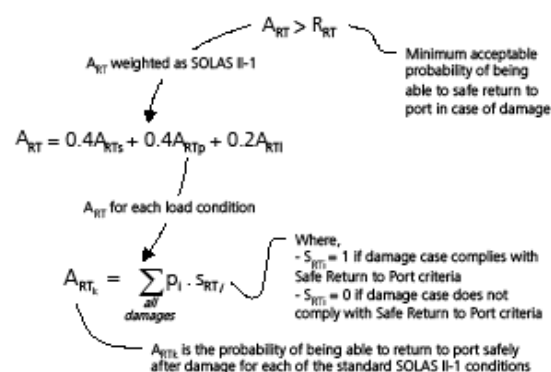


Fig.2 Return to port attained and required index

One aspect clearly identified by the paper is the notable effect of the range on defining a criteria threshold.

Figure 3 provides a graph taken from the paper showing the GZ Curve Range. The reference proposed is to have a GZ curve range of not less than 30°, as a minimum from the IS Code requirements. It can be noted in the graph that it is a quite onerous requirement that few cases comply with.

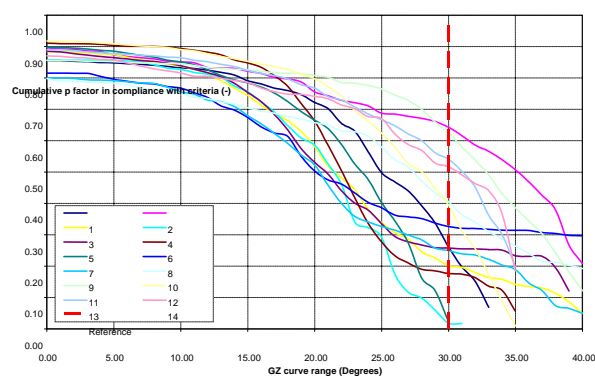


Fig. 3 GZ Curve range

This approach is based on zones as opposed to watertight compartments and therefore not immediately in line with the application of system redundancy. The positive side is the methodology is simple and aligned with the established SOLAS damage stability requirements.

As it stands, there is insufficient ship data to consider this as a robust proposal. Also, the ship designs are from an early period in the adoption of the probabilistic methodology. Therefore, it is possible the data will be impacted on as more experience is gained in application and interpretation of the regulations.

#### **DEVELOPMENTS BY GERMANY**

In 2009 Germany submitted a paper to IMO SLF going forward with an approach based on that mentioned above but in relationship to compartments as opposed to zones. It embraces a wider variety of available and acceptable damage cases.

This proposal provides results for four ships together with a practical solution in graphical form for visual support to the Master.

Since the opinion at the time of submission to IMO was focussed on support to the Master, this paper was not discussed in detail.

#### **GUIDANCE**

Guidance or rather support information for the Master is currently being developed at IMO for incorporation into MSC.1/Circ.1245.

The objective is to provide the Master with assistance on how to ascertain the immediate condition of the ship and, if satisfactory, what actions may be taken to improve the safety for the voyage back to port.

It is generally decreed that the information should not contain decision criteria but there are views that reference points for the master which could provide information on certain parameters, e.g., stability characteristics associated with the s-value or intact requirement value, could be useful for comparison to the ship's residual stability. A slight majority was against providing such reference points because these could not provide for all actual parameters and could be misleading. A particular reason for not including references is that at present there are no predominant solutions presented that have been rigorously debated.

Defining a level of stability in the traditional sense is not straight forward bearing in mind the numerous permutations and combinations of damage scenario, prevailing weather conditions and areas of operation. There is a lack of statistical information of how a damaged ship manoeuvres in a real sea way. Traditional methods of applying the roll period coefficients are not applicable. Although a damaged ship generally provides more damping there are other associated factors to consider such as the time to restore equilibrium following imposed angles of heel.

#### **ALTERNATIVE APPROACHES**

SSRC propose a ship specific method which determines the likelihood of capsizing associated with the global range of damages using numerical simulations. This product is used by some owners to support confidence with early implementation of safe return to port in new designs. The complexity in this approach makes it more difficult to encompass into the regulatory framework but is none the less a method to investigate in providing viable solutions.

#### **CONCLUSIONS**

To move forward with a design criteria or reference points for stability under specific casualty situations we need to identify under what conditions a vessel should be capable of returning to port and the level of acceptable risk. This may well be variable depending on operations and ship types.

More immediately, what support can be offered to the master? Diagrams similar to those proposed in the German paper are already supported in certain areas of the shipping industry. Any supporting information has to be clear and immediately available.

In designing solutions, the practicalities of implementation by the industry as a whole, should be considered but this does not mean moving ahead with technology.

Measuring the ability of a ship to safely return to port as a function of the damages cases

forming the subdivision index in Chapter II-1 SOLAS2009 is clean and efficient. Perhaps this is an easy way to measure the future design trend.

We should question whether a return to port requirement should be imposed that can override the safety levels assumed by the subdivision requirements currently adopted. Perhaps this philosophy is more relevant.

This remains a complex concept to embrace and there is no obvious and easy solution. Novel approaches and an open mind are required in the ultimate aim to turn potential accidents into controlled incidents.

## REFERENCES

International Maritime Organization, Sub-Committee on Stability Load Lines and on Fishing Vessel Safety 'A survey of residual stability margin' - SLF 52/8/1, 26 October 2009

International Maritime Organization, Sub-Committee on Stability Load Lines and on Fishing Vessel Safety 'Results of an investigation into the casualty threshold methodology by Lloyd's Register' - SLF 51/11/1, 10 April 2008

International Maritime Organization, Sub-Committee on Stability Load Lines and on Fishing Vessel Safety 'Possible option for SOLAS regulation II-1/8-1 amendment' - SLF 51/11/3, 6 May 2008

International Maritime Organization, Sub-Committee on Stability Load Lines and on Fishing Vessel Safety 'Stability and sea keeping characteristics of damaged passenger ships in a seaway when returning to port by own power or under tow' - SLF 50/8/1, 23 February 2007

International Maritime Organization, Sub-Committee on Stability Load Lines and on Fishing Vessel Safety 'Report on SDS Correspondence group' - SLF 49/4/1, 21 April 2006

International Maritime Organization, 'Adoption of Amendments to the International Convention for the Safety of Life at Sea, 1974, As Amended', MSC Res.216(82), 8 December 2006

International Maritime Organization, 'Explanatory Notes to the SOLAS Chapter II-1 Subdivision and Damage Stability Regulations', MSC Res.281(85), 4 December 2006

International Maritime Organisation, MSC.1/Circ.1245 'Guidelines for damage control plans and information to the master'

## DISCLAIMER

Lloyd's Register, its affiliates and subsidiaries and their respective officers, employees or agents are, individually and collectively, referred to in this clause as the 'Lloyd's Register Group'. The Lloyd's Register Group assumes no responsibility and shall not be liable to any person for any loss, damage or expense caused by reliance on the information or advice in this document or howsoever provided, unless that person has signed a contract with the relevant Lloyd's Register Group entity for the provision of this information or advice and in that case any responsibility or liability is exclusively on the terms and conditions set out in that contract.

## **Damage Stability of Ro-Pax Ships with Water-on-Deck**

A. L. Scott

UK Maritime and Coastguard Agency

### **ABSTRACT**

Currently European ro-ro passenger ships constructed after 1 January 2009 must comply with both the new SOLAS2009 probabilistic damage stability requirements and the Stockholm Agreement allowing for water accumulation on the vehicle deck (WOD). Doubts in some European states over whether SOLAS2009 makes sufficient provision for WOD led to the EU decision to retain Stockholm; this was partially reinforced by results from three new research projects, completed in 2009, which revealed potential weaknesses in the probabilistic regulations, particularly for smaller ro-pax ships and those with long lower holds. This paper gives some historical background and outlines some of the steps being taken to rectify the current regulatory situation.

### **KEYWORDS**

Ro-Ro; Damage Stability; SOLAS; IMO.

### **INTRODUCTION**

This paper aims to supply some background to the current situation at IMO with respect to the safety of new ro-ro passenger ships constructed after 1<sup>st</sup> January 2009 following the introduction of the SOLAS2009 amendments. It includes a brief historical background and goes on to highlight some of the issues which have led to the current regulatory situation in which new ro-ro passenger ships operating in European waters must continue to comply with the Stockholm Agreement as well as with SOLAS2009.

There follows a short section on the ongoing work of the IMO SDS Correspondence Group in trying to address the technical issues underlying three research projects completed in 2009 which examined new ro-ro ship designs compliant with SOLAS 2009. These results, which revealed some weaknesses in the new regulations particularly for smaller vessels and those fitted with long lower holds, have led to the initiation of further research projects which are currently in progress. It is hoped that the results emerging from these new projects will eventually assist IMO in producing satisfactory

updates to the SOLAS2009 regulations and accompanying explanatory notes.

Since the task of harmonizing damage stability regulations based on probabilistic methods was initiated more than 15 years ago there have been immense improvements in the computer hardware and software tools available to investigate ship safety. It is hoped that these developments will be fully utilized in the latest research projects to increase our knowledge of the complex issues surrounding the survivability of ro-ro passenger ships. As an approving Authority, however, the MCA has some concern as to how to keep abreast of these developments especially if, in future, direct calculation methods are used to produce radical new designs which will require approval. Perhaps as an industry we need to consider further benchmarking procedures to increase our confidence in the results from, for example, the various numerical techniques currently being developed and used by different organisations.

The main objective of this paper is therefore to encourage dialogue between IMO and the research teams working on the latest ro-ro

damage stability projects so that members of the SLF correspondence group and working group, many of whom represent approving Authorities, can be kept fully informed of the latest developments.

### **HISTORICAL BACKGROUND**

The SOLAS regulations are subject to almost continuous review and updating to reflect changes in ship size, type and design and to meet demands for increased safety. Regrettably the regulations have had to be amended on occasions in the wake of a major disaster, indeed the origins of SOLAS can be traced back to the loss of the Titanic in 1912. The losses which particularly affected the regulatory regime for ro-ro passenger ships were the “HERALD OF FREE ENTERPRISE” in 1987 and the “ESTONIA” in 1994. The former led to the early implementation of the planned revisions known as SOLAS90 and the latter to the Stockholm Agreement, which was at the time applicable only to ro-pax vessels operating in N.W. European waters under a SOLAS dispensation allowing local regional agreements to be applied in sea areas considered to be particularly dangerous, whether for congestion or weather conditions.

The disquieting thing about ro-ro passenger ships is the suddenness of the loss following ingress of water onto the open vehicle deck area. The time from the initiating incident to ultimate loss can be so short (a matter of minutes) as to preclude the possibility of anyone being rescued by LSA, with only the fittest (and luckiest) standing any chance of survival. The measures taken in the 1990's to upgrade the existing ro-ro fleet to comply with the Stockholm Agreement and the recognition in new ships that the “water on deck” problem could best be addressed by increasing the residual freeboard after damage seems to have led to a reduction in ro-ro casualties, at least in European waters, but continual vigilance on both the design and operational fronts is necessary.

The collision damage scenarios envisaged by the SOLAS regulations and the Stockholm Agreement – namely side damage to 1 or 2 compartments with a maximum penetration depth of B/5 metres – were not the principal cause of the loss of either the “HERALD” or the “ESTONIA”. More recently the loss of the “AL-SALAM BOCCACCIO 98” was attributable to water accumulation on the car deck during fire-fighting operations rather than to collision damage. The common feature of all these tragedies is water accumulation on the vehicle deck. The survivability of a ship complying with the SOLAS90 regulations has not been fully tested in a severe real-life collision. To our knowledge, there has yet to be an incident involving major penetration past the B/5 limit on a ro-pax ship in EU waters - a limit which the accident statistics indicate has historically been exceeded in around 45% of side damage cases.

Concerns that the deterministic regulations only covered limited damage scenarios encouraged development of a new approach to try to deal more comprehensively and scientifically with the problem of damage stability after collision. Originally introduced in 1973 in IMO Res. A265(VIII), then in the 1992 dry cargo ship rules (SOLAS Chapter II-1, Part B-1, Regulations 25-1 to 25-9), the probabilistic approach aimed to remove the limitations of compliance with pre-determined damage scenarios, “outmoded” concepts such as 1 and 2 compartment damage, B/5, floodable lengths and margin line. Instead, formulae and a methodology encompassing a much wider range of damage scenarios derived from an updated and larger database of accident statistics was introduced. The “harmonized” regulations (which in one move replaced deterministic SOLAS90 for passenger ships, the probabilistic dry cargo ship regulations in SOLAS90 Part B-1 and IMO Res A.265) were brought into force in 1<sup>st</sup> January 2009 as the SOLAS2009 amendments.

To comply with these new regulations, a proposed design must achieve a required index, “R” based on a formula including ship length

and the number of persons carried. In general the more passengers carried and the greater the length, the higher “R” becomes. “R” was established using regression techniques on existing ships to try to give, on average, an overall safety level equivalent to that of the preceding deterministic SOLAS90 regulations (excluding, it is now widely believed, the Stockholm Agreement for ro-pax ships). The new design is analysed through subjection to a large number of damage stability cases, determined from damage probability distribution curves derived from the accident database, at 3 pre-determined draughts. Each damage case which survives to a degree determined by the so-called “s”-factor formula based on heel angle, residual GZ and range, then contributes towards a summated attained index, “A”, weighted according to draught, which must be equal to or exceed the “R” index for the design to be approved.

Perhaps because of the UK’s particular anxiety to avoid a repetition of the loss of the HERALD with its unhappy consequences, the MCA initiated a design study into the safety of several different ship types which would be required to comply with SOLAS 2009 [Ref. MCA project RP 552]. The conclusion was that there could be a particular problem with ro-ro passenger ships. Crucially, due to the nature of the probabilistic approach, SOLAS 2009 permits designs in which individual simple, feasible damage scenarios can result in the rapid capsize of a ro-ro passenger ship in spite of the inclusion of a regulation (8) to prevent minor damages from having major consequences. Under the SOLAS90 deterministic regulations such scenarios would have so severely constrained operability (in terms of draught, floodable lengths and/or limiting KG/GM) that design changes would usually have been enforced. The UK also believed that insufficient attention was paid before the introduction of SOLAS2009 to designing new ships exclusively to meet the new requirements which involved a step-change from previous methods. Some work on testing new designs was carried out within the

HARDER project, but the regulations for ro-ro ships were later changed considerably during adoption at IMO (for example by removal of the SEM).

These and some other concerns were raised at successive meetings of COSS in Brussels. Eventually the EC and EU member states, having been alerted to some worrying results emerging from a new research project (RP592), funded jointly by the UK and NL, in which two new ro-ro ships were optimized to meet SOLAS2009, submitted a paper (ref. MSC 84/12/12) to IMO MSC asking for the issue of ro-ro damage stability to be re-opened for discussion at SLF. In the meantime, as a temporary precautionary measure, the EC decided that new post-1/1/2009 ro-ro ships should continue to comply with the Stockholm Agreement as well as SOLAS2009.

#### **DEVELOPMENTS AT IMO**

At IMO in July 2008 the SLF 51 sub-committee responded to MSC 84/12/12 by tasking the SDS correspondence group with assessing the various technical issues raised by new ro-pax research projects then underway and due to complete in 2009. The CG submitted a report (ref. SLF 52/11/1) which concluded that some amendments to SOLAS2009 for ro-pax ships may be necessary and these should be based on further research in particular on smaller ships with fewer passengers and on ships with long lower holds especially those fitted with B/10 longitudinal bulkheads.

At the SLF 52 meeting in January 2010, the sub-Committee asked the correspondence group to continue the work of assessing the results of further new research projects investigating ro-ro passenger ship damage stability. These projects, notably GOALDS (the subject of another paper at this meeting) and a follow-up design project initiated by EMSA are not expected to conclude until 2011/12. It is hoped that the leaders of these projects will keep IMO regularly informed as to the progress being made.

## SOME DISCUSSION POINTS

As this is a workshop, a few points and questions follow which it is hoped may provoke further debate on some of the unresolved issues still surrounding ro-ro damage stability.

### *(1) Why Focus on Ro-Ro Passenger Ships?*

In the UK our concern was always that the loss mechanism for ro-ro passenger ships is quite different from that of conventional passenger ships. The latter can technically capsize (however that is defined) but stay afloat for a lengthy period thanks to the reserve buoyancy provided by the superstructure and the relatively slow speed of progressive flooding allowing more time for evacuation. A ro-pax ship in contrast can capsize and sink in a matter of seconds once sufficient water builds up on the large open car deck leading to potentially much higher casualty rates. The focus of our attention was therefore to seek assurance that the SOLAS2009 regulations are at least as effective in providing for the dangerous WOD effect in ro-pax ships as SOLAS90 and the Stockholm Agreement, imperfect as the latter combination may have been.

### *(2) Loss Mechanism for LLH Ro-Pax Ships*

There are two main designs of ro-pax ship – one which is entirely transversely sub-divided below the car deck (usually employed on short crossings with rapid turnaround times) and one which combines longitudinal and transverse subdivision forming a long, lower hold (LLH). The loss mechanism for a LLH ro-pax ship may be quite different from one which is only transversely sub-divided below the vehicle deck. An unpublished UK study (RP 564) carried out on an existing LLH ro-pax ship compliant with IMO Res A.265 showed that damaging the LLH, one wing compartment and the vehicle deck results in margin line immersion as the LLH slowly fills and then sudden loss as water rapidly spreads over the car deck. The vessel sank in less than 20 minutes (real time) in almost calm conditions, the primary cause being the immersion of the

margin line quickly followed by complete loss of reserve buoyancy.

At least two of the studies carried out in 2009 showed it is possible to design new SOLAS2009 LLH ro-ro ships which also sink rapidly in calm seas following penetration of the LLH, which raises the question of whether this possibility was considered when the SOLAS2009 regulations were being developed. Attention seems to have been focused on the residual GZ curve but if the vessel simply sinks without reaching equilibrium then no such curve exists ( $s = 0$ ). At present within SOLAS2009 there is no penalty for  $s = 0$  in individual damage cases as long as  $A \geq R$  and the minor damage regulation 8 is complied with. Whilst some of the  $s = 0$  cases may be associated with relatively gradual loss of stability, others could be due to rapid sinkage or capsize due to WOD with high casualties and should therefore not be lightly dismissed. The issue of whether SOLAS2009 has taken sinkage in calm conditions into account is to be examined in more detail in a new MCA-sponsored research project (RP 625) which should be completed by the end of 2010.

### *(3) Transversely Subdivided Ro-Pax Ships*

In contrast, the loss mechanism for a transversely sub-divided ro-pax may not necessarily involve margin line immersion at equilibrium in calm seas but usually arises from a low residual freeboard due to a combination of sinkage, trim and heel followed by gradual water accumulation onto the car deck through the damage opening due to wave action. Here there is some relationship between significant wave height, residual freeboard, residual GZ (dependent on initial KG and the extent of damage) and the amount of water accumulation. The simplified calculations in the Stockholm Agreement allow for these relationships whereas using the alternative model test approach it is considered satisfactory if the vessel survives all 5 test runs for a particular worst damage case for a period of 30 minutes real time in the appropriate sea-state. This loss mechanism was originally to be

accounted for in SOLAS2009 by the SEM (static equivalent method) or a method based on residual freeboard but these were both dropped at SLF 47 in favour of the so-called GZ approach advocated by Sigmund Rusaas as discussed below.

**(4) The s-factor – development of equation**

The key paper, “Review of WOD and the GZ Approach”, which led to the adoption of the current equation for  $s_{final,i}$  in SOLAS2009 Reg. 7-2.3

$$s_{final,i} = K \cdot \left[ \frac{GZ_{max}}{0.12} \cdot \frac{Range}{16} \right]^{\frac{1}{4}}$$

was presented by S.Rusaas to an SLF inter-sessional meeting in Malmo in December 2003. The graphs shown in fig. 1 and 2 of this paper show the relationship between residual GZ and critical wave height leading to capsizing ( $H_s$ ) for ro-ro and conventional passenger ships.

Given the following statement in an earlier HARDER paper incorporated into SLF 45/3/3 p.24 there seem to be some justifiable doubts as to its correctness:-

*“Alternatively [for ro-pax ships] the traditional GZ based formulation can be used as a correlation to the probability of survival from the model tests. A format similar to the current proposal in the harmonised regulations is possible:*

$$s = [(GZ_{max}/TGZ_{max}) \cdot (Range/TRange)]^{\frac{1}{4}}$$

*Where, TGZ<sub>max</sub> = 0.25m and GZ<sub>max</sub> not to exceed TGZ<sub>max</sub>*

*TRange = 16 degrees and Range not to exceed Trange”*

This question was investigated further in the jointly-funded UK/NL project RP592 in which it was shown that increasing TGZ<sub>max</sub> from 0.12 to 0.25 m for the two new S2009 ro-ro ships designed in the study would result in a

reduction of only around 1% in the Attained Index A - a figure apparently correctly predicted in Rusaas’ paper. In fact RP592 showed that the relative insensitivity of A to the TGZ<sub>max</sub> terms in the s-factor equation is attributable more to the fact that a large proportion of damage cases either have  $s = 0$  or  $s = 1$ . Only the relatively few cases where  $0 < s < 1$  would be influenced by changing TGZ<sub>max</sub> from 0.12 to 0.25m. It was argued in the report for RP592 that this could vary from ship to ship and that it would be more correct and conservative to use a TGZ<sub>max</sub> of 0.25 m.

Rusaas argued that 90% of the collisions in the accident database occurred in sea states with SWH < 2 m and virtually none with SWH > 4 m. Fig. 2 of the paper shows that the maximum difference in the s factor between a conventional and a ro-ro passenger ship (which is assumed to be attributable to the WOD effect) is around 10% and this is most pronounced when the GZ<sub>max</sub> for each type of ship is around 0.1 metres - equivalent to a critical sea state leading to capsizing ( $H_s$ ) of around 1.8 metres for a ro-ro ship and 3 metres for a conventional passenger ship. Where the GZ<sub>max</sub> is 0.05 m or less ( $H_s = 1$  m for both types) or 0.3 m and above ( $H_s = 3.9$  m for ro-ro’s and  $H_s > 12$  m for conventional passenger ships) the s factors are almost the same for both ship types. As both vessel types have equally low survivability at residual GZ<sub>max</sub> of 0.05 m and there are virtually no instances of collision damages occurring in high sea states such as 3.9 metres SWH and above (sea states in which there would be a pronounced difference between ro-ro and conventional passenger ship survivability), the paper concludes that outside a range of GZ<sub>max</sub> values between 0.05m and 0.20 m, there is virtually no difference in the s-factor between ro-pax and conventional ships and the WOD effect can therefore safely be neglected.

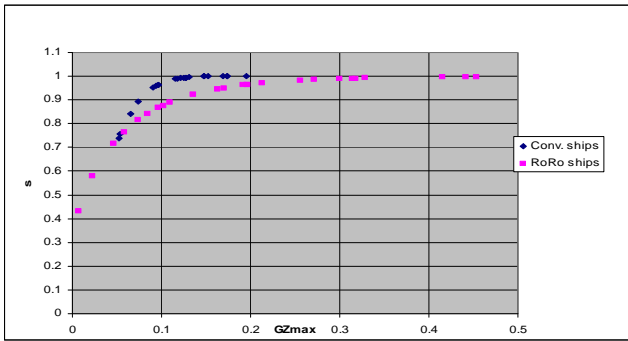


**Fig. 1:** From S. Rusaas’ paper “Review of WOD and the GZ approach” Dec. 2003 fig.2; s- factors for trendlines of Hs.

Rusaas’ paper, quoted in IMO SLF 47/3/9, persuaded the majority of member states at SLF to accept the adoption of the GZ approach using a value of GZmax of 0.12 in the above equation covering both ship types. The implication is that there is no evidence for any significant difference between the overall survivability of ro-pax ships and conventional passenger ships within a probabilistic framework and that the WOD can therefore be safely ignored.

The link, established in Stockholm, between residual freeboard and ro-ro survivability (the greater the residual freeboard and the lower the sea state, the less chance of water accumulation on the car deck) is not explicitly expressed in the adopted equation for s-factor.

**(5) The s- factor – based on limited data**

One major concern with Rusaas’ paper is that the conclusions have necessarily been drawn from a rather small set of data. Fig. 2 shows that 68% of the points are taken from model test results for one ro-pax ship (PRR-01). PRR-01 is a transversely sub-divided ro-pax (for full details and a GA see HARDER paper 3-31-D-2001-01-0) and was model tested for one asymmetrical damage case (midships, standard SOLAS extents) for 3 different draughts and trims and 4 different initial KG values. Dividing the data used to produce Fig. 2 into separate ships and fitting individual regression lines gives a truer picture of the variability of the relationship between Hs and GZmax.

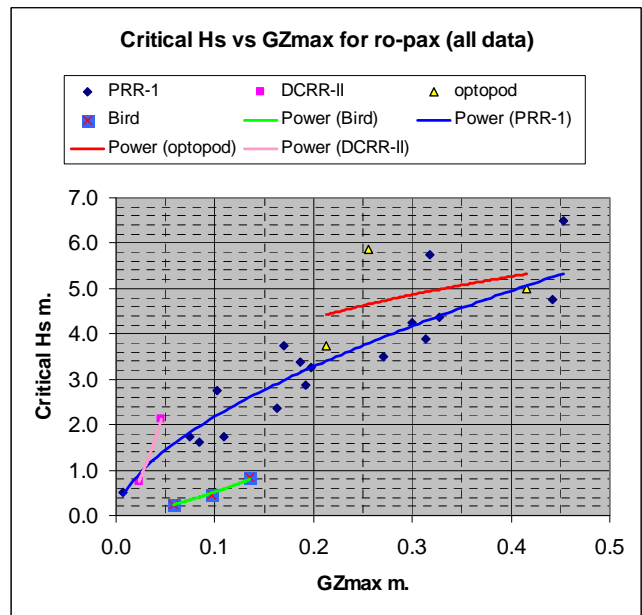


**Fig. 2:** From S. Rusaas’ paper “Review of WOD and the GZ approach” Dec. 2003 fig. 1. Re-drawn to show that 68% of points are for one ship (PRR-01) only tested for 1 midships damage case with penetration depth < B/5

This can be seen more clearly in Fig. 3 which presents curves of Hs against initial KG for PRR-01 for the 3 tested draughts and clearly shows the easily anticipated trend for decreasing survivability with increasing draught and initial KG for the particular damage case in question.

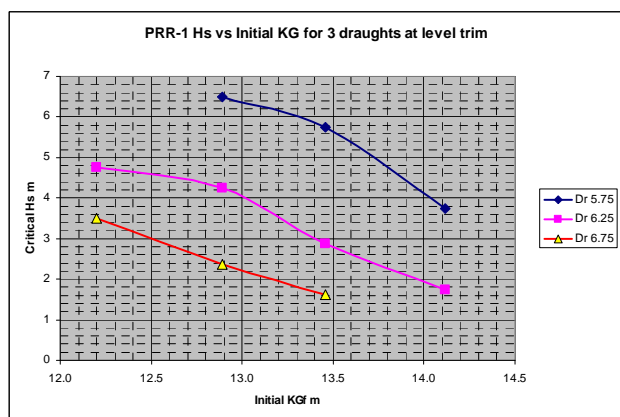
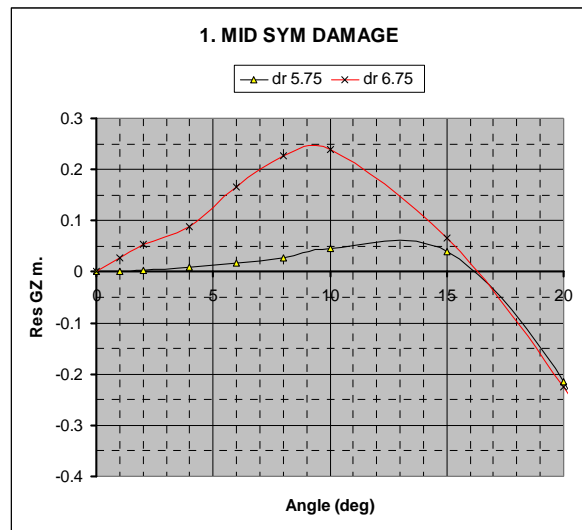


**Fig. 3:** PRR-01 data re-analysed to show relationship between initial draught, KG and Hs for the midships damage case.

**(6) The s-factor – residual range ensures large GZmax?**

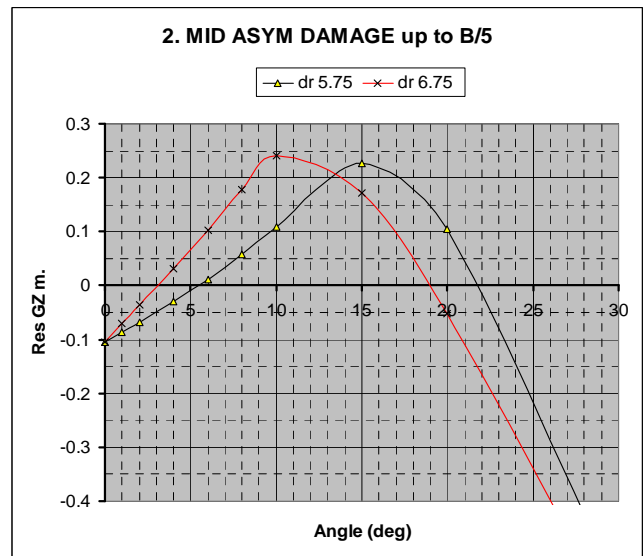
Rusaas also argues that residual range and GZmax are strongly linked (see fig. 3 in his paper) and that if a ro-pax has a residual range of 16 degrees, the GZmax is likely to be around 0.3 metres implying a critical wave height for capsizing of around 4 metres. As virtually no collisions have ever occurred in such high sea states the conclusion is drawn that the residual range term within the s-factor can be relied upon to predict the critical wave height for capsizing for a ro-pax with acceptable accuracy.

Our concern is, however, that the assumed general relationship between residual GZmax and range is based on data from only one damage case – at amidships, asymmetrical with penetration depth of B/5 – on a ship with mainly transverse subdivision below the car deck (PRR-01). To test whether the assumed 16 degrees / 0.3 metres relationship between residual range and GZmax is more widely applicable, we created 2 simple box-shaped computer models having the same principal dimensions as PRR-01. The first was purely transversely sub-divided so that a midships damage resulted in symmetrical flooding between transverse bulkheads; the second had a long lower hold 40% of LBP in length with B/5 longitudinal boundaries. The second model was subjected firstly to a B/5 asymmetrical damage to the wing tank then to a deeper damage penetrating into the LLH. In all cases the vehicle deck was damaged with 90% permeability. These damages were applied at a light draught of 5.75 m and a deep draught of 6.75 m and the resulting damage GZ curves (figs 4-6 below) were adjusted to give a residual range of approximately 16 degrees by varying the initial KGf to determine the corresponding GZmax.



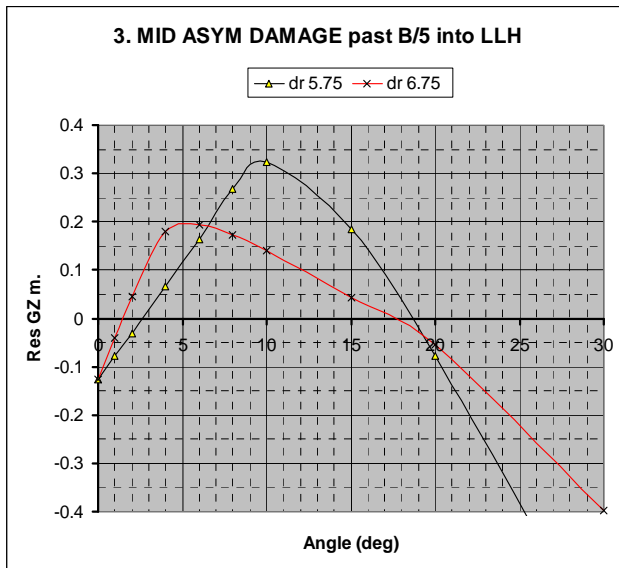
Draught	GZmax for 16 deg range	Hs m.	Initial KGf m
5.75	0.06	1.5	13.6
6.75	0.25	3.8	11.1

**Fig. 4:** Transversely subdivided box-shaped vessel – amidships symmetrical damage



Draught	GZmax for 16 deg range	Hs m.	Initial KGf m
5.75	0.225	3.5	12.85
6.75	0.240	3.7	10.85

**Fig. 5** LLH Box-shaped vessel – amidships asymmetrical damage up to B/5



Draught	GZmax for 16 deg range	Hs m.	Initial KGf m
5.75	0.323	4.3	10.75
6.75	0.193	3.2	7.7

**Fig. 6** LLH Box-shaped vessel – amidships asymmetrical damage past B/5 into LLH

This brief exercise appears to show that the GZmax/Residual Range relationship of 0.3 / 16 used to confirm that the equation for s-factor in the SOLAS 2009 Regulation 7-2.3 is equally applicable to ro-pax and conventional passenger ships, may well be valid only for the specific amidships asymmetrical damage case tested for PRR-01 in the HARDER project (corresponding approximately to case 2 in the above study). It therefore seems that a much wider spread of data involving more extensive damages to different ro-ro designs is needed. Perhaps basing the s-factor only on heel, MaxGZ and residual range is too simplistic especially as all these parameters are primarily dependent on initial draught, KG and the damage extent.

These problems may have been compounded by the possible neglect of sinkage as a loss mechanism in SOLAS 2009 - something clearly demonstrated in two of the ro-pax research studies completed in 2009. In our opinion, these uncertainties regarding the s-factor fully justify the extra research work now being undertaken.

## CONCLUSIONS

It is hoped that the new research projects - EMSA2, GOALDS, RP625 and FLOODSTAND - using the latest analytical tools will shed more light on some of the issues raised in this paper and eventually inform further discussions at IMO as we seek to ensure that the SOLAS2009 regulations for ro-ro passenger ships are fit for purpose.

Ro-ro vessels are fundamentally important to the economic activity of many countries and yet can remain a relatively vulnerable mode of transport if due precautions are not taken in their design and operation.

The common aim is that we all want to be convinced that new generations of post-2009 ro-ro passenger ships will be able to fully utilize the flexibility of design offered by the probabilistic approach or alternative methods and yet be safer for the travelling public than those built in preceding generations.

## REFERENCES

- Rusaas, "Review of WOD and the GZ Approach", presented to an SLF inter-sessional meeting in Malmo in December 2003.
- Jasionowski, Investigation into the Safety of Ro-Ro Passenger Ships fitted with Long Lower Holds – Phase II. MCA RP592, March 2009.
- The above papers and many others relevant to this issue can be readily accessed from the following MCA web-site:- <http://m3net.mcga.gov.uk/c4mca/imosdscg.htm>
- SOLAS Consolidated Edition, 2009

## GOALDS – Goal Based Damage Stability

Apostolos Papanikolaou<sup>1)</sup>, Christian Mains<sup>2)</sup>, Sigmund Rusaas<sup>3)</sup>,  
Rafal Szalek<sup>4)</sup>, Nikolaos Tsakalakis<sup>5)</sup>, Dracos Vassalos<sup>5)</sup>, George Zaraphonitis<sup>1)</sup>

<sup>1)</sup> National Technical University of Athens-SDL, <sup>2)</sup> Germanischer Lloyd,  
<sup>3)</sup> Det Norske Veritas, <sup>4)</sup> Safety at Sea, <sup>5)</sup> Universities of Glasgow & Strathclyde - SSRC

### ABSTRACT

*The new probabilistic damaged stability regulations for dry cargo and passenger ships (SOLAS 2009), which entered into force on January 1, 2009, represent a major step forward in achieving an improved safety standard through the rationalization and harmonization of damaged stability requirements. There are, however, serious concerns regarding the adopted formulation for the calculation of the survival probability of passenger ships, particularly for ROPAX and large cruise vessels; thus eventually of the Attained and Required Subdivision Indices for passenger ships. Furthermore, present damaged stability regulations account only for collision damages, de-spite the fact that accidents statistics, particularly of passenger ships, indicate the profound importance of grounding accidents. The present paper outlines the objectives, the methodology of work and early results of the EU funded, FP7 project GOALDS (Goal Based Damaged Stability, 2009-2012), which aims at ad-dressing the above shortcomings by state of the art scientific methods and formulating a rational regulatory framework, properly accounting for the for the damage stability properties of passenger ships.*

### KEYWORDS

Damage ship stability; probabilistic assessment, goal-based design; risk-based design; passenger ship safety.

A Attained Subdivision Index  
CDF Cumulative Distribution Function  
PDF Probability Density Function  
LRF Lloyd's Register Fairplay  
TTS Time To Sink

### 1. INTRODUCTION

In January 2009, the new harmonized probabilistic rules for ship subdivision became mandatory, initiating a new era in rule-making in the maritime industry in line with contemporary developments, understanding and expectations. This was the culmination of more than 50 years of work, one of the longest gestation periods of any other safety regulation. Considering that this is indeed, a step change in the way safety is being

addressed and regulated, “taking our time” is well justified (Papanikolaou, 2007).

One of the great achievements of this effort was thought to be the harmonization of standards for dry cargo and passenger vessels in a probabilistic frame-work which allows for a rational assessment of safety and design innovation. In this state of affairs, the EU-funded R&D project HARDER (1999-2003), created history at IMO by being the first externally funded research project to support specifically the IMO rule making process and to contribute massively to the successful development of the new rules.

However, with a number of ship owners opting to follow these new rules in advance and as of today, a number of issues were surfacing,

which require urgent consideration, as these affect the most safety-critical ships, namely large passenger ships, which are currently one of the fastest growing ship sectors and what is more important these ships constitute the core strength of the European shipbuilding industry. Also, great concerns were expressed by EU member states and the European Maritime Safety Agency (EMSA) regarding the abolishment of the Stockholm Agreement provisions for ROPAX ships, when the new SOLAS 2009 entered in to force; in fact, there was strong evidence that SOLAS 2009 does not satisfactorily cover Water On Deck effects on ROPAX survivability (e.g., HSVA, 2009). These concerns, which form the kernel of the rationale for the research reported in this paper, can be summarized as follows:

- As the required subdivision index was derived by harmonization (based on existing vessels, built in the 90ties), the new damage stability standard being statistical in nature (rather than performance-based) could not implicitly cater for the higher level of safety inherent (required) in mega-passenger ships; it rather maintains a safety level fit for the ships of a bygone era.
- In addition, lack of proper consideration (due to lack of availability) of large passenger ships in the sample studied in Project HARDER, raised concerns during the harmonization process as to the suitability for the developed standards for damage stability among the IMO delegates, leading to a strong and explicit recommendation in IMO SLF47 to undertake pertinent research to address the damage stability standards for these ships (specifically to reformulate the probability of survival in a damage condition – s factor).
- In addition, only survivability following *collision events* was addressed. A similar formulation for *grounding accidents* was not developed.
- Within the EU-funded R&D project SAFEDOR (2005-2009), a series of high-level formal safety assessments (FSA studies) were performed for cargo and passenger vessels. The FSA studies on cruise and ROPAX vessels both concluded that the risk to human life could be reduced cost-effectively by increasing the required subdivision index.
- The results of the FSA on cruise vessels performed within SAFEDOR show that a reduction of risk by 2.1 lives per ship per lifetime (30 years) may be achieved by increasing either GM or freeboard. Both design measures are shown to be cost-effective according to IMO criteria. However, due to the high-level approach within a FSA, only generic design measures were explored and found to be cost-effective. No complete new concept ship design was created to check the consequences of introducing higher subdivision requirements. Therefore, the FSA studies recommend undertaking research to investigate more thoroughly this issue.
- Recent experience in the design of new large passenger ships according to the forthcoming probabilistic rules, tend to emphatically reinforce the foregoing. The rules appear to be inconsistent with design experience for high survivability for these ships and the level of vessel achieved in some of these designs is far higher than the level demanded by the rules, suggesting that there is “room” for higher standard of safety for large passenger ships without penalizing other design considerations; this is in full support of the FSA findings.
- Developing SOLAS 2009 as a new damage stability global standard, the consideration of Water On Deck effects on the survivability of ROPAX vessels was not an issue, as this was covered by the Stockholm Regional Agreement; thus, inherently, SOLAS 2009 could never be an equivalent for SOLAS 90 + Stockholm Agreement provisions.
- Developments within SAFEDOR of holistic approaches in dealing with ship

safety have revealed that the risk to human life from flooding (resulting from collision and grounding accidents) dominates the safety of passenger ships (almost 90% of the total risk), thus making it imperative to “get damage stability right” (see, Vassalos D. in Papanikolaou (ed), 2009).

- Other developments within IMO concerning the safety of large passenger ships, led to concepts of progressively more holistic nature, namely “Safe Return to Port”, again with flooding (and fire) accidents at the very centre of such developments; this necessitating a more thorough understanding of how damage stability ought to be catered for in ship design and operation.
- Along similar lines, one of the top-agenda items at IMO, namely Goal-Based Standards is targeting in the longer term all ship types, with of course passenger ships being a main target, implicitly again pointing towards the need to sort out the damage stability standard for large passenger ships.

This latter point provided the inspiration for the title of the present research project, namely “Goal-Based Damage Stability” – GOALDS; it aims to contribute to IMO regulatory work in a similar fashion to HARDER supported by a consortium of partners that essentially comprises the same core partnership.

The project addresses the above outlined challenges by undertaking research to improve the current survivability formulation, to integrate collision and grounding damage events, to proceed to a risk-based derivation of a new subdivision requirement and conduct a series of concept design studies to ensure the practicability of the new formulation. Upon completion, GOALDS will submit key results to IMO for consideration in the rule making process. More specifically, GOALDS key objectives are to:

- Develop an enhanced formulation for the survival factor “s” accounting for key design parameters of passenger ships and for the time evolution of flooding

scenarios; it evident that the formulation of the new survival factor will cater for the design differences between cruise and ROPAX ships.

- Develop a new survivability formulation for flooding following grounding accidents.
- Integrate collision and grounding survivability formulations into a single framework
- Validate the new formulations by experimental and numerical analyses
- Develop a new damage survivability requirement in a risk-based context
- Evaluate the practicability of the new formulations by a series of ship concept design studies
- Upon completion, submit results for consideration by IMO

The project consortium consists of eighteen (18) European organizations<sup>1</sup>, representing all major stakeholders of the European maritime industry (yards, class societies, operators and flag states), research institutes and universities. Practically all project partners and in particular the major drivers of the project collaborated successfully in the past in the completion of the related projects SAFER-EURORO, HARDER and SAFEDOR. Also, an Advisory Committee has been formed composed of representatives of major public regulatory authorities and CESA, to the extent they are not already active partners in the project. The AC is meant as a sounding body for the consortium as well as a platform for early discussion of project results related to the

---

<sup>1</sup> National Technical University of Athens-Ship Design Laboratory (coordinator), Universities of Glasgow and Strathclyde-Ship Stability Research Centre, Germanischer Lloyd, Det Norske Veritas, Safety at Sea, Lloyds Register, Hamburg Ship Model Basin, Vienna Model Basin, Danish Maritime Authority, Maritime and Coastguard Agency, University of Trieste, STX Europe-France, STX Europe-Finland, FINCANTIERI, MEYER Werft, Color Line, Carnival PLC, Royal Cruises Lines, <http://www.goalds.org>.

preparation and consolidation of regulatory proposals to IMO<sup>2</sup>.

## 2. OBJECTIVES & EARLY RESULTS<sup>3</sup>

The project’s detailed objectives and work plan may be found in the public domain area of the project’s web site <http://www.golds.org>. In the following, some early scientific results of the project are presented.

### 2.1 Damage Statistics for Collision and Grounding

Some early work of the project is focusing on an update of the collision damage statistics compiled in the HARDER project; these statistical data were also subsequently updated by a number of flag state delegations as part of the rule making process at IMO; the aim of GOALDS is herein to collect and analyse latest damage data, available to the project, and to provide suitable probability distributions for collision damage characteristics pertinent to passenger ships. To this end the GOALDS database builds on the existing HARDER database, with additional data coming from all stakeholders participating in the project, as well as from other publicly available accident databases.

Whereas the earlier damage statistics were limited to collision damages only, in the present project we consider also grounding damages; this work was actually initiated but was never completed within the project HARDER. In this respect, emphasis will now be placed on the grounding damage characteristics of passenger ships, noting that grounding is a very serious hazard for passenger ships’ survivability.

The HARDER database includes casualties from 1944 up to the year 2000. To identify the casualties in the last 10 years, the Lloyd’s Register Fairplay database (LRF) has been used, whereas the characteristics of these

damages were deduced mainly from class societies’ records. A total number of 1587 casualties could be recorded in the updated database (349 GOALDS, 1238 HARDER). It was differentiated between collision, grounding and contact damages, as shown in below table (Table 1).

**Table 1: Collected damage data by hazard and origin for the period 1944 to 2010**

	Collision	Grounding	Contact
HARDER	891	312	35
GOALDS	185	160	4
database	1076	472	39

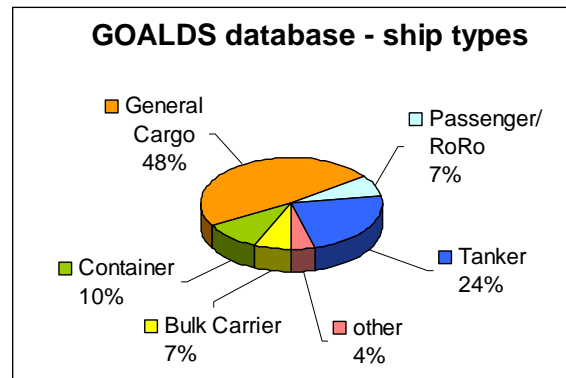


**Fig. 1: GOALDS database of damage statistics – Origin of damages by ship type**

The distribution of the ship types captured in the GOALDS database can be seen in the pie chart (Fig. 1).

The limited number of available damage data for passenger ships led to the conclusion that all damage data independently of ship type and time period should be considered; this was done likewise in previous relevant analyses (e.g., HARDER project). Some preliminary results of the data analysis are shown in the following graphs.

#### Collision:

A-1.1 non-dimensional damage position in longitudinal direction ( $f(x)$ =PDF;  $N_x$ =Number of casualties)

A-1.2 non-dimensional damage length  $f(x)$  = PDF,  $F(x)$  = CDF

<sup>2</sup> Association of European Shipbuilders CESA, flag states: Maritime Administrations of Norway, Sweden, Netherlands, Finland, Germany and USA, noting that the Maritime Administrations of Denmark and United Kingdom are already regular members of the consortium.

<sup>3</sup> At the time of preparing this paper, the project was practically 6 months underway, thus only some early results are herein presented.

**Grounding:**

A-1.1 nondimensional damage position in longitudinal direction ( $f(x)$ =PDF;  $N_x$ =Number of casualties)

A-1.2 nondimensional damage length  $f(x)$ =PDF,  $F(x)$  = CDF

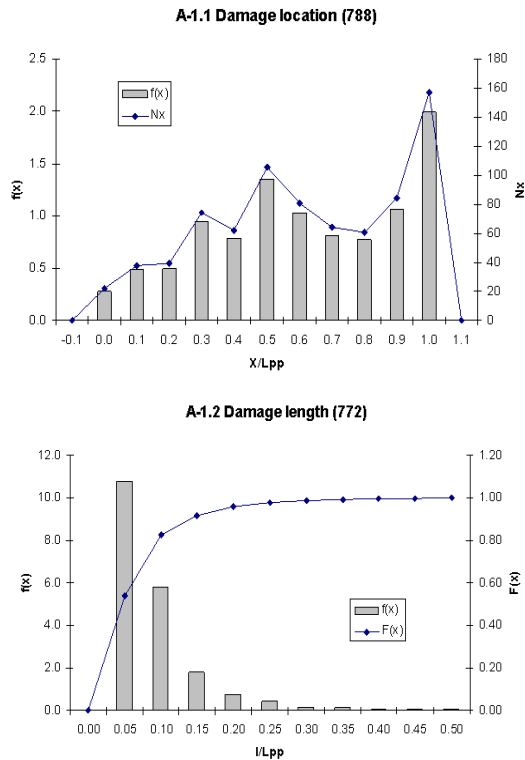


**Fig. 2: Damage location and length for collision damages according to GOALDS database**

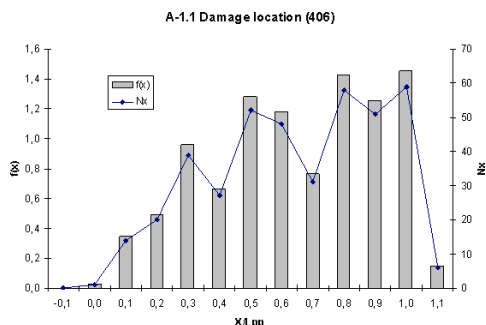


**Fig. 3: Damage location and length<sup>4</sup> for grounding damages according to GOALDS database**

**2.2 Numerical Studies on Survivability Benchmarking of Numerical Codes**

Project GOALDS has introduced a new era in damage survivability research. For the first time ever, numerical simulations will be utilised to produce the bulk of results, which will then be used for the development of the new s factor formulation, following validation through physical experiments. This is a sign of the confidence that the research community has gradually acquired in relevant simulation codes that pave arguably the way forward. Most of the partners involved in this project have long experience or are presently in the process of developing their own damage stability simulation codes. Thus, it is sensible to share the effort between those involved, firstly for efficiency and secondly for verification purposes.

However, before distributing project’s simulation effort to qualified project partners, a benchmarking of the employed numerical codes would be necessary. This is actually a verification of the outcome of earlier related damage stability benchmarks of codes, organised by ITTC and SAFEDOR (see, Papanikolaou, 2007). To this end, the ROPAX ship PRR-1, which has been used in a number of previous studies, was selected for benchmarking. Results for PRR-1 from

<sup>4</sup> Regarding the recorded damage length of groundings, special attention was paid to the consideration of multiple holes’ damages by an equivalent damage length

physical testing already exist from the HARDER project, a fact that makes this particular ship a good base for benchmarking studies. In addition to this, it is a typical example of a middle-sized ROPAX vessel, without the controversial feature of a long-lower hold.

**Table 2: PRR-1 main particulars**

Length over all	194.30	m
Length between perpendiculars	170.00	m
Subdivision Length	178.75	m
Breadth	27.80	m
Depth to subdivision deck (G-Deck)	9.00	m
Depth to E-Deck	14.85	m
Keel thickness	14.85	m
Service Draught	6.25	m
Displacement	17301.7	ton
KMT	15.522	m
KG	12.892	m
VCG	3.595	m
LCB	81.891	m

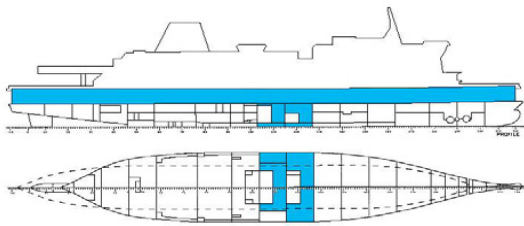


**Fig. 4: PRR-1 and Test Damage**

Obtained numerical results by two project partners (NTUA-SDL & SSRC) show reasonable convergence with respect to comparable experimental results, as well as among themselves. Static stability calculations seem to be in perfect match between the two simulation contributors so far (P1 & P2) as shown in Figs 5~6. Concerning the dynamic damage stability simulation results, both codes under-predict to a certain degree survivability, compared to available experimental results; this is less worrying as it places numerical results on the safe side, Fig. 7. Thus and pending verification by further benchmarks, numerical predictions appear to lead, in general, to conservative survival predictions.

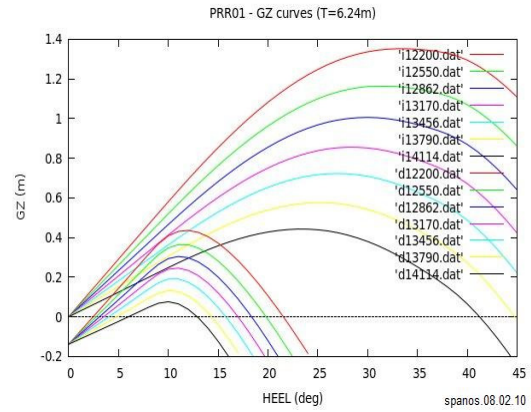


**Fig. 5: PRR01-GZ curves calculated by P1 code**

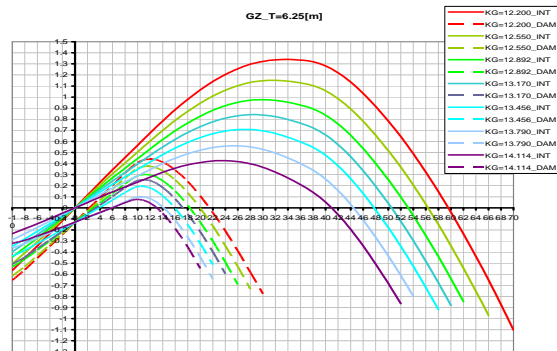


**Fig. 6: PRR1-GZ curves calculated by P2 code**

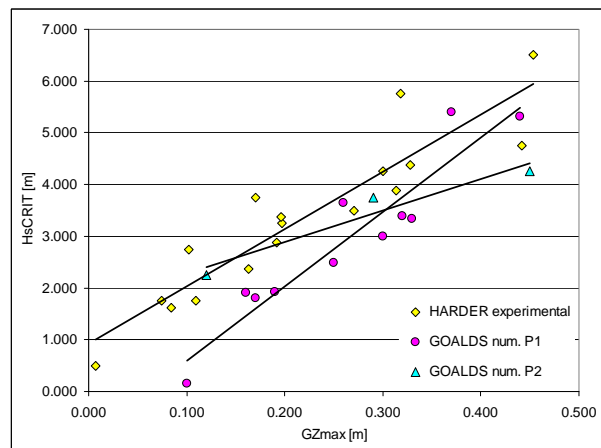


**Fig. 7: Experimental vs. numerically simulated results by codes P1 and P2**

**Table 3: PRR-1 Tests**

Model tests						Simulations (P1, P2)			
Init T	Init tr	KG	GZ <sub>MAX</sub>	Range	Hs <sub>CRIT</sub>	Init tr	KG	GZ <sub>MAX</sub>	Hs <sub>CRIT</sub>
[m]	[deg]	[m]	[m]	[deg]	[m]	[deg]	[m]	[m]	[m]
6.25	0	12.200	0.442	20.200	4.750	0	12.200	0.44	5.32
6.25	0	12.892	0.300	15.900	4.250	0	12.550	0.37	5.40
6.25	0	13.456	0.192	12.200	2.875	0	12.750	0.33	3.34
6.25	0	14.114	0.074	7.100	1.750	0	12.892	0.30	3.00
6.25	-1	12.200	0.314	16.600	3.875	0	13.170	0.25	2.48
6.25	-1	12.892	0.197	12.474	3.250	0	13.456	0.19	1.92
6.25	-1	13.456	0.109	9.000	1.750	0	13.790	0.10	0.16
6.25	1	12.200	0.328	18.800	4.375	<b>0</b>	<b>12.000</b>	<b>0.45</b>	<b>4.25</b>
6.25	1	12.892	0.196	13.930	3.375	<b>0</b>	<b>13.000</b>	<b>0.29</b>	<b>3.75</b>
6.25	1	13.456	0.102	9.800	2.750	<b>0</b>	<b>14.000</b>	<b>0.12</b>	<b>2.25</b>
6.25	1	14.114	0.007	2.400	0.500				
5.75	0	12.892	0.453	21.400	6.500	0	13.456	0.32	3.39
5.75	0	13.458	0.318	17.600	5.750	0	14.114	0.17	1.80
5.75	0	14.114	0.170	12.560	3.750				
6.75	0	12.200	0.271	14.000	3.500	0	12.200	0.26	3.65
6.75	0	12.892	0.163	12.150	2.375	0	12.892	0.16	1.90
6.75	0	13.456	0.084	6.800	1.625				

**Capsize Band**

Probably more important than the critical (survival) wave height per se, the search for the critical seastate has revealed something new about the nature of the capsize process. As is usually the case with boundary (extreme Limits) phenomena, ship survival is not a well-defined process. It appears that there is a band within which the transition from “safe” to “unsafe” takes place. This has been conventionally named “capsize band”. This band begins at the wave height where no capsizes are observed at all (given certain uncertainty levels) and finishes at that wave height where all realisations result in loss. In order to better describe the capsize band, another term has been introduced, the “rate of capsize” (PF). This is no more than the probability of capsize, given a seastate. So PF will be 0 at the lower end of the capsize band and 1 at the upper end. The point of the capsize band where PF = 0.5 is the critical wave height (Hs<sub>crit</sub>) and it is this value that is used by convention when referring to ship survivability.

The capsize boundaries are symmetrical, either side of the Hs<sub>crit</sub>, whilst the capsize band follows a specific pattern. Applying non-linear regression to the results from the simulations it seems that there is a perfect fit for a *sigmoid* distribution (Fig. 8).

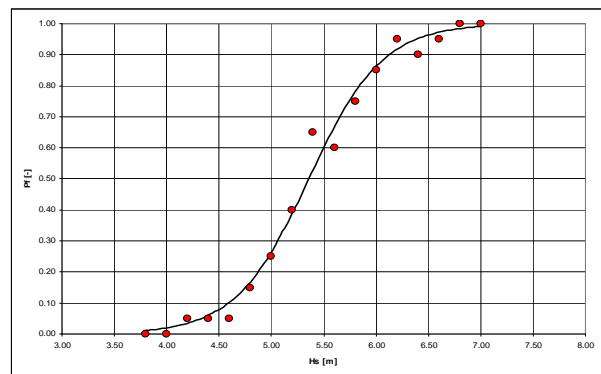


**Fig. 8: Capsize band and fitted sigmoid**

Another attribute of the capsize band is that it is varying with critical wave height. More specifically, the higher the critical wave height, the broader the bandwidth and visa versa. This is visible in Fig. 9, where the

capsize band has been established for various conditions for PRR-1. Appropriate curves have been fitted to make results clearer.

as well as characteristics of the ship geometry and loading condition.

The fitted sigmoid curves are described by four parameters:  $A_0$ ,  $A_1$ ,  $x_0$ ,  $dx$  that are lower  $P_F$  ( $=0$ ), upper  $P_F$  ( $=1$ ), critical wave height and bandwidth respectively. With  $A_0$  and  $A_1$  being predefined it is rather easy, having just two parameters, to express capsize band analytically. The solution put forward shall be based on those properties of the fitted curves,

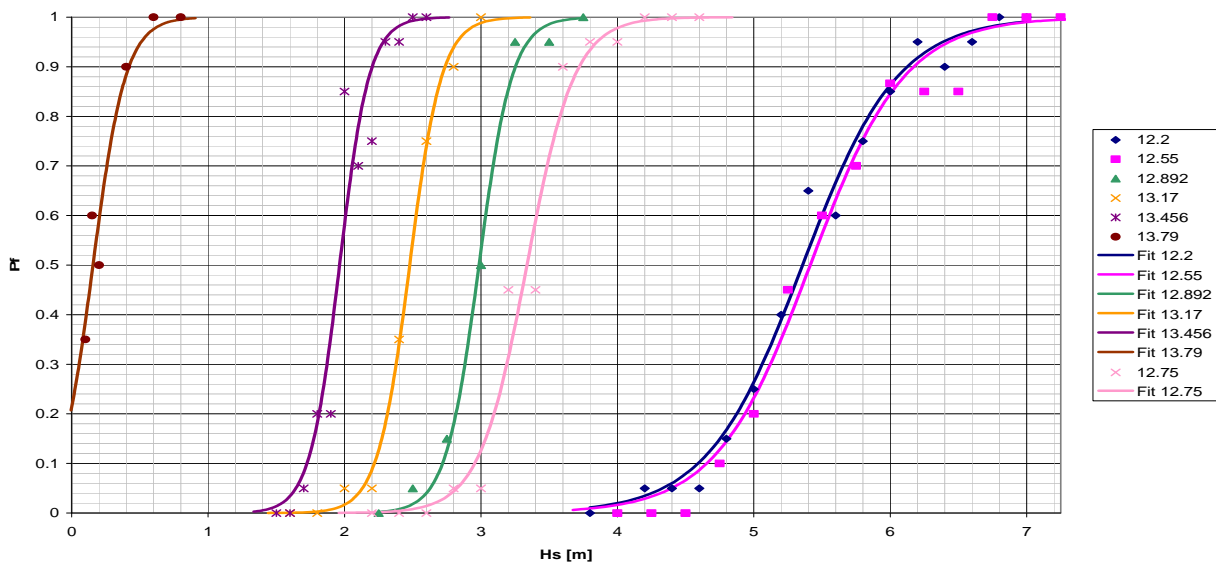


**Fig. 9: Variation of the capsize band for various critical wave heights**

### 2.3 Experimental Studies on Survivability

One of the main project's objectives is to provide experimental evidence on the process of ship stability deterioration after hull breach, typical for collision and grounding accidents. The evidence corresponds to the relation between specific set of damage and environmental conditions and the corresponding time it takes for the limit state condition to evolve (vessel losing its functional equilibrium attitude). Results will be used for the verification of related numerical predictions of the survival factor (s-factor), as outlined in the previous section.

The experiments will be undertaken for two representative large ROPAX and two Cruise Liner ships. Two model basins will conduct the model experiments, namely Vienna Model basin will build and carry out experiments for cruise vessels and HSVA (Hamburg) will be in charge of the ROPAX vessels. The main data of the sample vessels selected for the physical experiments are given in the following table (Table 4).

**Table 4: Main data of GOALDS test ships**

<b>Ship</b>	<b>Ropax (R1)</b>	<b>Ropax (R2)</b>	<b>Cruise ship (C1)</b>	<b>Cruise ship (C2)</b>
Number of passengers	1400	622	3840	2500
LOA	194.3 m	97.9 m	311.123 m	294.81 m
LBP	176.0 m	89.0 m	274.73 m	260.6 m
Breadth moulded	25.0 m	16.4 m	38.6 m	32.2 m
Deepest subdivision loadline	6.55 m	4.0 m	8.6 m	8.0 m
Depth to bulkhead deck	9.1 m	6.3 m	11.7 m	10.6 m
Displacement	16,558 tn	3,445 tn	62,459 tn	45,025 tn
Service speed	27.5 kn	19.5 kn	22.6 kn	22.0 kn

All sample vessels, the data of which were supplied by project partners, are ships designed in compliance with the deterministic SOLAS '90 damage stability regulations. The decision to select SOLAS 90 ships as a baseline for the development of the GOALDS damage stability standard was made after thorough discussions among the project partners; this, namely, ensured, a common baseline with comparable numerical and experimental data obtained in the HARDER project, whereas the harmonized probabilistic SOLAS 2009 was also developed on an equivalent basis with SOLAS 90.

#### Damage Selection

The selection of the damage location and extent for the model experiments is straightforward for the collision damages, in view of past experience with respect to the identification of worst damage; however, it is less clear with the groundings, for which less experience exists. Thus, the location of the grounding damages for the selected sample ships was specified on the basis of the statistical data collected by the project; for the critical grounding, it was

assumed that 4 compartments of the double bottom will be flooded, with the additional penetration of the centre watertight bulkhead above the inner bottom to allow for up-flooding.

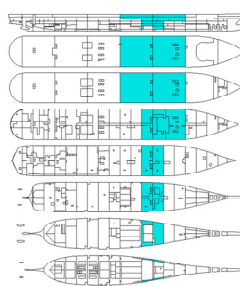
The location of the collision damage was derived using “worst SOLAS damage (2-compartment damage up to B/5,  $\pm 35\%L$  from amidships)” with regard to the minimum area under the residual positive GZ curve; this was cross checked with results of numerical simulations of same damages. Numerical simulations accounting for dynamic effects contributed to identifying additional damages, which would affect capsize and/or cause extreme roll motions.

The impact of the various explored damages was assessed by application of both SOLAS 90 provisions and numerical simulations; the results were graded with respect to their severity; for each vessel a comparative grading table was prepared, ranking the severity of the various damages (Table 5). The least sum resulting from the ranking of the severity according to both methods indicates the damage selected for experiments. It should be

noted that in case of test cruise vessels, a 3-compartment damage of outer shell will be used in order to approach the survivability boundary. In general it was agreed that for verification purposes suitable statistical damages beyond SOLAS 90 standard (i.e. increased penetration) will be included in the tests, to ensure that the formulation of the s factor will capture realistically the physics of related damages.

After the test damages were selected the corresponding model drawings were prepared and a test matrix for each vessel type was established. The first two vessels to be tested in summer 2010 are C1 and R2.

**Table 5: Ranking of damage cases according to severity**



Case	SOLAS '90	Simulations	Sum	35%
1-2	18	-	-	
2-3	16	1	17	
3-4	6	2	8	
4-5	14	15	29	Y
5-6	12	16	28	Y
6-7	8	3	11	Y
7-8	11	4	15	Y
8-9	9	14	23	Y
9-10	7	10	17	Y
10-11	10	13	23	Y
11-12	5	8	13	Y
12-13	13	5	18	Y
13-14	1	6	7	Y
14-15	3	9	12	Y
15-16	2	7	9	Y
16-17	4	11	15	Y
17-18	15	12	27	Y
18-19	17	17	34	
19-20	19	18	37	
20-21	20	-	-	

initially with maximum KG values (SOLAS 90); subsequently, the KG values will be increased in an attempt to capture the survivability boundary. Also, the significant wave height will be gradually increased to a maximum of Hs=4.0m.

**2.4 Risk-based Damage Stability Requirement**

A complete risk model considering both collision and grounding will need the following elements to be in place:

1. Collision and grounding frequency, i.e. how often a collision and grounding takes place.
2. Flooding frequency, i.e. how many of the collision or grounding cases actually lead to flooding.
3. Probability of not surviving the collision or grounding given flooding. This is ideally equal to 1-A, where A is the attained index according to the probabilistic rules.
4. Giving non-survival, how much time is available to evacuation.
5. Given the estimated time, what is the likely outcome of the evacuation?

This may be illustrated as follows, Fig. 10:

**Table 6: Typical sample ship test matrix**

		Irregular waves JONSWAP 1/25				
		H <sub>1</sub>	H <sub>2</sub>	...	H <sub>max</sub> = 4.0m	
Loading conditions	DL (1m trim)	(x)	(x)	...	(x)	
	DP (0 trim)	x	x	...	x	
	DS (0 trim)	x	x	...	x	
Damage location	Col 1	x	x	...	x	
	Col 2	-	-	...	-	
	Grounding	x	x	...	x	
Damage extent	2-comp <sup>+</sup>	x	x	...	x	
	3-comp <sup>++</sup>	x	x	...	x	
Penetration	Shell	x	x	...	x	
	B/5	-	-	...	-	
Centre of Gravity	KG1	x	x	...	x	
	KG2	x	x	...	x	
	KG3	x	x	...	x	
Transient	In waves	(x)	(x)	...	(x)	
	Calm water			x		

A typical Test Matrix (Table 6) includes testing of one collision and one grounding damage for each ship and for 3 draughts (DS, DP and DL),

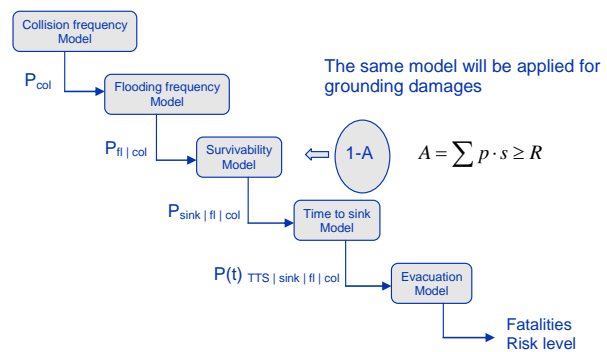


**Fig. 10: Model of risk-based damage stability requirement**

Some background information about the formulation of the risk-based damage stability requirement of GOALDS may be found in Skjong et al., 2006.

## **2.5 Innovative ship concept designs based on the new damage stability requirement**

In order to investigate the impact of the new formulation for the probabilistic damage stability evaluation of passenger ships on the design and operational characteristics of characteristic ROPAX and cruise vessels, it is planned to conceptually design and optimise innovative vessel layouts, meeting the new damage stability standard, while considering building cost and efficiency in operation.

An existing integrated design optimisation procedure (Zaraphonitis et al., 2003) of NTUA, encompassing the parametric design and optimization of ROPAX vessels, will be extended to account for cruise ship design layouts and adapted to the new damage stability standard. Participating industry will be providing expertise and empirical data, as necessary for the implementation of the developed procedure.

The resulting design concepts will be further elaborated to the preliminary stage by the participating shipyards, namely Fincantieri, Meyer Werft, STX Finland and STX France.

## **3. SUMMARY AND EXPECTED OUTCOME**

This paper presented the objectives and reviewed early results of the EU funded, FP7 project GOALDS. The main expected outcome of GOALDS is its contribution to enhanced safety of the passenger maritime transport and the facilitation of the application of rational, risk-based procedures to the design of ROPAX and cruise ships, a clear domain of the European shipbuilding industry. This will be achieved by delivering a rational, fully validated, robust and consistent method for assessing the safety of passenger ships in case of a collision or grounding. In this way, the project aims at further developing and complementing past work of the successful HARDER project, which decisively contributed to the development and the adoption of the new harmonized damage stability regulations pertaining to all types of

dry cargo and passenger ships. This project outcome is being sought not only by the European maritime community, but the entire international maritime community has been working in recent years on the further improvement of passenger ship's safety, especially in view of ultra large cruise ship designs and operations.

On the way to this goal, the project will deliver a whole array of useful applications and products. The project will provide a quantum leap in understanding the complex physics behind the behaviour of a damaged passenger ship, considering the fundamental differences in ROPAX and cruise ship design, and the unique concept of simplified generic models should enable designers and regulators with far better tools than before for making rational designs and regulations. New and updated damaged databases will be established, and unique tools for quantifying the probability of damage and calculating expected extent of damage following a collision or grounding will be exploitable by all parties.

The results are mainly targeted to assist regulators in their work with new and improved regulations for passenger ships covered by SOLAS, with an expected time for exploitation of maximum three years. The timing is very appropriate in light of the need for new passenger ships to comply with expected growth of the water-borne transportation in Europe and the international cruise business. By introduction of new and rational, risk-based criteria now, new passenger ships may be designed with greater flexibility without compromising safety.

The main product of GOALDS – a rational probabilistic approach to assessing collision and grounding of passenger ships and the rational criteria deriving there from - as well as the consequence analysis tools - may of course be exploited by the maritime community on a worldwide basis, but the detailed knowledge and understanding of the method remains within Europe, and thus providing the European maritime community with a significant technological edge. This is

especially valid for the shipbuilding industry, which will gain significant knowledge on how to apply the new approach on design of passenger ships following an improved probabilistic concept, better accounting for the special design features of ROPAX and cruise ships.

#### ACKNOWLEDGEMENTS

The presented work is being conducted within the EU funded project GOALDS (2009-2012), Contract No FP7-233876. The European Community and the authors shall not in any way be liable or responsible for the use of any knowledge, information or data of the present paper, or of the consequences thereof. The views expressed in this paper those of the authors and do not necessary reflect the views and policies of the European Community.

#### REFERENCES

- GOALDS (2009-2012). “Goal-based Damage Stability”, Project funded by the European Commission, FP7- DG Research, Grant Agreement 233876. <http://www.goalds.org>.
- HARDER (1999-2003). “Harmonization of Rules and Design Rational”. Project funded by the European Commission, DG XII-BRITE.
- HSVA (2009). “Research for the Parameters of the Damage Stability Rules including the Calculation of Water on Deck of Ro-Ro Passenger Vessels, for the amendment of the Directives 2003/25/EC and 98/18/EC”, Final Report Part I-II, funded by EMSA, July 2009, <http://www.emsa.europa.eu>.
- Papanikolaou, A. (2007). “Review of Damage Stability of Ships - Recent Developments and Trends”, Proc. PRADS 2007, Houston, October 2007
- Papanikolaou, A. (ed.), Guedes Soares, C., Jasionowski, A., Jensen, J., Mc George, D., Papanikolaou, A., Poylio, E., Sames, P., Skjong, R., Skovbakke-Juhl, J. and Vassalos, D (2009). “Risk-based Ship Design–Methods, Tools and Applications”, SPRINGER, ISBN 978-3-540-89041-6, February 2009.
- SAFEDOR (2005-2009). “Design, Operation

- and Regulation for Safety”, EU project, FP6-516278.
- SAFER-EURORO I and II (1997-2005). “Thematic Network, Design for Safety: An Integrated Approach for Safe European Ro-Ro Ferry Design”, Project funded by the European Commission,
- Skjong, R, Vanem, E, Rusaas, S and Olufsen, O (2006). “Holistic and risk based approach to collision damage stability of passenger ships”, Proc. 9<sup>th</sup> Int. Conf. on Stability of Ships and Ocean Vehicles, Rio de Janeiro, Brazil, 25-29 September.
- Zaraphonitis, G, Boulougouris, E. and Papanikolaou, A. (2003). “An Integrated Optimisation Procedure for the Design of Ro-Ro Passenger Ships of Enhanced Safety and Efficiency”, Proc. 8<sup>th</sup> IMDC Conference, Athens, May 2003.

# Application of Wave Groups to Assess Ship Response in Irregular Seas

Christopher C. Bassler, Vadim Belenky, Martin J. Dipper, Jr.

David Taylor Model Basin (DTMB), Naval Surface Warfare Center, Carderock Division

## ABSTRACT

A method using wave groups to evaluate ship response in heavy seas is presented. A ship sailing in a stochastic environment is difficult to model because of both the rarity and significant nonlinearity of the large motion responses. In the proposed method, wave groups which are critical to ship response are defined, separating the complexity of the nonlinear dynamics of ship response from the complexities of a probabilistic description for the response. In this formulation, wave groups may be considered as a possible method to solve the problem of rarity in a deterministic manner. Details of the procedure to obtain ship-specific thresholds and time-between wave groups are discussed. A procedure using wave groups to evaluate the probability of a rare event, the undesirable response, is also presented.

## KEYWORDS

wave groups, dynamic stability, seaway loads, problem of rarity, fold bifurcation

## INTRODUCTION

Severe wave conditions present increased risk to ships and other ocean-going vessels. These large waves, in particular sequences, or groups, may cause structural damage or stability failure for a ship operating in these conditions. Because of its significance as a sequence of excitation events, a wave group may present a higher probability of severe ship structural or stability response than a single large wave. Therefore, they must be considered when modeling severe wave environments and when identifying operational conditions where there is increased risk to the vessel. However, these wave groups, which are most critical to the ship dynamics performance, may differ from common oceanographic definitions of wave groups. A critical, or dynamically significant event, is based on a combination of initial conditions, sequence of excitations, and the duration of excitation. For ship designers, operators, and researchers, the important

practical matter remains: which waves or wave groups will result in a significant, or undesirable, ship response.

## BACKGROUND

Differences between wave groups, as considered in oceanography and in nonlinear ship response, are briefly discussed. A more detailed review of these differences can be found in Bassler, *et al.* (2010). The use of wave groups as a method to solve the problem rarity, with the possibility of experimental validation, is also discussed.

### *Wave Groups in Oceanography*

A wave group is defined as a series of waves, with wave heights larger than a specified threshold, and with approximately equal periods (Masson & Chandler, 1993; Ochi, 1998). Large-amplitude wave groups are often formed in developing seaways or by intersecting storms (Buckley, 1983; Toffoli, *et*

*al.*, 2004; Onorato, *et al.*, 2006), or due to the interaction effects of waves and currents.

Spectral shape can also significantly influence grouping; wave grouping increases as the wave energy spectrum becomes narrower (Goda, 1970; Goda, 1976). This spectral narrowing often occurs in a fetch-limited growing sea (Longuet-Higgins, 1976). Bimodal sea states, formed by wind generated waves and swell, are also much more likely to contain groups of large-amplitude waves (Rodriguez & Guedes Soares, 2001).

#### **Wave Groups and Nonlinear Ship Motions**

Accounts of ships experiencing groups of large waves, such as the “Three Sisters,” have been reported (Buckley, 1983, 2005). Because they may present a more serious risk to a vessel than single large-amplitude waves (Kjeldsen, 1984), groups of waves must also be considered in models of ship response to severe wave environments.

Su (1986) suggested that a wave group, with one or more extremely large waves, would provide a better environmental design scenario than a single extreme wave or a group of regular waves. Philips (1994) also expressed the need to develop a combined, spatially-temporally-defined extreme wave group for ship design

Tools have been developed for ship design where wave groups are used to induce a specific ship motion response. This approach was discussed by Blocki (1980) and Tikka & Paulling (1990) to study parametric roll, using wave groups to induce parametric excitation. Additional studies of the applications of wave groups to parametric roll response have been made by Boukhanovsky & Degtyarev (1996) and Spyrou (2004). Alford has used a design wave train method to produce a desired motion response (Alford, 2008). An assessment procedure for parametric roll in early-stage ship design was developed by Belenky & Bassler (2009), which consists of determining the response to a “typical” wave group. This paper also attempts to address some of the issues related to the definition of a “typical” wave group.

#### **Wave Groups and the Problem of Rarity**

Dangerous ship behaviors are caused by either extremely high or extremely steep waves, or a sequence of waves with particular frequencies. These waves, or their combinations, are rare and assessing their probability of occurrence remains a difficult problem.

Once these waves generate large excitation, a large-amplitude response may be expected. For a dynamical system that describes ship motions, this means that nonlinearities are significant for the response. If a dynamical system has significant nonlinearities, it becomes very sensitive to initial conditions. Depending on the initial conditions, very different responses may result: from merely tracking the contour of a large wave to catastrophic motions, including capsizing.

The main difficulty with the assessment of dynamically-related undesirable events, or dynamic “failures,” is both their rarity and significant nonlinearity, which need to be addressed simultaneously. Assessing the dynamical response to these wave sequences constitutes the general problem of rarity—when the time between events is long, compared to a relative time-scale (Belenky, *et al.*, 2008). The problem of rarity may be solved by separating the ship response into sub-problems, according to their time scale. The simplest example of implementation using this approach is the piecewise-linear method for calculating capsizing probability (Belenky, 1993; Paroka & Umeda, 2006; Paroka, *et al.*, 2006; Belenky, *et al.*, 2009). The same principle was also applied for nonlinear response using numerical simulations (Belenky, *et al.*, 2008a).

Consideration of groups of large waves is another way to separate the time scales, using the time between groups and the duration of a group. It is assumed that all important dynamic behavior occurs at the time while the group of waves passes the ship. This time is relatively short, and the group can be taken as a sequence of deterministic waves, which induce instability for a ship. Then the probability of encountering one of these critical wave groups

was computed for a given route and duration (Themelis & Spyrou, 2007; 2008). This approach was also used by Umeda, *et al.* (2007) for broaching assessment.

As a result of separating of the time scales, there are two problems. The first problem is evaluating the response of a nonlinear dynamical system to a group of large deterministic waves (the “rare” problem). The initial conditions of the dynamical system at the moment of encounter with this group are random. The probabilistic characteristics of these initial conditions must come from the solution of the second problem, which considers ship motions in less severe waves, during the time between the groups (the “non-rare” problem). Then the probability of encounter for the ship with this critical wave group must be calculated.

#### **Model Experiments**

One of the obvious additional advantages of the wave group approach over other methods to address the problem of rarity is that it can be used in model experiments, as well as numerical simulations. Because of this, some of the inherent difficulties with validation of ship response in random seas, which more closely approximate the ocean environment, can be addressed.

Completely random wave testing can be difficult because very long run times are needed to ensure extreme events with low probability of occurrence are realized, including large waves or wave groups. Realizations of the most severe wave conditions in a random seaway require long time durations and are generally not repeatable. Also, because of the temporal and spatial limitations of a basin, it is impractical to ensure the critical excitation events are realized with standard irregular wave model experiments.

A review of previous and existing techniques for ship motions and structural testing methods is given in Bassler, *et al.* (2009; 2010). An experiment was previously conducted to generate large-amplitude deterministic wave groups, with characteristics

similar to those observed in ocean measurements (Bassler, *et al.*, 2009).

#### **DEFINITION OF A WAVE GROUP**

Groups of large waves present a sequence of environmental conditions which may result in severe dynamic responses of a ship, either for the resulting ship motions, structurally, or both. However, not all wave groups will be significant in causing a severe response. Therefore, the definition of a wave group must be formulated from the perspective of ship dynamics.

Large-amplitude response, caused by the wave group, is likely to be nonlinear. However, methods with linear approximations are only applicable to relatively small-amplitude motions. Therefore, the wave elevation or wave slope angle resulting in significantly nonlinear response may be used as a threshold for the “ship dynamics” definition of a wave group.

One of the effects of nonlinearity is the dependence of the response on initial conditions. In order to consider the response to a wave group encounter as a single random event, the response to the current wave group should be independent from the response to the previous wave group. As a result, there should be enough time between these groups for the autocorrelation function of the response to effectively die out. Therefore, large waves that are close to each other in sequence should be considered as part of the same group, even if they are actually separated by a few small waves.

A sample wave group is shown in Fig. 1. As observed, the first group has three waves and all of them are above the threshold. The second group has six waves, of which four waves are above the threshold, and two waves are below the threshold. This example illustrates the difference between the “oceanographic” and “ship dynamics” definitions of the wave group. From the “oceanographic” point of view, the second group has only two waves (III) and (IV). The group is preceded by a single large wave (I) and is followed by a single large wave (VI).

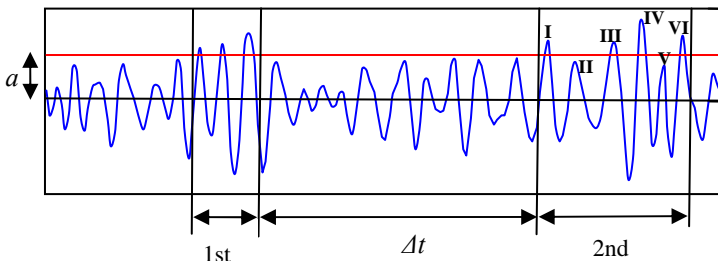


Fig. 1: Wave groups from a sample wave time-series realization, with specified amplitude threshold,  $a$ , and the time between wave groups,  $\Delta t$ .

However, from the point of view of the ship dynamics, all six waves must be considered together. Even if the wave (II) is small when the large wave (III) is encountered, the influence of the first large wave (I) still affects the motions. As a result, the “ship dynamics” wave group may have a more complex shape, but the encounter with a wave group becomes a Poisson flow event and time between them is expected to be distributed exponentially.

This definition of a “ship dynamics” wave group provides a generalized sequence of waves, resulting in nonlinear ship response. In the example shown for this paper, the threshold is only specified for wave crests. However, the same formulation may also be extended to wave troughs, and both the crests and troughs should be considered for a practical assessment.

### SPECIFICATION OF A THRESHOLD

The threshold,  $a$ , or minimum level resulting in significant response, may be different depending on which problem of dynamics is being evaluated and also depends on the relative size of the ship and the waves and operational conditions for the ship. Below this threshold, the ship response may be considered small, and modeled with linear methods.

As a simple example to examine this possible definition, a 1-DOF roll equation with linear damping and single-harmonic excitation is considered,

$$\ddot{\phi} + \delta 2\dot{\phi} + \omega_0^2 f(\phi) = \alpha_e \cos(\omega_e t) \quad (1)$$

where  $\delta$  is the damping ratio,  $\omega_e$  is the frequency of excitation, and  $\alpha_e$  is amplitude of excitation. The nonlinear stiffness may be considered in a form of a cubic parabola, which makes the system, (1), the Duffing oscillator.

Consider three different amplitudes of excitation:  $\alpha_1$ ,  $\alpha_2$  and  $\alpha_3$ . Below a critical response level,  $\alpha_1$ , the ship response is considered linear. Above this level, the system may exhibit some indication of nonlinear behavior, such as a fold bifurcation (Fig. 2). The Duffing oscillator is the simplest dynamical system capable of producing a fold bifurcation (Guckenheimer & Holmes, 1983; Thompson & Stewart, 1986; Spyrou, 1997). One of the justifications for such a definition is that the fold bifurcation for roll motion has been observed experimentally (Francescutto, *et al.*, 1994).

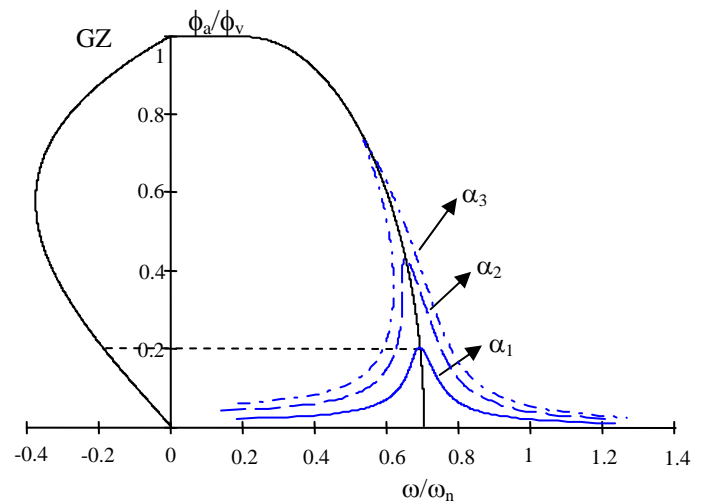


Fig. 2: Backbone curve and response curve for roll motion, with the ship-specific “GZ curve”, modeled using the Duffing oscillator. The transition between linear response,  $\alpha_1$ , and nonlinear response,  $\alpha_2$  and  $\alpha_3$ , where fold bifurcation is observed, is identified.

In this formulation, the amplitude of the wave slope that enables fold bifurcation to occur can be considered as the threshold,  $a$ , in the definition of the “ship dynamics” wave group. However, within the conceptual framework of this approach, other definitions for significant events should be considered and examined as well.

## TIME BETWEEN WAVE GROUPS

The time between wave groups,  $\Delta t$ , which can result in significant response events should be long enough so that these events can be considered independent. There are two reasons for this definition. First, by allowing enough time to pass between wave groups, the initial conditions for the wave group response become an objective of the “non-rare” problem and can be evaluated using, for example, frequency domain techniques. Second, it allows for the application of Poisson flow to the large response event caused by excitation from the wave group. The latter is very important, because it allows an explicit relation between the probability of failure and time of exposure.

To determine  $\Delta t$ , an autocorrelation function of roll response may be used. Because the time between groups is associated with small-amplitude response, the autocorrelation function,  $r(\tau)$ , can be easily computed from the response spectrum, available from the frequency domain calculations.

$$r(\tau) = \frac{1}{V} \int_0^{\infty} S_{\phi} \cos(\omega\tau) d\omega \quad (2)$$

where  $S_{\phi}$  is the roll response spectrum and  $V$  is the variance. The cross-correlation function,  $c(\tau)$ , is defined as:

$$c(\tau) = \frac{1}{V} \int_0^{\infty} S_{\phi} \sin(\omega\tau) d\omega \quad (3)$$

and used to obtain the envelope,  $e(\tau)$ , of the autocorrelation function of roll.

$$e(\tau) = \sqrt{r(\tau)^2 + c(\tau)^2} \quad (4)$$

Using the envelope of the autocorrelation function, a time can be identified when the autocorrelation function has decreased below a specified value, such as 5%. For the notional example presented (Fig. 3), the autocorrelation function for roll response from a Bretschneider sea state 8 spectrum will decrease to 5% after 94 seconds.

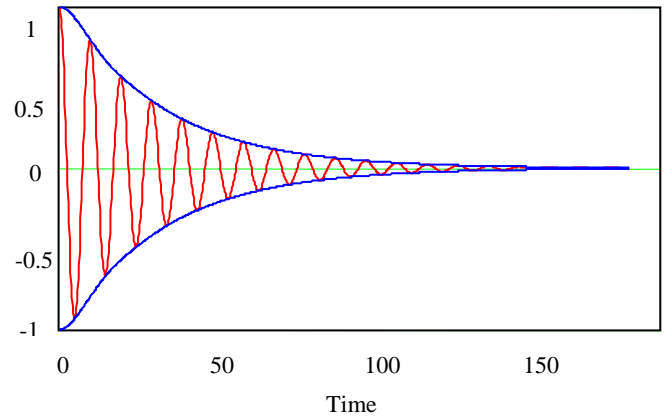


Fig. 3: Autocorrelation function of ship response, with envelope, which can be used to determine  $\Delta t$ .

## PROBABILITY OF FAILURE DUE TO ENCOUNTER WITH A WAVE GROUP

Assuming that Poisson flow is applicable to wave group encounters, then the probability of failure during exposure time,  $t_e$ , can be determined.

$$P_F(t_e) = 1 - \exp[-\lambda_{GS} P_{FE} \cdot t_e] \quad (5)$$

Here  $\lambda_{GS}$  is the rate of encounter of a critical wave event, either a single wave or a group, and  $P_{FE}$  is the probability of failure, once such critical wave event is encountered. As the mechanism of failure may be different when encountering a single wave or a group, it makes sense to express these quantities separately

$$P_F(t_e) = 1 - \exp[-(\lambda_G \cdot P_{FEG} + \lambda_S \cdot P_{FES}) \cdot t_e] \quad (6)$$

where  $P_F$  is the probability of failure,  $t_e$  is the time of exposure,  $\lambda_G$  is the rate of encounter of a wave group, and  $\lambda_S$  is the rate of encounter of a single wave.  $P_{FEG}$  is the probability of failure if a wave group is encountered and  $P_{FES}$  is the probability of failure if a single wave is encountered.

The rate of encounter of a wave group or single wave,  $\lambda_{GS}$ , may be estimated from a time series as:

$$\lambda_{GS}^* = \frac{m^*(N_{GS})}{t_e} = \lambda_G^* + \lambda_S^* \quad (7)$$

An asterisk is used to distinguish the statistical estimate from the theoretical value.  $N_{GS}$  is the total number of waves above the threshold, both groups and single waves, observed during a window of the duration,  $t_e$ , and  $m^*(N_{GS})$  is the estimate of the mean value of the total number of waves. The total number of waves above the specified threshold is given by

$$N_{GS} = N_G + N_S \quad (8)$$

where  $N_G$  is the total number of wave groups and  $N_S$  is the total number of single waves.

The total number of wave groups is given by

$$N_G = N_{GS} \cdot P_{EG} = N_{GS} \cdot \sum_{i=2}^{\infty} pmf(n_i) \quad (9)$$

where  $P_{EG}$  is the conditional probability of encountering a wave group, and  $pmf(n_i)$  is the probability mass function of the  $i$ th wave in a group.

The total number of single waves,  $N_S$ , above the specified threshold is given by

$$\begin{aligned} N_S &= N_{GS} \cdot pmf(n=1) = N_{GS} \cdot (1 - P_{EG}) \\ &= N_{GS} \cdot P_{ES} \end{aligned} \quad (10)$$

where  $P_{ES}$  is the conditional probability of encountering a single wave, and  $pmf(n=1)$  is the probability mass function of the number of single waves above the specified threshold.

In (7),  $\lambda_G^*$  is the rate of encounter for a wave group and  $\lambda_S^*$  is the rate of encounter for a single wave.

$$\lambda_G^* = P_{EG} \cdot \lambda_{GS}^* \quad (11)$$

$$\lambda_S^* = P_{ES} \cdot \lambda_{GS}^* = (1 - P_{EG}) \cdot \lambda_{GS}^* \quad (12)$$

## CHARACTERISTICS OF WAVE GROUPS

In order to examine the robustness of the method to characterize wave sequences of dynamical significance to ship response, or wave groups, a sample Sea State 8 wave data

set and arbitrary wave amplitude threshold and time between groups, were used to examine the distributions of these wave characteristics.

A sample set of 200 realizations, each 2600 seconds long, from a Bretschneider sea state 8 spectrum ( $H_s=11.5$  m,  $T_m=16.4$  s) was used. As an example to illustrate the method, the wave amplitude threshold was specified to be  $a=5$  m and the time between wave groups  $\Delta t=50$  seconds.

The encounter with a wave group is assumed to follow a Poisson flow event; therefore, the time between them is expected to be distributed exponentially. This is confirmed by the results of a Pearson chi-square goodness-of-fit test for the sample wave data set (Fig. 4).

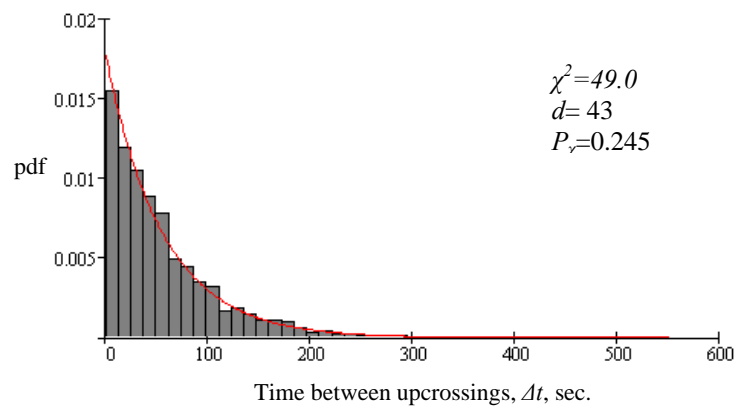


Fig. 4: Distribution of the time between wave groups,  $\Delta t$ , with an amplitude threshold of  $a=5$  m, and results from a Pearson chi-square goodness-of-fit-test for the sample Bretschneider sea state 8 data set.

## Number of Waves in a Group

The procedure for counting of number of waves in a group is straight forward, once the wave groups have been identified as described above. The histogram of the number of waves in a group is shown for the example data set (Fig. 5). The most outstanding feature of this histogram is a very tall first bin, which corresponds to the case where a “group” has only one wave. These are single large waves, and from the ship dynamics perspective may be considered separately. For actual wave groups

with two or more waves, the distribution appears similar to exponential.

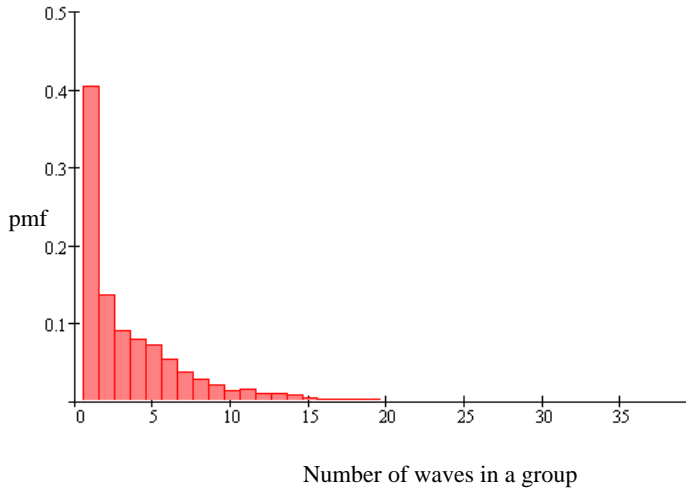


Fig. 5: Distribution of the number of waves in a group for the sample Bretschneider sea state 8 data set, with  $a=5\text{m}$  and  $\Delta t=50$  seconds.

The following additional parameters were obtained from the simulated wave data set: amplitude for the  $n$ th wave in the group, period for the  $n$ th wave in the group, and wave steepness of the  $n$ th wave in the group. Additional discussion of these characteristics is given in Bassler, *et al.* (2010).

## CONCLUSIONS

In this paper, a method to evaluate ship response in heavy seas using wave groups was discussed. The response for these events may be characterized by a high degree of nonlinearity. Modeling a significantly nonlinear system in a stochastic environment is difficult. Because of the rarity and significant nonlinearity for the large response, either numerical simulations and/or model tests must be used.

The principle idea behind using wave groups is to enable separation of the complexity of nonlinear dynamics of ship response from the complexities of a probabilistic description for the response. This separation may be achieved by considering irregular waves as a series of wave groups, which are capable of producing undesirable

response, interlaced with intervals of relatively benign waves. Then the nonlinearity of the response only becomes important during the duration of the groups, while the intervals of benign waves are only “responsible” for providing the initial conditions when encountering the wave group.

The wave group can be considered as deterministic sequence of waves exciting a nonlinear dynamical system. With this formulation, wave groups may be considered as a possible method to solve the problem of rarity and, with the wave group characteristics related to ship-specific properties, can be solved in a deterministic manner.

A wave group is defined as beginning with the first upcrossing of the specified threshold,  $a$ , and ending with a downcrossing, of the threshold, where the next upcrossing of the threshold occurs at a time greater than the specified minimum duration between groups,  $\Delta t$ . Both the threshold and duration can be specified based on the given ship type and seaway information. This method enables wave group characteristics to be obtained from time-series information, or from merely spectral information, which may be available from wave buoys in the area of operation for a ship. Using this method, a procedure to evaluate the probability of a rare event, the undesirable response, using wave groups is also presented.

For future work, a probabilistic model of wave groups will be obtained, by fitting distributions to the characteristics. Then realizations of wave groups with the representative probabilistic characteristics must be realized in the time-domain, using either numerical simulations or experiments, or both.

## ACKNOWLEDGEMENTS

The authors appreciate support of this work from Dr. John Barkyoumb, under the Naval Innovative Science and Engineering Program at NSWCCD. Earlier contributions related to this work have been supported by Dr. Pat Purtell (ONR) and Mr. James Webster (NAVSEA). The authors are also grateful to Prof. Kostas Spyrou (National Technical University of Athens, Greece) and Prof. Pol Spanos (Rice University, USA) for some helpful discussion related to the contents of this paper.

## REFERENCES

- Alford, L. K. (2008), Estimating Extreme Responses Using a Non-Uniform Phase Distribution, Ph.D. Dissertation, University of Michigan.
- Bassler, C. C., M. J. Dipper, and G. E. Lang (2009), "Formation of Large-Amplitude Wave Groups in an Experimental Basin," *Proc. 10th Intl. Conf. on Stability of Ships and Ocean Vehicles*, St. Petersburg, Russia.
- Bassler, C. C., V. Belenky, and M. J. Dipper (2010), "Characteristics of Wave Groups for the Evaluation of Ship Response in Irregular Seas," *Proc. 29th Intl. Conf. on Ocean, Offshore, and Arctic Engineering*, Shanghai, China.
- Belenky, V. L. (1993), "A Capsizing Probability Computation Method", *J. Ship Research*, Vol. 37, pp. 200- 207.
- Belenky, V., J. O. de Kat, and N. Umeda (2008), "Toward Performance-Based Criteria for Intact Stability," *Marine Technology*, 45(2).
- Belenky, V. L., Weems, K. M. and W. M. Lin, (2008a), "Numerical Procedure for Evaluation of Capsizing Probability with Split Time Method," *Proc. 27th Symp. Naval Hydrodynamics*, Seoul.
- Belenky, V. L., A. M. Reed, and K. M. Weems (2009), "Probability of Capsizing in Beam Seas with Piecewise Linear Stochastic GZ Curve" *Proc. 10th Intl. Conf. on Stability of Ships and Ocean Vehicles*, St. Petersburg, Russia.
- Belenky, V. and C. Bassler (2009), "Vulnerability Level 2 Criterion for Parametric Roll," *Intl. Workshop on Dynamic Stability Considerations in Ship Design*, Ilawa, Poland.
- Blocki, W. (1980), "Ship Safety In Connection with Parametric Resonance of the Roll," *Intl. Shipbuilding Progress*, 27(306), pp. 36-53.
- Boukhanovsky, A. V. and A. B. Degtyarev (1996), "Nonlinear Stochastic Ship Motion Stability in Different Wave Regime," *Proc. 3rd Intl. Conf. in Commemoration of the 300th Anniversary of Creating Russian Fleet by Peter the Great*, St. Petersburg, Russia.
- Buckley, W. H. (1983), "A Study of Extreme Waves and Their Effects on Ship Structure," Ship Structure Committee Report, SSC-320.
- Buckley, W. H. (2005), "Extreme Waves for Ship and Offshore Platform Design," SNAME T&R Report No. 57.
- Duffing, G. (1918), *Erzwungene Schwingungen bei Veranderlicher Eigenfrequenz*, Vieweg: Braunschweig.
- Francescutto, A., G. Contento and R. Penna (1994), "Experimental Evidence of Strong Nonlinear Effects in the Rolling Motion of a Destroyer in Beam Seas," *Proc. 5th Intl. Conf. Stability of Ships and Ocean Vehicles*, Melbourne, FL, Vol. 1, 13 p.
- Goda, Y. (1970), "Numerical Experiments on Wave Statistics with Spectral Simulation," PHRI Report, 9(3), pp. 38-43.
- Goda, Y. (1976), "On Wave Groups," *Proc. 1st Intl. Conf. on the Behavior of Offshore Structures*, Trondheim, Norway, pp. 115-128.
- Guckenheimer, J. and P. Holmes (1983), *Nonlinear Oscillations, Dynamical Systems, and Bifurcations of Vector Fields*, New York: Springer.
- Kjeldsen, S. P. (1984), "Dangerous Wave Groups," *Norwegian Maritime Register*, 112(2), pp. 4-16.
- Longuet-Higgins, M. S. (1976), "On the Nonlinear Transfer of Energy in the Peak of a Gravity-Wave Spectrum: A Simplified Model," *Proc. Royal Society of London A*, 347, pp. 311-328.

- Masson, D. and P. Chandler (1993), "Wave Groups: A Closer Look at Spectral Methods," *Coastal Engineering*, 20.
- Ochi, M. K. (1998), *Ocean Waves: The Stochastic Approach*, Cambridge, U.K.: The Cambridge University Press.
- Onorato, M., A. R. Osborne, and M. Serio (2006), "Modulational Instability in the Crossing Sea States: A Possible Mechanism for the Formation of Freak Waves," *Physical Review Letters*, 96.
- Paroka, D., Y. Okura, and N. Umeda (2006), "Analytical Prediction of Capsizing Probability of a Ship in Beam Wind and Waves", *J. Ship Research*, Vol. 50, No. 2, pp. 187-195.
- Paroka, D. & Umeda, N. (2006), "Capsizing Probability Prediction of the Large Passenger Ship in Irregular Beam Wind and Waves: Comparison of Analytical and Numerical Methods" *J. Ship Research*, Vol. 50, No. 4, pp. 371-377.
- Philips, O. (1994), "The Structure of Extreme Ocean Waves," *Proc. 20th Symp. on Naval Hydro.*, Santa Barbara, California, 21-26 August.
- Rodriguez, G. R. and C. Guedes Soares (2001), "Correlation Between Successive Wave Heights and Periods in Mixed Sea States," *Ocean Engineering*, 28(8), pp. 1009-1030.
- Spyrou, K. (1997), "Dynamic Instabilities in Quartering Seas- Part III: Nonlinear Effects on Periodic Motions," *J. Ship Research*, 41(3), pp. 210-223.
- Spyrou, K. J. (2004), "Criteria for Parametric Rolling?," *Proc. 7th Intl. Ship Stability Workshop*, Shanghai, China, 1-3 November.
- Su, M.-Y. (1986), "Large, Steep Waves, Wave Grouping and Breaking," *Proc. 16th Symp. on Naval Hydro.*, Berkeley, California, July.
- Themelis, N. and K. J. Spyrou (2007), "Probabilistic Assessment of Ship Stability," *Trans. Society of Naval Architects and Marine Engineers*, Vol. 115 pp. 181-206.
- Themelis, N. and K. J. Spyrou (2008), "Probabilistic Assessment of Ship Stability Based on the Concept of Critical Wave Groups," *Proc. 10th Intl. Ship Stability Workshop*, Daejeon, Korea, 23-25 March.
- Tikka, K. K. and J. R. Paulling (1990), "Predictions of Critical Wave Conditions for Extreme Vessel Response in Random Seas," *Proc. 4th Intl. Conf. on the Stability of Ships and Ocean Vehicles*, Naples, Italy.
- Toffoli, A., J. M. Lefevre, J. Monbaliu, and E. Bitner-Gregersen (2004), "Dangerous Sea-States for Marine Operations," *Proc. 14th Intl. Offshore and Polar Engineering Conf.*, Toulon, France, 23-28 May.
- Thompson, J. M. T. and H. B. Steward (1986), *Nonlinear Dynamics and Chaos*, New York: John Wiley and Sons.
- Umeda, N., M. Shuto, and A. Maki (2007), "Theoretical Prediction of Broaching Probability for a Ship in Irregular Astern Seas," *Proc. 9th Int. Ship Stability Workshop*, Germanischer Lloyd, Hamburg.



## Risk Based Analysis of Inland Vessel Stability

Milan Hofman,

Department of Naval Architecture, Faculty of Mechanical Engineering University of Belgrade

Igor Bačkalov,

Department of Naval Architecture, Faculty of Mechanical Engineering University of Belgrade

### ABSTRACT

The authors continue to investigate the problem of inland container vessel rolling due to influence of beam gusting wind. Previously developed risk based tools are used for the critical analysis of the new version of European Directive for Technical Requirements for Inland Waterway Vessels. It is shown that the Directive, concerning stability, freeboard and safety clearance of container vessels, is not strict enough. The vessels, satisfying all the requirements of the Directive, could be flooded through the open cargo hold, in some extreme but realistic storms. In addition, the risk based approach is applied to investigate the probability of sliding of unsecured containers, due to wind action and vessel rolling.

**KEYWORDS:** Probabilistic ship stability rules; Inland container vessels; Coupled nonlinear rolling; Stochastic wind action.

### INTRODUCTION

Severe rolling is commonly connected to the seagoing ships in waves, and not to the vessels sailing along inland waterways. However, inland vessels could also roll heavily, not due to waves, but due to (chaotic) gusts of strong beam wind. This especially applies to inland container vessels, as they have large lateral areas that could be exposed to wind. The problem of inland vessel rolling has already been investigated by the authors in a series of papers (Hofman et al 2005, 2006, Bačkalov et al 2008, 2010, Bačkalov 2010). A novel tool for risk based analysis of inland container vessel stability was developed, consisting (basically) of two parts: firstly, the coupled nonlinear equations of motion are solved numerically, giving the time history of vessel rolling due to beam gusting wind. Secondly, the vessel motion is analyzed statistically, and the probability of flooding of open container hold, found. It was shown that the method is

especially applicable to critical analysis of the existing stability rules. For instance, it was found (by a surprise) that the vessels satisfying some of the respectable inland stability standards could be flooded and eventually capsized due to severe gusts of beam wind!

The present paper continues the investigation of inland vessel rolling due to gusting beam gales. It is focused on critical analysis of the new version of European Technical Requirements for Inland Waterway Vessels (Directive of the European Parliament and the Council 2006/87/EC), and checks in detail the part of the Directive prescribing stability, freeboard and safety clearance of inland container vessels. It shows that the Directive, even more than some other stability standards analyzed previously, is (in this part) not strict enough. In aim of harmonization and simplicity, the dynamic wind effects are oversimplified, so the vessels satisfying the requirements of the Directive were found (in

some extreme cases) unsafe from the probabilistic point of view.

In addition to the critical analysis of EC Directive, the paper investigates the possibility of sliding of unsecured containers due to vessel rolling and the wind influences. Thus, for the first time, the usual practice on inland waterways – the transportation of unsecured (unlashed) containers – is put to test by the novel risk based tools.

### BASIC TOOLS

In the present investigation, vessel motion due to the influence of beam wind gusts is modelled by coupled, nonlinear differential equations of roll and sway, developed and explained in detail in Bačkalov et al (2010). So called “course keeping model” is used, in which the vessel is not allowed to drift freely due to the beam wind, but is forced to sway oscillatory about her prescribed straight route. The main feature of the approach is the treatment of the wind effects. The wind force and moment depend on the variable wind speed, which is obtained from the known, semi-empirical wind spectrum. More precisely, wind speed is presented as<sup>1</sup>

$$v(t) = \bar{v} - \dot{\eta} + v' = \bar{v} - \dot{\eta} + \sum_{n=1}^N v_n \cos(\omega_n t + \alpha_n),$$

and the amplitudes of gusting wind components  $v_n$  are obtained from the wind spectrum by the relation

$$v_n = \sqrt{2S(\omega_n) \cdot d\omega}$$

which follows from the definition of the spectrum.

As in the previous papers (Hofman et al 2005, 2006, Bačkalov et al 2008, 2010, Bačkalov 2010), Davenport wind spectrum is applied

$$S(\omega) = \frac{4\kappa \cdot \bar{v}^2 X^2}{\omega(1+X^2)^{\frac{4}{3}}}, \quad X = \frac{600\omega}{\pi \cdot \bar{v}}.$$

On the basis of the discussion given in Hofman et al (2006), the coefficient of terrain roughness appropriate for suburban areas  $\kappa = 0.015$  is applied.

The differential equations of motion are solved numerically by classical Runge-Kutta method, and the vessel roll and sway motions  $\varphi(t)$ ,  $\eta(t)$  are obtained. Stochastic analysis of these motions gives the mean value of roll, its standard deviation, and other statistical characteristics of vessel nonlinear, irregular rolling. Then, the most probable maximal heel in  $N$  cycles would be

$$\varphi_{max} = \bar{\varphi} + \sigma_{\varphi} \sqrt{2 \ln N},$$

while the probability that the angle of roll would reach some prescribed value  $\phi$  is

$$P \approx N \exp \left[ -\frac{1}{2} \left( \frac{\phi - \bar{\varphi}}{\sigma_{\varphi}} \right)^2 \right].$$

In the case that  $\phi$  is angle of flooding of the open cargo hold, the probability  $P$  would be called *the index of flooding*.

In addition to maximal heel and the index of flooding, the present investigation analyzes the condition in which the unsecured containers would slide due to the vessel motion and the wind influences. The analysis is straightforward once the vessel motions are known, so only the final formulas would be presented here.

The components of acceleration of centre of container mass could be obtained from vessel motion, in the form

$$a_y = \ddot{\eta} \cos \varphi - y_C \dot{\varphi}^2 - z_C \ddot{\varphi},$$

$$a_z = -\ddot{\eta} \sin \varphi + y_C \ddot{\varphi} - z_C \dot{\varphi}^2.$$

The total container reactions in  $y$  and  $z$  direction follow from Newton law as

$$F_y = ma_y + mg \sin \varphi - F_w \cos \varphi,$$

$$F_z = ma_z + mg \cos \varphi + F_w \sin \varphi.$$

The container is unsecured, just freely leaned to the box below, so the following restrictions in the supports apply

<sup>1</sup> The nomenclature is given at the end of the text

$$F_z \geq 0, \quad |F_y| \leq \mu F_z.$$

This leads to the condition under which the container would not slide:

$$\frac{|F_y|}{F_z} = \frac{|ma_y + mg \sin \varphi - F_w \cos \varphi|}{ma_z + mg \cos \varphi + F_w \sin \varphi} = f_s \leq \mu,$$

giving the probability of sliding of an unsecured container as

$$P_s \approx N \exp \left[ -\frac{1}{2} \left( \frac{\mu - \bar{f}_s}{\sigma_s} \right)^2 \right].$$

### **FREEBOARD AND STABILITY RULES**

As said, the present investigation offers a critical analysis of the new version of European Technical Requirements for Inland Waterway Vessels, which was accepted in 2006 and is obligatory since the beginning of 2009. The paper checks, by the risk based approach, the part of the Directive prescribing stability, freeboard and the safety clearance of inland container vessels.

The requirements prescribed by the Directive are, very briefly, the following.

The freeboard of vessels with open cargo holds should be, at least, **0.15 m**. This basic freeboard could be (somewhat) reduced on the account of the deck sheer and watertight superstructure.

The safety clearance (vertical distance from the waterline to the first unsecured opening) should be, at least, **0.5 m**.

Concerning stability, the Directive supposes that the vessel is subjected to the beam wind and (simultaneous) turning on a circular path. It recognizes the case of secured (fixed, lashed) and unsecured (non fixes) containers. For the case of unsecured containers (which is the usual practice on the major European inland waterways), the mean wind speed is supposed to be **18 m/s**, and the radius of the turning trajectory equal to  $2.5L$ . Under such joint action of wind and centrifugal force, the maximal static heel is restricted to **5°**. In addition, the edge of vessel deck should not be

submerged, and the metacentric height should not be less than **1 m**.

It should be noticed that the stability requirements are (for the sake of simplicity), reduced to the static requirements, only. Unlike some other inland stability rules, the Directive neglects all the dynamic effects. For instance, the Recommendations of UN Economic Commission for Europe, or Serbian Register of Shipping, do account wind gusts through (simplified) inland weather criterions. However, the requirement of the Directive that the edge of the main deck should not be submerged, does give some safety margin to cover the neglected dynamic effects. One of the tasks of the following analysis is to clarify if such simplified approach is sufficient and properly adjusted to insure the vessel's safety.

### **SAMPLE VESSEL**

The sample vessel of the present investigation is a typical European inland container vessel **110 m** long, **11.4 m** in beam, designed to carry up to **208 TEU** containers in **13 bays**, **4 rows** and **4 tiers**, in a single open cargo hold. The vessel has designed draught of **3.1 m** (typical for the Rhine vessels). In such, fully loaded condition, the average mass of TEU containers onboard is about **12.8 t**.

It is supposed that the vessel has freeboard of **0.15 m**, which is the minimal value required by the Directive. To satisfy the safety clearance requirement, the vessel would have to have watertight hatch coamings, at least, **0.35 m** high. However, the actual height of watertight hatch coamings is not yet specified, as it would be one of the variables in the oncoming calculations.

Since the angle of the deck edge submergence of the sample vessel equals **1.5°** (less than **5°**) it is the critical heeling angle according to the Directive. The angle of flooding of the cargo hold, in the case of minimal safety clearance (minimal watertight hatch coaming height) is **5.7°**. The residuary righting arm of the vessels, defined as

$$h' = h - GM \cdot \sin \varphi,$$

is presented in Fig. 1 and approximated by an odd polynomial of high order for the sake of numerical calculations. From the known  $h'$  curve, one can easily obtain total righting arm  $h$  for any prescribed value of  $GM$ . The critical heeling angles depend on the height of watertight hatch coamings, so are not yet specified.

It was found that the critical requirement - static heel smaller than  $1.5^\circ$  under combined action of wind, was satisfied if  $GM > 1.2 m$ . Being larger than  $1 m$ , that is the actual stability limitation prescribed the Directive.

To prevent eventual falling of crew into the cargo hold, the Directive (in the part not connected to freeboard, safety clearance or stability requirements) defines the minimal height of hatch coamings as  $0.7 m$ . However, there is no specific requirement for their water tightness, once the minimal safety clearance is satisfied!

To resume, the sample vessel, in the case of metacentric height over  $1.2 m$  and watertight hatch coaming height over  $0.35 m$ , would satisfy all the stability, freeboard and safety clearance requirements prescribed by the Directive.

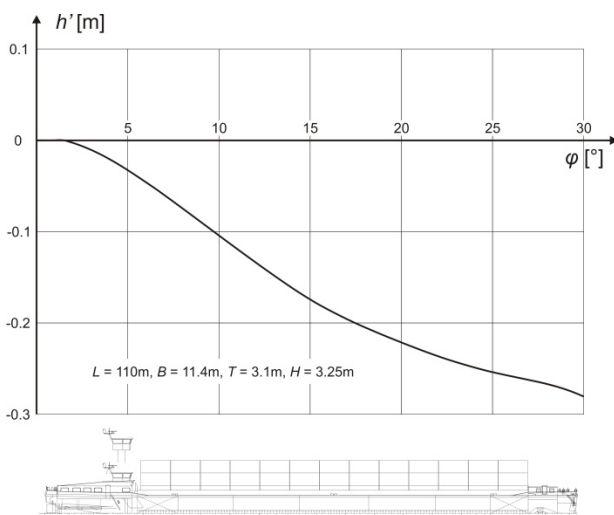


Fig. 1: Residuary righting arm of sample vessel

## NUMERICAL EXPERIMENTS

The explained risk based procedure was applied on the sample vessel, supposing that the mean wind speed is  $18 m/s$ , which is

exactly the one prescribed by the Directive. In applying the procedure, it was necessary to assess the appropriate period in which the vessel is exposed to the wind action. The choice of storm duration is closely related to the assessment of acceptable (permitted) index of flooding, as one of the most delicate tasks in the following analysis. In the present analysis, as in the previous investigation done by the authors, it is accepted that the storm lasts for 2 hours, and that in such circumstances the acceptable index of flooding is of  $O(10^{-3})$ . Although such choice is somewhat arbitrary, it is believed (as explained in Hofman at el 2006), that it provides a similar level of safety to inland vessels, as does the classical Weather Criterion to the seagoing ships.

The most probable maximal heel of the vessel satisfying the minimal requirements of the Directive, in two hours of storm, is obtained to be  $7^\circ$ . It is larger than  $5.7^\circ$ , implying that the cargo hold of such vessel would be flooded! So, the height of watertight hatch coamings has to be increased over the minimal value prescribed by the Directive, to ensure the vessel safety.

The obtained index of flooding of sample vessel for different metacentric heights and for different hatch coaming heights is presented in Fig. 2. Concerning the requirements of the Directive and the imposed risk based criterion, these diagrams could be divided into four Regions:

	Region I	Region II	Region III	Region IV
EC Directive Criterion	✓	✓	✗	✗
Risk based Criterion	✓	✗	✗	✓

The results falling into Region II demonstrate a possible situation in which the requirements of the Directive are fulfilled, while the risk based approach indicates that the vessel is not safe enough! In the case of examined vessel, this happens if the watertight hatch coamings are less than  $0.85 m$  high.

The part of the curves in Region IV show the opposite situation: there are cases in which the metacentric height could be reduced below the

requirements of the Directive, without endangering the vessel safety.

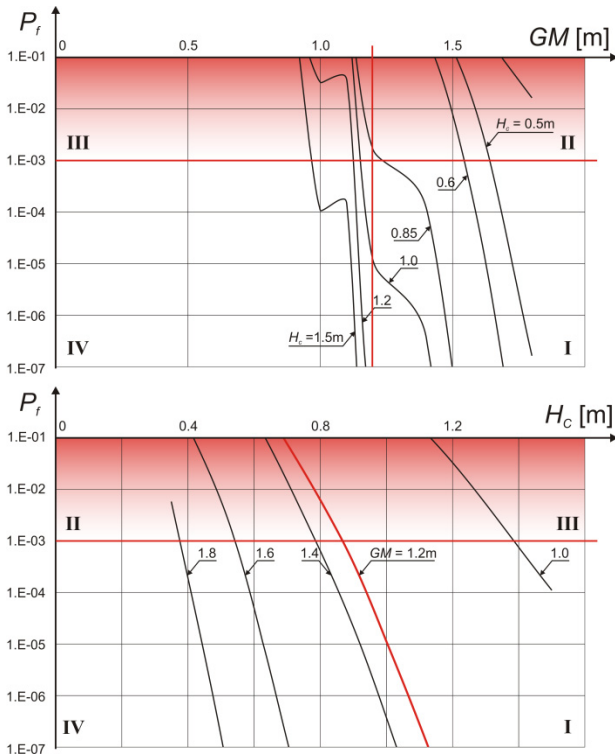


Fig. 2: Index of flooding of a typical inland container vessel

In addition to the index of flooding of the cargo hold, the probability that unsecured containers could slide in 2 hours of gusting wind action was calculated. A container in a side row of the highest tier was chosen as an example.

The results for the probability of sliding in case of different mean wind speeds, as a function of container mass and metacentric height, is presented in Fig. 3. The friction coefficient between the containers is supposed to be 0.4 (steel to steel, wet).

As expected, the diagrams show that the probability of sliding decreases with the increase of container mass. The most vulnerable are, therefore, the empty, 2 t containers. Still, even these containers do have acceptably small probability of sliding at mean wind speeds up to 18 m/s. It should be remembered: that is the wind speed prescribed by stability criterion of the Directive; at the stronger winds, the inland transportation is (usually) stopped. So, normally there is no danger of container sliding. However, if the

vessel (for some reason) sails in a bit stronger winds, the probability of sliding of containers could be dangerously increased.

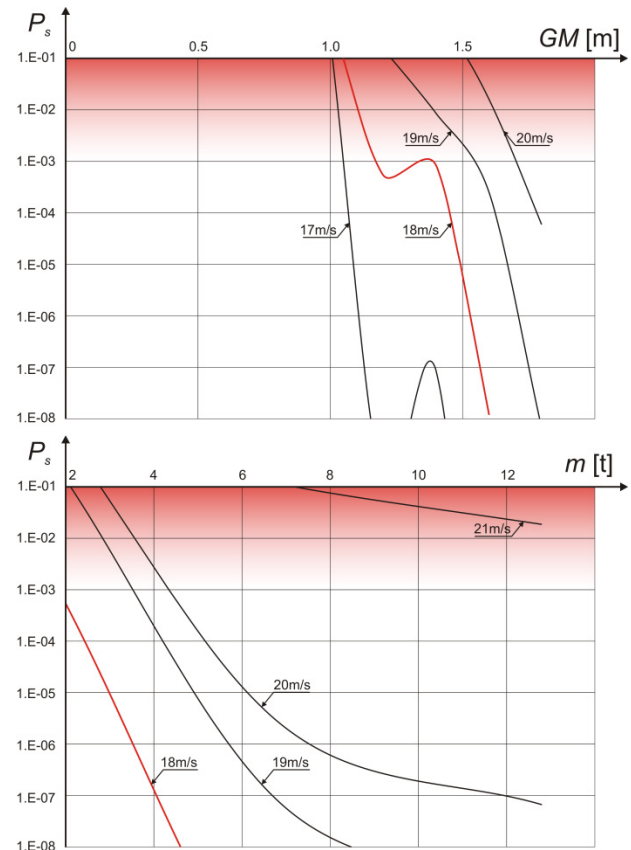


Fig. 3: Probability of sliding of unsecured container

## CONCLUSIONS

Introduced risk based procedure was applied on a typical, 110 m long inland container vessel, satisfying the minimal safety requirements of the European Directive for Technical Requirements for Inland Waterway Vessels. It was supposed that the vessel sails in beam storm prescribed by the Directive (mean wind speed 18 m/s), and found by numerical experiments that her cargo hold would be flooded in two hours due to heel and rolling caused by the gusting wind!

To prevent the flooding, the vessel's safety clearance would have to be increased over the minimal requirement prescribed by the Rules. The proposed risk based criterion (minimal index of flooding of  $O(10^{-3})$ ), indicates that such increase should be, at least, 0.5 m. This

could be done (for instance), by increasing the height of watertight hatch coamings.

In spite of disturbing findings of the numerical experiments, there seems to be no accidents that such results anticipate. Is that just a good fortune or the obtained results involved some improper assumptions and modelling?

The answer seems to lie in typical hatch coaming heights used on inland container vessels. Namely, apart from the safety clearance requirement, the vessels usually have hatch coamings of over 1 m because of strength (and other) reasons. Such high hatch coamings are typically made watertight, so they (unintentionally but fortunately) increase the vessel safety to the desired level!

The risk based approach proved that, in winds of mean speeds up to 18 m/s, there is no practical danger of container sliding. However, the results also show a high sensitivity of sliding risk on the wind speed. In the winds just a bit stronger than 18 m/s, the probability of sliding of empty containers in the upper tiers becomes dangerously high. So, the usual practice to stop inland traffic in wind speeds exceeding 18 m/s, seems to agree surprisingly well with the obtained risk based result.

## ACKNOWLEDGMENTS

The paper is a part of long-term project “Development of Safe, Efficient, Ecological (SE-ECO) Ships” executed by Department of Naval Architecture, Faculty of Mechanical Engineering University of Belgrade. The project is financed by Serbian Ministry of Science and Technology, Contract No. TR-14012.

## REFERENCES

- Bačkalov, I., Kalajdžić, M., Hofman, M., “On Safety of Inland Container Vessels Designed for Different Waterways”, FME Transactions, 2008, Vol. 36, No. 2, pp. 51-57.
- Bačkalov, I., Kalajdžić, M., Hofman, M., “Inland Vessel Rolling due to Severe Beam Wind: a Step towards a Realistic Model”, Journal of Probabilistic Engineering Mechanics, 2010, Vol. 25, pp. 18-25.
- Bačkalov, I., “Nonlinear Ship Rolling due to Wind and Waves”, Ph.D. Thesis, 2010, Faculty of Mechanical Engineering University of Belgrade.
- Directive of the European Parliament and of the Council 2006/87/EC on Technical Requirements for Inland Waterway Vessels.

Hofman M., Bačkalov I., “Weather Criterion for Seagoing and Inland Vessels – Some New Proposals”, Proceedings of International Conference on Marine Research and Transportation (ICMRT) 2005, pp. 53-62.

Hofman M., Maksić I., Bačkalov I., “Some Disturbing Aspects of Inland Vessel Stability Rules”, Journal of Ship Technology, 2006, Vol. 2, No. 2, pp. 1-14.

United Nations Economic Commission for Europe (UNECE), “Amendment of the Recommendations on Technical Requirements for Inland Navigation Vessels”, 2006.

Rules for Inland Waterway Vessels, Serbian Register of Shipping - Jugoregistar (in Serbian), 1994.

## NOMENCLATURE

$A_n$	wind-gust amplitude
$a_y, a_z$	acceleration components of container centre of mass
$C$	container centre of mass
$F_B$	vessel freeboard
$F_w$	wind force
$F_y, F_z$	container reactions
$g$	gravitational acceleration
$f_s$	container sliding function
$\bar{f}_s$	mean value of $f_s$
$G$	vessel centre of mass
$GM$	metacentric height
$h$	total righting arm
$h'$	residual righting arm
$H_c$	hatch coaming height
$L$	vessel length
$m$	container mass
$N$	number of cycles
$P$	probability
$P_f, P_s$	index of flooding and probability of container sliding
$S$	wind spectrum
$\sigma_\varphi, \sigma_s$	standard deviations of $\varphi$ and $f_s$
$t$	time
$v, \bar{v}$	wind speed, mean wind speed,
$v'$	fluctuating wind speed
$v_n$	amplitude of $n$ -th wind component
$x, y, z$	moving coordinate axes (centre in $G$ )
$y_C, z_C$	coordinates of centre $C$
$\alpha_n$	phase shift of $n$ -th wind component
$\phi$	prescribed angle of heel
$\varphi, \bar{\varphi}$	roll angle, heel, mean value of roll
$\varphi_f, \varphi_{max}$	flooding angle, most probable maximal heel
$\eta$	sway
$\kappa$	coefficient of terrain roughness
$\mu$	friction coefficient
$\omega, \omega_n$	wind frequency, frequency of $n$ -th wind component

## Melnikov's Method Applied to a Multi-DOF Ship Model

Wan Wu,

Leigh S. McCue,

Department of Aerospace and Ocean Engineering, Virginia Polytechnic Institute and State University, Blacksburg, VA, USA

### ABSTRACT

In this paper, a coupled roll-sway-heave model derived by Chen *et al* (1999) is studied. In order to address the small damping constraint, the extended Melnikov's method for slowly varying system is used by assuming the damping term is large. Using the extended Melnikov's method, the critical wave amplitudes are calculated. A phase space transport method has been applied. The ratios of erosion safe basin areas have been calculated based on the Melnikov's method and were compared with the results from numerical simulations.

### KEYWORDS

Multi-DOF Melnikov; Slowly-varying; Ship; Stability.

### INTRODUCTION

Six degree of freedom (DOF) vessel motion problems exhibit numerous complexities, particularly when studied analytically. Most previous work on multi-DOF vessel motions either reduced the problems to lower (one or two) DOF problems or used numerical simulations. In the work of ship motion analysis, compared to 1DOF problems, relatively little work have been done using analytical methods for multi-DOF ship motion problems.

In this paper, the extended Melnikov's method (Salam, 1987) is applied to a roll-sway-heave coupled ship model derived by Chen *et al.* (1999). By changing the coordinates and applying the singular perturbation technique, Chen showed the model can be simplified to a slowly varying system with three variables, which contain roll displacement and roll velocity as the fast varying variables and a slowly varying variable. This kind of system can be manageable using the Melnikov's method discussed by Wiggins and Holmes

(1987, 1988). But similar to the planar Melnikov's method, the constraint of this method is the small perturbation assumption. In order to address this constraint, the extended Melnikov's method for slowly varying systems is applied. The extended Melnikov's method developed in the literature by Salam (1987) has been recently applied to ship motions problems such as capsize (Wu and McCue, 2007, 2008, Wu, 2009) and surf-riding (Wu *et al.* 2010 and Wu 2009). The purpose of this work is to show the possibility of applying the extended Melnikov's method to multi-DOF ship models.

### MATHEMATICAL MODEL

The equations of motion for the coupled roll-sway-heave model in the earth-fixed coordinate system can be expressed in Eq.(1)

$$\begin{aligned}m\ddot{y}_c &= Y \\m\ddot{z}_c &= Z \\I_{44}\ddot{\phi} &= K\end{aligned}\tag{1}$$

in which,  $m$  is the mass of the ship,  $y_c$ ,  $z_c$  and  $\phi$  are sway displacement, heave displacement and

roll displacement, respectively.  $Y, Z$  and  $K$  are generalized forces. The prime denotes the derivative with respect to time  $t$ . Chen *et al.* (1999) transformed the model to a wave-fixed coordinate, in which the ship is viewed as a particle riding on the surface of the wave. The sway motion is now parallel to the local wave surface and the heave motion is perpendicular to the local wave surface. The equations of motion now can be expressed as in Eq.(2).

$$\begin{aligned} \dot{x}_1 &= x_2 \\ \dot{x}_2 &= f_1(x_1, y) + \varepsilon g_a(x_1, x_2, y, z_1, z_2, \tau) \\ \dot{y} &= \varepsilon g_b(x_1, x_2, y, z_1, z_2, \tau) \\ \dot{\varepsilon z}_1 &= z_2 \\ \dot{\varepsilon z}_2 &= f_2(z_1, z_2) + \varepsilon g_c(x_1, x_2, y, z_1, z_2, \tau) \end{aligned} \quad (2)$$

where  $x_1 = \phi$ ,  $x_2 = \phi'$ ,  $z_1 = z_0/h$  in which  $h$  is the draft of the ship.  $y$  is a transformed coordinate which contains sway velocity and other variables.  $z_0$  is small compared to  $h$ .  $(\dot{\cdot})$  is the derivative relative to  $\tau$ , where  $\tau = \omega_r t$ .  $\omega_r$  is the natural frequency of roll.

In Eq.(2), the heave motion is considered to exhibit fast dynamics compared to roll and  $y$ . Chen *et al.* (1999) used the singular perturbation theory to this system to show that  $z_1$  and  $z_2$  can be solved from the steady state equation and can be substituted into the slow dynamics. The dynamics of the whole system Eq.(2) can be represented by the reduced system Eq.(3).

$$\begin{aligned} \dot{x}_1 &= x_2 \\ \dot{x}_2 &= f_1(x_1, y) + \varepsilon g_a(x_1, x_2, y, \varepsilon, \tau) \\ \dot{y} &= \varepsilon g_b(x_1, x_2, y, \varepsilon, \tau) \end{aligned} \quad (3)$$

Chen *et al.* found that for the reduced system in Eq.(3), roll motions are the fast varying variables while  $y$  is the slowly varying variable. Systems like this are called slowly varying systems. When  $\varepsilon = 0$ , this is simply

the planar roll motion with zero forcing and zero damping. When  $\varepsilon$  is a small positive number, the  $y$  motion (which includes sway and other motions) becomes relevant. Because the sway motion is stable, the system will trend towards the invariant manifold of roll dynamics.

## THEORETICAL BACKGROUND

### *Melnikov's Method for Slowly Varying Systems*

Melnikov's method is one of few analytical methods that can be used to predict the occurrence of chaotic motions in nonlinear dynamic systems. Melnikov's method has been applied to a number of ship dynamics problems, such as capsizing in beam seas (Falzarano, 1990) and surf-riding in following seas (Spyrou, 2006). Most of these are treated as single DOF problems. Melnikov's method for multi-DOF problems has been introduced in several references including the works of Wiggins and Holmes (1987, 1988), who derived the Melnikov's function for slowly varying system in Eq.(3).

When  $\varepsilon = 0$ , the unperturbed system in Eq.(3) has a planar Hamiltonian, which contains a homoclinic (or heteroclinic) orbit. The Melnikov's function for this system is

$$M(t_0) = \int_{-\infty}^{+\infty} (\nabla H \bullet \vec{g})(q_0(t), t+t_0) dt \quad (4)$$

$$- \frac{\partial H}{\partial z}(\gamma(z_0)) \int_{-\infty}^{+\infty} g_b(q_0(t), t+t_0) dt$$

$\vec{g} = [0, g_a, g_b]$ .  $H$  is the Hamiltonian for the unperturbed system.  $q_0(t) = (x_1, x_2)$  is the coordinates of the homoclinic orbit for the unperturbed system. And  $\bullet$  is the dot product.

### *Melnikov's Method for Slowly Varying Systems with Large Damping*

When the damping term is assumed to be large, it is grouped in the unperturbed system. Therefore, the unperturbed system is no longer Hamiltonian due to the presence of  $x_2$  in  $\tilde{f}_1$ .

$$\begin{aligned} \bullet \\ x_1 &= x_2 \end{aligned} \quad (5)$$

$$\bullet \\ x_2 = \tilde{f}_1(x_1, x_2, y)$$

The homoclinic orbit, which is essential in the formation of Melnikov's function, disappears as well. Since the homoclinic orbit does not arise naturally, it has to be created artificially. Eq.(3) is then written in the form of Eq.(6).

$$\begin{aligned} \bullet \\ x_1 &= x_2 \\ \bullet \\ x_2 &= \tilde{f}_1(x_1, x_2, y) + \varepsilon \tilde{g}_a(x_1, x_2, y, \varepsilon, \tau) \\ \bullet \\ y &= \varepsilon g_b(x_1, x_2, y, \varepsilon, \tau) \end{aligned} \quad (6)$$

The Melnikov's function for this system is

$$\begin{aligned} M(t_0) &= \int_{-\infty}^{+\infty} \tilde{x}_2 \tilde{g}_a(q_0, t+t_0) \left\{ \exp \left[ -\int_0^t a(s) ds \right] \right\} dt \\ &+ \int_{-\infty}^{+\infty} \tilde{x}_2 \frac{\partial \tilde{f}_1}{\partial y} \int_0^t g_b(s+t_0) ds \left\{ \exp \left[ -\int_0^t a(s) ds \right] \right\} dt \end{aligned} \quad (7)$$

in which,  $\tilde{q}_0(t) = (\tilde{x}_1, \tilde{x}_2)$  is the coordinates of the new homoclinic orbit of Eq.(5).  $a(s)$  is the trace of the Jacobian matrix of Eq.(5). If the unperturbed system in Eq.(5) is Hamiltonian,  $a(s) = 0$ . Eq.(7) can be reduced to the same form as Eq.(4).

### Phase Space Transport

As mentioned earlier, the unperturbed system of Eq.(3) has a planar homoclinic orbit, which contains a stable manifold and a unstable manifold. Wiggins and Holmes (1987) pointed out that when  $\varepsilon$  is small enough, the perturbed system is  $\varepsilon$ -close to the local unperturbed manifolds in a small neighborhood. Outside of this region, the perturbed manifold is  $\varepsilon$ -close to the unperturbed manifold in finite time. The theory of phase space transport for planar systems is applied here to predict the safe region erosion in finite time.

For the unperturbed system, the inside of the homoclinic orbit is the safe region. When the homoclinic orbit is perturbed, the manifolds will intersect resulting in *lobes*. And some

initial conditions initially inside the safe region may be outside the safe region for the perturbed system (pseudoseparatrix) after some time. This phenomenon corresponds to a special lobe called *turnstile lobe* (Wiggins, 1992). The area of this lobe is given in Eq.(8) (Wiggins, 1992).

$$\mu(L_0) = \varepsilon \int_0^T M^+(t_0, \phi_0) dt_0 + O(\varepsilon^2) \quad (8)$$

in which  $M^+(t_0, \phi_0)$  is the positive part of the Melnikov's function,  $L_0$  represents the lobe,  $t_0$  is the parameter in the homoclinic orbit  $q_0(t_0)$  denoting different time in the Poincaré map.  $\phi_0$  is the phase difference with the external forcing.  $T$  is the period of the external forcing.

Phase space transport refers to the initial conditions transporting outside the safe region after several periods of external forcing. The amount of the transported phase space can be used to show the rate of safe area erosion. Chen and Shaw (1997) derived the estimate of erosion ratio as shown in Eq.(9).

$$\rho_e = \frac{3\mu(L_0)}{A_s} = \frac{3\varepsilon}{A_s} \int_0^T M^+(t_0, \phi_0) dt_0 + O(\varepsilon^2) \quad (9)$$

where  $A_s$  is the area of the unperturbed safe region,  $\rho_e$  is the ratio erosion area divided by the original safe region, and because  $\varepsilon$  is a small positive number,  $O(\varepsilon^2)$  term can be ignored. In this work, Eq.(9) is used to show the erosion of safe basin for the capsizing problem.

### APPLICATIONS

The data from twice capsized fishing boat *Patti-B* are used here for numerical investigation. Chen *et al.* (1999) proposed this model shown in Eq.(10).

$$\begin{aligned} f_1 &= k_{11} - x_1 + k_{12}x_1^2 + k_{13}x_1^3 \\ g_a &= \sigma_{41} \cos x_1 + \sigma_{42} \cos^2 x_1 - \delta_{42}y - \delta_{44}x_2 \\ &\quad - \delta_{44q}x_2|x_2| - \lambda f_1(x_1) \cos \Omega \tau + \gamma_{41} \sin \Omega \tau \\ g_b &= \sigma_{21} \cos x_1 - \delta_{24}x_2 - \delta_{22}y + \gamma_{21} \sin \Omega \tau \end{aligned} \quad (10)$$

$f_1$  is the restoring moment in the roll motion, which includes the effect of bias.  $-\delta_{44}x_2 - \delta_{44q}x_2|x_2|$  is the nonlinear roll damping.  $\Omega$  is the non-dimensional wave frequency. Other coefficients come from hydrodynamic forces, wind forces and wave forces.

### Melnikov's Function

The extended Melnikov's method is applied here by assuming the roll damping terms are large. For the slowly varying system, it is essential to have a homoclinic orbit in order to calculate the Melnikov's function (Wiggins, 1987). If the linear damping term is assumed to be large, the center in the unperturbed system will become a sink, which makes it impossible to have a homoclinic orbit. In this work, the following damping term is assumed for roll

$$B(x_2) = \delta_{44}x_2 + bx_2^2 + cx_2^3 \quad (11)$$

where  $b$  and  $c$  are coefficients.

Although it is physically unrealistic to have quadratic damping term in roll, it is used here to show the possibility of using the extended Melnikov's method to multi-DOF problems.

In order to form the homoclinic orbit for the unperturbed system, the quadratic damping term is assumed to be large. The unperturbed system is now

$$\begin{aligned} \dot{x}_1 &= x_2 \\ \dot{x}_2 &= k_{11} - x_1 + k_{12}x_1^2 + k_{13}x_1^3 + bx_2^2 - \delta_{42}\bar{y} \end{aligned} \quad (12)$$

where  $\bar{y} = \frac{\sigma_{21}}{\delta_{22}} \cos \bar{x}_1$  is the sway variable

obtained from averaging.  $\bar{x}_1$  is the coordinate of the saddle point, which can be calculated by setting  $\dot{x}_1 = 0$  and  $\dot{x}_2 = 0$ . Eq(12) contains a homoclinic orbit starting from a saddle connecting to itself, as shown in Figure 1. The solid line in the figure is the homoclinic orbit for Eq.(12), while the dashed line is the homoclinic orbit for the unperturbed system in Eq.(3) without the quadratic damping term. These two homoclinic orbits start from the

same saddle point, and are close to each other. The Melnikov's function can be calculated using Eq.(7). Numerical integration can be carried out without difficulty.

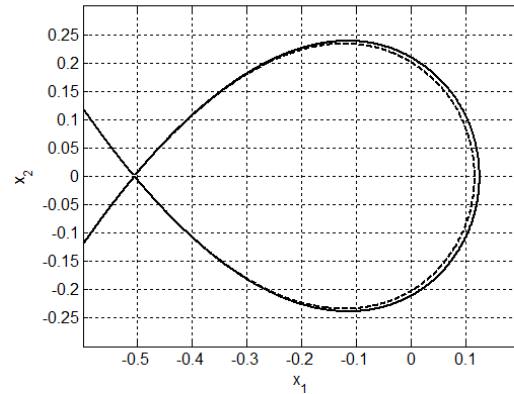


Fig. 1: Homoclinic orbit for the unperturbed system

### Numerical Results

Chen *et al.* (1999) have found the hydrodynamic and hydrostatic coefficients in Eq.(10) for *Patti-B* at wave frequency  $\omega_w = 0.6 \text{ rad/s}$ . In this work, the simulation is carried out for the case when the center of gravity has slight bias  $y_G = 0.025$ . The wind forces are assumed to be zero. The quadratic damping coefficient is set to  $b = 0.1$ . Melnikov's functions for both the standard and extended methods can be calculated using Eqs (4) and (7), respectively. When  $M(t_0) = 0$ , this corresponds to the critical wave amplitude  $a$  beyond which the chaotic motion and capsize may occur. The critical wave amplitude  $a$  has been calculated for both Melnikov's methods listed in Table 1.

As shown in the table, the extended Melnikov's method predicted the critical wave amplitude slightly higher than the standard Melnikov's method for the case studied here.

Table 1: Critical wave amplitude for two Melnikov's methods

Method	a (m)
Standard Melnikov	0.1792
Extended Melnikov	0.1826

Numerical simulations are carried out to obtain safe basins of the 3DOF system with the damping terms shown Eq.(11) and with original damping term. The safe basins are calculated by integrating a grid of  $100 \times 100$  points in roll plane with  $y, z_1$  and  $z_2$  initial conditions equal to 1. Every initial condition is integrated until a roll angle is greater than the angle of vanishing stability ( $0.5063rad$ ), thus capsizing occurs or through 10 cycles of external forcing, thus deemed safe. Capsizing was checked every  $dt = 0.01s$ . Figure 2(a) is the system with quadratic damping and Figure 2(b) is the original system. In both cases, the wave amplitude  $a = 0$ .

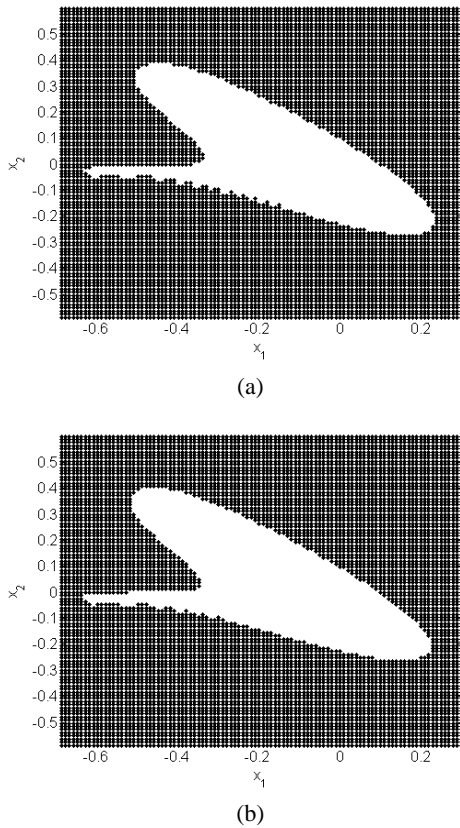


Fig. 2: Safe basins for different models (The white areas are the safe basins, and the dark areas are capsizing area.) (a). Safe basin for system with quadratic damping included. (b). Safe basin for original system.

The ratio of erosion area has been calculated using Eq.(9) for both Melnikov's function defined by Eqs.(4) and (7). Numerical simulations are also carried out for the 3DOF system to compare the results. Chen and Shaw

(1997) pointed out that in order to implement phase space transport methods, the dynamics should be studied on the invariant manifold where lobes can be defined. Therefore, similar to their work, the initial conditions for the numerical simulations have been chosen as 1720 points on the invariant manifold of roll dynamics, which are obtained by numerically calculating the safe points for the unperturbed system (basically the homoclinic orbit). Two points are picked on every direction of  $y, z_1$  and  $z_2$ . A grid of  $(1720 \times 2 \times 2 \times 2)$  points are used as the initial conditions. For the numerical data, the ratio of erosion area is calculated using the points capsized in 10 cycles of external forcing divided by the total number of points.

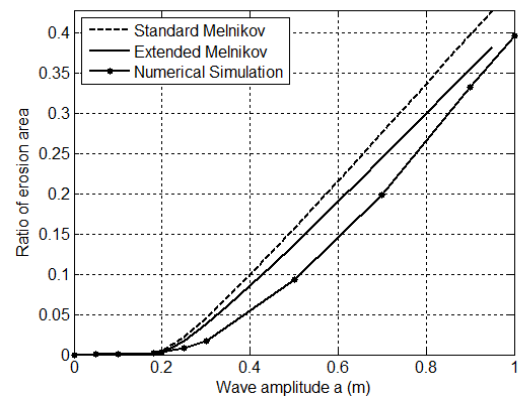


Fig. 3: The ratio of erosion area for different methods.

Figure 3 shows the ratio of erosion areas for different methods. The results from both Melnikov's methods are conservative compared to the numerical simulation results. And the results from the extended Melnikov's method are more accurate than those from the standard Melnikov's method, especially for larger wave amplitudes. Compared to the time-consuming 3DOF numerical simulations, the method of phase space transport based on the extended Melnikov's method provides a fast way to estimate ratio of erosion with reasonable accuracy.

## CONCLUSIONS REMARKS

In this paper, the extended Melnikov's method has been used to a roll-sway-heave coupled

model which can be reduced to a slowly varying system. In order to obtain the homoclinic orbit, a quadratic damping term is treated as large. Although it is physically unrealistic to have a quadratic term in roll damping, it is used here just to demonstrate the feasibility of the method. Coupled with the method of phase space transport, this results in a fast and effective way to estimate the ratio of erosion with apparently conservative accuracy. This work is the first step of applying the extended Melnikov's method to a special form of multi-DOF dynamical systems. It provides the possibility of applying the method to other multi-DOF problems in ship dynamics.

#### ACKNOWLEDGMENTS

This work has been supported by Dr. Patrick Purtell under ONR Grant N00014-06-1-0551 and Dr. Eduardo Misawa under NSF Grant CMMI 0747973.

#### References

- Chen, S.L.; Shaw, S.W. and Troesch, A.W.: A Systematic Approach to Modelling Nonlinear Multi-DOF Ship Motions in Regular Seas. In: *Journal of Ship Research*. 43 (1999) 25-37.
- Chen, S.L. and Shaw, S.W.: Phase Space Transport in a Class of Multi-Degree-of-Freedom Systems. In: *Proceedings of 1997 ASME Design Engineering Technical Conferences (DETC97)*
- Falzarano, J.M.: Predicting Complicated Dynamics Leading to Vessel Capsizing. PhD dissertation, University of Michigan, Ann Arbor, 1990.
- Salam, F.M.: The Melnikov Technique for Highly Dissipative Systems. In: *SIAM Journal on Applied Mathematics*. 47 (1987) 232-243.
- Spyrou, K.J.: Asymmetric Surging of Ships in Following Seas and its Repercussions for Safety. In: *Nonlinear Dynamics*. 43 (2006) 149-172.
- Wiggins, S.; Holms, P.: Homoclinic Orbits in Slowly Varying Oscillators. In: *SIAM Journal of Mathematical Analysis*. 18(3) (1987) 612-629.
- Wiggins, S.: Chaotic Transport in Dynamical Systems. (1992) Springer-Verlag, New York.
- Wiggins, S.; Holms, P.: Errata: Homoclinic Orbits in Slowly Varying Oscillators. In: *SIAM Journal of Mathematical Analysis*. 15(9) (1988) 1254-1255.
- Wu, W. and McCue, L.S.: Melnikov's Method for Ship Motions Without the Constraint of Small Linear Damping. In: *Proceedings of IUTAM Symposium on Fluid-Structure Interaction in Ocean Engineering*, (2007), Hamburg, Germany.
- Wu, W. and McCue, L.S.: Application of the extended Melnikov's Method for Single-degree-of-freedom Vessel Roll Motion. In: *Ocean Engineering*. 35 (2008) 1739-1746.
- Wu, W., Spyrou, K.J. and McCue, L.S.: Improved Prediction of the Threshold of Surf-riding of a Ship in Steep Following Seas. In: *Ocean Engineering*. (2010) doi:10.1016/j.oceaneng.2010.04.006
- Wu, W.: Analytical and numerical methods applied to nonlinear vessel dynamics and code verification for chaotic systems. PhD dissertation, Virginia Tech, Blacksburg, 2009.

## **Freak waves and capsizing accidents**

Takuji, Waseda,

Graduate School of Frontier Sciences, University of Tokyo

Takeshi, Kinoshita,

Institute of Industrial Sciences, University of Tokyo

### **ABSTRACT**

Marine accidents, possibly caused by encounters with the “freak waves”, are investigated. The result of the studies at the laboratory tank of the University of Tokyo revealed that the probability of freak waves increases when the directional spectrum narrows. Sea states during five marine accidents near Japan were analyzed using the third-generation wave model and suggested the narrowing of the directional spectrum. Based on the estimated information of the directional wave spectrum and other parameters during the marine accident, the possible causes of the accident will be discussed in the context of slamming, broaching and other possibilities.

### **KEYWORDS**

Freak wave; Marine Accident; Directional Spectrum; Benjamin-Feir Instability; Tank Experiment

### **INTRODUCTION**

Records of freak wave or rogue wave in the ocean are documented by seafarers as well as by scientists using advanced instrumentations (Kharif et al. 2009). Records reveal that the freak waves appear like a wall of water unexpectedly to the seafarers navigating in otherwise tractable sea states. The generation mechanism of the freak waves has become apparent in the last 10 years or so. One of the well studied mechanisms is the manifestation of the modulational instability of weakly nonlinear wave train in a random directional sea (Janssen 2003, Onorato et al. 2004,). Instability of random sea was suggested theoretically by Albers (1973) and has been elaborated by Yuen and Lake (1982) but it is only in the last decade that people associated this mechanism to the freak wave generation. However, this mechanism is not effective in realistic directional seas (Soquet-Juglard et al. 2005). Systematic studies in laboratory wave tank varying the directionality of the wave

spectrum revealed that the probability of the freak wave gradually increases as the directionality narrows; i.e. as the crest length gets longer (Waseda et al. 2009ab, Onorato et al. 2009ab). Waseda et al. (2009a) suggested that such sea state is possible from hindcast wave field. The key is then to predict the meteorological condition forming a sea state with directionally narrow wave spectrum. Tamura et al. (2008) showed that the marine accident near Japan occurred when the directional spectrum narrowed due to swell and wind-sea interaction. In this paper, we analyse five other marine accident cases using the wave model outputs to estimate the freak wave indices.

### **FREAK WAVE OCCURRENCE AND THE DIRECTIONAL SPECTRUM**

#### *Tank Experiment*

The Ocean Engineering Tank of the Institute of Industrial Science of the University of Tokyo (Kinoshita Laboratory and Rheem Laboratory,

50 m long, 10 m wide, 5 m deep) is equipped with a multi-directional wave maker with thirty-two 31 cm-wide triangular plungers that are digitally controlled to generate regular as well as random waves in ranges of wave periods (0.5 ~ 5 s). The JONSWAP-Mitsuyasu type directional wave spectrum was generated:

$$S(\omega) = \alpha g^2 (2\pi) \omega^{-5} \exp\left\{-\frac{5}{4}\left(\frac{\omega}{\omega_p}\right)^{-4}\right\} \gamma \exp\left\{-\frac{(\omega-\omega_p)^2}{2\sigma^2\omega_p^2}\right\} \quad (1)$$

$$G(\theta) = G_n \cos^n(\theta) \quad (2)$$

The peak frequency was set to 1.2389 Hz (wavelength 1 m), the value of  $\alpha$  was adjusted for the significant wave height in the range of 3 cm and 6 cm, and the peakedness parameter  $\gamma$  was set to 3.0, a typical value in growing sea. The most relevant control parameter in this experiment is the exponent  $n$  of the directional spreading function  $G(\theta)$ ;  $n = 3 \sim 250$ . The spectral evolution was measured by an array of wave wires at 5 m interval along the tank and the directional wave array of 6 sensors (a pentagon and its centroid). The directional wave spectrum was estimated using the wavelet detection method (WDM). Each run is an hour long.

#### Exceedence probability and the Kurtosis

The probability of freak wave in random directional sea is quantified by the probability density function of the wave height. Onorato et al. (2004) have demonstrated experimentally that the probability of the freak wave occurrence increased as the frequency bandwidth narrowed; i.e. as the value of the peakedness parameter  $\gamma$  increased. They have also demonstrated that the value of the Kurtosis of the surface elevation increased due to quasi-resonance down the tank. The value of the Kurtosis depends on both frequency bandwidth of the spectrum and wave steepness and their ratio was coined the BFI by Janssen (2003).

$$BFI = \frac{ak}{\mathcal{E}/f_0} \quad (3)$$

The *BFI*, representing the relative significance of nonlinearity and dispersion, is a useful index

in estimating the freak wave occurrence for a given uni-directional wave. Mori and Janssen (2006) derived an expression for the probability of the freak wave including the kurtosis as a parameter correcting linear theory. Based on these pioneering works, Waseda et al. (2009ab) and Onorato et al. (2009ab) independently conducted tank experiment to study the effect of directionality. Using the Kurtosis as an indicator, a steep reduction of the freak wave probability was found when the directional spectrum narrowed (Fig. 1).

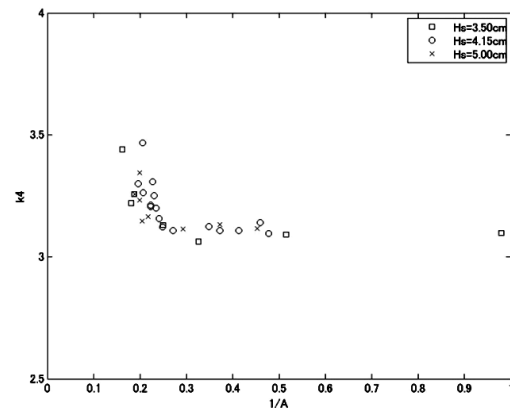


Fig. 1: Kurtosis plotted against directional spreading ( $1/A$ ) where  $A$  is defined as  $A \cdot K(\theta; f) \equiv G(\theta; f)$ , and  $G(\theta; f)$  is the directional distribution function satisfying  $\max[K(\theta; f)] = 1$ ; circle 35-40 m, square 14-15 m fetch. The figure is reproduced from Waseda et al. (2009a).

The BFI was extended in Waseda et al. (2009a) to include the effect of directionality:

$$BFI_{eff} = \frac{\mathcal{E}_{eff}}{\sqrt{(\delta k/k)^2 - 2(\delta l/k)^2}} \quad (4)$$

Effective BFI ( $BFI_{eff}$ ) makes use of the effective spectral bandwidth (the denominator) introduced by Alber (1978) and also the resonant interaction coefficient that reduces as the resonance condition departs from the singularity along the resonance manifold (the numerator). The observed variation of Kurtosis was characterized as a single-valued function of the  $BFI_{eff}$ . Arbitrariness in the determination of the effective spectral bandwidth remains, and will be discussed further in the freak wave index section.

## WAVE FORECASTING/HINDCASTING

### Model description

The model is based on WavewatchIII<sup>TM</sup> (WW3) and covers a region near Japan at a quarter degree horizontal resolution nested within the coarse Pacific basin model (one degree). The Pacific model is forced by the U. S. Navy Operational Global Atmospheric Prediction System (NOGAPS) wind, and the Japan model is forced by the Japan Meteorological Agency Meso-Scale Model (MSM) wind. The model is configured at a default WW3 setting. Tamura et al. (2008) improved the model replacing the nonlinear source term from the default DIA method to the SRIAM method. Some of the marine accident analyses make use of this improved WW3 with SRIAM. In et al. (2009) compared the performance of the SRIAM and DIA in estimating various freak wave indices and concluded that qualitative assessment can be made using the conventional DIA. Note that, regardless of the nonlinear source terms used, the third generation wave model tends to produce broader directional spectrum than the observation (e.g. Tamura et al. 2010). The forecast model is in operation since April 2009 and the nowcast data are archived as hindcast product. The hindcast product is analyzed in this study.

### FREAK WAVE INDICES

#### Geometry of the directional spectrum

The BFI and its extension, conveniently relates the geometry of the spectrum (frequency bandwidth and average steepness) to the probability of the freak wave. The parameters characterizing the spectral geometry are the steepness (5), the frequency bandwidth (6), and the directional spreading (7):

$$ak_s = \left( \frac{H_s}{2} \right) \left( \frac{2\pi}{\lambda_m} \right) \quad (5)$$

$$Q_p = 2m_0^{-2} \int_0^\infty \sigma \left[ \int_0^{2\pi} F(\sigma, \theta) d\theta \right]^2 d\sigma \quad (6)$$

where

$$m_0 = \int_0^{2\pi} \int_0^\infty F(\sigma, \theta) d\sigma d\theta$$

$$\sigma_\theta = \left[ 2 \left\{ 1 - \left( \frac{a^2 + b^2}{E^2} \right)^{\frac{1}{2}} \right\} \right]^{\frac{1}{2}} \quad (7)$$

where

$$a = \int_0^{2\pi} \int_0^\infty \cos(\theta) F(\sigma, \theta) d\sigma d\theta$$

$$b = \int_0^{2\pi} \int_0^\infty \sin(\theta) F(\sigma, \theta) d\sigma d\theta$$

These parameters can be derived from the directional spectrum  $F(\sigma, \theta)$ . Waseda et al. (2009a) further attempted to combine  $Q_p$  and  $\sigma_\theta$  to estimate the effective spectral bandwidth  $\sqrt{(\delta k/k)^2 - 2(\delta l/k)^2}$  but had to include an arbitrary constant which needs to be calibrated.

#### The $Q_p - \sigma_\theta$ plot

Numerous studies suggested that the correlation between BFI (ratio of  $ak_s$  and  $Q_p$ ) and the probability of freak wave was poor. On the other hand, Tamura et al. (2008) focused attention only on the directional property of the spectrum (i.e.  $Q_p$  and  $\sigma_\theta$ ) and demonstrated that the trajectory of the spectral property in the  $Q_p - \sigma_\theta$  space can indicate a dangerous sea state. The  $Q_p - \sigma_\theta$  diagram is reproduced in Fig.2 supplemented with annotations. In et al. (2009) further utilized the  $Q_p - \sigma_\theta$  diagram suggesting possible seasonality of the freak wave occurrence near Japan. The  $Q_p - \sigma_\theta$  diagram will be utilized in the investigation of the marine accident cases.

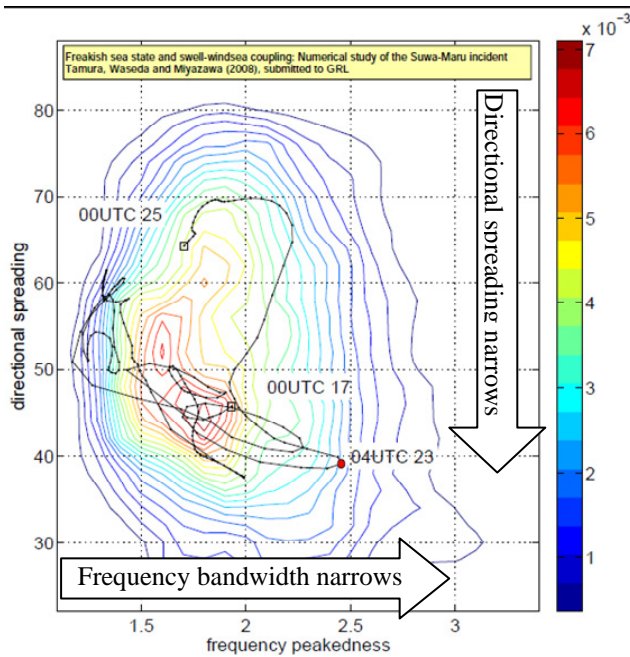


Fig. 2: The trajectory of spectral property in the  $Q_p - \sigma_\theta$  diagram. The occurrence of freak wave is highest in the lower right corner and lowest in the upper left corner. The figure is reproduced from Tamura et al. (2008). Case 1 in this paper.

## MARINE ACCIDENT CASES

### Summary of the cases studied

Six marine accident cases were studied. In chronological order of the incident, the gross tonnage of the vessel and the wave parameters estimated from the wave model are summarized in Table 1. Except for the fifth case, all the other cases occur when the probability of freak wave was high judged from the trajectory on the  $Q_p - \sigma_\theta$  diagrams (Fig.3). The accidents occur (red dot) when the directional spectrum was narrow.

Table 1: Summary of the gross tonnage, description of the accident, and relevant wave parameters (significant wave height, mean period, mean wavelength, steepness, directional spreading, frequency bandwidth) from the wave model at the time of the marine accident cases.

GRT	accident	Hs	Tm	Lm	ak	$\sigma_\theta$	$Q_p$
33,833	loss of bow	8.2	12.4	240	0.11	25	2.5
135	capsize	3.8	9.5	141	0.08	38	2.5
19	capsize	7.9	9.9	154	0.16	25	2.8
7,910	load shift	6.0	9.7	145	0.13	21	2.4
121	capsize	2.5	5.8	52	0.15	45	2.1
113	capsize	1.7	4.9	38	0.14	29	2.4

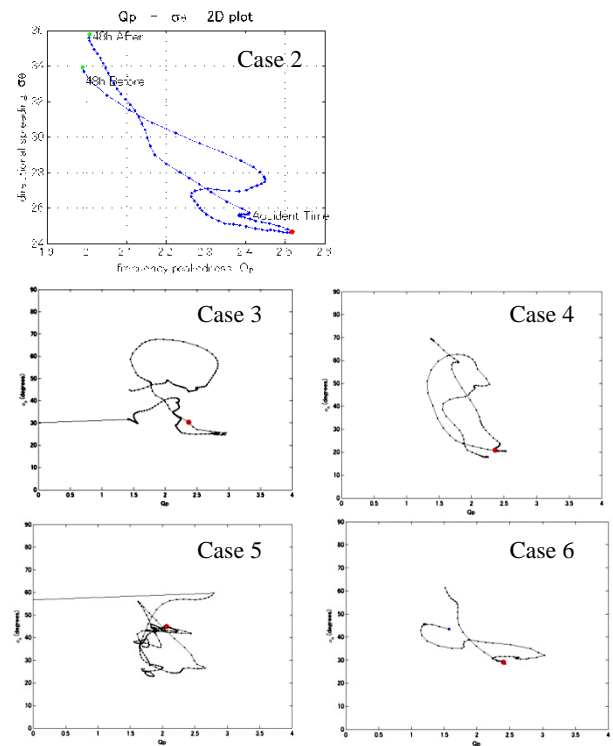


Fig. 3: The trajectory of the spectral property in the  $Q_p - \sigma_\theta$  diagram for cases 2 to 6. Except for the fifth case, the accident occur (red dot) at the lower right corner of the diagram when the directional spectrum is narrow.

### Case 1: Bulk carrier Onomichi (1980.12.30)

After the loss of her bow at 156.2E and 31.0N, south of the Kuroshio Extension, Onomichi had survived for two months until it finally sunk. The damaged bow has been observed and photographed, and after an intensive study of the structural strength of the hull, Yamamoto et al. (1983) concluded that the ship must have encountered a wave of height exceeding 20 m. Possible impact force due to slamming is considered to be the cause of the structural damage. The reproduced wave field suggests that the significant wave height was around 8 m or so, suggesting that the wave 20 m high is a freak wave. The possible meteorological cause of the freak wave in this case is the Eastward propagation of a strong westerly wind (In et al 2009).

A tank experiment was conducted at the Ocean Engineering Tank of the University of Tokyo, studying the bending moment on a 2m model ship encountering extreme waves generated by dispersive focusing (chirped wave group) and Benjamin-Feir wave train. The

study revealed that the midpoint bending moment of the ship hull was unbounded, and increased with the encounter wave height. Both the sagging bending moment and the hogging bending moment did not saturate (Fig.4). For a 280 m long vessel, the result suggests that the bending moment did not saturate even for waves as high as 35 m. From the result of this tank experiment, we conclude that it is possible that the bottom slamming due to encounter with a wave over 20 m in height has damaged the bulk-carrier Onomichi.

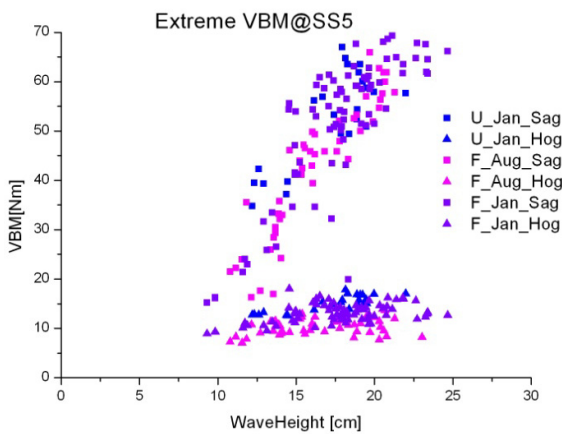


Fig. 4: The extreme vertical bending moment plotted against the encountered wave height for sagging bending moment (squares) and hogging bending moment (triangles).

**Case 2: Fishing vessel (2008.6.23)**

A large fishing vessel of 135 GRT capsized at 144.5E and 35.5N, North of the Kuroshio Extension, due to encounter with two consecutive extreme waves according to the survivor of the sunken ship. The meteorological conditions that lead to the formation of a freakish sea condition is the coexistence of the Baiu/Meiyu front and the depression. Peculiar spectral evolution of swell and wind-sea interaction is reported by Tamura et al. (2008). The height of the freak wave is estimated to be around 8 m based on the significant wave height of 4 m from the wave model. It is said that the sunken ship was using a para-anchor at the time of the incident. The interval between the two consecutive extreme waves (as reported) is unknown. If they were waves within a single wave group, the interval would have been around 10 seconds or so, but if they were waves from two independent groups, the interval could have

been around 120 seconds or so. The combined effect of the use of para-anchor and the encounter with two consecutive extreme waves could have possibly led to the capsizing of the vessel.

**Case 3: Fishing vessel (2009.10.25)**

A small fishing vessel (19 GRT and LOA 19 m) capsized at 138.5E and 33.0N near the Hachijo Island during a severe sea condition of 8 m in significant wave height. The characteristic meteorological condition leading to this incidence is the stationary front south of Japan. In between the front and the Japanese archipelago, a gale condition of 10 m/s East-North-East wind and 20 m/s gust developed within 10 hours. The spectral evolution suggests a freakish sea state.

**Case 4: Ferry (2009.11.12)**

A large ferry boat (LOA 167 m, D 6 m) experienced a serious load shift at 136.3E and 33.6N of the coast of the Kii Peninsula, heeled at large angle, drifted and eventually collided with a reef. The significant wave height was 6 m, and average wavelength was 145 m. The wave analysis suggests a freakish sea state but the estimated freak wave of 12 m height does not seem to be a threat for LOA 167 m ship. However, because the ship was sailing to the southwest followed by westward propagating wave, the possible scenario of the large heel can be the loss of transverse stability due to passage of the freak wave from the portside.

**Case 5: Fishing vessel (2009.12.20)**

A large fishing vessel of 121 GRT sunk during a gale condition of 15 m/s West-North-West wind at 130.0E and 35.0N near Tsushima strait. The reported significant wave height was 4 m and from the wave model was 2.5 m because of the short fetch from the coast of South Korea. The wave spectrum did not indicate a freakish sea state either. Possibility is that the spatial resolution of the numerical model was insufficient to resolve high frequency wind, for example, the gap winds from the valleys in the Korean peninsula.

**Case 6: Fishing vessel (2010.1.12)**

A large fishing vessel of 131 GRT sunk at 127E and 33N in the East China Sea. A possible green water loading was reported from the ship in the last radio contact. The estimated significant wave height is only 2 m. The wave spectrum suggests a freakish condition. The ship was unloaded since she was on her way to the fishing ground. Therefore, even with the possible encounter with the freak wave, it is difficult to explain the capsizing. The incident occur South-East of the Cheju Island, where the wind from the North-West can be intensified in the East side as it blows around the Island. Such wind condition is not resolved in the MSM wind product we used for the wave simulation.

**CONCLUSIONS**

Result from the experimental work hinted us the possibility of abnormal meteorological condition as a precursor to the development of freakish sea state when the directional spectrum narrows. Among the six incidents studied, 5 of them suggested that the sea state was freakish. In the first case, the ship experienced bottom slamming. In the second case the ship lost its stability due to combined influence of sea-anchor and green-water loading. In the third case the ship capsized because she encountered an enormous wave compared to her size. In the fourth case the ship lost its stability and healed because of the freak wave in following sea. The reason for the sink of the fifth and the sixth case is unknown because the estimated wave height is rather small. In both cases, the incidents occur close to the land where the resolution of the wind product is insufficient.

**ACKNOWLEDGMENTS**

The work was supported by the grant-in-aid for scientific research, MEXT.

**REFERENCES**

Alber, 1978, The effects of randomness on the stability of two-dimensional surface wavetrains, Proc. R. Soc. Lond. A. 363, 525-546

In, Waseda, Kiyomatsu, Tamura, Miyazawa, and Iyama, 2009 Analysis of a marine accident and freak wave prediction with an operational wave model, Proceedings, June, ISOPE-Osaka

Janssen, 2003, Nonlinear four-wave interactions and freak waves, J. Phys. Oceanogr., 33, 863-884

Kharif, Pelinovsky and Slunyaev, 2009, Rogue waves in the Ocean, Springer, 219pp

Mori & Janssen, 2006, On Kurtosis and occurrence probability of Freak Waves, J. Phys. Oceanogr., 36(7), 1471-1483

Onorato, Osborne, and Serio, 2002: Extreme wave events in directional, random oceanic sea states, Physics of Fluids, 14 (4), 25-28

Onorato, Osborne, Serio, Cavaleri, Brandini, Stansberg, 2004, Observation of strongly non-Gaussian statistics for random sea surface gravity waves in wave flume experiments, Phys. Review E, 70, 067302

Onorato et al. 2009a, Statistical properties of mechanically generated surface gravity waves: a laboratory experiment in a three-dimensional wave basin, J. Fluid Mech., 627, 235-257

Onorato, Waseda, Toffoli, et al. 2009b, On the statistical properties of directional ocean waves: the role of the modulational instability in the formation of extreme events, Phys. Rev. Letters, 102(11), 114502

Soquet-Juglard, Dysthe, Trulsen, Krogstad, and Liu, 2005, Probability distribution of surface gravity waves during spectral changes, J. Fluid Mech., 542, 195-216

Tamura, Waseda, Miyazawa and Komatsu, 2008: Current-Induced Modulation of the Ocean Wave Spectrum and the Role of Nonlinear Energy Transfer. J. Phys. Oceanogr., 38, 2662-2684

Tamura, Waseda, & Miyazawa, 2009, Freakish sea state and swell-windsea coupling: Numerical study of the Suwa-Marui incident, Geophys. Res. Letters, 36, L01607

Tamura, Waseda and Miyazawa, 2010, Impact of the nonlinear energy transfer on the wave field in the Pacific hindcast experiment, J. Phys. Oceanogr., to be published

Waseda, Kinoshita & Tamura, 2009a, Evolution of a random directional wave and freak wave occurrence, J. Phys. Oceanogr., 39 (3), 621-639

Waseda, Kinoshita & Tamura, 2009b, Interplay, J. Phys. Oceanogr., 39 (3),

Yamamoto, Otsubo, Iwai, Watanabe, Kumano, Fujino, Fukasawa, Aoki, Ikeda, and Kuroiwa, 1983. Disastrous Damage of a Bulk Carrier due to Slamming, The lecture of The Society of Naval Architects of Japan in 1983.

Yuen and Lake, 1982: Nonlinear dynamics of deep-water gravity waves, Adv. Appl. Mech., 22, 67-229

## Assessment of Short-Term Risk with Monte-Carlo Method

Bradley Campbell, Vadim Belenky

Naval Surface Warfare Center, Carderock Division

### ABSTRACT

The paper describes a method for the direct assessment of the probability of partial stability failure for an intact ship. The method is essentially a statistical extrapolation, allowing explicit account of influence of nonlinearity of GZ curve on roll distribution. It is achieved by using a Peaks-Over-Threshold method for extrapolation. The method is also capable of simultaneously treating large port and starboard roll angles. To avoid possible inapplicability of Poisson flow, an envelope approach is used. A partial stability failure is associated with the upcrossing of the dangerous level by the envelope. The proposed method is called “Envelope Peaks over Threshold” (EPOT). Application of EPOT is demonstrated with simulated wave elevations.

### KEYWORDS

Problem of Rarity, Principle of Separation, Partial Stability Failure, Statistical Extrapolation

### INTRODUCTION

The main principle that allows solving the problem of rarity is separation. Instead of one problem with very rare events, two or more related problems are considered: “non-rare” and “rare”. The “non-rare” problem is crossing a threshold that is low enough that a statistically significant number of crossings can be observed in a model test or numerical simulation. The “rare” problem is a statistical extrapolation of the data above this threshold, see Figure 1.

Nonlinearity is accounted for by separating small and large-amplitude motions with the threshold. If any sort of statistical fit is used on roll motion data in its entirety, the resulting fit will be dominated by the small-amplitude motions where the roll motion is still relatively linear, and the influence of nonlinearity will generally be not represented properly. The threshold must therefore be high enough, so that the influence of nonlinearity above that threshold can be considered substantial. It cannot be chosen based purely on statistics. Physical considerations based on the shape of the GZ curve must be included as well, however setting particular limits on a threshold

is outside of scope of this paper; these limits are assumed to be given.

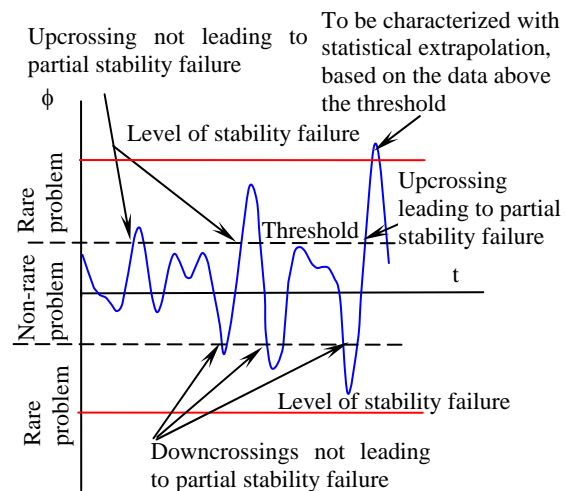


Figure 1 Summary of the current method: separation principle

### BOTH-SIDES CROSSING

Partial stability failure in a form of a large roll event is equally dangerous on either side of a ship. Therefore, a random event of upcrossing is not yet a complete model of partial stability failure. A complete model of the partial stability failure should include both

upcrossing of a specified level on the positive side and downcrossing of the specified level on the negative side. This random event can be written as:

$$X = ((\phi(t) < a) \cap (\phi(t + dt) \geq a)) \cup ((\phi(t) > b) \cap (\phi(t + dt) \leq b)) \quad (1)$$

Here  $X$  is a random event associated with partial stability failure;  $a$  is a positive level of exceedance and  $b$  is negative level of exceedance. Obviously, if the mean value of roll is zero and requirements are the same for the both sides:

$$\text{if } (m(\phi) = 0) \Rightarrow a = -b \quad (2)$$

If the distribution of the roll and roll rate are symmetric, the rate of both-sides crossings can be expressed as:

$$\lambda_{ab} = 2f(a) \int_0^{\infty} f(\dot{\phi}) \dot{\phi} d\dot{\phi} \quad (3)$$

In particular, for the generic normal process  $x(t)$ :

$$\lambda_{ab} = \frac{1}{\pi} \sqrt{\frac{V_{\dot{x}}}{V_x}} \exp\left(-\frac{a^2}{2V_x}\right) \quad (4)$$

Where  $V_x$  is the variance of the process and  $V_{\dot{x}}$  is the variance of it derivative.

The random event of both-side crossing does not follow Poisson flow, as the independence condition is difficult to meet. The autocorrelation function will not die out during the half a period; so if there was an upcrossing through the positive thresholds, the downcrossing through the negative threshold is more likely.

## ENVELOPE APPROACH

The ability to apply Poisson flow is important, as it is difficult to provide an explicit relationship with time outside of the Poisson flow assumption. Belenky & Breuer (2007) used the envelope of the roll process to overcome similar difficulty while dealing with parametric roll; such a process usually has a very narrow spectrum. The narrow spectrum results in significant clustering (or grouping) of

the high peaks. As a result, even one-sided upcrossings become dependent on neighboring cycles, as once upcrossing occurs, it is very likely that it will occur again on the next period of motion.

The envelope  $a(t)$  is defined as

$$a(t) = \sqrt{\phi^2 + \psi^2} \quad (5)$$

Where  $\psi$  is a complimentary process that can be obtained with Hilbert transform.

An additional difficulty here is that the spectrum of roll motions is not necessarily narrow and the envelope cannot be considered as a slowly changing function. In some cases this can result in the envelope peaking higher than the process itself (due to the behavior of the complimentary process). The envelope can then cross the level of interest while the process does not, see Figure 2.

To avoid this artificial crossing, the piecewise linear approximation of the envelope is used, also shown in Figure 2. Values for this “peak-based” envelope are calculated using linear interpolation between the absolute values of peaks or zero-crossing peaks of the process. Using absolute values ensures that both-sides crossing are taken into account as opposed to just upcrossing. This approach is also helpful while dealing with relatively narrow-banded processes, such as ship motion in following and stern-quartering seas.

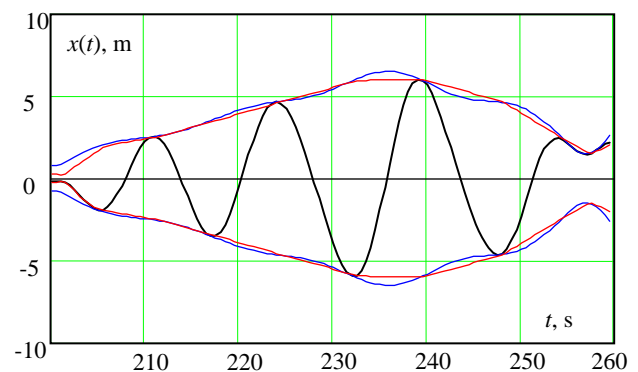


Figure 2. Zoomed in envelope (blue) peak-based or piece-wise linear approximation of the envelope (red) evaluated for wave elevations (Bretshneider spectrum at typical sea state 8)

## ENVELOPE PEAK OVER THRESHOLD

The main challenge that the problem of rarity poses comes from the nonlinear nature of large-amplitude roll motions. It is well known that large-amplitude roll motions cannot, in general, be characterized by normal distribution (Belenky & Sevastianov, 2007). The type of distribution depends strongly on the shape of the ship's righting arm curve, which may change significantly in waves. It is also difficult to fit a distribution with simulated or measured data; because only the large-amplitude motions carry information on the nonlinearity of the motion and they are rare.

For the same reason it is also difficult to fit the extreme value distribution. Because the dynamical system possesses significant nonlinearity, any statistical fit based on all the data may be misleading, as these data may be dominated by relatively mild nonlinearity. The resulting distribution fit may not reflect the physical properties of the dynamical system for large displacements.

The envelope-peaks-over-threshold method enables the implementation of the principle of separation and avoids the inapplicability of Poisson flow. Then, the probability of at least one large roll event during time  $T$  is as follows:

$$\begin{aligned} P(T | E > a_2) &= 1 - \exp(-\lambda T) \\ \lambda &= \xi \cdot P(E > a_2 | E > a_1) \end{aligned} \quad (6)$$

Here  $\xi$  is the rate of upcrossing through the threshold  $a_1$ , while  $a_2$  is the level of stability failure.

The objective of the non-rare problem is finding the rate of upcrossing,  $\xi$ , of a given threshold,  $a_1$ , by the peak-based envelope. The objective of the rare problem is to find conditional probability,  $P(\phi > a_2 | \phi > a_1)$ , that the envelope exceeds the level of partial stability failure,  $a_2$ , once a given threshold,  $a_1$ , is crossed.

The value of the threshold plays an important role in separating small and large-amplitude motions. The threshold must therefore be high enough, so that the influence of nonlinearity above that threshold can be considered substantial.

## NON-RARE PROBLEM

The most direct way to estimate upcrossing of the peak-based envelope is direct counting; then the mean number of events can be estimated as:

$$m_U^* = \frac{1}{N_R} \sum_{j=1}^{N_R} N_{Uj} \quad (7)$$

Where  $N_{Uj}$  is the number of events observed during record  $j$ . The estimate of rate of upcrossing is:

$$\xi^* = \frac{m_U^*}{T_R} \quad (8)$$

Where  $T_R$  is duration of the record.

The confidence interval for estimate (8) can be found using auxiliary random variable (Kramer & Leadbetter 1968):

$$U_{i,j} = \begin{cases} 1 & E_{i,j} \leq a_1 \cap E_{i+1,j} > a_1 \\ 0 & \text{Otherwise} \end{cases} \quad (9)$$

$i = 1, \dots, n; \quad j = 1, \dots, N_R$

If the upcrossings are independent, this auxiliary random variable has a binomial distribution with parameter  $p$  – probability that an upcrossing occurs in a particular time instant. It can be estimated as:

$$p^* = \frac{1}{nN_R} \sum_{i=1}^n \sum_{j=1}^{N_R} U_{i,j} \quad (10)$$

The number of upcrossings observed during record  $j$  can be expressed through this auxiliary variable as:

$$N_{Uj} = \sum_{i=1}^n U_{i,j} \quad (11)$$

The number of upcrossings can be related to the estimate of the upcrossing rate.  $N_{Uj}$  is the sum of independent variables with a binomial distribution, each of which has the same parameter,  $p$ . This sum also has a binomial distribution with the same parameter  $p$ , but with  $n$  equal to the sum of the number of cases (time steps).. In the case of  $N_R$  records, the total number of cases becomes:

$$N = N_R \cdot n \quad (12)$$

Then, the probability that  $N_R$  records, each with

$n$  time steps, will contain  $k$  upcrossings can be expressed as:

$$P(k) = \frac{N!}{k!(N-k)!} p^k (1-p)^{N-k} \quad (13)$$

Formula (13) also can be interpreted as the probability mass distribution for the number of upcrossings for all the records. The number of upcrossings  $k$  is related to the estimated rate of upcrossing as:

$$\xi^* = \frac{k}{T_R n} \quad (14)$$

Boundaries of confidence interval for  $\xi^*$  are expressed as:

$$\xi_{low}^* = \frac{1}{T_R n} Q\left(\frac{1-\beta}{2}\right); \quad \xi_{up}^* = \frac{1}{T_R n} Q\left(\frac{1+\beta}{2}\right) \quad (15)$$

Where  $Q(P)$  is an inverse to the cumulative distribution function (CDF) for  $P(k)$  and  $\beta$  is a given confidence probability.  $Q(P)$  is often referred to as the Quantile function.

#### RARE PROBLEM: DIRECT FIT

The objective of the rare problem is to find the probability of the envelope crossing the given level of stability failure,  $a_2$ , if the threshold,  $a_1$ , was already exceeded. This probability can be trivially found if the distribution of envelope peaks over the threshold is known:

$$P(E > a_2 | E > a_1) = 1 - F(E_m | E_m > a_1) \quad (16)$$

Here  $F(E_m | E_m > a_1)$  is the CDF of the envelope peaks over the threshold (see Figure 3). It can be found through a Weibull fit to the available statistical data, using the method of moments or the maximum likelihood method (Cohen 1965), see Figure 4.

Both figures use a dataset of wave elevations simulated with a Bretshneider spectrum for a typical sea state 8.

$$f(x) = \begin{cases} \frac{k}{\alpha} \left(\frac{x-\theta}{\alpha}\right)^{k-1} \exp\left(-\left(\frac{x-\theta}{\alpha}\right)^k\right) & x \geq \theta \\ 0 & x < \theta \end{cases} \quad (17)$$

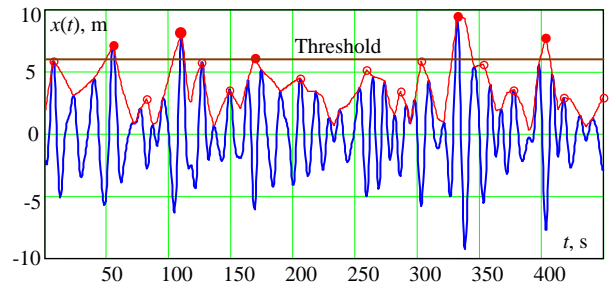


Figure 3 Envelope Peaks over Threshold (filled circles)

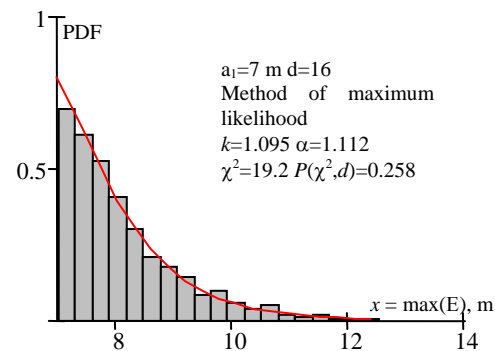


Figure 4 Weibull Fit for Envelope Peaks over Threshold

The width of bins for the histogram in Figure 4 was calculated with the following formula (Scott, 1979):

$$W = \frac{3.5\sigma}{\sqrt[3]{N_p}} \quad (18)$$

Where  $\sigma$  is standard deviation and  $N_p$  is the number of available data points.

Both distribution fitting methods use statistical data to find the parameters of the distribution (17). Therefore these parameters are random values, which mean the rate of upcrossing is also a random number. The confidence interval must therefore be evaluated to reflect statistical uncertainty. In fact, the easiest way to evaluate the confidence interval for the upcrossing rate is to compute it for the distribution (17) using the method described in (Belenky & Weems, 2008); sample results are shown in Figure 5 and Figure 6. The confidence interval widens as the threshold is raised since there are less data points available.

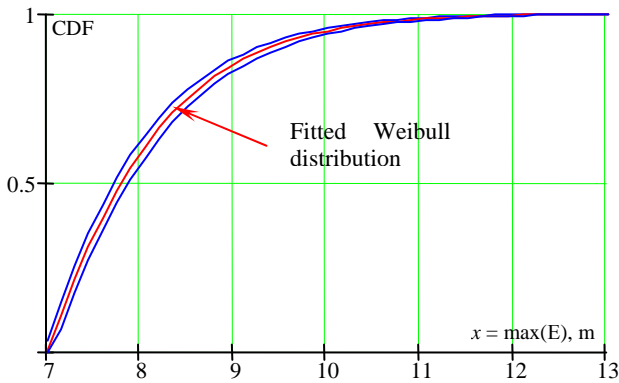


Figure 5 Weibull CDF with Confidence Interval Fitted for Envelope Peaks Exceeding the Threshold of 7 m

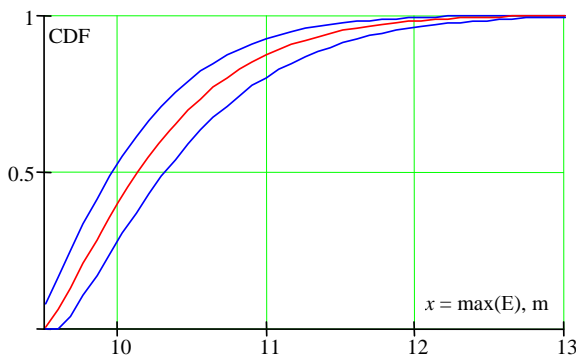


Figure 6 Weibull CDF with Confidence Interval Fitted for Envelope Peaks Exceeding the Threshold of 9.5 m

As a result, it is possible to propagate statistical uncertainty throughout the method and obtain the final result (6) with a confidence interval.

A series of results for these calculations done for 200 simulated records of wave elevations of 30 min durations each (Bretshneider spectrum at typical sea state 8, with significant height 11.5 m and modal period 16.4 sec) was calculated for different threshold values and are shown in Figure 7.

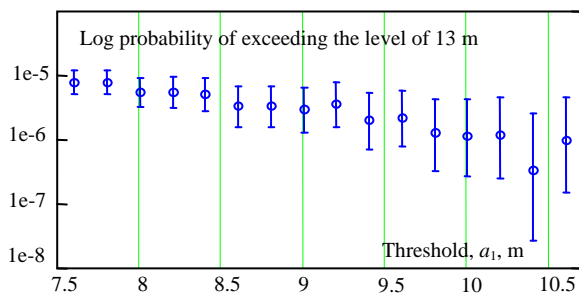


Figure 7 Statistical Extrapolation of Upcrossing Rate

Figure 7 shows some variability of the extrapolated estimate. As the threshold increases, the estimate shows some decrease, while the confidence interval becomes wider.

In principle there can be two tendencies affecting the result. The accuracy of the Weibull fit is better for extrapolation if the data points are closer to the target, but the uncertainty is larger as there are fewer and fewer data points available. The optimum is achieved somewhere in the middle. Therefore averaging the results from different thresholds may be useful:

$$\lambda_a = \frac{1}{N_{a1}} \sum_{i=1}^{N_{a1}} \lambda(a_{1i}) \quad (19)$$

As the first expansion, averaging was also applied to the boundaries of the confidence intervals:

$$\lambda_a^{low} = \frac{1}{N_{a1}} \sum_{i=1}^{N_{a1}} \lambda^{low}(a_{1i}) \quad (20)$$

$$\lambda_a^{up} = \frac{1}{N_{a1}} \sum_{i=1}^{N_{a1}} \lambda^{up}(a_{1i})$$

### RARE PROBLEM: EXTREME VALUE FIT

The solution of the rare problem involves the evaluation of the probability using the tail of the distribution. Difficulties with predicting the behavior of the tail of fitted distributions are not new. These difficulties were one of the motivations for the development of extreme value theory; therefore it is quite logical to try to use extreme distributions for the rare problem. In its classic interpretation, the extreme value distribution describes probabilistic properties of an extreme value observed during a given time.

To fit an extreme value distribution a time window  $T_W$  is introduced; the largest value observed during this time represents one data point, see Figure 8.

The Weibull distribution can be fit using these data points. The resulting distribution will be a conditional distribution, as only points above the given thresholds are used. By the definition of the cumulative distribution function:

$$F_{EV}(a_2 | a_1, T_W) = P(E \leq a_2 | E > a_1, T_W) \quad (21)$$

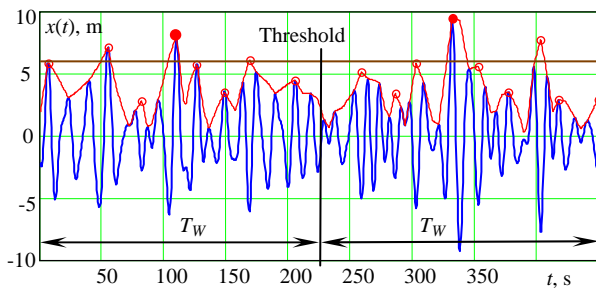


Figure 8 Data Points for Extreme Value Distribution of Envelope

The probability of exceedance of the level  $a_2$  during time  $T$  is expressed as:

$$P(E > a_2 | T_W) = P(E > a_1 | T_W) \cdot P(E > a_2 | E > a_1, T_W) \quad (22)$$

Here  $P(E > a_1 | T_W)$  is the probability of at least one exceedance of the given threshold, while  $P(E > a_2 | E > a_1, T_W)$  is the conditional probability of an exceedance of the level  $a_2$  once the threshold  $a_1$  has been crossed. The latter is a probability of a random event, complimentary to (21) and therefore it can be expressed through conditional CDF as:

$$P(E > a_2 | E > a_1, T_W) = 1 - F_{EV}(a_2 | a_1, T_W) \quad (23)$$

The probability of at least one exceedance of the given threshold can be expressed using Poisson flow, as the rate of upcrossing through the threshold  $a_1$  is the solution of the non-rare problem:

$$P(E > a_1 | T) = 1 - \exp(-\xi T_W) \quad (24)$$

A similar expression can be written for the probability of at least one exceedance (or upcrossing) of the level  $a_2$ :

$$P(E > a_2 | T) = 1 - \exp(-\lambda T_W) \quad (25)$$

The rate of events  $\lambda$  is the final objective; substitution of equation (23-25) into (22) allows expressing it through the extreme value CDF:

$$\lambda = -\frac{1}{T_W} \ln(\exp(-\xi T_W) + (1 - \exp(-\xi T_W)) F_{EV}(a_2 | a_1, T_W)) \quad (26)$$

Taking into account (6) the solution for the rare problem (independent of time of exposure,  $T$ ) is expressed as:

$$P(E > a_2 | E > a_1) = -\frac{1}{\xi T_W} \ln(\exp(-\xi T_W) + (1 - \exp(-\xi T_W)) F_{EV}(a_2 | a_1, T_W)) \quad (27)$$

The result of sample calculations are shown in Figure 9 and, as expected, the variability of is less (at least visually) in comparison with the fit of Weibull distribution to peaks, as shown in Figure 7. Nevertheless using an averaging procedure (19-20) seems to be reasonable for this case as well.

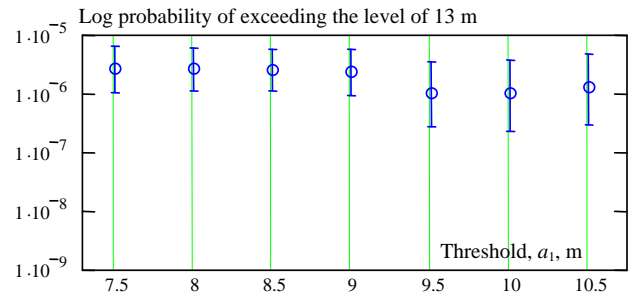


Figure 9 Statistical Extrapolation of Upcrossing Rate Using Extreme Value Distribution Fit for Rare Problem

## COMPARISON WITH THEORETICAL SOLUTION

Simulated wave elevations were used as a numerical example. As this is a normally distributed process the theoretical solution may exist.

However, the failure event is associated with an upcrossing of the peak-based envelope through a certain level. The probability of this event cannot be exactly expressed in closed form, as there is a subtle difference between the peak-based envelope and theoretical envelope defined by formula (5).

Nevertheless, for a relatively high level of upcrossing, the difference between the probability of upcrossing of the theoretical envelope and the peak-based envelope may not be that significant, as a large peak of the process belongs to both the theoretical and peak-based envelopes. Therefore the first candidate for the theoretical solution is the rate of upcrossing of the theoretical envelope

$$\lambda_e = a \sqrt{\frac{(\omega_2^2 - \omega_1^2)}{2\pi V_x}} \exp\left(-\frac{a^2}{2V_x}\right) \quad (28)$$

Where  $\omega_1$  is the mean frequency,  $\omega_2^2$  is the second moment of the spectral area, normalized by the variance of the process  $V_x$ ;  $a$  is the level of crossing. The derivation of this formula is trivial as the distribution of the envelope is Rayleigh and its derivative is normal.

For the very same reason, the Rayleigh distribution can be assumed for the rare solution. The upcrossing rate in the non-rare solution can be approximated as:

$$\xi = \exp(c_0 + c_1 a_1 + c_2 a_1^2) \quad (29)$$

For the purpose of numerical example the coefficients  $c_0$   $c_1$   $c_2$  are evaluated from statistics with a least-squares method.

For the very large level of crossings, it may also be possible to use formula (4); it may be so rare that crossing occurs only on one side.

All three these theoretical solutions, nevertheless, remain approximations. However comparisons with extrapolation results may be used as a very coarse verification. The comparison is shown in Figure 10 and confirms the ability of the proposed method to yield reasonable predictions with statistical extrapolation.

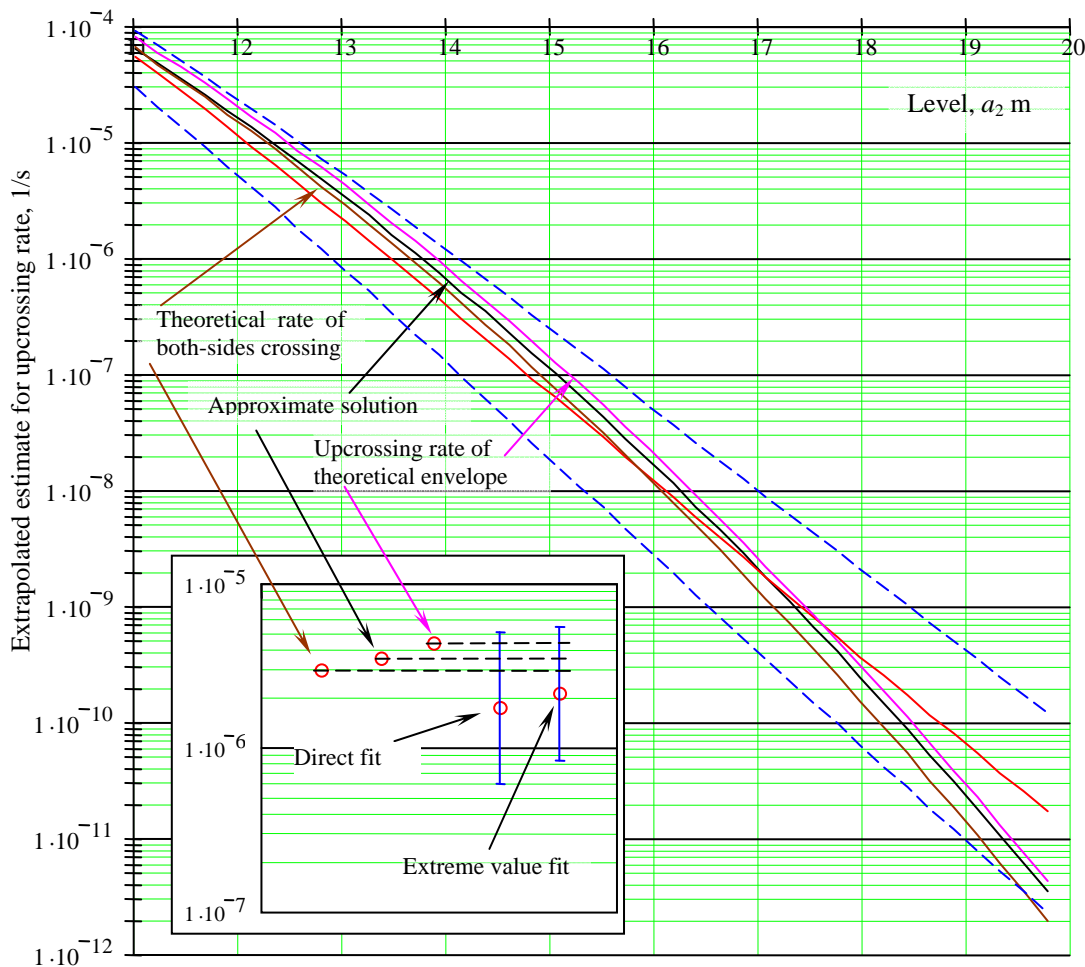


Figure 10 Averaged estimate of rate of upcrossing of the peak-based envelope extrapolated using extreme value distribution. Insert shows the extrapolation for the level of 13 m using both direct and extreme value fit of Weibull distribution.

## SUMMARY

The EPOT method offers several advances in the context of the direct assessment of partial stability failure. The use of the data exceeding the threshold accounts for the non-linearity of a ship's roll motion as the linear portion of the response does not dominate the distribution fit. Use of the envelope handles both port and starboard rolls ensuring the applicability of the Poisson Flow. The envelope also accounts for the dependence of subsequent roll cycles; this is important for narrow banded processes, such as roll motion of a ship operating in following and quartering seas.

The EPOT method can be used for the direct assessment of stability failures for ships. It may be used with simulation data as well as model tests data.

The EPOT method is still under development. Future work includes evaluating the performance of the algorithm when non-linearity of the roll response becomes severe, such as happens near the peak of the righting arm curve.

## ACKNOWLEDGEMENTS

The authors wish to thank J. Brown for his support and patience in bring this work to fruition. The authors are grateful to

Dr. Arthur Reed and Prof. Pol Spanos for their support and guidance in this work. The authors also wish to thank George Hazen for his insight and work in connecting extreme value theory with exceedance rate.

## REFERENCES

- Belenky, V. & A. Breuer (2007) Intact and Damage Stability of Ships and Offshore Structures—Bridging the Gap. *Proc. PRADS 2007*, Houston, Texas.
- Belenky, V. L. & N. B. Sevastianov (2007) *Stability and Safety of Ships: Risk of Capsizing*. SNAME, Jersey City, ISBN 0-939773-61-9
- Belenky, V., and Weems, K.M., (2008) "Procedure for probabilistic evaluation of large amplitude roll motions," *Proceedings of OC2008: Osaka Colloquium on Seakeeping and Stability of Ships*, Osaka, Japan
- Cohen, C. A. (1965) Maximum Likelihood Estimation in the Weibull Distribution Based on Complete and On Censored Samples. *Technometrics*, 7(4):579–588.
- Kramer, H. and Leadbetter, M.R. (1967). *Stationary and related stochastic processes*, John Wiley, New York
- Scott, D. W (1979) On Optimal and Data-based Histograms. *Biometrika*, 66(3):605–610

## Tolerable Capsize Risk of a Naval Vessel

Andrew Peters

QinetiQ, UK

### ABSTRACT

Many of the operations and duties conducted by naval ships involve a degree of risk. This risk is somewhat unavoidable due to the nature of operating a warship at sea, where operational requirements can put the vessel and crew in harms way. One of the hazards that the crew are subjected to while on operations is that of the weather.

The objective of this paper is to discuss the tolerable risk associated with the loss of a naval vessel due to the weather conditions. A review of tolerable risk and potential methodologies of calculating an annual probability of loss of the vessel which uses time domain simulations and statistics of observed weather conditions aboard naval ships are presented.

### KEYWORDS

Tolerable risk, Damage ships, Vessel loss.

### INTRODUCTION

Many of the operations and duties conducted by navies involve a certain degree of risk. This risk is somewhat unavoidable due to the nature of operating a naval vessel at sea, where operational requirements can put the vessel and crew in harms way. One of the continual hazards that the crew are subjected to whilst on operations is that of the weather.

Many navies, such as the UK's Royal Navy, now have a duty of care to ensure the level of risk they expose the ship's company to is commensurate with the benefits gained. It is this basis which is the principle of tolerable risk [1]. Navy ships are exposed to many hazards when at sea, like most commercially operated ships, but unlike commercial ships they may not be able to avoid heavy weather conditions due to operational requirements.

By using the theory and application of risk tolerability principles, as used by the UK's Health and Safety Executive (HSE) and adopted in most industries, an assessment of tolerable risk can be made [2]. This

methodology is available for any business that deals with risk to the workforce or to the general public, including the UK MoD. The UK MoD assess the tolerability of risks associated with all areas of military equipment and operations. These tolerability principles could be applied to provide a suitable tolerable risk for the annual capsizes risk of a naval vessel.

In 1990, the Cooperative Research Navies (CRNAV) Dynamic Stability group was established with the aim of deriving dynamic stability criteria for naval vessels. To derive such criteria, the group needed to evaluate in-service and new ship designs in moderate to extreme seas, in terms of their relative safety and probability of capsizes. This would ensure that new vessels continued to be safe, whilst avoiding high build and life-cycle costs associated with over-engineering.

To achieve these objectives, the numerical simulation program FREDYN was developed and continues to be applied extensively both to intact and damaged ships. This time-domain

program is able to take account of nonlinearities associated with drag forces, wave excitation forces, large-angle rigid-body dynamics and motion control devices. The current CRNAV group comprises of representatives from UK MoD, Naval Sea Systems Command (NAVSEA), the Australian, Canadian, French and the Netherlands navies, as well as the U.S. Coast Guard, Defence Research & Development Canada, (DRDC), Maritime Research Institute in the Netherlands (MARIN), Naval Surface Warfare Center Carderock Division (NSWCCD) and QinetiQ.

The objective of this paper is to discuss the concept of tolerable risk, which is the willingness to live with a risk so as to secure greater benefits. Using an accepted framework known as the Tolerability of Risk (TOR), decisions as to whether risks from an activity are unacceptable, tolerable or broadly acceptable can be made. These principles of tolerable risk are examined in association with the loss of a naval vessel due to the weather conditions.

### **BROAD PRINCIPLES OF RISK ASSESSEMENT**

Some may argue that any risk is unacceptable, but in reality the risk of suffering harm is an unavoidable part of living in the modern world. However, some risks can indeed be deemed acceptable for the following reasons [3]

- Threshold condition: A risk is perceived to be so small that it can be ignored.
- Status quo condition: A risk is uncontrollable or unavoidable without major disruption in lifestyle.
- Regulatory condition: A credible organisation with responsibility for health and safety has established an acceptable level of risk.
- De Facto condition: An historic level of risk continues to be acceptable.
- Voluntary balance condition: The benefits are deemed worth the risk by the risk taker.

In recent times there is an expectation for a society free from involuntary risk. The concept of risk is often used in everyday discussions where people often describe taking a risk in relation to taking a chance of adverse consequences to gain some benefit. Risk, however, is defined as ‘the combination of the likelihood and consequence of an unplanned event leading to loss or harm’ [1,2]. The way in which society treats risk depends upon the individual perception of how the risk relates to them. There are many factors involved and it is down to how well the process giving rise to the risk is understood, how equally the danger is distributed and how individuals can control their exposure [1]. Studies have shown that hazards give rise to concerns which can be put into two categories:

#### *Individual Concerns:*

This is associated with how the hazard affects an individual and all things that they value personally. Individuals are more likely to happily accept higher risks of hazards that they choose to accept rather than any hazards imposed upon them, unless they are considered negligible. If the risks provide benefits they will want the risks to be kept low and be controlled [2].

#### *Societal Concerns:*

This is the impact of hazards on society and if they were to happen would result in a socio-political response with repercussions for those responsible for controlling the hazard. These concerns are often associated with hazards that if they were to occur would cause significant damage and multiple fatalities. Examples would include Nuclear Power stations, rail travel and genetic engineering. Concerns due to multiple fatalities from a single event/effect are known as societal risk [2].

### **CHARACTERISING THE ISSUES IN TERMS OF RISK**

To examine the risk associated with the loss of a naval vessel the first stage must involve framing the issues relating to the risk. This will

result in characterising the risk both quantitatively and qualitatively to look at how it may occur and what effect it will have on those involved and society at large.

A risk assessment is normally conducted when characterising the issues affecting the risk, which includes identifying the hazards which would lead to harm, what the likelihood of it occurring would be and what harm and consequences would be experienced if it was to happen.

This stage of the assessment often assesses the individual risk and then moves to look at the effect on societal concerns to first identify if the hazards should be considered at all or could be regulated sufficiently.

The analysis of this for the loss of a naval vessel in heavy weather can be, in some cases, simplified in certain aspects. The outcome of a vessel capsizing in bad weather will inevitably result in the fatalities or extreme harm to the majority of the crew onboard and would result in the material loss of the platform. An event of this type leads towards examining the societal risk aspects due to the outcome resulting in multiple deaths and loss of a naval asset. The additional repercussions that the navy and government would have to deal with are also associated with societal risk.

### **TOLERABILITY PRINCIPLES**

Once a risk has been assessed it must be examined to identify if the level of the risk is broadly acceptable, tolerable or unacceptable and whether the hazard should be even considered. It is therefore not surprising that a lot of work in determining criteria for these acceptability levels has been conducted [2].

Criteria used by regulators in the health and safety field have shown that the criteria can fall into three ‘pure’ criteria [2]:

#### *Equity based criteria*

These have the premise that individuals have the unconditional right to a certain level of protection, i.e. which is usually acceptable in normal life. This often results in a level of risk that can not be exceeded. If the risk level after analysis is above this level and suitable control measures can not be introduced to lower the risk, the risk is deemed unacceptable. For naval vessels these criteria will be relevant.

#### *Utility based criteria*

These criteria apply to the comparison between incremental benefits of the measures to reduce the risk, the risk of injury and the costs of the benefit. These criteria therefore look at comparing, in monetary terms, the cost of the benefits (statistical lives saved) of the preventative measure compared to the cost of implementing it.

#### *Technology based criteria*

These criteria essentially reflect that a satisfactory level of risk is obtained when ‘state of the art’ measures are employed to control the risks. For a naval vessel this could include advanced heavy weather training or onboard operator guidance systems.

### **TOLERABILITY OF RISK**

These criteria described above can be used on their own although a combination is often a better approach. The HSE have incorporated them in a framework known as the Tolerability Of Risk. This methodology breaks the level of risk down into three regions. These are described in figure 1 with the ‘ALARP triangle’ and are described in detail as follows :

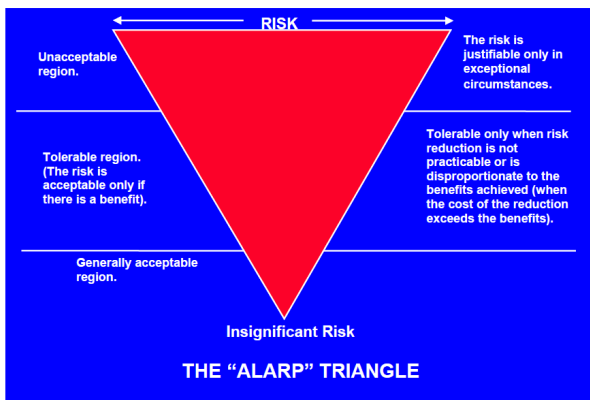


Figure 1 – ALARP triangle

*Broadly acceptable risk region*

Risks that fall into the broadly acceptable risk region are deemed insignificant. Regulators would not require any additional measures to reduce the risks further than they already are. Further actions would only be required if lowering the risk was practical or where there is a legal requirement to lower it further. Regulators are required to regularly monitor the risk to ensure that it remains in this region. The level of risk at this level is comparable to what people regard as insignificant or trivial in their day to day lives [2].

*Tolerable risk region (As Low As Reasonably Possible - ALARP)*

This region lies between the broadly acceptable and intolerable regions. Risks in this region relate to those risks that people are willing to tolerate in order to gain from the benefits. This means that the risk is deemed tolerable where society desires the benefits of the activity and only if further risk reduction is impracticable or the penalties are grossly disproportionate to the improvement gained. The levels of the risks must be assessed and the results used correctly to determine control measures. The assessment method must use the best available scientific knowledge [2].

*Intolerable risk region*

The risk in this region cannot be justified except in extraordinary circumstances. Control

measures are required to drive the risk downwards into one of the lower risk regions.

The aim for any activity would be to have the risks fall into the broadly acceptable region. However, the practicability of achieving this, for example with a naval vessel operating in open ocean conditions, may be difficult to achieve without unacceptable restrictions on the ship and operation. Therefore as the intolerable region by its nature can not be acceptable in anything but extraordinary circumstances, the As Low As Reasonably Possible (ALARP) region is realistic for naval vessels, with measures such as training and heavy weather guidance to assist in controlling the risk of capsize.

**TOLERABILITY LIMITS – INDIVIDUAL RISK BOUNDARIES**

The term ‘Individual risk’ is used to describe the level of risk of fatality of an individual that is exposed to a particular activity. UK HSE guidelines state that an annual 1 in a million probability of fatality is a very low level of risk and should be used to define the boundary between the broadly acceptable and the Tolerable regions of risk [2].

The UK HSE guidelines [2] for a hypothetical person exposed to hazards in the workplace have defined the maximum tolerable risk of fatality as 1 in 1000 per year ( $10^{-3}$ ) and 1 in 10000 ( $10^{-4}$ ) for the risk of fatality to a member of the general public. This is referred to as the basic safety limit and is the cumulative value of risk an individual is exposed to. This measure is applied to investigate the risk to a hypothetical worker working in a particular industry, such as offshore for example, and used to compare to levels in other industries. It provides a base line for comparison and assessment of changes to the level of risk.

Individual risk however can not be used on its own for larger events which, if they occur, will result in higher numbers of fatalities. Group risk or societal risk as it is commonly known is used to describe the relationship between the

probability of an unplanned event and the number of people affected by the event. It applies to those activities which present major implications for society such as a high number of fatalities, the loss of a major asset, environmental and political damage. Societal risk is not just calculated by taking the individual risk and multiplying it by the total number of fatalities from a single event, but is often complex and has many influences on its level.

### **TOLERABILITY LIMITS – SOCIETAL RISK BOUNDARIES**

For large events which impact on society as a whole, the societal risk will be the dominating factor rather than individual risks. Events which involve multiple fatalities will attract wide social interest and the societal risk encompasses both societal risk and society's reaction to an event.

When considering what society considers tolerable, there are several aspects which influence the response of society to the event and hence certain events are considered more tolerable than others. For example:

1. Acts by God or nature are considered more tolerable than those of human error.
2. Risks are more tolerable if we have control or have had participation in the decision leading to the risk e.g. car accidents are deemed more tolerable than aircraft accidents.
3. Risks are not tolerable if we cannot see the benefit for ourselves.
4. Familiarity makes a risk more tolerable. For example, a car accident is more tolerable than a nuclear radiation accident.
5. A large number of accidents spread over a fairly long period of time is more tolerable than a large number of incidents in close succession.
6. Less tolerable with risk towards the innocent and vulnerable.
7. Personal experience.

These and many other factors come into the society's response to an incident; particularly the knowledge of the hazard, whether the hazard was man made or natural and whether the potential victims are particularly vulnerable, e.g. children and the elderly [1].

Media coverage can significantly influence society's level of tolerability to a risk. For example, there are few car crashes reported in the press. However, aeroplane crashes or passenger ship accidents always are, when there are far fewer of these incidents. This makes society much more wary of ships and aeroplanes than driving a car.

The loss of a naval vessel due to capsizing in heavy weather would be classed as a significant event, due to the loss of a high proportion of the crew, the naval asset and the political damage associated with it. However, the hazard in this case is from nature and it is understood by society that naval personnel are exposed to greater risks whilst on operations, such as a search and rescue mission in heavy weather, and may accept a higher risk as being tolerable in that case.

The complexity of developing tolerable limits for events that would raise societal concerns is complex, so a way of conveying this information has been accepted. It uses the concept of FN curves, where the F denotes frequency and the N denotes the number of fatalities. These diagrams provide relationship data on the frequency of the fatal accident (plotted on the y axis) and the number of fatalities resulting from it (plotted on the x-axis). These curves can be used to graphically describe limits of risk acceptance. The curves can be generated by defining different combinations of consequence (i.e. fatalities) and the related frequency that gives negligible, acceptable and unacceptable risk respectively.

The UK HSE [2] have realised the complexity involved in analysing societal risk and have produced guidelines to define the acceptable borders between the tolerable and intolerable regions. This guidance is based on a FN criteria

point for a single accident which occurs with a frequency of  $2 \times 10^{-4}$  events per year (1 in 5000) which results in 50 fatalities. This result is then extended on the FN diagram by applying a line with a slope of -1, using logarithmic scales on both axes, which is then defined as the risk neutral line i.e. a linear relationship between frequency and consequence. The broadly accepted region is taken as 2 orders of magnitude below this criteria ( $<1$  in 500,000). These zones of tolerability are shown pictorially in figure 2. This FN diagram provides a framework in which to assess the risk tolerability of society of a particular event.

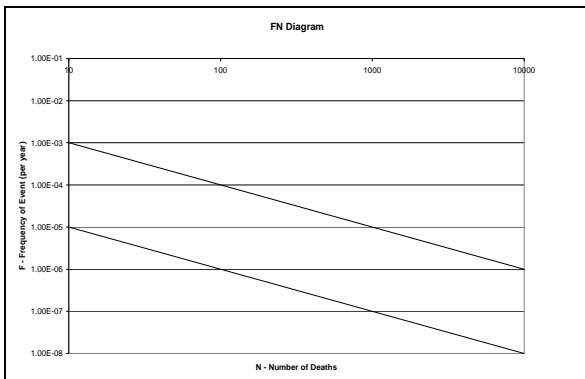


Figure 2 - FN diagram

In assessing an event such as the capsizing of a naval vessel, both the individual and societal risks need to be evaluated as they incorporate different concepts.

Excluding the other hazards that the crew onboard Royal Navy warships are exposed to in this study, the HSE guidelines can be used to assess what could be used as the tolerable risk of loss of a naval vessel.

### RISK ASSOCIATED WITH TRANSPORTATION

Examining various forms of transport, identifying how these industries deal with risk and what society deems acceptable allows direct comparison for what could be deemed acceptable to society for the maritime industry and naval vessels.

The risks involved in the air transportation industry are those which most people are aware of and accept when they fly. An accident survey of 1,843 aircraft accidents from 1950 through 2006 determined the causes of the accidents to be as follows:

- 53%: Pilot error
- 21%: Mechanical failure
- 11%: Weather
- 8%: Other human error (air traffic controller error, improper loading of aircraft, improper maintenance, fuel contamination, language miscommunication etc.)
- 6%: Sabotage (bombs, hijackings, shoot-downs)
- 1%: Other cause

(The survey excluded military, private, and charter aircraft.)

However, the risk of being involved in a crash on a single flight is, on average, 1 in 6 million [4,5], depending upon airline, in comparison to the likelihood of dying in a car journey of 1 in 5000. This means that for anyone flying, the individual is much more likely to die on the journey to the airport rather than during the flight itself. Fear of flying is common, mainly due to lack of personal control, understanding and the general concept of being at high altitude. People are perfectly happy to drive cars frequently, as they are in control and are happy to disregard the fact that there are 50,000 fatalities on highways every year. To put this into perspective, statistically a person would have to fly once a day every day for over 15,000 years in order to be involved in an aircraft accident.

When discussing modes of transport, there are a number of ways in which to define a fatality risk measure. The potential loss of life (PLL) measure is a basic measure of risk of fatality per year that is often used to define accident rates. However, this criterion has the short coming of not incorporating any exposure time into the measure. It is also important to make the distinction between individual and societal

risk. The most common risk measures for individual risk are the Average Individual Risk (AIR) and Fatal Accident Rate (FAR). The AIR measure is calculated by dividing the PLL measure by the number of people exposed e.g. the number of crew on a naval ship. The FAR measure is calculated by dividing the PLL value by the total number of man hours of exposure and multiplying by a  $10^8$  scaling factor. This gives the number of fatalities per  $10^8$  hours of exposure to the hazard.

These measures provide a good means of comparing risks from travelling by various modes of transport, as shown in table 1.

**Table 1 - Individual risk of fatality for transport modes**

<b>Travel Mode</b>	<b>Fatalities per <math>10^8</math> passenger KM</b>	<b>Fatalities per <math>10^8</math> passenger hour (FAR)</b>
Motorcycle	9.7	300
Bicycle	4.3	60
Foot	5.3	20
Car	0.4	15
Van	0.2	6.6
Bus/coach	0.04	0.1
Rail	0.1	4.8
Water	0.6	12
Air	0.03	15

As can be seen from table 1, travelling by sea is one of the least risky modes of transport. The FAR value can be calculated for travelling on UK ferries and is 8.8 fatalities per  $10^8$  hours of exposure [6]. Compared to the other modes of

transport, UK ferries can be seen to be one of the safest forms of transport.

Regarding the risk of capsizing of a navy vessel, consideration should be made to the exposure time and particularly the exposure to the heavy weather conditions where capsizing is more likely to occur.

Other areas of the marine industry and other wider industries can be used to provide further comparison of the level of risk a person working in that industry is exposed to during their working life. These results for wider industry provide an indication to what society generally regards as acceptable.

The UK HSE [7] provides statistics comparing the risk of fatalities in various UK industries, table 2:

**Table 2 - Individual risk of fatality in UK Industries**

<b>Industry</b>	<b>Annual Individual Risk of Fatality</b>
Agriculture	$8.10 \times 10^{-5}$
Construction	$3.70 \times 10^{-5}$
Offshore	$4.00 \times 10^{-5}$
Services	$0.35 \times 10^{-5}$

These UK statistics are lower when compared with statistics from other parts of the world, table 3 [6].

**Table 3 - Individual risk of fatality in industries worldwide**

Industrial Activity	Fatalities per 1000 worker-years
Mining	0.9 - 1.4
Construction	0.3
Industry	0.15
Shipping	1.9 – 2.1
Fishing on the Continental self	2.3
Fishing	1.5

These statistics illustrate that the highest individual risks in UK industry are generally around  $10^{-5}$  -  $10^{-4}$  fatalities per year, compared to the  $10^{-3}$  to  $10^{-4}$  level for industries worldwide which are at the tolerable limit defined by the UK HSE.

Over the last few decades, extensive resources have been used to reduce the risks involved with the shipping industry. The long term trend of loss frequency has been studied [8] and it was concluded that the annual loss rate had been reduced by a factor of 10 in the twentieth century, from more than 3% in 1900 down to 0.3% in 1990. However, the greatest level of reduction was early in the century and the level of reduction has levelled off in recent years.

Investigations into the risk of loss of merchant vessels using Lloyd’s world casualty statistics has been conducted [9]. In that study, the total loss rate for different types of merchant ships are analysed, table 4.

**Table 4 – Commercial vessel annual risk of vessel loss**

Vessel Type	Total loss rate (per 1000 ship years)	Annual probability of ship loss
General Cargo	5.4	$5.4 \times 10^{-3}$
Bulk Dry	3.3	$3.3 \times 10^{-3}$
Oil Tanker	1.5	$1.5 \times 10^{-3}$

On examination of fatalities from the loss of these different vessel types, it was found that there were 170 fatalities per year on general cargo ships that were lost. This relates to 1.8 deaths for every complete vessel loss. Taking the typical number of crew on this type of vessel, the individual risk of death for a general cargo ship crew member is calculated as  $3.7 \times 10^{-4}$  [9]. This is the highest of the vessel types, with many of the other vessel types having a probability of individual risk of death close to the  $1 \times 10^{-4}$  level. RoRo passenger vessels were found to have a individual death risk of  $7 \times 10^{-5}$ . The relatively large public focus on marine accidents reflects society’s considerable awareness of these fatalities.

As described above, regarding multiple fatalities and societal risk, an FN diagram is often used to convey acceptable risk levels for events with multiple fatalities. However, the FN diagram can be used to describe both required and the prescribed risk levels.

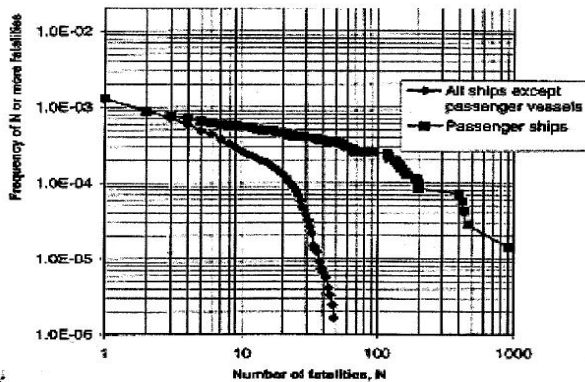


Figure 3 – Frequency of accidents involving  $N$  or more fatalities DNV 1998 [10]

Figure 3 is based on data from DNV in 1998, which shows the observed FN values for passenger ship accidents (upper curve) and cargo ships accidents (lower curve). For the passenger ships, it can be seen that small single fatality incidents occur with a frequency of approximately  $10^{-3}$  per year, whereas an extreme casualty event (approximately 1000 casualties) occur with a frequency of  $10^{-5}$  per year.

### TOLERABLE CAPSIZE RISK OF A NAVAL VESSEL

It cannot be assumed that the loss of a frigate from capsizing would result in an approximate 10% fatality rate among the crew onboard, as found in the commercial vessels statistics. As the duty stations of the crew on naval ships are distributed throughout the vessel, many are below the weather deck which is quite different to commercial vessels where the majority of the crew will be in the vessel's superstructures. It therefore can be assumed that the loss of at least 50% of the crew would be a more realistic value, as the crew stationed below 2 deck on a frigate would be unlikely to escape if the vessel capsized.

From the commercial vessel statistics, the probability of loss of the vessel is in the order of  $10^{-3}$ , table 1. This is just within the tolerable region, with up to 10 fatalities from any incident. From the loss of the general cargo vessels, the average fatality rate has been found to be 1.8 deaths per vessel loss. For the capsizing

of a naval vessel the number of fatalities would be significantly higher.

The FN diagram statistics for passenger ships, figure 3, show a probability of  $8.5 \times 10^{-3}$  for 100 fatalities and  $1 \times 10^{-4}$  for 200 fatalities per year. A passenger ship could be considered to be similar to a naval vessel, as there are a high number of personnel onboard compared to a cargo ship. As this is the observed level of probability, it could be taken that this is acceptable to society, as it is a historically accepted level of risk.

From the risk analysis, it is clear that the capsizing of a naval vessel will result in a significant number of fatalities, as a medium sized vessel (such as a frigate) could have approximately 200 crew members. Based on the HSE tolerability limits, this would require the probability of the loss of the ship to be  $6 \times 10^{-5}$  per year to be within the tolerable region. This is slightly higher than the credible failure risk assumed for submarines, which is taken as a minimum of  $10^{-6}$  for a 90 day patrol, where a failure event will also likely result in the fatalities of the entire crew [11]. This  $10^{-6}$  value is on the tolerable and generally acceptable regions boundary of the UK HSE FN diagram.

Having around 100 fatalities (50% of a frigate crew) in the tolerable risk region would require an annual probability vessel loss of less than  $1 \times 10^{-4}$ . The generally acceptable region would require annual probability of loss of less than  $1 \times 10^{-6}$ . This would also result in an individual risk to the crew members at a similar magnitude as other areas of the marine and wider UK industry.

Considering all these points, it is suggested that a tolerable region boundary of  $1 \times 10^{-4}$  would be a suitable level for the annual risk of loss of a navy vessel in heavy weather and would be comparable to other areas of the marine industry and other major events. A value of  $1 \times 10^{-4}$  annual capsizing risk was therefore found to be a suitable level for the tolerable risk boundary for the loss of a naval frigate at sea.

However, the manner in which extremely rare independent events are combined adds a final additional complexity to the problem, as probability theory has the combined probability of different independent events defined as the sum of the independent risks. This suggests that the other potential risks of loss of the ship and crew at sea should therefore be considered and subtracted from the  $1 \times 10^{-4}$  risk level to produce the tolerable limit of annual loss of the frigate and crew due to capsize. If these other potential risks have a probability of occurrence that is several orders of magnitude lower than the vessel capsizing, then tolerable risk value presented could still be closely related to that of the vessel capsizing. In a similar way to capsizing, naval vessels have almost never been known to be totally lost to fire, for example, while at sea (in peace time in recent years). Further investigation is required to identify the other potential risks of loss for a warship while at sea to identify how these risks realistically combine to produce an overall capsize risk that compares with other areas of industry.

### ASSESSING THE RISK OF CAPSIZE OF A NAVAL VESSEL

Assessment of the probability of a vessel capsizing is a significant aspect of assessing the risk. Calculating the probability of the vessel capsizing can be conducted with modern computational tools, such as FREDYN, which can model a vessel in extreme wind and waves. However, there are many areas of uncertainty that are inherent in the calculations that require careful consideration.

In order to accurately calculate the capsize probability of a naval vessel, a simulation tool is required to examine all possibilities of sea state and operational loading conditions to provide assessment of all realistic operational scenarios. The numerical simulation program FREDYN was developed by the Maritime Research Institute Netherlands (MARIN) for the Cooperative Research Navies working group and continues to be applied extensively to both intact and damaged ships. This time-

domain program is able to take account of nonlinearities associated with drag forces, wave excitation forces, large-angle rigid-body dynamics and motion control devices. The FREDYN program permits investigations into the dynamics of intact and damaged vessels operating in realistic environments.

### CALCULATION OF ANNUAL CAPSIZE RISK PROBABILITY

FREDYN simulations can be used to evaluate the critical roll (capsize) behaviour of a vessel in a range of realistic operating load conditions. This procedure was developed by McTaggart [12] in 2002 and is described further in his paper [13]. The method, adopted by the CRN working group, is largely based upon the method described fully in his report [12] and is used for evaluating capsize risk of intact ships in random seas. This approach for predicting ship capsize risk combines the time domain simulation program FREDYN with probabilistic input data for wave conditions and ship operations (speed and heading). For a ship in a seaway of duration  $D$  (e.g. 1 hour) the probability of capsize  $P(C_D)$  is:

$$P(C_D) = \sum_{i=1}^{N_v} \sum_{j=1}^{N_\beta} \sum_{k=1}^{N_{H_s}} \sum_{l=1}^{N_{T_p}} P_v(v_{s,i}) P_\beta(\beta_j) P_{H_s, T_p}(H_{s,k} T_{p,l}) P(C_D | V_s, \beta, H_s, T_p) \quad (1)$$

Where:  $V_s$  = ship speed,  $\beta$  = wave heading relative to ship,  $H_s$  = wave significant height,  $T_p$  = wave modal period.

The last term is a conditional probability of capsize in a given wave condition and ship heading relative to the waves.

Limited Gumbel distributions are used to fit to the maximum roll angles recorded in each of the seaway conditions, in order to calculate the capsize probabilities. A second, distribution free method, is also possible and was investigated with a new set of data calculated in a recent study. However, the limited Gumbel

distributions have been shown by members of the CRN group to provide the best data fit and better predictions at the higher roll angles, which is the area of most interest for capsizing prediction [12]. The Gumbel fit uses the upper 30 degree range of the simulation and fits to a minimum of 10 data points. This work was validated on large numbers of simulations (400+) by McTaggart [12]. However this number of runs was not feasible for any routine calculations, as the time to compute would be very lengthy. Realistically, the number of simulations has to be between 10-50. The sensitivity of using this number of runs was also investigated by McTaggart and was shown to give very good results [12]. Recent studies with the CRN group have shown that for other frigate types there may be a need for a greater number of simulations to produce statistically reliable results. Current investigations by CRN members are onward to identify if using the peaks over threshold methodology produces better fidelity of results, as the roll motion peaks during the whole simulation are used in the calculation of the capsizing probability rather than just the maximum roll angle in each simulation.

The probability of capsizing is calculated based on a time period of 1 hour and can be computed using equation 1. The associated annual probability of capsizing can be calculated from the following equation, using the 1 hour capsizing risk [7]:

$$P(C_{annual}) = 1 - [1 - P(C_D)]^{\alpha \times 1 \text{ year} / D} \quad (2)$$

Where  $\alpha$  is the fraction of time spent at sea and  $D$  is duration (hours).

### UNCERTAINTY IN RISK CALCULATION

In the assessment of uncertainty and the application of safety factors to areas of uncertainty, HSE recommends making use of sensitivity analysis and comparative risk

assessments for novel hazards that have a similarity to the case under investigation [2]. In the engineering world, safety factors are calculated to take into account the uncertainties in materials, calculation methods, etc. This principle is particularly exploited in the world of ship structures. In general engineering, safety factors between 1.25 and 5 are often used, dependant on the level of knowledge and uncertainty of the material and the environment, stress and load a structure is to be subjected to. The aerospace and automotive industry use factors in the region of 1.15 and 1.25, due to the costs associated with structural weight. The testing and quality control is also higher in these industries, with significant modelling (computationally and physically) of the material stresses involved.

The submarine world uses safety factors of a similar magnitude to the aerospace world, with significant physical and computational models used to ensure accurate understanding of the influences.

When assessing risks, it is usually required for uncertainty in the calculations to be taken into account when there is lack of, or incomplete data [2].

When examining the risk of loss of a naval vessel, the uncertainty in the outcome of the event i.e. what would happen if the vessel was to capsize, is actually very low due to the fact that it would result in the inevitable total loss of the vessel and a large number of the crew onboard. However, the uncertainty associated with the calculation of the probability of the event occurring is greater and must be adequately handled in order to calculate realistic values of risk for the vessel.

Knowledge uncertainty is one of the areas that must be dealt with [2]. This occurs when there are sparse statistics or random errors; for example, in experiment data used to define the probability of the event occurring [2]. Although many commercial vessels are lost each year and the statistics are available, in the case of the loss of a naval vessel in heavy

weather, the statistics are very sparse and mainly representative of outdated designs of hullforms.

Modelling uncertainty is the term given to the uncertainties in the mathematical terms used in a numerical model used to assess risks. This is also closely linked with limited predictability associated with an outcome that is sensitive to the assumed initial conditions of the system under investigation and affects the final state i.e. the initial conditions of the ship affecting whether it capsizes in a certain wave condition or not.

It is clear that there are potential levels of uncertainty in the modelling of the risk of loss of a naval vessel using simulation tools such as FREDYN. Some of the main areas of uncertainty are related to the following:

- The probability of the vessel being in the waves and level of exposure.
- The probability of the speed and heading combinations in heavy weather.
- The simulation time i.e. the length of time the ship is in the waves.
- The number of simulations used in the prediction of the capsize event.
- The vessel loading condition.
- The angle used to define the capsize event.
- The autopilot in the simulations.
- Roll damping characteristics.

Techniques have been developed under what is defined as the ‘precautionary principle’ to handle uncertainty when dealing with calculating risk [2]. Uncertainty can be overcome by constructing the most credible scenarios of how the hazards might be realised.

#### *Sensitivity of the annual capsize risk calculation*

The variables listed above, which are input parameters into the FREDYN capsize simulations, can be investigated using standard sensitivity type approach to assess the

sensitivity of the inputs on the output probability of the capsize event. This would allow scenarios from the most likely to the worst case to be established and allow suitable safety factors to be derived and accounted for in the assessments.

The probability of the vessel being in the waves can cause unrealistically high probabilities of capsize by using the equation 2. A Bales wave climate statistics table [14] for the North Atlantic is often used to provide the probability of the waves occurring during the year, which is multiplied by the probability of the capsize event in those conditions. This can cause an unrealistically high annual probability of loss of the vessel, as the probability of the largest waves occurring with a high probability of loss of the vessel have a large influence on the overall annual capsize risk.

The capsize risk associated with the current calculations suggests that the probability of the vessel actually encountering the worst sea conditions is over estimated in the scenarios. A more realistic probability of the vessel encountering the waves is required.

A study was made for the UK MoD [15] which analysed the wave condition records made by the RN bridge teams in the 6 hourly records, which are kept by all Royal Navy ships whilst at sea. This data was collected for 78 Royal Navy vessels from 1968 to the present day. The data was also analysed from 1985 to the present day, to reflect the change in conditions encountered following the end of the cold war. This equates to over 168 years of Royal Naval ships at sea, which provides a substantial data set of more realistic wave statistics for the calculation of an annual capsize risk.

Using this wave height data and the Bales wave scatter table to provide the distribution of wave periods at each wave height condition resulted in a factored wave scatter table with a more realistic probability distribution for the vessel encountering the waves in a year. The change in probability distribution of wave height from

the new data compared to the standard Bales scatter table is shown in figure 4 below:-

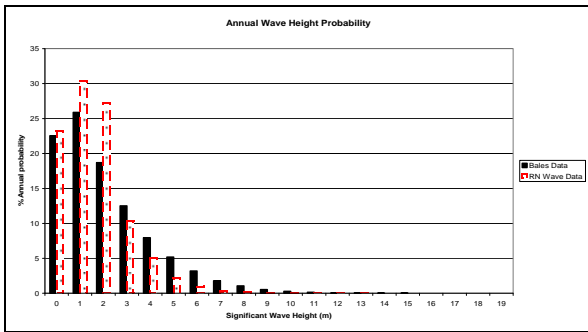


Figure 4 – Wave Height Probability of Encounter

It is clear from figure 4 that there is a distinct difference in the distribution of the wave height data that vessels have historically encountered compared to the annual probability of the waves occurring. The main significant factor is that the Royal Navy ships do not historically experience the larger waves as the standard annual wave statistics would suggest. This could be partly due to avoiding storms in certain cases, but not completely.

In equation 2 above for the calculation of the annual capsizes risk, the hourly capsizes risk that is generated from the simulations is effectively extrapolated up for each hour the vessel spends at sea. In the moderate wave heights, the maximum roll angles that are recorded are used to predict the probability of exceeding the 70 degree capsizes angle. The wave height conditions recorded on the navy ships are made every 6 hours, which is also a realistic time frame for a large storm sea to remain relatively constant. Calculating results for the probability of capsizes over 6 hours simulations may provide better results, which would equal the time between measurements made onboard. With a naval ship at sea approximately 30% of the year this equates to 440 6hr time periods.

To evaluate the effect of the simulation time, a number of calculations have been performed with different simulation run lengths, from 30 minutes to 6 hours, as well as different numbers of realisations between 10 and 50.

The results show that the effects on the annual capsizes risk are very small after 2 hours of simulation and increasing the number of simulations makes little difference to the annual capsizes risk at this run length, figure 3. This shows that this has little effect on the probability of the capsizes event for this vessel. A wider study is required to identify if this is the same for other vessels and load conditions.

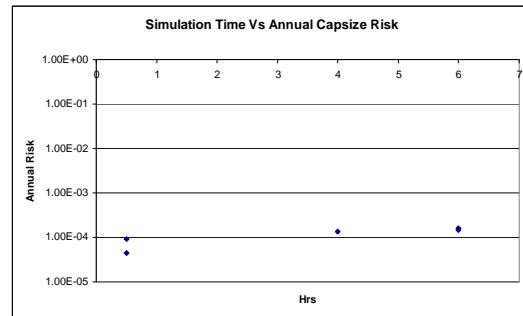


Figure 3 – Effect of simulation time on annual capsizes risk

The selection of the ship speeds can have a large effect on the capsizes risk and unrealistic speeds should be avoided in the simulations. To achieve the most realistic annual capsizes probability, the actual operation of the ship in heavy weather is required to be accounted for in the calculations. Standard heavy weather seamanship training instructs operators to not go faster than 60% wave speed in heavy weather. This means that the vessel speed selection should be made as realistic as possible. Selecting speeds above 90% wave speed (30% safety factor for the operator) is unrealistic and will result in unrealistic capsizes probabilities.

An even probability of heading is also usually assumed for the simulations. This could be considered to be precautionary, as in the very worst conditions the operator would avoid stern sea condition based on their experience, which is difficult to account for. Variation in the risk should be reviewed by removing certain headings, such as stern seas in the worst wave conditions. Selecting the accurate point this decision is made will require further discussion with operator training schools.

The roll damping characteristics of the model in the simulation will require investigation as to how it effects the risk calculation. The damping characteristics will be required to be set up as close as possible to the real vessel by comparing roll decay and roll period information. A systematic variation of the damping input parameters would provide the influence of the results to a specified variation of the damping characteristics. A suitable safety factor could then be derived to account for the variation on the modelling of the roll damping.

The autopilot control in the simulation will have an effect on the survival of the vessel. Using a systematic variation of the autopilot control parameters, the variation in risk could be derived based on those changes to the autopilot. A factor could then be derived based on the variation of the autopilot parameters.

The load condition of the vessel also needs to be considered in the annual capsizing probability, as a vessel in a deep loading condition will often be inherently safer than in a light seagoing condition. It is therefore important to calculate at least two load conditions and use the typical operational profile to define the time the vessel would spend at each loading condition. This can then be realistically accounted for in the annual capsizing probability. Operational procedures to ballast down with the forecast of heavy weather should also be accounted for in the calculations.

## CONCLUSIONS

In reviewing current Health and Safety guidelines, along with comparison with other modes of transport, other industries and the commercial marine industry guidelines for individual and societal risk have been described and can be used to examine the acceptable level of risk for capsizing in heavy weather for the loss of a naval vessel. A value of  $1 \times 10^{-4}$  annual capsizing risk was found to be a suitable level for the tolerable risk boundary for the loss of a naval frigate at sea. The magnitudes and method of combining other

very low risks of loss of the ship and crew at sea, needs to be further investigated and considered in defining the tolerable limit of annual capsizing loss. If the other potential risks of vessel loss are found to be several orders of magnitude lower probability of occurring than the vessel capsizing, then the tolerable risk value presented will still relate predominantly to that of the vessel capsizing. Therefore, this could provide an overall capsizing risk that can be compared with other areas of industry.

In order to calculate suitable levels of capsizing risk, sensitivity analysis is required to assess the input parameters to identify the most realistic scenarios and the potential variation in the capsizing risk due to realistic variation of the input parameters. By undertaking this analysis, realistic risk levels and safety factors can be calculated to evaluate the annual capsizing risk of a naval vessel for comparison with the tolerable risk level deduced.

## ACKNOWLEDGMENTS

The author would like to gratefully acknowledge the permission granted by the CRNAV working group for publishing this investigation.

## REFERENCES

- [1] Tolerability Principles – Warships in Harbour, MoD internal publication
- [2] HSE Reducing Risks, Protecting People, Crown Copyright 2001
- [3] Rowe W.D Acceptable levels of Risk for Undertakings. Colloquium Ship Collisions with Bridges and Offshore Structures . Copenhagen.
- [4] [http://www.livescience.com/environment/050106\\_odds\\_of\\_dying.html](http://www.livescience.com/environment/050106_odds_of_dying.html)
- [5] <http://winter-travel.org/travel-news/risk-of-dying-in-plane-crash-compared-to-other-activities/>
- [6] Kristiansen, S, Maritime Transportation, Safety Managements and Risk Analysis, 2005
- [7] HSE Website Statistics 2009

- [8] Lacaster J, Engineering Catastrophies : Cause and Effect of Major Accidents, 1996
- [9] MSC 77/25/4 Comparison of general cargo ship losses and fatalities- 2003 - RINA
- [10] DNV 1998, FSA of passenger vessels Report no. 97-2503
- [11] MAP 01-73 UKMoD
- [12] McTaggart K.A, 'Ship Capsize Risk in a Seaway using fitted Distributions to Roll Maxima, May 2000, Transactions of ASME, Journal of Offshore Mechanics and Artic Engineering.
- [13] McTaggart K.A, DeKat J.O 'Capsize Risk of Intact Frigates in Irregular Seas', SNAME Transactions 2000.
- [14] Bales S.L, Lee, W.T. and Voelker J.M. (1981) Standardised Wave and Wind Environments for NATO Operational Areas
- [15] 40 years of wave conditions, BMT report 2006



## **Climatic Spectra and Long-Term Risk Assessment**

Alexander B. Degtyarev

Professor, St.Petersburg State University, Russia

Vladimir V. Mareev

Associate Professor, St.Petersburg State University, Russia

### **ABSTRACT**

Modern information technologies enable a radically different approach to research on the dynamical behavior of complex marine objects. In order to utilize high-performance computational architectures effectively, it is necessary to consider alternative approaches to the mathematical formulation of these problems. In particular, new statements of a problem can be formulated which were senseless earlier, but now appear effective with these computational environments. This paper considers the problem of code development, based on potential flow formulations. It is shown that a new approach for obtaining the pressure-field in time-domain simulations could be very effective for long-term risk assessment.

### **KEYWORDS**

ARM of wind waves; long-term ship motion simulation; high-performance computer architectures.

### **INTRODUCTION**

Long-term risk estimation for operations in various regions of the Ocean demands the reliable consideration of the behavior of objects in specific sea areas during particular seasons, or periods, of operation. An integrated approach for the description of external excitations, on the basis of spectral approximations which account for a small amount of characteristics (more often in this aspect significant wave height and less often the average period is also considered), can result in the underestimation of risk and the loss of essential features of the estimated region. It is quite clear that the wind wave spectrum, with a particular significant wave height, will vary both for geographic location (e.g Black Sea and North Sea), resulting in different responses for the same object. Even greater variability result if we consider the wave regime – storm characteristics, superposition of different wave systems, alternation of

storms and quiet weather, etc. The qualitative consequences of failing to consider these characteristics are shown in Boukhanovsky et al. (2000).

However, earlier risk estimation methods, from probability theory, and forecasting of rare events were applied exclusively. Statistical data were used only to provide estimations of one or other likelihood characteristics (moments, correlations, laws of distribution). The continued development of powerful computer resources allows one to consider alternative approaches to this problem. Such resources enable the consideration of these problems from other approaches than just the traditionally known mathematical methods. Now, the absolutely separate direction of complex problems may be considered to obtain solutions. Mapping of the problems onto particular computer architectures, especially parallel or distributed, dictates which methods are appropriate for a specific problem decision. Compared to traditional rea-

soning approaches (consecutive and analytical) this may seem a little bit unusual. Let us consider the general approach to the problem of computing the long-term pressure distribution under the wave surface, in both the spatial and time-domain.

### STATEMENT OF THE PROBLEM

The most general description of behavior of a sea object under the action of waves may be obtained by solving the Navier-Stokes equation with traditional boundary conditions on the wave surface and the submerged portion of the body. Because the formation of waves is practically completely determined by gravitational forces, and the influence of viscosity is important to consider close to a surface of a body, in naval hydrodynamics potential flow formulations are traditionally used.

Let us follow the assumption that wave motion is irrotational and can be described by only the wave potential. In this case, the general problem is formulated by the following equation and boundary conditions:

$$\Delta\varphi = 0$$

$$\frac{\partial\varphi}{\partial t} + \frac{1}{2}\left(\left(\frac{\partial\varphi}{\partial x}\right)^2 + \left(\frac{\partial\varphi}{\partial y}\right)^2 + \left(\frac{\partial\varphi}{\partial z}\right)^2\right) + g\zeta = p_0 \quad (1)$$

$$\frac{\partial\zeta}{\partial t} + \frac{\partial\zeta}{\partial x}\frac{\partial\varphi}{\partial x} + \frac{\partial\zeta}{\partial y}\frac{\partial\varphi}{\partial y} = \frac{\partial\varphi}{\partial z} \quad \text{at } z = \zeta$$

where  $\zeta(x,y,t)$  is the free surface,  $\varphi$  is the wave potential, and  $p_0$  is the atmosphere pressure

The determination of the spatio-temporal distribution of the potential (to be exact, its derivatives) around the investigated object enables the determination of the field of hydrodynamic pressures, which when integrated on the body gives the forces and moments necessary for modeling ship behavior.

$$p(\mathbf{r}) = -\rho\frac{\partial\varphi}{\partial t}\Big|_{\mathbf{r}} - \rho g z_0 - \frac{\rho}{2}\left(\left(\frac{\partial\varphi}{\partial x}\Big|_{\mathbf{r}}\right)^2 + \left(\frac{\partial\varphi}{\partial y}\Big|_{\mathbf{r}}\right)^2 + \left(\frac{\partial\varphi}{\partial z}\Big|_{\mathbf{r}}\right)^2\right)$$

$$\mathbf{F} = -\int_{S_0} p \cdot \mathbf{n} dS$$

$$\mathbf{M} = -\int_{S_0} p \cdot (\mathbf{r} \times \mathbf{n}) dS'$$

where  $S_0$  is the wetted ship surface,  $\mathbf{n}$  is the outward normal vector, and  $\mathbf{r} = \{x_0, y_0, z_0\}$  is a radius-vector of the wetted ship surface.

Eq. (1) is the linear problem with nonlinear boundary conditions and an unknown boundary. The last aspect makes the problem very difficult.

Therefore, the general solution for the potential is obtained only in some special cases, and first of all only for a sinusoidal wave. Accounting for the randomness of waves makes the analytical solution of the potential for a stochastic problem practically useless for applications in problems of naval hydrodynamics.

In both cases the unknown border,  $\zeta(x, y, t)$ , is defined in the process of the problem solution. For example, in the linear definition of the problem

$$\zeta(x, y, t) = -\frac{1}{g} \frac{\partial\varphi}{\partial t},$$

where the derivative of the potential with respect to time is considered on an unperturbed wave surface. Therefore, in practice other approaches are applied.

### COMPUTATIONAL APPROACH: MAPPING OF THE PROBLEM

On the other hand, the problem (1) could be seriously simplified if the spatio-temporal realization of random wave field is known *a priori*. From the analytical point of view, it does not give any special advantages, but for direct modeling it permits the development of effective computing procedures. The question of reconstructing random spatio-temporal wave-fields depends on its hydrodynamic adequacy, i.e. the waves simulated by any others means should fit the physical laws presented in problem (1). At the same time, such a wave model should be effective from computational point-of-view and enable one to reproduce not only a stationary wave process, but also the evolution of waves in time.

We can consider as one of criteria for assessing the hydrodynamic adequacy of the generated random wave-field, corresponding to natural observations, the statistical wave characteristics which are not used as input data for the wave generation procedure. For example, if we use the correlation surface only, its frequency directed spectrum, for free-surface generation, after statistical processing of the model realization we should obtain both the higher moments and laws of distribution for the other wave elements.

It has been shown that it is possible to obtain such a result in the specification of a model using the classical scheme of autoregression – the moving mean (Davidan 1988; Rozhkov and Trapeznikov 1990). Such a wave model is in the form of a class of linear differential systems with distributed parameters and a random input signal of type of a field of white noise:

$$\left[ \prod_{k=1}^N L_k \right] \zeta(\mathbf{v}) = \left[ \prod_{k=1}^N Q_k \right] \varepsilon(\mathbf{v}), \quad (2)$$

where  $L, Q$  are differential operators.

Stationary solutions of the differential equations of type (2) define a class of random fields with the generalized rational spectral density:

$$S_{\zeta}(\vec{\omega}) = \frac{1}{2\pi} \frac{\left| \sum_{j_1=0}^{P_1} \dots (N) \dots \sum_{j_n=0}^{P_n} C_{[j_1 \dots j_n]} i^{\sum j_m} \prod_{k=1}^N \omega_k^{j_k} \right|^2}{\left| \sum_{j_1=0}^{N_1} \dots (N) \dots \sum_{j_n=0}^{N_n} B_{[j_1 \dots j_n]} i^{\sum j_m} \prod_{k=1}^N \omega_k^{j_k} \right|^2} \quad (3)$$

Thus it is possible to show that the model of three-dimensional waves, traditionally put into practice offered by Longuet-Higgins, represents model of a moving mean. Therefore, in the limiting case, both of the considered approaches could be considered as equivalent. However, the field model of moving mean has weak convergence. Because of computing difficulties for the application of Longuet-Higgins model for sea waves generation (especially three-dimensional), the combined model of au-

toression can be used to establish a nonlinear procedure for parameter assessment.

Therefore, the field autoregressive model is more attractive, and can better characterize the processes. It is known, that the procedure of a moving mean is the best way which is applicable for processes with uniform spectral density, whereas autoregression model is more suitable for processes with strongly pronounced peaks (Box and Jenkins 1970).

For the proper development of a computing process for the model, it is necessary to transition from a continuous model to a model with discrete arguments. So, for example, a finite-difference equation of wave can be defined as

$$\zeta_{(x,y,t)} = \sum_{i=0}^{N_x} \sum_{j=0}^{N_y} \sum_{k=0}^{N_t} \Theta_{(i,j,k)} \zeta_{(x-i,y-j,t-k)} + \varepsilon_{(x,y,t)} \quad (4)$$

where  $\Theta(i,j,k)$  are generalized coefficients of autoregression and  $\varepsilon(x,y,t)$  is a field of white noise.

Procedures for autoregression parameters and the variance of white noise field assessment are developed based on a generalized Yule-Walker equations system:

$$K_{\zeta}(x, y, \tau) = \sum_{i=0}^{N_x} \sum_{j=0}^{N_y} \sum_{k=0}^{N_t} \Theta_{i,j,k} K_{\zeta}(x-i\Delta_x, y-j\Delta_y, \tau-k\Delta_t) \quad (5)$$

The variance of the white noise field can be determined from equation (5), when  $i,j,k=0$ :

$$\sigma_{\varepsilon}^2 = D[\zeta] - \sum_{i=0}^{N_x} \sum_{j=0}^{N_y} \sum_{k=0}^{N_t} \Theta_{i,j,k} K_{\zeta}(i\Delta_x, j\Delta_y, k\Delta_t) \quad (6)$$

It is possible to see from (4) that the autoregressive model is capable of modeling ergodically, at minimal computing expense, a periodic realization of a random process, which its stochasticity is limited only by the period of the pseudo-random number generator. Additionally, the model does not use the property of the likelihood of convergence, Gaussian assumption, as, for example, Longuet-Higgins model

or other known models. It allows effective application to the research of extreme events, both in oceanography, and in naval hydrodynamics. It is also important that, on the basis of linear inertial transformation, the model can be used to easily construct nonlinear inertia-less transformations to any law of distribution.

In Degtyarev and Boukhanovsky (1996) it is shown that this model is hydrodynamically adequate, as compared to natural conditions. For the verification of the field autoregressive model, a series of tests for complete analysis of wind and complex sea has been carried out. In addition, the analysis of wind-wave evolution in storm and with spatially non-uniform current was carried out. The latter showed that the autoregression model, together with nonlinear inertia-less transformation (Degtyarev and Boukhanovsky 1996; Boukhanovsky et al. 2000) can successively reproduce nonlinear wind-waves when the distribution law of ordinates is distinct from normal.

As a test, simulated aerial images were used (Degtyarev and Boukhanovsky 1996). Statistical characteristic of the visible waves were used for verification. The criterion of verification was the agreement of the cdf and the joint distributions and conditional moment curves between the measured waves and simulated waves.

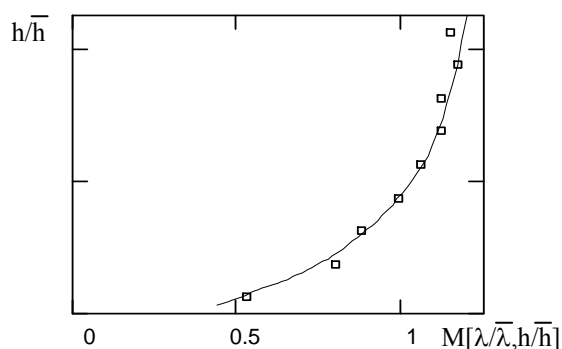


Fig. 1: Regression of lengths and heights of waves.  $\square$  – model, line – experiment

All experimental results concerning the distributions of visible wave's elements have been confirmed. In particular, the characteristic form of a curve of the conditional variance of wave-lengths from their heights (Fig. 2) has been

presented. Such agreement cannot be achieved by any of known ways of wave modeling, including the Longuet-Higgins model.

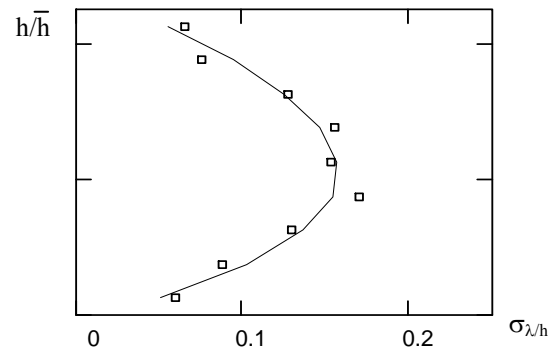


Fig. 2: Scedastic curve of lengths and heights of waves

Modeling of a complex sea has also been carried out. Some variants of wind-waves and systems of swell have been investigated. It is shown that the distribution law of the wave periods of a complex sea, represents a combination of Weibull laws with various parameters (Rozshkov 1990). The number of elements of a combination is equal to the number of wave systems. For the usual wind-waves distribution law of periods, the solution is well-smoothed on a grid, using a Weibull law with  $k=3$ , however at narrowing, a spectrum parameter of distribution law increases, approaching 4.

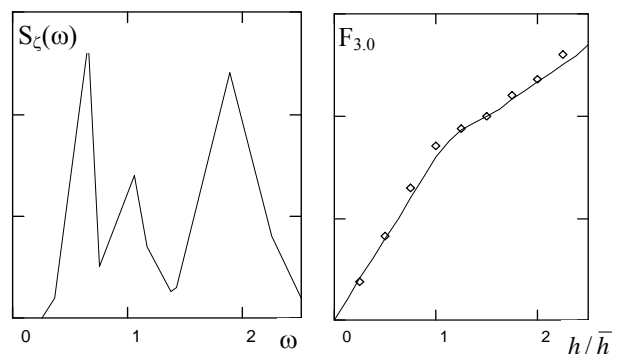


Fig. 3: Spectrum with two swells and distribution of wave periods

On the basis of the obtained results, it is possible to discuss the high physical adequacy of the presented model of sea waves on quasi-stationary time-domain. In Fig. 3, one of the interesting examples of three investigated wave systems is shown.

To analyze the abilities of the model to generate a non-stationary wave-field, we considered a number of storm types. As the first, Hurricane "Belief" (Davidan 1988), which took place in the central part of the North Atlantic on September 2-6, 1966 was chosen.

Besides the model of non-stationary, the wave-field on a longer time interval: July 5-17, 1986 (Rozhkov 1990) has also been verified. The interval of wave evolution has been broken into thirty-six 8-hour sites, where each had waves that were assumed as quasi-stationary. The evolution of the average wave height during a storm is shown in Fig. 4. The strong agreement between experimental measurements and the model results is encouraging for the ability of the model to produce high quality results in a range of synoptic variability.

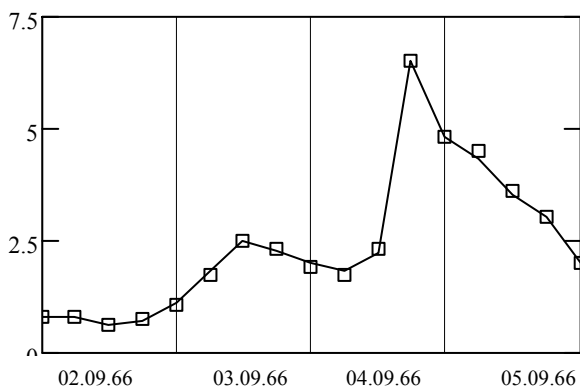


Fig. 4: Diagram of average wave height variation during hurricane "Belief"

All these results inspire confidence that this effective computing procedure allows us to generate a hydrodynamically adequate wave surface, and also possesses the ability to evolve the solution in time.

For the description of such transformation, it is necessary to address questions of wave-weather scenario modeling. Some details related to this question were presented at the Stability Workshop in 2005 (Degtyarev 2005). During the evolution of sea waves, the spectral density randomly varies in time, i.e. for description of such an evolution the spectral density should be represented by a stochastic function. One of the ideas formulated in Degtyarev (2005) consists of the parameterization of  $S_{\zeta}(\omega)$ . In this

case, we consider it as a deterministic function with a set of random variables:

$$S = S(\omega, \theta, \Xi) \quad (7)$$

The feasibility of an approach like (7) obviously depends on the level of accuracy used to specify the spectrum  $S_p(\omega, \theta)$ . This may be specified by the parameters  $\Xi_p$  taken from their multidimensional distribution  $F_{\Xi}(\xi)$ .

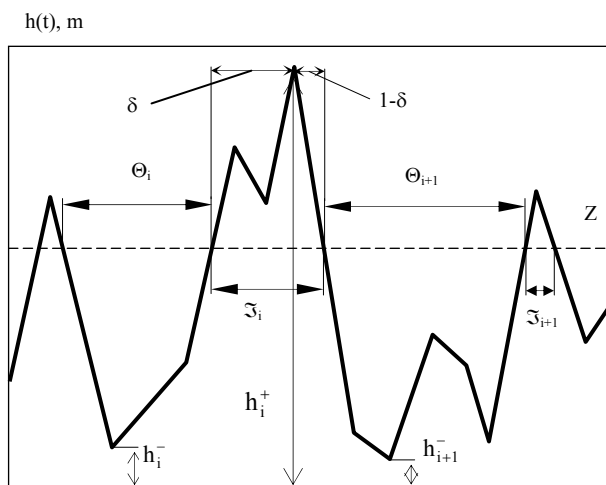
In the present study, parameters of the spectrum related to wave height, spectral shape, the frequency of the spectral peak,  $\omega_{\max}$ , and the main wave direction,  $\theta_{\max}$ , are selected as parameters in  $\Xi$ . The single field model spectrum may be formulated

$$S_p(\omega/\omega_{\max}, \theta - \theta_{\max}, \Xi_r),$$

where  $\Xi_r$  signifies the rest of the parameters. More general spectra,  $S(\omega, \theta)$ , are obtained as

$$S(\omega, \theta) = m_{00} \sum_{p=1}^N \gamma_p S_p \left( \frac{\omega}{\omega_p}, \theta - \theta_{\max}, \Xi_r \right) \quad (8)$$

where  $m_{00}$ , the 0<sup>th</sup> moment of the spectrum, is equal to the total variance of wave field,  $N$  is the number of wave fields (peaks in the spectrum), and  $\gamma_p$  are weight factors for each system so that,  $\sum_{p=1}^N \gamma_p = 1$ .



Using this approach, a procedure for a 5 t, days  
 Fig.5. Parameters describing storms and weather windows  
 (Божиковацкая et al. 2000, Degtyarev 2005).

A time-series of wind-wave heights in the mid-latitudes and subtropical areas of the World Oceans can be used as alternating sequences of storms and weather windows. We define a storm of duration  $\mathfrak{T}$  and intensity  $h^+$  as a situation when random function  $h(t)$  exceeds a pre-defined value  $Z$ . The period  $\Theta$ , during which the wave height is less than this threshold, will be called a weather window of intensity  $h^-$ . The parameter  $\delta$  shows the asymmetry of the storm:

$$\delta = (t_p - t_b) / \mathfrak{T}$$

$t_b$ ,  $t_p$ ,  $t_e$  are times of storm start, the maximum, and the end, respectively. Fig. 5 clarifies these definitions.

Such a parametrization of wave evolution permits one to simulate variations of the spectrum parameters in (7). Examples of procedures of storms classification for specific regions are shown (Boukhanovsky et al. 2000, Degtyarev 2005, Belenky and Sevastianov 2007). The uniform approach to waves, modeling (2) - (4), and its evolution, permits one to develop a set of nested autoregressive models for generation of continuous realization of spatio-temporal wave-field, in a given region of the Ocean.

At the quasi-stationary and synoptic intervals of variability, the wave process is best described by the stationary auto-regression model AR(p) of order p, namely

$$\xi_t = \sum_{k=1}^p \phi_k \xi_{t-k} + \varepsilon_t, \quad \zeta_t = f(\xi_t) \quad (9)$$

where  $\phi_k$  are coefficients to be computed using the correlation function  $K_\xi(\tau)$ , and  $\varepsilon_t$  is white noise with a given distribution function, which has to be compatible with the nonlinear functional transformation  $f(\bullet)$  of function  $\xi_t$  into, respectively, the Rayleigh or log-normal distribution of  $\zeta_t$ . In Lopatoukhin et al. (2001) it is shown that a stationary pulse-like random process is a good model for a sequence of storms and fair weather intervals.

The actual generation of a series of random storms and weather windows is based on a Monte-Carlo approach. Thus, it becomes pos-

sible to reproduce the whole variety of values of  $\{h^+, h^-, \mathfrak{T}, \Theta\}$ :

$$\begin{aligned} \mathfrak{T}_k &= F_{\mathfrak{T}}^{-1}(\gamma_1^{(k)}), \Theta_k = F_{\Theta}^{-1}(\gamma_2^{(k)}) \\ h_k^+ &= F_{h^+|\mathfrak{T}}^{-1}(\gamma_3^{(k)} | \mathfrak{T}_k), h_k^- = F_{h^-|\Theta}^{-1}(\gamma_4^{(k)} | \Theta_k) \end{aligned} \quad (10)$$

Here  $\{\gamma_i^{(k)}\}$  denotes a system of four pseudo random numbers.

A stochastic model for extra-annual rhythms could be written as follows:

$$\zeta(t) = m(t) + \sigma(t)\xi_t \quad (11)$$

Here  $m(t)$  and  $\sigma(t)$  are periodic functions, and  $\xi_t$  is a non-stationary process AP(p) so that

$$\xi_t = \sum_{k=1}^p \phi_k(t)\xi_{t-k} + \varepsilon_t \quad (12)$$

and the coefficients  $\phi_k(t) = \phi_k(t+T)$  are periodic functions of time.

A model that is capable to describe year-to-year variability of the monthly mean wave heights will therefore require twelve values of  $m(t)$  and 78 values of  $K(t, \tau)$ . It is possible to reduce the number of dimensions by considering the following representation of periodically correlated stochastic processes (PCSP):

$$\zeta(t) = \sum_{k=-\infty}^{\infty} \eta_k(t) \exp(i\omega_k t) \quad (13)$$

So with the help of such nested autoregression models, it is possible to reconstruct conditions of a hypothetical (artificial) weather scenario, at a specific location of interest. The idea is to look at a situation that did not yet happen, but in principle, can happen.

## CONCLUSION

One of the most promising applications of the autoregression model is for advanced hydrodynamic codes. These codes are tradi-

tionally based on potential flow and external models for vortex and viscosity forces. They use Longuet-Higgins model for wave elevations and pressures, which put a limit on the length of irregular wave realizations that can be efficiently used for simulations. Another limitation is for the modeling non-stationarity. The latter one may be especially important for dynamic stability, as growing seas increase the probability of encounter for steep waves, which may represent significant danger, in terms of roll motions. The application of the autoregression model naturally solves both problems. As it was shown, the autoregression model offers a very natural way to present non-stationarity. However, for use of the autoregression model in a potential hydrodynamic code, wave pressures also need to be evaluated. Several options can be considered for pressures. The most natural way is to use formulation (1). The autoregression model of wave elevations becomes the boundary condition. Another option is use autoregression model itself for the pressures as well. In the latter case, it needs to be related with the wave elevations and a given spectrum.

## REFERENCES

- Belenky V.L., Sevastianov N.B. Stability and safety of ships: Risk and capsizing. Second Edition SNAME, Jersey City, NJ, 2007
- Boukhanovsky A., Degtyarev A., Lopatoukhin L., Rozhkov V. Stable states of wave climate: applications for risk estimation. //Proceedings of the International conference STAB'2000, Launceston, Tasmania, Australia, 2000, vol.2, pp.831-846
- Boukhanovsky A., Rozhkov V., Degtyarev A. Peculiarities of Computer Simulation and Statistical Representation of Time-Spatial Metocean Fields. //in book "Computational Science - ICCS 2001", LNCS 2073, Springer, part I, pp.463-472
- Box G., Jenkins G. Time series analysis. Forecasting and control. Holden-Day, SF, 1970
- Davidan I.N.(ed.) Theoretical foundation and calculation methods for wind waves. Gidrometeoizdat, Leningrad, 1988 (in Russian)
- Degtyarev A.B. New approach to wave weather scenarios modeling. //Proceedings of 8<sup>th</sup> International Ship Stability Workshop, Istanbul, Turkey, October 2005, paper No 3.2
- Degtyarev A.B., Boukhanovsky A.V. Probabilistic modelling of stormy wave fields. //Proceedings of International Conference "Navy and Shipbuilding Nowadays", St.Petersburg 1996, February 26-29, Vol.2, A2-29 (in Russian)
- Lopatoukhin L., Rozhkov V., Ryabinin V., Swail V., Boukhanovsky A., Degtyarev A.. Estimation of extreme wind wave heights. WMO/TD-N 1041, 2001
- Lopatoukhin L., Rozhkov V., Boukhanovsky A., Degtyarev A., Sas'kov K., Athanassoulis G., Stefanakos Ch, Krogstad H. The spectral wave climate in the Barents Sea. //Proceedings of the conference OMAE'2002, OMAE2002-28397, Oslo, Norway, 2002
- Rozhkov V.A., Trapeznikov Yu.A. Probability models of oceanological processes. Gidrometeoizdat, Leningrad, 1990 (in Russian)
- Rozhkov V.A.(ed.) The results of oceanological research in tropical East Pacific. Gidrometeoizdat, Leningrad, 1990 (in Russian)



# Developing a Shared Vision for Naval Stability Assessment.

Doug Perrault<sup>1</sup> Tristram Hughes<sup>2</sup> Steve Marshall<sup>3</sup>

on behalf of the

## Naval Stability Standards Working Group

<sup>1</sup>Defence Research & Development Canada – Atlantic

<sup>2</sup>Senior Naval Architect, Salvage Division, SMIT International; Formerly Project Officer Hydrodynamics, Naval Platform Research and Development, Royal Netherlands Navy

<sup>3</sup>Surface Ship Hydromechanics, Directorate of Sea Systems, MoD

### **Abstract**

Surface combatants are required to operate in conditions of high military threat and be capable of deployment to any area of conflict or crisis at any time. This requirement calls for the vessel and crew to be capable of safely contending with the full range of environmental conditions that may be encountered while pursuing their primary objective. Achieving and maintaining this capability is strongly influenced by the application of naval stability standards, many of which have a common origin, based on experiences from World War II and before. Although such standards have apparently served the navies admirably over many years, there are many reasons to question their limitations and applicability in the context of modern ship design and procurement. This paper addresses presents the efforts to date of the Naval Stability Standards Working Group to investigate the relationship between existing intact stability standards and capsizing risk with respect to frigate forms.

### **1. Introduction**

The maintenance of a maritime strategic capability demands the ability to rapidly deploy to any area of conflict or humanitarian crisis. The attainment and maintenance of this capability is strongly influenced by the application of naval stability standards. Over half a century of warship design and operational experience has led many navies to adopt and apply very similar standards to design and life-cycle management of stability.

The stability standards have apparently served the navies admirably over the last forty years or so; they appear to have resulted in warship designs having a low level of capsizing risk. Despite this apparently good service there are many reasons to investigate their validity and applicability, including:

- The level of safety assured by compliance with such standards is unknown.

- It is questionable whether the essentially static measures truly reflect the dynamic behaviour in extreme conditions.
- Modern naval hull forms are becoming increasingly less similar to those against which such standards were originally developed.

### **2. The Naval Stability Standards Working Group**

The Co-operative Research Navies (CRNav) Dynamic Stability group was established in 1989 to undertake research into the underlying physical phenomena and characteristics of dynamic stability. The work has led to the development and application of suitable dynamic stability simulation tools in pursuit of this objective. In light of the significant advances made by the group, the concerns with current stability standards could now be investigated in more detail.

The Naval Stability Standards Working Group (NSSWG) was formed in 1999 from the naval members of the CRNav group. The objective of the group is *'To develop a shared view on the future of naval stability assessment and develop a Naval Stability Standards Guidelines document which can be utilised by the participating navies at their discretion.'*

At a practical level, this involves identification of methods of relating stability criteria to risk. In the short-term, this means identification of level of safety extant in the current standards, focusing on the strengths and weaknesses of existing standards, and using a standard set of environmental conditions. In the long term, it means developing methodologies for assessing stability characteristics and practical limits for both design and life-cycle management.

### **3. Background**

Currently, the stability of naval vessels is assessed using hydrostatic criteria and methodologies based on concepts that date back over two centuries. The hydrostatics-based standards (e.g., [1], [2], [3], [4], [5] and [6]) have attempted to incorporate some consideration of

dynamic issues through the application of gust factors to wind heeling levers, the use of roll back angles, and in some cases the consideration of the diminution of the righting arm when the vessel is balanced on a wave [3][4].

It is known that the static stability criteria values include some margin to account for the relatively crude nature of the calculation methods employed at the time of their inception. However, the exact rationale behind the determination of these factors and other approximations is no longer clear. It is this lack of clarity in conjunction with the apparently good service provided by such standards over the last forty years that has resulted in situations where strict compliance to a standard is demanded by the stability authority, with extremely small short-falls against even a single criterion considered unacceptable. At the same time, it is not unusual to see the same set of intact stability criteria being rigorously applied to vessels ranging from harbour tugs to aircraft carriers. It is assumed that this broad brush application also results from the lack of alternatives and the perception of good service rendered by the standard.

**3.1 The Impact of Modern Ship Designs**

Radical departures from conventional displacement designs are now becoming increasingly common. These include the application of 'tumble home', deep 'V' and wave-piercing bow forms, and the inclusion of more hull integrated watertight superstructure. There are also gradual changes such as the evolution of aft body design, with notably wider transom forms emerging in modern ship designs. It is questionable if the types of vessels against which Sarchin and Goldberg [7], for example, developed their criteria (two designs pre-dating WWII), exemplify their modern equivalents.

**3.2 Changing Procurement**

Increasingly, commercial standards are being adopted in place of defence standards, with the rationale being that they offer better value for money. This may indeed be true in many instances, provided the role and fitness for purpose of the commercial standards are fully compatible with the required naval capability. Understanding the level of safety inherent in the stability standard used – whether commercial or military – and how that level of safety varies with changes in the values of the constituent

criteria (both individually and jointly) is required for rational and cost-effective assessment of the dynamic stability of a vessel.

**3.3 Through Life Stability Management**

While total compliance may be easily achievable at the start of a warship's life, maintaining full compliance becomes increasingly difficult later in life due to increases in KG and displacement. To facilitate a balanced and efficient approach to through-life stability management, it is imperative to know how "growth" affects the ability of the stability standard criteria's ability to indicate risk.

**4. Approach**

The work to date concentrates on investigating the level of safety associated with current standards. Figure 1 maps the process adopted. This approach uses an extensive series of FREDYN (v 8.2) time domain ship motion simulations coupled with probabilistic data describing the environment and the vessel operating parameters. An explanation of this time domain tool is given in reference [8].

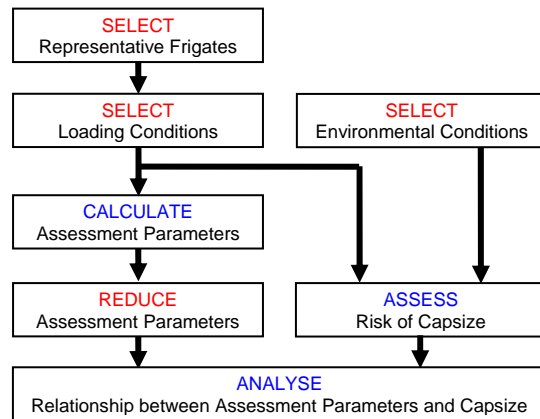


Figure 1 . Schematic view of approach adopted.

**4.1 The Probabilistic Methodology**

The probability of capsizing is directly related to the probability of exceeding a critical roll angle:  $P(\phi > \phi_{critical})$ . The methodology employed in determining the probability of exceeding a critical roll angle in a particular loading condition is that described by McTaggart and de Kat [9]. Time domain simulations from FREDYN [8] are combined with probabilistic input data for the wave conditions and heading and speed of the ship via the programs Pcapref and Pcapsize, collectively known as the PCAP analysis [9]. The probability of exceeding the critical roll angle within a given time is given by:

$$P(\phi > \phi_{crit}) = \sum \sum \sum \sum p(V)p(\beta)p(H_s, T_p) \times P(\phi > \phi_{crit} | V, \beta, H_s, T_p)$$

where  $V$  is the vessel's speed,  $\beta$  is the vessel's heading,  $H_s$  is the significant wave height,  $T_p$  is the peak wave period, and their joint probability density is  $p(H_s, T_p)$ . The final term is the conditional probability of exceeding the critical roll angle given a specific combination of speed, heading, and seaway conditions,  $P(\phi > \phi_{critical} | V, \beta, H_s, T_p)$ . It is determined from the FREDYN numerical simulations based on the maximum roll angles.

**4.2 Assumed Distributions**

**4.2.1 Operational Conditions.**

There are two basic operational probability distributions assumed. The first,  $P(V)$ , is a discretised distribution for calm water speeds derived from a representative naval frigate operational speed profile. The second is  $P(\beta)$ , a uniform distribution of headings. It is important to note that these operating distributions are independent of any operator action; there are no voluntary heading related speed reductions. Therefore the probability of exceeding the critical roll angle determined should be considered a baseline and reflects only the influence of the 'quasi-static' stability standards and hull form characteristics, and not the added influence of the good seamanship of the operator.

**4.2.2 Environmental Conditions.**

Intact capsize is clearly related to encountering a critical environment in manner such that one or a number of capsize mechanisms are invoked. The probability of exceeding the critical roll angle is therefore related to the probability of occurrence of a given environment (see Equation (1)). For the purposes of this study the Bales North Atlantic scattergram [10] was modified slightly [9] and used to define the probability distribution of unidirectional Bretschneider wave spectra.

Since the wind conditions are typically related to the wave conditions, an approximation was employed that assumed that winds were not only collinear with waves but related to the significant wave height via a linear relationship [9][10].

**4.3 The Frigates**

A total of twelve frigates representing all participant navies were selected. Table 1 shows the range of basic form parameters of the selected frigates. Each vessel is of a class that is either currently in service or that

has seen significant periods of service. The designs can be considered to span at least the last 40 years. Some of the designs predate the inception of the Sarchin and Goldberg criteria, but were required to meet them later in life. The majority of the vessels were designed from the outset to meet either Sarchin and Goldberg or derivatives of that standard.

Table 1. Range of Basic form Parameters.

Parameter:	Min	Max
Displacement (tonnes) - $\Delta$	2478	5490
Length at Waterline (m) - L	106.68	124.50
Beam at Waterline (m) - B	12.19	15.23
Draft (m) - T	3.81	5.33
Depth (m) - H	8.89	11.69
Vert. Center of Gravity (m) - KG	5.00	7.20
Metacentric Height (m) - GM	0.250	1.649
$C_B = \nabla / (L * B * T)$	0.440	0.548
$C_{WP} = A_{WP} / L * B$	0.718	0.810
$C_{VP} = C_B / C_{WP}$	0.593	0.698
L/B	7.873	9.160
KG/H	0.539	0.738
KG/B	0.404	0.497
KG/T	1.120	1.671
GM/B	0.020	0.121

$A_{WP}$ : Waterplane Area  
 $\nabla$ : Volumetric Displacement

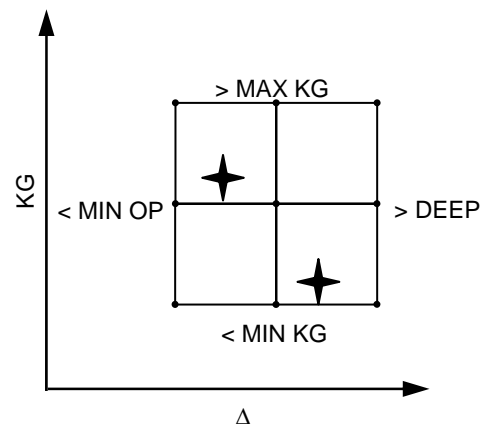


Figure 2 . The Conceptual Matrix of Loading Conditions.

Each navy selected a matrix (3 displacements x 3 KGs) of loading conditions for their vessels. The matrix bounded actual operating load conditions, whether they were driven by intact stability considerations or those of damage stability. The outer boundaries of the matrix were required to include combinations of KG and displacement that would fail a number of criteria in order to expose their associated probability of capsize (see Figure 2).

#### 4.4 GZ Parameters

A set of ‘quasi-static’ measures that represent the majority of the criteria used to evaluate stability performance in the various naval and commercial standards was assessed. The selected GZ assessment parameters can be considered, or categorised, by the degree by which the dynamic environment is considered.

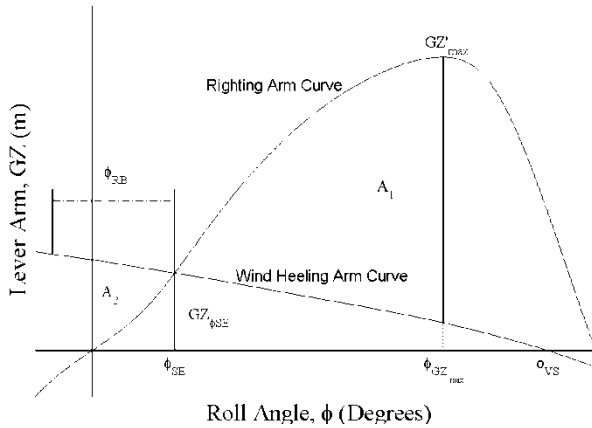


Figure 3. Typical GZ Curve with Wind Heeling

##### 4.4.1 Fully Static

At the most basic level we have the fully static approach whereby the shape (Table 2) and area (Table 3) characteristics of the calm water righting curve are assessed.

Table 2 . Fully Static Shape Parameters.

Parameter	Description
GM	The metacentric height (fluid) (metres).
$\phi_{GZmax}$	The angle at which the maximum righting lever arm occurs (degrees).
RPS	Range of positive stability (degrees).
$GZ_{max}$	The maximum righting lever arm (metres).
$GZ_{30^\circ}$	The righting lever arm at 30° (metres).

Table 3 . Fully Static Area Characteristic.

Parameter	Description
$A_{0^\circ-30^\circ}$	The area under the GZ curve between 0° and 30°. (m-rad)
$A_{0^\circ-40^\circ}$	The area under the GZ curve between 0° and 40°. (m-rad)
$A_{30^\circ-40^\circ}$	The area under the GZ curve between 30° and 40°. (m-rad)

A further set (Table 4) of fully static assessment parameters were derived by the CRN group [8] through an extensive series of FREDYN simulations of the dynamic behaviour of 30 frigate type hulls.

Table 4 . Further Parameters.

Parameter	Description
$A_{\phi_{SE}-\phi_{VS}}$	Total (dynamic stability) area under the GZ curve. (m rads)
$C_{VP}$	Vertical prismatic coefficient

##### 4.4.2 Energy Balance

The set of terms in Table 5 assess the relationship between the characteristics of the calm water righting curve and an induced wind heeling curve. It is this set of criteria from Sarchin and Goldberg [7] that has formed the basis, or core, of the majority of current naval stability standards. In the original criteria and therefore DDS 079-1 [1] (the US navy standard), these parameters are related to the application of a 100 knot beam wind heeling lever.

Table 5 . Energy Balance Parameters.

Parameter	Description
$\phi_{SE}$	The angle of intersection of the wind heeling lever with the GZ curve. (degrees)
$\frac{GZ_{\phi_{SE}}}{GZ_{max}}$	The GZ at $\phi_{SE}$ divided by the maximum GZ.
$A_1$	The area between the GZ curve and the wind heeling lever between $\phi_{SE}$ and the down flooding angle. (m rad)
$A_2$	The area between the GZ curve and the wind heeling lever between $\phi_{SE}$ and a roll back angle of 25°. (m rad)
$A_1 / A_2$	The ratio of the $A_1$ to $A_2$

##### 4.4.3 Wave Adjusted

The final set of parameters (Table 6) are those that, in place of the calm water righting curve, employ a righting curve determined from the vessel being balanced in a trough and/or on the crest of a wave of wavelength proportional to the vessel length. Such standards [4] also tend to apply an energy balance assessment.

Table 6 . Wave Adjusted Parameters.

Parameter	Description
$GZ'_{\phi_{REF}}$	The residual righting lever arm at $\phi_{REF}$ with a beam wind.
RRPS	The residual range of positive stability.
$A'_{\phi_{SE}-\phi_{VS}}$	The residual area under the GZ curve, above the wind heeling lever arm curve, and above the $GZ = 0$ axis.

##### 4.4.4 Form Parameters

A number of hull form parameters were also selected for inclusion in the analysis in order to allow the differentiation between traditional and

more modern forms. These include basic particulars, form coefficients, and characteristic ratios.

#### 4.5 Performance Assessment

A total of 124 ship loading conditions representing 12 ships were investigated. It is to be noted that all analysis undertaken assumes that superstructure is included with respect to the determination of the wind heeling lever only. It was excluded from consideration with respect to buoyancy since it was considered that its inclusion would obfuscate the important issues of hull geometry.

The above parameters were determined for each ship loading condition. A comprehensive regression analysis was undertaken, the objective of which is to allow the determination of the ability of measures, either individually or in combination, to reflect dynamic stability.

#### 4.6 Collation of 'Quasi-Static' and Probabilistic Data

The outputs from PCAPSIZE and FREDYN, along with externally-calculated, wave-balanced GZ curves and the North Atlantic scattergram information, are post processed using MATLAB.

##### 4.6.1 Conditional Probabilities

In addition to the probability of exceeding the critical roll angle within one hour under all sea conditions, the probabilities of exceeding the critical roll angle within one hour given a specific sea state were also calculated. The classic sea state definitions [11] are used with the selected (North Atlantic) scattergram [10]. These probabilities can be further discriminated by ship speed and/or heading, allowing the identification of significant speed-seaway or heading-seaway combinations.

Further, in order to gain an insight into those combinations that were most likely to be the cause of extreme dynamic events, an approach was employed that determined those speeds, headings, and wave parameters that were associated with highest (hourly) conditional probability given capsizing. The parameters exposed in this manner are as follows:

- Significant wave height (m).
- Peak wave period (s).
- Nominal wave steepness –  $H_s/\lambda$ .
- Speed (knots).
- Heading (degs).

#### 5. General Results

The parameters associated with current stability standards show mixed results. The results of this study indicate reasonable relationships, in many instances, between risk of exceeding the critical angle and those GZ parameters that are employed in current naval standards. This tends to validate the use of these parameters. The variation in relative ranking of the parameters for each ship, however, would indicate that few if any of the parameters can be used across all ships.

In general, the van Harpen criteria (wave balanced GZ curves) provided stronger results than the nominal (no wave balancing) GZ curve parameters.

It should also be noted that the form parameters are less useful than GZ parameters for indicating the risk of extreme motion. This may be because risk of capsizing is related to geometry and inertial properties of the ship, and the latter are not reflected in the form parameters.

The study has also shown that, on an individual parameter basis, many naval standards employ criteria, or measures, that are superfluous or redundant due to collinearity. Additionally, although many standard parameters show high linear correlation with probability of extreme motions, there are other parameters, not currently used in the standards, that have higher correlation.

When the ships are considered as a group, none of the standard parameters have a strong correlation with the probability of exceeding the critical roll angle.

#### 6. Discussion

Loading conditions used in the present study do not necessarily reflect real working conditions for the ships involved. The loading conditions used are intended to give broad indication of risk of capsizing, and in some cases may even be outside the bounds of proper and normal operation of the ship.

There has been some debate over the probability values determined in the PCAP analysis (Pcapref and Pcapsize). It is generally felt that the PCAP method over-predicts capsizing in the long term (e.g., one year). Although the issue is primarily apparent in the long-term probabilities, the debate has fostered a desire to look at alternative probability methods. It has also lowered the confidence in the current probability values.

FREDYN 8.2 and the inherent assumptions in the strip theory employed therein, may cause

inaccuracies in some of the simulation results, also affecting the probability results.

Taken together, this means that the regression analysis results cannot be taken to be accurate, and thus the relative strengths and weaknesses of GZ parameters for indicating risk of exceeding the critical roll angle are not strictly valid. The methodology, however, is a reasonable process, and further work is warranted.

## **7. Recommendations**

Capsize risks determined on the basis of FREDYN version 8.2 simulations should be used in a relative manner, for assessing the relevance of ship stability parameters. Absolute values of capsize risks are likely to be inaccurate due to limitations in FREDYN 8.2 accuracy and some uncertainty in the probability methodology employed.

The investigation into the level of risk accepted by using current naval standards should use a FREDYN version 9.8 or higher where the approach based on the long wave assumption is replaced by a three-dimensional panel methodology for the determination of Froude-Krylov forces. Furthermore, the panel method for determination of the wave radiation and diffraction forces should be used.

A selected number of the original ship set should be chosen for further simulations with their actual operational minimum and maximum loading conditions and an intermediate 50% condition. In order that they truly reflect accepted levels of capsize risk, said cases should be, where practically possible, those used in practice, whether driven by intact or by damage stability.

## **References:**

1. Navy(Australia) Standard A016534, Material Requirements for RAN Ships, Submarines and Systems, 'Naval Architecture Requirements - Stability of RAN Ships and Boats', 1999.
2. C-03-001-024/MS-002, 'Stability and Buoyancy requirements Canadian Armed Forces Surface Ships', 1979.
3. BV1033, Bauvorschrift für Schiffe Bundeswehr - Marine. '1033 Stabilität der Überwasserschiffe', Bundesministerium der Verteidigung, German Federal Navy.
4. van Harpen, N.T., 'Eisen te stellen aan de stabiliteit en het reserve-drijfvermogen van bovenwaterschepen der Koninklijke Marine en het Loodswezen', April 1970. Corporate source: Royal Netherlands Navy.
5. Naval Engineering Standard N.E.S. 109 Part 1 Issue 4, 1999, Stability Standards for Surface Ships Part 1, Conventional Ships. U.K. Ministry of Defence.
6. Naval Ship Engineering Centre, Design Data Sheet – Stability and Buoyancy of U.S. Naval Surface Ships, DDS 079-1, U.S. Navy, Naval Sea Systems Command, Washington DC. 1 August 1975.
7. Sarchin, T. H., and Goldberg, L. L., 'Stability and Buoyancy Criteria for U.S. Naval Surface Ships', SNAME Transactions, New York, Vol. 70, 1962.
8. De Kat, J. O., Brouwer, R., McTaggart, K.A., and Thomas, W.L., 'Intact ship survivability in extreme waves: New Criteria From a research and naval perspective'. Fifth International Conference on Stability of Ships and Ocean Vehicles, STAB '94 Conference, Melbourne, Florida, Nov. 1994.
9. McTaggart, K.A., De Kat, J. O., 'Capsize Risk of Intact Frigates in Irregular Seas', SNAME Transactions. 2000.
10. Bales, S.L., Lee, W.T., and Voelker, J.M. (1981). 'Standardized Wave and Wind Environments for NATO Operational Areas'. DTNSRDC. (Report DTNSRDC/SPD-0919-01).
11. 'Standardized Wave and Wind Environments and Shipboard Reporting of Sea Conditions', STANAG 4194, edition 1, North Atlantic Treaty Organization (NATO), 6 April 1983.

## Approaches for Evaluating Dynamic Stability in Design

Philip R. Alman<sup>1</sup>, Naval Sea Systems Command, for,  
The Naval Stability Standards Working Group

### ABSTRACT

*There are many ways of treating dynamic stability. No single approach is always best, but must be defined relative to each design and each yields a fidelity proportionate to resources and technological maturity. During the ship design process choices must be made that balance the approach within a wide trade space encompassing ship design characteristics, operational doctrine, technical risk management, operational safety, cost and schedule. Existing static approaches do not directly account for ship dynamics. There is a clear need to develop a frame work for integration of technical approaches into the ship design/acquisition process. The objective of this paper is to define a basis for outlining the range of intact dynamic stability methodologies that can be employed to naval ship design that address dynamic stability in such a way as to minimize technical and safety risks in an economical manner. The paper summarizes ongoing work by the Naval Stability Standards Working Group (NSSWG), and outlines relevant technical approaches suitable for employment on naval ship designs from preliminary/concept design stages through to operator guidance.*

**Keywords:** *Dynamic Stability, Risk Management, Naval Stability Standards Working Group, Static Stability, Probabilistic, Empirical, Criteria*

---

<sup>1</sup> The opinions expressed in this paper are those of the author and not necessarily those of the Naval Sea Systems Command or the United States Navy.

### Background

There is no single approach that is best for addressing dynamic stability as part of a ship design effort. Many factors encompassing design characteristics, technical maturity, methodology, resources, cost, and safety must be balanced to find the most appropriate treatment. Risk management techniques are well suited to defining the most cost-effective approach for treating dynamic stability in the design process.

The Naval Stability Standards Working Group (NSSWG) has worked to define these issues over a number of years. The NSSWG has representatives from Canada, Great Britain, Australia, France, United States, and the Netherlands. The development of specific methodologies addressing dynamic stability has been in the work plan for that group since its inception. As efforts have progressed, it has become increasingly clear that a wide range of approaches would have to be defined to meet all the requirements of every Navy.

Historically, dynamic stability has been represented by static measures including GZ area margins, and variation of GZ on prescribed waves, and other empirical rules. This approach is relatively simple and the least onerous for cost and schedule. Treatment of dynamic stability based on vessel dynamic response is still in the research and development stages. Even so, there are many approaches that can yield useful information, but no means to knit them into a coherent process. Thus there is a clear need to develop a

framework for integration of intact dynamic stability assessment into the ship design/acquisition process.

### NSSWG Definitions for Intact Dynamic Stability

There are three principle factors affecting dynamic stability:

1. The static restoring moment
2. The dynamic response (including damping and added moment of inertia)
3. The hydrodynamic forces on the vessel from waves/wind

Estimating and understanding these three factors and their relationship to stability failure modes, and developing appropriate safety margins governing allowable KG and Displacement for the ship design forms the basis for risk control in the acquisition process.

The Naval Stability Standards Working Group (NSSWG) uses the categories below as the basis for stability discussion.

**Static Capsize** - A static capsizes may occur suddenly when a disturbance is encountered that is sufficient to overcome the ship's inherent ability to remain in an equilibrium state at or near upright. The event has traditionally been characterized by parameters which relate to a reduction in the righting arm lever (or GZ curve) which represents the static stability of a vessel

independent of forward speed and time. Conditions that could lead to static capsize include improper loading, lifting or topside icing (increasing VCG); towing, wind, or load shift, (increasing heel angle); trapped fluids on deck (increasing free surface effects); and loss of watertight integrity (loss of buoyancy/water plane area).

**Dynamic Capsize** - A Dynamic Capsize is defined as a very large amplitude roll caused principally by seaway and wind excitation on a moving vessel or as a function of time. This wind and wave action may lead to equipment damage, personnel injury, loss of system functionality and/or weather-tight/watertight integrity from which the ship is unable to maintain its intact upright state. A dynamic capsizes is characterized as a time-dependent event occurring in unrestrained 6 degrees of freedom motion. The loss of dynamic stability may occur under a variety of conditions (intact or damaged) once the forcing function exceeds the available restoring force.

**Large Amplitude Motions** - Large amplitude motions are a part of dynamic stability considerations and include large roll angles, “knock downs”, yaw, lateral accelerations, pitch, etc. These motions are caused by the dynamics of the vessel as it is excited by wind and seaway. Large amplitude motions in the non-linear range tend to be in the range of roll angles where the GZ curve is softening but still able to provide sufficient restoring force to resist capsize. Dynamic capsizes occurs once roll has reached an extreme point on the GZ Curve, and restoring force can no longer bring the ship back to an upright position.

**Static Stability Standards and Practice**

Navies assess stability using static methodologies. Existing stability criteria are a composite based around compliance with specific safety elements. In the case of the DDS-079-1 these are the following:

*Principal Safety Elements in DDS-079 Criteria*

Intact Ship

- Beam Winds Combined With Rolling
- Lifting of Heavy Weights
- Crowding of Passengers to One Side
- High Speed Turning
- Topside Icing

Damaged Ship

- Stranding Involving Moderate Flooding
- Bow Collision
- Battle Damage Involving Extensive Flooding

Flooded Ship

- Beam Winds Combined With Rolling
- Progressive Flooding

Each of the safety elements listed above is defined through various criteria. Naval ships must comply with

the most restrictive limit resulting from the application of several criteria such as beam wind, passenger crowding, icing, high speed turning, and damage stability [1].

In general a range of loading conditions is bounded by the envelope established by the governing limits. This limit becomes a composite curve as shown in the Figure 1 below. An acceptable loading condition is one which the KG is below the limiting curve.

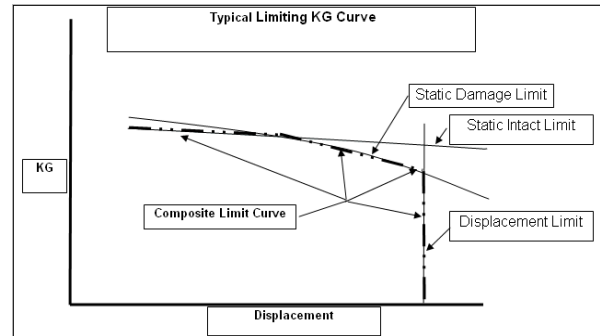


**Figure 1 Typical Limiting KG Curve and Components**

Historically static stability criteria do not directly address dynamic stability and large amplitude motion; although it is generally acknowledged that the margin of safety for seaway motions is included as the A1/A2 area ratio and roll back angle. The historical record supports the adequacy of this approach. However, the adequacy of such factors of safety using static methods may not be adequate when applied to hull forms with novel features. Consequently there is a need to integrate dynamic stability methodologies into the criteria stability criteria.

**Intact Dynamic Stability Assessment Methodologies**

There are many ways to categorize dynamic stability assessment methodologies, the definitions of which are still under discussion. Discussion of these methodologies is best handled in the context of a risk management process.

The starting point is to form a lexicon by which everybody involved in the risk management process can talk from the same common understanding.

One example is provided in Belenky, DeKat, Umeda [2]. Four basic approaches were described which can be summarized as: probabilistic performance-based criterion, deterministic performance-based criterion, probabilistic parametric criterion, and deterministic parametric criterion.

Within the NSSWG, ongoing efforts have been based around a categorization of dynamic stability methodologies as “Empirically Based Rules”, “Rules Based on Probabilistic Dynamic Approaches”, “Direct Probabilistic Assessment” and “Relative Probabilistic Based Assessment. Although these don’t agree exactly

with those of Belenky, DeKat, Umeda, they are complimentary and generally convey the similar concepts based on naval ship stability practices. The NSSWG categorizations are defined as follows:

*1. Empirically Based Rules* - Development of criteria based on a set of “rules” established from a study of hull form characteristics using engineering principles based on evaluation of design characteristics such as the GZ curve. A suitable body of ships is assessed to form the basis for establishing criteria. The resultant criteria are typically binary and expressed as “pass/fail” and will have factors of safety to account for physical properties which can not be fully modeled. Typically static stability criteria fall into this group. This rules-based methodology is largely based on heuristics – experience with previous designs. It may not be readily applicable to evolutionary or novel designs.

*2. Rules Based on Probabilistic Dynamic Approaches* - A probabilistic study for a series of ship types is used as the basis to determine suitable design characteristics to be used as part of dynamic stability criteria. Design characteristics are identified as being the most closely correlated to capsizing probability for the type of ship assessed. A suitable criterion is then derived for the design characteristics identified which provides a reasonable mitigation of capsizing risk. The NSSWG has been actively developing this approach as reported in Perrault et al. [3]

*3. Direct Probabilistic Assessment* - Direct determination of a capsizing probability for seaway environments using a validated simulation tool and/or a series of model tests. The resultant capsizing probability is assessed as acceptable or unacceptable based on some risk level established for specific seaway operations or for lifetime risk. Some risk comparison can be made using tools such as Farmer’s curves (Ayyub [4]) to establish acceptable risk levels in comparison to other occupation or modes of transportation. In Peters [5] a discussion is provided on approaches to establish acceptable risk levels for naval frigates. The authors conclude that an acceptable risk of capsizing for a naval frigate on an annual basis could be approximately  $1 \times 10^{-4}$ .

*4. Relative Probabilistic Assessment* - A probability index is established based on comparisons of the design ship capsizing probability to a known baseline ship operating in identical conditions. The resultant probability index is assessed as acceptable or unacceptable based on a relative measure against the baseline. A probability index must be developed for the baseline ship as part of the comparison. The assessment is done for the baseline ship when in compliance with an existing static criteria. The index must not only have the baseline determined by the existing ship, but must have a rationally derived scale in order to provide meaningful comparisons between the existing ship and

the design ship. Note that the baseline ship will have been assessed by one of the above methods by necessity.

**The Intact Dynamic Stability “Tool Kit”**

The categories defined above provide the building blocks from which integration of dynamic stability into the design process can begin. The integration is centered on developing a measure of the risks associated with the proposed hull form, definition of the tools available, their fidelity and the resources necessary to use them. Thus a “Tool Kit” of technical approaches is developed. Each tool in the kit has a fidelity and cost associated with its application.

The dynamic stability risk characterization of the hull form should be made through a set of measures. The characterization can be made qualitatively at initial stages but should move into development of quantitative (e.g., probabilistic) measures as the design develops. These risk measures can be broadly characterized as follows.

- Heuristic/Historical Experience (Qualitative)
- Early design assessment/rules of thumb developed from simple design parameters. (Qualitative/Quantitative)
- Simulation and/or Test Data (Quantitative)

Determination of the appropriate approach might be accomplished in the context of a risk assessment. The “tool kit” represents the means by which hazards and consequences can be quantified and managed.

For example, the use of vulnerability criteria as proposed by Bassler [6] very good starting point establishing both the early stage risk and mitigation through the level 1 and level 2 vulnerability criteria.

The risk characterization should be revisited several times as the design matures.

Measures for risk mitigation must also be considered along with the risk. In a formal sense risk may be thought of as fitting into the following. Ayyub [4].

- Risk Reduction or Elimination
- Risk Transfer
- Risk Avoidance
- Risk Absorbance

For dynamic stability, some of the most prominent mitigation measures can be generally thought of as follows:

- Criteria (Risk Reduction)
- Operational Restrictions (Risk Avoidance)
- Operator Guidance (Risk Avoidance)
- Training (Risk Avoidance)

The addition of training and operator guidance specifically to reduce or avoid a dynamic stability risk is an attractive option. In general operator guidance can be as follows:

- Simple rules of thumb compiled from historical experience/data
- Operator guidance based on dynamic stability assessment to produce either polar plots and/or rules of thumb based on specific loading conditions, speeds, headings and environmental conditions, and vulnerabilities.
- Training involving real time simulation and classroom lectures.

Each has an associated cost, fidelity and effectiveness.

**Process for Dynamic Stability Risk Characterization**

In broad terms there are several types of risk. Also interrelated are the risks associated with technological maturity and programmatic costs.

Early in a design it may not be possible to develop a quantitative risk assessment for dynamic stability due to a lack of available data. Decisions may have to be made based on judgment, past experience and historical evidence. For some designs this may be sufficient and the process can end there with the application of static criteria. More radical hull form designs may have to be approached with the object of developing a quantitative risk assessment.

The quantitative risk assessment should consider several factors some of which are outlined below.

1. Dynamic Stability Risk Inherent in the Hull Form
  - a. Quantification of Risk
    - i. Data
    - ii. Availability and Reliability of Data
    - iii. Historical Experience
  - b. Maturity of Technology
    - i. ‘Measures’ of Risk; i.e., Criteria
    - ii. Fidelity of Risk Assessment
  - c. Resource Requirement
    - i. Cost of R&D
    - ii. Cost of Implementing
2. Measures for Risk Mitigation
  - a. Criteria
  - b. Operator Guidance
  - c. Operational Limits
  - d. Design Changes

A technical risk assessment team should be established. This team would be composed of a group of subject matter experts covering stability, seakeeping, analytical tools, model testing and ship handling.

The team starts by attempting to quantify the technical risk associated with the hull form. The risk is estimated based on availability of data; historical, analytical or model testing. Lack of available data (“Unknown”) for an informed judgment could make the risk high. Other sources of data and their fidelity are evaluated accordingly. Mitigations are also identified. The process is iterated until the risk is considered to be in an acceptable range (Figure 2 below)

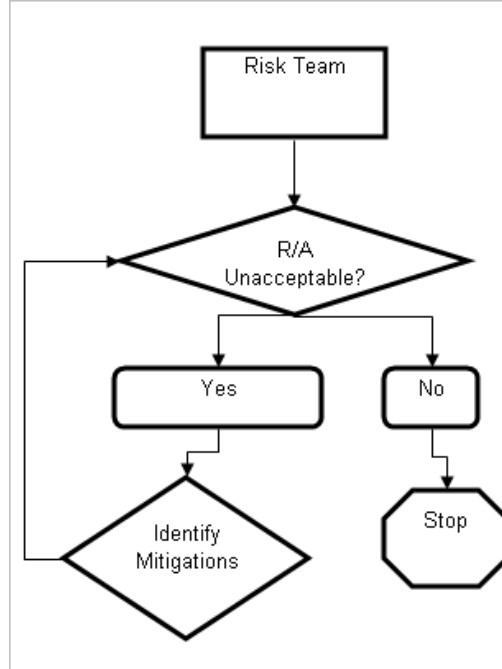


**Figure 2 Dynamic Stability Risk Assessment Process**

The results of an initial risk estimate for a hull form “A” might look like figure 3. In this case a review of available data suggests that there is a “likelihood” of a “critical” dynamic stability failure in a specified operational time frame.

Hazard: Dynamic Stability Failure					
Severity	Likelihood				
	Unlikely	Seldom	Occasionally	Likely	Frequent
A. Catastrophic					
B. Critical				X	Initial Estimate
C. Serious					
D. Moderate					
E. Marginal					

**Figure 3 Initial Hull Form Risk Assessment**

It is also important to consider available technology and its fidelity or ‘maturity’ as part of this process. The available “tools” may be categorized as follows:

- Heuristics/historical studies
- Simulation-based methods
- Systematic Model testing in regular, unidirectional waves to develop an index
- Direct results of (extensive) model testing in irregular, multidirectional waves

The team must answer the question “how much do I believe the data and what is the cost impact”? Table 1 below illustrates how a series of methodologies or “tools” might be ranked for fidelity and cost in developing the risk of dynamic stability failure. Actual metrics would have to be developed for a ranking process.

Hull Form A		
Notional Tool Fidelity for Risk Estimation		
Method	Effectiveness Cost	
1	Limited	Less
2	Medium	Moderate - High
3	High	High
4	Very High	Very High

1 - Heuristics/Historical Studies
2 - Simulation Based Methods
3 - Systematic Regular Wave Tests
4 - Extensive Random Wave Testing

**Table 1 Notional Tool Fidelity Ranking**

The process of developing the data required to assess the dynamic stability risk may require a considerable outlay of resources involving personnel and lead time and funding. This should be assessed early on in the design when it is still possible to make hull form changes. The cost of developing the required methodology to refine the risk estimate needs to be addressed and balanced against the benefit of the hull form.

Mitigations should be defined and addressed immediately. The mitigations are defined such that the severity and probability of the risk may be controlled or reduced. The mitigations are also developed based on an understanding of the nature and the magnitude of the assessed risk for the hull form.

In many cases the outcome should simply be a validation of existing practice. For instance an assessment of a conventional hull form ‘should’ confirm the adequacy of existing stability techniques in managing the risk. In other cases, the risk assessment should serve as a warning flag of potential dynamic stability problems and provide a basis from which to develop an outline of the technical and programmatic challenges associated with addressing dynamic stability for the proposed design. Cost benefit analysis should be developed for the decision process.

Specific risk management techniques for ranking dynamic stability methods and mitigations should be developed according to the needs of the Navy or organization conducting the assessment. There are many references covering application of specific risk management ‘tools’. A good example of the application

of risk management to submarine weight engineering is provided by Tellet [7]. Similar approaches could be adapted to dynamic stability risk management.

**Example Approaches for Defining Dynamic Stability Risk Mitigation**

1. *Early design assessment/rules of thumb developed from simple design parameters* - This approach uses simple design parameters resulting from studies of static stability characteristics on waves, or model test/simulation data using one of the criteria-based approaches. Results may include rules of thumb for distribution of waterplane area, vertical prismatic coefficient, specifications for righting energy and minimum positive GZ. The results are used for guidance during design but not as specific criteria to set the displacement/KG curve. The displacement/KG curve is developed based solely on compliance with unmodified intact static/ damage static criteria in the traditional manner. This approach is fairly easy to implement providing sufficient studies have been conducted to provide a basis for the rules of thumb. While it can provide design guidance, these approaches are most useful in highlighting design characteristics which may be problematic from a dynamic stability perspective and will require more rigorous investigation. An example of the structure of such an approach can be found in Belenky [8].

2. *Integrate dynamic stability into existing stability criteria to produce a unique dynamic stability limit or modified static stability limit.* - In this approach dynamic stability becomes one of the safety elements in the existing criteria. This results in a more formalized process. Consequently some strategy to augment existing criteria must be found by identifying the safety element associated most closely associated with dynamic stability. That safety element can be modified by one of the four methodologies defined above to address dynamic stability. This then produces a new dynamic stability limit as a function of mass properties and KG. This new limit is used in combination with the intact, damage and other limits to set the displacement/KG limit for the operation of the ship.

It is interesting to note that the watertight/weather tight boundaries used for static stability assessments may not directly coincide with the weather deck of the ship. This can make integration of dynamic stability/ static stability limits problematic as the buoyant volume and restoring force and wave forcing used in large amplitude motions may not match that of the static criteria limits.

In the modified criteria, mass properties are maintained within the resulting envelope throughout service life as shown in Figure 4 below.

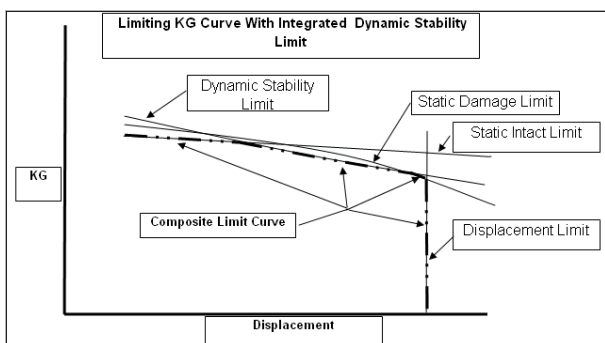


**Figure 4 Typical Limiting KG Curve with Integrated Dynamic Stability Limit**

The complexity of the criteria in both definition and implementation is directly related to the methodology. Criteria-based approaches using design parameters, and GZ curve assessment techniques are more readily implemented and socialized throughout the design community, although they may not provide sufficient flexibility to address designs outside of the data base from which they were developed.

Novel hull forms will rely more heavily on relative probabilistic and direct probabilistic approaches as they are likely outside of any data base used for development of criteria. [9] There may also be methodologies based on a ‘simplified deterministic waves approach’. [6] These approaches provide for the greatest flexibility but are the most challenging to implement as criteria and enforce through out the acquisition process. The cost associated with these approaches can be daunting as extensive engineering and risk studies are necessary to demonstrate compliance.

The complexity of the approach chosen bears a direct relationship to the perceived risk and/or the factors of safety assigned. Table 2 illustrates a notional ranking for effectiveness of criteria in mitigating dynamic stability risk on a design for a notional hull form “A”.

Hull Form A		
Notional Criteria* Fidelity for Risk Mitigation		
Method	Effectiveness Cost	
1	Limited	Less
2	Medium	Moderate - High
3	High	High
4	Medium-High	High

1 - Emperically Based Rules
2 - Rules Based on Probabilistic Dynamic Approaches
3 - Direct Probabilistic Assessment
4 - Relative Probabilistic Assessment

\* Criteria using mitigation method 2

**Table 2 Notional Criteria Ranking**

3. *Operator guidance based on dynamic stability assessment to produce either polar plots and/or rules of thumb based on specific loading conditions, speeds, headings and environmental conditions and/or Operability Envelopes* - Another complimentary approach is to provide operator guidance as a means of risk mitigation for dynamic stability. Dynamic Stability operator guidance may be as simple as rules of thumb or it may involve a direct probabilistic assessment of dynamic capsize risk or large amplitude motions risk. Key motion parameters are identified and assessed for specific seaway environments, and limits are imposed based on application of risk methodologies. These limits are displayed as polar plots and form the basis for operational guidance to the ship handler.

CG370 Full Load SS8  
Sig. Wave Ht (m): 11.50 Modal Period (sec): 16.4 (BRETSCHEIDER)  
Response: CAPSIZE

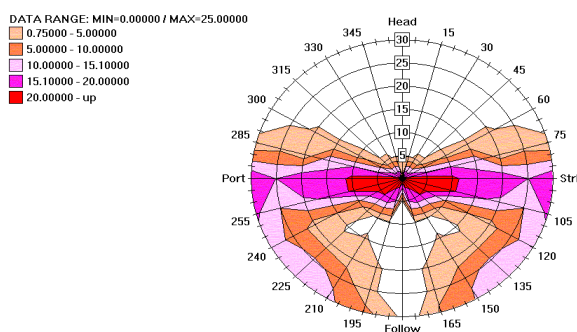


**Figure 5 Example Capsize Risk Polar Plot**

In some cases when operator guidance is provided, it may be considered sufficient to minimize dynamic stability risk without new dynamic stability criteria. Simulation or model testing maybe required developing the appropriate polar plots. Some training and socialization is required to implement the operator guidance.

There appears to be an unquantified margin between safe operability and acceptable intact stability implied by current standards. In many cases, safe operability is determined by practice of good seamanship. In spite of the margin being unquantified, it is relatively easy to determine operability envelopes and specify them as part of an acquisition. Dynamic stability events occurring inside the operability envelope would be expected to have a very low probability of occurrence and this may be checked by simulation and/or model testing as required and supplemented by existing operability criteria (e.g., IMO/SLF 49). The operability approach doesn't rely on an annual or lifetime risk which is likely to be non-discriminate (i.e. in all headings, sea states, etc) without the influence of the operator or operability factors, and therefore very high.

In development of the operability envelope approach three questions should be addressed:

- What is tolerable from a corporate and societal viewpoint?
- What inherent level of risk is associated with current standards?
- What level of risk is inherent in good ship-handling (reaction to cues)?

Training for the crew should be developed which addresses the use of the operator guidance system, identification of cues, and how to identify and manage risk when in heavy weather. Shaw[10] The Operator Guidance and Training Working Group (OGTWG) is a group of naval operators convened by invitation of the NSSWG to provide input and insight into the issues involved with operating ships in high seas. Work done to date by the OTGWG has identified appropriate classroom and simulator curricula associated with specific bridge team positions.

Table below lists a notional ranking of operator guidance/operational limits that may be identified for the risk assessment.

Hull Form A		
Notional OG/SOE Fidelity for Risk Mitigation		
Method	Effectiveness Cost	
1	Limited	Less
2	Medium	Moderate - High
3	Medium-High	High
5	High	Low-Moderate

1 - Emperically Based Rules of Thumb
2 - Polar Plots/Rules of Thumb
3 - Polar Plots/Training
4 - SOE Restrictions

**Table 3 Operator Guidance SOE Ranking**

4. *Changes to Hull Form* - If approached early in the design the most effective mitigation may be the identification of specific design changes that reduce the dynamic stability risk. However it may not be possible to make sufficient geometry changes or mass property changes and still meet requirements for the overall design. In that case some combination of approaches to dynamic stability risk mitigation should be identified that includes hull form changes to the extent possible, coupled with operator guidance, operational limits and criteria.

**Final Hull Form Risk Ranking**

Finally, a combination of options assembled from the tables could be assessed for mitigation effectiveness and cost. The best combination will be the one that provides the most effective risk reductions and least cost, taking into account the limitations on both these measures.

Risk reduction/cost plots can be used as a tool to select the best combination of options. For notional “Hull Form A”, it could be determined that the best options are achieved using a combination of the following

- Rules Based Probabilistic Dynamic Approaches
- Polar Plots/Rules of Thumb

It may take several iterations to finally get to an acceptable risk for the hull form as shown in Figure 6 below.

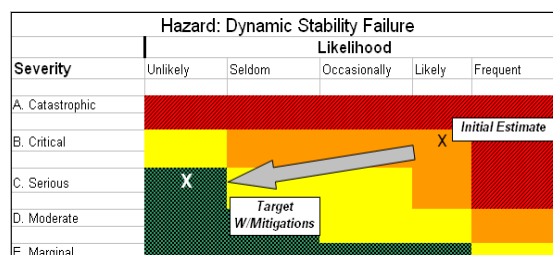


**Figure 6 Estimated Reduction in Hull Form Risk After Mitigation**

**Conclusion**

The process of developing rational approaches for consideration of dynamic stability is in its infancy. Through intelligent use of analytical tools, test data, and historical evidence it is possible to establish a rational process to manage and reduce the risk of a dynamic stability event occurring at sea. The tools employed to accomplish this should be used carefully and with an eye to economy without sacrificing safety. Risk management techniques provide a rational framework to accomplish this goal. Although not addressed in this paper, similar processes can be tailored to damage dynamic stability.

**Acknowledgements**

The Naval Stability Standards Working Group, David Tellet for his inspiration and advice, Martin Rennilson, Doug Perrault, Steve Marshall, Karl Stambaugh, Brad Campbell for their thoughts and discussions.

**References**

1. Alman, P.R., Minnick, P.V., Sheinberg, R., Thomas, W. L. III; “Dynamic Capsize Vulnerability: Reducing the Hidden Operational Risk”, SNAME Transactions, Society of Naval Architects and Marine Engineers, Vol. 107, New York, 1999.
2. Belenky, DeKat, Umeda; “Toward Performance-Based Criteria for Intact Stability”, SNAME 2008
3. Perrault, Hughes, Marshall; “Developing a Shared Vision for Naval Stability Assessment”, STAB 2010
4. Ayyub; “Risk Analysis in Engineering and Economics”, pages 95-109, 2003, Chapman and Hall/CRC

5. Peters; "Tolerable Risk of Capsize of a Naval Vessel", STAB 2010
6. Bassler, Belenky, Bulian, Franscscutto, Spyrou, Umeda; "A review of Available Methods for Application to Second Level Vulnerability Criteria", STAB 2009
7. Tellet, Cimino; "Marine Vehicle Weight Engineering", pp231-245, 2007, SAWE
8. Belenky, Bassler, Spyrou; "Dynamic Stability Assessment in Early Stage Ship Design", STAB 2009
9. Ayyub, Kaminsky, Alman, Engle, Campbell, Thomas; "Assessing the Probability of the Dynamic Capsizing of Vessels", Journal of Ship Research, SNAME, December 2006, 50(4), 289-310
10. Shaw, CDR, (USCG); "Practical Experience and Operational Requirements for Onboard Risk Management Under Marginal Stability Conditions", STAB 2001

## Operator Guidance for French Mine Hunters

Jean-François LEGUEN, Christophe CAQUINEAU, Emmanuel MOGICATO, Thierry DUPAU,  
Emmanuelle RÉGNIER, Pierre VONIER, Hervé, DISPA, François, LORIN

DGA Hydrodynamics (ex Bassin d'essais des carènes),

Chaussée du Vexin – BP 510 – 27105 Val de Reuil Cedex - FRANCE

### ABSTRACT

STEREDENN is a monitoring system dedicated to stability installed on a French navy mines hunter. It includes several functionalities as hydrostatic calculation and sea states estimator. For the evaluation of capsizes risk, numerical calculations (with FREDYN from CRNAV), model experiments and sea trials were performed by DGA hydrodynamics

### KEYWORDS

MONITORING ; OPERATIONAL LIMITS ; OCEAN BASSIN ; SEA STATES ESTIMATOR

### INTRODUCTION

The French navy ship CMT class (see Fig1) is mine hunters built in cooperation between Belgium, Netherlands and France. Those ships and their conceptions are quite old now. Naval stability standards and their use have also changed and been reinforced. Therefore modifications for the improvement of the stability (mainly after damage) of those mines hunters could be considered in the near future. Modifications have been or will be carried out independently in each country.

SSF is the part of the French ministry of defence which is in charge of the maintenance of the fleet. Preliminary to the planned modifications and in order to characterise more precisely the current ships, SSF asks DGA Hydrodynamics to assess the dynamics stability of CMT.

Following this study SSF and ALFAN (Navy headquarters) decided to reinforce operational limits for CMT before modifications. In order to help the crew to follow those operational limits instrumentation and screenplay were installed on board in the wheelhouse. This prototype system named STEREDENN is

described in this paper. First feed back are encouraging in the use of this prototype. Are such operation systems useful for security improvement?



Fig. 1: CMT "Croix du sud" (French navy).

### STEREEDEN: GENERAL ARRANGEMENT

STEREDENN is linked to one motions sensor (speed and 6 degrees of freedom) and includes four functionalities. The first one is a numerical tool (FASTABI). Using the mass distribution given by the crew it computes the hydrostatics characteristics of the ship. The second one is a sea states estimator (SSE) based on a comparison of motion measurements to numerical calculations. By using real time measurement of the roll period, STEREDENN

is able to estimate the vertical position of the centre of gravity. These parameters which are those mainly necessary to assess the risk of capsizing by numerical calculations are used to choose the corresponding polar plot which is indicated to the crew (Fig2). This information can help them to select a safer route (speed and relative heading).

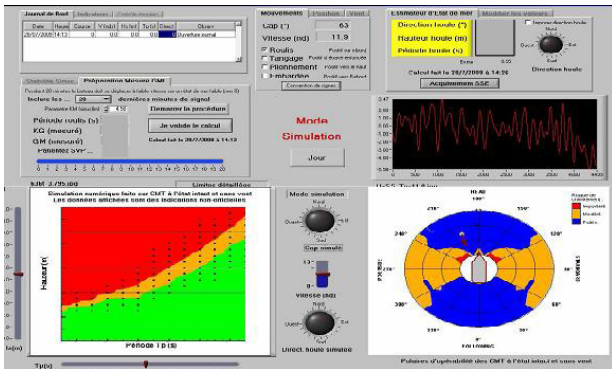


Fig. 2: Screen on the wheel-house

The four functionalities are described below.

**FIRST: FASTABI**

FASTABI is a numerical code that has been internally developed by DGA Hydrodynamics. The programming language is VB8 (Microsoft Visual Basic 2005) which makes maintenance easy and ensures a long lifetime. The code is run through DOS interface, using a mesh defining the hull forms and a series of input files made of various command lines. This type of input data has been adopted to facilitate the learning of the software and its integration in a numerical process of optimisation which necessitates to put a great number of computations in parallel, or in a system such as STEREDENN.

The software presently contains the following modules:

- A loading case being given, searching for the static equilibrium of the ship in draught, heeling and trim for various static wave configurations,
- Starting from the values read on the draught scales, searching for the corresponding load

case (displaced volume), which is numerically equivalent to a stability experiment,

- Computation of the internal efforts supported by the hull girder (shearing forces and bending moment),
- Intact stability analysis using the naval ships regulation issued by Bureau Veritas (BV Naval Rules),
- Intact and damage stability analysis using the civil regulations issued by International Maritime Organisation (IMO)
- Computation of tank tables to be used by the hydrodynamic code called FREDYN, that deals with dynamic stability on waves,
- Computation of the various hydrostatic data for the studied hull.

If needed, the free surface effects can be taken into account.

**FASTABI processing**

To evaluate the stability of a given ship, the displaced volume, the location of the centre of buoyancy, the location of the centre of floatation and the associated inertias of the floatation surface are needed. To get some of these values, volume integrals are to be derived, which can bring some difficulties. To avoid this problem, the hull is modelled using a surface mesh made of a multiple polyhedrons, which allows the volume integrals to be transformed in surface integrals, using the divergence theorem. Going further, the surface integrals are themselves reduced to line integrals applied to the contours of the polyhedrons, using the Green's theorem. The mathematical problem is then quite simple, consisting in multiplications and additions. To be able to enforce this method, it is nevertheless necessary to have a totally closed mesh, that is without any free edge and the elementary faces of the mesh have to be oriented in the same way. Hence, for FASTABI, each normal of the mesh points outwards.

FASTABI then automatically computes the displaced volume that balances the weight of the ship (defined by the mass and the location of the centre of gravity) using a converging method by limiting the global mesh to the floatation surface, the latter representing still water or waved surface.

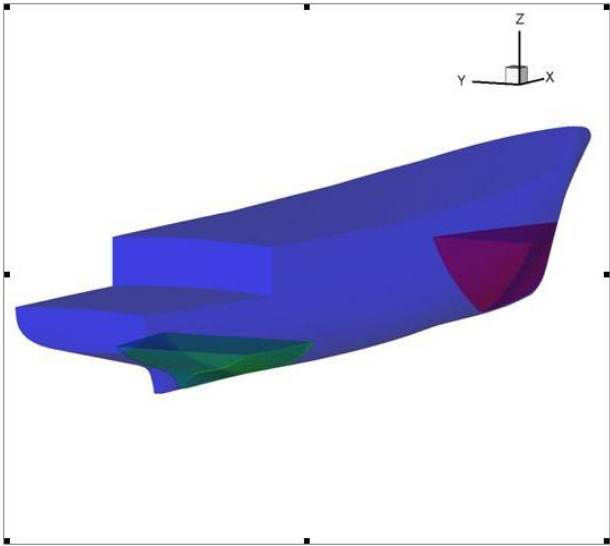


Fig. 3: CMT mesh used by FASTABI

The free surface effect resulting from liquid taking place in tanks is taken into account by meshing the latter and filling them up to the actual level. Each type of tank of the ship can also be automatically meshed by FASTABI, assuming that the walls located in the hull are planar surfaces.

Hence for a pure parallelepiped, 6 planes are used to define the tank, while for which some walls are common with the hull, such as the green and purple ones on Fig. 3, the closed contour is obtained by intersecting limiting planes with the global mesh of the hull. More complicated tanks are obtained by successive removals of smaller tanks from primary one.

As soon as the closed contour is obtained, FASTABI automatically meshes the outer surfaces using the so-called “ear cutting” algorithm, which is a triangle based method.

This meshing technique developed in FASTABI allows to quickly model each tank with a degree of precision at least equal to that

of the mesh of the hull and avoids the use of heavy codes dedicated to meshing operations.

The free surface effect is then automatically computed and taken into account at each step of the converging method when determining the global equilibrium of the ship. Hence, results are greatly improved when comparing with methods that traditionally represent the free surface effect through simple formulations.

### *Damage stability*

A given damage in the hull is considered in FASTABI as the loss of buoyancy volume. The damage is modelled exactly in the same way as the tanks are, and then removed from the global mesh of the ship, providing a new hull with which any computation can be performed. Tanks that are located in the damaged area can be removed or taken into account, being empty or loaded by their filling liquid. In the latter case, the buoyancy of the tank is included in the calculations.

The damaged analysis is carried out on intact situations that satisfy the stability criteria. The computations are made exactly in the same manner as in the intact situation, except that the criteria to be observed are modified.

It can be noted that concerning STEREDENN presently installed on board CMT “Aigle”, the possibility to perform damaged stability analysis is not used.

### **SECOND: GM ESTIMATOR**

The Sea State Estimator (SSE) module used in STEREDENN has already been briefly described in previous papers (Leguen 2007). It is based on a mathematical model of the ship (Transfer functions) that gives the ship's motions on any sea state. The SSE varies the significant height, the period and the heading of the swell till it fits the measured motion of the ship. The ship is modelled through her transfer function and the SSE searches the sea state that minimises the error between the theoretical response and the measured one. The

sea state is modelled through a Bretschneider spectrum whose parameters are:

- Significant wave height ( $H_s$  in m)
- wave period (peak period  $T_p$  or zero up-crossing period  $T_z$  in s)
- wave heading (in deg).

Transfer function of the ship are computed thank to the software PRECAL (seakeeping code developed by the CRS, Cooperative Research Ships). What we are interested in are the significant height and the peak period correlation coefficients of the 6 degrees of freedom. Computations are made for each wave period (from 5 to 8s each 1s), each heading (from 0 to 180deg each 15deg) and for several speeds (from 0 to 12knt each 2knt). All the results are gathered in a database stored on-board by STEREDENN. To achieve the estimate, the characteristic values of the measurements ( $H_s$ ,  $T_p$  and correlation coefficients) are compared to the values of the database. For each period and heading, the difference between theoretical and measured value of  $H_s$ ,  $T_p$  and the correlation coefficients are computed. The estimated sea state is the one with the smallest total error.

The motions used to estimate the sea state have an impact on the accuracy of the results. Building from its own experience, for this study DGA Hydrodynamics made the choice to use heave, pitch and sway motions. Heave and pitch are used for comparison of  $H_s$  and  $T_p$  because these motions are quite linear. The Pitch/Heave correlation is used to differentiate in an efficient way head seas and following seas. The sway/Heave correlation is used to identify if the swell comes from starboard or from port side. Those choices have been validated thank to seas trial aboard a CMT.

### THIRD: GM ESTIMATOR

A functionality of the system was developed in order to help the crew to validate the input data of the risk analysis. One of those input data is the vertical position of the centre of gravity. One way to estimate the  $GM$  value is to measure the roll period (for example Cotta 1985). If the displacement, the position of

centre of buoyancy, the mass inertia in roll and the added inertia in roll are known then it is possible to estimate the  $GM$  value using (1).

$$T_{\phi} = 2\pi \sqrt{\frac{I_{xx} + I_{xx}^a}{GM \cdot \Delta \cdot g}} \quad (1)$$

The difficulty is to know the inertia and the added inertia. To obtain those values, the best way seems to be to use measurements made during a stability experiments require by rules for  $GM$  evaluation. If during one of those experiments the roll period is measured, than it is possible to have the inertia on that day. Then as displacement, inertia can be deduced from this day to another day using mandatory stability package.

Formula (1) is often compressed in formula (2), and called Doyère formula.

$$T_{\phi} = k \sqrt{\frac{B^2 + 4KG^2}{GM}} \quad (2)$$

Inertia is included in the determination of the value of parameter  $k$ .

By inversion of (2) the position of centre of gravity is obtain with (3) from roll period measurement.

$$KG = \frac{-T_{\phi}^2 + \sqrt{T_{\phi}^4 - 16k^2(B^2k^2 - KM.T_{\phi}^2)}}{8k^2} \quad (3)$$

This methodology does not give measurement with so good accuracy than the usual way, but can be useful for the crew to check their estimation of  $KG$ .

## FOUR: RISK ESTIMATOR

### Seakeeping calculations

Seakeeping calculations (including occurrence of capsizing in severe seas) are performed with FREDYN version 9.9 (developed by CRNAV). Only cases without damage were performed (including limited cases with wind). In total 228288 (33x76x7x13) run of 1 to 8 hours (depending of the occurrence of capsize).

- 33 different displacements
- 76 sea states  $T_p$  from 5 and 17s and  $H_s$  from 2.5 to 17m
- 7 speeds
- 13 wave heading

Two months of calculation on a PC cluster were needed.

### Operability polar plot

Results were presented as one polar plot for each sea states displacement and wind conditions (see Fig 4).

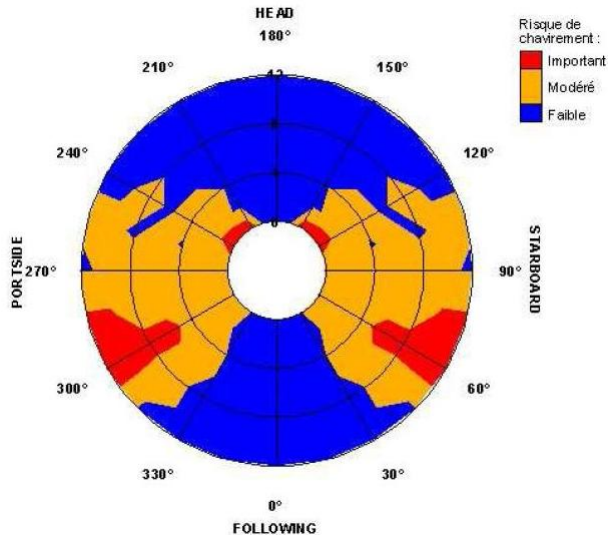


Fig. 4: Operability polar plot

Risk is assessed as the probability of capsizing in the following hour (with same condition). Risk is divided into three levels:

- Blue : low risk
- Orange : moderate risk
- Red : High risk

### Experimental validations

Because FREDYN is more dedicated to frigates hull forms, validation was needed for smaller ships as the mine hunters.

Beforehand roll damping was determined in order to include it directly in the code rather than use empirical estimations included in FREDYN. The estimation was determined during sea trials with extinction tests.

Two campaign were performed on two model sizes (1/12 and 1/36 scale). The first was used to validate moderate motions without speed while the small model was used with forward speed. In order to validate the occurrence of capsize it was mandatory to find at least on for the model. Those capsizes occurred on severe seas with low forward speeds and following seas.

## CONCLUSIONS

The system STEREDENN was tested at sea for a year. First feed-backs and validations of the SSE are confident. It seems that the information given to the crew is useful for them, even if they have always to make the final decision to evaluate the situation and the risk.

## ACKNOWLEDGMENTS

DGA Hydrodynamics wishes to thank SSF and ALFAN for given us this study which allowed the realisation of the prototype.

## REFERENCES

- Leguen J-F., Bourdon O., Dispa H. ; Hull Monitoring of a French Frigate, Description, Treatments and Applications ; ISOPE 2007
- Cotta A. ; GM\_METER. Appareil automatique de mesure en continu du module de stabilité des navires ; ATMA 1985
- FREDYN Version 9.9 User's manual, MARIN 2008



## Landing Craft Stability Standard

Jeremy Atkins

BMT Defence Services Ltd

Steve Marshall

Sea Systems Group, UK Ministry of Defence

Nick Noel-Johnson

BMT Defence Services Ltd

### ABSTRACT

The same stability criteria are applied to large and small naval ships and have served them well for many years. Landing craft are very different to warships (around which the standard was designed) putting into question the applicability of naval stability criteria and the assumptions regarding the risk of craft loss. A research programme to derive a new stability standard for UK landing craft is described. Detail is provided regarding the method for establishing operational doctrine, the associated landing craft specific stability hazards and the derivation of new stability criteria that will form a key element of the future standard.

### KEYWORDS

Craft; Doctrine; Dynamic; FREDYN; Freeboard; Landing; Stability; Standard.

### INTRODUCTION

Landing craft are complex marine vehicles. They are required to operate in a range of sea environments both independently and from motherships and beaches. Whilst doing this they must carry a wide variety of payloads including passengers. As a consequence of these factors the craft operate under limitations on deadweight and environment.

Accordingly, the safety standards for landing craft have to adequately address all these roles and activities. Stability criteria applied to Royal Marine landing craft have traditionally been a derivative of Def Stan 02:109. These in themselves are derived on longstanding criteria developed by Sarchin & Goldberg based on WWII frigate hullforms. Whilst their applicability to landing craft may not be inappropriate, although challenging (e.g. achieving the max GZ >30 degrees), the levels

of risk and robustness of the individual criteria and criteria set are not known.

The design of landing craft is often challenging as the craft when operated from motherships (e.g. Landing Platform Docks (LPD)) have a constrained size envelope. Some of the other factors influencing the design are:

- Draught constrained by depth of water over mothership dock sill;
- Weight constrained by davit launch;
- Beam constrained by mothership dock dimensions;
- Range & speed requirements;
- Cargo weight & load and offload arrangements;
- Crew access.

This paper describes the considerations, methodology and process for the development

of a bespoke stability standard for landing craft. The scope of the standard will address all the performance requirements of the Naval Ship Code (2009). The key lines of development described in this paper are focussed on the unique aspects of landing craft and thus the aspects requiring special consideration. In doing so the foundation of the development has been the doctrine for operation of landing craft.

## DOCTRINE

To inform the development of the standard and ensure that it adequately addresses the primary stability hazards it was necessary to verify the current understanding of landing craft operational doctrine. This was done through engagement with Landing Craft Utility (LCU) and Landing Craft Vehicle and Personnel (LCVP) coxswains in a series of stability related doctrine capture workshops.

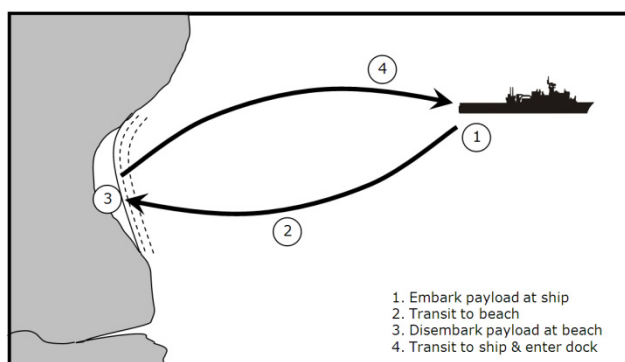


Fig. 1: Vignette used in operator doctrine capture workshops.

Each of the workshops adopted a common format and question set to ensure a consistent approach and thereby allow comparison to be drawn across the three groups of operators visited. A key element of the workshops was use of a common vignette against which the questions were pitched (Figure 1). These questions were designed to determine the doctrine employed during normal and wartime operation and their experience of landing craft operation. From their responses it was possible to establish a common picture of the evolutions that could be expected to occur.

Key conclusions specific to landing craft operation and design drawn from the exercise are as follows:

- There was a consistent approach to landing craft operation across each group of operators;
- The coxswains' recollections of landing craft handling, seakeeping and cues to adjust heading and speed are the same;
- The actions taken by the coxswains following these cues were broadly similar;
- The LCU Mk10 does not suffer from regular green seas whilst operating within the prescribed operational envelope;
- Green sea events are used as a primary indicator to the coxswain to change course/speed.

Potential stability safety hazards associated with the operational doctrine were identified during the exercise. These hazards are being used to inform the development of the new stability standard. Some examples of these hazards are illustrated in Table 1, below.

**Table 1: Stability hazards identified during doctrine capture workshops.**

Key Event	Hazard(s)
Interpretation of Sea Conditions	The provenance of surf height limits for landing craft is not known.  Inaccurate sea state assessment.
Damage / Loss of Watertight Integrity	The internal geometry / constrained compartments of landing craft prevents effective damage control.  Raking damage that affects two compartments (including main engine room).
Beach Approach and Departure	Insufficient power or propulsor emergence and subsequent loss of control in surf zone.  Capsize in surf zone on approach to beach due to wave action.  Capsize in surf zone during 180 degree turn due to wave action.
Green Seas / Water in Well Deck	Effect of green seas and the ability to remove entrained water.
Loss of Power / Steerage	Loss of propulsive power during operation (transit/open water and surf zone).
Payload Unloading, Loading, Positioning & Securing	Embarking unknown vehicle weight/VCG (e.g. due to payload of vehicle).  Retraction through surf zone with unknown trim / list / draught.

## STABILITY STANDARD STRUCTURE

### *Watertight Integrity*

The programme will develop standards for each of the performance requirements for watertight integrity. Whilst most of these are relatively straight forward some require special

attention due to the design and operation of landing craft.

The standard will address the need for protection of the forward part of the ship from both collision with floating objects (e.g. whilst entering an LPD) and from grounding (e.g. on unsurveyed rocks).

The open nature of the typical craft with high bulwarks requires the drainage of the cargo deck to be efficient as trapped water on deck leads to a reduction in stability. The study has focussed on researching the sizing of freeing ports stipulated by different Administrations for a variety of craft. A direct approach to sizing freeing ports relating the height of bulwarks, deck area and possible reduction in stability has proved unsuccessful. No direct relationship to the sizing required by Load Line and stability parameters could be derived.

Green water is one of the key cues to handling of the craft and heading and speed would be altered to remove the frequency of such events. Current arrangements on UK LCU Mk10's are designed to Load Lines rules and it was reported during the doctrine workshops that when water enters the deck it drains away quickly and efficiently.

The design constraints for landing craft results in some challenges for the protection of vents. Bespoke arrangements are normal practice and designs must consider the operational environment and additional influences such as accidental damage from payload handling, operation in cold weather and damage from debris.

### *Reserve of Buoyancy*

A range of areas are being developed to support the requirements for reserve of buoyancy, such as the construct of loading conditions and the subdivision of landing craft. The programme will also review the damage extents currently applied to landing craft and

develop requirements that better reflect the hazards from operation e.g. damage from grounding. The outcome will also define a distinction between safety (damage from grounding & collision) and capability (damage from hostile action).

A further key line of development surrounds the performance requirements for freeboard. A ship's freeboard provides a safety margin for buoyancy and stability above that required for static equilibrium in calm seas to allow the ship to operate in a seaway. Freeboard has a direct effect on the relative height of the gunwale and wave crests; it can therefore influence the incidence and quantity of green seas. Altering freeboard also allows the designer to influence intact stability, damaged condition reserve of buoyancy and damaged stability.

Construction of the requirements for freeboard consisted of firstly defining the performance requirement associated with freeboard; and secondly, arriving at a consistent definition for how freeboard is measured that can be applied to the wide range of landing craft designs that the standard is intended to cover.

Considering first the performance requirements, these have been developed to support the functional objective that the ship shall have sufficient freeboard to prevent excessive shipping of green seas in any foreseeable operating condition. This in turn leads to performance requirements that can be summarised as:

- Have a minimum freeboard to ensure an adequate reserve of buoyancy. As a minimum, the freeboard shall meet the requirements of the Merchant Shipping (Load Line) Regulations (1998);
- Have a minimum height of side to limit the shipping of green seas to a level at which, any resulting entrapped water does not

threaten the stability and buoyancy of the vessel;

- Remain afloat following the loss of hull integrity resulting from foreseeable damage and following shipping of green seas.

The second area of development concerned the consistent definition of freeboard. Whilst at face value, this may appear a simple task it is much complicated by the variable nature of landing craft designs.

Both the Naval Ship Code and the Merchant Shipping (Load Line) Regulations both use a similar definition for freeboard that refers to freeboard as the distance measured vertically downwards at amidships from the upper edge of the deck-line to the load line.

In the case of landing craft, the freeboard definition can become a significant design driver. The lowest deck exposed to the external environment is invariably the vehicle deck (Figure 2), the height of which can prove critical to achieving a balanced design. In the example in Figure 2, increasing freeboard and consequently vehicle deck height, results in raising the payload centre of gravity which may result in an associated reduction in stability. Furthermore, it may also limit the capability of the landing craft as vehicle deck height can drive bow ramp length and gradient, or can limit the beach gradient on which the landing craft payload can be disembarked. These competing design requirements may result in a solution where the vehicle deck is placed as low as possible.

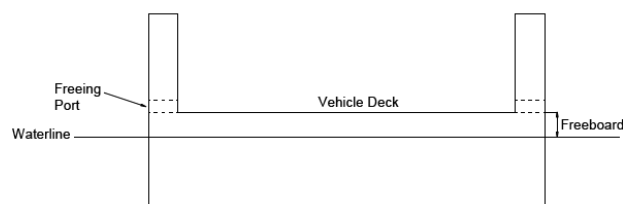


Fig. 2. Freeboard measured to vehicle deck.

In extreme cases this can result in landing craft designs where the vehicle deck is below

the waterline, for example the UK LCVP Mk5. Applying the existing freeboard definition in this instance, results in a negative freeboard value.

A more suitable definition of freeboard was required to allow the design requirements to be articulated appropriately. A solution was found in the Maritime and Coastguard Agency definition for Small Commercial Vessels and Pilot Boats (2004):

*“Freeboard means the distance measured vertically downwards from the lowest point of the upper edge of the weatherdeck to the waterline in still water or, for an open vessel, the distance measured vertically downwards from the lowest point of the gunwale to the waterline.”*

An open vessel being in this case a landing craft that may not be fitted with a watertight weatherdeck over part of its length.

It is not appropriate to always measure freeboard to the top of the bulwark as Regulation 2 of the Landing Craft Stability Standard requires all exposed decks to have an efficient means of drainage. This may take the form of freeing ports or a pump arrangement. In the case of freeing ports, unless they have a watertight closure, water is able to enter the vehicle deck as well as drain from it which limits the reserve of buoyancy.

However, a bulwark with openings such as freeing ports can still be effective at minimising the shipping of green seas. This is particularly true where openings are arranged or provided with suitable protection to prevent ingress of water during transient immersion.

Therefore freeboard is defined to ensure adequate reserve of buoyancy and the height of side is defined to limit shipping of green seas.

### ***Reserve of Stability***

The goal of the research is to develop quasi-static stability criteria similar to the scope that are currently employed on such craft. These will be based on a dynamic analysis and capsize risk methodology using FREDYN that has been benchmarked against model tests.

A 1/16<sup>th</sup> scale model of a generic LCU-type hull was constructed and tested in large seas to measure seakeeping data for FREDYN validation and to assess the dynamic stability of landing craft (Figures 3 & 4). The model was tested at a single displacement with multiple VCGs and two different sizes of freeing ports. The model scale was chosen to provide a nominal model length of 1.5m.

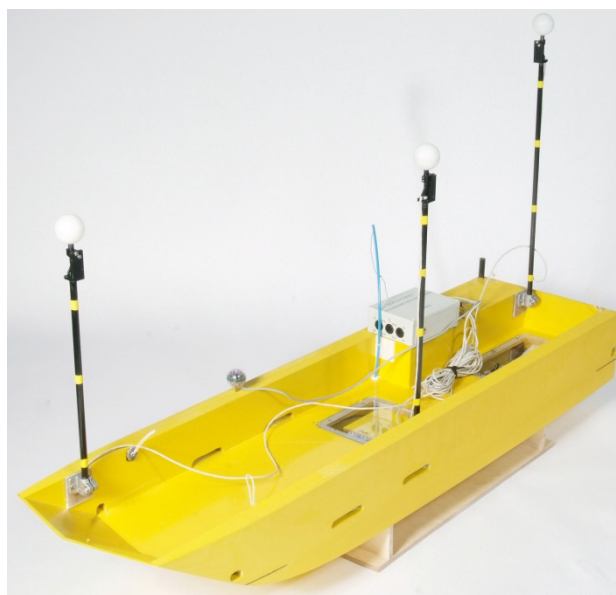


Fig. 3: Free running experiment model.

This set of model tests was undertaken in the Ocean Basin at QinetiQ Haslar during June 2009. For this study, the model was tested in stern and stern quartering seas in the intact condition. It was predominantly tested in stern seas, since these were considered most likely to induce broaching motions and water on deck problems; particularly in the steep, near shore wave conditions. The tests were conducted at close to 5 and 10kts (full scale) in order to capture any dynamic stability effects, such as broaching. Different sized freeing ports were

achieved by commencing the experiments with one size of freeing ports and then permanently making the ports larger part way through the tests. This change in size represented an increase in freeing port area of 50%. The model was run at two relative wave headings, two speeds and in five combinations of regular wave frequency and height. Steep, irregular waves representing sea states 4 and 5 were also tested.

Two loading conditions were tested with the VCG of the first set at the limiting value for compliance with Def Stan 02:109, the second was set with an increase of 0.4m at full scale. The model did not demonstrate any instability in the load conditions initially chosen, and so additional experimental runs would be conducted at the 30 degree heading (stern quartering seas) and at 10kts with higher VCGs, in order to determine the point of vessel capsize.

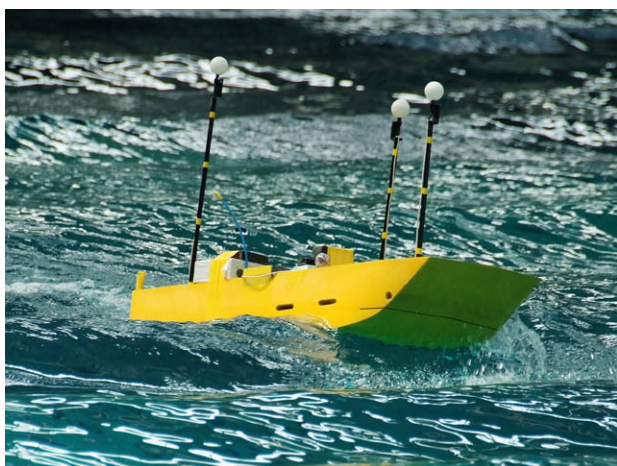


Fig. 4: Free running experiment model

Due to the relatively unusual box shape of the LCU hull design, the original SHIPMO calculation method in FREDYN for added mass and damping calculations was not considered accurate enough in FREDYN. The new SHIPMO2006 code can account for more unusual ship forms and was considered as being more pertinent for use for this shape of hull form. The internal arrangement of the vessel was modelled in FREDYN, based on the

Paramarine model. The vehicle deck region was modelled in FREDYN as a large damage compartment with openings above the side deck edge; this allowed water to flow on and off the vehicle deck in a realistic manner during FREDYN simulations.

A selection of static and dynamic roll decay data from the experiments was used to compare and tune the FREDYN model for the generic LCU. FREDYN was originally developed for frigate forms. As the generic LCU is quite different in shape, there was a need to perform some tuning of the roll decay characteristics of the FREDYN model.

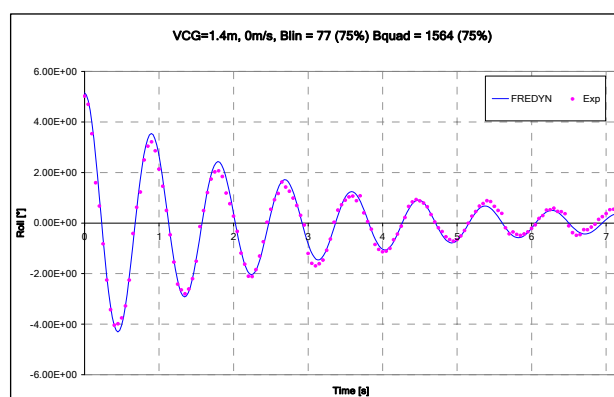


Fig. 5: Static roll decay comparison.

A direct comparison between the motions recorded during the experiments and the motions predicted within FREDYN was undertaken. For regular seas, in addition to RMS values, the period of oscillation and correlation of the time based traces of roll, pitch and heave were used to characterise the quality of the FREDYN simulations in the more stable conditions. In the high VCG conditions, the comparisons were more related to the prediction of motion 'events', such as large roll angle excursions and capsize events.

Difficulties were experienced achieving adequate replication of the tank model track due to the manoeuvring model in FREDYN and its constraints on waterjet bucket angles. Once these were addressed a good correlation of the track lead to a good correlation with the model tests.

The higher VCG runs showed more frequent capsize with a similar time trace prior to capsize and then a good correlation of the capsize mode between FREDYN and experiment. A point to note is that the LCU experiment model often survived more wave encounters prior to capsize, whereas the FREDYN simulation predicted capsize earlier, although following the same capsize mode as the experiment.

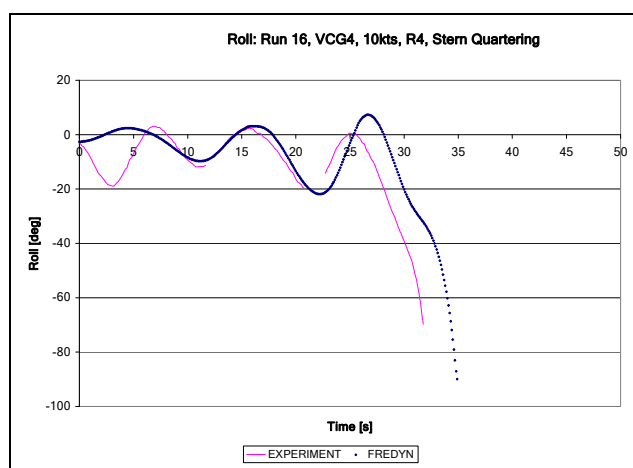


Fig. 6: Capsize model test/FREDYN comparison.

As part of this phase of work, an initial computational study using probabilistic risk calculations to investigate the envelope of the dynamic stability performance, based on the way in which the vessel is operated, is to be investigated. By varying the vessel load conditions (displacement and vertical centre of gravity), the static stability parameters used in the current intact criteria assessment will vary. Conducting simulations for a number of loading conditions will provide probabilities of loss of the vessel due to loss of buoyancy or stability in all these conditions.

Information from the doctrine workshops on how the operators selected speeds and headings and the cues they used were distilled down into a set of realistic scenarios and input parameters for use in the simulations.

It was clear from the workshops that there are two distinct phases to the operation of the

landing craft: the transit from mothership to shore in open ocean and the time spent in surf conditions near to the beach.

To investigate the performance in the transit phase, the intact stability study involves running the CRNavies PCAPREF program, which utilises FREDYN as a subroutine, to calculate probabilities of intact vessel loss in a seaway. Two speeds were identified from the workshops, 5.0 and 7.5kts, with the lower speed only used in bow and bow quartering seas. The headings were found to be of equal probability, so a range of headings from 0 to 180 degrees in 30 degree intervals are being calculated.

Two displacements were selected, with four VCG conditions that span the current intact stability criteria from pass to fail. A full and reduced freeboard height was also created for four of the conditions to identify the effect that freeboard height has on the heavy weather survivability. Based on the current guidelines and the workshop discussion, the wave condition limit for these craft is currently sea state 5; if encountered, the craft should head for shelter. Taking this into consideration, a maximum significant wave height of 5m would be used in the simulation, which actually equates to a sea state 6, in order to extend the operational envelope in the simulations. The wave height condition is varied in 0.5m increments. A cut down wave scatter table was selected and the probabilities factored to produce a value of 1 for these craft.

For the definition of the capsize point in the PCAPREF calculations, a value equal to the roll angle at which the gunwale would submerge was selected, as it has been seen in the experiments that a substantial intake of water onto the vehicle deck rapidly leads to loss of the vessel. These capsize risk calculations will be reported in future papers.

### ***Safety of Embarked Persons***

The performance requirements of the Naval Ship Code stipulate the assessment of the impact of craft behaviour on personnel activities and safety arrangements. This aspect of the programme is envisaged to adopt current standards with little development needed.

### ***Preservation of Life***

The landing craft should provide a safe haven for those onboard following an extreme event until the point of evacuation. Craft similar in size to landing craft have little survivability beyond damage to a single compartment. The craft are limited in range and at present have a limitation of 20nm from a safe haven or mothership. It would possibly be at disproportional cost to require enhanced survivability for such simple craft. The focus of this research line is to ensure that the escape and evacuation arrangements are balanced with the craft ultimate stability performance.

### ***Provision of Operational Information***

The role of these craft as highlighted in the vignette (Figure 1) is complex and the payload may vary greatly and also the weight of vehicles may, on occasions, not be known. One of the challenges is determining if the craft are overloaded. A load line mark is not appropriate as the craft is loaded when aground and not in environmental conditions where the draughts can be read to any reliable accuracy. The operator guidance provided to the coxswain needs to reflect closely how the craft are operated, as such the format of traditional Stability Information Books is not appropriate. The key facets of operator guidance are:

- Clear and concise instruction on stability and maintaining watertight integrity;
- A matrix of payloads, their locations and particular fluid restrictions;
- A simple method of determining the stability of unique payloads.

The impact on the designer is ultimately a greater range of loading conditions for assessment and conversion of the output to a form that is simple to interrogate by the coxswain. This in itself is a great challenge for naval architects who in the main design operator guidance that has to meet often a conflicting role for both Administration plan approval and use by the operator.

### **CONCLUDING REMARKS**

The risks associated with the application of traditional warship, frigate based, stability criteria to small craft with different L/B ratios is under development. Landing craft although they look simple are complex to design, having to satisfy a number of key constraints. Furthermore, the role of carrying a wide variety of cargos and the environment they operate in has lead to the need assess the risks associated with the application of current standards and to derive a bespoke cohesive stability standard. The key knowledge vacuums where resource is being concentrated are:

- Operator influences and ship-handling cues;
- Freeboard requirements;
- Stability criteria;
- Damage extents;
- Operator guidance.

This paper has described the progress made so far on understanding the influences on the stability of landing craft. Adopting the systems approach to developing a new bespoke standard should provide coherency and transparency encompassing all areas of the NATO Naval Ship Code Chapter III performance requirements.

### **DISCLAIMER**

The statements and opinions made in this paper are those of the authors and may not represent those of the UK Ministry of Defence or BMT Defence Services Ltd.

**REFERENCES**

MCA MGN 280 (M) Small Vessels in Commercial Use for  
Sport or Pleasure, Workboats and Pilot Boats - Alternative  
Construction Standards, 2004

Merchant Shipping (Load Line) Regulations 1998

Naval Ship Code, Allied Naval Engineering Publication 77,  
December 2009



## On the Time Dependent Survivability of ROPAX Ships

Dimitris A. Spanos

Apostolos Papanikolaou

*The Ship Design Laboratory of the National Technical University of Athens*

### ABSTRACT

The time dependent survivability of ROPAX vessels is herein investigated by use of numerical simulations of ship motion and flooding in waves. Present studies further confirm that characteristically a ROPAX ship capsizes fast when sustaining damages leading to capsize. The time dependent survivability is estimated by applying Monte Carlo probability simulation, and was found to be limited within short times after the damage event. Finally, the survive wave height, unconditional to damage opening and loading condition, is approached.

### KEYWORDS

Time to capsize; survivability; capsize; simulation; flooding; damage stability; ROPAX

### GENERAL

The time a ship survives after a casualty of flooding has become an explicit design objective for passenger ships through the SOLAS amendments, *IMO* (2006), and the introduced concept of *safe return to port*. The purpose of the regulations is to establish design and operational criteria so that when a passenger ship is subject to flooding of any single watertight compartment then vital systems and services will remain operational for the safe return to port with its own propulsion and the ordered evacuation and abandonment of people on board. These regulations will be applicable to all passenger ships (of length 120 m and over) built on or after July 1, 2010 (one week after the date of the present workshop).

Implications on the ship design will be mainly related to the rearrangement of systems and services in order to provide the required redundancy for machinery and propulsion. New designs are expected to be, in principle, of improved safety with respect to flooding (and fire, which is regulated accordingly). However the watertight subdivision remains the basic approach to control the time to survive after a casualty.

The prime assumption of the safe return is that the ship is able to survive the flooding of one compartment for sufficient time, and then, safety concerns can be reduced to the loss of operability of the systems installed inside. The time dependent survivability of ships has been addressed both by setting a time threshold of 3 hours (*IMO*, *MSC.78*) for the development of the relevant regulations, as well as through the time requirements which are derived from the evacuation procedure and ordered abandonment for a passenger ship separately.

For ROPAX ships, and differently to other ship designs, to survive one compartment damage for sufficient time requires additional considerations, because ship's survivability is strongly dependent on the possible flooding of the large vehicle space, which is located above the calm water free surface. For such arrangements, the damage openings are likely extended above the subdivision deck (car deck). Then, even if one compartment below the main deck is damaged, the vehicle space may also be flooded because of the action of waves, which may lead to ship capsize if the floodwater exceeds some critical amount. Hence, additionally to the transverse and longitudinal watertight subdivision, the horizontal subdivision is of importance for

ROPAX vessels and has to be thoughtfully considered in connection to the one compartment damage.

The amount of water on deck that a ROPAX vessel may sustain is characteristic to each ship loading condition and damage case. This critical amount has been extensively investigated over the last decades and was regulated with SOLAS'95 (Stockholm Agreement provisions). There, the damage stability is evaluated in the presence of a critical amount of water on deck that may potentially be accumulated. Nevertheless, it is still unknown how long a ship that complies with the provisions may survive after damage.

The flooding rate of the vehicle space eventually determines the time to flood the deck, up to the critical amount. Obviously if the rate happens to be slow, because of a small damage opening or low wave heights, then a long time is required for the water on deck to grow up to the critical amount and to approach critical stability. However, in earlier work of *Spanos & Papanikolaou (2007)*, it was pointed out that the flooding of the vehicle deck is a relatively fast process, characterized by limited probability of ship loss in later times. These observations, which were related to the worst SOLAS damage, are herein further verified by analyzing another typical ROPAX, and by investigating the more general situation, where the parameters of the damage case are randomized too.

#### TIME TO CAPSIZE FOR DAMAGED ROPAX

Numerical simulation methods for the motion of the damaged ROPAX ships in waves may today provide excellent guidance in related studies and investigations. Herein the simulation method by *Spanos (2002)* is applied to analyze the time aspects of the complex flooding process and the dynamic stability in waves.

Figure 1 presents the time to capsize of a ROPAX vessel in beam waves versus the significant height of the incident waves.

Numerical simulation results in comparison with experimental data from recent tank model tests by *Rask (2010)* are presented, referring to developed seas of *JONSWAP* spectrum and slope  $H_s / \lambda = 0.04$ .

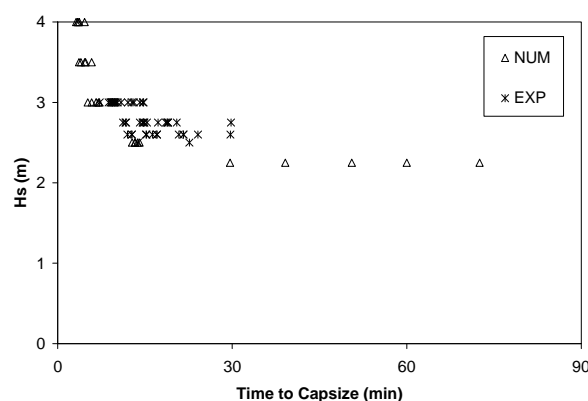


Figure 1 Numerical simulation and experimental data.

The time estimations regard a typical two compartments damage case as demonstrated in Figure 2. This is a ROPAX vessel of 137 m length, (geometrically similar to the ROPAX *Estonia*, lost on 1994) having damaged the two shaded compartments aft amidships plus the vehicle space. The fore compartment corresponds to the main engine room. Inside the aft compartment there is an intact side tank which causes an asymmetric damage case. The assumed damage opening, according to SOLAS'95 (B-II Reg.14), is located on the port side.

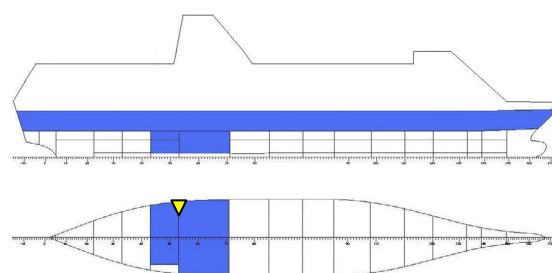


Figure 2 Typical damage case.

Figure 1 suggests a high correlation between the numerical results and the experimental data. The measurements in the tank are stopped after 30 min, hence there are no data for later times. A limit survive wave height at 2.25 m is identified from the numerical simulations as an asymptotic below which no capsize events may

occur. The corresponding height for the tank tests is estimated at 2.50 m, thereof a difference within tolerance is observed.

For wave heights just below the survive limit, the flooding process reaches some average balance between the water inflow and outflow on the deck area, maintaining some average floodwater on deck, which is not enough to lead to any capsize and the vessel survives for long. For even smaller waves no floodwater could reach the deck, as a result of large damage freeboard compared to the incoming waves.

Some basic difference between the presented physical and numerical tests is that in numerical simulation the ship moves in 3 degrees of freedom (that of heave, roll and pitch) whereas in the tank the ship model freely moved in 6 degrees and drifted downstream in beam waves. This fact, together with the ideal test conditions with the computer simulation, may explain the different scatter of the times to capsize.

Figure 1 is characteristic for damaged ROPAX ships, according which, the ship survives infinite time for waves heights up to the survive limit and capsizes above that limit in a fast mode, in the particular case in less than 30 min. Half hour is considered a fast capsize in view of the required time for an ordered evacuation, in addition to the time needed to evaluate a damage and make any decision for evacuation.

### SENSITIVITY OF THE SURVIVE TIME

Sensitivity studies based on numerical simulation have shown that the time to capsize keeps the characteristic behaviour of Figure 1 in the variance of the basic parameters of the damage cases. The ship loading condition, the sea state and the possible shape of damage opening may affect either the survive limit of wave heights or directly the time to capsize.

Regarding the incident waves, the time to capsize was found to be insensitive with

respect to two different wave spectra, namely that of *JONSWAP* and *Pierson-Moskowitz* types of equal spectrum parameters. It was also insensitive to the wave heading for changes up to 20 degrees from beam waves. While a delay of capsize and simultaneously increase of survive limit could be observed for the longer waves, as shown in Figure 3. Another basic parameter, the *GM* also affects the time to capsize, also presented in Figure 3. By increasing the *GM* (by 0.5 m) an increase of both the survive limit (by 0.5 m) as well as a double time to capsize has resulted.

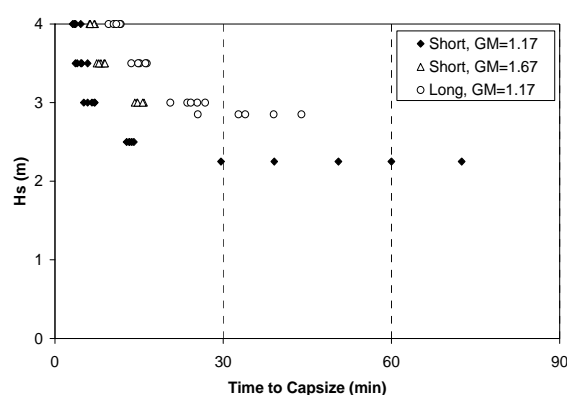


Figure 3 Effect of *GM* and wave periods on time to capsize.

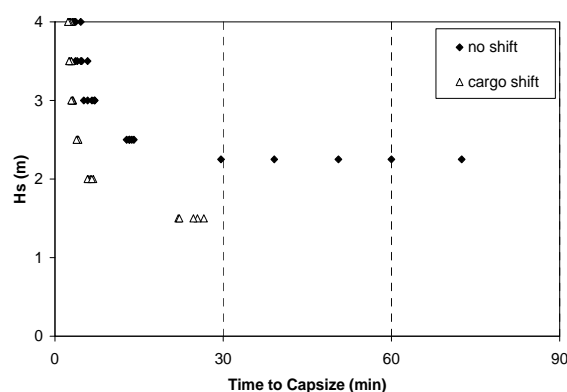


Figure 4 Shift of cargo strong effect on TTC.

Another notable effect could be observed for the transverse centre of gravity TCG of the ship, which may be due to some shift of cargo, Figure 4. Then a substantial decrease of the survive wave height and notably faster capsize observed. This change is actually an effect of ship loading condition and change of corresponding residual stability; however, the characteristic behaviour of the time to capsize remains still unchanged.

### TIME DEPENDENT SURVIVABILITY

The parameters that practically affect the time to capsize, and discussed above, were the assumed sea state (significant wave height and period), the ship loading condition (as expressed through *GM*) and of course the size of the damage opening. For small sizes of the opening delayed capsizes or even not capsize at all is expected, while large openings may lead to fast capsizes.

To estimate the probability distribution of the time to capsize for the studied damage case in the most generic situation, a probability simulation has been applied by use of Monte Carlo method. The parameters that affect the time to capsize are assumed to be random variables of given probabilities. In particular, rough waves up to 4.0 m of significant wave height were assumed and of a probability distribution according to that of collision statistics. The waves were assumed of *JONSWAP* spectrum with slope  $H_s/\lambda$  uniformly distributed between 0.018 and 0.050. The metacentric height *GM* of the intact ship was assumed also uniformly distributed between 1.00 m and 2.75 m. And finally, the damage opening was of rectangular shape with dimensions that follow the statistical distributions of collision damages (see, Lutzen 2001).

The results of the probability simulation are summarized in Figure 5, which are the fit curves of the numerical statistics. The unimodal probability distribution has the peak at 10 min and thereafter it continuously decays. The probability to capsize within 30 min from the damage event equals 80% and it reaches almost 95% within 60 min.

Given the probability of the time to capsize then the time dependent survivability of the ship can be directly estimated, and it is presented in Figure 6 below. This is the probability to survive the damage case of Figure 2. The probability to survive *s* is a function of time, and asymptotically converges to 0.981. This limit is the survivability,

unconditional to the time as well as to the damage opening, sea state and *GM*. If the survivability would be defined with respect to the 30 min limit, as used to be in SOLAS, then the it would slightly increase and reach a value of  $s=0.985$ . Apparently, the time dependence of survivability is limited to below 60 min, and remains practically independent of time for times longer than 1 hour.

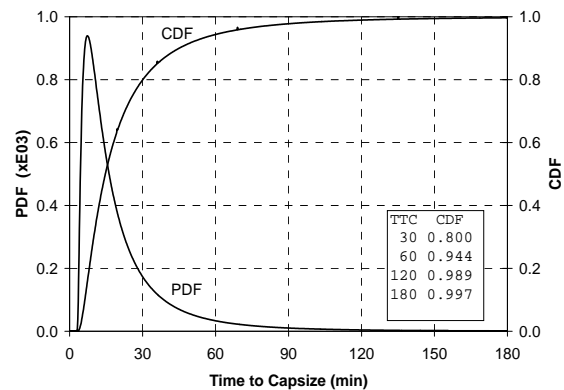


Figure 5 Probability of Time to Capsize in rough waves.

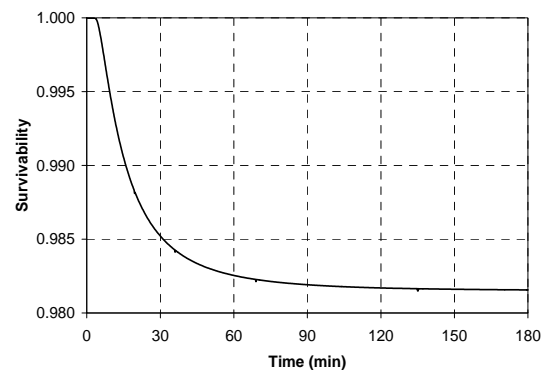


Figure 6 Time dependent survivability of the ship for the specific damage case.

According to SOLAS (2009, Part B1, reg.7.2) the survivability in waves for this particular damage case equals  $s=0.836$  (with  $GZ_{max}=0.10$  m and range 9.4 deg). This is notably different from the above *s*-factor, which was estimated by numerical simulation. This underestimation of survivability according to the SOLAS regulations confirms (at least in this case) the conservative nature of stability and safety regulations. However, the more than eight times higher value of the probability to capsize *c* (which is  $c=1-s$ ) resulting from the two estimations, namely 16% against 2%,

reinforces the necessity to sustain investigation on the survivability models.

### **CLOSING REMARKS**

The survivability of a damaged ROPAX in waves has been analyzed in the most generic damage situation. It was confirmed that capsizing may occur due to floodwater accumulated on the vehicle deck and that capsizing is then fast.

Survive limits could be clearly identified for each particular investigated condition. Below that limit a ship capsizing does not occur.

Taking into account the random nature of the main parameters, like the damage opening and loading condition, a generic survive limit could be still detected, below which no capsizing events could occur and above which capsizing was always a likely event.

It was also demonstrated that the survivability of a ROPAX ship is weakly dependent for times between 30 and 60 min, and practically time independent for times later than 1 hour. On the basis of the so far studies and evidences, the survivability of ROPAX ships may be regarded as time independent.

Finally, the survivability of the investigated ROPAX in collision damages is significantly underestimated by the present SOLAS 2009, which is an additional evidence for the necessity for further evaluation and possible improvement of these regulations.

### **ACKNOWLEDGEMENTS**

The herein presented results were deduced from studies conducted within the European Commission research projects FLOODSTAND (Integrated Flooding Control and Standard for Stability and Crises Management, SCP7-GA-2009-218532), and GOALDS (Goal Based Damage Stability, FP7-SST-2008-RTD-1-233876). The European Commission and the authors shall not in any way be liable or responsible for the use of any knowledge, information or data presented, or of the consequences thereof.

### *References*

- IMO, Resolution MSC.216 (82), Adoption of Amendments to the International Convention for the Safety of Life at Sea, 1974, as amended, December 8, 2006.
- Lutzen, M., Ship collision Damage, PhD thesis, Dept. of Mechanical Engineering, Technical University of Denmark, December 2001.
- Rask, I., Benchmark data on time to capsize for a free drifting model, E.U. research project FLOODSTAND, Integrated Flooding Control and Standard for Stability and Crises Management, FP7-RTD-218532, Rep.4.1.a, rev.2, 2010.
- Spanos, D.A., Time Domain Simulation of Motion and Flooding of Damaged Ships in Waves, Doctoral Thesis, Ship Design Lab., National Technical University of Athens, 2002.
- Spanos, D.A., Papanikolaou, A., On the Time to Capsize of a Damaged RoRo/Passenger Ship in Waves, 9<sup>th</sup> Inter. Ship Stability Workshop, Hamburg, 2007.



## Comparison of $s$ -factors according to SOLAS and SEM for Ro-Pax vessels

Maciej Pawłowski

School of Ocean Engineering and Ship Technology,  
TU Gdansk, Poland

### ABSTRACT

The paper discusses differences between the  $s$ -factors for ro-pax vessels, calculated according to the SOLAS methodology and the SEM for a middle sized Polish ferry “Polonia” and for a box-shaped vessel. Three major conclusions can be drawn from numerical results. 1) the  $s$ -factors according to the SOLAS Convention are *smaller* than or equal to the  $s$ -factors according to the SEM, 2) the smaller the damage stability, the greater the difference between them, which results from the fact that the SOLAS  $s$ -factor is much more sensitive to stability than the  $s$ -factor based on the rational SEM, 3) the SOLAS Convention underestimates the real safety of ro-pax vessels, and 4) the degree of underestimation increases with the ship size.

### KEYWORDS

subdivision, damage stability,  $s$ -factor

### INTRODUCTION

Since 1996 a rational methodology for the prediction of the  $s$ -factor has been known, which means the probability of surviving the ship with a given compartment or a group of compartments flooded. The method, developed originally for RO/RO vessels at Strathclyde University, has been known as the static equivalent method (SEM), see Vassalos *et al.* (1996, 1997), Pawłowski (2004, 2007a, b). IMO (1997), however, was in favour of adopting for the  $s$ -factor a simplistic methodology, based on the  $GZ$ -curve, reflecting so-called good engineering judgement. The original formulation was this

$$s = C(\frac{1}{2}GZ_{max}Range)^{1/2}, \quad (1)$$

where the coefficient  $C$  accounts for the effect of the final angle of equilibrium, with  $C = 1$ , if the final angle of equilibrium  $\phi_e \leq 25^\circ$ ,  $C = 0$ , if  $\phi_e > 30^\circ$ , and  $C = [(30 - \phi_e)/5]^{1/2}$ , otherwise.  $GZ_{max}$  is the maximum righting lever (metres) within the range as given below but not more than 0.1 m.  $Range$  is understood as the range of positive righting levers beyond the angle of equilibrium but not more than  $20^\circ$ , and not more than to the angle of immersion of non-weather-tight openings.

Some years later, influenced by the HARDER project (2003), IMO (2009) decided to modify the

above formulation, keeping on the same format, embedded in the  $GZ$ -curve, as follows

$$s = C(\frac{25}{48}GZ_{max}Range)^{1/4}, \quad (2)$$

where  $GZ_{max}$  is not to be taken more than 0.12 m, and  $Range$  not more than  $16^\circ$ . The above formulation has been derived using the standard IMO distribution of sea states at the moment of collision. Therefore, it is invalid for other sea state distributions. Further, it provides no information, whether the ship is safe at the given sea state after collision.

### ORIGINAL SEM FOR RO/RO SHIPS

Prior to 1996, over thirty years of research failed to develop rational and accurate damaged stability criteria to predict the capsizal resistance of damaged RO/RO vessels, despite great efforts (Middleton and Numata 1970, Bird and Browne 1973). The SEM for RO/RO ships postulates that the ship capsizes in a way that is quasi-static and based on the heeling moment of the elevated water on the vehicle deck. This method was developed following observations of the behaviour of damaged ship models in waves. Among the most important observations from these model tests and subsequent investigations (Vassalos *et al.* 1996, 1997) are:

1. As the ship reaches the *point of no return* (PNR) it behaves quasi-statically, with marginal transverse stability and very subdued roll motions.

2. The PNR (the critical heel) generally occurs at an angle very close to  $\phi_{max}$ , the angle where the static  $GZ$  curve for the damage ship reaches maximum.
3. The critical amount of water on the vehicle deck can be predicted from static calculations by pouring water onto the undamaged vehicle deck until the heel angle reaches  $\phi_{max}$ .
4. The critical and unique measure of the ship's survival capability is the level  $h$  that this critical water is elevated above the sea level at the point of no return, as shown in Figure 1. This simple fact was unknown until 1996 and was the prime reason why the previous model tests were inconclusive.

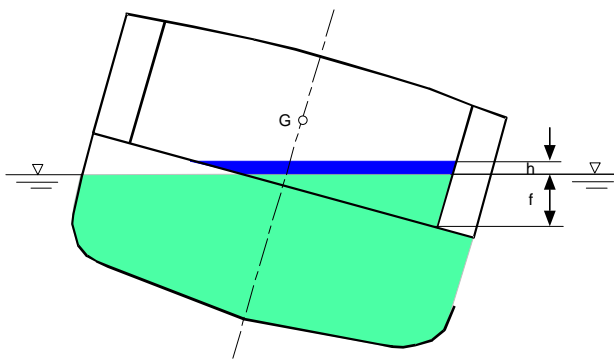


Figure 1. A damaged RO/RO ship with a rise of water on the car deck at the PNR

5. The model tests and subsequent simulations indicated that this elevation of water on deck  $h$  could be directly linked to the sea state, or  $H_s$ .
6. The higher the water elevation  $h$  at the point of no return, the higher the sea state needed to elevate the water to this level and capsize the ship.
7. Generally, the size of the damage opening, the trim and damage freeboard of the ship do not affect the survival capability.

Subsequent investigations have indicated that the immersion of the deck edge  $f$  at the damage opening is relevant to some extent, and several refinements and enhancements in the SEM are, therefore, possible based on the theoretical model for water on deck accumulation, as developed by Pawłowski (2001a, b, 2003). This effect, however, is of little importance and can be ignored.

Hence, the sought boundary stability curve may take the form of:

$$h = 0.085 H_s^{1.3}, \quad (3)$$

where both quantities are in metres,  $h$  is the elevation of water on the vehicle deck above sea level at the critical heel angle, obtained by static calcula-

tions, and  $H_s$  is the median sea state the ship can withstand with given stability, termed also as the critical sea state.

The critical heel angle (PNR) is understood here as the heel angle induced by the elevated water on deck at which the equilibrium of the ship is unstable. This angle is crucial for the SEM, as the elevation of water is calculated just at that angle, which in turn defines the critical  $H_s$ .

It is possible to find the critical heel angle, equal the angle  $\phi_{max}$ , with the omission of the  $GZ$ -curve, which is particularly useful for flooding cases with trim. This characteristic value is such for which the heeling moment produced by elevated water reaches a maximum. In this concept it is sufficient to find for each amount of water on deck the  $GZ$ -lever at the angle of loll over a range of heel angles, and to choose the one with a maximum  $GZ$ -lever. To do these calculations effectively, knowledge of principal axes of inertia for actual damaged waterplanes is needed. The entire known commercial software does not provide these characteristics.

Equation (3) provides on the whole a first-rate prediction, with deviations in a large majority of cases less than the sea state resolution used to derive  $H_s$ , which was 0.5 m. The above equation is universal, i.e. independent of ship size, the type of ship subdivision, compartment flooded, loading condition, etc. The critical wave height  $H_s$  depends solely on the elevation of water at the critical heel angle, and nothing else. More details and advances in knowledge on damaged ship safety can be found in the publications of Pawłowski (2004, 2007a, b, 2008), and Bulian (2008), shedding more light on the SEM and proving its robustness.

Knowing the critical sea state  $H_s$  from equation (3) for a given damage case, the factor  $s$  (probability of collision survival) can be readily obtained from the distribution of sea states occurring at the moment of collision. The probability of collision survival equals simply the probability that the critical significant wave height  $H_s$  is not exceeded at the moment of collision. Thus, the factor  $s$  equals CDF for given  $H_s$ . For this purpose, the CDF of sea states, proposed by the IMO could be used, as shown in Figure 2.

It is noteworthy that the distribution of sea states at the moment of collision is different from the sea state distribution, obtained from regular weather statistics. In a large majority of cases, collisions happen in the

proximity of ports, in confined waters, and in fog, typically associated with calm weather. It is understandable, therefore, that in such circumstances sea states are on the whole lower than those in regular weather statistics. The sea state distribution, however, may differ for certain regions.

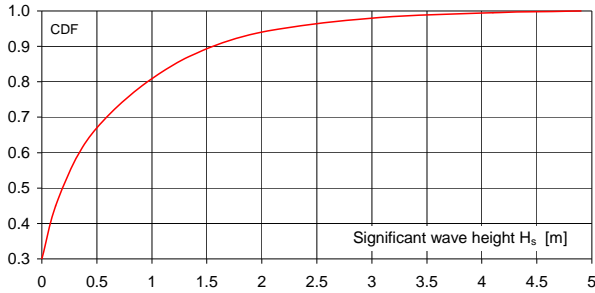


Figure 2. IMO distribution of sea states occurring at the moment of collision

Using the sea state distribution as shown in Figure 2, a very good approximation of this curve for  $H_s$  up to 5 m, which is identical with the factor  $s$ , is given by

$$s = (0.7494x^3 - 2.4095x^2 + 2.6301x + 0.0148)^{1/3}, \quad (4)$$

where  $x = H_s/4$  is in meters. For  $H_s > 5$  m,  $s = 1$ . Specific applications could consider actual distributions of sea states at the moment of collision, appropriate for the area of ship operation.

## COMPARISONS

To see the differences between the two methodologies described briefly above, the  $s$ -factor has been calculated for a box shaped vessel, and for a medium-sized Polish ferry “Polonia”. In all the cases investigated midships floodings were considered only, to ease the calculations. The box-shaped vessel had no double bottom, whereas the height of the double on the ferry was 1.85 m. In the latter case the damage extended from the double bottom upward above the car deck. Both ships had a single hull.

Particulars of the ferry “Polonia” are as follows:

$$\begin{aligned} L_{oa} &= 169.90 \text{ m} & T &= 6.20 \text{ m} \\ L_{pp} &= 159.00 \text{ m} & h_0 &= 4.067 \text{ m} \\ B &= 28.00 \text{ m} & m &= 18\,186 \text{ ton} \\ D &= 8.65 \text{ m} & z_G &= 11.42 \text{ m} \end{aligned}$$

Two compartments below the car deck of various lengths were flooded. In the case of the ferry a shorter compartment of length 24 m extended between  $x_1 = 67.5$  m and  $x_2 = 91.5$  m, measured from the aft perpendicular. A longer compartment of length 30 m

extended between  $x_1 = 64.5$  m and  $x_2 = 94.5$  m. Five flooding scenarios were considered with various transverse arrangements below the car deck, including a transverse compartment, and a wing compartment with two widths:  $b = 0.1B$  and  $0.2B$ , see Figure 3. The simultaneous flooding of the wing and the adjacent central compartment was also considered. Space above the car deck was open, with no provisions for reserve buoyancy, allowing for large scale flooding.

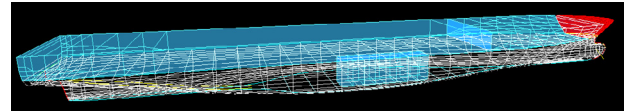


Figure 3

Particulars of the box-shaped ship were as follows:

$$\begin{aligned} L &= 143.00 \text{ m} & T &= 5.75 \text{ m} \\ B &= 28.00 \text{ m} & h_0 &= 1.835 \text{ m} \\ D &= 8.00 \text{ m} & z_G &= 12.00 \text{ m} \end{aligned}$$

Two transverse compartments below the car deck were flooded of length 16.5 m and 18.5 m.

The  $s$ -factors for the two ships according to SOLAS and SEM are compiled in Table 1 and Figure 4. As can be seen, the two  $s$ -factors equal each other only if they equal 1, i.e., if damage stability is sufficient. For deficient stability the SOLAS  $s$ -factor is *always* smaller than the  $s$ -factor based on the SEM, and the difference increases the more deficient the stability is.

Table 1

Polonia	$h$ (m)	factor $s$ SEM	range	$GZ_{max}$	factor $s$ SOLAS
<b>24 m</b>					
C	0.580	0.997	15.6	0.381	0.994
0.1B	0.990	1.000	22.6	0.540	1.000
0.1B+C	0.436	0.991	12.2	0.243	0.934
0.2B	0.605	0.997	15.4	0.300	0.990
0.2B+C	0.290	0.969	8.4	0.131	0.851
<b>30 m</b>					
C	0.365	0.984	11.3	0.265	0.917
0.1B	0.797	1.000	20.4	0.462	1.000
0.1B+C	0.263	0.960	6.2	0.087	0.728
0.2B	0.356	0.983	10.6	0.155	0.902
<b>Box ship</b>					
	0.415	0.990	9.81	0.114	0.874
	0.441	0.992	10.13	0.133	0.892
	0.308	0.973	8.46	0.056	0.705
	0.300	0.971	7.4	0.056	0.682

The above stems from the fact that the SOLAS  $s$ -factor is much more sensitive to damage stability than the  $s$ -factor based on the SEM, clearly seen in Figure 4, reflected by a very steep trendline for the two  $s$ -factors. If this could be taken as a rule, it would mean that the SOLAS Convention largely underestimates the safety of damaged ships.

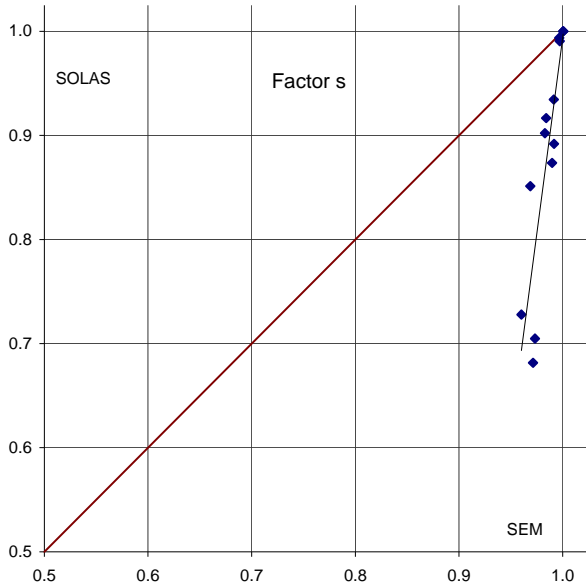


Figure 4. Factors  $s$  according to SOLAS and SEM

The large insensitivity of the SEM  $s$ -factor to damage stability explains Figure 5. If water elevation  $h$  is larger than about 0.15 m, the SEM-based  $s$ -factor is larger than 0.9. As can be seen from Table 1, to have the water head  $h \approx 0.15$  m, the righting arm curve would have to be marginal, yielding a marginal  $s$  according to SOLAS. Hence, in the light of the SEM the  $s$ -factor is to a large extent of binary nature, which agrees with common sense.

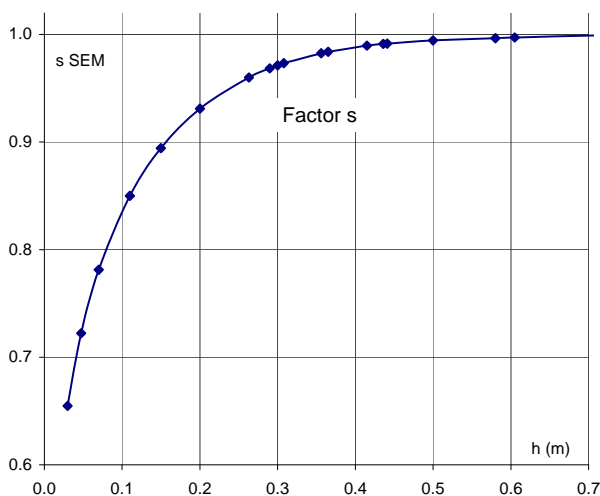


Figure 5. Variation of SEM  $s$  with water elevation

Water elevation  $h$  is a rational (physical) measure of a ship's resistance against capsizing, independent of the ship size. It is understandable that the same elevation of water on deck can occur with various  $GZ$ -curves, depending on the ship size. This in turn yields various  $s$ -factors according to SOLAS, smaller for large ships, though in the light of the rational SEM a ship's survivability remains the same for the same water head. This alone indicates that the SOLAS formulation for  $s$  is deficient, *panelizing* large ships. Hence, the degree of underestimation of ship safety increases with the ship size, which clearly contradicts reality.

We have to tell loudly that clinging to the  $GZ$ -curve in the SOLAS Convention has led IMO to a deceptive  $s$ -factor, allowing for a false effect of the ship size on subdivision index, panelizing large ships.

## CONCLUSIONS

Based on the results and arguments presented in this paper the following conclusions can be drawn:

- for deficient stability the  $s$ -factors according to the SOLAS Convention are *smaller* than the  $s$ -factors according to the SEM
- the smaller the damage stability, the greater the difference between them
- the SOLAS Convention underestimates the safety of damaged vessels
- the degree of underestimation increases with the ship size

## ACKNOWLEDGEMENTS

Dr Andrzej Laskowski of the Polish Register of Shipping is acknowledged for carrying out calculations of the  $s$ -factor for the ferry "Polonia".

## REFERENCES

- Bird, H., and Browne, R. P. 1973: Damage stability model experiments, *RINA Transactions*, pp. 69–91.
- Bulian, G. 2008: Time-based damaged ship survivability: a quasi-static equivalent method, *Int. Shipbuilding Progress*, Vol. 55, No. 3, pp. 183–226.
- HARDER – Harmonisation of Rules and Design Rationale, EU Contract No. GDRBCT-1998-00028, Final Technical Report, 31 July 2003
- IMO 1997: SOLAS Consolidated Edition (International Convention for the Safety of Life at Sea, 1974, as amended)
- IMO 2009: SOLAS Consolidated Edition (International Convention for the Safety of Life at Sea, 1974, as amended)

- Middleton, E. H., and Numata, E. 1970: Tests of a damaged stability model in waves, *SNAME Spring Meeting*, paper No. 7, 14 pp.
- Pawłowski, M. 2001a: Analytical studies for water on deck accumulation, *Transactions*, Schiffbautechnische Gesellschaft E.V., Sommertagung, Danzig, TU Gdansk, Poland.
- Pawłowski, M. 2001b: The capsizal resistance of RO/RO vessels, Task No. 3.4 on “Generalized s Factor”, EU project on Harmonization of Rules and Design Rationale “Harder”, Reference No.: [3-34-T-2001-01-0](#).
- Pawłowski, M. 2003: Accumulation of water on the vehicle deck, *Proceedings of the Institution of Mechanical Engineers, Part M, J. Engineering for the Maritime Environment*, Vol. 217 (M4), pp. 201–211.
- Pawłowski, M. 2004: Subdivision and damage stability of ships, Euro-MTEC book series, Foundation for the Promotion of Maritime Industry, Gdansk, ISBN 83-919488-6-2, 311 pp.
- Pawłowski, M. 2007a, A modified static equivalency method for roll-on/roll-off vessels, *Journal of Ship Research*, Vol. 51, No. 1, March 2007, pp. 39–46.
- Pawłowski, M. 2007b: Survival criteria for passenger roll-on/roll-off vessels and survival time, *Marine Technology*, Vol. 44, No. 1. January 2007, pp. 27–34.
- Pawłowski, M. 2008: Closure on survival time, *Proceedings*, 10<sup>th</sup> Int. Ship Stability Workshop, Daejeon, Korea, paper 8-3, 5 pp.
- Vassalos, D., Pawłowski, M., and Turan, O.: A theoretical investigation on the capsizal resistance of passenger Ro–Ro vessels and proposal of survival criteria, Final report, Task 5, The North West European R&D Project, March 1996
- Vassalos, D., Turan, O., and Pawłowski, M. 1997: Dynamic stability assessment of damaged passenger RO/RO ships and proposal of rational survival criteria, *Marine Technology*, Vol. 34, No. 4, pp. 241–266; see also: Criteria for survival in damaged condition, *Proceedings*, Int. Seminar on the Safety of RO/RO Passenger Vessels, RINA, London, June 1996, 15 pp.



## **A Study on the damage stability requirements for Ro-Ro passenger ships**

Yoshitaka Ogawa,

National Maritime Research Institute, Japan.

Shingen Takeda,

Mitsubishi Heavy Industries, Ltd.

### **ABSTRACT**

With regard to the middle and the small size Ro-PAX ferry, the safety levels of the SOLAS 2009 and the SOLAS 1990 regulations in association with the Stockholm Agreement (SA) was examined. Firstly, calculation of the required GM by applying SOLAS 2009 and SOLAS 1990 with SA was carried out. It is clarified that the required GM of the present calculated ship in SOLAS2009 is larger than, or at least equivalent to, in SOLAS90 with SA. It is also clarified that we should take such difference of philosophy into account in the further consideration of the safety levels of the SOLAS 2009. Secondly, model tests were conducted with the middle-size Ro-PAX ferry. It is rational to compare safety level of the SOLAS 2009 with that of the SOLAS 90 with SA adjusted by model tests.

### **KEYWORDS**

Damage Stability; Ro-PAX ferry; SOLAS 2009; Stockholm Agreement.

### **INTRODUCTION**

With regard to the damage stability requirements of the SOLAS 2009 amendments on RO-PAX ships, the IMO had started comprehensive examination on whether or not the safety levels of the SOLAS 2009 and the SOLAS 1990 (SOLAS90) regulations in association with the Stockholm Agreement (SA) are generally equivalent.

It is believed that the examination should be based on comprehensive research work. Based on this background, intentional studies have been conducted (e.g. EUROYARDS Stability

Group, 2009). As a preliminary result, it is confirmed that, in terms of large Ro-PAX ferries, safety level of the SOLAS 2009 is more stringent than that of SOLAS90 with SA because the philosophy of each regulation is different, particularly the difference of the definition of damage extent and the increase of required index in the SOLAS2009 (EUROYARDS Stability Group, 2009).

In the meanwhile, it is considered that there are some points for further examination. One is the further comparison of the safety levels between the SOLAS 2009 and the SOLAS90 with SA

particularly in terms of the middle and the small size Ro-PAX ferry.

Another is the comparison of safety level between numeric standards and model tests adjustment in SA. It is considered that accumulated water on deck stipulated in SA may be overestimated in numeric standards and therefore it may often need to be adjusted by a model test to satisfy SA.

Based on this background, firstly, calculation of the required GM by applying SOLAS 2009 and SOLAS 90+SA was carried out. With regard to the subjected Ro-PAX ferries, it is clarified that the required GM of the present calculated ship in SOLAS2009 is larger than, or at least equivalent to, in SOLAS90 with SA. It is also found that such difference can be attributed to the difference of philosophies between SOLAS 2009 and SOLAS 90, in particular to the difference of definition of damage extent and required index in SOLAS2009.

Secondly, model tests were conducted with the middle-size Ro-PAX ferry. It is clarified that there are a certain difference between the safety levels of SOLAS 90 with SA obtained by the numerical standards and that obtained by model tests because accumulated water on deck stipulated in SA is overestimated in the numeric standards.

#### **CALCULATION OF THE REQUIRED GM BY APPLYING SOLAS2009 AND SOLAS90+SA**

##### ***The Subject Ships***

For the comparison of required safety level by applying SOLAS2009 and SOLAS90+SA, two model ships of RO-PAX ferry were prepared

based on typical existing ones complying with damage stability requirements of the SOLAS2009. One of them is middle-size Ro-PAX ferry. Principle particular is shown in Table 1. The subdivision of this Ro-PAX ferry is shown in Figure 1. Another one is small-size Ro-PAX ferry. Principle particulars and the subdivision of this ship are shown in Table 2 and Figure 2, respectively.

Within the framework of the SOLAS2009, RO-PAX ferry with long lower hold (LLH) especially that fitted with B/10 longitudinal bulkheads can be considered. It was found that we couldn't find such ferries within the Japanese Ro-PAX ferries. However, it is considered that the safety level examined by means of the present two ferries could describe the average safety level of the middle-size and the small-size RO-PAX ferry.

##### ***Calculation of the required GM of middle-size Ro-PAX ferry***

Table 3 shows the calculated required GM, which indicates that, in the Partial and Light Service cases, the required GM is larger in the SOLAS2009 than in the SOLAS 90 with SA. Table 3 also shows that, in the case of the deepest subdivision, the required GM in the SOLAS2009 is almost the same as that in the SOLAS90 with SA. Thus, it is clarified that the required GM of the present calculated ship in SOLAS2009 is larger than, or at least equivalent to, in SOLAS90 with SA. Findings drawn from the calculation are similar with that drawn from the study by the EMSA (EUROYARDS Stability Group, 2009).

**Table 1: Principle particulars of a middle-size RO-PAX ferry**

Subdivision length (Ls) (m)	199.2
Breadth(B) (m)	27.0
Number of persons on board (persons)	850

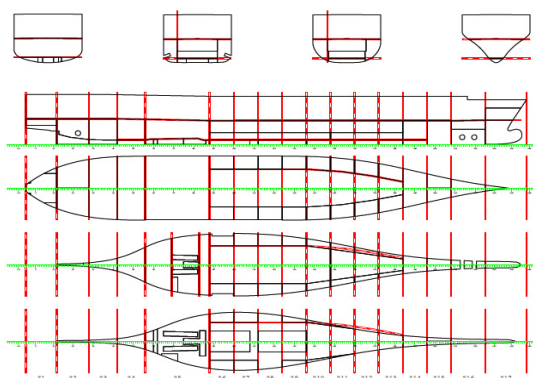


**Fig. 1: The Subdivision of middle-size Ro-PAX ferry.**

**Table 2: Principle particulars of the small-size RO-PAX ferry**

Subdivision length (Ls) (m)	100.0
Breadth(B) (m)	17.8
Number of persons on board (persons)	218

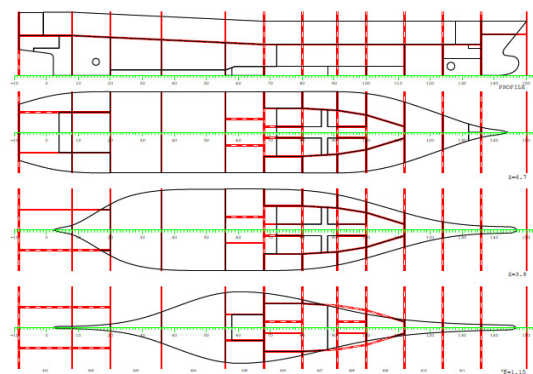


**Fig. 2: The Subdivision of small-size Ro-PAX ferry.**

Such difference of the required GM can be attributed to the difference of the philosophy of each regulation, in particular to the definition of damage extent. As the number of passenger increases, the required Index in the SOLAS2009 increases and the required GM of every loading condition increases. For the compliance with such a severe required index, flooding of more than two compartments is required to be taken into account in the SOLAS2009. On the other hand, in the SOLAS90, although the number of passengers has impact on the subdivision coefficient (Cs) which defines the number of damage compartment, most of the damage case results in two compartment damage. This implies that it becomes relatively easy for larger ship to comply with SOLAS90. Consequently, the number of passenger has little effect on the required GM in the SOLAS90.

Because of such difference in philosophy of both regulations, it is clarified that safety level of the SOLAS2009 of a relatively large ship becomes higher than that of the SOLAS90 with SA.

**Table 3: Required GM of the middle-size RO-PAX ferry for SOLAS2009, SOLAS90 and SOLAS90+SA.**

	Light service dl	Partial dp	Deepest ds
Draught (m)	5.7	6.4	6.9
Required GM (m)			
CASE1 SOLAS2009	2.5	1.3	1.73
CASE2 SOLAS90	1.4	1.19	1.33
CASE3 SOLAS90+SA	1.44	1.25	1.65

**Calculation of the required GM of small-size Ro-PAX**

The required GM of small-size Ro-PAX is also calculated. In this calculation, the required GM is calculated based on the SOLAS2009 Reg.7 (Probabilistic requirement) and Reg.8 (minor side damage requirement), separately. To examine the effect of accumulated water based on SA, assumed wave height and derived accumulated water are varied in this calculation. Figure 3 shows the calculated required GM, which indicates that, in all loading case, the required GM in the SOLAS2009 is almost the same as that in the SOLAS90 with SA, which corresponds to the case of 4m significant wave height in Fig.3, because the requirement in regulation 8 in SOLAS2009, minor damage requirement, is similar to that in SOLAS90. It is found that minor damage requirement is dominant to the small-size Ro-PAX. It is clarified that the required GM of the present calculated small-size Ro-PAX ferry in SOLAS2009 is almost same as in SOLAS90 with SA.

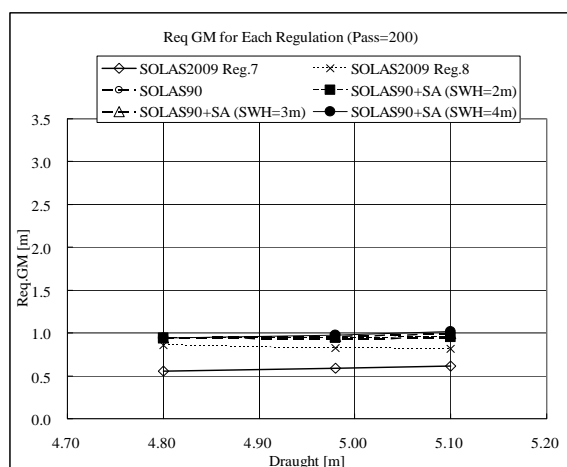


Fig. 3: Required GM of the small-size RO-PAX ferry for SOLAS2009, SOLAS90 and

SOLAS90+S.A. (N=200).

Furthermore, the effect of number of persons on board on the required GM is examined. Figure 4 shows the required GM under the assumption of increase of number of persons on board. It is found that, in the case of the deepest subdivision, the required GM in the SOLAS90 with SA is significantly larger than that in SOLAS2009. The assumed damage extent in SOLAS90 and SOLAS2009 reg.8 increases due to the increase of number of person on board (more or less than 400 persons). It is found that such an increase has effect on the required GM in the SOLAS90 with SA. It is clarified that we should take such difference of philosophy into account in the further consideration of the safety levels of the SOLAS 2009.

Particularly, it should be considered that operational factor such as the number of persons on board has much relation with the safety level of small-size Ro-PAX ferry.

**CONSIDERATION OF ACTUAL SAFETY LEVEL ENSURED BY THE STOCKHOLM AGREEMENT**

*Comparison of Safety level between Numeric Standards and Model Tests Adjustment*

It is considered that accumulated water on deck stipulated in SA may be overestimated in numeric standards. Consequently, it may often need to be adjusted by a model test to satisfy SA. This means that there may be a certain difference between the safety levels of SOLAS90 with SA obtained by the numerical standards and that obtained by model tests.

Therefore, model test was conducted to investigate the difference of required GM between SOLAS90+SA in numeric standards and that adjusted by model test and to find out whether the ship designed according to SOLAS 2009 would survive in model tests carried out according to the guidelines in the Annex of the Stockholm Agreement or according to the Directive 2003/25/EC, as amended. Therefore, model tests were carried out with various loading conditions (GM=1.0, 1.2 and 1.4m)

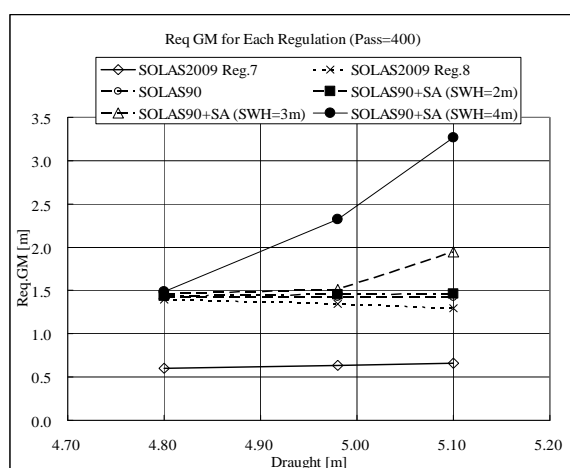


Fig. 4: Required GM the small-size RO-PAX ferry for SOLAS2009, SOLAS90 and SOLAS90+S.A. (N=400).

#### Overview of Model Tests

Model tests were conducted with the middle-size Ro-PAX ferry, which is mentioned above section, in accordance with “Revised Model Test Method Under Resolution 14 of the 1995 SOLAS Conference” (MSC.141(76)). The width of the damage openings and all conditions of experiments are determined based on this guideline.

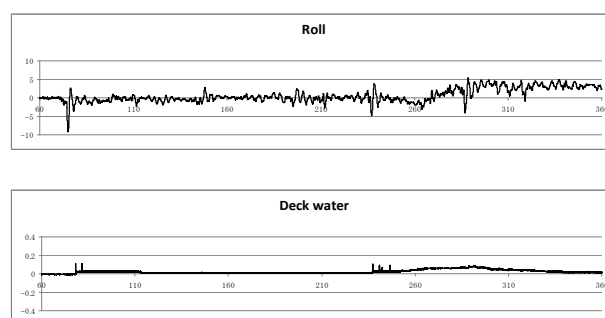
The tests were carried out in the towing tank in National Maritime Research Institute of Japan.

About 5 m long model, which corresponds to a model scale of 1:40, was used. Damaged compartments and ro-ro spaces are modelled with the correct surface and volume permeability ensuring that floodwater mass and mass distribution are correctly represented. Ventilating and cross-flooding arrangements are constructed to represent the real situation of the subject Ro-PAX ferry.

The irregular beam seas were generated with the JONSWAP spectrum. The 200 m long test basin provided sufficiently long measurement duration practically free of wave reflection. Ship motion including roll, incident wave and water height on Ro-Ro deck were measured by means of gyro and wave probes.

#### Results of Model Test

Figure 5 shows the example of time histories of roll motion, water height on Ro-Ro deck and incident waves. In the case of GM=1.2m, it is clarified that the present Ro-PAX ferry did not capsize in different ten 30 minutes realisations although water piled up on Ro-Ro deck and induced the certain heel to lee side. In the meanwhile, in the case of GM=1.0m, ship capsized because GM after damaged became almost zero. Therefore, it is clarified that the required GM exists between 1.0m and 1.2m.



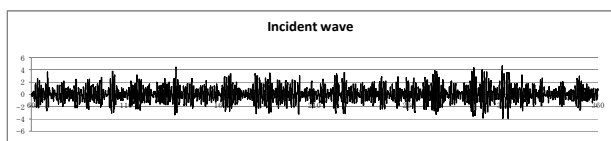


Fig. 5: Sample of time history of roll motion, water height on RoRo deck and incident wave (GM:1.2m, Significant wave height :4m ).

The result shows that the required GM exists between 1.0m and 1.2m, which demonstrates that the required GM based on the numeric standards in SA as described in Table 3 (1.65) is larger than the required GM revealed by the model test. Therefore, because the accumulated water on deck stipulated in SA is overestimated in numeric standards, it is clarified that there is a certain difference between the required GM based on the numeric standards and that based on the model test.

Therefore, it should be considered preferable to compare safety levels of the SOLAS2009 with that of the SOLAS90 with SA using model test adjustment.

**Table 4: Comparison of Required GM based on the numeric standards in SA with the required GM revealed by the model test.**

	Numeric standards	Model test
GM (m)	1.65	1.0<GM<1.2

## CONCLUSIONS

As a result of the present study, the following conclusions are obtained;

1. With regard to the subjected Ro-PAX ferries, the required GM in the SOLAS2009 is larger than, or at least equivalent to, in the SOLAS 90 with SA in all the loading cases defined in the

SOLAS2009. Such difference can be attributed to the difference of philosophies between SOLAS2009 and SOLAS90, in particular to the difference of definition of damage extent. Therefore, it is important that we should take such difference of philosophy into account in the further consideration of the safety levels of the SOLAS2009.

2. It is clarified that there are certain differences between the safety levels the of SOLAS90 with SA obtained by numerical standards and that obtained by the model tests because accumulated water on deck stipulated in SA is overestimated in numeric standards. It is same findings of the study conducted by the EMSA/HSVA. Hence, it is rational to compare safety levels of the SOLAS2009 with those of the SOLAS90 with SA adjusted by model tests.

## ACKNOWLEDGMENTS

The present study was carried out in cooperation with the Japan Ship Technology Research Association through the part of the Japanese project for the stability safety that is supported by the Nippon Foundation.

## REFERENCES

- EUROYARDS Stability Group, Comparison of RoPax Designs -SOLAS 90 and SA vs SOLAS2009-, Technical Report of EUROYARDS Stability Group, 2009
- Revised model test method under resolution 14 of the 1995 SOLAS conference (MSC.141(76)), IMO, 2002

## **FLOODSTAND – Integrated Flooding Control and Standard for Stability and Crises Management**

Risto P. S. Jalonen,

*Aalto University School of Science and Technology, Espoo, Finland*

Andrzej Jasionowski,

*Ship Stability Research Centre, Universities of Glasgow & Strathclyde, UK*

Pekka Ruponen,

*Napa Ltd, Helsinki, Finland*

Nicolas Mery,

*Bureau Veritas, Neuilly-Sur-Seine Cdx, France*

Apostolos Papanikolaou,

*National Technical University Athens, Greece*

Anna-Lea Routi,

*STX Finland Oy, Turku, Finland*

### **ABSTRACT**

This paper presents an overview of the research project FLOODSTAND, which is targeted to develop and increase reliability of flooding simulations and of assessments of large passenger ship performance in safety-critical crises. The gaps in existing data will be filled and uncertainties in the current knowledge can be rectified by experiments and computational methods. The aim of the project is to develop guidelines and standards, in connection to damage stability, a crucial element of ship safety. This paper presents the background, objectives and structure of the project as well as the applied methods and expected results.

### **KEYWORDS**

damage stability, progressive flooding, time-to-capsize, decision support, rescue, passenger ship

### **INTRODUCTION**

The size of large passenger ships has grown up to measures that are bigger than ever. Thus, the need to develop assessments related to ship safety has also become more important than ever. Simulations are widely used today to support decision-making in various problems,

related to some special issues e.g. in the design process of a large cruise passenger ship or a ROPAX-vessel. If the calculation routines are reliable and fast enough, they may offer help in potential crises, too. The growing need and interest for flooding simulations has increased the requirements regarding the capability and the reliability of many elements in simulations.

General arrangement of a large passenger ship is very complex. Internal subdivision of a watertight compartment of a cruise vessel with all the non-watertight boundaries has some effect on the progress of flooding, but today it is yet almost practically an impossible task to be exhaustively modelled; this may also be meaningless. However, the behaviour of some leaking structures, whether described by the rate of their leakage and/or by their collapse at a certain level of loading, may have a definite effect on the ship's survivability, in damaged condition. Thus, it is an important topic for experimental research, like the behaviour of a damaged vessel in waves is. Research, related to the known lacks of knowledge, to required data and to novel methods to facilitate reliable assessments of ship safety, on various levels of detail, is carried out in this project.

Guidelines and standards, based on reliable data and methods, following commonly agreed & accepted criteria, form a solid base for sound development. The expected results of the new FP7 project FLOODSTAND are planned to help in, and they also form part of the development of flooding simulations and of ship safety assessments. Multifaceted contemplation and utilisation of both bottom-up and top-down approaches, on various levels of detail and for various purposes will further improve the evolution of methodology and standards used to guarantee ship safety.

#### DESIGN AND APPLICATION (WP1)

The main objective of the first Work Package, WP1, of project FLOODSTAND is to produce sufficient amount of documentation and data of the selected sample ships of different size for further use in WP2 and WP3. The shipyards developed and provided two representative sample ship designs for typical state-of-the-art cruise vessels to be used for flooding simulation purposes, see Fig. 1.

The new concepts of inner design will be developed considering the weak points of the original designs. Naturally, they have still to comply with actual statutory rules but the real flooding behaviour has to be improved.

The main focus is on two different aspects;

1. Flooding of void spaces through structural ducts
2. Flooding of cabin structures

New arrangements of voids and cabins, staircases and other non watertight spaces will be developed and considered, too.

The different new concepts will be analyzed further with the flooding simulation tools and compared with the design practises in current use. The main objective for the judgement of the designs is the stability during and after the flooding as well as the remaining time to escape from the flooded rooms.

Based on the conclusions of the other work packages, different design concepts for spaces below and on the bulkhead deck will be analysed at a later stage of the project.

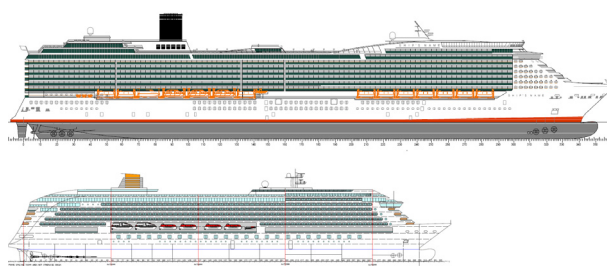


Fig. 1: Above: Post-Panama sized cruise ship; 125000 GT, L = 327 m, B = 37.4 m, T = 8.8 m, and below: a medium sized cruise vessel: 63000 GT, L = 238 m, B = 32.20 m, T = 7.4 m.

#### EXPERIMENTAL AND NUMERICAL TESTS (WP2)

Flooding progression modelling is studied in several ways in FLOODSTAND. The scope of modelling extends from single openings and structural elements to partitions and compartments up to a whole ship section. The applied approaches to produce new knowledge include experimental and numerical methods.

The behaviour of many structures, typically used in passenger ships, like semi-watertight doors, cross-flooding hatches, wall panels and windows, is not always well known in the case of flooding. Numerical data, related to the actual leakage and/or collapse under water pressure, does not exist or has not been known

widely enough to make it possible to be taken into account in flooding simulations, see IMO SLF47/INF.6 (2004). Therefore, experimental research on the leakage and collapse of such structures, under controlled conditions of a test laboratory, was considered to be an important topic to be investigated.

A watertight tank, that would facilitate tests with many interchangeable structures under relevant water pressure and destructive loading, was designed and built. It was fitted with a system for static water pressure adjustment and equipment for measurements and monitoring arrangement for acquiring stress distribution within the tested structure and for measuring of the flow rate through the leakages during the phases of the tested structure's collapse.

Two shipyards provided ship structures that were prepared beforehand for testing, as well as information and data related to them. The results of these tests (see Fig. 2), soon fully completed, will be published soon.



Fig. 2 A non-watertight wall panel leaking in the tests at CTO.

Numerical methods offer another important research method related to the mechanisms of failure of the doors and the other structural components for the assessment of their effects on the flooding. Thus, simulations, carried out using explicit finite element (FE) codes (LS-Dyna, MSC Patran/Nastran) were included in the research program. Utilization of explicit code provides much efficient opportunities of modeling of the failure propagation.

It is expected that two main pressure values will describe the failure process. The failure process begins when the structure loses its watertight integrity and starts to leak - this stage is described by the leakage pressure. Failure process continues until the collapse of the structure, which is described by the collapse pressure. At any time, the extent of failure can be described by the area of leakage opening. Computations will be validated with the experiments conducted. Based on the experiments and the FE-simulations, estimated risk criteria for leakage and collapse of doors and other structural elements will be proposed.

#### *Experimental and computational studies on pressure losses*

Experimental studies on the pressure losses in manholes were performed in scales: 1:1, 1:2 & 1:3, to obtain numerical data for validation of CFD-calculations. These test were continued by systematic tests with different modifications of a typical arrangement of a cross-flooding duct of a large passenger ship, with the interest in deriving conclusions on the effects of some parameters, such as the number of girders and openings on the pressure loss.

A number of CFD computations on the previously described parts of the ship have been carried out. These CFD computations will be used to provide a global and simplified flooding simulation tool with unknown coefficients (e.g. pressure loss in various openings). Both RANSE solver ISIS-CFD of CNRS and Fluent will be used.

Dedicated CFD simulations will be also carried out in order to assess the pressure losses in typical air pipes from the voids since during flooding the counter pressure of air can have a significant effect on the cross-flooding time.

#### *Effects of air pressure, level of detail, scale etc.*

Air compression inside the damaged ship can have a notable effect on the flooding progress. In model tests this factor has usually been neglected by using large ventilation pipes. In the novel model tests at MARIN a large vacuum tank is used to properly scale the air pressure outside the model. This provides a

unique opportunity to test the air compression effects on flooding in model scale. The floating position is kept fixed but several combinations of heel and trim angles are tested. Water heights and air pressures are measured in many compartments. In addition also the forces and moments acting on the model are recorded. The results of these challenging tests will provide data for further validation of numerical simulation codes. Two models with different levels of detail are used.

Input parameters of flooding simulations will be systematically varied in order to assess the sensitivity of the simulation results on these parameters. The sample ship designs produced in the WP1 will be used for this purpose. Guidelines for the preferred accuracy of the input data along with simple error estimations will be provided.

### **FLOODING CONTROL ONBOARD (WP3)**

Currently the available tools for damage control onboard the ships are mainly papers showing pre-calculated results of pre-defined damage cases. Obviously, the real damage is arbitrary. In addition the loading condition and the statuses of the doors (open/closed) can be different. In fact, the number of combinations is practically unlimited. This means that the starting point for the assessment of damage and flooding extent has to be based on the information from various monitoring systems (flood sensors, tank sounding devices, door status, etc.).

The WP3 focuses on studying how the limited information, received from flood level monitoring systems, can be utilized in the assessment of damage extent and time-domain flooding simulation for estimating the time-to-flood and the stability of the ship. The objective is to develop a flood sensor data interpreter for instantaneous use in flooding prediction tools, as well as to derive methods for assessment of uncertainty in such data interpretation. Furthermore, based on the improved knowledge in assessing leaking and collapsing of non-watertight structures and pressure losses in various openings (WP2), the

results of the flooding simulation tool are expected to be much more reliable.

Finally, some guidelines and principles for the design of flood water sensor systems will be developed. The main task is to find the optimum locations for the sensors. Some preliminary results are presented in Penttilä and Ruponen (2010). The developed methods will be implemented in a decision support system for demonstration and testing purposes.

### **STOCHASTIC SHIP RESPONSE MODELLING (WP4 & WP6)**

Current damaged ship stability standards represent some consensual degree of ability for a ship to attain a state of functional equilibrium if disturbed from it; however, this ability has never been resolved into practical information, such as:

- (a) Should the ship return to port after a collision incident when it is half a nautical mile from the port or should it be abandoned immediately? Or
- (b) Should the ship return to port after a collision in a “bad” weather when it is 200 miles from the nearest port, e.g. northern ice regions, or should the potentially thousands of persons onboard be asked to abandon the vessel?

Weighing of information for a decision in both these cases will be different and must be precise. And today such weighing for a decision is left to the discretion of ship’s crew with similarly discretionary advice from far-away onshore supporting teams.

The FLOODSTAND project sets to devise basis, *a standard*, for such decisions, so that either the crew or the on-shore team advises accordingly to rigorous criteria accommodating for all information that is relevant to such decision making at every instant of time, as well as for all the uncertainties associated with eventually committing to this decision. The decision making process will thus be limited to providing with accurate assessment of all the relevant input information, rather than

judgement if these or the other ship states are better for this or the other decision. The judgement element will be replaced with reading of the standard's recommendation. The crew's responsibility would thus be limited to provision of as representative information of the casualty as is possible and then timely execution of the recommendation.

It is proposed that the judgement standard is based on the concept of *conditional risk*. The decision to be executed will always be that which results in the least risk at given instant of time. From the point of view of development within the proposed project, the risk will be considered as a mathematical expectation of the loss conditional on a specific decision option available and relevant to a specific casualty case (damage characteristics, ships systems availability, evacuation systems, rescue proximity, ship state e.g. watertight doors closed, etc), as is shown schematically in Figure 4 and concept equation ( 1 ).

$$E(loss|decision_i) = \sum_j loss(j) \cdot p_{N_i}(j|decision_i) \quad (1)$$

For  $j=1...N_{max}$  and where  $N_{max}$  is total number of persons onboard.

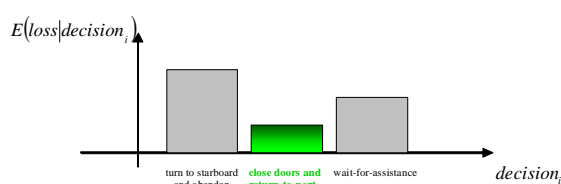


Fig. 3: The FLOODSTAND concept of the “least risk” to be used as the decision merit function.

Furthermore, it is proposed that this casualty mitigation standard be directly used for revision or, indeed, setting of design standards. For instance it could be required that a ship is designed so, that the expected loss for every one of a set of specific damage cases (e.g. every damage leading to 3-compartment flooding) and given specific mitigation action (e.g. stay onboard) is not more than a given acceptable level.

Such precise estimates of underlying stochastic process of capsizes, supported with precise estimates of actual conditions, also accounting for expected uncertainties in assessing such actual flooding states, can be built into a rational standard for decision making during crises as well as for informing the crew at all times of ship criticality during operation, so as to enhance crew preparedness for such crises.

### MUSTERING-ABANDONMENT-RESCUE MODELING (WP5)

One of the tasks to be carried out in the project FLOODSTAND is to determine standards for developing Mustering, Abandonment and Rescue models that would integrate the most significant factors accounting for the potential degradation of people's health and eventually provide as an output, the risk (in terms of safety) for passengers to abandon the ship. This risk should be easily converted into an input for a decision support system aiming at helping masters to adopt the best options for ensuring passengers' safety in case of a flooding event onboard a large passenger vessel. Moreover, standards for assessing the uncertainty bounds associated with the models will also be determined since a decision support system can be considered effective at the condition that it provides the decision-maker with a clear indication of the uncertainties attached to its output information/advice.

Concerning the aspects focussed on in this section, the first year of the project FLOODSTAND was mainly dedicated to collecting and analysing data from different sources in order to address the different aspects of evacuation in case of a flooding event. Amongst these aspects are the detection of flooding, the assessment of damage by the crew, the assessment of the situation by the master, the decision to stay onboard or abandon the ship, the effects of flooding on evacuation, the launching of life-saving appliances (LSA) while the vessel is listing because of flooding or the recovery of LSA by the Search and

Rescue (SAR) services. During this period several passenger ships' masters and SAR personnel were interviewed and/or answered a questionnaire. This feedback from 'in field' people brought precisions on the actual decision making process in case of flooding as well as the practical needs faced by these persons when it comes to real massive evacuations of cruise and passenger ferry ships. Accident and evacuation drill reports were also analysed and a regulatory review, setting the minimum regulatory requirements for crisis management onboard passenger ships, was performed.

Moreover, the core concepts underpinning the development of the mustering, abandonment and rescue (MAR) models were also defined. They were adapted from a combination of the SAFECRAFTS FP6 EC funded project's results (SAFECRAFTS, 2008 & SAFECRAFTS, 2008), and the current state-of-the art practice for ship evacuation simulation. They are based on the principle that health can be a relevant indicator of the success of the ship abandonment. During the process of mustering, abandonment and rescue, the health of passengers and crewmembers is a variable that is likely to degrade as they go through MAR obstacles. At the end of the process, the final health of passengers is compared to their initial one, which provides a good indication on how risky it is to abandon the ship. The potential number of fatalities is directly derived from this indicator and will be the preferred input for the loss function embedded in the decision support system.

#### DEMONSTRATION (WP7)

The last WP of the project deals with the demonstration and exploitation and dissemination of results. In the framework of project's demonstration activities, it is planned to test within a realistic working environment the effectiveness of the developed standard in rating different decisions for various casualty cases and for a series of hypothetical as well as real-life (historical) scenarios; independently, demonstration and testing should include the

implementation of the approach in the design process.

WP7 is composed of three tasks referring to the benchmarking of data on casualty mitigation case, the demonstration of the casualty mitigation standard and the demonstration for use as a design standard. In this respect, characteristic benchmark scenarios will be developed, that will be used in the testing of the standard in typical ship operational conditions and in the ship design process. The results will provide feedback to other WPs for modification, improvements or fine-tuning of the proposed standard.

As the basic criterion for the crisis management the *loss function*  $L$  will be used:

$$L = TTE - TTS, \quad (2)$$

where TTS: Time to Survive;

TTE: Time to Evacuate

Time data for ship flooding and probability of survival, evacuation, abandonment and rescue of people on board will put together to derive the loss function in terms of a balance between survive and evacuation time, for given casualty scenario.

The benchmark scenarios will address characteristic time aspects of the ship flooding process. The basic frame of each scenario is determined by the set of parameters that will remain fixed throughout the testing process, e.g. ship type (ROPAX and cruise ship), damage type (collision and grounding), hull subdivision, etc., whereas other parameters are characterized by increased uncertainty will be emulated, e.g. damage size, sea state, internal openings, time to evacuate, etc. The available information during an emergency situation, like flooding, forms the actual conditions for which a decision support has to be developed. Without such conditional environment any decision remains rather generic and consequently of low practical usefulness.

## CONCLUSIONS

The objectives of project FLOODSTAND include development of new data to improve the knowledge related to damaged ship stability and progressive flooding. Its purpose is to create useful data and methods, apply the new information in developing new guidelines and decision support tools for both designers and operators. The project was started in 2009. So, some of the results of the project<sup>1</sup>, described just briefly above, have already been generated and the dissemination process, via various publications etc., has started.

## ACKNOWLEDGMENTS

Although the opinions professed in this paper represent those of the individual authors, the team of which was selected from each WP-leader organisation of FLOODSTAND, the paper strives to objectively describe the whole collaborative project. The project would not have been possible without the efforts of the whole Consortium<sup>1</sup> or without the financial support from the EC to this three-year research

project FLOODSTAND (Grant Agreement Number 218532, SCP7-GA-2009-218532), making the described work possible, and that the authors want to express their gratitude for.

## REFERENCES

- IMO SLF47/INF.6 (2004). Large Passenger Ship Safety: Survivability Investigation of Large Passenger Ships, submitted by Finland, 11. June 2004.
- Penttilä, P., Ruponen, P. (2010) Use of Level Sensors in Breach Estimation for a Damaged Ship, Proceedings of the 5th International Conference on Collision and Grounding of Ships 14-16.6.2010, Espoo, Finland.
- SAFECRAFTS, 2008, "Quantitative assessment of two existing rescue systems and identification of critical areas", Deliverable D4.2 of the EC funded project "Safe Abandoning of ships" (SAFECRAFTS)
- SAFECRAFTS, 2009, "Quantitative assessment of two novel concepts of rescue systems and identification of critical areas", Deliverable D4.4 of the EC funded project "Safe Abandoning of ships" (SAFECRAFTS).

---

<sup>1</sup> For more information of the project FLOODSTAND, it's results and the Consortium (consisting of: AALTO University (ex. Teknillinen korkeakoulu, previously also known as Helsinki University of Technology), Finland; STX Finland; CNRS, France; CTO, Poland; DNV, Norway; BMT, United Kingdom; MARIN, The Netherlands; MEC Insenerilahendused, Estonia; Meyer Werft GmbH, Germany; Napa Ltd, Finland; SSPA, Sweden; SF-Control, Finland; NTUA, Greece; Bureau Veritas, France; SSRC, United Kindom; S@S, United Kindom; Maritime and Coastguard Agency, United Kindom), see the web-site: <http://floodstand.tkk.fi/> .



## Calculation method to include water on deck effects

Nicolas F.A.J. Carette,

MARIN, Netherlands

Frans van Walree,

MARIN, Netherlands

### ABSTRACT

Green water is an important issue regarding ships stability as it may dramatically change the loading of the ship compared to its dry deck condition. Until now, computational methods capturing this event are very time consuming as they often try to capture the complete dynamics of the flow over the vessel's structure and deck using CFD. Such methods are not practical when dealing with numerous lengthy time domain simulations for long term stability assessments. MARIN has developed a fast method to be implemented in its 6 DOF time domain program FREDYN . This method has as objectives to be as fast as possible, even real time if achievable, but at the same time take into account correctly the mass of water flooding on the deck during green water events. The method is based on pre-computing the steady forward speed wave pattern and diffracted and radiated waves. The steady wave is computed for a series of sailing conditions using the in-house 3D linear panel code DAWSON. The diffracted and radiated waves are pre-computed using in-house 2D strip theory potential code SHIPMO for a series of frequencies and sailing conditions. A ship generated wave is then computed at each time step during the simulation using the current position and motions of the ship. This improves the computation of a realistic wave elevation consisting of the incident, steady, diffracted and radiated waves along the hull of the ship. This wave profile is then used to feed our flooding module which computes flows in tanks, compartments and through openings. This flooding model is based on a quasi-static Bernoulli formulation and empirical discharge coefficients. It is used to compute the flow over the bulwarks and through the freeing ports to the deck.

### KEYWORDS

Time domain, green water, capsizes, calculations, FREDYN.

## INTRODUCTION

The capsize envelope obtained using time domain calculations appeared to be rather conservative during several risk analysis studies. This appeared to be strongly related to green water events happening too easily, too extremely and too often.

Until now, the Froude-Krylov forces were computed in FREDYN using the instantaneous waterline taking into account the ship motions and undisturbed incoming wave, and by this way these forces are taking care of the green water events. This is most of the time a conservative approach as it neglects diffraction, radiation and the forward speed wave which reduce the critical relative wave heights, this mostly for positions aft of the bow area.

The present new implementation proposes as first step to take into account the vessel and its motions on the water. The objective is to have a better estimation of the waterline to improve the calculation of the hydrostatic forces, including water on the deck.

## METHOD

The effect of the ship on the water surface is divided in three components:

- Static forward speed wave
- Diffracted wave
- Radiated wave

Each component is computed separately at the beginning of the time step at several positions along the ship. By summing the three waves we obtain the perturbation wave profile that can be summed with the incoming wave. Points between calculation locations are obtained by spatial linear interpolation. If the point lies outside the waterline contour, for instance in case of bulb, closest approximation is used. By points we mean any location where the water height is needed such as, for instance, a panel on the hull for the Froude-Krylov forces or an opening into a flooded compartment.

### *Static forward speed wave*

The static wave is obtained by linear interpolation between series of wave profiles computed at different speeds, drafts and heel angles. The actual position and speed of the ship is then used to pick up the right databases. Draft and heel values must be extracted from low frequency motions. Wave patterns are computed once before the calculations using a 3D potential solver. From the patterns, only the values along the vessel are extracted to obtain the waterline.

### *Diffraction wave*

The diffracted wave profile is obtained for each section of the ship using databases of linear potential diffraction.

Using MARIN's 2D strip theory code SHIPMO, the diffraction potential is extracted at each section, at the waterline, for a series of wave frequencies, headings and speeds. The potential is saved as a complex number to allow for linear interpolation between the databases without losing the phase information. It is converted to a wave amplitude response operator in m/m. At each time step of the calculation a database of diffraction potentials is made, depending on the actual speed and heading of the ship. Then, for each incoming wave component  $n$  and at each section  $i$ , the instantaneous diffracted wave profile at each section is computed using (1).

$$\tilde{\zeta}_i = \sum_n \tilde{\zeta}_{in} z_n \sin(\omega_n t - \kappa_n + \varepsilon_n + \tilde{\varepsilon}_{in}) \quad (1)$$

The diffracted waterline is then used further during the time step using spatial linear interpolation to every panel of the ship. The error in this case by the spatial interpolation is rather limited as the triggering factor for water on deck is the waterline itself which is as precise as there were sections in the calculations; the diffracted wave is not needed

outside the ship where the spatial interpolation would introduce large errors.

Such pre-calculation followed by some spatial interpolation is used to save computation time as the sum of wave components is done only twice per section, one for port and one for starboard side, instead of doing it for every panel, relative location and flooding opening. Diffracted wave is actually the only wave that could be really computed at any point but the calculation time would be excessive using fine meshes and wave spectra.

### **Radiation wave**

The radiation wave is basically obtained in the same way than the diffraction wave except that there is here the need for retardation functions to go to the time domain.

For each section and wave encounter frequency, the radiation potential is extracted from potential solutions, for instance a SHIPMO calculation. The potential is converted to a wave amplitude response. Then a method similar to what is done with the added mass and damping is applied:

- The real part of the amplitude is divided by  $\omega^2$
- The imaginary part is divided by  $\omega$

We have thus similarly as for added mass and damping terms the following formula for the radiation wave components:

$$a_i(\omega) = \frac{Re(\phi_{rad_i}(\omega))}{\rho g \omega^2} \quad (2)$$

$$b_i(\omega) = \frac{Im(\phi_{rad_i}(\omega))}{\rho g \omega} \quad (3)$$

Converted to time domain functions using (4) and (5), they give “added mass” and

“retardation function” of radiation wave amplitude.

$$A_i = a_i(\omega_\infty) + \frac{1}{\omega_\infty} \int_0^\infty B_i(\tau) \sin \omega_\infty \tau d\tau \quad (4)$$

$$B_i(\tau) = \frac{2}{\pi} \int_0^\infty (b_i(\omega) - b_{i_\infty}) \cos \omega \tau d\omega \quad (5)$$

The retardation functions are saved for each section and side for the whole calculation. Using correlation with the time history of motions we can thus compute the radiated wave at each section using (6).

$$\zeta_i(t) = A_i \ddot{x} + B_i(\infty) \dot{x} + \int_0^\infty B_i(\tau) \dot{x}(t - \tau) d\tau \quad (6)$$

As for the diffracted wave, the radiated wave profile is saved for each section at the waterline for both sides during a complete time step and spatially interpolated to any point on the ship.

### **Calculation**

When using only the static wave correction, the calculation can still be done in real time on a PC with a quad core CPU at 2.66 GHz.

The diffraction calculation strongly depends on the number of wave components. On a dual core PC, the calculation time doubles with 80 wave components compared to the calculation without correction. The difference tends to reduce as the interpolation between the databases becomes less and less the bottleneck.

The radiation correction has not been fully tested but non constant time step is the most expensive factor as the retardation functions have to be recomputed for each section every time it changes. Otherwise it costs at every time step two correlations per section.

## TANK TESTING

The validation of the present method is based on a series of tests carried out at MARIN using a model of the DDG51 (European version) beginning of 2009. Tests were carried out with a captive and free sailing model. The loading condition was such that stability was low giving a high capsizing risk.

### *Captive tests*

The tests with a captive model were done to look at steady forward speed wave and diffracted wave. The tests were done at different speeds and heel angles in regular waves of various frequencies and amplitudes. Relative wave elevation were recorded at several locations along the model.

**Table 1: Regular wave captive tests.**

Speeds	18, 24	knots
Heel angles	10, 20	deg
Amplitudes	1.25, 1.875	m
Frequencies	0.546, 0.598, 0.661, 0.739	rad/s

### *Free sailing tests*

Free sailing tests were done, in high stern quartering seas to look at green water events. Conditions were such that capsizing risk was high during the standard time domain simulations but rather low during the tests. Tests were done at two headings (300 and 330 deg) and three speeds (12, 18 and 24 knots) in irregular waves.



Fig. 2: High roll motion without capsizing and very low amount of green water in stern quartering seas.

## VALIDATION

### *Steady wave*

The steady wave implementation was validated by comparing the wave profile computed to the average wave elevation during the tests. At the speeds of interest one can observe a large trough at amidships increasing the margin against green water events. This was until now absolutely not taken into account. One can also notice that the heel angle does not have a strong effect on the wave profile in these conditions. The method clearly improves the estimation of the waterline to the original undisturbed wave compared with the experimental measurements.

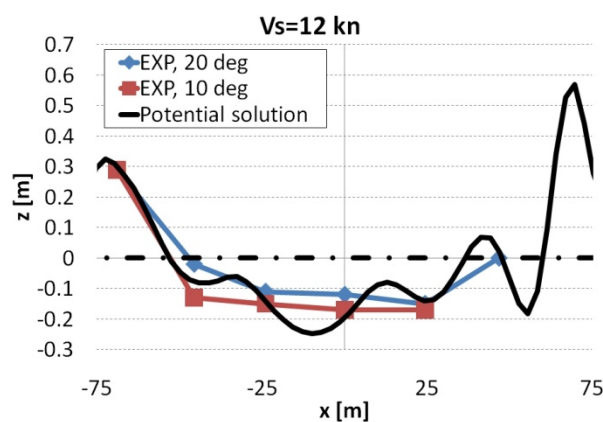


Fig. 3: Computed waterline compared to experimental steady wave profile during captive tests for different heel angles at 12 knots.

**Diffraction wave**

The maximum wave measurements along the hull have been compared to the maximum amplitude of the potential diffracted wave summed to the incoming and steady waves. The following figures give the profiles of maximum wave elevation along the ship for different conditions during experiments and calculations compared to the deck line and incoming wave for both leeward and windward sides.

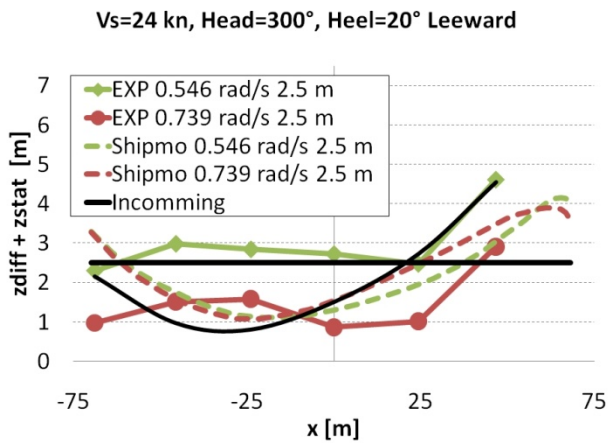


Fig. 4: Maximum wave elevation along captive vessel in regular waves: experimental and computed (leeward).

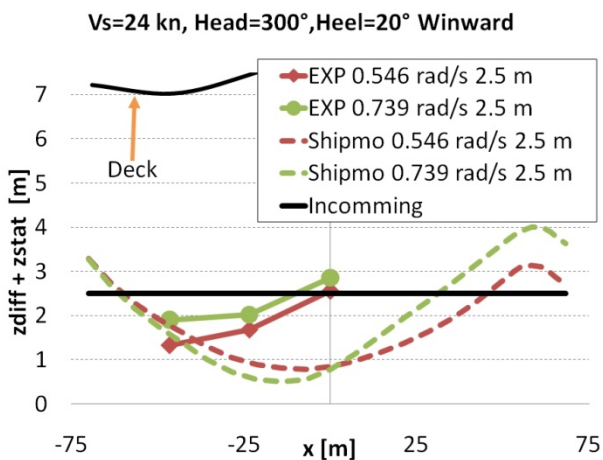


Fig. 5: Maximum wave elevation along captive vessel in regular waves: experimental and computed (windward).

In case of large roll angles, taking diffraction and steady wave into account improves the estimation of the green water events (see Fig. 4). The diffraction most of the time reduces the water elevation along the vessel, and combined with the steady wave very often avoids the water to flood on the deck. However, the effect of the frequency on the diffraction seems often underestimated by strip theory. The diffracted wave is also overestimated at the aft of the ship, but this is a typical drawback from linear theory with forward speed.

Finally, the disturbed wave amplitude on windward seems underestimated for some configurations, this appeared using both strip theory or 3D diffraction (PRECAL), but this is not critical when looking at capsizing risk due to green water as most capsizing over predictions are on the leeward side.

**Radiation wave**

The radiation was not used during these calculations as first attempts gave unrealistically high waves. This probably comes from a lack of a forward speed correction. The radiation potential is solved for a series of encounter frequencies but is valid at zero speed, the effect of radiated waves being washed backwards when sailing is not taken into account. Depending of the velocity, the retardation function at one section should become more and more dependent of the ones in front. Another solution would be to compute the potential radiation wave databases at forward speed using an exact solution and have a set of retardation functions for different speeds as it is done for the damping.

**RESULTS**

A series of free sailing time domain calculations were done with and without steady and diffracted wave correction. For each condition a series of five runs of half an hour was done.

Without correction, almost in all conditions very high capsizes risk is observed. Most of the capsizes happen very soon and fast. They are always due to excessive amounts of water on deck. For most simulations the deck is almost constantly wet on the leeward side. As the encounter frequencies were quite low, if a wave crest exceeds the freeboard at amidships, it will stay there and induce large and increasing roll angle until capsizes occurs. This process appears as a static loss of stability triggered by the first freeboard exceedance event.

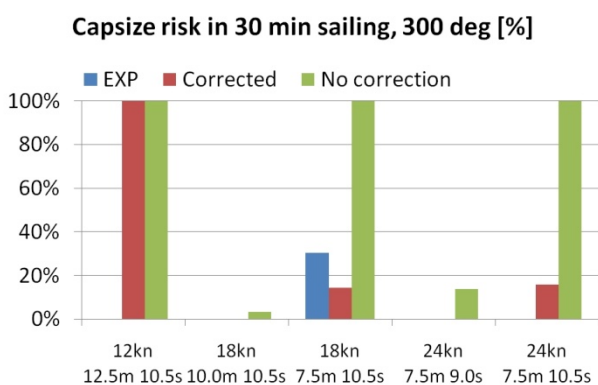


Fig. 6: Capsize risk with and without wave correction for 30 minutes sailing at 300 deg heading compared to experiments.

When the correction is applied, the threshold of the capsizes event is definitely increased. One can observe much less capsizes, most of the time those capsizes are now due to broaching. If water on deck occurs, the volume of trapped water is maybe still overestimated due to the absence of a model computing the well known dam break motion of the green water which retards the progression of the water at the beginning of the green water event. This may explain why the correction seems still not sufficient in very large waves. However in those cases, they were also very steep and breaking, which anyhow cannot be captured with linear waves.

Capsizes risk in 30 min sailing, 330 deg [%]

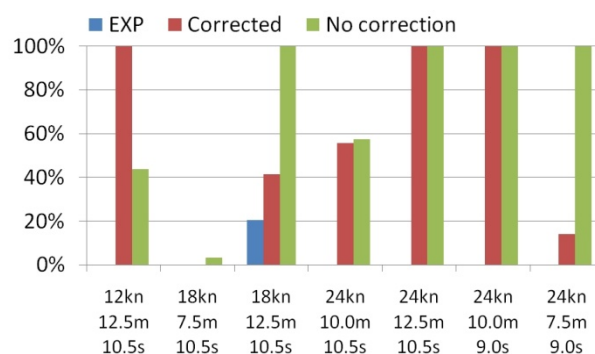


Fig. 7: Capsizes risk with and without wave correction for 30 minutes sailing at 330 deg heading compared to experiments.

The reduction of capsizes risk is of course accompanied by a reduction of the roll. We can see that this reduction results in a better matching of the experiments most of the time.

RMS Roll, 330 deg [deg]

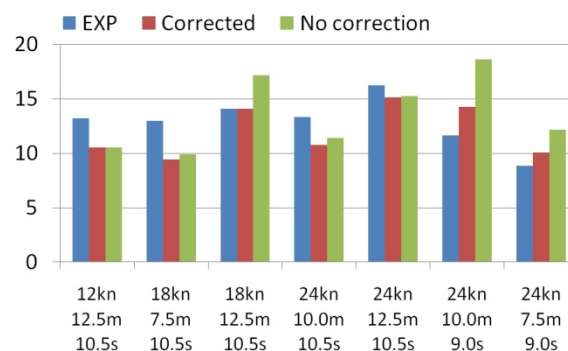


Fig. 8: Standard deviation of roll with and without wave correction compared to experiments.

## CONCLUSIONS

The correction of the waterline for forward speed gives, for a very reasonable computation time, a much better threshold for freeboard exceedance. This helps improving capsizes risk analysis at high speeds. The effect of the heel angle on the wave profile is limited in a normal rolling range. This should be checked up to

very high heel angles to know if the database really needs to depend on the heel angle. A dependence on trim could be easily included but raises the question of how to extract its value from the pitch and wave slope.

The correction for the diffraction slightly improves the asymmetry of the waterline between wind- and leeward sides. This would be even more important for headings closer to beam seas and slightly higher wave frequencies. The correction improves the capsize risk prediction by lowering the waterline in the conditions tested.

As already mentioned, the radiation was not used during these calculations as first attempts gave unrealistically high waves, probably due to a wrong forward speed effect when using strip theory. Two ways are seen, either a correction on the retardation functions or a corrected potential solution.

The case of very high or breaking waves seems still to be an issue. This could maybe be corrected by applying the radiation correction as large amplitude motions generally push the water away from the deck, retarding the flooding. Another correction could also come from a larger database of radiation and steady waves for very large heel angles. Finally, representing the deck by a floodable compartment might introduce some delay in the flooding of this one by using appropriate discharge coefficients and openings representing the flow over the bulwarks. On the other hand, breaking waves cannot be computed using linear wave spectra whatever method is used to correct them.

As this new method relies on steady, diffraction and radiation databases, any improved method to estimates these components would immediately improve the calculation of the instantaneous waterline without need of a reimplementatation.

## ACKNOWLEDGMENTS

This research is performed for the Cooperative Research Navies. The permission of the CRN to publish the results is gratefully acknowledged.

## NOTATIONS

$z$	Incoming wave	[m]
$\tilde{\zeta}$	Diffacted wave	[m]
$\check{\zeta}$	Radiated wave	[m]
$\omega$	Wave frequency	[s <sup>-1</sup> ]
$\kappa$	Wave number	[-]
$n$	Index for frequency	[-]
$i$	Index for section	[-]
$\varepsilon$	Incoming wave phase	[-]
$\tilde{\varepsilon}$	Diffraction wave phase	[-]
$\phi_{rad}$	Radiation potential	[kg/ms <sup>2</sup> ]



# **An Approach to the Validation of Ship Flooding Simulation Models**

Egbert L. Ypma

MARIN, the Netherlands

Terry Turner

Defence Science & Technology Organisation (DSTO), Australia

## **ABSTRACT**

A methodology has been developed to validate a Ship Flooding simulation tool. The approach is to initially validate the flooding model and the vessel model separately and then couple the two models together for the final step in the validation process. A series of model tests have been undertaken and data obtained has been utilised as part of the validation process. Uncertainty in the model test measurements and the geometry of the physical model play a crucial role in the validation process.

This paper provides an overview of the methodology adopted for the validation of the ship flooding simulation tool and presents some of the preliminary results from this study.

## **KEYWORDS**

Time domain, flooding, simulation, damaged stability, validation, uncertainty determination

## **INTRODUCTION**

To accurately predict the progressive flooding of a damaged vessel and its effect on the ships motion two tightly coupled methods are required to be developed. If the vessel changes its orientation, the internal floodwater distribution changes and vice versa. In addition, the changing distribution of the floodwater changes the dynamics of the vessel (centre of gravity, total mass and mass inertia). All these effects have to be taken into account in the modelling process.

An added complexity in trying to accurately simulate the flooding phenomenon is the highly non-linear chaotic nature of the flooding process. Small variations in this flooding

process, e.g. how the water progresses through an opening, can influence the final result.

Due to the highly chaotic nature of the flooding process it is vital that the numerical model represents the experimental model as closely as possible. To obtain an exact numerical representation of the physical model is very difficult. Differences may occur due to the limited accuracy of the production process of the physical model, modelling errors made in the translation from 'real' world to 'simulated' world, and the uncertainty (or limited accuracy) of the measurements. All these factors must be considered.

When there is a requirement to numerically model an actual full scale vessel other factors

also must also be considered. The internal geometry of a full scale ship is extremely complicated and it would be very difficult to account for all the small details that may influence the flooding process. Issues such as leaking doors and collapsing air ducts are highly random events that can never be accounted for numerically. For this reason several “acceptable” assumptions are required to be made when numerically modelling full scale ships.

Due to the highly chaotic nature of the flooding process and the various areas of uncertainties in both model scale and full scale vessels, a method for progressive flooding tools must be developed to account for these uncertainties at an acceptable level. The following three questions need to be carefully considered when defining this method:

1. How can a validation process be defined such that it is possible to conclude whether a simulation tool is sufficiently accurate?
2. Is it possible to define general rules to model the internal ship-geometry in such a way that the simulation tool predicts extreme events sufficiently accurate (both statistically and in magnitude)?
3. What is the best way to deal with uncertainties in the validation process?

This paper will provide a brief overview of the numerical tool Fredyn [see Fredyn v10.1 2009] and its progressive flooding modelling capability and will also outline the approach undertaken by both The Maritime Institute Netherlands, (MARIN), and The Defence Science and Technology Organisation, (DSTO) for the validation of the progressive flooding module.

## **SHIP MOTION AND PROGRESSIVE FLOODING SIMULATION MODEL**

### ***Background***

The Cooperative Research Navies group, (CRNav), was established in 1989 to initiate a research program focussed on increasing the understanding of the dynamic stability of both intact and damaged naval vessels. The group has representatives from Australia, Canada, France, The Netherlands, the United Kingdom and the United States. The CRNav aims to increase the understanding of the stability of Naval vessels from a more physics based approach rather than an empirical derived one. To manage this process the CRNav has formed the Naval Stability Standards Working Group (NSSWG). The objective of the NSSWG is to investigate the applicability of the quasi-static, empirical based Sarchin and Goldberg stability criteria for modern Navy vessels and to develop a shared view on the future of naval stability assessment.

Until recently, the main focus of the NSSWG has been on intact stability and so far this has been a fairly comprehensive and complex task. However with the recent development of the new flooding module within Fredyn, future programs of work will be focused on the damage stability of naval vessels.

The flooding simulation model was developed and implemented by MARIN and funded by the CRNav group. In 2009 a collaboration agreement was signed between the CRNav and the Cooperative Research Ships, (CRS), working group ShipSurv II to jointly develop and validate the flooding module. In 2009 and 2010, the Defence Science and Technology Organisation, (DSTO), Australia, in collaboration with The Australian Maritime College, (AMC), have undertaken a research program to support MARIN in the validation of the progressive flooding module.

In theory the flooding module can be interfaced to any 6D vessel (large) motion simulation

program. Currently, however, it is interfaced to Fredyn, jointly developed by MARIN with the CRNav, and PRETTI (jointly developed by MARIN and the CRS group). Fredyn was used for all the examples in this paper.

### The Simulation Model

To enable an accurate simulation of the flooding of a damaged vessel operating in waves the simulation model describing the motions of the vessel and the model that determines the progressive flooding mechanism must be closely coupled to each other. Figure 1 shows an example of the typical information that is required to be interchanged between the simulation models..

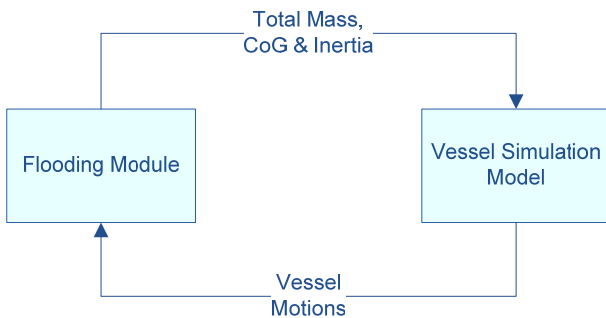


Figure 1 Interface Vessel model and flooding model

In the scenario with significant flooding onboard a vessel, it is not unusual for sudden large changes in the vessels motions to occur. For an accurate simulation of this event both the flooding model and the vessel motion model must take this into account. The simulation must also be able to calculate a changing mass, centre of gravity and inertia over time. The accuracy of the roll damping model utilised is also vital in modelling this scenario. The relative wave height at the damage location is also required to be accurately predicted.

### FREDYN<sup>®</sup>

FREDYN<sup>®</sup> is an integrated sea keeping and manoeuvring ship simulation tool capable of predicting large ship motions in extreme conditions. The development of FREDYN was jointly funded over the last 20 year period by

MARIN and the CRNav. Over the years a substantial effort was made to validate and improve the code with model test experiments.

FREDYN uses the frequency domain tool Shipmo2000 as a pre-processor to calculate the frequency dependent added mass and damping coefficients. Using a panellised hull form the program is capable of calculating the Froude-Krylov forces on the instantaneous wetted hull. An appropriate roll damping model can be selected which can be tuned to satisfaction when roll decay data is available. The standard vessel manoeuvring model is based on a frigate hull form but can be replaced with a dedicated, specifically tuned model when required. A wide variety of simulation components is available to model the vessel's propulsion and manoeuvring: rudders, fins, skegs, bilge keels, various propeller types, waterjets, trim-flaps, etc. The forces calculated by these sub-models are partly empirical based. A separate module is used to control the vessel's heading and/or attitude.

The environment can be modelled by wind and by various wave systems coming from different directions. The wind and wave systems can be specified by making a selection from one of the available spectra. Together with the user specified parameters this will generate a (random) wave sequence (or varying wind speed).

The equations of motions are based on Newton's second law: the forces and moments of all the sub-models are calculated, transferred to the space-fixed reference frame attached to the ship's centre of gravity, and summed. It eventually results in the momentum rate. Fredyn allows for time-varying mass properties to be able to deal with the potentially large mass fluctuations caused by the flooding process.

To increase the flexibility a (python) scripting module allows to interact with the simulation program without altering its code. The scripting functionality can be used to program

vessel trajectories, implement speed pilots or do more advanced logging.

Over the last year the software was completely restructured resulting in a very modular and highly configurable simulation program that can be very easily extended by additional modules. More recently, efforts are made to incorporate the steady forward wave and the diffracted and radiated wave patterns to improve the calculation of the wave profile close to the moving hull.

### ***Flooding Module***

The flooding module is used to calculate the flow of water and air through a user specified geometry. It assumes a horizontal fluid surface at all times. The effect of air-compressibility and its effect on the flow of water is fully taken into account.

The compartment geometry is represent by tank-tables that are generated prior to the simulation. A tank-table for a compartment tabularises the relation between heel, trim of the vessel, level of the fluid in the compartment and the volume of the fluid, centre of gravity and inertia matrix. Interpolation on actual heel, trim and level values is used to find intermediate values.

Any number of openings can be specified connecting two tanks or a tank to the sea. A single opening consists of four corner-points that specify the size and orientation of the opening. For each opening a constant discharge coefficient for water and a separate discharge coefficient for air has to be specified. If required, the user can specify a leaking pressure and area, a collapse pressure and a start- and/or stop time. An opening either connects two tanks or connects a single tank to the sea.

It is also possible to define a duct between two tanks, or between a tank and the sea.

Bernoulli's equation for incompressible media is used to determine the flow velocity of fluid

along a stream line from the centre of a compartment (A) to the opening (B)

$$p_B - p_A + \frac{1}{2} \cdot \rho_w \cdot v_B^2 + g \cdot \rho_w \cdot (h_B - h_A) = 0 \quad (1)$$

In this application of Bernoulli's equation the  $\rho$  is constant and the velocity in point A, the centre of the compartment, is neglected. The variables  $p_A$  and  $p_B$  are the air pressures above the fluid in the compartment (A) and on the other side of the opening (B). After determining the velocity in the opening the mass flow through an entire opening is determined by integration over the height of the opening (along the local vertical):

$$\dot{m}_w = \rho_w \cdot C_{d,w} \cdot \int_0^H width(z) \cdot v_B(z) \cdot dz \quad (2)$$

Where  $C_d$  is the discharge coefficient specified by the user for this opening. It takes all the losses into account caused by contraction, pressure losses etc.

A similar procedure is used to determine the mass flow of air through an opening and the Bernoulli's equation for compressible flow is used:

$$\frac{P_0}{\rho_0} \cdot (\ln(p_B) - \ln(p_A)) + \frac{1}{2} \cdot v_B^2 = 0 \quad (3)$$

The flooding process is considered isothermal, hence Boyle's law applies and thus the density of air is assumed to vary linearly with the pressure.

The pressure correction method developed for air and water flows by Ruponen [see Ruponen 2007] is used to solve the coupled flow of fluid and air through a complex user defined geometry. The pressure correction method is using the equation of (mass)continuity and the linearised equations of Bernoulli to correct the water levels and air-pressures in an iterative method until the error in mass flow drops

below a user specified minimum. Upon conversion both the equations of mass continuity and momentum are satisfied.

### **FREDYN FLOODING MODEL VALIDATION**

As previously discussed it is extremely difficult to model and capture all the phenomena that occur during the flooding of a vessel. For this reason there will always be slight variations in the experimental results when compared to the numerically predicted results. There are several factors that contribute to the differences observed. These include:

- Measurement accuracy (motions, levels)
- Determination of the hydrostatic & dynamic properties of the model
- Production accuracy of the test model (both internal & external)
- Choices made during the modelling of the internal geometry (deck and bulkhead positions, permeability)
- Imperfections caused by mathematical modelling (empirics!)

These uncertainties can be grouped in 3 main categories:

- Uncertainties caused by the physical model & the measurements
- Uncertainties caused by flooding model
- Uncertainties caused by the vessel model.

The first category plays a role during the model testing, the second two are tightly coupled and play a role during the simulations. The result of the validation process will be a comparison between the measurements and the simulation data. In general, when they are ‘acceptably’ close then the conclusion is justified that the simulation application performs well. The first key problem in view of the nature of the process and the uncertainties that play a role is how to define ‘acceptable’. The second key problem is that if the result is not ‘acceptable’ then which sub-model has to be changed to improve the result.

The issue with the uncertainty covered by the physical model and measurements can be solved by firstly having a clear understanding of the uncertainties involved and secondly by undertaking a series of simulations to determine the influence that these uncertainties have on the overall result.

The uncertainty in both the flooding and vessel motion models can be solved by separating the validation of the flooding model and the vessel simulation model. The validation process can then be split into several phases:

#### *1. Fully constrained model.*

Fully constraining the model in a pre-described heel, trim and draft allows for a check of the flooding module without the dynamics of the vessel. By using a heel and trim value different from zero the performance of the flooding module for inclined openings can be validated. In addition, the geometry of the numerical model can be verified.

#### *2. Force the measured motions from the model test upon the flooding module.*

In this validation process the motions measured experimentally are prescribed onto the numerical model and the water levels and volumes in each compartment are determined. These levels and volumes are then compared to those obtained experimentally. If the flow rate into a compartment is different between the measured and the predicted, then the opening coefficient(s) of the compartment openings can be tuned. However, for complex geometries this might become a very difficult task. This process is a verification that the flooding model is working correctly. This approach is shown in Figure 1.

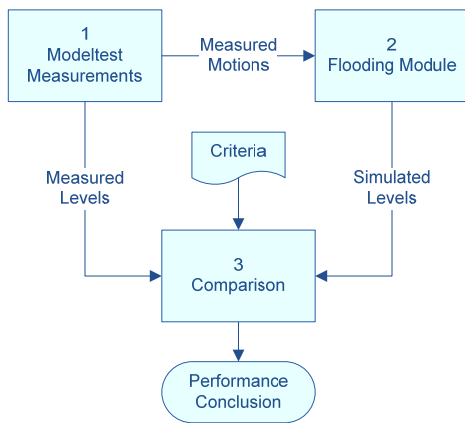


Figure 1 Flowchart showing the approach for the Prescribed Motion Phase

3. Use the result of step 2 (a time-varying, ‘wandering’ mass of all the flood-water) and use it to excite the dynamic vessel model.

When the outcome of step 2 is summed it can be replaced by a single, time-varying mass (having a centre of gravity, inertia and a weight) that moves over and throughout the vessel. This approach is allowed as long as the vessel is only excited by this wandering and changing floodwater mass and will not be applicable when the vessel is also subject to other external forces such as waves.

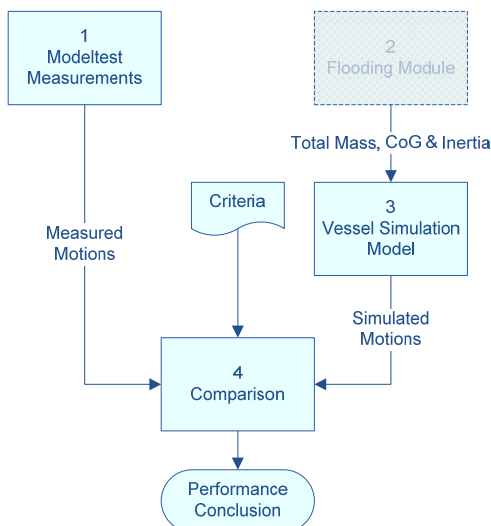


Figure 2 Flowchart showing the approach for the Moving Mass Phase

The outcome of this step (vessel motions) can be compared with the measured vessel motions

during the model test. A schematic showing this process is shown in Figure 2. It is a test of the quasi-static flooding model approach and of the interface between the flooding module and the vessel simulation program.

4. Close the loop and combine both models

The final step in the validation process is to undertake a simulation with the complete model i.e. vessel model and flooding module, and compare the predicted levels and motions with the measured modeltest data. A schematic outlining this process is shown in Figure 3.

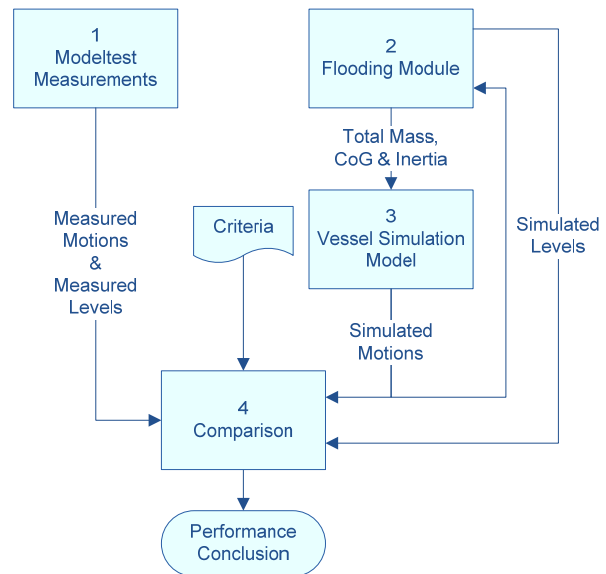


Figure 3 Flowchart showing the approach for the Full Simulation Phase

### Component & interface verification

Prior to using the measurements in this approach, the validation method was verified by replacing the model test measurements with the data obtained from the fully coupled system. The process flow of this test is shown in Figure 1.

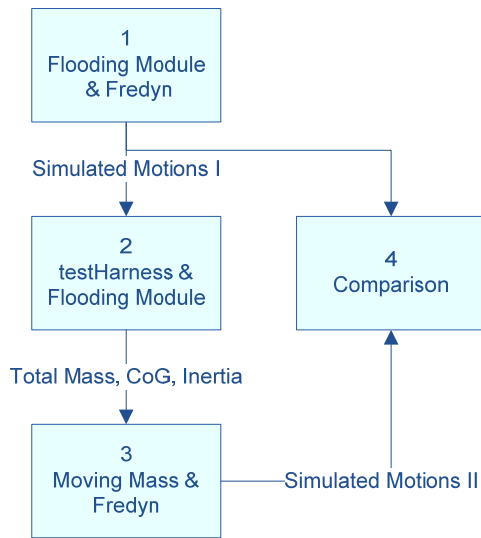


Figure 4 Component Verification

The motions as calculated by step 1 and 3 should compare very well as modeling errors play no role. It is a test of the interfaces and coordinate transforms involved.

### MODELTESTS

The model tests undertaken at AMC were performed in two phases. Prior to undertaking these experiments, it was expected that the tests were going to be complex and the lessons learned from Phase 1 would be incorporated into the second phase of testing. The test program was set up in such a way that the complexity of the scenario was gradually increased. A priori simulations were performed to determine the most interesting loading conditions. Prior to the flooding tests roll decays at zero speed were undertaken, in both damaged and intact condition. The roll decay data was used to tune the roll damping of the simulation model. Fully constrained model tests were performed with a initial heel and trim of zero. In later tests a series of runs were performed with a range of non zero initial heel and trim combinations.

The experimental model used, shown in Figure 5, was a generic destroyer design (scale 1:40, length approx. 3.0 meters) with a detailed internal geometry. The model was built in such a way that the damaged compartment block could be replaced with a more complex

compartment arrangement at a later stage. The compartment block was located aft of amidships.



Figure 5 A photograph of the generic destroyer model

Two compartment arrangements were constructed and are referred to as simple and complex compartments. The difference between the simple and the complex model was the addition of (longitudinal and athwart) gangways. These arrangements comprised of 3 decks, 19 compartments of which 6 had level measurements and 2 had air pressure measurements. In addition to these measurements the 6 motions of the vessel were also recorded along with both internal and external video.

The flooding was initiated by puncturing a latex membrane that covered the large damage opening as seen in Figure 6.

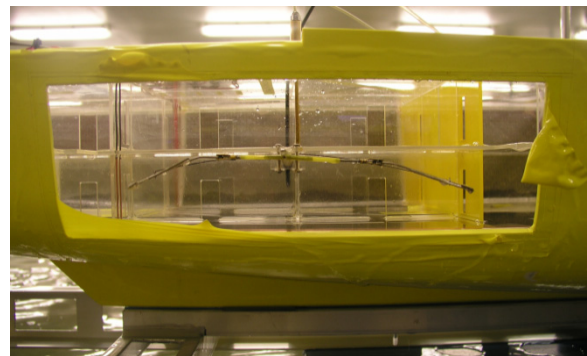


Figure 6 The A photograph showing the generic destroyer damage opening

During the model tests many precautions were taken to reduce the uncertainty of the results. After each run a calculation tool was used to check the equilibrium levels in each (measured) tank with respect to each other and to the still water plane. After each run a check of the (level) calibration was done. A run was repeated when spurious results were suspected.

After the tests the model was carefully re-measured to ascertain the ‘as build’ situation.

### VALIDATION RESULTS

The validation methodology approach, as previously described, has been applied to the data obtained with the first phase of the model test done at AMC. The results described in this paper are preliminary due to the final set of data (of phase II) not being available at the time of the analysis. The validation was performed in following steps:

1. Component & interface verification
2. The vessel roll damping
3. Vessel hydrostatics
4. Fully Constrained
5. Forced Motions
6. Moving Mass
7. Unconstrained Analysis

All plots and other data are given in full scale.

#### *Component & interface verification*

The roll angle was selected as performance indicator for this step. Both data sets lie on top of each other, indicating a successful check.

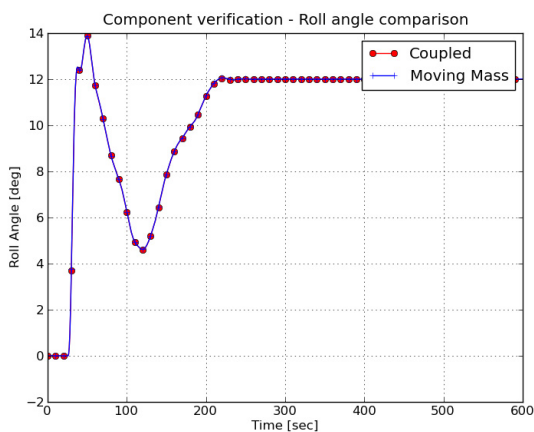


Figure 7 Component verification - Roll angle comparison

#### *Vessel roll damping model*

The roll decay data was used to tune the roll damping model. All flooding tests were done at zero speed hence only the roll damping for that speed required to be tuned. Several roll decays

were performed, each with a different initial angle. Only slight tuning of the radius of gyration,  $k_{xx}$ , value was required to have a good resemblance of the measured and the simulated data for all initial roll angles. A typical comparison between the numerically predicted and the experimentally obtained roll decay is shown in Figure 8.

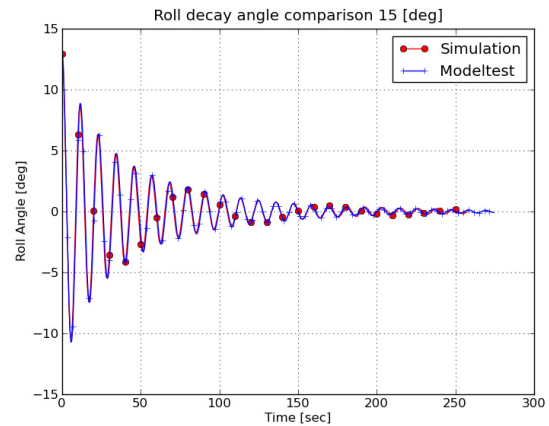


Figure 8 Roll decay for initial angle of 15 degrees

#### *Vessel hydrostatics & tanktables*

To check the hydrostatics of the simulation model, each tank was filled individually at 50%, 100% and at an intermediate value determined by an unconstrained simulation run. This was done both in FREDYN and PARAMARINE<sup>®</sup>, [see PARAMARINE<sup>®</sup> 2009] the latter program was used to generate the tanktables used in the flooding simulation. The equilibrium values for heel, pitch, draft and tank centre of gravity were compared. Slight differences were found. After completion of Phase 2, the actual dimensions of the experimental model were verified and slight differences were observed to those dimensions used in the preliminary analysis. Verification of the hydrostatics will be repeated using the re-measured dimensions.

#### *Fully Constrained*

During the model test the model was fully constrained at zero heel and trim. This test gives an indication of the performance of the flooding module. The influence of the motions of the vessel on the flooding process is not considered at this stage due to the model being

fully constrained in all six degree of freedom..

Figure 9 shows an example of both the simulation and experimental time traces of the water level in a compartment that floods through a number of openings and other compartments. The air pressure in this compartment remains ambient as the compartment is open to the outside. The discharge coefficient for all the openings are set to a default value of 0.58.

The simulation of the flooding of this compartment shows excellent comparison to the experimental data. The arrival of the water at the position of the probe, the filling rate of the compartment and the final equilibrium level are all predicted extremely well.

A full uncertainty analysis was undertaken, which incorporated the uncertainties for level and calibration measurement and uncertainties in the as-build situation. The 95% values ( $2\sigma$ ) used in the calculation of uncertainties are 2.0 mm for the level sensor accuracy and 4.0 mm for the geometry uncertainty (model scale values). Preliminary results from the model tests suggest that the 2.0 mm might be too low. The 95% range appeared to be around  $\pm 0.20$  m (full scale) and is indicated by the unconnected dots shown in Figure 9.

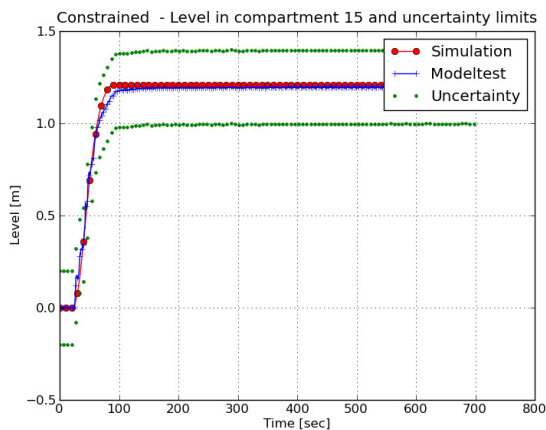


Figure 9 Comparisons between predicted and experimental compartment water levels.

**Forced Motion**

For the forced motion analysis the

experimental model motions (heave, pitch roll) were used to drive the flooding module. To be able to do this a small test Harness application was created which loads a file with motion data and the flooding component. Figure 10 shows a comparison between the simulation and model tests results along with the expected uncertainty.

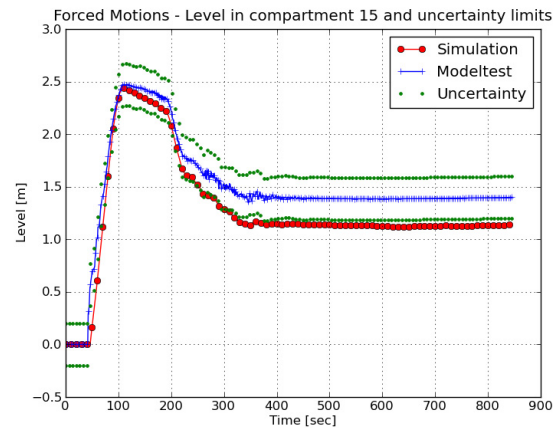


Figure 10 Comparisons between predicted and experimental compartment water levels.

There is a difference between the model test and the simulation slightly outside the limits of uncertainty. The difference is approximately constant as soon as the equilibrium is reached. The compartment which Figure 10 is referring to is connected to the sea and is fully ventilated, therefore at equilibrium, the distance between the water level in the compartment and the still water plane should be zero.

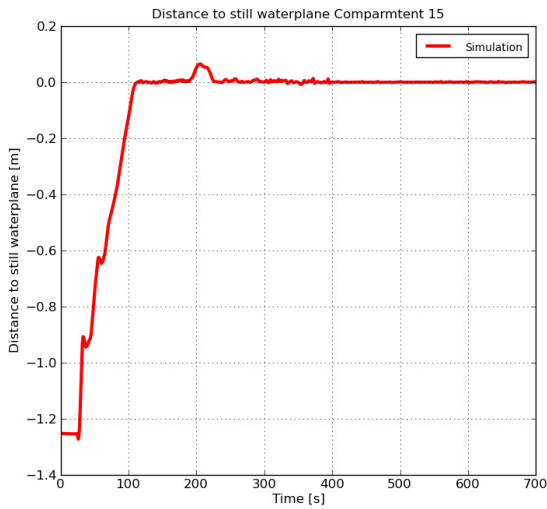


Figure 11 Distance to still-water plane (simulation)

Figure 11 shows the distance between the water level within the compartment and the still water plane over time. It is evident that the simulation is predicting the water level within the compartment accurately.

When the experimental data is used (level, heel, pitch, heave and draft) and the equilibrium value for the distance to the still water plane is calculated, then the difference is 0.23 [m], full scale. It should be noted that after undertaking this preliminary analysis the physical experimental model was re-measured and slight differences in the geometry details used in this analysis were found. It is planned to undertake this analysis again with the new geometry details.

Figure 12 shows the water level within a different compartment over time for both the simulation and model tests.

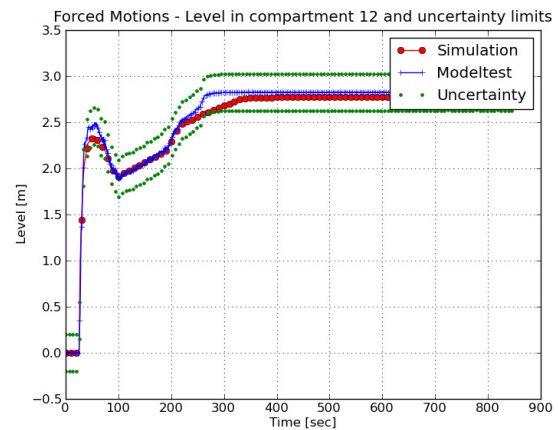


Figure 12 Comparisons between predicted and experimental compartment water levels

This compartment is located adjacent to the damage opening. When the equilibrium measurement for this compartment is used, then the calculated difference between the compartment water level and the still water plane is 0.03 [m], which is well within the estimated uncertainty limits.

### Moving Mass

Using the results from the forced motion runs a time record of the total flooding mass and its center of mass can be determined. These values are then used to excite the vessel model. The roll, pitch and heave motions of the simulation vessel can then be compared against the modeltest values. Figure 13 shows the comparison between the experimental and simulated results.

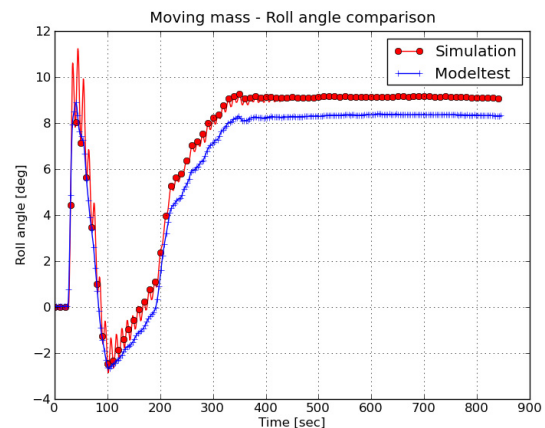


Figure 13 A comparison between the roll versus time for both the simulated and experimental analysis.

The initial numerically predicted roll angle is larger than the measured value. This result is consistent with that shown in Figure 8. This compartment is on the port side of the vessel. The simulation predicts a smaller volume, (mass), of water in this compartment hence resulting in an increase roll to starboard, (roll angle is positive to starboard). Initially, also some fluctuations are visible. This is an indication that the experimental model has more internal damping. It will also be caused by the quasi-static approach in the flooding module for this highly dynamic model test.

Figure 14 shows a good agreement between the numerically predicted magnitude of pitch compared to that obtained experimentally.

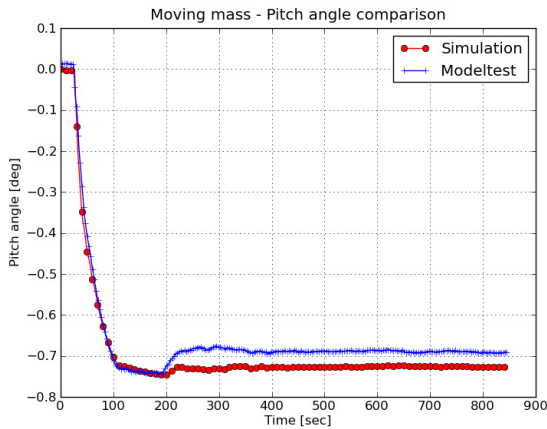


Figure 14 Comparison of pitch motion

**Unconstrained run**

The final stage in the validation methodology is the complete coupling of the numerical flooding model with the numerical vessel model. Figure 15 and Figure 16 show a comparison between the numerically predicted roll and pitch motions compared with the experimentally obtained values.

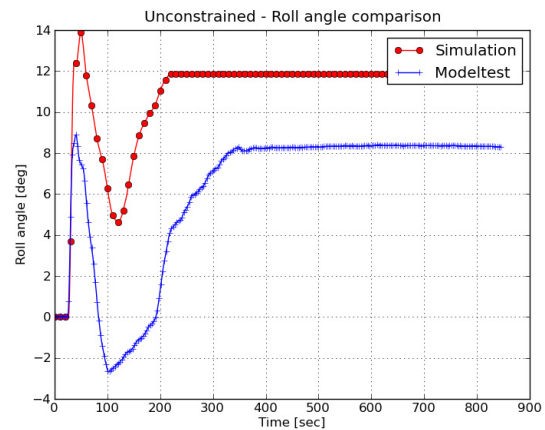


Figure 15 A comparison between the roll versus time for both the simulated and experimental analysis

It is evident that there is a significant difference between the numerically predicted and the experimental results. As stated previously, the comparisons shown in this paper are using the assumed geometry arrangement but the re-measuring of the model upon completion of the experimental phase has shown some slight variations in the assumed geometry. These slight variations at model scale may have significant effect on the results when modelling full scale. It is planned to undertake the complete validation process again using the updated geometry.

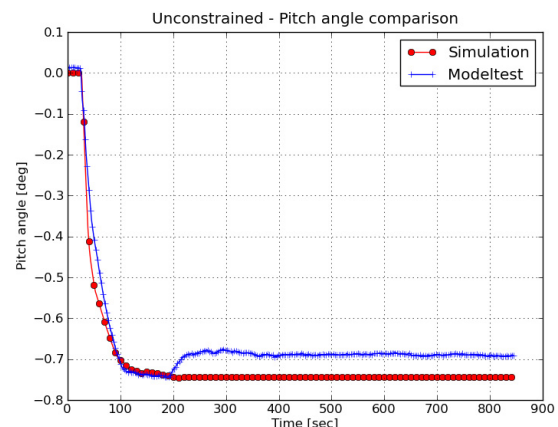


Figure 16 A comparison between the pitch versus time for both the simulated and experimental analysis

## CONCLUSIONS

This paper has provided an overview of the methodology that has been adopted by MARIN and DSTO to validate the progressive flooding modelling capability within Fredyn. This methodology included a phased approach where initially both the flooding model and the vessel model were validated separately and then coupled together for the last validation stage. A series of model tests were undertaken in support of this validation process.

Preliminary findings have shown reasonably good results but have also highlighted the need to clearly identify the source and extents of uncertainties in the experimental program. This information can then be utilised to determine what is an “acceptable” level of agreement between the numerical predictions and the experimental results.

The results presented in this paper are based on an assumed geometry of the experimental model and post trial geometry verification have shown slight differences in the geometry details. Ongoing validation studies are planned using the new geometry definitions.

## REFERENCES

- Fredyn v10.1, Theory & user Manual, MARIN, the Netherlands, 2009
- PARAMARINE© v6.1, User Manual, GRC Ltd, United Kingdom, 2009
- Ruponen, Pekka, Progressive Flooding of a Damaged Passenger Ship, Doctoral Dissertation, Helsinki University of Technology, 2007

## TEMPEST — A New Computationally Efficient Dynamic Stability Prediction Tool

William F. Belknap, Arthur M. Reed  
Carderock Division, Naval Surface Warfare Center

### ABSTRACT

The US Navy has embarked upon the development of a new computational tool for simulating the responses of a ship operating in severe sea states. This new tool, TEMPEST, is designed to be computationally efficient to support real-time training simulators as well as high-resolution evaluation of surface-ship, dynamic-stability performance across a wide range of possible environmental conditions. TEMPEST aims to improve the state-of-the-art for real-time computations through the inclusion of nonlinear (body-exact) hydrodynamic perturbation forces and physics-based, viscosity-influenced lift and cross-flow drag forces. Slender-ship and low-aspect-ratio lifting-surface theories provide the ability to maintain computational efficiency while including the dominant nonlinearities within the dynamic stability problem. This paper argues for the efficacy of TEMPEST's theory in reconciling the need for accurate predictions with computational efficiency.

### KEYWORDS

Large amplitude motions, nonlinear dynamics, body-exact hydrodynamics, bilge-keel forces, TEMPEST, maneuvering in waves

### INTRODUCTION

Ship operability and safety are often linked to its motions in waves and eventually to its dynamic-stability risk. Evaluation of dynamic-stability risk is primarily achieved through the gathering of performance data in the wave environment and speed-heading condition of interest. The performance data can be obtained from model tests or simulations. Model tests are expensive, limited in flexibility (wave conditions, run length), and can have scale effects. If the design changes, or even the loading condition changes, an entire new model test needs to be executed. Simulations offer the opportunity to include scale effects, provide nearly any environmental input desired, and are generally easier to re-run when geometry or loading conditions change. However, there is a significantly higher burden on simulations to validate the theory for full-scale ship performance. Regardless, there remains a need for the designers or regulatory authorities who need to evaluate dynamic-stability risk to have several tools at their disposal. Model tests,

high-fidelity computational tools (like CFD), and fast simulations all have their roles.

The number of conditions that must be simulated depends upon the resolution to which dynamic stability needs to be characterized. If the failure modes are not known *a priori*, it may be necessary to obtain motion statistics over a complete range of environmental and ship operating conditions. If the matrix of conditions includes multi-directional seas with two or more wave systems (swell is more than likely not correlated to the wind-driven system), the total number of simulations quickly grows. For a nominal speed-heading resolution of every 5 knots and 15 degrees, each environmental condition could have approximately 150 conditions for which extreme value statistics need to be generated. Because of this, there is a need for computational efficiency. However, computational speed does not provide the designer or regulatory authority any benefit if the answer is wrong. The goal then is to generate sufficiently accurate results as computationally efficiently as possible. The evolu-

ing understanding of the relevant physics allows for theory to be only as complex as needed. It is with this objective that the U.S. Navy has embarked upon the development of a new dynamic-stability simulation tool called TEMPEST.

**PHYSICAL PROBLEM**

A simulation tool needs to be able to include the physical phenomena that are relevant to the full-scale problem. As such, the first step in developing a computational tool is to identify what the physical problem is and decompose it in a manner that can be modeled. At the highest level, the physical problem can be described by the ambient environment, the ship control condition, and the forces acting on the ship. **Figure 1** illustrates the physical problem to be modeled.

*Environment*

The definition of the ambient environment for the dynamic stability problem must include both the wind and wave environments. In realistic sea conditions, the wave environment is generally considered multi-directional. An example polar spectrum showing two distinct wave systems is shown within **Figure 1**. It is important to be able to include multiple wave directions in a computational model because of the unique physics that occur in such a situation. For example, one wave system may

degrade transverse hydrostatic stability while another may provide a rolling moment.

Another aspect of the wave environment that is strongly correlated to dynamic-stability risk is the steepness of the seas. Steep seas have a more significant impact on the change in wetted geometry, which has a large effect on the forces felt by the hull. Within steep seas, nonlinear effects become stronger, such as the asymmetry of the wave profile and the nonlinear pressure and particle kinematics.

The wind environment may or may not be aligned with the wave systems, which produces another variable in the dynamic stability assessment matrix. Therefore, in addition to a reference mean speed, the wind environment includes a mean direction.

In order to determine the force on the ship due to wind in high sea states, the wind profile must be understood at the “local” scale, meaning that the effect of the nearby wave shadowing is included. This results in an apparent gustiness from the effect of being in the trough versus being on the crest. It is unclear whether or not capturing these effects has a significant effect on the final ship-motion results, but it has been decided that the effects should be included until otherwise deemed unnecessary.

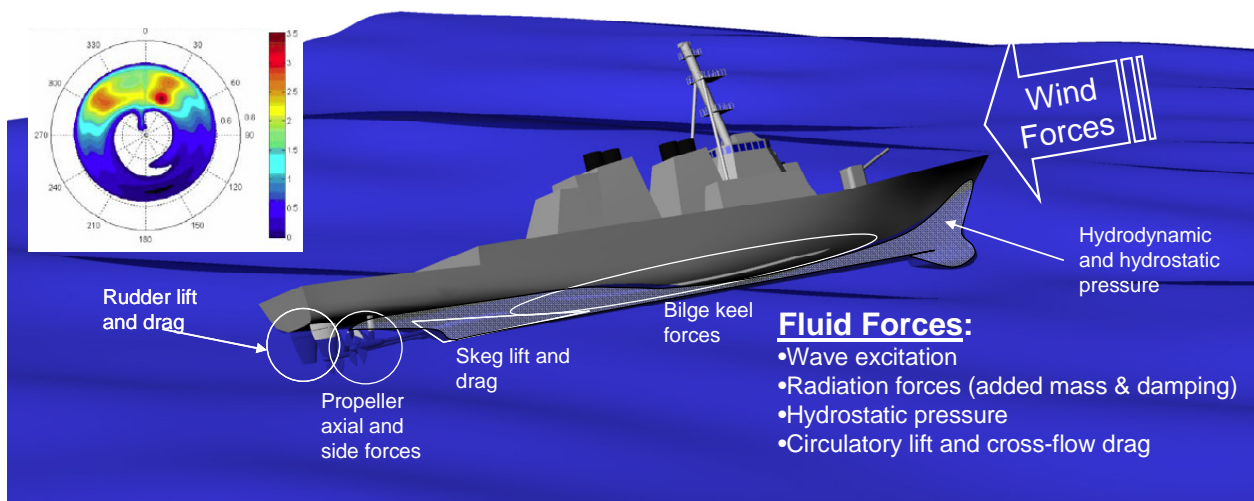


Figure 1: Illustration of the physical problem to be simulated

### **Ship control**

In a traditional “seakeeping” framework, the ship’s speed and heading is considered known or prescribed. The solution of the seakeeping problem is the characterization of the motions about this nominally constant speed and heading. This framework is adequate and appropriate for determining the non-rare motion statistics, such as the RMS or significant values.

In the characterization of the large amplitude, or rare motion problem, it is necessary to consider the forces and responses that arise from large deviations from the constant speed-heading condition. These may include, but are not limited to, surf-riding and broaching. To allow for these, the ship must be *self-propelled* and *self-steered*. As such, the physical problem is best characterized as the maneuvering-in-waves problem.

To be self-propelled means that a propulsor model of some sort provides a thrust to balance the resistance forces present due to the air and water. Rather than prescribing a speed, the thrust and resistance, both of which can be time-dependent, determine the speed.

Self-steered means that a rudder, azimuthing propulsor, or other steering device is used to provide a yaw moment that counters a yaw moment induced by the aerodynamic and hydrodynamic forces on the hull. The time-changing balance of these forces and moments leads to the time-changing heading of the ship.

### **Forces**

The forces acting on the vessel in the defined ambient environment for the ship under self-propulsion and self-steering control largely follow from the typically understood seakeeping and maneuvering problems. The unique aspects of the dynamic stability problem are the coupling of the forces and the effect of large amplitude motion and/or large amplitude waves.

The fluid forces on the hull consist of hydrostatic pressure, wave excitation (Froude-Krylov and diffraction), radiation forces (*i.e.*, the added-mass and wave-making damping effects), resistance forces, and circulatory lift

and cross-flow drag that arise from viscosity. In a high sea state, these forces can act on a hull with large changes in wetted geometry.

In the special case that the deck is submerged, the fluid flow must be treated as a “green water” problem. The green water problem describes the time delay in the force due to the time it takes for the fluid to cover the deck, as well as the shipping of water as the deck reemerges.

In addition to the bare hull, the bilge keels provide a lifting force or a cross-flow drag, as well as contribute to the added mass. As with other parts of the hull, the bilge keels can exit and re-enter the free-surface.

Propeller forces depend on the advance coefficient,  $J$ , which in turn is affected by the ambient environment (via wave-orbital velocities) and ship motions. In large waves the propellers can exit and re-enter the water, which will affect thrust and consequently speed of the ship. Furthermore, in the extreme motion and wave conditions present, large inflow angles of attack can result that lead to side forces that can be up to 40% or more of the axial force.

The rudder forces are coupled both with the propeller thrust and the ambient wave environment. As with other appendages, the rudders are subject to exit and re-entry through the free surface.

Finally, the wind environment imparts forces and moments on the exposed parts of the hull. The wind loads are dependent upon the time-changing, wind-speed profile acting on the ship.

### **IMPORTANCE OF NONLINEARITY**

There are a number of nonlinearities that manifest themselves in the prediction of motions of ships in extreme seas and dynamic stability. These range from: the equations of motion, to the geometry of the vessel, to the hydrodynamics as exemplified by the nonlinear free-surface boundary condition applied to the ambient wave field and the hydrodynamic disturbance (radiated and diffracted waves), and to Bernoulli’s equation for pressure. The use of the fully nonlinear equations of motion is

endemic among dynamic-stability codes, but otherwise there are as many differences as there are choices as to which nonlinearities are important and need to be included.

### ***Hydrostatics and Froude-Krylov***

That nonlinearities are important for large-amplitude motion predictions has been recognized for many years, and is illustrated by the extensive use of “blended” methods that combine linear and nonlinear forces to predict large-amplitude vessel motions (Beck & Reed, 2001). Blended methods typically incorporate nonlinear hydrostatic-restoring forces and nonlinear Froude-Krylov exciting forces due to the incident waves, with linear radiation and diffraction forces. Both the nonlinear hydrostatic-restoring forces and Froude-Krylov exciting forces account for body nonlinearities, particularly in the presence of large-amplitude waves and extreme motion responses.

The nonlinear hydrostatic-restoring forces arise from integrating the  $gZ$  term in Bernoulli’s equation over the instantaneous wetted surface of the vessel in the incident waves, so there is little ambiguity as to what is to be computed (cf, de Kat & Paulling, 1989). The issue here is how is the “incident wave” defined—is it purely linear, or does it include nonlinear (second-order or higher) terms? Since the mid 1800’s, it has been known that steep second-order waves have higher crests and shallower troughs than linear waves (Stokes, 1847), which will clearly affect the instantaneous wetted surface of the vessel and thus the hydrostatic-restoring force on the vessel. (More on the ambient wave description later in this section.)

The Froude-Krylov contribution to the exciting forces results from integrating the hydrodynamic terms of Bernoulli’s equation ( $\phi_t + 1/2\nabla\phi\cdot\nabla\phi$ ), which result from the incident waves over the immersed surface of the ship’s hull. In this case, it is not as clear what terms should be integrated as it was for the hydrostatic term. Many codes linearize Bernoulli’s equation to either  $\phi_t$  or  $\phi_t + U\phi$ , where  $U$  is the forward speed of the vessel, either instantaneously or on the average. This leaves the

possibility of significant variation in results for the Froude-Krylov component of the force without even considering the representation of the incident wave. Telste & Belknap (2008) present and discuss some examples of this type of variation. The representation of the wave which will be presented later adds even more variation.

### ***Hydrodynamic Forces***

To develop an understanding of the hydrodynamic forces and moments on a vessel undergoing large-amplitude motions, a numerical experiment was performed using a variety of computational tools. These computational tools ranged from linear, to blended, to fully nonlinear. The complete experiment is documented in a massive report (15,240 p.), Telste & Belknap (2008). Belknap & Telste (2008) and Reed (2009) contain summaries of the results.

In the numerical experiment, thousands of the force and moment calculations were made and compared for two hulls: oscillating in various modes of motion in calm water (Task 1), fixed in waves (Task 2), and simulating large-amplitude motions by contouring waves (Task 3). The results are presented in the form of time-history plots showing simulated forces and moments at two speeds, for a variety of headings and wave/motion amplitudes. It was not the purpose of the study to evaluate any one code relative to another, but rather to evaluate the differences between various complexities of theory; and in general, codes with a consistent level of theory produced quite consistent results.

Figure 2 shows a time history of ship-fixed vertical force from predictions for a hull undergoing forced heave in calm water at  $F_N = 0.3$  and  $\omega = 1.1$  rad/sec, with heave amplitude/draft of 0.8. Many of these Task 1 force and moment predictions demonstrate the importance of nonlinearity in the radiation forces. An obvious indicator of nonlinearity is the departure of the components of force and moment from a simple sinusoidal form. This is seen in the predictions by the three nonlinear codes shown in Figure 2. A surprising finding was

that the body-exact strip theory is capable of capturing these important nonlinearities—comparable to the two fully nonlinear, 3-dimensional codes. This result provides hope for the development of fast codes to predict dynamic-stability failures on the order of real time.

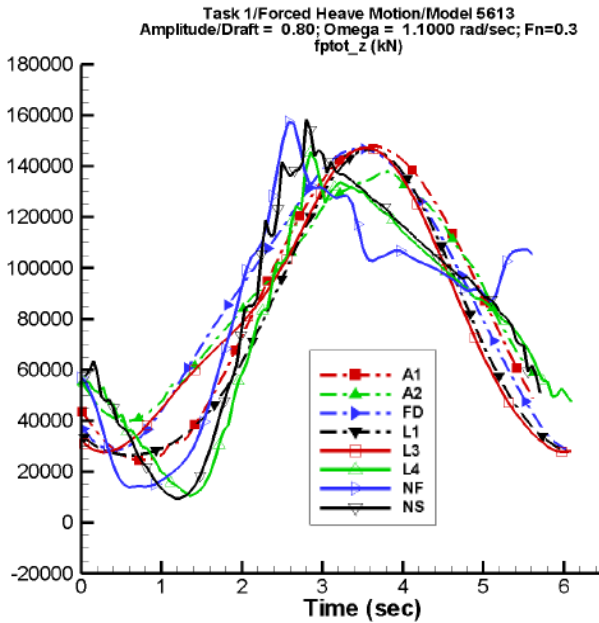


Figure 2: Time-history of ship-fixed vertical force from Task 1 predictions for ONRTH hull undergoing forced heave at  $F_N = 0.3$  and  $\omega = 1.1$  rad/sec, with heave amplitude/draft of 0.8. (Belknap & Telste, 2008)

Figure 3 provides a time-history of ship-fixed vertical forces [hydrodynamic (*i.e.*, radiation and diffraction); Froude-Krylov; hydrostatic] on a hull which is contouring waves in following seas at  $F_N = 0$ ,  $\lambda/L = 2$ , and  $H/\lambda = 1/20$ . From these Task 3 computations, it was found that the hydrostatic and Froude-Krylov forces are an order of magnitude greater than the hydrodynamic forces. The hydrostatic and Froude-Krylov forces calculated by all of the codes are in remarkable agreement—there is no difference in the hydrostatic force, and the differences in the Froude-Krylov force predictions are small. The hydrodynamic forces show significant variation between the codes. As it was impossible to distinguish between the radiation and diffraction components of the hydrodynamic force, one cannot identify the sources of the difference. However, the hydrostatic and Froude-Krylov forces are 180° de-

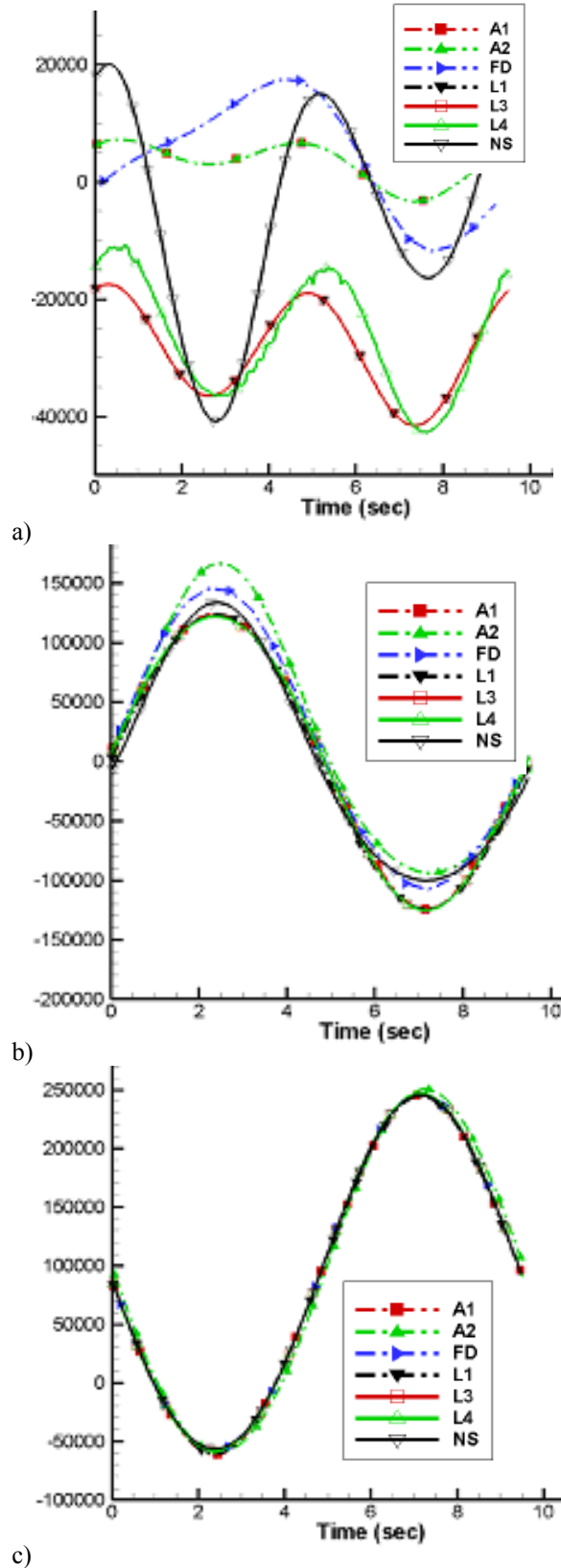


Figure 3. Time history of ship-fixed vertical force from Task 3 predictions for Model 5514 hull, while contouring following seas at  $F_N = 0$ ,  $\lambda/L = 2$ ,  $H/\lambda = 1/20$ , a) hydrodynamic force, b) Froude-Krylov force, c) hydrostatic force. (Belknap & Telste, 2008)

grees out of phase with each other, so they largely cancel each other. Thus the difference between the hydrostatic and Froude-Krylov forces is the same order of magnitude as the hydrodynamic force, which means an accurate calculation of the hydrodynamic force is very important.

### Second-Order Waves

As discussed earlier, nonlinear ambient-wave models have the potential to significantly influence predictions of dynamic stability. Two aspects of this are important: the shape of the wave profile; and the pressure within the wave. Stokes (1847) showed that the second order waves had steeper crests and shallower troughs than linear waves. According to linear theory, the pressure in wave crests (that portion of the wave above the calm free surface) is not zero at the free surface, which leads to significant errors in the predicted forces and moments on the ship's hull, particularly when the ship is in the wave crest in steep waves.

Figure 4 illustrates this for a wave of steepness ( $H/\lambda$ ) of 1/10. It shows the pressure contribution from the zeroth- [ $p_0/(\rho g) = -z$ ], first- [ $p_1/(\rho g) = 2Ae^{vz} \cos \theta$ ], and second-order [ $p_2/(\rho g) = -2vA2e^{2vz}$ ] terms in the pressure. As can be seen, the sum of the zeroth- and first-order pressure terms ( $p_0 + p_1$ ) differs significantly from zero—providing an over prediction of the actual pressure at the free surface.

One method of dealing with this discrepancy with linear waves is the so called Wheeler stretching (Wheeler, 1970), where the origin of the vertical coordinate is essentially shifted to the wave surface from the calm-water equilibrium surface, resulting in zero pressure at the free surface. The Wheeler-stretching approximation leads to much more realistic pressure distributions, and thus forces, than those forces which result from no stretching.

In the case where one is employing second-order wave theory to obtain realistic wave profiles in extreme seas, the use of second-order theory for the wave pressures leads to accurate predictions of the pressure within the wave

profile for regular waves.<sup>1</sup> The sum of the zeroth-, first-, and second-order pressure terms ( $p_0 + p_1 + p_2$ ) in Figure 4 provides an example of the second order pressure distribution, which comes quite close to zero at the free surface, much closer than the first-order approximation ( $p_0 + p_1$ ).

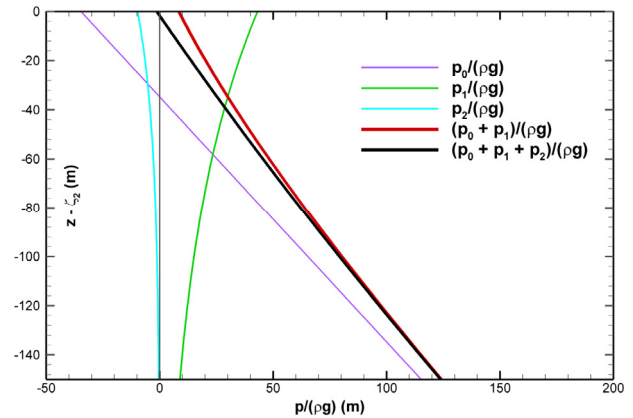


Figure 4: Pressure under a wave crest through second order divided by  $\rho g$ , as a function of the distance below the crest:  $H/\lambda = 1/10$ ,  $\zeta_1 = 2A \cos \theta$ ,  $\zeta_2 = 2A^2 v \cos(2\theta)$ ,  $p_0/(\rho g) = -z$ ,  $p_1/(\rho g) = 2Ae^{vz} \cos \theta$ ,  $p_2/(\rho g) = -2vA2e^{2vz}$  (Courtesy of J. Telste)

A consistent implementation of second order wave theory for irregular seas leads to sums containing exponentials of sum- and difference-frequency terms. The exponential sum terms can become quite large near the wave crests, resulting in extremely unrealistic pressures near the free surface of wave crests. This is illustrated in Figure 5 for two waves of differing frequencies such that the ratio of their wavelengths is 10.

There are several possible approaches that can be used to resolve the sum-frequency issue for irregular seas. One suggestion is to use a 2- or 3-term Taylor series expansion of the exponential rather than an exact function evaluation. Stansberg, *et al.* (2008) propose the use a low-pass filter applied to the linear horizontal velocity. The reason for such a filter is given by Gudmestad (1993), who states that the exponential term becomes very large near wave crests if the low-pass filter is not used.

<sup>1</sup> The second-order pressure equation does not require second-order wave theory, it can be used with linear wave theory.

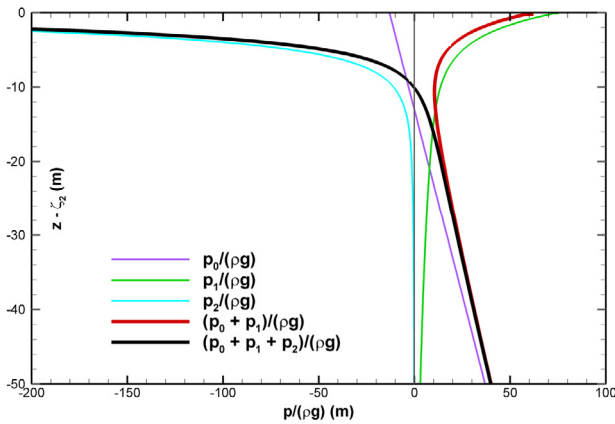


Figure 5: Pressure under a wave crest through second order,  $(p_0 + p_1 + p_2)/\rho g$ , for the sum of two waves versus the distance below the crest,  $z - (\zeta_1 + \zeta_2)$ , for two frequencies:  $\lambda_1/\lambda_2 = 10$ ,  $H/\lambda = 1/10$ ,  $(\theta_1, \theta_2) = (0, 0)$ . (Courtesy of J. Telste)

### Second-Order Forces

As a ship maneuvers in steeper and steeper waves, there are greater and greater interactions between seakeeping and maneuvering, to the point that one cannot predict maneuvering in steep waves by simply superimposing seakeeping and maneuvering in a linear fashion (cf, Reed, 2009). One of the reasons for this is the fact that in steep waves the second-order hydrodynamic forces and moments (second-order drift forces and moments, and added resistance in waves) begin to play a significant part in the maneuvering behavior of the ship—slowing it down and speeding it up as it executes a turn in waves (Skejik & Faltinsen, 2008). For this reason, it is important to have a comprehensive model of the physics that includes these forces. The Froude-Krylov forces and moments capture a portion of these forces and moments, but only the component due to ambient waves. There is a significant hydrodynamic component that must be captured accurately.

### Nonlinear Dynamical System

Finally, it needs to be recognized that a ship undergoing large-amplitude motions in extreme seas represents a nonlinear dynamical system. As a consequence, the vessel response can change drastically with small increases in excitation—this is particularly true near and beyond the peak in the righting-arm curve,

where the restoring moment remains essentially constant or even decreases as the heel angle (roll angle) increases. Conceptually this is easy to understand in calm water, but in a seaway, there is even more variability due to the ship's being posed on a wave—as the wave passes along the hull the magnitude of the righting arm will fluctuate relative to the calm-water righting arm and the angle corresponding to the peak of the righting arm will vary. Whether the peak of the righting-arm curve increases or decreases in magnitude and the angle at which the peak occurs is a function of the shape of the hull above and below the calm-water waterline and the phase of the wave along the hull. Statistically, this says that there will be significant uncertainty as to the response of the ship under these circumstances. This has significant implications for the validation of computational tools and it is important for one to understand these concepts when validating the tools.

### CODE APPROACH OPTIONS

Having identified the components of the maneuvering-in-waves physical problem and understanding the importance of nonlinearity within the dynamic-stability problem, several modeling approaches were evaluated for implementation in TEMPEST. Vassalos, et al. (1998) provide an overview of the numerical tools and approaches available for predicting dynamic stability events. Further evaluation of options relied on experience with existing ship-motion computational tools, though physical considerations played a large role as well. One reason for this is that existing tools are fallible; *e.g.*, some of the tools may not have been adequately verified, meaning that seemingly poor validation results can not be separated from potential bugs in the code. A key argument for developing a tool from scratch is that it allows for best verification practices (thorough documentation, unit tests, etc.) to be built in from the beginning.

Perhaps the first high-level-approach question to consider is whether to follow a complete flow solver (such as RANS or Euler VoF) or a potential flow-based track. While the option to

compute a total solution of the fluid flow is attractive because it would include nearly the entire physical problem in a single computation, the computational cost is prohibitive given the number of conditions that need to be simulated. For that reason, a framework that follows the traditional seakeeping decomposition of a radiation and diffraction potential-flow solution added to a circulatory-lift solution is the only practical path. The argument for such an approach is that there is weak and/or one-way coupling between the hull radiation and diffraction (or “hydrodynamic disturbance”) force and the lift and cross-flow drag on the appendages and the hull itself. While this assertion requires validation, there is no apparent alternative that meets computational speed requirements.

There are two basic paths that can be followed within the framework described above. One approach is to combine a maneuvering theory with a seakeeping theory, such as the two-time scale model employed by Skejik & Faltinsen (2008) that attempts to break the problem into its low-frequency part (maneuvering) and high-frequency part (seakeeping). The difficulty with this approach is avoiding any double-counting of forces. The attractiveness of this option is that trusted maneuvering models can be used. The second approach is to attempt to model the circulatory lift problem by itself, thereby avoiding double-counting issues. The challenge then is providing a robust model for this force.

Table 1: Computational efficiency (computational seconds / simulated seconds)

	Linear	Blended	Nonlinear
<b>2D</b>	$O(10^{-3})$	$O(10^{-1})$	$O(10^0)$
<b>Slender ship</b>			<i>est. <math>O(10^1)</math></i>
<b>3D*</b>	$O(10^1)$	$O(10^1)$	$O(10^3)$

\* Time-domain solution of hydrodynamic disturbance for Linear and Blended methods

Within the community of potential flow approaches, a code can be described in simple terms by how 3-dimensional it is and how much nonlinearity is captured. In general, the

more 3-dimensional and the more nonlinear a code, the less computationally efficient it will be. Table 1 provides a high-level view of the computational expense within the matrix of nonlinearity and slenderness assumption ranges. “Linear” denotes potential flow codes that are completely linear, whereas “Blended” includes nonlinear (body-exact) hydrostatic and Froude-Krylov forces. The term “Nonlinear” refers to codes with nonlinear hydrodynamic-disturbance forces as well as nonlinear hydrostatic and Froude-Krylov forces. Slender-body approximations range from “2D”, which is strip theory, to “Slender ship”, which includes some 3D effects, to a fully 3D code. The cells of the table are colored green if the computational speed is considered acceptable for providing a sufficient level of data resolution for dynamic-stability risk characterization while red is considered unacceptable.

Table 2 is organized identically to Table 1, but rather than color-coding according to computational speed, the cells are color-coded based on an intuitive assessment of the code’s ability to capture the relevant physical phenomena. This assessment largely follows the arguments laid out on the importance of nonlinearity to the dynamic stability problem.

Table 2: Capturing physics & nonlinearity

	Linear	Blended	Nonlinear
<b>2D</b>			
<b>Slender ship</b>			
<b>3D</b>			

These tables may provide simplistic views of the code-approach options for the solution of the hydrodynamic forces, but they help the theory developer navigate the solution space.

### TEMPEST APPROACH

The philosophy driving the development of TEMPEST’s theory was to include all aspects of the maneuvering in waves physical problem as described earlier and model these components such that they capture the important nonlinearities. The review of code-

approach options has given the development team confidence that a computationally efficient approach is feasible as long as the simplifying assumption of ship slenderness is adopted. This is supported by Table 3, which provides an estimated composite ranking of the hydrodynamic-solution approaches within the criteria of accuracy and speed. As noted earlier, accuracy is weighted more heavily than speed, because quick but incorrect data is of no value to the user. The result is that the TEMPEST approach is based on a fully body-nonlinear hydrodynamic solution with advanced models: for the environment; for circulatory lift and for cross-flow drag on the hull and appendages; and for other superimposed forces.

Table 3: Estimated composite ranking of computational efficiency and ability to capture the relevant physics

	Linear	Blended	Nonlinear
<b>2D</b>			
<b>Slender ship</b>			
<b>3D</b>			

**Environment**

As input to the force models, the modeling of the environment becomes just as important as the force models themselves. While the user generally describes the wave spectrum and wind speed, it is the environmental models that interpret these higher level inputs to provide ambient pressures and velocities at many places on the hull at every time step.

Waves In TEMPEST, the seaway is modeled by second-order waves with arbitrary directionality. Though the modelling of second-order waves adds significant computational cost relative to linear waves, it was determined that the steep waves that lead to dynamic-stability events are best captured by a second-order model. It is believed that the pressure and particle-velocity profiles obtained from the second-order model, while requiring additional validation, are more accurate than

linear waves with Wheeler stretching in the “surf zone” above  $z = 0$ .

To alleviate some of the computational cost, FFT techniques are used to accelerate the computations. An additional feature of the TEMPEST wave model is the availability of an integral-equation iterative solution in the special case of unidirectional seas to find the linear input spectrum, when given the target second-order spectrum.

Long-term solutions may include a higher-order wave model that solves for the evolving wave field. This may significantly increase computational time, but may be necessary if the pressures and velocities are found not to be accurate enough in the steepest waves using lower-order wave models.

Wind The TEMPEST ambient wind environment model defines the vertical wind speed profile above the free surface at any point in space and time. The notable attribute of the TEMPEST wind model is that it attempts to account for the effects of shadowing near large steep waves. This model is currently in development using environmental data obtained from a North Sea oil rig.

**Hydrodynamic Forces**

The hydrodynamic forces acting on the ship are composed of:

- Hydrostatic & Froude-Krylov
- Hydrodynamic disturbance (radiation & diffraction)
- Green water on deck
- Resistance
- Bilge-keel
- Hull circulatory lift and cross-flow drag
- Propeller
- Rudder
- Wind

In all the force components, the effect of geometric nonlinearity is included by accounting for the position of the hull and appendages relative to the incident waves.

Froude-Krylov and Hydrostatic Forces The Froude-Krylov and hydrostatic forces are obtained by integrating the ambient-wave dynamic and static pressures, respectively, over

the instantaneously wetted hull. The wetted hull is determined by the position of the ship and the undisturbed incident wave. To best capture the longitudinal force, the pressures are evaluated on 3D panels. An illustration of the body-exact Froude-Krylov plus hydrostatic pressure on a 3D mesh is given in Figure 6.

Hydrodynamic-Disturbance Forces The force that captures the traditional seakeeping radiation and diffraction forces is the hydrodynamic-disturbance force. TEMPEST obtains this disturbance force by solving the time-domain potential-flow boundary-value problem on the time-changing wetted surface of the hull. The conclusion of the theory development team was that applying a slender-ship approximation would still capture the dominant physics while allowing the computations to occur at or near “real-time” speed. The theory behind this approach is given in a report to be published by Sclavounos, *et al.* (2010).

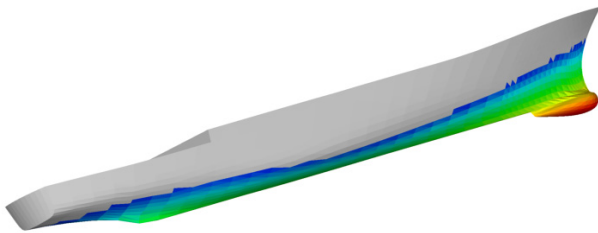


Figure 6: Sample ambient-wave pressure on a 3D meshed hull

The body-exact hydrodynamic disturbance solution in TEMPEST is being implemented in a two-phase process. In Phase 1, a strictly 2D approach is taken via a body-exact strip theory. Phase 2 implements a slender-ship theory, built upon body-exact strip theory that incorporates 3D effects.

The body-exact strip theory in Phase 1 follows the theoretical and numerical approach presented by Bandyk (2009). In this approach, impulsive and wave-memory problems are solved on 2D strips at each time step, an example of which is shown in Figure 7. The boundary value problem is numerically solved by a 2D Rankine panel method where the body section has sources distributed on 2D panels and the free surface uses desingularized panels. An

example of this is shown in Figure 8. Memory effects are automatically captured in the solution of the free-surface panels’ source strengths.

In the Phase 2 hydrodynamic-disturbance potential solution, 3D effects are added through the use of a 3D time-domain Green function that operates on the impulsive source strengths determined on 2D sections. While this approach is presumably more computationally intensive than the body-exact strip theory, it may include 3D effects that are significant to the dynamic-stability problem. In this approach, as opposed to the body-exact strip theory in Phase 1, the wave-memory effects are obtained through evaluations of convolution integrals within the Green function. To address the computational burden, efficiency may be gained by simplifying the convolution integral functions and/or determining equivalent impulsive source-dipole line distributions within the interior of the wetted hull.

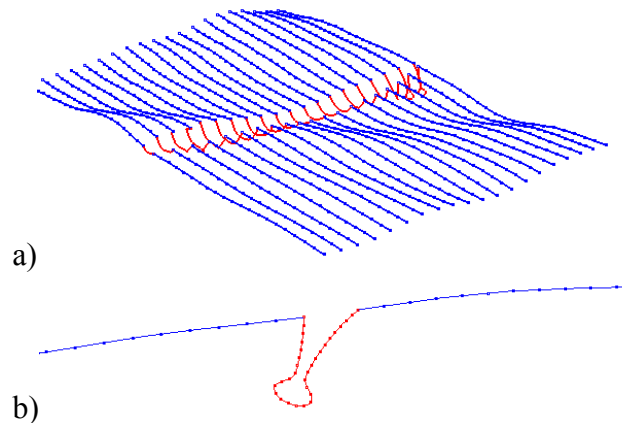


Figure 7: Illustration of the body-exact strip theory problem for a) the entire ship, and b) a single 2D section.

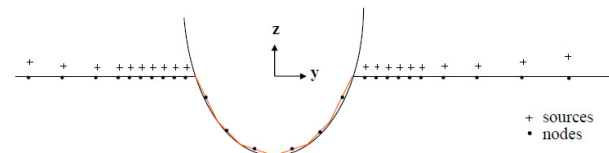


Figure 8: Numerical solution of the time-domain boundary value problem for an example section (from Bandyk (2009)).

In both implementations of the body-exact hydrodynamic-disturbance problem, the force can be calculated from the velocity potentials

through pressure integration or a momentum formulation. Calculating pressure for the 2D problem involves the difficult task of determining  $x$ -derivatives. Bandyk (2009) describes the use of radial-basis functions to overcome this difficulty. The momentum formulation (see Sclavounos, *et al.* 2010) simplifies the force evaluation by requiring only a time-derivative on the integrated potentials.

Finally, hydrodynamic-drift forces that arise from the disturbed free-surface elevation are included. This is done in a simplified manner by evaluating a waterline integral that provides a hydrostatic correction due to the disturbance-wave elevation around the hull.

Green Water on Deck To account for the physics of deck submergence and re-emergence, a semi-empirical green-water model is included. This model has been implemented and successfully tested in LAMP (Liut, *et al.* 2002). This model uses empirical relationships to get water height on deck given the deck-edge exceedance following Zhou, *et al.* (1999). A notable attribute of this model is that it does not capture the lag in elevation across the deck due to the flow of water on and off the deck. However, until it can be shown that the lag effect is important to the dynamic-stability problem, computational efficiency requirements dictate the use of the semi-empirical model.

Ship Resistance The TEMPEST resistance model uses a user-supplied resistance curve with the wave drag removed via a series of speed-calibration runs. The calibration runs remove any double-counting with the hydrodynamic disturbance force. To account for body nonlinearity, the resistance curve is modified to account for the instantaneous wetted surface. The quasi-steady resistance is then obtained based on the instantaneous velocity through the water which includes the influence of wave orbital velocities.

Bilge-Keel Forces Low-aspect-ratio lifting-surface theory is the foundation of the TEMPEST bilge-keel force model (cf, Greeley & Peterson, 2010). The work of Bollay (1936) inspired the model by showing that the trailing vortex sheet comes off the edge of the surface

at an angle equal to half the angle of attack. By prescribing this trajectory of a trailing vortex sheet, a vortex-lattice method can be used to solve for the circulation strength and determine the (quasi) steady and unsteady forces due to lift. This method breaks down at angles of attack greater than about 50 (generally low-ship-speed conditions) where there is no true lift, so a Morison equation-based model is used. An “instantaneous” Keulegan-Carpenter (KC) number is estimated through the use of a short-time spectral analysis of normal velocity using a discrete Fourier transform. In large amplitude roll cases, the effect of the bilge keels piercing the free surface is captured by means of a piece-wise damping model that accounts for various pieces of the hull entering and leaving the water (Bassler, *et al.*, 2010).

Hull Lift and Cross-Flow Drag Similar to the hydrodynamic disturbance force, the hull lift and cross-flow drag force model is being implemented in a two-phase manner. The initial model uses low-aspect-ratio lifting-surface theory to estimate time-changing (due to waves and motion) side force and yaw moment coefficients. These coefficients are calibrated based upon user-supplied coefficients. This lift force is phased out over increasing drift angle,  $\beta$ , through a  $\cos^2 \beta$  multiplier that approximates stall. A cross-flow drag force is also calculated at each section for the time-changing geometry. This force follows a  $\sin^2 \beta$  behavior due to the fact that the only influence is the square of the cross-flow velocity. The cross-flow drag coefficients can be user-supplied or estimated based on shape coefficients. Reynolds number dependence of cross-flow drag coefficients is included.

The second phase of the hull lift and cross-flow drag force model implementation will apply the vortex-lattice techniques developed for the bilge-keel force model.

Propeller Forces The propeller forces are included as external forces to the hull. The key attribute of the TEMPEST propeller-force model is that it includes not just the axial force but also side forces when the inflow velocity provides an angle of attack to the propeller.

The inflow velocity includes the effects of body velocity (including rotations), wave orbital velocities, and an estimate of the viscous wake due to the presence of the hull.

The forces developed by the propellers due to the time-varying inflow are determined by a blade-element model. The blade-element model will properly account for partial or full emergence of the propeller. Pending more study, scale effects may be included to account for loss of thrust due to cavitation

Rudder Forces The TEMPEST rudder-force model provides the forces due to lift and drag only. The contribution to the radiation and diffraction problem is not considered. To account for body-nonlinearity, the rudder force is scaled by the immersed area of the rudder.

Wind Forces Wind forces are determined on the hull following a horizontal strip-theory approach similar to that given by Gould (1982). The benefit to a strip-theory approach is that it allows the use of an arbitrary wind-speed profile while still taking advantage of calibrated wind-drag and moment coefficients. Given the need to include non-traditional wind profiles due to the local presence of large, steep waves, such an approach is necessary.

## CONCLUSIONS

TEMPEST is a new dynamic-stability simulation tool currently in development by the US Navy. The requirements of the tool are accuracy and computational speed.

After careful study of the physical problem, a comprehensive set of environment and force models has been described that is expected to provide a viable solution to the dynamic-stability prediction problem that advances the state-of-the-art. The fundamental argument behind the TEMPEST approach is the requirement for body-nonlinearity in all force models, including the hydrodynamic-disturbance force (radiation and diffraction).

The TEMPEST development will be followed by extensive validation at the component level and as a system.

## ACKNOWLEDGEMENTS

The authors would like to acknowledge the contributions of John Telste and Dr. Mike Hughes (NSWCCD), Dr. Dave Greeley (Applied Physical Sciences); and Prof. Paul Sclavounos (MIT), Prof. Bob Beck (U. Michigan), and the other members of the TEMPEST Theory Advisory Panel (TAP), who have contributed to the development of the TEMPEST theory. Dr. Pat Purtell (ONR) and Jim Webster (NAVSEA) have supported the TEMPEST effort.

## REFERENCES

- Bandyk, P. (2009) A Body-Exact Strip Theory Approach to Ship-Motion Computations. Ph.D. Thesis, Univ. Michigan, Dept. Naval Architecture and Marine Engineering.
- Bassler, C. C., A. M. Reed & A. J. Brown (2010) A Method to Model Large-Amplitude Ship Roll Damping. *Proc. 11th Int'l Ship Stability Workshop*, 10 p.
- Beck, R. F. & A. M. Reed (2001) Modern Computational Methods for Ships in a Seaway. *Trans. SNAME*, 109:1–51.
- Belknap W. & J. Telste (2008) Identification of Leading Order Nonlinearities from Numerical Forced Motion Experiment Results. *Proc. 27th Symp. Naval Hydro.*, Seoul, Korea, 18 p.
- Bollay, W. (1936) A New Theory for Wings with Small-Aspect Ratio. Ph.D. Thesis, Caltech, ii+86 p.
- de Kat, J. O. & J. R. Paulling (1989) The simulation of ship motions and capsizing in severe seas. *Trans. SNAME*, 97:139–68.
- Gould, R. W. F. (1982) *The Estimation of Wind Loads on Ship Superstructures*, Maritime Technology Monograph No. 8, The Royal Institution of Naval Architects.
- Greeley, D. S. & B. J. Petersen (2010) Efficient Time-Domain Computation of Bilge Keel Forces. *Proc. 28th Symp. Naval Hydro.*, Pasadena, CA, 17 p.
- Gudmestad, O. T. (1993) Measured and Predicted Deep Water Wave Kinematics in Regular and Irregular Seas. *Marine Structures*, 6:1–73.

- Liut, D. A., K. M. Weems, and W. M. Lin (2002) Nonlinear Green Water Effects on Ship Motions and Structural Loads. *Proc. 24th Symp. Naval Hydro.*, Fukuoka, Japan.
- Reed, A. M. (2009) A Naval Perspective on Ship Stability, *Proc. 10th Intl. Conf. Stability of Ships and Ocean Vehicles*, St. Petersburg, Russia.
- Sclavounos, P. D., J. G. Telste & A. M. Reed (2010) Nonlinear Response Modeling of a Vessel in Steep Random Waves. Carderock Division, Naval Surface Warfare Center Report NSWCCD-50-TR-2010/039.
- Skejic, R. & O. M. Faltinsen (2008) A unified seakeeping and maneuvering analysis of ships in regular waves. *J. Mar. Sci. Tech.*, 13:371-394., DOI 10.1007/s00773-008-0025-2
- Stansberg, C. T., O. T. Gudmestad & S. K. Haver (2008) Kinematics under Extreme Waves. *J. Offshore Mechanics and Arctic Engineering*, 130(2) 020201.1–021013.8.
- Stokes, G. G. (1847) On the theory of oscillatory waves, *Trans. Cambridge Philosophical Society*, Vol. 8, Part IV, No. XXXIII, pp. 441–455.
- Telste, J. G. & W. F. Belknap (2008) Potential Flow Forces and Moments from Selected Ship Flow Codes in a Set of Numerical Experiments. Carderock Division, Naval Surface Warfare Center Report NSWCCD-50-TR-2008/040, 15,240 p.
- Vassalos, D., M. Hamamoto, J. O. de Kat, D. Molyneux & A. Papanikolaou, (1998) The State of the Art in Modelling Ship Stability in Waves, *Proc. 25th ATTC*, Iowa City, Iowa, 8 p.
- Wheeler, J. D. (1970) Method for calculating forces produced by irregular waves. *J. Petroleum Technol.*, **249**:359–367.
- Zhou, Z.Q., J. O. De Kat, and B. Buchner (1999) A Nonlinear 3-D Approach to Simulate Green Water Dynamics on Deck, *Proc. 7th Int'l Conf. Numerical Ship Hydro.*, Nantes, France.



## Heavy Weather Ship-Handling Bridge Simulation

Mr Stephen Marshall CEng RCNC

Sea Systems Group, DE&S, Ministry of Defence, UK

### ABSTRACT

The Naval Stability Standards Working Group (Australia, Canada, France, Netherlands, UK, USA) is examining the accepted risk associated with naval intact stability standards in extreme environmental conditions. Part of this programme is the inclusion of the assessment of the influence of the operator on capsize risk. Operator Workshops held by the Royal Netherlands Navy in 2005 & 2007 proved the feasibility of linking a bridge simulator and the dynamic stability tool FREDYN to achieve this goal. Building on the knowledge and recommendations from the Netherlands workshops the MoD held a Heavy Weather Ship-Handling Workshop at the TRANSAS bridge simulator, Portsmouth on 15-16th December 2009. The objective was primarily to benchmark the simulations with ship characteristics using Royal Navy Ship-handling doctrine. Whilst some further development is required on cues e.g. spray and ship manoeuvring characteristics the workshop successfully demonstrated, the integration of FREDYN v10, state of the art simulator graphics and the characteristics of heavy weather doctrine.

### KEYWORDS

Ship-handling, Heavy Weather, Bridge Simulator.

### INTRODUCTION

Modern Naval stability standards have had an exemplary record to date. These standards were developed over 40 years ago on hullforms different from today's. It is the goal of the Naval Stability Standards Working Group (Australia, Canada, France, Netherlands, UK, USA) to understand the strengths and weaknesses of current criteria applied to today's hullforms. In doing so, assumptions have been made about the influence of the operator in extreme seas. It is an unassailable fact that safety in such conditions is strongly influenced by good seamanship and command decisions. A series of Naval Operator Ship Handling Workshops were held at the Royal Netherlands Naval College bridge simulator facility (2005 & 2007). The basic intent of such has been twofold; firstly to allow insight into the beneficial effect of good seamanship upon

the risk of capsize, and secondly introduce, to the naval operator training fraternity, the potential of the latest technological advances in heavy/extreme weather ship simulation and ship board operator guidance as a viable supplement to sea time experience.

The influence of the operator, derived from such a simulator, will be translated to scientific parameters such as the intensity of different cues to select speed and heading. These parameters will be used in FREDYN dynamic stability risk calculations to minimise or discount the probability of unreasonable speeds and headings in extreme environments.

This paper describes the findings of a workshop held by the Sea Systems Group to benchmark with operator experience the bridge simulator visual, audio cues together with FREDYN ship handling and motions characteristics

## THE APPROACH

The goal was achieved through the integration of FREDYN v10 via a dll with the TRANSAS NTPRO 5000 software. The following architecture was used

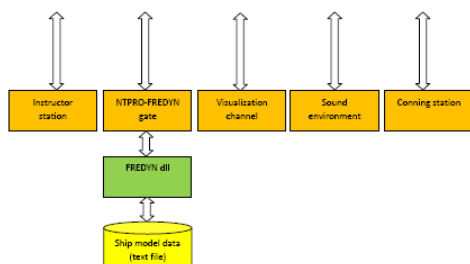


Figure 1: FREDYN/NTPRO Integration structure

On initialisation of the FREDYN program, data was passed to the NTPRO simulator based on the information defined in the FREDYN input files. This data consisted of the wind speed and direction, wave direction and the frequency, phase and amplitude of all of the wave components used to define the sea conditions. Other ship data parameters at time zero were also passed to the NTPRO simulator, such as ship attitude, initial velocities and RPM settings. Once the simulation was underway the visualisation parameters in the simulator could be modified to change the appearance of the visual effects to reduce visibility and change weather and light conditions

The following cues had been incorporated in the simulator triggered by FREDYN:

- Slamming noise
- Bow Spray & green seas ( Figure 2)
- Propeller racing (temporary increase in RPM on bridge readouts and sound effect)
- Hull creaking

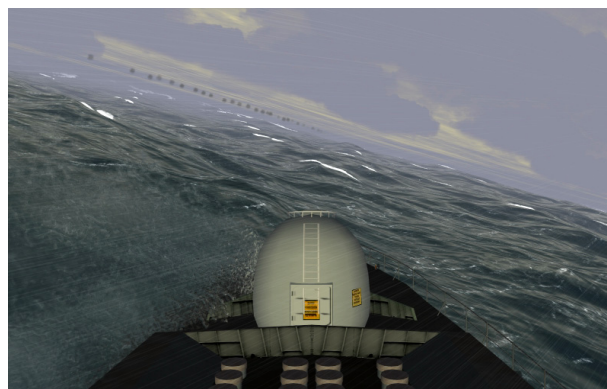


Figure 2: Bow Spray on SAR Stage 4

FREDYN provided the wave field and calculated the motions to suite in real time, triggering cues accordingly. A NTPRO overlay was applied to the waves to provide realism of definition such as white crests and streaking on the waves.

## THE SIMULATIONS

The scenarios used a T23 frigate in ship conditions that are representative of the ship as compliant with its stability standard.



Figure 3: T23 frigate

The serials used selected environmental and ship conditions to best illustrate the handling behaviour of the ship. The key characteristics selected for demonstration were:

- Pitching (the effect of trim and speed)
- Rolling (the effect of wave period & speed)
- Stern to sea ship handling (avoiding broaching & pooping)
- Turning across a sea (starting into and down sea with wind)

A scenario was also exercised dedicated to combining the above characteristics into a

Search & Rescue and Storm scenario as described below.

### SEARCH & RESCUE SERIAL (SAR)

The goal of the scenario was to exercise ship-handling doctrine benchmarking in an operational environment. It provided insight into operational considerations and the impact on ship-handling and the environment. The environment is progressively worsened throughout the serial although there was a necessary pause between each to facilitate reloading FREDYN. Wind was in the direction of waves and changed to deliver spreading and gusting in FREDYN.

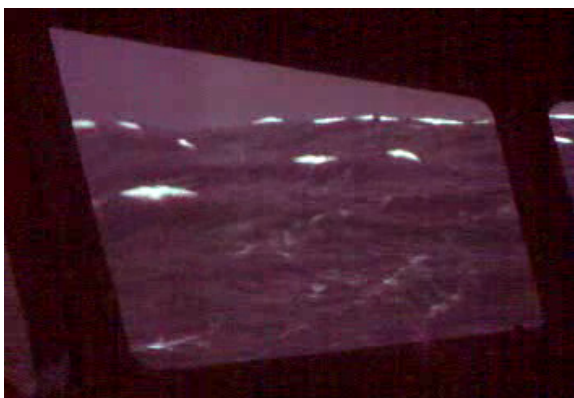


Figure 4: View from the bridge

Stage 1: Pilotage from Devonport with an Auxiliary ship to steam to Gibraltar at best speed. Building SAR scenario with 2 vessels in difficulty.

Stage 2: Low Sea State 6 (Hs=4m, Tm=10secs), Wind 30Kts. Goal to achieve best speed in bow quartering seas. Ship advised to proceed to sunken yacht to pick up life raft and person in water.

Stage 3: High Sea State 7 (Hs=9m, Tm=13.6secs), Wind 45Kts. Line of sight to casualty across the sea. Ship to adopt best speed to pick up casualties. Officer of the Watch (OOW) assesses conditions and adopts

either a bow or stern quartering course. Scenario provided an opportunity to position ship for either deployment of rescue boat or swimmer of the watch.



Figure 5: SAR Stage 3 completion

Stage 4: Mid Sea State 8 (Hs=11m, Tm=15secs), Wind 45Kts. New casualty, tanker on fire ship advised to proceed at best speed to tanker and to standby vessel on arrival. Line of sight to casualty is stern quartering seas. OOW assesses conditions and selects a best speed whilst minimising motions and ensuring ship has steerage.



Figure 6: SAR Stage 4 Auxiliary ship Helo returning from tanker & smoke from tanker seen in the distance.

Stage 5: High Sea State 8 (Hs=13m, Tm=16secs), Wind 45Kts. SAR complete and

ship to rejoin original track, OOW to advise best speed in conditions head seas. Man Over Board (MOB) from flight deck then reported and thus turning across the sea is exercised.

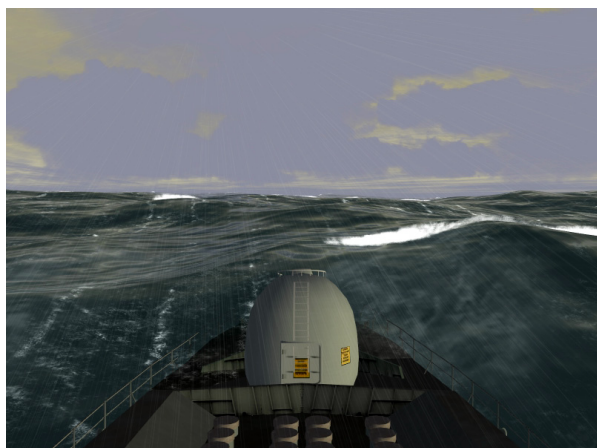


Figure 7: SAR Stage 5 Head Seas.

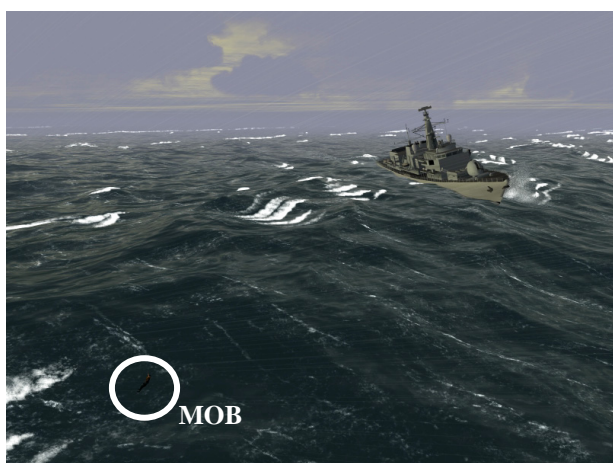


Figure 8: SAR Stage 5 Man Overboard (MOB).

The operators concluded “ I certainly feel I have been through a storm”. The simulations as they stood exercised all the ship-handling characteristics of naval doctrine. It was a significant step forward in technological development in heavy weather ship-handling using a bridge simulator.

The workshop also highlighted additional influences on ship-handling such as the command structure on the bridge and also machinery configuration and response times. For example in stern seas where the guidance advises 60% of wave speed, this speed whilst providing more responsive course-keeping,

may not be adopted as it is not an economical speed.

## CONCLUSIONS

In the development of the heavy weather simulator capability a much improved level of understanding of the effect of good seamanship upon the risk of capsize has been gained. Further advancement of the visual & audio cues, bridge environment and FREDYN code is required before the heavy weather simulator can be deemed benchmarked. The key enhancements required are:

### Essential:

- Spray cues & impact on bridge windows.
- Slamming audio cues
- Validation of ship manoeuvrability & the effect of wind and waves
- Wind spreading and gusting including an audio cue.

### Desirable:

- Inclinator
- Small OOW motion platform
- Slam judder.
- Noises associated with machinery e.g. propeller racing, gas turbine

## ACKNOWLEDGEMENTS

Thanks are made to Mr T Marchant (BMT Defence Services Ltd), Mr B Mills (Transas Marine) & Mr A Peters (QinetiQ) in making the workshop a success.

## DISCLAIMER

The statements made in this paper are those of the author and may not represent that of the Ministry of Defence.

## Further Perspectives on Operator Guidance and Training for Heavy Weather Shiphandling

Commander Laurie J. Van Buskirk,  
*U.S. Navy (Retired)*

Philip R. Alman,  
*U.S. Naval Sea Systems Command*

Captain James J. McTigue,  
*U.S. Navy (Retired), U.S. Naval Sea Systems Command*

### ABSTRACT

Historically, mariners have received minimal formal training in heavy weather shiphandling, relying on mentoring and hands on experience to develop shiphandling skills for dangerous environmental conditions. Maritime organizations are increasingly turning to technology to reduce the inherent risks of heavy weather, including operator guidance systems and simulation to train watch personnel. Shiphandling simulators are on the cusp of extending training capabilities from simple maneuvering situations to highly realistic heavy weather scenarios, resulting in vastly improved training effectiveness. This is especially critical as actual time spent afloat may represent proportionately less of a mariner's total career.

### KEYWORDS

**Shiphandling simulation; heavy weather training; operator guidance**

---

*Note:* The opinions expressed in this paper are those of the authors and not necessarily those of the Naval Sea Systems Command or the United States Navy.

### INTRODUCTION

Heavy weather presents mariners with significant risk of structural damage, loss of cargo, crew injury, and the potential for environmental damage (e.g., oil spills). Damage from heavy weather incurs significant costs to the maritime industry, both in property and environmental damage. In most cases, ships try to avoid heavy weather if possible, but some storms cannot be avoided, or prove to be worse than originally forecasted, leaving shiphandlers to deal with seas and winds for which they may have received little formal training.

All ships can be at risk of capsizing in extreme seas, and that risk can be exacerbated

by poor shiphandling decisions. Current heavy weather training follows two basic precepts: avoid extreme weather, and if the weather cannot be avoided, adhere to "rule of thumb" procedures and techniques to assist in safely riding out the storm. Advances in meteorological technology have significantly enhanced the ability to avoid severe weather by providing concise, real time understanding of the current and predicted weather environments, as well as storm mapping. However, on occasion, seamen must face the elements. It is at this point that correct and time-sensitive shiphandling decisions must be made, often in a high-stress environment that increases the potential for human error, and heavy weather training becomes critical.

## SHIPHANDLING TRAINING

Historically, shiphandling training has focused on building skill sets for normal seaway and restricted maneuvering situations, such as entering and exiting ports and special evolutions at sea. The focus has been on understanding basic shiphandling characteristics and techniques as bounded by a ship's size, propulsion, ship control, and steering capabilities. Mariners have received minimal formal training in heavy weather shiphandling, relying instead on personal mentoring and hands on experience in specific ship types or classes with known handling characteristics to impart the ability to cope with difficult and dangerous environmental conditions. The reality of shiphandling in heavy weather is that normally only the most experienced shiphandlers are engaged in ship control in severe weather, so junior officers get little actual hands-on experience. Because heavy weather is normally avoided, even the most seasoned mariners may have only limited experience in higher sea states. This training gap in appropriate shiphandling procedures in heavy seas contributes to a higher risk of damage and loss when heavy weather is encountered.

### *Heavy Weather Shiphandling Training Objectives*

In addition to the paucity of actual heavy weather shiphandling experience facing many of today's mariners, the advent of a variety of new hull forms makes it increasingly important to educate shiphandlers on the unique handling characteristics of these designs, particularly in higher sea states. In some cases, traditional shiphandling methods may not be appropriate for some of the more innovative designs, so relying on traditional responses in emergency situations may in fact exacerbate the danger. This is an important consideration in the training solution, as care must be taken to mitigate the possibility of negative transfer between traditional shiphandling techniques and those required for non-traditional hull forms. Shiphandling training, and in particular,

heavy weather shiphandling training, should focus on providing tools that complement existing training and focus on ensuring the safety of ship and crew.

Regardless of the hull form, mariners must have a practical knowledge of sea characteristics and the ability to "read" and predict conditions based on clues ascertained from the surrounding environment. This type of information can be covered through classroom training, is currently included in most shiphandling training programs, and provides the foundation for heavy weather operations. Higher sea states, however, require separate skills outside of the scope of shiphandling in calm seas. Certain standard operating procedures can improve the likelihood that at-sea maneuvering events do not result in catastrophic loss or damage. To effectively train for heavy weather, the shiphandler must learn to correctly interpret several basic elements of dynamic information (presented either by display or visual/physical recognition):

- Own ship stability data
- Wave direction, length, height, and periodicity
- Wind speed and direction
- Ship motions (roll, pitch, yaw, surge, sway, and heave)
- The combined dangers/effects of all of the above (slamming, pounding, pooping, surf-riding, broaching, and ultimately, capsizing)
- Appropriate mitigation techniques
- Casualty situations (structural damage, flooding, loss of power/steering, etc.)

Each hull form has its own unique stability characteristics. Factors such as list, trim, displacement, ballasting, KG, and GZ are all important for the shiphandler to know and understand in order to successfully maneuver in heavy weather. Paramount for the shiphandler is the ability to understand the combined effects of environmental conditions

and how they impact the unique shiphandling characteristics of the ship. A dynamic capsize can seem to be the result of unrelated events, but in reality, it is comprised of a cascading series of events and conditions that must be understood in order to properly interrupt the sequence and avoid catastrophic consequences.

There are basic tenets of good shiphandling that hold true in any situation, such as maintaining power, buoyancy, and stability; avoiding beam seas; and adjusting course and/or speed to minimize pitch and slam. However, once in heavy weather, understanding the combined effects of wind and waves on the specific hull form is critical (Alman, P. R., Minnick, P. V., Sheinberg, R., Thomas, W. L. III; 1999). Simple classroom training can provide a basic understanding of these effects, but the best form of instruction is simulation, through which the trainee can practice decision-making skills and experience the results of both correct and incorrect actions. These aerodynamic and hydrodynamic effects were heretofore difficult to simulate, but modern advances in physics-based ship motion software coding are now providing critical enhanced capability. This opens up the potential for rigorous hands-on training in a simulated environment, allowing routine training in the most dangerous of sea conditions, without jeopardizing personnel or ships.

Heavy weather training curricula should also include instruction on the use of basic calculations for estimating wave encounter period. This can be a useful tool during heavy sea states when technology is unreliable and/or unavailable. When simulation opportunities are added to this type of training, they allow the operator to effectively test his/her understanding of the principles, and to practice mitigation strategies appropriate for the ship type. This type of training helps solidify appropriate reactions when faced with time-sensitive decisions in actual heavy weather situations. There are basic mitigation strategies, or “rules of thumb,” to assist the operator in

maintaining a stable ship environment, such as the International Maritime Organization’s “Revised Guidance to the Master for Avoiding Dangerous Conditions in Heavy Seas.”<sup>1</sup> Guidance of this nature is useful, but should directly relate to the specific characteristics of the ship in question. For instance, some of the newer container ships appear to be susceptible to head sea parametric rolling, something not historically noted as a shiphandling concern. The magnitude of risk of a stability failure or capsize event can vary significantly between ship designs, as can the mode of failure. Consequently, the criticality of being able to recognize potentially severe conditions and make the correct judgment call with respect to the shiphandling decisions needed to mitigate risks assumes a degree of importance that cannot be underestimated.

The shiphandler should be trained to recognize ‘cues’ or precursors leading to an imminent dynamic stability event such as wave capture, bow plunging, or broaching to name a few, and understand the correct action necessary to get the ship out of danger in these situations. Ship motions are multi-dimensional, and shiphandlers need to thoroughly understand the implications of their ship’s response to heavy weather (i.e., its motions), the dangers certain combinations present, and how to correct for them. For many ships, the arrangement of hull and superstructure create significant windage and there may be large differences across various load conditions. The lateral distribution of windage can create lee/weather helm characteristics similar to that of a vessel under sail. A ship trying to ride out a storm in head seas may need sufficient headway to maintain controllability, but at the same time, may suffer significant or dangerous structural damage as a result of wave impact, making it necessary to come about into stern seas. A ship with insufficient power may get

---

<sup>1</sup> *Revised Guidance to the Master for Avoiding Dangerous Situations in Adverse Weather and Sea Conditions*. Ref. T1/2.04 (11 January 2007). MSC.1/Circ. 1228.

caught “in irons” if trying to steer thorough head seas and come around to a new course. Multiple factors are in play at any given time, and maneuvering decisions need to be balanced against handling capabilities accordingly. The shiphandler must weigh the amount and rate of turn to minimize slamming or pounding when turning into the wind, and rolling when turning away from the wind. Each ship motion imparts key information to the shiphandler. For instance, a long-hanging roll implies a loss of stability in following seas, but might be interpreted by an inexperienced shiphandler as an improvement on how the ship is riding. Avoiding a roll event may be as simple as altering course to ensure the period of encounter is as different as possible from the ship’s natural roll period, while in the same situation, changing speed alone will not correct for roll occurrence.<sup>2</sup> Here again, the opportunity to test these skills in a simulator allows the shiphandler to hone his “seaman’s eye” and get an accurate assessment of what can and cannot be done safely, so that when faced with an actual emergency, appropriate decisions can be made.

Over the past several years, the authors have worked with the Operator Guidance and Training Working Group (OGTWG), part of Cooperative Research Navies (CRNAV), to help define heavy weather shiphandler training objectives for the Naval Watch Officer. In addition to basic shiphandler objectives already routinely contained in shiphandlering curricula, the following recommended additions have been identified: better meteorological training; training on available decision aids; enhanced static, dynamic, and damaged stability training (including how to avoid/escape from hazardous situations, recognizing and understanding non-survivable conditions, and consequences of damage or system failures in heavy weather); and

discussions/assignments on heavy weather stability. Several workshops have been held over the years using full mission bridge simulators with heavy weather simulation capability. During these workshops, a number of simulator scenarios were tested to help develop these recommendations. Additional benefit can also be gained by using a full-mission shiphandlering simulator with enhanced heavy weather rendering and ship capsize modeling, and (if possible) by incorporating a classroom physics-based model simulator with an interface that can support changing factors such as course, speed, KG, wave height, etc.

One key advantage of adding simulator training is that it allows a scenario to be replayed (multiple times if desired) and the operator to practice different mitigation techniques as environmental conditions change. If a “bad” decision is made, the consequences should be clearly apparent, and the operator can try again and experience the results from a different set of shiphandlering maneuvers. Repetition can progressively enhance the degree of training transfer, while the risk of transfer failure is reduced (Foxon, M.; 1993). The trainee can also dissect the actions taken to better understand when naval architectural limits are reached and resulting damage can be anticipated. This type of training experience can provide lasting impressions on trainees, and can also facilitate development of a shiphandlering “fault tree” specific to each ship type.

### *Training Proficiency*

One of the main issues with any type of proficiency is the rate at which it decays when it is not used. Higher order cognitive skills and team behaviors (such as shiphandlering in heavy weather) are extremely perishable (Cannon-Bowers, J. A., Burns, J. J., Salas, E., and Pruitt, J. S.; 1998). The infrequency with which most shiphandlering have to face severe weather puts them at risk of having a much lower proficiency level than would be desired when confronted by those conditions. Today,

---

<sup>2</sup> *Revised Guidance to the Master for Avoiding Dangerous Situations in Adverse Weather and Sea Conditions*. Ref. T1/2.04 (11 January 2007). MSC.1/Circ. 1228.

maritime organizations (including navies) are increasingly turning to simulation tools as a means of providing required training to watch officer and bridge personnel in order to meet qualification requirements.

The effectiveness of training transfer is directly linked to how well training devices duplicate the actual environment (e.g., simulation fidelity).<sup>3</sup> Simulators have long been used in the aviation world as a principal (and economical) form of training. Airlines have been able to amortize the cost of a simulator in less than two years. For instance, Boeing 767 aircraft full flight simulator training costs approximately \$400 per hour, while actual aircraft training time costs between \$7000 and \$8000 per hour (Thompson, T. N.; Carroll, M. B.; and Deaton, J. E.; 2009). Simulator use has also increased significantly over the past 20+ years for shiphandling, though primarily for such tasks as open water and harbor maneuvering, man overboard practice, and for naval vessels, steaming in formation, and special evolutions. Shiphandling simulation also has to incorporate the element of motion in a seaway, which is difficult to accurately model in higher sea state conditions. Recent improvements in software coding capabilities are redefining the limits of shiphandling training possibilities. Shiphandling simulators are beginning to have the technical capacity to extend their training capabilities from providing traditional calm water/low sea state and restricted waters maneuvering to presenting highly realistic heavy weather scenarios, resulting in improved knowledge and effectiveness under the most severe circumstances. This is especially critical as, in many contemporary instances, actual time afloat may represent proportionately less of a mariner's total career. Consequently, the integration of a heavy weather shiphandling training capability into an overall maritime training program should be

approached carefully, with a structured set of goals.

### *Simulator Fidelity*

Simulation quality and human capabilities are critical factors in training effectiveness and efficiency. Simulator fidelity is potentially the most important aspect of simulator quality, and is also a critical factor in the cost effectiveness of simulation device design. It is normally understood to mean the degree to which the simulation replicates the actual environment, and there is a strong link between it and transfer of training (Liu, D., Macchiarella, N. D., and Vincenzi, D. A.; 2009). There are two principal aspects of simulator fidelity – physical fidelity (the replication of sights, sounds, and the “feel” of the actual environment), and psychological or cognitive fidelity (the replication of such things as communication, situational awareness, etc.), and these aspects have subsets which are not mutually exclusive, but rather, have a large degree of overlap. These include: visual and auditory fidelity (how well the simulation replicates known visual and auditory stimuli of the actual environment); equipment fidelity (how well the simulator replicates the actual equipment/systems the operator is expected to use); motion fidelity (how well motion cues experienced in the actual environment are replicated); task fidelity (the tasks and maneuvers executed by the user); and functional fidelity (how the device functions and provides realistic stimuli in the simulated environment). All of these must be considered in the overall simulation solution equation.

Shiphandling simulators have become quite good at representing most of these aspects of simulation. Technology has significantly enhanced visual fidelity in recent years. For instance, harbors now used in simulators are extremely realistic, with recognizable structures, piers, buoys, lights, navigational aids, etc. Environmental factors such as fog, low light levels, rain, lightning, thunder, and other characteristics can be added into the

---

<sup>3</sup> Allen, (1986); Alessi, (1988); Hays and Singer, (1989); Gross, et al, (1999).

simulation, as can other vessels, numerous types of aircraft, small boats, and even birds and people in the water. Ship sounds, such as whistles and alarms, and communications equipment have been accurately replicated. Equipment fidelity, the extent to which a simulator can emulate or replicate the equipment being used, which includes all the software and hardware components of the system (Zhang, B.; 1993), can prove to be more of an issue for some ship classes that have unique bridge or engineering equipments, but most bridge equipments are of sufficient similarity to provide adequate training transfer for routine evolutions. However, portraying realistic sea conditions in higher sea states has proven to be a challenge.

#### *Heavy Weather Simulator Models*

To provide accurate seaway representations, a heavy weather shiphandling simulator must be driven by a physics-based hydrodynamics model (such as FREDYN) which is capable of providing non-linear, six degree of freedom motion in the large amplitude motions resulting from exposure in a severe seaway. A principal requirement for the hydrodynamics model is that it should be executable in time domain at a time scale that is at least as fast as real time and validated for use in training. Development of numeric codes providing this capability is an evolving science. The non-linearities associated with seakeeping computations are associated with viscosity, pressure, free surface, and body geometry. Currently, fully non-linear codes are not suitable for integration into the simulator environment because excessively long execution times are in excess of real time. Some codes have adopted short cuts by blending linear and non-linear theories. These blended codes are significantly faster and are capable of engineering accuracy (Beck, R. F., and Reed, A. M.; 2001). The code used also must be capable of fidelity that can replicate behavior characteristics for specific ship classes in the heavy weather environment. These general characteristics are a functional

requirement of the previously identified training objectives.

Numerous commercial shiphandling simulation tools are available. Determination of the appropriateness of any simulator should include the verification, validation, and accreditation (VV&A) of the model used to run the simulation. The VV&A of the model is a necessity, and should include conceptual validation, design verification, code verification, results validation, and accreditation, which must be specific for the application. Specific intended uses of the tool should be clearly defined as part of this process. This will help ensure that desired training transfer can actually be achieved by the simulator.

#### **OPERATOR GUIDANCE**

There are several commercially available systems designed to provide operator guidance on ship motions and limitations, give warnings of impending difficulties, and serve as decision aids in situations such as extreme roll motions/parametric rolling, bow impact, green seas on deck, and broaching. These are real-time systems that display the ship's position in relation to pre-calculated sea-keeping operational risk limits. Some can also be interfaced with weather routing systems to predict ship motions based on forecasted weather under different motion parameters, and define the operational limits for route planning, as well as recommend tracks that avoid areas with forecasted excessive motion.

The emergence of these new operator guidance systems also supports the inclusion of heavy weather shiphandling into training curricula. These capabilities offer shiphandlers a tool that can automatically calculate safe operating environments and provide course and speed options to minimize hazards based on real-time wind and sea data. This can improve operational safety and provide an enhanced capability to continue a ship's mission in certain situations. More importantly, these

operator guidance tools can incorporate actual hull form data for unique ship types and help prevent catastrophic consequences for an operator who does not have a significant experiential base in that platform. When coupled with physics-based ship motion simulator training opportunities, this decision aid can significantly enhance the overall training experience, allowing the operator to test the limits of the ship and “experience” the consequences of erroneous shiphandling decisions, even taking the ship to the point of capsizing to better understand the dynamics of each shiphandling decision.

## CONCLUSION

Current technology advances are beginning to offer the ability to integrate multiple simulators, which create even greater “virtual reality” potential for heavy weather training. Simulation of various casualties can provide shiphandlers with training opportunities to better prepare them for decision-making under duress. Decision aids in the form of operator guidance capabilities are becoming more refined, and combining these capabilities with heavy weather shiphandling training could significantly reduce the incidence of mishaps in heavy weather.

As we look to the future, the potential for heavy weather simulator training is extremely encouraging, and this valuable resource should be a standard part of all shiphandling training. Simulators are on the cusp of providing highly realistic heavy weather scenarios, resulting in vastly improved knowledge and effectiveness under the most severe circumstances.

## List of References

- Alessi, S. M. (1988). “Fidelity in the Design of Instructional Simulations.” *Journal of Computer-Based Instruction*, 15(2), 40-47.
- Allen, J. A. (1986). “Maintenance Training Simulator Fidelity and Individual Difference in Transfer of Training.” *Human Factors*, 28(5), 497-509.
- Alman, P. R., Minnick, P. V., Sheinberg, R., Thomas, W. L. III (1999). “Dynamic Capsize Vulnerability: Reducing the Hidden Operational Risk”, *SNAME Transactions*, Society of Naval Architects and Marine Engineers, Vol. 107, New York.
- Beck, R. F., and Reed, A. M. (2001). “Modern Computational Methods for Ships in a Seaway,” *SNAME Transactions*, Society of Naval Architects and Marine Engineers, Vol. 109: 1-51, Jersey City, NJ.
- Cannon-Bowers, J. A., Burns, J. J., Salas, E., and Pruitt, J. S. (1998). “Advanced Technology in Scenario-Based Training”. In Cannon-Bowers, J. A., and Salas, E. (Eds.) *Making Decisions Under Stress* (pp. 365-374), Washington, D.C.: American Psychological Association.
- Foxon, M. (1993). “A Process Approach to the Transfer of Training.” *Australian Journal of Educational Technology*, 9(2), 130-143.
- Gross, D. C.; Pace, D., Harmoon, S.; and Tucker, W. (1999). “Why Fidelity?” In the Proceedings of the Spring 1999 Simulation Interoperability Workshop.
- Hays, R.T.; and Singer, M.J. (1989). *Simulation Fidelity in Training System Design*. New York: Springer-Verlag.
- Liu, D., Macchiarella, N. D., and Vincenzi, D. A. (2009). “Simulation Fidelity” in D. A. Vincenzi, J. A. Wise, M. Mouloua, and P. A. Hancock (Eds.) *Human Factors in Simulation and Training*. Boca Raton, FL: CRC Press.
- Revised Guidance to the Master for Avoiding Dangerous Situations in Adverse Weather and Sea Conditions. Ref. T1/2.04 (11 January 2007). MSC.1/Circ. 1228.
- Thompson, T. N., Carroll, M. B., and Deaton, J. E. (2009). “Justification for Use of Simulation” in D. A. Vincenzi, J. A. Wise, M. Mouloua, and P. A. Hancock (Eds.) *Human Factors in Simulation and Training*. Boca Raton, FL: CRC Press.
- Zhang, B. (1993). “How to Consider Simulation Fidelity and Validity for an Engineering Simulator.” *American Institute of Aeronautics and Astronautics*, 298-305.



## Decision Support for Crisis Management and Emergency Response

*Andrzej Jasionowski, The Ship Stability Research Centre, Naval Architecture and Marine Engineering, University of Strathclyde*

### ABSTRACT

Decision support systems for onboard use are many and varied. Primary role of such systems is to alleviate burden of processing of ship and environment data and ultimately to help crew in making informed decisions. Effectiveness of such processing could not be more important than during crises situations. This article presents with a prototype of an ergonomic decision support function for provision of advisory to the crew for enhancing their instantaneous preparedness for response to a distressed flooding situation. It is argued that automated inculcation of crew preparedness is the most effective tool for avoiding and managing crises, should they occur.

### KEYWORDS

Crisis management, emergency response, decision support, stability, survivability, flooding.

### INTRODUCTION

Technological advances in computing hardware over the last decades have facilitated solution of many problems in ever decreasing amount of time. However, the progress in technical calculus, involving modelling based on the fundamental physical laws, has been just as significant, and despite the availability of very powerful computers, many cases of numerical approximations to reality remain impractical to compute.

It is for this reason that advanced prognosis have only had limited success in proliferating the field of instantaneous decision support.

Although highly advanced computerised safety management systems (SMS), have found accelerated support, their advisory functionality are mostly limited to detection only, with more sophisticated prognosis capabilities remaining at prototyping and development stages.

Such prototype simulation approaches available for use in prognosis comprise a range of phenomena such as (a) flooding progression, modelled through various but direct solution to conservation of momentum laws, Papanikolaou

et al, 2000, Schreuder 2008, de Kat 2002, Jasionowski 2001, Petey 1988, or through quasi-static iterative approximations, e.g. Varela et al, 2007; (b) structural stress evolution under flooding, Bole, 2007, (c) mustering process, Vassalos et al, 2001, Piñeiro et al, 2005, (d) fire and smoke spread, Guarin et al 2004, and other.

Some of the reasons inhibiting their more wide use for decision support arise due to a series of practical problems in addition to sheer computational effort, such as the following:

- Each of these processes may vary at any instant of time due to changing conditions.
- The input is subject to considerable uncertainty.
- For any set of input information the outcome is random due to computational and modelling uncertainties as well as due to random nature of environmental or process conditions themselves.
- Each may be seriously influenced by decision choices.

These would imply that the projection functionality would be iterated for a range of uncertain conditions of either of the scenarios occurring as well as for a range of decision

options, so that the best choice can be identified with controllable degree of confidence.

This, in turn, implies that the computational task of scenario projection in real time in support of decision making will likely remain a serious challenge, as most of these analyses require substantial amount of processing time, usually measured in hours.

This is in contrast to real life cases of casualty scenarios, which in many occasions evolve in a matter of minutes, during which decisions could prove critical. The following recent casualties can be viewed to elaborate the issue.

**MV Estonia, 1994, 852 fatalities**

852 human lives were lost when the passenger Ro-Ro ferry MV Estonia sank on the night of 27/28<sup>th</sup> of September 1994 in the Baltic Sea, while on route between Tallinn, Estonia, and Stockholm, Sweden, Bergholtz at all 2008, Jasionowski et al 2008. The notable observation is that most of the 137 survivors are those that reacted fast, within the first approximate 10-20 minutes into the casualty.

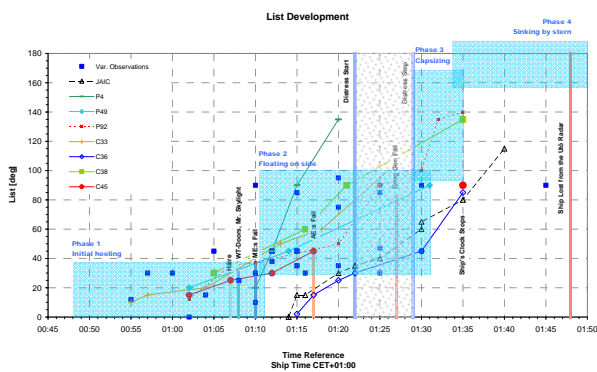


Figure 1 MV Estonia, statements by survivors on the heel angle experienced during abandonment, Bergholtz at all 2008.

Perhaps if crew were aware of what “to expect” they could have reacted quicker to casualty or averted it in the first place.

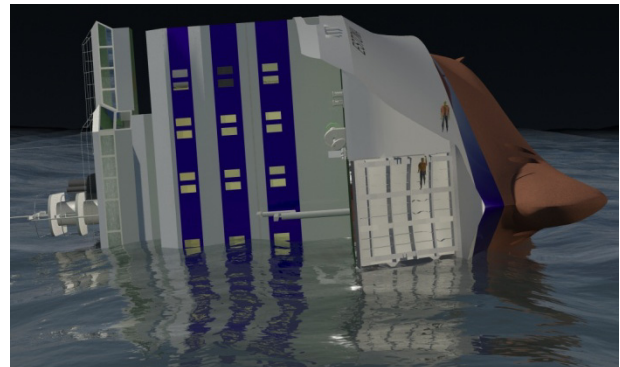


Figure 2 MV Estonia, Jasionowski et al 2008. At some instant two survivors managed to climb down the closed ramp, using its stiffening arrangement and abandon the ship. Heel angle 93deg.

**Monarch of The Seas, 1998, no fatalities**

According to the accident report by Paulsrud et al 2003, “At about 0130 hours, ..., the Monarch of the Seas raked the Proselyte Reef at an approximate speed of 12 knots without becoming permanently stranded”. Subsequently, “At 01:35 hours and owing to the water ingress, all watertight doors were closed from the bridge ...” and “At 01:47 hours the general emergency signal, seven short and one long blast, was given ...”. See Figure 3.

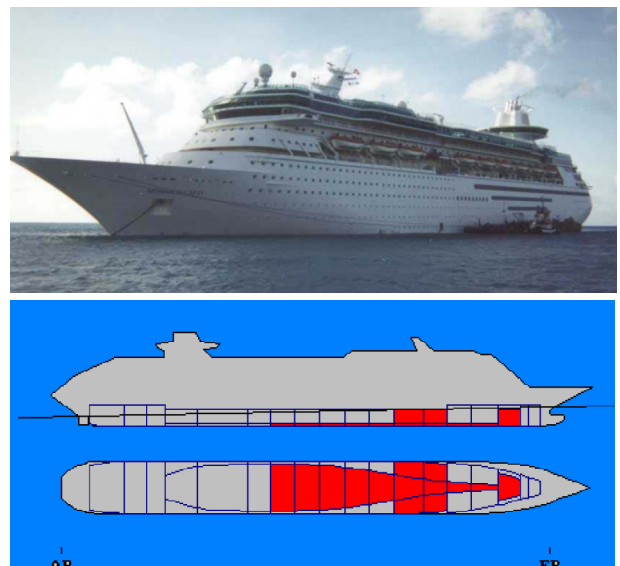


Figure 3 Monarch of the Seas, actual casualty in 1998 and flooding extent, Paulsrud et al 2003.

It appears that it took the crew 5 minutes to decide about closure of water tight doors (WTD), and 17 minutes to inform the persons

onboard of the casualty. Whilst this accident resulted in no fatalities, it should be clear that this time might as well not have been available, was the damage more severe. Decisions before as well as during every minute of the accident could have proven far more critical to this accident. A decision support system might have informed the crew if the situation is critical or not, and in this particular scenario it would have need to have been shown as moderate or perhaps not critical, after the watertight doors closure.

Of note is the fact that even though importance of WTD closure is identified in the report as critical, none of the ultimately recommended 20 safety actions, nor the pointed 20 lessons to be learned, mentioned issue of ship watertight integrity explicitly, highlighting only importance of SMS (Safety Management System) procedures.

### **Rockness, 2004, 18 fatalities**

On the 19 of January 2004 the Antigua & Barbuda flagged cargo vessel MV 'Rocknes' capsized within a number of minutes in a strait south of Bergen, Norway, resulting in 18 fatalities, see Figure 4. At the time, the ship was loaded with stones and pebbles that were to be delivered in Emden, Germany.



Figure 4 MV Rocknes, actual casualty in 2004, Jasionowski et al 2005.

The crew had perhaps 2-3 minutes into the casualty, for making their minds up on what, or if, any action was to be taken, as the rate of ship capsize was very high, see Figure 5.

Perhaps all these lives could have been saved if the crew was informed at all times of the vulnerability of the vessel to any flooding extent that was feasible, allowing them to react instantly at the first sign of distress.

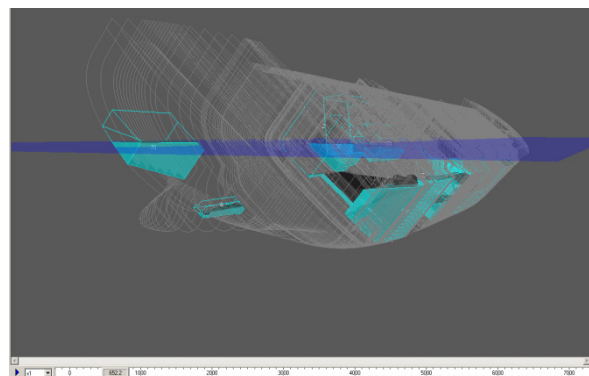


Figure 5 MV Rocknes, numerical reconstruction when heeling to 42 degrees during capsizing process. The vessel capsizes in 2 minutes. Visible in a light blue colour are the intact ship free surface tank loads as well as compartments flooded due to damage, Jasionowski et al 2005.

It can be seen that decisions for crises management in either of these different ship scenarios would need to be made virtually within first vital minutes from the very instant of loss of watertight integrity.

Indeed, it could be argued, that even more effective would have been for the crew to know beforehand the crises occurring, as to how to react to the situation.

This is the principle, in the search of which the VLog functionality has been developed as a possible ergonomic solution for sustaining the crew's preparedness for response to a crises situation, as described next.

### **VULNERABILITY LOG (VLog)**

Vulnerability Log, or VLog for short, is hereby proposed to be the functionality to inform the crew at all times on the instantaneous vulnerability state of the vessel, considering its actual loading conditions, the environmental conditions and the actual watertight integrity conditions. The vulnerability is proposed to be measured by means of the probability that a

vessel might capsize within given time when subject to any feasible flooding scenario.

Since before casualty occurs it is impossible to guess what kind of damage a ship might suffer, it seems plausible that the crew is made aware of what actually “can” happen, and if it did, what impact on the ship it can have? They would immediately be able to infer how critical a situation evolving is and hence what possible actions to follow.

Such impact will of course vary from a flooding case to a flooding case, and subject to what condition the vessel operates at, at which environment and what is the watertight integrity status. All these must, therefore, be considered.

The following framework outline, see equations ( 1 ) and ( 2 ), is all that is required to provide with this functionality, whereby VLog refers to  $F_T$  logged continuously in real ship-operation time.

$$F_T(t|Hs) = \sum_j p_j \cdot F_{T|*}(t|Hs, j) \quad (1)$$

Where:

$$F_{T|*}(t|Hs, j) = 1 - \left( 1 - \Phi \left( \frac{Hs - H_{crit,j}}{\sigma} \right) \right)^{30} \quad (2)$$

$$Hs_{crit,j} = 4 \cdot \frac{GZ_{max,j}}{0.12} \cdot \frac{Range_j}{16} \quad (3)$$

$$\sigma_r(Hs_{crit,j}) = 0.039 \cdot Hs_{crit,j} + 0.049 \quad (4)$$

More details of the model itself can be found in Jasionowski 2006a and 2007, and Tagg 2002. It is hereby referred to as a framework, as even though extremely straightforward, its essential details as well as its uncertainty measures are all under research and development. However, it is sufficient to demonstrate and then explain how the VLog functionality would work in

practice, including giving practical interpretations of  $F_T$  as well as  $F_{T|*}$ .

### CASE STUDY

A case of MV Estonia is hereby used to demonstrate the VLog functionality. Loading condition at the time of the loss of the vessel in 1994 were used, see Table 1 and Figure 6.

Table 1 MV Estonia, ship particulars.

L <sub>bp</sub>	137.4m
B	24.2m
Displacement	11,930 [m <sup>3</sup> ]
Draught mean	5.39m
Trim	0.435m aft
GM	1.17m
KG	10.62m

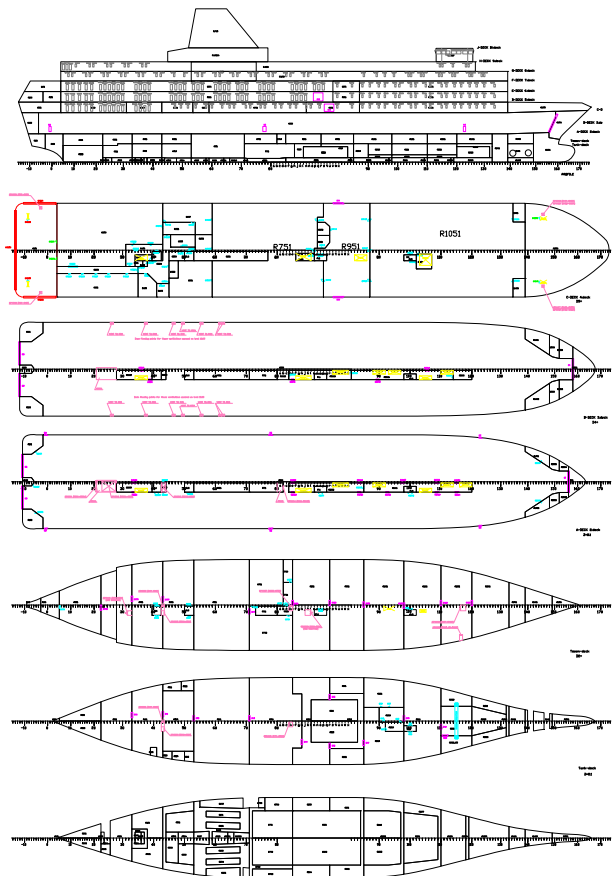


Figure 6 The GA of MV Estonia assumed for numerical modelling.

The following figures are presented to allow for interpretation of the VLog functionality.

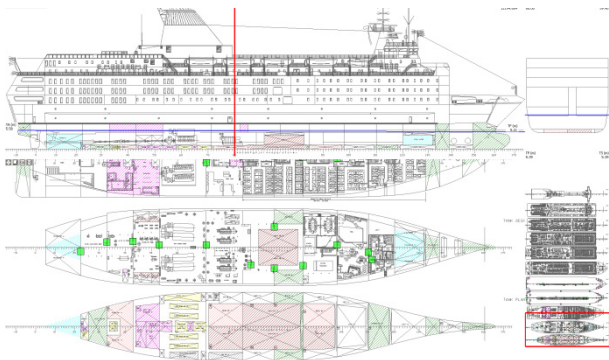


Figure 7 Ergonomic communication interface, model of MV Estonia, screenshot of watertight doors (WTD) closure status, green indicates “closed”, red “opened”.

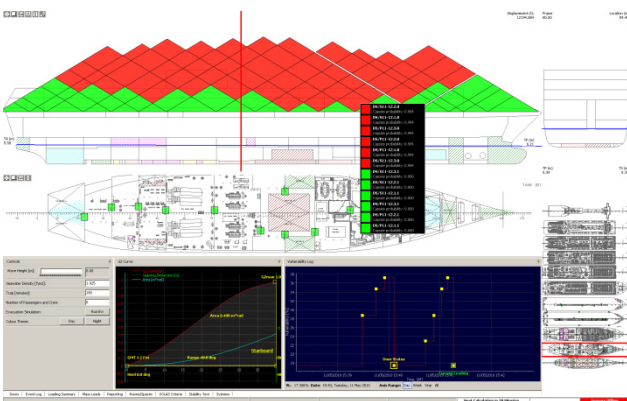


Figure 8 Vulnerability information, screenshot of the colour-coded values of  $F_{Tj^*}(3hrs|Hs=0m, j)$  for each of the  $j=1...1368$  flooding cases, each represented by a “diamond”, as well as  $F_T(3hr|0m)=17.38\%$  of ship overall vulnerability, all logged down at 15:40:06 hours (example time marked by the yellow square at 15hrs 40min 06seconds). For overlapping “diamonds” (e.g. multiple penetration or vertical extent for the same length of flooding case), the worst cases are shown.

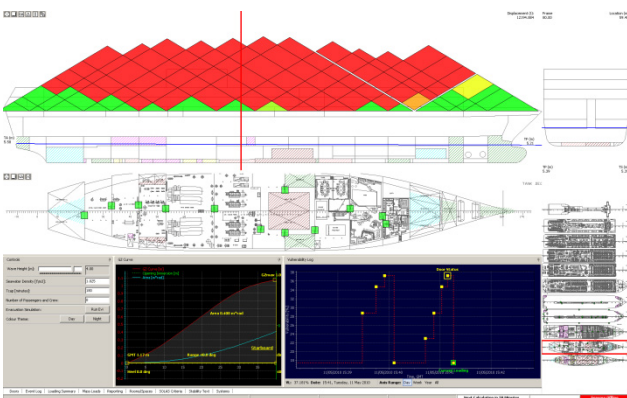


Figure 9 Screenshot of the colour-coded values of  $F_{Tj^*}(3hrs|Hs=4m, j)$  for each of the flooding cases, ship vulnerability  $F_T(3hr|4m)=37.18\%$  (purple window), logged down at 15:41:09 hours (example time marked by the yellow square at 15hrs 41minutes 09seconds). The green coloured “diamonds” indicate  $F_{Tj^*}=0\%$ , and red  $F_{Tj^*}=100\%$ . GZ

curve and draught marks shown for the ship in intact condition. Sea state  $H_s$  manual input shown in the left lower corner.

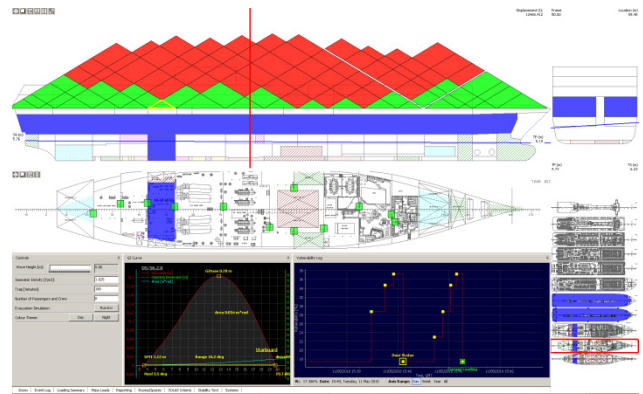


Figure 10 Flooding extent for damage case  $j=702$ , DS/S6.2.0, (diamond/triangle in yellow frame), with corresponding GZ curve logged at 15:40:06, see Figure 8. Ship vulnerability  $F_T(3hr|0m)=17.38\%$ . Note that draught marks correspond to ship condition of the most recent log at 15:41:16.

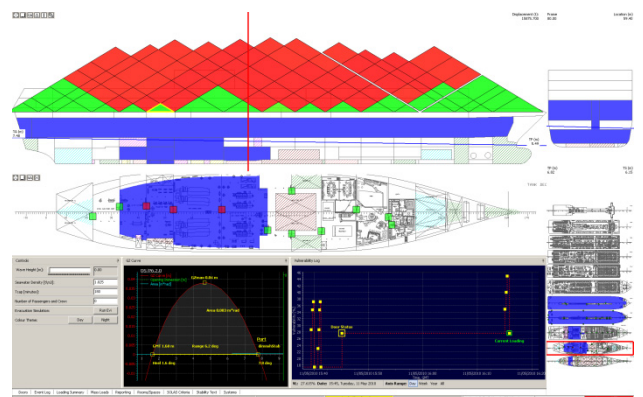


Figure 11 Flooding extent for damage case  $j=702$ , DS/S6.2.0, (diamond/triangle in yellow frame), with corresponding GZ curve logged at 15:45:09, ship vulnerability  $F_T(3hr|0m)=27.61\%$ . Note the three watertight doors, #216, #217 and #218, on the tank deck opened with the ensuing impact on the flooding extent. Note again  $H_s=0m$ .

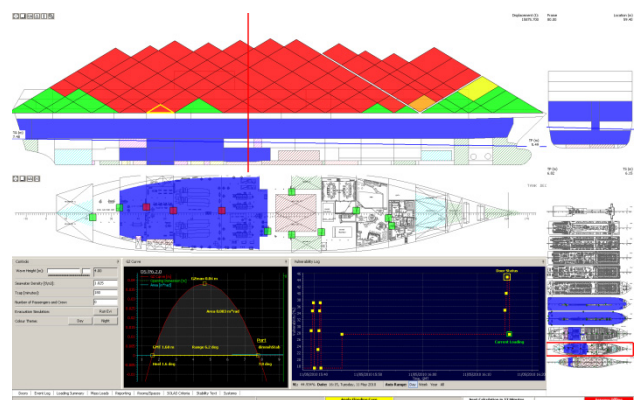


Figure 12 Flooding extent for damage case  $j=702$ , DS/S6.2.0, (diamond/triangle in yellow frame), with corresponding GZ curve logged at 16:15:28, ship vulnerability  $F_T(3hr|4m)=44.93\%$ . Note  $H_s=4m$ .

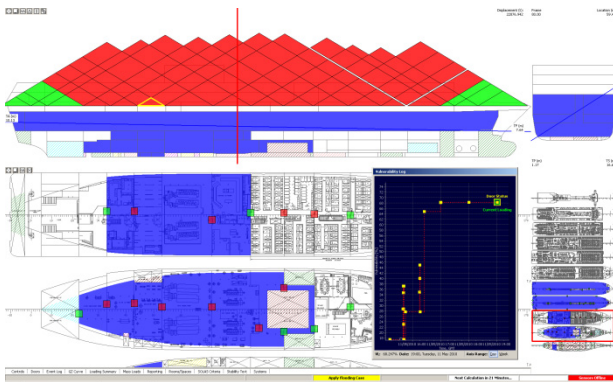


Figure 13 Flooding extent for damage case  $j=702$ , DS/S6.2.0, (diamond/triangle in yellow frame), with corresponding GZ curve logged at **19:00:30**, ship vulnerability  $F_T(3hr|4m) = 68.24\%$ . Note  $H_s=4m$  and many WTD opened. Very likely state of the vessel on the night of the ship loss in September 1994.

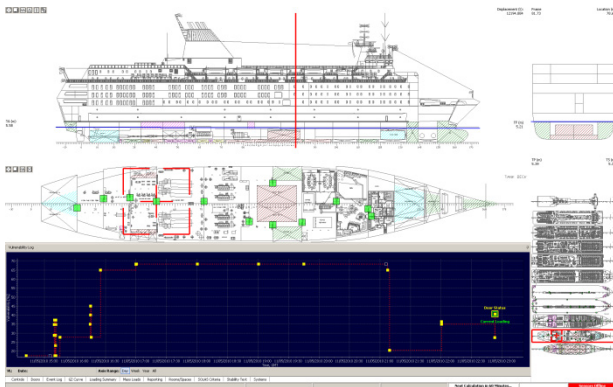


Figure 14 Sample of 8 hours vulnerability log (VLog).

The above figures should suffice to demonstrate the principle of the proposed VLog functionality for decision support, as discussed next.

## DISCUSSIONS

The first element worth mentioning is the interpretation of “vulnerability”. As mentioned earlier, ship vulnerability to flooding is proposed to be measured by means of the probability that an event of ship capsizing within given period of time occurs, subject to status assumptions.

For a flooding scenario resulting to final floating attitude, it is expected that ship’s residual stability will be sufficient to sustain its functional attitude for a level of environmental excitation. The relationship between residual

stability and the environment has been derived in project HARDER, as reported in Tagg 2002, and as given here by equation ( 3 ). It has subsequently been shown in the project SAFEDOR, Jasionowski at al 2006a, 2006b, 2007, that this relationship can be used to describe stochastic nature of ship capsizes for any given environment, and that it can be marginalised for all feasible flooding scenarios.

Thus, for an example of a specific flooding case  $j$ , a vulnerability of  $F_{Tj}(3hrs|H_s = 2m, j) = 40\%$  recorded in a given instant of time, implies probability of 40% that a ship may capsize in 3 hours, when subject to specific environmental conditions of  $H_s=2m$ . In other words, should the vessel suffer 10 accidents involving **exactly** flooding extent  $j$ , and each time at sea state of  $H_s=2m$ , it would be expected to observe 4 capsizes within less than 3 hours. This vulnerability can be derived for any feasible flooding extent for given ship design, and it can be conveyed to the crew in an ergonomic manner by means of colour coding, see the colourful “diamonds” in either of Figure 8 to Figure 13.

Furthermore, the vulnerability can be “averaged” for all flooding cases with “weights” corresponding to likelihood of any flooding extent occurring, in the marginalisation process. Thus, an example of an overall vulnerability of  $F_T(3hr|4m) = 70\%$ , indicates probability of 70% that a ship may capsize in 3 hours, when subject to specific environmental conditions of  $H_s=4m$  and for any among the many feasible flooding extents a ship might suffer. In other words, should the vessel suffer 10 accidents involving **any** flooding extent, and each time at sea state of  $H_s=4m$ , it would be expected to observe 7 capsizes within less than 3 hours. This “overall” vulnerability can be derived periodically for given ship conditions and conveyed to the crew in an ergonomic manner as a time-log, see Figure 14.

It can be noted in Figure 14 the “enormity” of the extent to which operation can have on the ship’s instantaneous vulnerability, that is its

ability to sustain stable attitude when subject to loss of watertight integrity. The vulnerability can increase from some 18% to nearly 70%, for the sample study cases used. The various conditions leading to this dramatic variation can again be found from Figure 8 to Figure 13.

The variation in time reflects changes to ship loading conditions, environment conditions  $H_s$ , as well as watertight integrity through opening of watertight doors.

The very process of logging in time of quantified and meaningful measure of vulnerability allows for auditing of the “goodness” of the operation. Such information, easily inferable from typical on-board computer display, allows for development and sustaining of understanding on what to expect, should flooding casualty occur.

For instance, given the vulnerability of MV Estonia on the night of the loss as shown in Figure 13, it can easily be seen that the vessel is extremely likely to capsize due to flooding.

The fact that specific type of flooding which is thought to have happened on the night of the casualty is not taken into account in cases used in Figure 13 is immaterial. The crew would not know what was happening exactly, but given projections as shown in Figure 13 with vulnerability of 70%, it would be instantly obvious that immediate action is required at the first sign of problems. More importantly, the crew might have taken greater vigil, were they aware of how vulnerable their ship can be, and how this can be managed through their own actions.

#### **ON-GOING WORK**

The framework for vulnerability assessment given above by models ( 1 ) and ( 2 ) is very simple. However, it appears to serve as a very informative model for use in the context of decision making. It reflects fundamentals of physical processes governing ship stability in waves and explicitly acknowledges uncertainty of such predictions by exploiting probability theory. Therefore, research efforts are ongoing to establish and verify practicalities of the

principles of the proposed functionality, as well as to assess impact of all engineering approximations that are to be used in application of the proposed model. Many such aspects are under study, with key focus on uncertainty in the widest sense, pertaining to its both aleatory as well as epistemic types. Example impact of treatment of actual tank loads in assessing stability, effects of damage character, relative importance of transient flooding stages, accuracy of physical experimentation used as basis data, or simple elements such as effect of computational speed on functionality of the whole proposition, or ergonomics of the conveying techniques used. The prime objective is to find solution acceptable for wider industrial application.

#### **CONCLUSIONS**

This article outlined a concept of an active through-life decision support and crises management principle. The key feature is provision of ergonomic information to the crew on the instantaneous ship vulnerability to flooding.

Such information allows the crew to have notion at all times on ships capacity to cope with any feasible flooding scenario, and thus allows for making informed and instant decisions on how to respond with mitigating actions at the first sign of distress.

Most importantly, the crew can take precautionary actions at any time of the ship operation to knowingly reduce vulnerability to the lowest levels possible for a particular ship design.

Therefore, crew preparedness for response to distressed situation can be promoted at all times.

#### **ACKNOWLEDGMENTS**

This research has been supported directly by EC FLAGSHIP (TIP5-CT-2006-031406) and EC FLOODSTAND (SCP7-GA-2009-218532). The financial support of the EC, as well as cooperative efforts among the consortium

members are hereby gratefully acknowledged. Many colleagues that have contributed with advice, expertise, research, development or analysis efforts in these ongoing projects are, in no particular order, Anthony York, Luis Guarin, Jonathan Logan, Jerzy Prigara and Piotr Dolebski from Safety At Sea Ltd, and Dracos Vassalos, Phil York, Jakub Cichowicz, Sara Locke, Qi Chen, Yasmine Hifi, Sandy Day and Andrew Pennycott from The Ship Stability Research Centre, Department of Naval Architecture and Marine Engineering, University of Strathclyde, whose varied valuable contributions and work are all hereby acknowledged.

## REFERENCES

- Bergholtz, J, Rutgersson, O, Schreuder, M: "WP2.1 Review of evidence Report No. 2 Conceivable course of events", Department of Shipping and Marine Technology, Chalmers, Technical Report, March 2008.
- Bole Marcus, "Introducing damage structural assessment to onboard decision support tools", Graphics Research Corporation Ltd, UK, ca 2007.
- Guarin Luis, Jayanta Majumder, Vladimir Shigunov, Guro Vassalos and Dracos Vassalos, "Fire and flooding risk assessment in ship design for ease of evacuation", Design for safety Conference, Osaka, 2004.
- Jasionowski, A, "An integrated approach to damage ship survivability assessment", PhD thesis, University of Strathclyde, 2001.
- Jasionowski Andrzej, Khattab Omar, "Time Domain Simulation of the Dynamics of Progressive Flooding and Capsizing MV Rockness", TQRN01-RE-001-AJ, 12 September 2005.
- Jasionowski A, Bulian G, Vassalos D, Francescutto A, Pawlowski, M, Maccari A, "Modelling survivability", EC SAFEDOR, D2.1.3., November 2006a.
- Jasionowski Andrzej, Dracos Vassalos, "Conceptualising Risk", 9th International Conference on Stability of Ships and Ocean Vehicles, Rio de Janeiro, September 2006b.
- Jasionowski Andrzej, Dracos Vassalos, Andrew Scott, "Ship Vulnerability To Flooding", 3rd International Maritime Conference on Design for Safety, Berkeley California, Sept 26 28th, 2007.
- Jasionowski, A, Vassalos, D: "[Technical Summary of the Investigation on The Sinking Sequence of MV Estonia](#)", Safety at Sea Report No VIES01-RE-005-AJ, May 2008, [Technical Summary of the Investigation on The Sinking Sequence of MV Estonia](#).
- de Kat Jan O, Peters Andrew J, "Model experiments and simulations of a damaged frigate", IMAM 2002 congress, Crete, May 2002, No. 129.
- Papanikolaou A, Zaraphonitis G, Spanos D, Boulougouris V, Eliopoulou E, Investigation into the capsizing of damaged Ro-Ro passenger Ships in Waves, Proc. 7th Inter. Conf. On Stability of Ships & Ocean Vehicles STAB2000, Australia, Tasmania, 2000.
- Paulsrud Finn, Farley J Timothy, Norwegian/US Coast Guard, "Report of investigation into the circumstances surrounding the grounding of the Monarch of The Seas on proselyte reef in Great Bay, Philipsburg, St Maarten, Netherlands Antilles on December 15, 1998, resulting in major vessel damage, no loss of life and minor pollution", 10 April 2003.
- Petey, F, "Ermittlung der Kentersicherheit lecker Schiffe im Seegang", *Schiffstechnik* 35, 155-172, 1988.
- Piñeiro A Lopez, F Perez Arribas, R Donoso, R Torres, "Simulation of Passengers Movement on Ship Emergencies: Tools for IMO Regulations Fulfillment," *J. Maritime Research*, vol. 2, no. 1, 2005, pp. 105-125.
- Schreuder, M, Numerical Simulations Of Foundering Scenarios, Research Study Of The Sinking Sequence Of M/V ESTONIA. Research Report No.134, SSPA, Göteborg, Sweden, 2008.
- Tagg R, Tuzcu C, "A Performance-based Assessment of the Survival of Damaged Ships – Final Outcome of the EU Research Project HARDER", Proc. of the 6th Intern. Ship Stability Workshop, Webb Institute, 2002.
- Varela Jose M, G Guedes Soares, "A virtual environment for decision support in ship damage control", August 2007, IEEE Computer Society.
- Vassalos Dracos, Hyunseok Kim, Guro Christiansen and Jayanta Majumder, "A Mesoscopic Model for Passenger Evacuation in a Virtual Ship-Sea Environment and Performance-Based Evaluation", Pedestrian and Evacuation Dynamics – April 4-6, 2001 – Duisburg.

# A Method to Model Large Amplitude Ship Roll Damping

Christopher C. Bassler, Arthur M. Reed

David Taylor Model Basin (DTMB), Naval Surface Warfare Center, Carderock Division

Alan J. Brown,

Virginia Tech

## ABSTRACT

A method is proposed to model large amplitude ship roll damping, with considerations for large amplitude roll motion effects, such as bilge keel interaction with the free-surface. The method is based on consideration of distinct ship-specific physical phenomena, such as bilge keel emergence and deck submergence. Abrupt physical changes occur with these events, resulting in significant changes in the damping of the system. Without these considerations, roll motion may be under-predicted. Additional considerations for practical implementation of the proposed method are also discussed.

## KEYWORDS

roll damping, bilge keels, nonlinear oscillators, piecewise methods

## INTRODUCTION

Roll damping is a complex process of energy transfer which affects the amplitude of ship motion. Bilge keels have been used on ships since the late 19th century to increase damping and reduce the severity of roll motions experienced by a ship in waves (Froude, 1865; Bryan, 1900; Martin, 1958; Kato, 1965). Because ship motions are more severe and large roll angles may occur in moderate to extreme sea conditions, it is important to understand and accurately model damping for these conditions to predict ship motions (Beck & Reed, 2001). In these conditions, the effectiveness of the dominant mechanism of roll damping, bilge keels, is reduced. This paper presents a method to model large amplitude roll damping, with consideration of the effectiveness of bilge keels at large roll angles.

## BACKGROUND

### *Ship Roll Damping*

In the classical model of ship motion as a spring-mass-damper system, damping is proportional to velocity and characterizes the energy dissipation of the system. Existing theoretical models for roll motion consider physical processes related to roll motion damping, using various mechanisms of energy dissipation. These include friction, lift, wave-making, and vortex generation from the hull, as well as the vortex generation and influence of deeply submerged bilge keels (Ikeda, 1978; Schmitke, 1978; Himeno; 1981). For ship roll motion, the effects of the bilge keels account for the largest component of energy dissipation and are most effective for small and moderate roll motion at low speeds (Ikeda, 1978; Himeno, 1981). At higher speeds, lift damping becomes more dominant (Baitis, *et al.*, 1981). Although larger size bilge keels are typically more effective, some constraints, due to hull

geometry and structures, limit the practical span of bilge keels.

In most modern potential flow codes, used to predict ship motion performance, roll damping is determined using the well-known Ikeda's method (Ikeda, *et al.*, 1978), or results from roll decay experiments to obtain ship-specific damping. These methods assume small amplitude roll motion, where the bilge keels are considered to be deeply submerged and smooth changes occur between the geometry of the body and the fluid domains.

Additional work has been performed to extend the application of the component based damping model. De Kat (1988) computed roll damping coefficients at the natural roll frequency and then applied these for other roll frequencies. Blok & Aalbers (1991) decomposed the roll damping due to bilge keels into two components, the lift on the bilge keel and the eddy generation from the bilge keels. Other methods have been developed where each component is determined for zero speed and then forward speed corrections are applied. Ikeda (2004) also detailed improvements to his method to determine optimal location for placement of the bilge keels. Changes have also been made to extend Ikeda's method to high-speed planing craft, with modifications to the lift component (Ikeda & Katayama, 2000), and high-speed multi-hull vessels, with modifications to the wave-making, eddy, and lift components (Katayama, *et al.*, 2008). For these high-speed vessels, predictions were performed for speeds up to  $Fn=0.6$ . Additional studies have also examined some of the limitations of Ikeda's method for application to ships with buttock flow stern geometries (Kawahara, *et al.*, 2009) and large bilge keels (Bassler & Reed, 2009).

Large ship motions result in abrupt changes in the geometry of the body relative to the fluid domains, which must be considered to accurately determine the properties of the dynamical system modeling ship roll motion (Bassler & Reed, 2009; Reed, 2009). Because existing theoretical models were developed for small to moderate roll motions, the amount of energy dissipation for large amplitude roll

motion may be over-estimated, resulting in under-predicted roll motion.

For large amplitude ship roll motion, the bilge keels become less effective, due to their interaction with the free surface and, for more severe motions, due to possible emergence. An example of this occurrence is shown (Fig. 1) for the ONR Topside Series tumblehome configuration (Bishop, *et al.*, 2005). In this example, the forward section of the starboard bilge keel has emerged, the midsection is shipping water, and the aft section remains submerged.

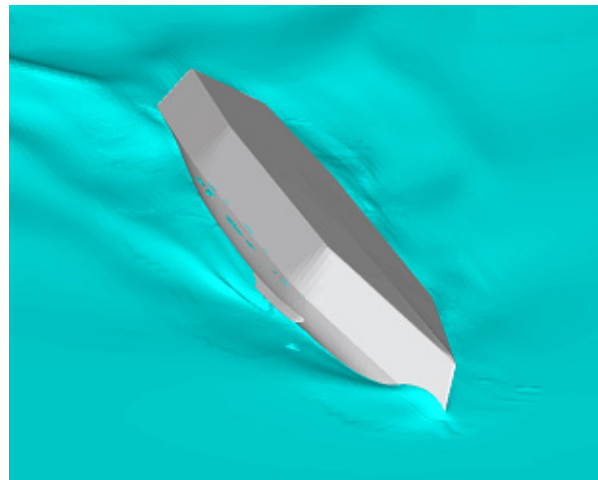


Fig. 1: DTMB Model #5613-1 at  $Fn = 0.30$ ,  $\phi = 30$  deg. For these conditions, the bilge keel is observed to be partially emerged from the water (Miller, *et al.*, 2008).

### ***Physical Phenomena in Large Amplitude Roll Motion***

When a ship experiences large amplitude roll motion, additional physical phenomena occur which are not considered in traditional roll damping models. These include asymmetric bilge keel interaction with the free surface, where water shipping occurs for bilge keel emergence, impact loading occurs upon re-entry, and air bubble entrainment occurs under the bilge keel after re-entry.

Observations of these physical phenomena were made during a series of forced roll motion experiments, at zero forward speed, performed at DTMB (Bassler, *et al.*, 2010). Force and moment measurements on both the hull and bilge keels were obtained for a model of the midship section of the ONR Topside Series,

Flared and Tumblehome configurations (DTMB Models #5699 and #5699-1). Particle Image Velocimetry (PIV) was used to measure the generated vortex-field (Fig. 2).

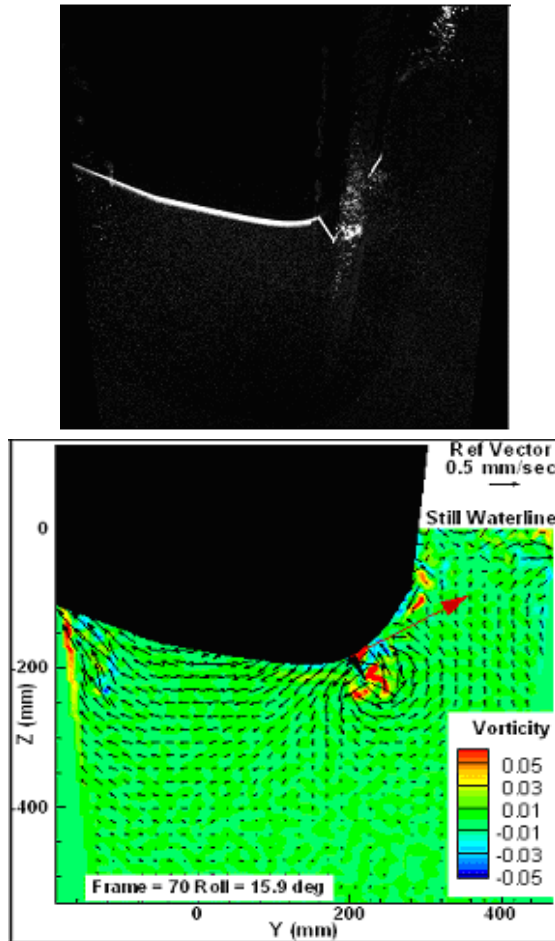


Fig. 2: Experimental measurements with DTMB Model #5699-1,  $\phi_a = 45$  deg,  $\omega=2.5$  rad/s. Air bubble entrainment is observed after bilge keel re-entry (top). Velocity-field measurements and bilge keel normal force measurements (red vector) are shown after bilge keel re-entry (bottom).

The individual physical phenomena that occur for large amplitude roll motion are highly nonlinear. However, the primary consideration of these events for ship roll motion prediction is their effect on the significant changes in the dynamical properties of the system. For example, it may not be necessary to explicitly model the localized nonlinear occurrence of bubble dynamics generated by the bilge keel upon re-entry after a large roll event. To enable modeling of these events in fast numerical

simulation codes, simplifying assumptions must be made, attributing the effects of these nonlinearities to the non-smooth transition at the boundary of the fluid domains.

### Motivation

By including the non-smooth transition, and subsequent changes in damping, which occur at large roll angles, more accurate ship roll motion predictions can be obtained. Without these considerations, the total roll damping may be over-estimated and the resulting ship roll motion may be under-predicted.

## THEORETICAL APPROACH

### Overview

The proposed procedure for predicting large amplitude roll damping is based on the modeling the abrupt physical changes in the dynamical system, which correspond to events such as bilge keel emergence or deck submergence (Fig 3). For large amplitude roll motion, an explicit dependence exists between roll damping and roll angle. From these events, distinct physical regions may be identified, which are dependent on the ship-specific geometry, where a significant change in damping of the system occurs.

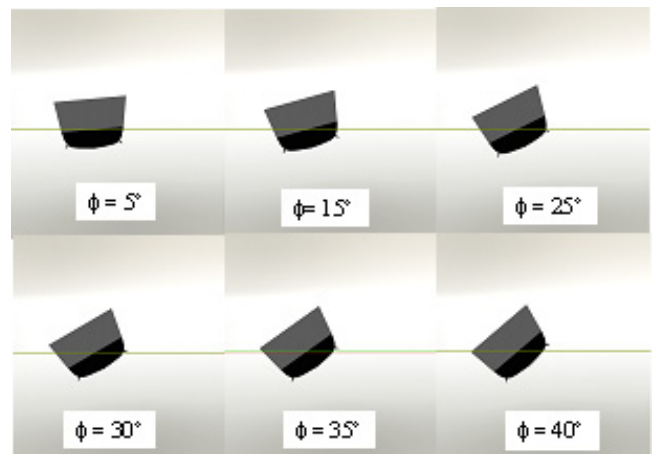


Fig. 3: Ship-specific abrupt physical changes due to variation in heel angle. For the midship section of the ONR Topside Series, flared configuration, bilge keel emergence is observed at 30 deg and deck submergence at 40 deg.

The roll angle can be used as a boundary to create a division of physical regions corresponding to abrupt physical changes associated with transition between the fluid domain boundaries. An example modeling the effect of bilge keel emergence and re-submergence on damping is considered in this paper.

### *Piecewise Methods*

Piecewise methods are a mathematical tool that can be used to model abrupt changes in system properties. Some well known dynamical systems in mechanics with these abrupt changes are dry friction, or Coulomb damping, and clock theory (Andronov, *et al.*, 1966). Because of the abrupt physical changes, oscillator systems with this behavior must be modeled explicitly. A piecewise linear approach has also been used to model the ship motion behavior associated with changes in the GZ curve for large amplitude roll motion (Belenky, 2000; Belenky & Sevastianov, 2007).

### *Application to Nonlinear Damping*

A piecewise method can be used to model mechanical oscillator systems with distinct physical regions, such as the interaction of the bilge keels or deck edge with the free surface. For initial consideration, single degree-of-freedom ship roll with a sinusoidal forcing function representing regular waves, is assumed. For this system a roll angle,  $\phi_t$ , can be specified which represents a physical threshold given by the ship-specific geometry. The transition across the physical boundary for each region, from small to large amplitude damping, can be considered to occur at a discrete instant in time.

Therefore, the change in damping during this process may be modeled as a “jump” for the non-smooth transition of a component of the body, such as the bilge keel or deck edge, out of the water (or into the water). The time-scale of this transition is small compared to the time-scale of the motion of the body, such as the roll period.

Based on this formulation of the problem, a system of algebraic equations may be determined and then solved simultaneously to obtain the damping for the large amplitude region.

## **A METHOD FOR LARGE AMPLITUDE SHIP ROLL DAMPING**

### *System of Equations*

The single degree-of-freedom ship roll equation is

$$\ddot{\phi} + 2\delta(\phi)\dot{\phi} + c(\phi) = F(t) \quad (1)$$

where  $F(t)$  is the forcing function from waves, given by

$$F(t) = \alpha \sin(\omega_e t) \quad (2)$$

where  $\alpha$  is the excitation amplitude and  $\omega_e$  is the frequency of excitation. The nonlinear stiffness,  $c(\phi)$ , is given by

$$c(\phi) = \omega_n^2 \frac{GZ(\phi)}{GM} \quad (3)$$

and the roll amplitude dependent damping,  $\delta(\phi)$ , is given by

$$\delta(\phi) = \begin{cases} \delta_1 & \text{if } \phi < |\phi_t| \\ \delta_2 & \text{otherwise} \end{cases} \quad (4)$$

where  $\delta_1$  is the damping for the small amplitude mode, below a specified physical threshold,  $\phi_t$ , and  $\delta_2$  is the damping for the large amplitude mode. The method may be implemented to obtain equivalent linear damping coefficients for each physical region. However, the damping formulation for each region is not limited to a linear formulation (4), and may include the use of more realistic models, such as a nonlinear formulation (5),

$$\delta(\phi)\dot{\phi} = \delta_a(\phi)\dot{\phi} + \delta_b(\phi)|\dot{\phi}| + \delta_c(\phi)\dot{\phi}^3 + \dots \quad (5)$$

where  $\delta_a$ ,  $\delta_b$ , and  $\delta_c$  are linear, quadratic, and cubic damping coefficients for that particular physical region (Dalzell, 1978; Cotton & Spyrou, 2000; Spyrou & Thompson, 2000).

These multiple sets of  $\delta_a$ ,  $\delta_b$ , and  $\delta_c$  can then be combined with the piecewise method to characterize damping for large amplitude roll.

This formulation may be further extended to model additional physical thresholds which will alter the damping characteristics of the ship in roll, such as deck edge submergence. Although nonlinear damping will most likely be used in any practical method for large amplitude roll motion; as a first step, in order to examine the ability of the piecewise model to reproduce the dynamic behavior of large amplitude roll motion, only linear damping coefficients are considered in this study.

An example of single degree-of-freedom large amplitude steady-state roll oscillation, with considerations for bilge keel emergence is shown (Fig. 4). The system is characterized by a natural roll frequency,  $\omega_n$ , frequency of excitation,  $\omega_e$ , and amplitude of excitation,  $\alpha$ , and amplitude of response,  $\phi_a$ . In this example, two transition points are identified, where one bilge keel re-enters the free surface after emergence, 1, and where the opposite bilge keel emerges, 2. In this example, the damping of the system is characterized by one set of coefficients,  $\delta_1$ , in the small amplitude mode, and another set of coefficients,  $\delta_2$ , in the large amplitude mode.

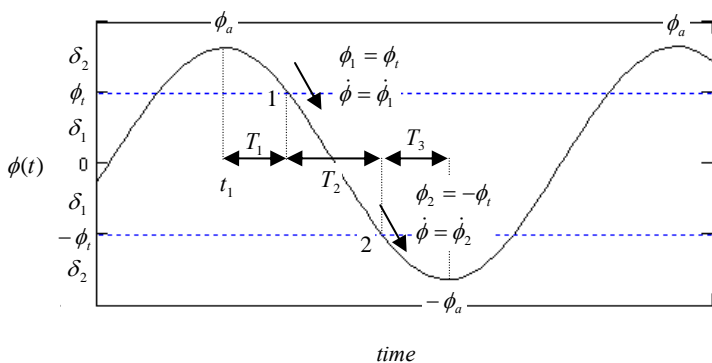


Fig. 4: 1DOF roll oscillation with amplitude,  $\phi_a$ , for one damping physical threshold. Locations (1) and (2) indicate threshold crossings at  $\pm\phi_1$  (e.g. bilge keel interaction with the free-surface).

As shown in Fig. 4,  $t_1$  is the time of the maximum amplitude,  $T_1$  is the time between the maximum amplitude and the first threshold

crossing (e.g. when the bilge keel re-enters the water),  $T_2$  is the time of the second threshold crossing (e.g. when the opposite bilge keel emerges) and  $T_3$  is the time of the maximum amplitude in the opposite direction. The roll angle and roll rate at the first threshold crossing, 1, are given as  $\phi_1$  and  $\dot{\phi}_1$ , respectively. The roll angle and roll rate at the second threshold crossing, 2, are given as  $\phi_2$  and  $\dot{\phi}_2$ . Because the process is periodic, a system of equations describing the half-period behavior of the system can be determined.

Formulae (6–8) express the roll and roll rate processes as solutions to ordinary differential equations for a system with linear damping in each physical region. The system of equations can also each be represented numerically, using a Runge-Kutta solver for each formula. Numerical evaluation for each equation enables a more robust model, and the use of varied nonlinear damping formulations for each physical region.

The transition from the maximum roll amplitude to the first threshold crossing, the re-submergence of the bilge keel, is given by

$$\begin{aligned} \phi_2(\phi_a, \dot{\phi}_a = 0, t_1, t_1 + T_1) &= \phi_1 = \phi_1 \\ \dot{\phi}_2(\phi_a, \dot{\phi}_a = 0, t_1, t_1 + T_1) &= \dot{\phi}_1 \end{aligned} \quad (6)$$

where  $\phi_2$  is the roll process using the second region damping coefficient,  $\delta_2$ .

The transition from the first threshold crossing to the second crossing, the emergence of the opposite bilge keel, is given by

$$\begin{aligned} \phi_1(\phi_1, \dot{\phi}_1, t_1 + T_1, t_1 + T_1 + T_2) &= \phi_2 = \phi_1 \\ \dot{\phi}_1(\phi_1, \dot{\phi}_1, t_1 + T_1, t_1 + T_1 + T_2) &= \dot{\phi}_2 \end{aligned} \quad (7)$$

where  $\phi_1$  is the roll process using the first region damping coefficient,  $\delta_1$ .

The roll process from the second threshold crossing to the maximum amplitude at the opposite side of the roll cycle is given by

$$\begin{aligned} \phi_2(\phi_2, \dot{\phi}_2, t_1 + T_1 + T_2, t_1 + T_1 + T_2 + T_3) &= -\phi_a \\ \dot{\phi}_1(\phi_2, \dot{\phi}_2, t_1 + T_1 + T_2, t_1 + T_1 + T_2 + T_3) &= 0 \end{aligned} \quad (8)$$

In order to demonstrate the method, a solution for the amplitude (the direct problem) was obtained. Given the solution for amplitude, the system of equations was then solved for damping (the indirect problem).

#### ***Solution for Amplitude- The Direct Problem***

For the direct problem, the evaluation of amplitude, in addition to the system of equations given by (6)–(7)–(8), the times corresponding to the threshold crossings,  $T_1$ ,  $T_2$ , and  $T_3$ , must also be included. Because the roll process considered in the model to obtain the damping coefficients is periodic, the times can be obtained with the inclusion of the following additional equation, where  $T_e$  is the roll excitation period.

$$T_1 + T_2 + T_3 = \frac{T_e}{2} = \frac{\pi}{\omega_e} \quad (9)$$

The values for  $\omega_n$ ,  $\omega_e$ ,  $\alpha$ ,  $\delta_1$  and  $\delta_2$  are specified and the values for  $\phi_1$  and  $\phi_2$  ( $=\pm\phi_t$ ), and  $\dot{\phi}_a$  are known. The system of equations (6)–(9) is solved to obtain  $\phi_a$ ,  $t_1$ ,  $T_1$ ,  $T_2$ ,  $T_3$ ,  $\dot{\phi}_1$  and  $\dot{\phi}_2$ .

#### ***Solution for Damping- The Indirect Problem***

In this system model, the first region, or small amplitude, damping,  $\delta_1$ , can be determined using Ikeda's method or from experimental measurements, such as roll decay tests. For the piecewise linear formulation discussed in this paper, the use of the equivalent linear damping coefficient formulation enables continuity with existing methods, which have traditionally been very appropriate for their intended use— modeling small to moderate amplitude roll motions.

Large amplitude forced oscillation tests may be carried out using experiments (e.g. Bassler, et al., 2007; 2010) or high-fidelity simulations tools, such as RANS (e.g. Miller, et al., 2008). In these tests, the maximum amplitude of the forced oscillation,  $\phi_a$ , and frequency of oscillation,  $\omega_e$ , are specified and the physical threshold,  $\phi_t$ , is known from the ship-specific geometry. Because forced oscillation is used, the amplitude of wave excitation and phase become virtual quantities.

Therefore, the excitation,  $\alpha$ , the time of the maximum amplitude,  $t_1$ , and the large amplitude, or second region damping,  $\delta_2$ , are unknowns and are determined from the solution to the system of equations using the indirect problem formulation.

For the indirect problem,  $\omega_n$ ,  $\omega_e$ ,  $\delta_1$ , and  $\phi_a$ , are specified and the values for  $\phi_1$  and  $\phi_2$ ,  $\dot{\phi}_a$ ,  $\dot{\phi}_1$ ,  $\dot{\phi}_2$ , and  $T_1$ ,  $T_2$ , and  $T_3$  are known. These values can be obtained from forced oscillation tests, using either experiments or high-fidelity simulations tools, such as RANS solvers. The system of equations is then solved to obtain  $\alpha$ ,  $t_1$ , and  $\delta_2$ . The system of equations (6)–(8) is over defined, which enables robust solutions to be obtained with very approximate initial values.

#### **ADDITIONAL CONSIDERATIONS FOR A PRACTICAL METHOD**

The procedure presented in this paper to model the change in roll damping for bilge keel interaction with the free-surface in large amplitude roll motion may also be extended to include additional physical regions which may significantly affect damping based on the ship-specific hull geometry, such as deck-in-water effects (Grochowalski, 1990; Grochowalski, et al., 1998).

Several additional considerations are needed in order to implement the method in time-domain numerical simulations and use the procedure for practical prediction of ship roll damping. These include multiple degree-of-freedom ship motions (such as heave and pitch), forward speed, irregular waves, and roll frequency dependence.

The use of a sectional approach in the time-domain, with the instantaneous relative position of the ship section and the free-surface from irregular waves near the ship (Fig. 5), may provide more accurate determination of when the physical threshold for a given ship section is crossed and which corresponding damping should be used. By integrating the sectional damping along the hull at each time-

step, the ship-specific roll damping for large amplitude ship motions can be determined.

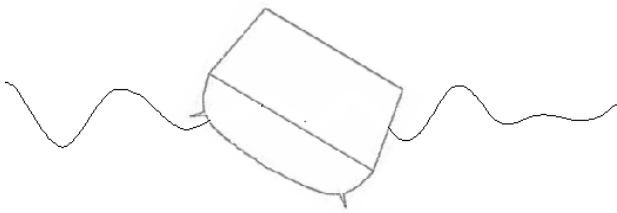


Fig. 5: Sectional view of the instantaneous relative position of the ship and irregular waves for determining roll damping at a given time-step.

## SUMMARY

A method for modeling large amplitude roll damping has been presented, based on modeling the abrupt physical changes that occur with events, such as bilge keel emergence or deck submergence. When these events occur, a significant change in damping of the system occurs that can be modeled explicitly using a piecewise approach.

By considering the discrete physical events in the time-domain, which alter the damping properties of large amplitude ship roll in waves, a series of damping coefficients for these different regions can be obtained. These can then be included in a look-up table and used in sectional time-domain evaluation. An example, with considerations for bilge keel emergence, was shown using the method. Despite the formulation of the method to only consider periodic roll, similar to excitation from regular waves, the damping coefficient information can be used to predict ship motion from a stochastic excitation. However, some additional considerations must still be addressed for practical implementation.

To examine the feasibility of the proposed method for modeling large amplitude roll damping, comparisons will be made to experimental measurements (e.g. Bassler, *et al.*, 2010). The suitability of the damping formulation for each region, small and large, and the frequency dependence of large amplitude damping will also be investigated. As mentioned previously, in order to develop a practical method using this theoretical model

for large amplitude ship roll damping, several additional issues must still be examined. The ability to account for additional ship motions, forward speed effects, and the local wave-field, may be possible using a sectional time-domain approach.

## ACKNOWLEDGEMENTS

The authors appreciate the support of this work from Dr. Pat Purtell (ONR) and Dr. John Barkyoumb and the NSWCCD Independent Applied Research (IAR) program. The authors would also like to thank Dr. Vadim Belenky (NSWCCD) for several helpful technical discussions.

## REFERENCES

- Andronov, A., S. E. Khaikin & A. A. Vitt (1966) *Theory of Oscillators*, New York: Dover Publications (Reprint, 1987).
- Bassler, C., J. Carneal & P. Atsavapranee (2007) "Experimental Investigation of Hydrodynamic Coefficients of a Wave-Piercing Tumblehome Hull Form," *Proc. 26th Intl. Conf. Offshore Mechanics and Arctic Engin.*, San Diego, CA.
- Bassler, C. C. & A. M. Reed (2009) "An Analysis of the Bilge Keel Roll Damping Component Model," *Proc. 10th Intl. Conf. Stability of Ships and Ocean Vehicles*, St. Petersburg, Russia.
- Bassler, C. C., A. M. Reed, & A. J. Brown (2010) "Characterization of Energy Dissipation Phenomena for Large Amplitude Ship Roll Motions," *29th American Towing Tank Conf. (ATTC)*, Annapolis, MD (in publication).
- Baitis, A. E., W. G. Meyers & T. R. Applebee (1981) "Validation of the Standard Ship Motion Program, SMP: Improved Roll Damping Prediction," Hydromechanics Dept. Technical Report, DTNSRDC Report SPD-0936-02.
- Beck, R. F. & A. M. Reed (2001) "Modern Computational Methods for Ships in a Seaway," *Trans. SNAME*, 109, pp. 1–51.
- Belenky, V. L. (2000) "Piecewise Linear Approach to Nonlinear Ship Dynamics," *Contemporary Ideas on Ship Stability*, New York: Elsevier, pp.149–160.

- Belenky, V. & N. B. Sevastianov (2007) *Stability and Safety of Ships: Risk of Capsizing*, Jersey City, NJ: SNAME, pp. 128–130.
- Bishop, R. C., W. Belknap, C. Turner, B. Simon & J. H. Kim (2005) “Parametric Investigation on the Influence of GM, Roll Damping, and Above-Water Form on the Roll Response of Model 5613,” Hydromechanics Dept. Technical Report, NSWCCD-50-TR-2005/027.
- Blok, J. J. & A. B. Aalbers (1991) “Roll Damping Due to Lift Effects on High Speed Monohulls,” *Proc. FAST '91*.
- Bryan, G. H. (1900) “The Action of Bilge Keels,” *Trans. Royal Inst. Naval Arch.*, 4.
- Cotton, B. & K. J. Spyrou (2000) “Experimental and Theoretical Studies of Large Amplitude Ship Rolling and Capsize,” *Proc. 7th Intl. Conf. on Stability of Ships and Ocean Vehicles*, Launceston, Australia
- Dalzell, J. F. (1978) “Note on the Form of Ship Roll Damping,” *J. Ship Res.*, 22(3):178–185.
- de Kat, J. (1988) “Large Amplitude Ship Motions and Capsizing in Severe Sea Conditions,” Ph.D. Thesis, U. California, Berkeley.
- Froude, W. (1865) “On the Practical Limits of the Rolling of a Ship in a Seaway,” *Trans. Inst. Naval Arch.*, 6.
- Grochowalski, S. (1990) “Hydrodynamic Phenomenon Generated By Bulwark Submergence and its Influence On Ship Susceptibility to Capsizing,” *Proc. 4th Intl. Conf. Stability of Ships and Ocean Vehicles*, Gdansk.
- Grochowalski, S., C. C. Hsiung, Z. J. Huang & L. Z. Cong (1998) “Theoretical Modeling of Ship Motions and Capsizing in Large Steep Waves.” *Trans. SNAME*, 106:241-267.
- Himeno, Y. (1981) “Prediction of Ship Roll Damping-State of the Art,” U. Michigan Dept. of Naval Arch. and Marine Engin., Report 239.
- Ikeda, Y., Y. Himeno & N. Tanaka (1978) “A Prediction Method for Ship Roll Damping,” Osaka Prefecture University, Dept. of Naval Arch., Report No. 00405.
- Ikeda, Y. & T. Katayama (2000) “Roll Damping Prediction Method for a High-Speed Planing Craft,” *Proc. 7th Intl. Conf. Stability of Ships and Ocean Vehicles*, Tasmania, Australia.
- Ikeda, Y. (2004) “Prediction Methods of Roll Damping of Ships and Their Application to Determine Optimum Stabilization Devices.” *Marine Tech.*, 41(2):89–93.
- Katayama, T., T. Taniguchi & M. Kotaki (2008) “A Study on Viscous Effects of Roll Damping of a High-Speed Catamaran and a High-Speed Trimaran,” *Proc. 6th Osaka Colloq. Seakeeping and Stability of Ships*, Osaka, Japan.
- Kato, H. (1965) “Effect of Bilge Keels on the Rolling of Ships.” *J. Soc. Naval Arch., Japan*, 117:93–114.
- Kawahara, Y., K. Maekawa & Y. Ikeda (2009) “A Simple Prediction Formula of Roll Damping of Conventional Cargo Ships on the Basis of Ikeda’s Method and Its Limitation,” *Proc. 10th Intl. Conf. on Stability of Ships and Ocean Vehicles*, St. Petersburg, Russia.
- Martin, M. (1958) “Roll Damping Due to Bilge Keels.” U. Iowa Institute of Hydraulic Research, Report.
- Miller, R. W., C. C. Bassler, P. Atsavaprane & J. J. Gorski (2008) “Viscous Roll Predictions for Naval Surface Ships Appended with Bilge Keels Using URANS,” *Proc. 27th Symp. Naval Hydro.*, Seoul.
- Reed, A. M. (2009) “A Naval Perspective on Ship Stability,” *Proc. 10th Intl. Conf. Stability of Ships and Ocean Vehicles*, St. Petersburg, Russia.
- Schmitke, R. T. (1978) “Ship Sway, Roll, and Yaw Motions in Oblique Seas.” *Trans. SNAME*, 86:26-46.
- Spyrou, K. J. & J. M. T. Thompson (2000) “Damping Coefficients for Extreme Rolling and Capsize: An Analytical Approach.” *J. Ship Res.*, 44(1):1–13.

## Some Topics for Estimation of Bilge-keel Component of Roll Damping

Toru Katayama, Yuuki Yoshioka, Takahiro Kakinoki, and Yoshiho Ikeda

Graduate school of Engineering, Osaka Prefecture University

### ABSTRACT

In this paper, two topics of roll damping estimation problems are introduced. In these topics, bilge-keel component of roll damping is focused, because the component is generally most part of viscous roll damping. First topic is the bilge-keel component of roll damping under shallow draft and large amplitude roll motion, and a prediction model of the draft effects for Ikeda's prediction method is proposed. Second topic is the bilge-keel component of roll damping under transitional rolling, and a prediction method of roll damping for transitional rolling is proposed.

### KEYWORDS

bilge-keel component, parametric rolling, relative draft, low Keulegan-Carpenter number, drag coefficient, transitional motion

### INTRODUCTION

In order to guarantee the safety of vessels, it is very important to understand the characteristics of roll motion and to estimate roll motion adequately. However, it is very complicated to calculate it because of difficulty of roll damping prediction due to significant viscous effects depending on vortex shedding.

It is well known that there is a prediction method of roll damping proposed by Ikeda et al. (1976)(1977)(1978). However, some estimation problems are indicated in the previous studies (Tanaka et al., (1981)(1982), (Ikeda et al.,(1994), Hashimoto et al.,(2008)(2009)) .

In this paper, two topics of roll damping estimation problems are introduced and bilge-keel component of roll damping is focused mainly, because the component is generally the largest part of total roll damping. In the first topics, the effects of shallow draft are investigated. A forced rolling test is carried out. And a simplified prediction method of the effects is proposed. In the second topics, the effects of transitional motion are investigated.

First, under transitional motion, the characteristic of drag coefficient of flat plate in the region of low  $Kc$  number is experimentally measured. Second, using the forced oscillation device, the characteristic of drag coefficient of flat plate under transitional condition in periodic motion is measured. Finally, based on the results of these experiments, a prediction method based on Ikeda's method is proposed.

### EFFECTS OF SHALLOW DRAFT

#### *Forced Rolling Test*

In the previous study by Tanaka et al. (1981), it is pointed out that bilge-keel component decreases when the draft is shallow. However, no formulation is proposed. Then, in this study, a forced rolling test is carried out by using two-dimensional model, and the characteristics of the effects of shallow draft on bilge-keel component is investigated to propose an empirical formula.

Table 1 shows the principal particulars of the model with bilge keel. Fig. 1 shows some parameters for explaining experimental conditions. The measurements at

systematically changed roll amplitudes, roll periods, drafts and height of roll axis (the center of rolling) are carried out. Bilge-keel component is obtained from subtraction measured data of hull without bilge keel from measured data of hull with bilge keel at the same condition.

Table 1 Principle particulars of two-dimensional model.

length: $L$	0.80m
breadth: $B$	0.237m
depth: $d$	0.14465m
block coefficient: $C_B$	0.8m
bilge radius	0.035m
length $\times$ breadth	0.01m $\times$ 0.80m

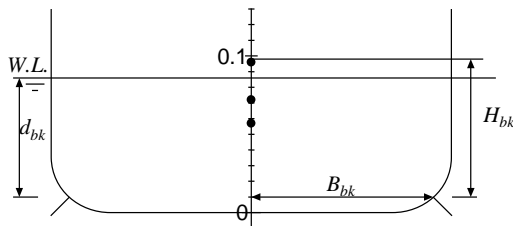


Fig. 1: Cross section of two-dimensional model.

**Empirical Formula**

Figs. 2-4 show the ratio of the predicted results by the measured ones. Horizontal axis shows  $d_{bk} / B_{bk}$ . Each figure shows the results of different  $H_{bk} / B_{bk}$ . Where  $d_{bk}$ ,  $B_{bk}$  and  $H_{bk}$  are shown in Fig.1. Measured results are indicated by different marks for different roll amplitude. The maximum roll amplitudes is different for each height of roll axis and they are 17.71, 18.57, 21.0 degrees respectively.

Fig. 2 shows that the ratio increases linearly with increase of draft. For different roll amplitudes, the tendency is almost same quantitatively. Fig. 3 shows that the ratio is almost same for different roll amplitudes. And the ratio increases linearly and its inclination is higher than Fig. 2. Fig. 4 shows that the similar tendency as Fig. 2. And its inclination is the highest of all. If draft is deep enough, the estimation results can be agree with the

measured results. It means that the ratio does not exceed 1.0 with increase of draft. Moreover, above-mentioned characteristics are not almost affected by roll period.

A fitting curve is obtained from the measured data. Correction factor's formula (1) is expressed as following equation.

$$\begin{aligned}
 C_{bk} = & \left( 3.615 \frac{H_{bk}}{B_{bk}} - 1.227 \right) \frac{d_{bk}}{B_{bk}} \\
 & + \left\{ 3.29 \left( \frac{H_{bk}}{B_{bk}} \right)^2 - 5.35 \frac{H_{bk}}{B_{bk}} + 1.98 \right\} \phi_a^2 \\
 & + \left\{ 2.48 \left( \frac{H_{bk}}{B_{bk}} \right)^2 + 1.90 \frac{H_{bk}}{B_{bk}} - 11.6 \right\} \phi_a \quad (1) \\
 & + \left\{ 2.77 \left( \frac{H_{bk}}{B_{bk}} \right)^2 - 3.27 \frac{H_{bk}}{B_{bk}} + 1.14 \right\} \\
 & \leq 1.0
 \end{aligned}$$

where  $\phi_a$  is in radian. Bilge-keel component is obtained by multiplying correction factor by bilge-keel component of Ikeda's roll damping prediction method.

**Calculated Results**

For a post panamax container ship (Hashimoto et al.,(2008)(2009)), roll damping is calculated by Ikeda's method with the correction factor. When parametric rolling occurs at high wave height in head waves, large relative draft change is caused. In the roll damping calculation, the relative draft of each cross section at the moment, where roll is upright, is used. Fig. 5 shows the calculated results. Total roll damping decreases 6% at roll amplitude  $\phi_a = 8.59\text{deg}$ , 11% at  $\phi_a = 14.38\text{deg}$ , and 19% at  $\phi_a = 20\text{ deg}$ , for the results without considering the relative draft change. Shallow draft due to draft change in waves affects on bilge-keel component significantly.

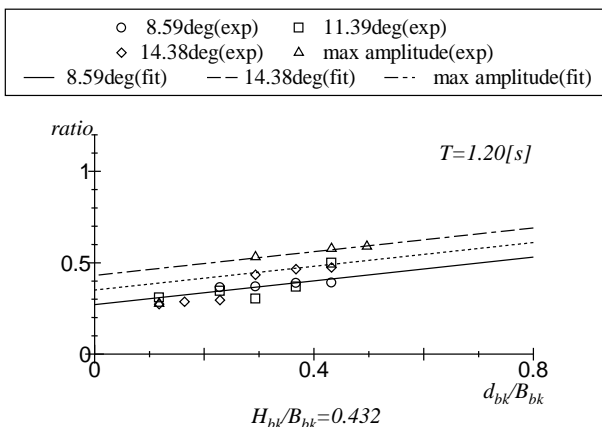


Fig. 2: Ratio of experiment of bilge-keel damping component to prediction at height of roll axis  $KG=57\text{mm}$ .

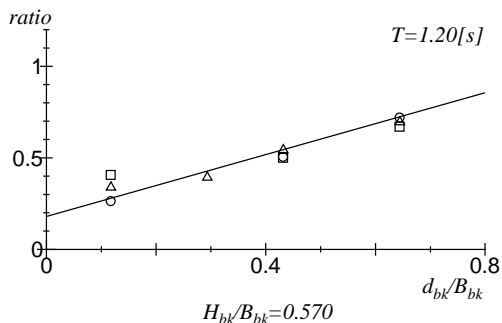


Fig. 3: Ratio of experiment of bilge-keel damping component to prediction at height of roll axis  $KG=72\text{mm}$ .

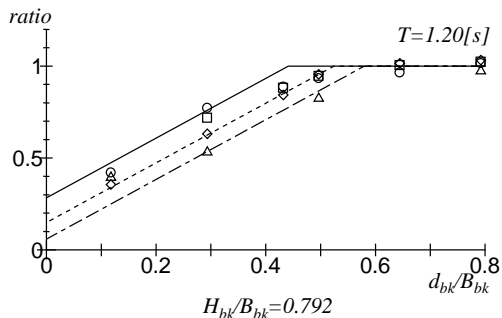


Fig. 4: Ratio of experiment of bilge-keel damping component to prediction at height of roll axis  $KG=96\text{mm}$ .

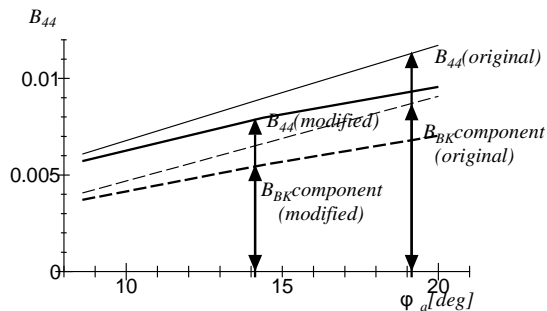


Fig. 5: Prediction result of roll damping including relative draft effects.

## EFFECTS OF TRANSITIONAL AND NON-PERIODIC ROLLING

### Drag Coefficient in Uniform Flow

First, drag coefficient of a flat plate, which is assumed as bilge keels, in uniform flow is measured. A strut and a flat plate are fixed by a load cell (shown in Fig. 6), and it is towed at constant forward speed. Towing speeds are from  $U = 0.1$  to  $1.0\text{m/s}$  at  $0.1\text{ m/s}$  space. Drag force acting on a flat plate  $D$  is obtained from deducting measured drag without the flat plate. Drag coefficient is calculated with the following equation.

$$C_D = \frac{D}{0.5\rho S U^2} \quad (2)$$

where  $D$ ,  $\rho$ ,  $S$  and  $U$  denote drag force, density of fluid, area of flat plate and towing speed. In order to avoid low  $Kc$  number effects, measured data in the region  $Kc > 100$  are used in the analysis of drag force.  $Kc$  number is expressed as follows,

$$Kc = \frac{2\pi x}{D_p} \quad (3)$$

where  $x$  and  $D_p$  denote forward distance and height of a flat plate shown in Fig. 6 ( $L_p/D_p = 11$ ).

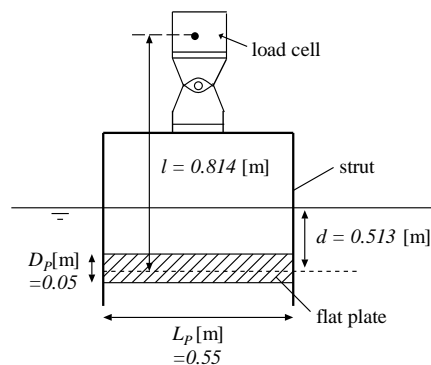


Fig. 6: Schematic view of the experimental device.

Fig. 7 shows the results. Drag coefficient of a flat plate ( $L_p \gg D_p$ ) measured by Hoerner (1993) is also shown in Fig. 7. In order to remove low Reynolds number effects on drag force, drag force of a tapered flat plate is also measured. From this figure, it is confirmed that drag coefficients of a tapered flat plate is constant for change in forward speed, even if it is lower than Hoerner's results. In this study, a tapered flat plate is used.

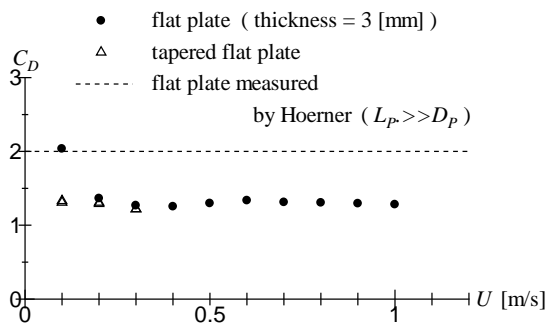


Fig. 7: Drag coefficients of flat plates in uniform flow.

### Drag Coefficient in Oscillatory Flow

It is known that drag coefficients on oscillating flat plate at low  $Kc$  number ( $Kc < 10$ ) is significantly changed by a slight change of  $Kc$  number (Tanaka et al.,(1980), Kudo et al.,(1980)).  $Kc$  number of oscillating flat plate is expressed as follows,

$$Kc = \frac{2\pi y_A}{D_p} \quad (4)$$

where  $y_A$  is amplitude of oscillation. However, the experimental results at low  $Kc$  number ( $Kc < 3$ ) is not found because of difficulty of measurement. Then, drag force of a flat plate at low  $Kc$  number is carefully measured.

The experimental device shown in Fig. 6 is oscillated and hydrodynamic force and forced motion are measured. Drag force, which is proportional to motion velocity, is obtained from these data. Drag coefficient is calculated with the following equation.

$$C_{D_{peri}} = \frac{F_p}{0.5\rho S(y_A \omega)^2} \quad (5)$$

where,  $\omega$  is circular frequency of forced oscillation, and  $F_p$  is drag force acting on a flat plate.  $F_p$  is obtained from deducting drag force without flat plate.

Fig. 8 shows the results. Drag coefficient is about 20 at  $Kc = 0.5$ , and decreases with increase of  $Kc$  number, and becomes the value in uniform flow at about  $Kc=250$ . As the results, a fitting curve of drag coefficient Eq. (6) is determined, and it is shown in Fig.8 as a dotted line.

$$\frac{C_{D_{peri}}}{C_{D0}} = (20.0e^{-1.23Kc} + 2.86e^{-0.174Kc} + 1) \times \left( 0.908 + \frac{1.2}{1+1.01^{Kc}} \right) \quad (6)$$

( $0 < Kc \leq 250$ )

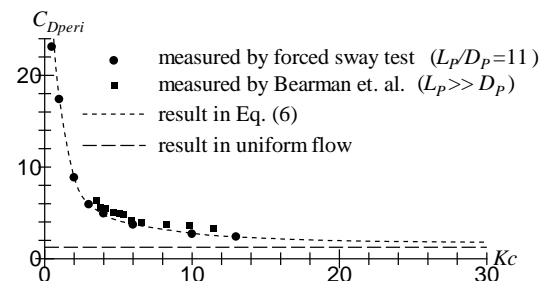


Fig. 8: Drag coefficients of flat plates in oscillatory flow.

### Drag Coefficient under One Direction Accelerating

Experimental device shown in Fig. 5 is towed horizontally by a method of free fall of a weight shown in Fig. 9. In order to obtain drag force acting on a flat plate, two measurements with and without flat plate are carried out, and these data are analysed by deducting inertia components, respectively. Drag coefficients in the both cases are obtained and fitting curve (7) and (8) are determined respectively.

$$\frac{C_{D(S+P)acc}}{C_{D0}} = \left( \begin{array}{l} 4.76e^{-0.279Kc} \\ + 20.6e^{-2.06Kc} + 1.168 \end{array} \right) \times \left( 0.908 + \frac{1.2}{1+1.01^{Kc}} \right) \quad (7)$$

(0 < Kc ≤ 250)

$$\frac{C_{DSacc}}{C_{D0}} = (17.0e^{-1.89Kc} + 2.72e^{-0.50Kc} + 0.168) \times \left( 0.908 + \frac{1.2}{1+1.01^{Kc}} \right) \quad (8)$$

(0 < Kc ≤ 250)

where Kc number obtained from Eq. (3). From Eqs. (7) and (8), drag coefficient of a flat plate at one direction accelerating is calculated with the following equation and the results are shown in Fig. 10.

$$\frac{C_{Dacc}}{C_{D0}} = \frac{C_{D(S+P)acc}}{C_{D0}} - \frac{C_{DSacc}}{C_{D0}} \quad (9)$$

(0 < Kc ≤ 250)

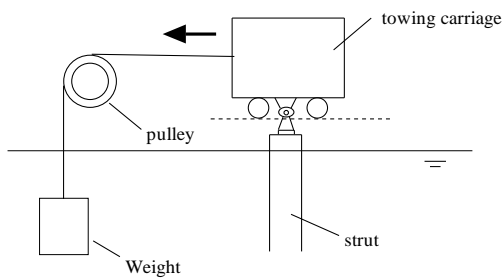


Fig. 9: Schematic view of experiment towed by free fall of a weight.

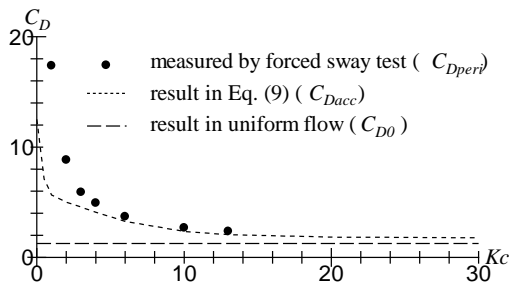


Fig. 10: Comparison of drag coefficients of a flat plate by forced sway test and by direction accelerating test.

### Drag Coefficient under Transitional Condition in Oscillatory Flow

In this section, using the forced oscillating device, measurements of forces acting on a flat plate in each swing from rest is carried out.

Figs. 11 and 12 show the results. Drag coefficient is gradually increasing from the first swing to the fourth swing. After the fourth swing, drag coefficient becomes constant. From the results, the formula of drag coefficients including the number of swing from rest is decided as the following equation.

$$C_{Dn} = C_{Dacc} + (C_{Dperi} - C_{Dacc}) \frac{n-1}{3} \quad (10)$$

where n is the number of swing (n = 1, 2, 3 and 4), and Kc number obtained from Eq. (4).

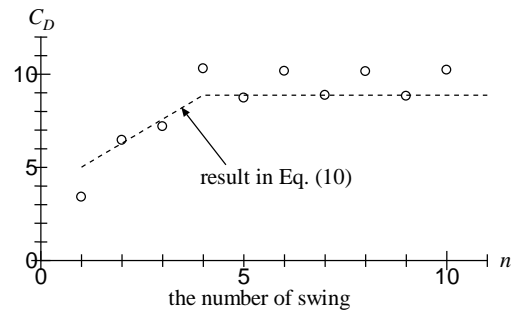


Fig. 11: Drag coefficient of flat plate vs. the number of swing at Kc = 2.0.

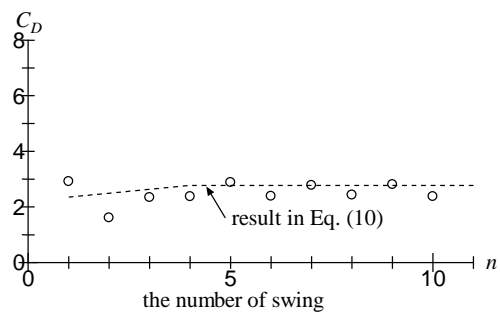


Fig. 12: Drag coefficient of flat plate vs. the number of swing at Kc = 10.0

## CONCLUSION

In this paper, two topics of roll damping estimation problems are introduced.

In the first topics, the effects of shallow draft are investigated. Bilge-keel component of roll damping by Ikeda's prediction method is overestimated for lower roll axis and shallow draft. Based on the measured results, an empirical formula to the bilge-keel component is proposed.

In the second topics, the effects of transitional motion are investigated. In the region at  $Kc < 250$ , drag coefficient of a flat plate under one direction accelerating is larger than that in uniform flow and smaller than that in steady oscillatory flow. Moreover, in transitional condition under forced oscillation, the drag coefficients from 1<sup>st</sup> swing to 3<sup>rd</sup> swing are smaller than that in steady oscillatory flow. These facts may indicate that the characteristics of drag coefficient affect transitional and non-periodic rolling. Based on the results, an empirical formula to the bilge-keel component by Ikeda's prediction method is presented.

## Reference

- H. Hashimoto and N. Umeda, "Preventing Parametric Roll with Use of Anti-Rolling Tank for a Large Containership in Head and Following Waves," The 4<sup>th</sup> Asia Pacific Workshop on Marine Hydrodynamics, 2008, pp73-78.
- H. Hashimoto and Y. Sanya, Research on Quantitative Prediction of Parametric Roll in Regular Waves," Journal of the Japan Society of Naval Architects and Ocean Engineers, 2009, Vol.8, pp361-364.
- K. Kudo, A. Kinoshita and M. Nakawatari, Experimental Study on Hydrodynamic Viscous Force Acting on Oscillating Bluff Body, Journal of the Kansai Society of Naval Architects, Japan, 1980, Vol. 177, pp. 83-90.
- N. Tanaka, Y. Himeno, Y. Ikeda and K. Isomura, Experimental study on Bilge-Keel Effect for Shallow-Draft Ship, Journal of the Kansai Society of Naval Architects, Japan, 1981, Vol. 180, pp. 69-75.
- N. Tanaka, Y. Ikeda and H. Okada, Study on Roll Characteristics of Small Fishing Vessel Part I Measurement of Roll Damping, Journal of the Kansai Society of Naval Architects, Japan, 1982, Vol, 187, pp. 15-23.
- N. Tanaka, Y. Ikeda and Y. Himeno, Experimental Study on Hydrodynamic Viscous Force Acting on Oscillating Bluff Body, Journal of the Kansai Society of Naval Architects, Japan, 1980, Vol. 179, pp. 35-43.
- S. F. Hoerner, Fluid Dynamic Drag, 1965.
- Y. Ikeda, Y. Himeno and N. Tanaka, On Roll Damping Force of ship : Effects of Friction of Hull and Normal Force of Bilge Keels, Journal of Kansai Society of Naval Architects, Japan, 1976, Vol. 161, pp. 41-49.
- Y. Ikeda, K. Komatsu, Y. Himeno and N. Tanaka, On Roll Damping Force of Ship : Effects of Hull Surface Pressure Created by Bilge Keels, Journal of Kansai Society of Naval Architects, Japan, 1977, Vol. 165, pp. 31-40.
- Y. Ikeda, Y. Himeno and N. Tanaka, On Eddy Making Component of Roll Damping Force on Naked Hull, Journal of The Society of Naval Architects, Japan, 1977, Vol. 142, pp. 54-64.
- Y. Ikeda, Y. Himeno and N. Tanaka, Components of Roll Damping of Ship at Forward Speed, Journal of The Society of Naval Architects, Japan, 1978, Vol. 143, pp. 113-125.
- Y. Ikeda, T. Katayama, Y. Hasegawa and M. Segawa, Roll Damping of High Speed Slender Vessels, Journal of the Kansai Society of Naval Architects, Japan, 1994, Vol. 222, pp. 73-81

## Approximation of the non-linear roll damping

Maciej Pawłowski

School of Ocean Engineering and Ship Technology,  
TU Gdansk, Poland

### ABSTRACT

The paper discusses how to get the proper estimation of the non-linear damping moment in ship roll with the help of free roll tests. It demonstrates two major points, 1° that the damping moment in terms of approximation is an odd non-analytic function, 2° the standard method based on the ratio of two consecutive amplitudes is of limited meaning for non-linear roll. A new method is proposed, based on approximation of free roll, using the instantaneous values of the logarithmic decrement of damping. It is assumed that the instantaneous values are identical with the equivalent values, obtained from equating work done over one cycle.

### KEYWORDS

ship roll, non-linear damping, simulations of ship motions

### INTRODUCTION

It is well known that roll damping is non-linear. Damping is needed for simulations of ship motions. In equations of motion a normalized damping is normally used, understood as the ratio between the damping moment and the virtual moment of inertia around the longitudinal axis of rotation. This characteristic value is typically approximated by an odd quadratic polynomial of the form:

$$b_1 \dot{\phi} + b_2 \dot{\phi} |\dot{\phi}|,$$

the second derivative of which with respect to the speed of roll does not exist at  $\dot{\phi} = 0$ . Consequently, this type of approximation is non-analytic.

Damping is an odd function of the speed of roll  $\dot{\phi}$ . In general, it seems natural to use odd polynomials for approximating odd functions. In the case of normalized damping, this is an odd polynomial of the speed of roll  $\dot{\phi}$ :

$$b_1 \dot{\phi} + b_3 \dot{\phi}^3 + b_5 \dot{\phi}^5 + \dots,$$

where the coefficients  $b_1, b_3, b_5, \dots$  are constant.

The same applies to other odd functions, as, for instance, the *GZ*-curve, which is an odd function of the angle of heel (roll). Consequently, it should be approximated resorting to odd polynomials (or sine

sums) of the angle  $\phi$ , as discussed by Pawłowski (1987).

The above matter seems obvious to mathematicians. Therefore, McCue (2007) in her noteworthy paper did not hesitate at all to use odd polynomials for approximating odd functions. She did this despite the fact that in the original paper she used for reference, non-analytical approximations were employed both for damping and the *GZ*-curve.

### BASIC ASSUMPTION

The damping coefficient is normally denoted by  $N$ . In the case of non-linear damping, this coefficient is amplitude dependent, normally established with the help of free roll tests, varying from oscillation to oscillation. Work dissipated by the damping moment over one cycle during a forced motion can be calculated as follows:

$$L = \int_0^{2\pi} M d\phi = \int_0^{2\pi} (N_1 \dot{\phi} + N_3 \dot{\phi}^3 + N_5 \dot{\phi}^5 + \dots) d\phi, \quad (1)$$

where the expression in the parentheses is the damping moment  $M$ . Assuming that the forced motion is harmonic, that is  $\phi = a \sin \omega t$ , where  $a$  is the amplitude of roll, and  $\omega$  is the circular frequency of oscillation, then  $\dot{\phi} = \omega a \cos \omega t$ . Since  $d\phi = \dot{\phi} dt$ , the following results from equation (1)

$$L = N_1(\omega a)^2 \int_0^T \cos^2 \omega t dt + N_3(\omega a)^4 \int_0^T \cos^4 \omega t dt + N_5(\omega a)^6 \int_0^T \cos^6 \omega t dt + \dots \quad (2)$$

where  $T = 2\pi/\omega$  is the period of oscillations. Introducing notation

$$I_n = \int_0^T \cos^n \omega t dt,$$

the above integrals can be easily calculated by the recurrence equation  $I_{n+2} = \frac{n+1}{n+2} I_n$ , which results from integration by parts. Since  $I_0 = T$ , the first integral in equation (2) equals  $\frac{1}{2}T$ , the second equals  $(\frac{1}{2} \cdot \frac{3}{4} = \frac{3}{8})T$ , the third equals  $(\frac{3}{8} \cdot \frac{5}{6} = \frac{5}{16})T$ , and so on. Hence, equating work done over one cycle yields

$$N_1(\omega a)^2 \frac{1}{2}T + N_3(\omega a)^4 \frac{3}{8}T + N_5(\omega a)^6 \frac{5}{16}T + \dots = N(\omega a)^2 \frac{1}{2}T, \quad (3)$$

where  $N$  is the equivalent linear coefficient of damping, amplitude dependent. For linear damping  $N = const$ , which means independence of the amplitude of oscillations, whereas for non-linear damping  $N$  is a function of the amplitude of roll  $a$ . Equation (3) yields an even polynomial relative to the amplitude of roll for the equivalent coefficient of damping:

$$N = N_1 + \frac{3}{4}N_3(\omega a)^2 + \frac{5}{8}N_5(\omega a)^4 + \dots, \quad (4)$$

where  $N_1 = const$  is a linear part of the equivalent coefficient of damping, independent of amplitude, whereas the other part is non-linear, dependent on the amplitude  $a$ . Similar considerations can be found in Błocki (1977, 1980). It is noteworthy that using only two terms in equation (4), frequently found in literature, is insufficient for proper approximation of

the non-linear damping, shown later.

A graph of  $\nu \equiv \frac{1}{2}b$  versus the amplitude  $a$  is normally obtained experimentally from free roll tests; in physics the quantity  $\nu$  is termed the logarithmic decrement of damping. It is assumed that the experimental value of  $\nu$  is identical with the equivalent one. Having found a polynomial approximation of the logarithmic decrement, equation (4) says how to get the coefficients  $N_1, N_3, N_5, \dots$ , needed in computations. Dividing the above equation throughout by the virtual moment of inertia  $J_x + m_{44}$ , we get

$$b = b_1 + \frac{3}{4}b_3(\omega a)^2 + \frac{5}{8}b_5(\omega a)^4 + \dots, \quad (5)$$

where  $b_1, b_3, b_5, \dots$  are constant, independent of  $a$ .

### FREE ROLL

It is worth recalling that damping is very difficult to obtain from experiments with reasonable accuracy. Normally, free roll tests are used for this purpose. A typical run of such a roll, carried out at CTO in the 'dry' condition for a ro-pax vessel used for surviving tests, is shown in Figure 1. The scale of the model was 1:50, and vessel's particulars were these:

$L_{oa} = 169.90$ m	$C_b = 0.628$
$L_{pp} = 159.00$ m	$h_0 = 3.46$ m
$B = 28.00$ m	$m = 16\,500$ ton
$T = 5.73$ m	$z_G = 12.40$ m

Measured values, recorded every 0.02 s with resolution of  $0.1^\circ$  are marked by dots, whereas solid lines correspond to approximated values, based on two different methods, discussed below. Some non-harmonic character of roll, clearly visible for small amplitudes, can be attributed to the presence of water that leaked to the hull during earlier tests of the model in damaged conditions.

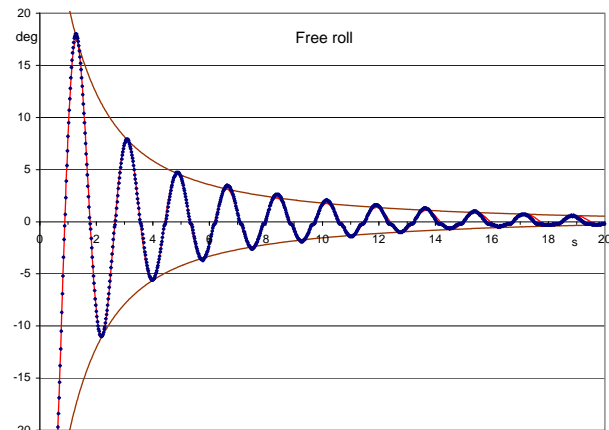
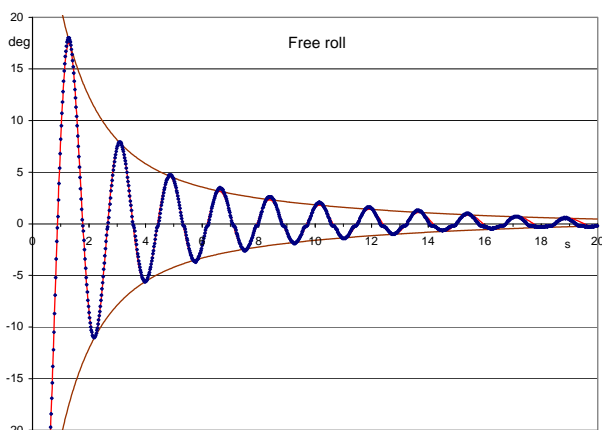


Figure 1. Free roll of a vessel in the intact condition and the run of instantaneous amplitudes

Linear free roll of the ship is described by the equation

$$\phi = \phi_0 + \alpha e^{-\nu t} \cos(\omega t + \varepsilon), \quad (6)$$

where  $\phi_0$  is a bias (initial heel),  $\alpha$ ,  $\nu$ , and  $\varepsilon$  are constants,  $\omega = (\omega_0^2 - \nu^2)^{1/2}$  is the circular frequency of free roll,  $\omega_0^2$  equals the coefficient of stability  $Dh_0$  related to the virtual moment of inertia around the longitudinal axis  $J_x + m_{44}$ , and  $\nu$  is the logarithmic decrement of damping. The last characteristic value is defined by the equation:  $2\nu = N/(J_x + m_{44})$ , where  $N$  is the damping coefficient. The first two factors in equation (6) can be treated as amplitude at given time instant:

$$a = \alpha e^{-\nu t}. \quad (7)$$

For non-linear free roll with finite initial amplitude, the logarithmic decrement of damping  $\nu$  varies in the course of time. How it varies, it is not easy to establish, since the problem is ill conditioned. One possibility is to replace the exponent  $\nu t$  in equation (6) and (7) by the integral (cumulative) curve of the logarithmic decrement

$$C = \int_0^t \nu(\tau) d\tau = \bar{\nu} t, \quad (8)$$

and approximate  $C$  versus time, which can be done through regression. The quantity  $\bar{\nu} = C/t$  is the mean cumulative decrement, whereas  $\dot{C} = \nu$  is the instantaneous (actual) decrement of damping. As the actual decrement  $\nu$  and amplitude  $a$  are both functions of time, this indirectly defines the instantaneous  $\nu$  as the function of the instantaneous amplitude of roll  $a$ .

Similarly, as the circular frequency of free roll slightly varies in the course of time, the quantity  $\omega t$  in equation (6) should be also replaced by the integral curve of the circular frequency

$$\Omega = \int_0^t \omega(\tau) d\tau = \bar{\omega} t, \quad (9)$$

where  $\bar{\omega} \approx (\omega_0^2 - \bar{\nu}^2)^{1/2}$ , which can be proved rigorously. In other words, in the case of non-linear free roll  $\omega t$  is replaced by  $\bar{\omega} t$ .

### APPROXIMATIONS

Various approximations can be used for  $C = C(t)$ , either by approximating the mean cumulative decrement  $\bar{\nu}$ , or the actual decrement  $\nu$ . Best results in both cases give the exponential approximation

$$\nu = \nu_\infty + \beta e^{-\gamma t}, \quad (10)$$

where  $\nu_\infty$ ,  $\beta$  and  $\gamma$  are constants, which can be found with the help of the least squares method, using e.g. Solver in Excel. When the mean cumulative decrement  $\bar{\nu}$  is approximated, the actual decrement is obtained from the equation  $\nu = \dot{C} = d/dt(\bar{\nu}t)$ . When the actual decrement  $\nu$  is approximated, the mean cumulative decrement  $\bar{\nu}$  is obtained from equation (8).

The exponential approximation for the mean accumulated decrement is shown in Figure 1 on the left, and for the actual decrement on the right for the same run of free roll. As can be seen, both provide exceptionally good approximations, nearly identical with the real run, proving validity of equation (6) also for non-linear roll, with  $\nu t$  replaced by the integral  $C$ .

Graphs of the mean cumulated and actual decrements as the function of time are shown in Figure 2. Curve 1 concerns approximation of the mean decrement, and curve 2 the instantaneous decrement. As can be seen, the two approximations provide almost identical runs of the coefficients  $\bar{\nu}$ . The same applies to runs of the instantaneous values of  $\nu$  for about half of time, when amplitudes of roll are large. Afterwards the two curves diverge. Curve 1 for the instantaneous values of  $\nu$  falls below its asymptotic value, which is wrong. And this can be taken as a rule – approximations of the mean cumulated decrement do not guarantee that the instantaneous decrement will fall monotonically to its asymptotic value. For this reason, it is better to approximate the run of the actual rather than mean decrement. For the latter case the asymptotic value  $\nu_\infty = 0.225/s$  and for the former  $\nu_\infty = 0.134/s$ .

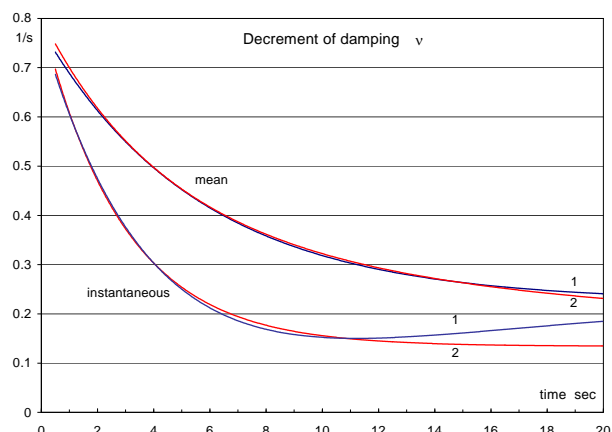


Figure 2. Decrement of roll damping  $\nu$  as function of time

The resulting prediction of the actual logarithmic decrement  $\nu$  as the function of the instantaneous amplitude of roll is shown in Figure 3 along with

values obtained from the ratio of amplitudes for each cycle, normally used in tests. Using equation (6), with  $\nu t$  replaced by the integral  $C$ , yields

$$\nu^* = (1/T) \ln(a_n/a_{n+1}), \quad (11)$$

where  $T$  is a period of roll, and  $a_n/a_{n+1}$  is the ratio of two consecutive amplitudes, understood as two consecutive extreme values of roll of the same sign. The quantity  $\nu^* = (C_{n+1} - C_n)/T$  is nothing other than the mean decrement of damping over one cycle. These values, taken at the average amplitude  $\frac{1}{2}(a_n + a_{n+1})$ , are marked with triangles in Figure 3, and approximated by a quadratic curve.

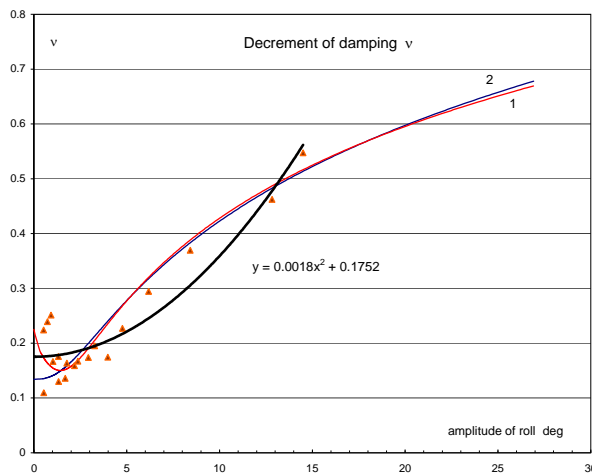


Figure 3. Decrement of damping  $\nu$  versus roll amplitude along with measured values and a quadratic approximation

As can be seen, the two approximations provide almost identical prediction of the coefficient  $\nu = \nu(a)$ , except the initial value, well supported by measured values. Curve 1, based on approximation of the mean cumulated decrement has clearly an incorrect run in the neighbourhood of zero, as it falls below the initial (asymptotic) value. On the other hand, curve 2, based on approximation of the instantaneous decrement has an ideal run in the neighbourhood of zero, with vanishing odd derivatives at zero, as in the case of even functions. However, a quadratic approximation is clearly insufficient for that purpose. Things look better, if a biquadratic approximation is used, as shown in Figure 4.

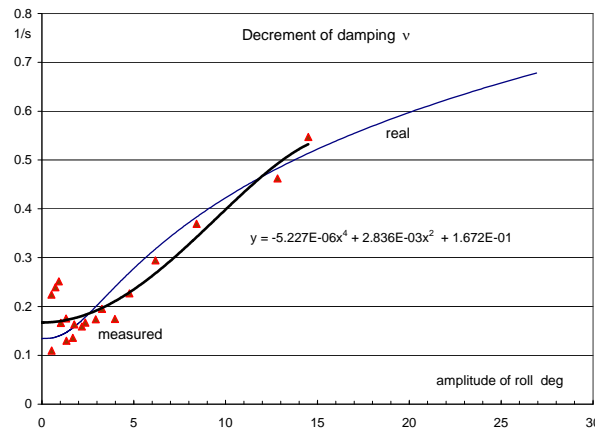


Figure 4. Biquadratic approximation of measured values versus the real run of  $\nu$  as function of amplitude of roll

The existence of a plateau in the neighbourhood of zero is self-explanatory, if someone realises that for small amplitudes of roll the logarithmic decrement of damping  $\nu = const$ . On this ground we can expect that all the odd derivatives vanish at zero and the function  $\nu(a)$  is even.

Sometimes the coefficient  $\nu = \nu(a)$  is found for each half cycle

$$\nu^* = (2/T) \ln(a_{n+1/2}/a_n), \quad (12)$$

where  $a_{n+1/2}/a_n$  is the ratio of two consecutive amplitudes, understood as two consecutive extreme values of roll, of opposite sign. But this does not help at all. Because measurements of roll are of limited accuracy, a pretty high scatter of points is then obtained, particularly when the amplitude of roll becomes small. Therefore, using half cycles for calculating the coefficient  $\nu$  is not recommended.

Looking at the measured values someone could think that a linear approximation would be best, as shown in Figure 5, supporting the current generally accepted assumption that damping moment in ship roll is an odd quadratic expression

$$M = N_1 \dot{\phi} + N_2 \dot{\phi} |\dot{\phi}|,$$

where  $N_1$  and  $N_2$  are constants. Ikeda (1978) provides a method for the prediction of the two coefficients.

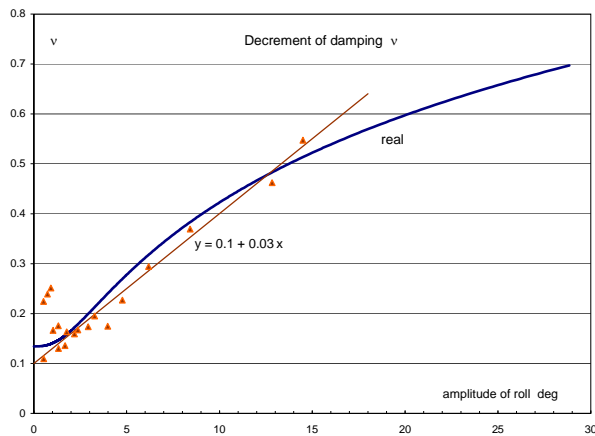


Figure 5. Linear approximation of measured values of  $v$

Regarding measured values of the actual decrement, using the instantaneous amplitudes we can get the actual values of decrement almost as the continuous function of time. To this end equation (11) should be applied to any two amplitudes taken at time instants far away each other by  $T$  seconds. Values calculated this way are shown in Figure 6, which are almost identical with the instantaneous values of decrement  $v$ .

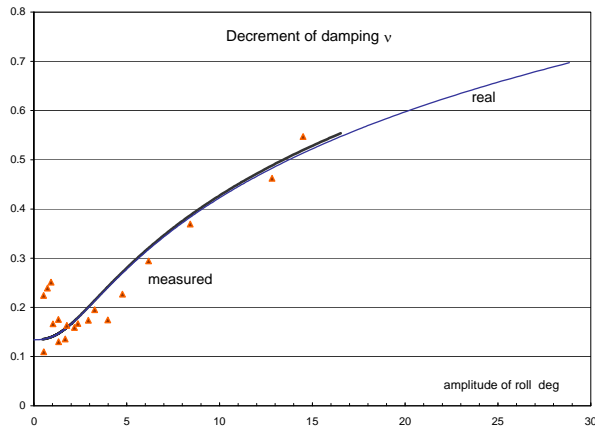


Figure 6. Characteristic and real values of  $v$

Although the actual decrement is an even function, it is extremely difficult for approximation with the help of even polynomials. Use of three terms, i.e. applying a biquadratic approximation, as shown in Figure 7, is clearly inadequate, whereas using more terms creates numerical problems with definition of high degree polynomials and is undesirable in applications. For that reason we are forced to resort to odd non-analytical polynomials with  $||$ .

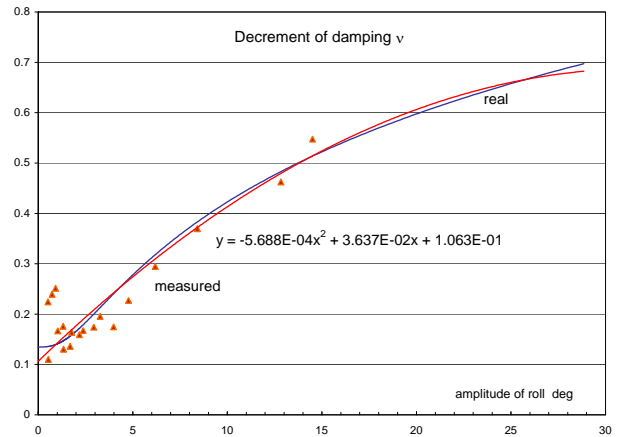


Figure 8. Quadratic approximation of actual values of decrement of damping

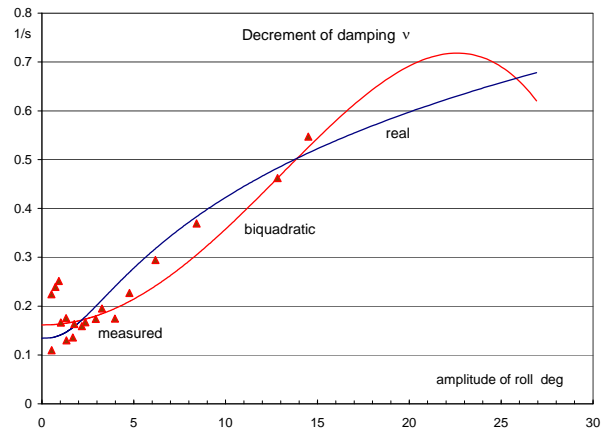


Figure 7. Biquadratic approximation of actual values of decrement of damping

If we abandon the condition of symmetry and use regular polynomials, the instantaneous decrement of damping can be very easily and accurately approximated by quadratic polynomials, as shown in Figure 8. The differences are hardly visible. Numerical quality of approximation is impressive, particularly if compared with Figure 7, though in both cases the same number of terms (three) is used. Application of regular polynomials is contradictory with the basic assumption made earlier, but is necessary due to practical reasons.

### REALISTIC ASSUMPTION

Adopting regular polynomials for the coefficient  $v = v(a)$  is equivalent to the assumption that the damping moment is a non-analytic odd function of the speed of roll  $\dot{\phi}$ , that can be expanded into a power series, containing even terms with  $||$

$$M = N_1 \dot{\phi} + N_2 \dot{\phi} |\dot{\phi}| + N_3 \dot{\phi}^3 + N_4 \dot{\phi}^3 |\dot{\phi}| + N_5 \dot{\phi}^5 + \dots \quad (13)$$

Equating work done, as before, over one cycle yields

$$N_1 (\omega a)^2 \frac{1}{2} T + N_2 (\omega a)^3 \frac{4}{3\pi} T + N_3 (\omega a)^4 \frac{3}{8} T + N_4 (\omega a)^5 \frac{16}{15\pi} T + N_5 (\omega a)^6 \frac{5}{16} T + \dots = N (\omega a)^2 \frac{1}{2} T, \quad (14)$$

Recalling the previous recurrence identity, it is easy to find the coefficients at even damping coefficients  $N_2, N_4, N_6, \dots$ . Since  $I_1 = \frac{2}{\pi} T$ , the coefficient at  $N_2$  equals  $\frac{2}{3} \cdot \frac{2}{\pi} = \frac{4}{3\pi}$ , at  $N_4$  equals  $\frac{4}{5} \cdot \frac{4}{3\pi} = \frac{16}{15\pi}$ , at  $N_6$  equals  $\frac{6}{7} \cdot \frac{16}{15\pi} = \frac{32}{35\pi}$ , and so on.

Equation (14) yields a polynomial for the equivalent coefficient of damping relative to the amplitude of roll:

$$N = N_1 + \frac{8}{3\pi} N_2 (\omega a) + \frac{3}{4} N_3 (\omega a)^2 + \frac{32}{15\pi} N_4 (\omega a)^3 + \frac{5}{8} N_5 (\omega a)^4 + \dots, \quad (15)$$

In most cases it is sufficient to take four terms in the above expansion. Dividing the above equation throughout by the virtual inertia  $J_x + m_{44}$ , we get

$$b = b_1 + \frac{8}{3\pi} b_2 (\omega a) + \frac{3}{4} b_3 (\omega a)^2 + \frac{32}{15\pi} b_4 (\omega a)^3 + \frac{5}{8} b_5 (\omega a)^4 + \dots, \quad (16)$$

where  $b_1, b_2, b_3, \dots$  are constant, independent of  $a$ . As dimension of  $b$  is 1/s, the same dimension has the coefficient  $b_1$ , the coefficient  $b_2$  has no dimension, dimension of  $b_3$  is s,  $b_4$  is s<sup>2</sup>,  $b_5$  is s<sup>3</sup>, and so on. Because  $b = 2\nu$ , therefore

$$\nu = \frac{1}{2} b_1 + \frac{4}{3\pi} b_2 (\omega a) + \frac{3}{8} b_3 (\omega a)^2 + \frac{16}{15\pi} b_4 (\omega a)^3 + \frac{5}{16} b_5 (\omega a)^4 + \dots, \quad (17)$$

A graph of  $\nu$  is needed from free roll tests, as shown in Figure 8. In this case a two-degree approximation fits almost perfectly the run of instantaneous values of the decrement  $\nu$ .

### USE OF THE APPROXIMATION

Knowing polynomial approximation of the experimental decrement  $\nu$  relative to the amplitude of roll, as shown in Figure 8, the coefficients of damping  $b_1, b_2, b_3, \dots$  can be easily defined by comparing expansion (17) with the approximation of  $\nu$ . By doing so, we have to remember that the amplitude  $a$  in equation (17) is in radians, whereas in Figure 8 – in degrees. Hence,

$$\begin{aligned} \frac{1}{2} b_1 &= 0.10632/s \\ \frac{4}{3\pi} b_2 \omega &= 0.036370 \cdot (180/\pi)/s, \\ \frac{3}{8} b_3 \omega^2 &= -0.00056883 \cdot (180/\pi)^2/s, \end{aligned}$$

The mean circular frequency for the model investigated equals  $\omega = 3.54/s$ . Hence, the coefficients  $b$  for the model are, as follows

$$\begin{aligned} b_1 &= 0.21264/s, \\ b_2 &= 1.3870 s, \\ b_3 &= -0.39737 s^3. \end{aligned}$$

For the ship, they have to be rescaled according to the laws of modeling. Since the model is in the scale 1:50, one second in real scale is  $50^{1/2} \approx 7.07$  longer than in model scale. Therefore, the coefficients  $b$  for the vessel are, as follows

$$\begin{aligned} b_1 &= 0.0301/s, \\ b_2 &= 1.3870 s, \\ b_3 &= -2.8098 s^3. \end{aligned}$$

The virtual moment of inertia for the ship around the longitudinal axis equals  $J_x + m_{44} = 2204569 \text{ ton m}^4$ . Hence, the two first damping coefficients are these:  $N_1 = 66295 \text{ ton m}^4/s$ , and  $N_2 = 3057718 \text{ ton m}^4$ .

According to Ikeda, the two values are, as follows:  $N_1 = 61900 \text{ ton m}^4/s$ , and  $N_2 = 1120682 \text{ ton m}^4$ . They amount to 93.4% and 36.7% of the real values. In model scale, they correspond to  $b_1 \approx 0.199/s$ ,  $b_2 \approx 0.508$ . Such coefficients give a straight line in Figure 5 described by the equation:  $\nu = 0.0993 + 0.0133a$ . It crosses the ordinate axis at a point  $\nu \approx 0.099/s$ , practically the same as for the subject model, but with inclination merely 44.3% (more than twice smaller) of the inclination for the linear regression, shown in Figure 5. It happens despite the fact that the Ikeda's coefficient  $N_2$  includes the effect of bilge keels.

Knowing the damping moment, it is easy now to get the equation for free roll

$$(J_x + m_{44}) \ddot{\phi} + M + Dh_0 \phi = 0,$$

where  $M$  is the damping moment, given by equation (13). Dividing it throughout by the virtual moment of inertia  $J_x + m_{44}$ , we get

$$\ddot{\phi} + b_1 \dot{\phi} + b_2 \dot{\phi} |\dot{\phi}| + b_3 \dot{\phi}^3 + b_4 \dot{\phi}^3 |\dot{\phi}| + b_5 \dot{\phi}^5 + \omega_0^2 \phi = 0, \quad (18)$$

where  $b_1, b_2, b_3, b_4, b_5$  are the normalized coefficients of damping, as derived above. The angle  $\phi$  is in ra-

dians. To get roll simulations in degrees, the angle  $\phi$  should be replaced by  $\phi \cdot \pi/180$ .

It is worth noting that the virtual moment of inertia  $J_x + m_{44}$  corresponds to a virtual (physical) axis of rotation, located at the virtual ship mass centre (the mass centre for the ship along with the added mass in sway), as discussed by Balcer (2004). For the ship investigated, the virtual axis lies 2.79 m below the ship centre of gravity.

Using free roll tests we get the virtual moment of inertia related to the virtual axis of rotation. By calculations, this quantity value is provided normally for the axis passing through the mass centre of the ship. If this is the case, we have to remember to transform it to the virtual axis.

The above coefficients of damping have been derived based on equation (16), valid for a forced harmonic roll with constant amplitude of roll. Here arises a question, if they are valid for free roll, with gradually decaying amplitude and damping? For free roll equation (16) is still valid provided that we take the mean values for  $a$  and  $b$  at given cycle. A graph of the mean decrement of damping  $\nu$  versus the mean amplitude  $a$  is, however, exactly the same as graphs based on instantaneous values, termed 'real', shown on the previous figures. On this basis we can expect that damping coefficients are valid not only for free roll but also for roll in natural conditions.

## CONCLUSIONS

Based on the results and arguments presented in this paper the following conclusions can be drawn:

- from the theoretical point of view, the damping moment is an odd *analytic* function, which is, however, difficult to expand into a power series, containing odd terms only
- in terms of approximation the damping moment behaves as if it was an odd *non-analytic* function that can be neatly expanded into a power series, containing even terms with ||
- the standard method for definition of  $\nu$ , based on the ratio of two consecutive amplitudes is correct also for non-linear roll, but of limited meaning
- approximation of free roll can provide robust values for the instantaneous decrement  $\nu$  as a function of the instantaneous amplitude of roll
- assuming that the instantaneous decrement is identical with the equivalent value, obtained

from equating work done over one cycle, allows for definition of the coefficients of non-linear damping, needed in simulations of ship motions.

## ACKNOWLEDGEMENTS

This work evolves from discussion that took place after the 9<sup>th</sup> Stability Workshop in Hamburg, 2007. Dr Andrzej Laskowski of the Polish Register of Shipping is acknowledged for providing a number of free roll simulations with a quadratic decrement of damping, as in Figure 3. The simulations were not very satisfactory, particularly for large amplitudes at the beginning of roll, which encouraged the author for further analysis, presented in this paper.

## REFERENCES

- Balcer, L.: Location of ship rolling axis, Polish Maritime Research, No 1(39), 2004, Vol. 11, pp. 3–7, [http://www.bg.pg.gda.pl/pmr/pdf/PMRes\\_2004\\_1.pdf](http://www.bg.pg.gda.pl/pmr/pdf/PMRes_2004_1.pdf)
- Blocki, W.: Bezpieczeństwo statku związane z rezonansem parametrycznym (Safety of the ship related to parametric resonance), PhD thesis, TU Gdansk, 1977, 106 pp.
- Blocki, W.: Ship safety in connection with parametric resonance of the roll, *International Shipbuilding Progress*, Vol. 27, No. 306, February 1980, pp. 36–53.
- Ikeda, Y.: A prediction method for ship roll damping, Report No 00405, Dept. of Naval Architecture, University of Osaka Prefecture, 1978.
- McCue, L., and Campbell, B.: Approximation of ship equations of motion from time series data, 9<sup>th</sup> Int. Ship Stability Workshop, Hamburg, Germany, August 2007, Paper 20, 9 pp.
- Pawłowski, M.: An approximation to the righting arm curve, Technical Report, NAOE–87–50, Dept. of Naval Architecture & Ocean Eng., University of Glasgow, 1987, 28 pp. ■



## **Flooding simulations of ITTC and SAFEDOR benchmarks test cases using CRS SHIPSURV software**

Philippe Corrigan,  
Bureau Veritas

Ana Arias,  
Navantia

### **ABSTRACT**

SHIPSURV is a project of the Cooperative Research Ships (CRS) community, devoted to the development of tools and methodologies for the assessment of the survival capability of a ship after damage. This paper describes results obtained during one task of the ongoing validation process of the developed tool Pretti-flooding, which couples a seakeeping code with a progressive flooding simulation module. The task consisted in simulating test cases of the ITTC benchmark (flooding of a box shaped barge in calm water) and test cases of the benchmark carried out in the SAFEDOR project (determination of the survival wave height for a damaged RoPax in waves).

### **KEYWORDS**

Damage stability; progressive flooding; numerical simulation.

### **INTRODUCTION**

The SHIPSURV project of the Cooperative Research Ship community aims at providing ship designers and operators with a methodology to identify which measures can be taken to increase the survivability of a damaged ship experiencing flooding after an accident such as grounding or collision. One of the major objectives was to develop and validate a numerical tool for the prediction of the damaged ship motion and internal loads on a seaway. In this purpose, a flooding simulation tool was developed by MARIN with funding of the CRNav (Cooperative Research Navies) and has been made available to the CRS community via a collaboration agreement signed between the CRNav and the CRS SHIPSURV working group. Then a validation process of this software, called Pretti-flooding, has started.

One of the first validation tasks consisted in performing numerical simulations for test cases

defined in previous flooding software international benchmarks, namely: ITTC benchmark (model tests performed by the University of Helsinki on a barge) and SAFEDOR benchmark (model tests performed on the Ropax ship “PRR02” in the EU HARDER project).

This paper presents comparisons of the obtained results with the numerical results and/or available experimental data published for these benchmarks.

### **NUMERICAL METHOD**

SHIPSURV Pretti-flooding software is a time domain simulation code for the prediction of the behaviour of a damaged ship experiencing progressive flooding. The program consists of a time domain 6 DOF seakeeping code. The actual waterline is evaluated at each time step. Hydrostatic and wave pressures are integrated over the actual wetted surface. Diffraction forces are obtained by solving the potential

flow problem. Radiation forces are calculated using the Cummins equations. Additional forces from water ingress and progressive water flooding through the ship are included using a hydraulic flooding water model, based on the Bernoulli equation, with discharge and head loss coefficients defined respectively in openings and in ducts. The free surface in flooded compartments is assumed to remain horizontal at any time. Air compression effects can be modelled. Thus, a complete calculation is performed in three successive steps: hydrodynamic coefficient frequency domain calculation, floodable compartments tank tables calculation and time domain seakeeping and progressive flooding calculation.

**ITTC BENCHMARK**

**Benchmark description**

Following an invitation from the 48<sup>th</sup> session of the IMO/SLF sub-committee, the ITTC Stability in Waves committee organised a benchmark test of time domain flooding simulation tools (see *ITTC (2007)*). The benchmark consisted in modelling the time domain behaviour of a box shaped barge in six different flooding scenarios in calm water, which had been previously modelled experimentally by the Technical University of Helsinki (see *Ruponen (2006)*).

The study performed in SHIPSURV consisted in reproducing these six scenarios and in comparing the time domain behaviour with experimental measurements.

**Barge model tests description**

The barge considered as the basis for the study was a box shaped barge with a chamfer in the bilge as shown in Fig.1. The model scale was 1:10 with a corresponding model length of 4 m and an initial transverse metacentric height of 0.11 m. The barge was arranged with eight floodable tanks (see Fig.2) located slightly forward from the midsection to reach various trim angles in flooded condition. All these compartments were opened to the atmosphere with the exception of the two ones located in the double bottom (DB1 & DB2) which were airtight.

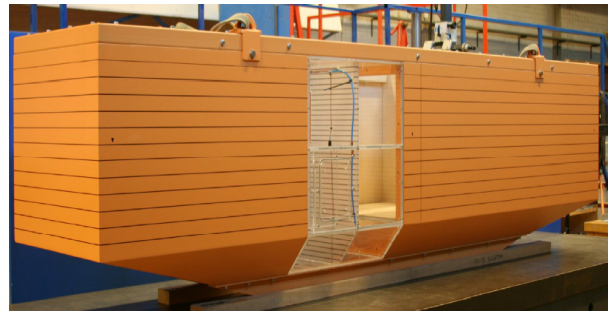


Fig. 1: Damage case arrangement

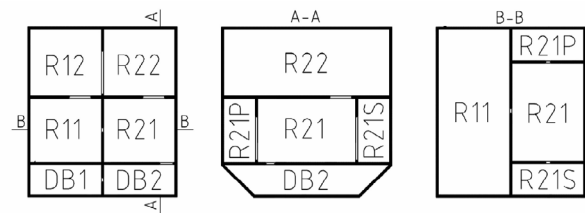


Fig. 2: Floodable compartments arrangement

The compartments were fitted with water level sensors. The double bottom compartments were also instrumented to allow air pocket pressure measurement. In addition the model heel, trim angles and draught were recorded.

The six flooding scenarios are described in Table 1. They correspond to combinations of damage location (bottom DB2 or DB1, side), size (small/large), opening between R12 and R22 (modelling a watertight door opening), allowing to obtain cross flooding and vertical flooding configurations.

**Table 1: Barge test cases:**

Name:	Damage case:	R12-R22 opening:	Special:
Test 1	Bottom DB2 small	Closed	Fixed floating pos.
Test 2	Bottom DB2 small	Closed	
Test 3	Bottom DB2 small	Open	
Test 4	Bottom DB2 large	Closed	
Test 5	Bottom DB1 large	Closed	
Test 6	Side R21S large	Closed	DB1 and DB2 not floodable

**Numerical modelling**

The barge has been modelled at full scale. Like for model tests, upper compartments R12 and R22 were fully vented and side compartments R21S and R21P were vented by pipes connected to the atmosphere. Discharge coefficients of openings and head loss coefficients of pipes identified by

Ruoponen (2006) have been used for simulations. A roll decay test was also available in Ruoponen (2006). However, the corresponding experimental roll damping ratio (1.9%) was smaller than the calculated potential roll damping ratio (6.2%). Consequently, no viscous roll damping has been added in simulations. Finally, simulations have been carried out with three free degrees-of-freedom (heave, roll and pitch), except for Test 1 performed with no free degree-of-freedom (fixed barge).

**Results**

For modelling reasons, comparisons have been performed at full scale, by extrapolating model test results using Froude scaling. This does not allow to fully correctly scale air compression effects. In addition, calculated free surface levels in flooded compartments had to be post-processed to obtain water heights as delivered by Ruoponen (2006) and defined as the free surface height above the keel line amidships.

Test 3 (bottom damage), whose comparison with experimental results is representative of those obtained also for Tests 2, 4 and 5, and Test 6 (side damage) are presented hereafter.

**Test 3 (bottom damage)**

Test 3 is a bottom (DB2) damage case. The corresponding flooding sequence is illustrated on Fig.3.

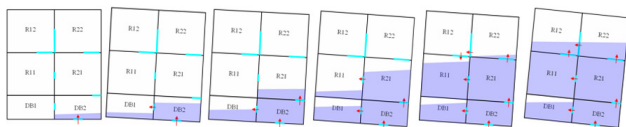


Fig. 3: Test 3 flooding sequence

A good agreement is obtained between predicted and measured trim and heave time histories, as shown on Fig.4.

Fig.5 shows that predicted water height in DB1 is very close to the experimental one. The predicted maximum height corresponds to the fully filled condition, which is not the case for the measurement. R21 water height predictions are also very close to experimental ones, with

again a maximum consistent with a fully filled compartment. For DB2, the same maximum values are reached at the equilibrium. However, the calculated height rises earlier and quicker than the measured one. According to the modelling, the water height in DB1 should increase as soon as the free surface in DB2 reaches the opening between these compartments and water starts flooding DB1.

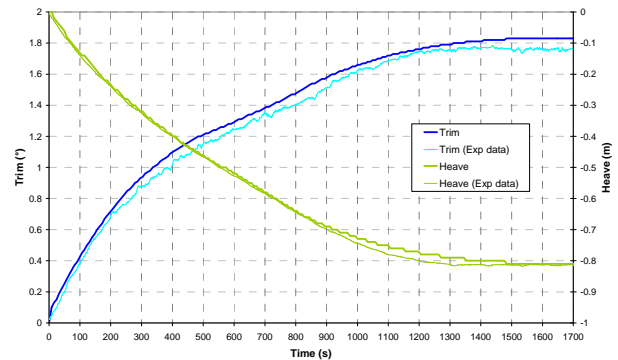


Fig. 4: Test 3 predicted vs exp. trim and heave

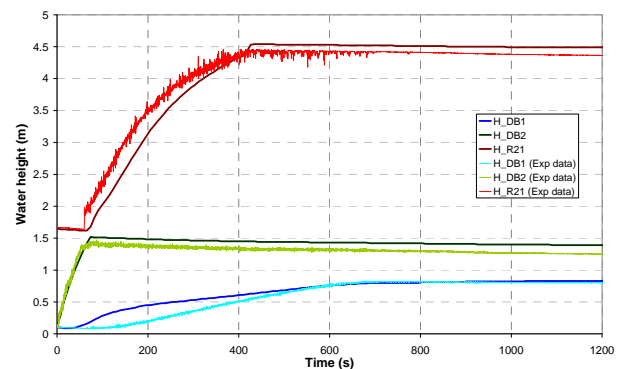


Fig. 5: Test 3 predicted vs exp. water height (DB1, DB2, R21)

This is observed on the predicted DB1 water height, but not on the measured one. This phenomenon has been encountered for all tests with damage in DB2, but not on Test 5 with a damage in DB1, which could suggest a relation with the water height measurement in DB1 and/or the modelling of the start of flooding of DB1 through the side opening.

In other compartments R11, R21 and R22, fairly good agreement is obtained between predicted and measured water heights (see Fig.6).

Finally, similar trends are obtained on pressures on the top of the two double bottom

compartments (see Fig.7). The predicted pressure difference between the two compartments at equilibrium (5480 Pa) is consistent with the predicted difference of water heights inside these compartments (0.55 m), whereas the difference in measured pressures (650 Pa) is not consistent with the difference in measured water heights (0.42 m).

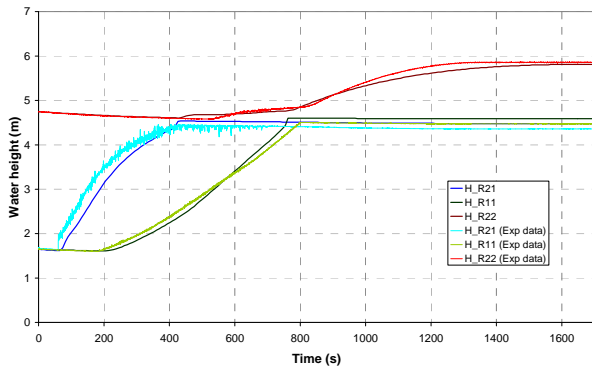


Fig. 6: Test 3 predicted vs exp water height (R11,R21,R22)

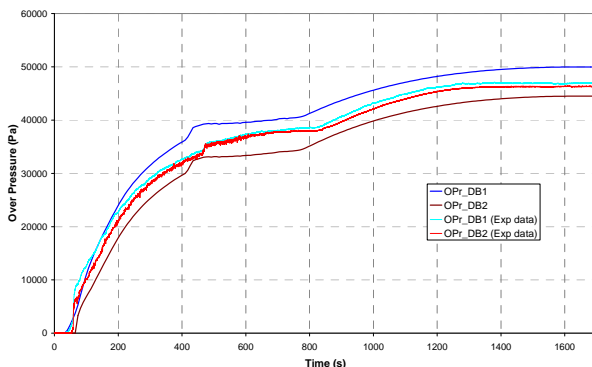


Fig. 7: Test 3 predicted vs exp. tank top pressure (DB1, DB2)

**Test 6 (side damage)**

Test 6 is a side (R21S) damage case, leading to an unsymmetrical flooding yielding roll motion in addition to heave and pitch.

Good agreement between predicted and measured draught and trim angle at equilibrium has been obtained, with discrepancies of 4.5% and 2.7% respectively. A larger difference is observed on roll motion with a predicted peak roll angle almost five times the measured one (see Fig.8). In addition, the measured roll motion exhibits an unexpected and unpredicted oscillatory behaviour, with a period (5.7 s) lower than the roll natural period of the barge (between 5.9 and 6.3 s).

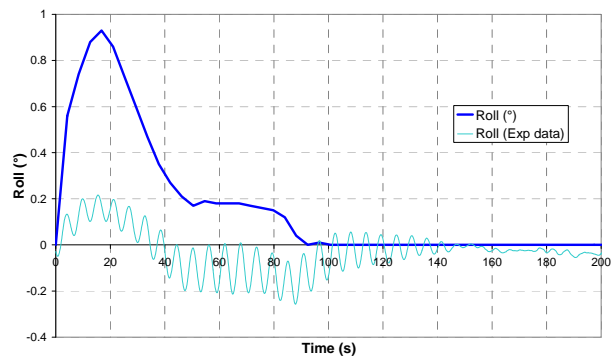


Fig. 8: Test 6 predicted vs exp. roll motion

Significant differences have also been obtained on the water heights in compartments R21S, R21 and R21P (see Fig.9). Predicted water heights in R21S and R21P are respectively larger and lower than the measured one, which is consistent with the larger predicted roll motion towards the damage.

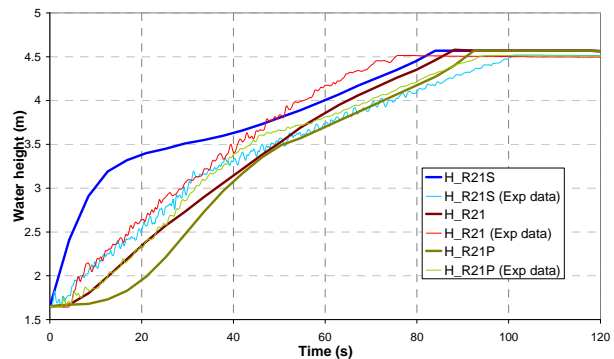


Fig. 9: Test 6 predicted vs exp. water height (R21S,R21,R21P)

Better agreements have been obtained in other compartments, as shown on Fig. 10.

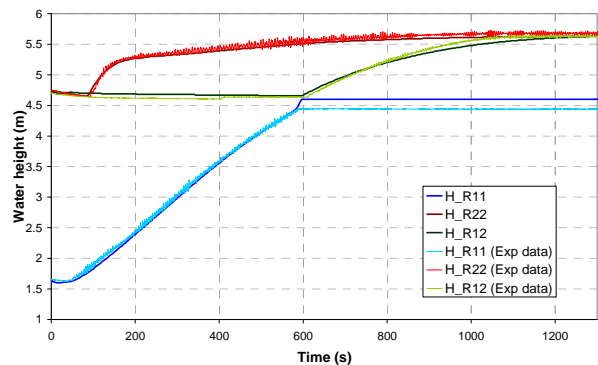


Fig. 10: Test 6 predicted vs exp. water height (R11,R12,R22)

## SAFEDOR BENCHMARK

### Benchmark description

The EU project SAFEDOR organised an international benchmark study on numerical codes for the prediction of the motions and flooding of damaged ships in waves. The study, which is described by *Spanos & Papanikolaou (2008)*, consisted in comparing the performance of four software codes to simulate the response of a damaged ROPAX on beam irregular waves, for five specified numerical cases and one specified additional case for which model experimental data were available. For the five numerical cases, the study consisted in comparing the prediction of the so-called survival boundary  $H_{s_{surv}}$ , defined as  $P(\text{capsize} | H_s \leq H_{s_{surv}}) \leq 5\%$  made by each code. For the sixth case (“Seakeeping test”), the predicted ratios of roll motion *rms* value in intact condition to roll motion *rms* value in damage condition have been compared to the experimental one.

The study performed in SHIPSURV consisted in comparing, for three out of the first five test cases, the survival boundary obtained by Pretti-flooding with the ones obtained in SAFEDOR with the four codes, and, for the sixth case, in comparing the ratio of roll motions in intact/damage conditions predicted by Pretti-flooding, with the experimental ones.

### Test cases description

Tests are performed on the PRR02 ROPAX ferry which has been investigated before within the European research project HARDER (2000-2003). It is designed according to SOLAS 90 stability standard, with main particulars as given in Table 2:

**Table 2: PRR02 main particulars:**

Length, $L_{pp}$ (m)	174.80
Beam, $B$ (m)	25.0
Draft, $T$ (m)	6.40
Depth, $D$ (m)	9.10
KG (m) / $i_{xx}$ (m) basic / GMt	12.33 / 10.5 / 2.1
KG (m) / $i_{xx}$ (m) reduced / GMt	11.33 / 10.1 / 3.1

The ship is equipped with bilge keels. The damage case refers to the damage of two adjacent compartments located amidships and corresponds to the worst SOLAS 90 damage case. The length of the damage opening is 8.25 m ( $3\%L+3.00$  m), with a triangular penetration and unlimited vertical extent causing damage to the vehicles space on the main deck too. This arrangement leads to seven floodable compartments (see Fig.11).

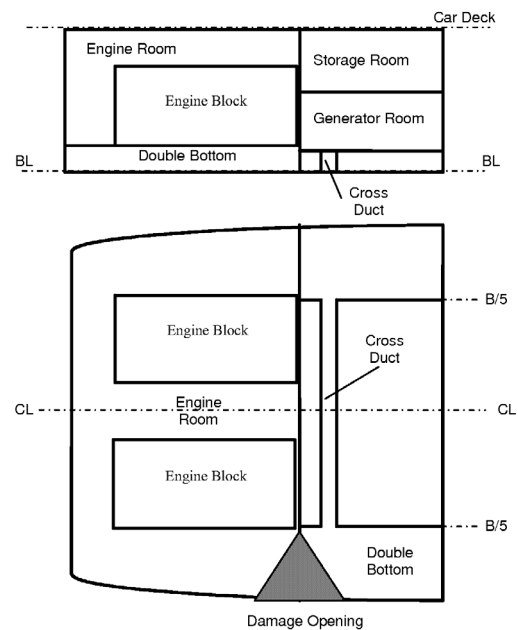


Fig. 11: Damage case arrangement

Tests are performed on irregular beam waves. Table 3 below describes the four cases that have been used in SHIPSURV.

**Table 3: SAFEDOR benchmark test conditions used in SHIPSURV:**

Test	Reference	Description / difference wrt Test 1
1	Basic	$KG=12.3m$ , $T_p = 4\sqrt{H_s}$ , $\gamma=3.3$ , $B44_{v-basic}$ , $C_{discharge-basic}$
4	High roll viscous damping	$B44_{v'}=2 \times B44_{v-basic}$
5	Reduced $C_D$	$C'_{discharge}=0.5 \times C_{discharge-basic}$
6	Seakeeping	$KG=11.3m$ , $T_p=10.4s$ , $\gamma=1$ , $H_s=3m$ , damage 30min after simulation starts

### Numerical modelling

In Pretti-flooding, openings are geometrically described by four corners, and characterised by a discharge coefficient. The V-shaped damage opening was thus modelled by a series of horizontal triangular elements and vertical rectangular elements, as described on Fig.12.

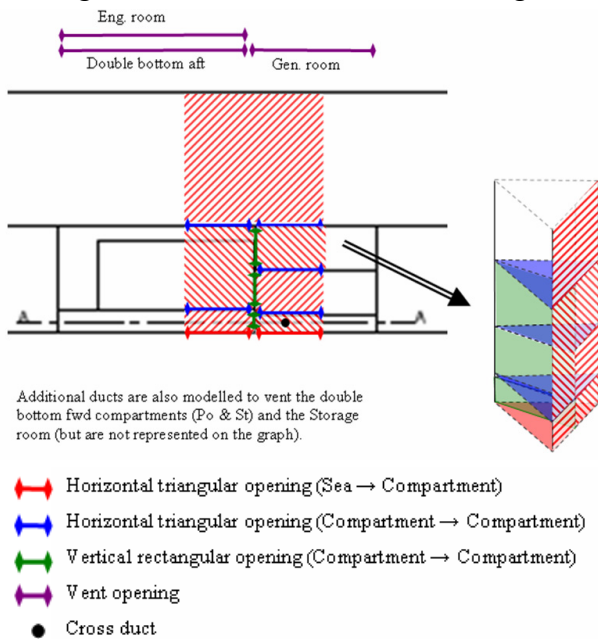


Fig. 12: Modelling of damage opening & compartments venting

A discharge coefficient value of 0.6 has been used for all these elements. For the duct connecting the two double bottom compartments, a head loss coefficient of 1.78 has been used.

All compartments have been vented to remove air compression effects.

A linear plus quadratic formulation has been used for modelling the ship roll damping. The corresponding terms have been identified, for both KG conditions, from the roll decay test presented in *Spanos & Papanikolaou (2008)*.

A spring and dashpot have been added in the transverse horizontal direction in order to leave the model free from swaying, while removing the drift due to wave forces. The added stiffness and damping have been adjusted to obtain a sway natural period of 120 s with a 10% damping ratio.

Before running flooding simulations on irregular waves, preliminary checks have been performed on the calculated GZ curve and natural roll frequency in intact condition. The calculated GZ curve lies within the ones calculated by the four SAFEDOR benchmark codes (see Fig.13).

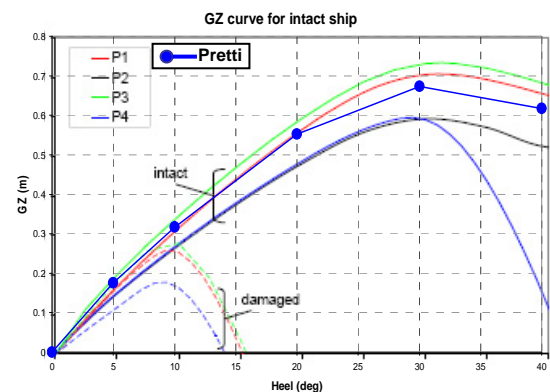


Fig. 13: GZ curves for intact ship calculated by Pretti and other SAFEDOR codes

**Table 4: Comparison between calculated and experimental roll natural frequencies:**

KG (m)	Roll natural frequency		
	Calculated (rad/s)	Experimental (rad/s)	Difference (%)
12.33	0.395	0.388	1.8
11.33	0.492	0.491	0.2

In addition, differences lower than 2% have been obtained between the calculated and the experimental roll natural frequencies (see Table 4).

### Results of irregular wave tests

Simulations have been performed by considering, as in SAFEDOR benchmark, that the ship capsizes if the roll angle exceeds 30 deg, or if the average roll angle over a period of 30 minutes exceeds 20 deg.

Five significant wave heights have been tested for tests 1, 4 and 5.  $H_s$  values have been determined iteratively by starting, for each test, with the lower and higher  $H_{s,surv}$  obtained in SAFEDOR, and then, according to the results obtained with Pretti-flooding, by dichotomy in order to bound  $H_{s,surv}$  until five wave heights have been tested. For each  $H_s$ , ten 30 minutes duration simulations have been performed: five runs by opening the damage at the start of the

simulation and five runs with a damage opened 2000 s after the start of the simulation. New wave spectrum random phases have been generated for each simulation.

The capsizing probabilities obtained for the three test cases are presented on Fig.14.

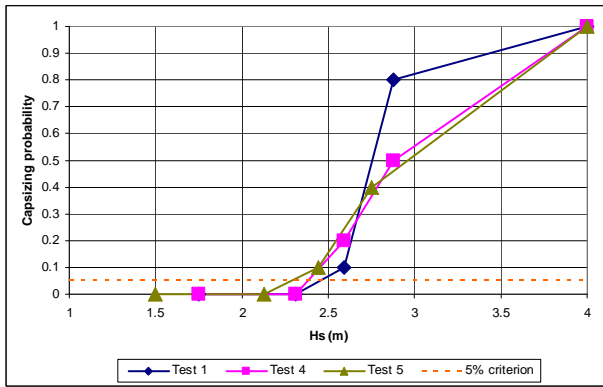


Fig. 14: Capsizing probabilities obtained with Pretti-flooding  
The corresponding 5% probabilities derived from Fig.14 are compared to the ones obtained in the SAFEDOR benchmark on Fig.15.

Pretti-flooding predictions are in the lower range of the SAFEDOR codes ones. In addition, the effect of doubling the viscous damping or dividing by two the discharge coefficients does not seem significant.

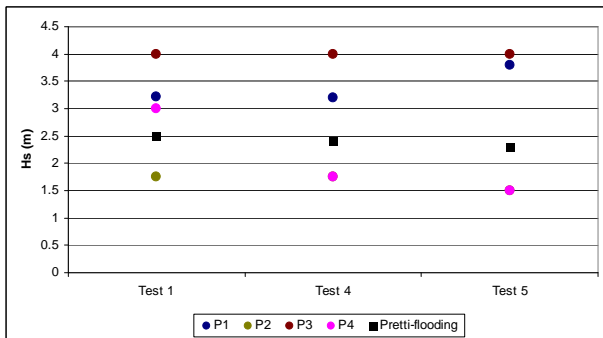


Fig. 15: Predicted 5% capsizing probabilities  
The capsizing mechanism predicted by Pretti-flooding is very similar for tests 1, 4 and 5. The amount of flooded water oscillates around an average value which is reached quickly after the damage is opened. Capsizing is then observed when a larger wave train floods the main deck.

Test 6 corresponds to a simulation on long waves. The damage is opened after 30 minutes simulation in intact condition, and is continued for additional 30 minutes. The experiments

report a 1/3 reduction of the roll *rms* value in damaged condition, with time trace of Fig.16:

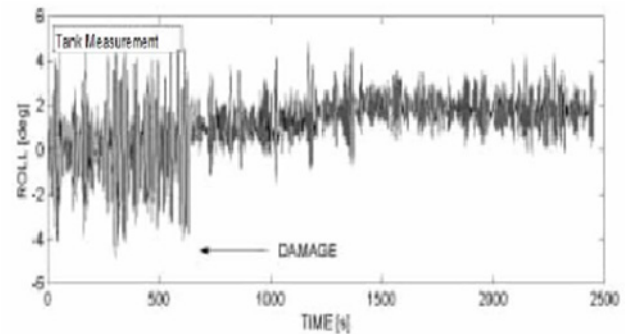


Fig. 16: Test 6: experimental roll motion before/after damage  
A similar roll response is predicted by Pretti-flooding as shown on Fig.17:

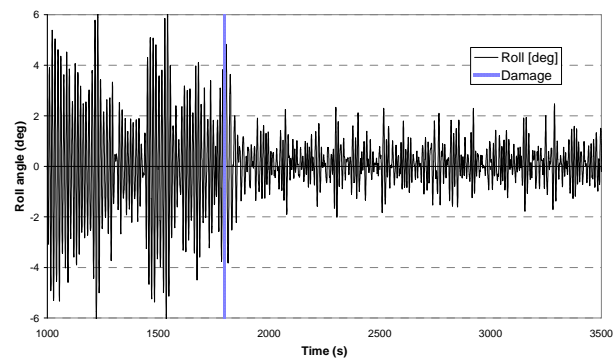


Fig. 17: Test 6: predicted roll motion before/after damage  
Pretti-flooding seems to provide a satisfactory prediction of the damaged ship roll damping, with a ratio of roll *rms* values after/before damage of 0.35, which is closer to the experimental observations than the predictions of the SAFEDOR benchmark code (see Table 5).

**Table 5: Test 6 – predicted roll rms values by SAFEDOR benchmark codes and Pretti-flooding:**

Code	Roll rms intact (deg)	Roll rms damaged (deg)	Roll rms ratio
P1	2.61	1.91	0.73
P2	2.72	2.37	0.87
P3	1.58	1.02	0.64
P4	1.84	1.80	0.98
Model tests	-	-	~0.33
Pretti-flooding	2.28	0.80	0.35

## CONCLUSION

The ITTC benchmark test cases provide relatively simple validation scenarios on calm water and with limited ship dynamics.

Good agreement has been generally obtained between Pretti-flooding predictions and model test measurements. In all cases, the results predicted by Pretti-flooding seem consistent with the assumptions on which the flooding model is based. However, some deviations in results suggest that more validation in configurations of air compression coupled with air evacuation trough openings as well as configurations of unsymmetrical flooding should be carried out.

The SAFEDOR benchmark test cases complement the above validation cases by adding the influence of irregular waves, in situations of larger ship dynamics.

The survival wave height boundary obtained for the three first test cases selected in SHIPSURV were well in the range of the values predicted by the four codes tested in the SAFEDOR benchmark.

Larger discrepancies have been obtained on predicted roll motions for the fourth “seakeeping” test, with, however, a reduction of rms roll angle between intact and damage situation closer to the available experimental data than the reductions predicted by the four codes of the SAFEDOR benchmark. It should be noted that the mechanics of capsizing, which, according to experiments, correspond to a gradual increase of floodwater, is not observed in the simulations performed with Pretti-flooding; as a matter of fact, the quantity of floodwater always reached quickly an almost constant volume, and capsizing seemed to occur after a large wave train flooding the car deck was encountered.

Further validation work, which will also include internal loads prediction, will be performed in 2011, using new model tests that will be specifically carried out in this purpose within SHIPSURV.

## ACKNOWLEDGEMENT

This work has been carried out within the SHIPSURV project of the Cooperative Research Ships ([www.crships.org](http://www.crships.org)).

## REFERENCES

- ITTC, Time dependent survivability of passenger ships in damaged condition, Progress report on benchmark testing of numerical codes for time-to-flood prediction, SLF 50/8, 2007
- Ruponen, P., A. Model tests for the Progressive Flooding of a Box-Shaped Barge, M-292, 2006
- Spanos, D.A., Papanikolaou, A. Benchmark Study on Numerical Codes for the Prediction of the Motions and Flooding of Damaged Ships in Waves, Safedor report SAFEDOR-R-7.3.4-2008-05-31.NTUA.rev-0, 2008

## **Study on the motions and flooding process of a damaged ship in waves**

SeokKyu, Cho, *MOERI/KORDI*

HongGun, Sung, *MOERI/KORDI*

SaYoung, Hong, *MOERI/KORDI*

BoWoo, Nam, *MOERI/KORDI*

YoungSik, Kim, *MOERI/KORDI*

### **ABSTRACT**

To study the motions and flooding process of a damaged cruiser, a series of experiment and numerical calculation have been performed in calm water and in waves. Two damaged parts are selected to investigate damage effects; mid section and fore section. The results of the experiment, quasi-static model and quasi-dynamic model are compared. The numerical simulation is conducted using quasi-static model and quasi-dynamic model. The quasi-dynamic model adopts the mass-spring system for internal water motion description. The model considers the dynamics of free surface as ship motion.

### **KEYWORDS**

Cruiser, Damaged, Flooding, Experiment, Sloshing

### **INTRODUCTION**

The ship accidents occurred due to various reasons; collision, running a ground, malfunctioning of an engine, attack, etc. When a ship is damaged for certain reason, she loses her function and safety. So, the evaluation of the motions and assessment of stability is very important. Many efforts have been also made for the development of numerical methods for the behaviour of damaged ship. These numerical methods have been validated and improved by the international benchmark studies such as those done by ITTC and HARDER project. Up to now it is believed that the numerical methods are able to predict the overall tendency of the damaged ship motions and flooding process to an extent when compared with experiments. But reliable

prediction is difficult because the underlying phenomena are very complicated and highly nonlinear due to the various factors such as geometry of damaged compartment, flooding process and waves etc. To improve the accuracy of the numerical methods and the understanding of the mechanism of flooding process, data of various damaged scenario need more through numerical methods and experiments. Also it is generally believed that the physics of damaged ship can be analyzed by experiments more realistically.

In this study a series of experiment and numerical analysis have been carried out for the behaviour of a damaged cruiser in waves. Two damaged configurations are selected to study the damage effects. The one is mid section part which has 6 compartments. The

second is fore section part which has 4 compartments. The position of damage is starboard in both damage conditions. The flooding tests were performed for the transient process and the flooding water height was measured by 19 water height sensors. The flooding test results can also be used for the validation data of numerical codes and the enhancement of understanding. To study the effect of flooding water and damage compartment, model tests were carried in various wave conditions. The motion tests in waves were carried out after the compartments are completely flooded. The experiments indicate that the internal compartment influences the transient flooding process and roll motion. When there is shallow water in compartment and the ship moves as natural frequency of internal water in compartment, the coupling of internal water and ship motion occurs. The numerical simulation is conducted using quasi-static model, quasi-dynamic model and CFD. The quasi-dynamic model adopts the mass-spring for internal water motion description. The model considers the dynamics of free surface as ship motion. This mass-spring equation is explicitly coupled with ship motion equation. The quasi-dynamic model shows the intermediate results of CFD and quasi-static model.

## MODEL EXPERIMENTS

The model tests were performed in MOERI ocean engineering basin ( $L \times B \times D$ :  $56 \times 30 \times 4.5$  m). The model ship is a cruiser and the hull data of cruiser is provided by SSRC. The contents of model test are as follows.

- Motion in regular and irregular waves
  - Intact, damaged
- Flooding process in calm water
  - Intact, damaged
- Free decay in calm water
  - Intact, damaged (opened, closed)

## Ship model

The target ship is a cruiser. The main particulars are summarized in Table 1 and Figure 1 and Figure 2 show lines and model of cruiser. The model was fitted with bilge keels. Its length is 75 m and height is 0.50 m in prototype. They are symmetrically located about the mid ship at half the bilge girth. The inclination with the vertical is 45 deg. The model was around 5 m long corresponding to a scale of 50.

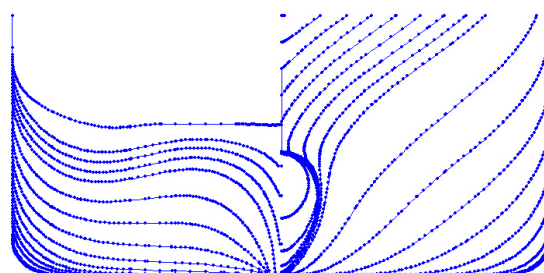


Fig. 1: Lines of cruiser



Fig.2: Cruiser model

Table 1: Particulars of cruiser

Items	
Length, $L_{pp}$	247.2 m
Beam, $B$	35.5 m
Draft, $T$	8.3 m
Displaced weight	56541.5 ton
KG	16.393 m
GM	2.388 m
Natural roll period	21.07 m
Gyration of roll	14.814 m
Gyration of pitch	61.925 m

### Damage compartment

Two damaged scenarios were chosen. The one (DAM1) is that mid section part is damaged which has 6 compartments. The second (DAM2) is that fore section part is damaged which has 4 compartments. These damaged parts are little different with original inner compartment of the cruiser. The compartments were simplified for model test. The opening of damaged compartment is located starboard side, the length is 6 m and the height is 5 m. The general arrangement of the damaged compartment is shown in Figure 3.

The damage model is shown in Fig 4. The material of damaged model is acryl and thickness is 5 mm. The coordinates of compartments and inner connection are listed in Table 2 & 3. The origin is midship (10 St.) in x, center in y and baseline in z direction. The opening of DAM1 is located above free surface, 8.3 m. The top of opening from the keel is 8.4 m. The top of DAM2 opening from the keel is 8.05 m. The opening is pulled out in an instant for flooding test. The coordinate of wave probes in each compartment is listed in Table 4.

### Environmental conditions

The characteristics of damaged cruiser in waves are investigated. To study the effects of flooding water and in/out flow through opening, motions in regular and irregular waves are measured. In order to study the effects of wave height, 4 heights (1, 3, 5, 7 m) of regular waves are used. The wave conditions are as follows.

- Regular waves

Frequency: 0.2 rad/s ~1.1 rad/s

Height: 1, 3, 5, 7 m

- Irregular waves: JONSWAP( $\gamma=3.3$ )

Irreg1:  $H_{1/3}=1$  m,  $T_p=5\sqrt{H_{1/3}}$

Irreg2:  $H_{1/3}=3$  m,  $T_p=5\sqrt{H_{1/3}}$

### Measurement system

To analyze the behaviours of damaged ship, the motions of ship and water in compartment must be measured. The 6 dof motion of ship are measured by non-contact optical system

(RODYM6D). The flooding flow is measured by capacity type wave probe. The number of wave probe used is 10 in CP10/11 and 6 in CP17. Video cameras are used to record the flow of flooding process. The RBM1 is in CP10-R1S next to damage opening. The location of wave probes can be found in Cho et al (2009).

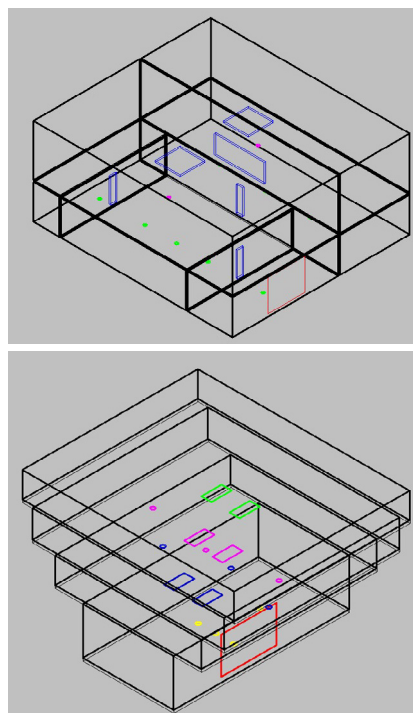


Fig.3: Arrangement of damage compartments (CP10/11, CP17)

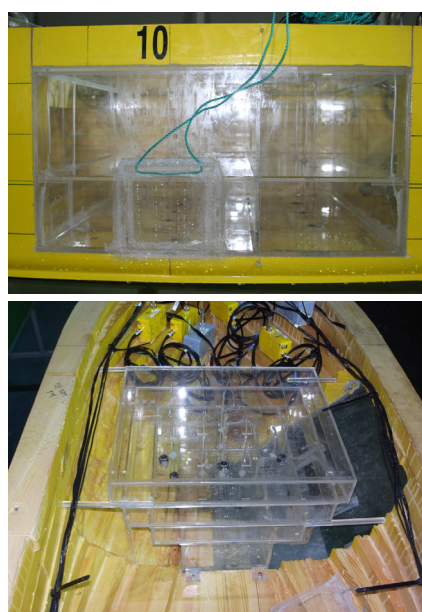


Fig.4: Damage compartment model

## NUMERICAL METHOD

In order to analyze the flooding, use the quasi-static model (Cho et al, 2009) and quasi-dynamic model. The quasi-dynamics model is lumped mass-spring system for free surface. This model calculate the free surface angle which is flat, that is mean sense as the ship motion. Fig 5 shows the concept of quasi-static, quasi-dynamic and CFD model. The quasi-dynamic model equation coupled with ship motion is flows. The 4<sup>th</sup> order Runge-Kutta method is used for time integration.

$$a_1 \ddot{y} + a_2 \dot{y} + a_3 y = -b_1 \ddot{x} - b_3 x \quad (1)$$

where  $y$  is free surface angle,  $x$  ship roll,  $a$  and  $b$  equation coefficients.

$$\begin{aligned} v &= \dot{y} \\ \dot{v} &= \frac{-b_1 \ddot{x} - b_3 x - a_2 v - a_3 y}{a_1} \end{aligned} \quad (2)$$

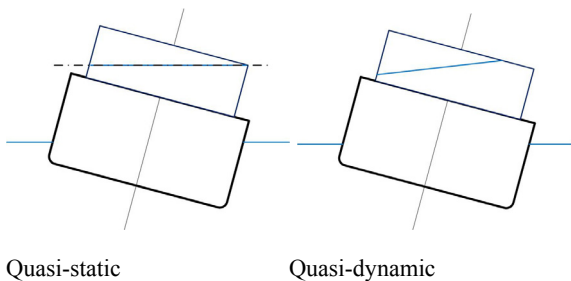


Fig 5: Free surface model

## TEST RESULTS & DISCUSSION

### Experimental results

Fig 5 shows the roll free decay test results. The natural roll period for DAM1 decreases about 1 sec due to flooding, heeling, free surface etc. The quadratic damping for DAM1 is different with intact. When opening is open condition, damaged part is not symmetric and flow in/out occurs in the CP10-R1S. This indicates that the estimation of damping is difficult when a damaged part is severe. The closed condition is flooded with closed opening. So, there is no flow in/out through opening. The motions are

affected by only internal water motion. Roll of close condition is similar with intact.

The flooding test was performed in calm water for DAM1 and DAM2. Fig 5 and Fig 6 shows the results for DAM1. The flooding through the opening starts at CP10-R1S (RBM1) and continues to CP10-R1C (RBM2,3,4) and CP10-R1P(RBM5). The water instantly fills up CP10-R1S. After filling of CP10-R1S, water propagates into other compartments. The RBM6, 7 and 8 show the flow from CP10 to CP11. The required time for flooding second floor, CP10/11-R2 is about 240 sec and the steady state value of roll angle is 5.14 deg. Fig 6 shows the motions with flooding. Roll motion begins at the same time with flooding and reaches the steady state (~400 sec) after filling of CP10-R1S/C/P. The flooding process of DAM2 is shown in Fig 7 & 8. The flooding process and motions are quite simple due to simple geometry and configuration. The flooding starts at CP17-R1 and flooding water reaches to the bottom of CP17-R2. The amount of water in CP17-R2 is small.

The motion tests in waves were carried out in the condition that the compartments were flooded. This gives the same situation at initial condition. The results of motions in waves are shown in Fig 9~12. The wave amplitudes are 1, 3, 5, 7 m to assess the effect of nonlinearity of the incident waves. The heave RAO shows there is no effect of wave amplitude and damage. But the roll motion is significantly influenced by wave amplitude and damage conditions. Interestingly enough, the effect of wave amplitude on roll motion also appears in intact condition. The peak value of roll RAO decreases at resonance frequency when wave amplitude increases. In case of DAM1, roll RAOs are changed due to internal water motion and inflow/outflow. The resonance frequency moved from 0.3 rad/s to 0.33 rad/s due to sloshing. The effect of internal water motion appears for wave amplitude 3, 5, 7 m and sloshing occurred in CP10/11-R2. This is sloshing in low filling ratio. When wave amplitude is 1m, the internal water motion is small and sloshing doesn't occur. In order to excite sloshing in a considerable level, waves

more than 3 m should be incident because the ship heels 5.14 deg to starboard. Fig 14 shows the sloshing by roll motion. In case of DAM2, roll RAOs is similar to intact RAOs. Although sloshing in CP17-R2 occurs, there is no significant influence of flooding because of small amount of water. Fig 13 shows the effect of opening and in/outflow.

Fig 15, 16 & 17 show the roll motion and internal water motion in CP10/11-R2. The position of water height measurement (RBM9/10) is in the middle. The initial value of water height is zero in flooded situation. The positive value stands for increasing and negative value decreasing. When wave height is 1 m, flooding water doesn't reach to port side wall and sloshing doesn't occur. But in case wave height 5 m, flooding water reached port side wall. When wave frequency is 0.33 rad/s, the coupling of sloshing and roll is strong. Table 2 shows the phase of roll and incoming wave due to sloshing.

**Table 2: Phase of wave and roll**

Frequency	0.2~0.25 rad/s	0.3~0.36 rad/s	0.4 rad/s ~
Intact	90 deg	0 deg	-90 deg
DAM1	90 deg	180 deg	-90 deg

Fig 15 and 16 show the irregular test results for intact and DAM1. The flooding affects the roll motion and the roll motion decrease. Also the motion of flooding water is clear at 0.3 rad/s.

### *Numerical simulation results*

Fig 17~21 show the results for ITTC tanker model. The free decay results of quasi-dynamic model are pretty similar to experiments and CFD. This indicates that the quasi-dynamic model can calculate the dynamics of free surface. Also regular wave test shows the reasonable results. The merit of quasi-dynamic model is fast calculation. The required time is almost same as quasi-static model.

The damaged problem is calculated by quasi-dynamic model. The results are shown in Fig

23~26. The transient flooding process is represented by the model. The flooding heights are compared and the numerical results agree with experiments. But the roll is different at flooding beginning. This difference is due to the different amount of flooding water in CP10R1S. The increase of numerical result in CP10R1S is almost step and CP10R1S is full. But experiment shows CP10R1S is not filled once and is full after 150 sec. This lag may be occurred by air compression and numerical model limit. Fig 25 and 26 show the regular wave results. Roll RAOs show similar tendency of experiments.

## CONCLUSIONS

The experiments and numerical analysis have been performed for the behaviour of damaged cruiser in waves. The influences of damage configuration, internal water motion, wave height and flow in/out are considered. The transient process and motion behaviour in waves are analyzed. The transient flooding process is measured in each compartment. The effect of flooding on the ship motion appeared in roll motion. Although the amount of water in upper compartment is small, the sloshing is occurred and the effect is significant. Quasi-dynamic model show quite good results. For more precise estimation, the improvement of model is needed.

## ACKNOWLEDGMENTS

This study is a part of research program, "Development of simulation technologies for dynamics stability of ships" supported by Ministry of Knowledge Economy of Korea and "Development of Extreme Response Analysis Technologies for Offshore Structures" supported by Korea Research Council of Fundamental Science and Technology.

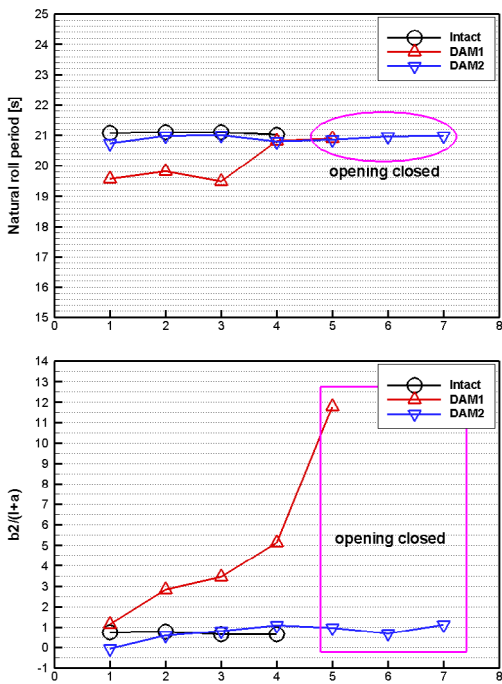


Fig 6: Results of free decay

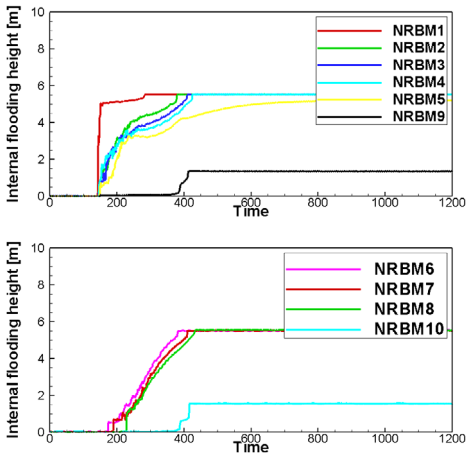


Fig 7: Flooding process of DAM1

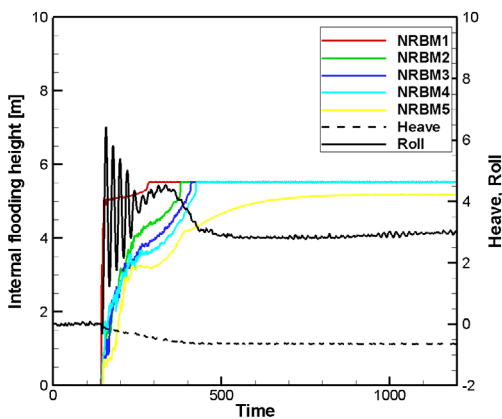


Fig 8: Motions with flooding of DAM1

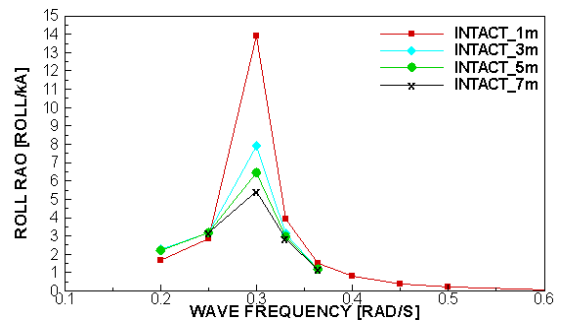


Fig 9: Roll RAO of intact

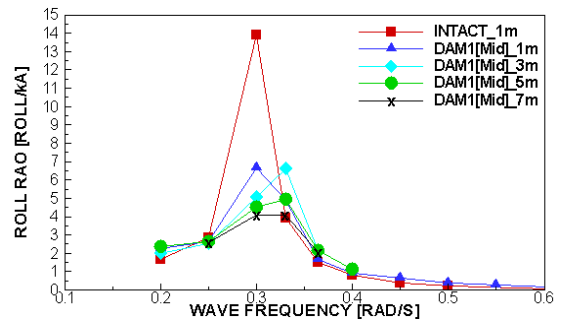


Fig 10: Roll RAO of DAM1

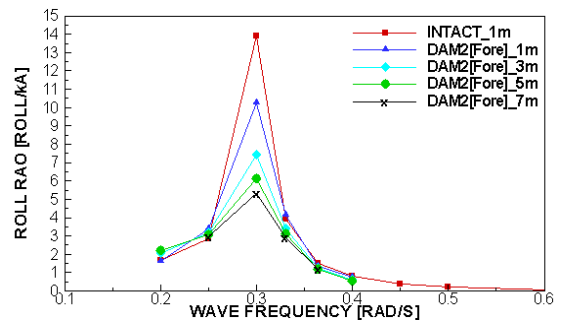


Fig 11: Roll RAO of DAM2

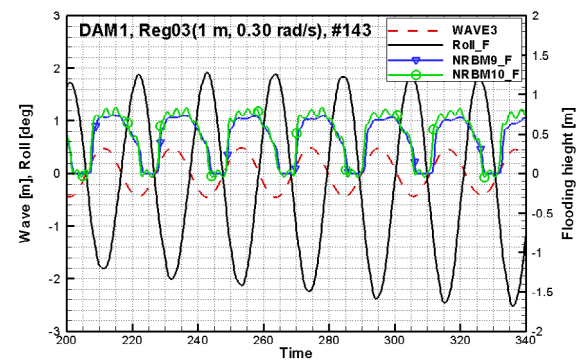


Fig 12: Motion and flooding of DAM1 (wave height 1m,  $\omega=0.3$  rad/s)

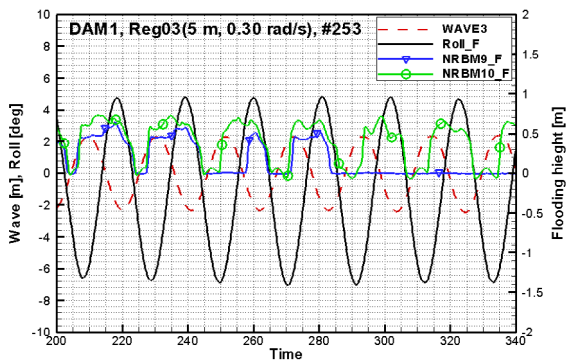


Fig 13: Motion and flooding of DAM1(wave height 5m,  $\omega=0.3$  rad/s)

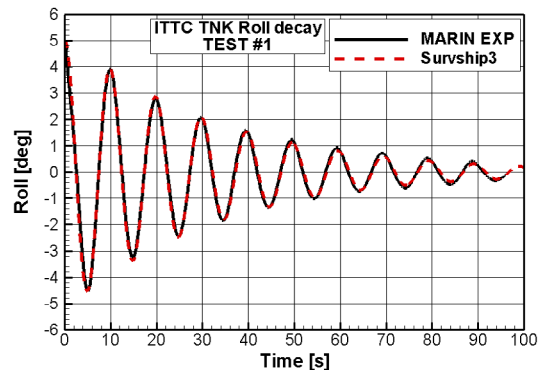


Fig 17: Free decay( $h=0$ m)

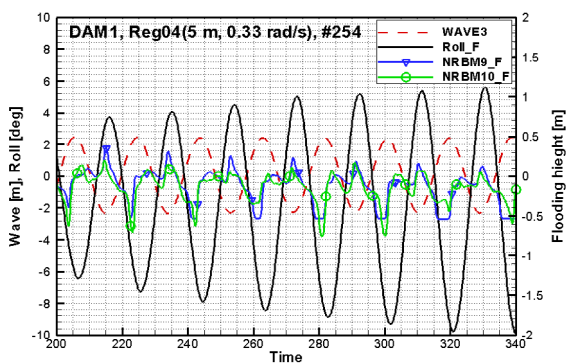


Fig 14: Motion and flooding of DAM1(wave height 5m,  $\omega=0.33$  rad/s)

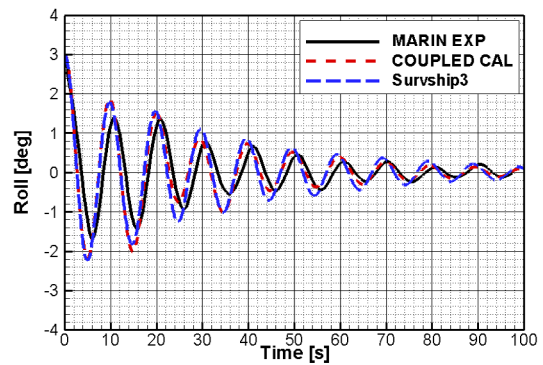


Fig 18: Free decay-sub resonance( $h=3$ m)

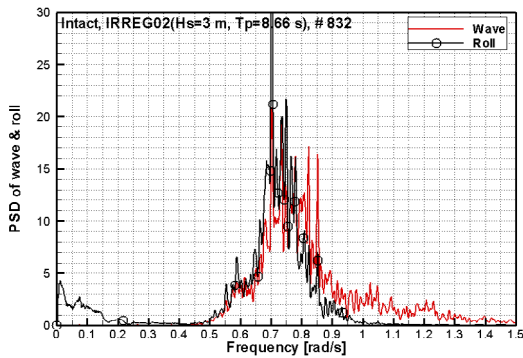


Fig 15: PSD of intact in irregular wave( $H_s=3$  m)

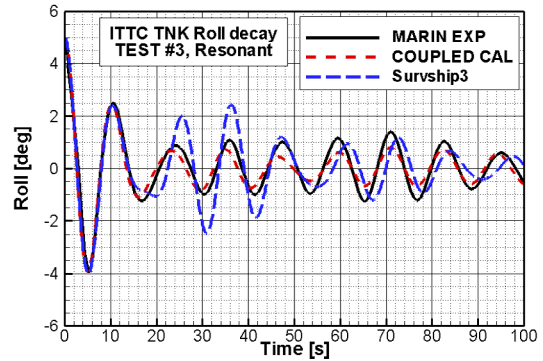


Fig 19: Free decay-resonance( $h=4$ m)

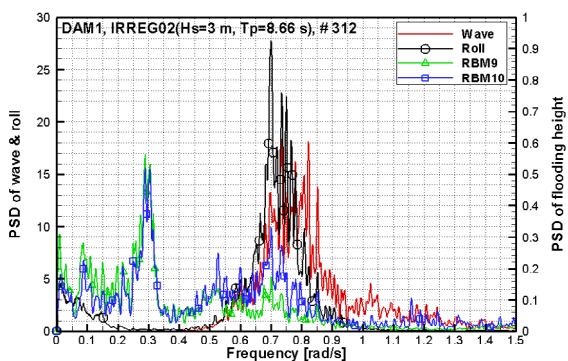


Fig 16: PSD of DAM1 in irregular wave( $H_s=3$  m)

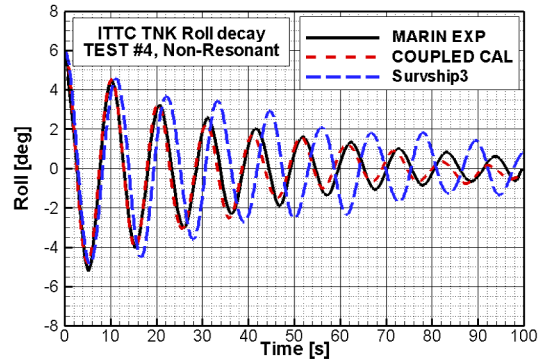


Fig 20: Free decay-non-resonance( $h=16$ m)

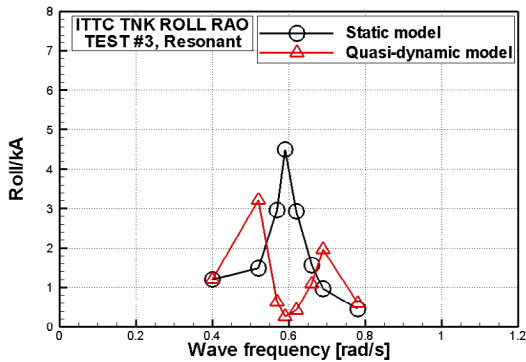


Fig 21: Roll RAO-resonance(h=4m)

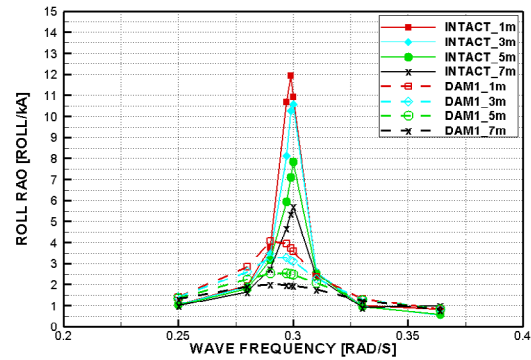


Fig 25: Roll RAO for intact and DAM1-Quasi-dynamic model

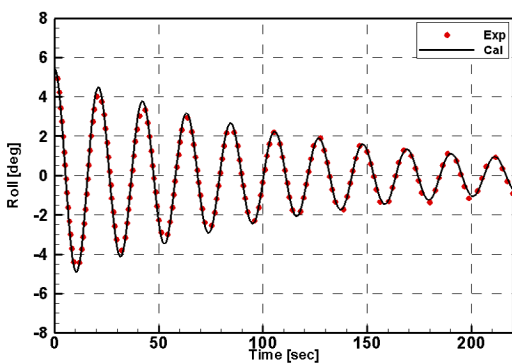


Fig 22: Roll free decay of cruiser

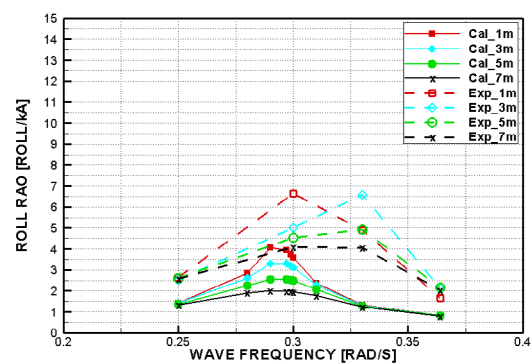


Fig 26: Roll RAO comparison for DAM1-Quasi-dynamic model

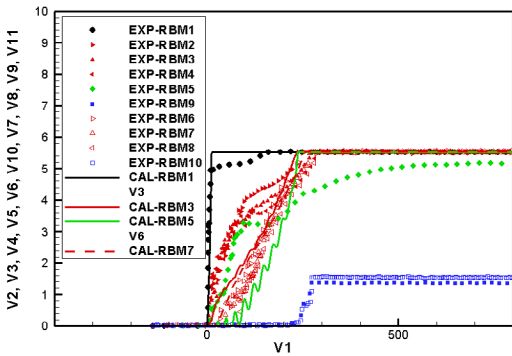


Fig 23: Comparison of flooding height for DAM1

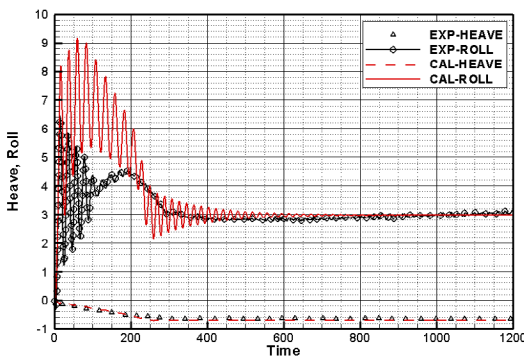


Fig 24: Comparison of motions for DAM1

## REFERENCES

- Cho, S., Sung, H., Nam, B., Hong, S. and Kim, K., 2009, "Experimental Study on Flooding of a Cruiser in Waves", Proc. 10th International Conference on Stability of Ships and Ocean Vehicles, St. Petersburg, pp. 747~753.
- Palazzi L. and De Kat J., 2004, "Model Experiments and Simulations of a Damaged Ship With Air Flow Taken Into Account", Marine Technology, Vol. 41, No. 1, pp. 38-44.
- Papanikolaou, A. and Spanos, D., 2002, "On the Modelling of Floodwater Dynamics and its effects on Ship Motions", Proc. 6th International Ship Stability Workshop, Webb Institute, New York.
- Papanikolaou, A. and Spanos, D., 2005, "24th ITTC Benchmark Study on Numerical Prediction of Damage Ship Stability in Waves Analysis of Final Results", Proc. 8th International Ship Stability Workshop, Turkey.

Ruoponen, P. 2007, "Progressive flooding of a damaged passenger ship", Doctor thesis, Helsinki university of technology.

van Walree F. and N. Carette, 2008, "Benchmark study of numerical codes for the prediction of time to flood of ship-phase 2", Proc. 10th International Ship Stability Workshop, Daejeon, Korea.



# An Application of the DOE Methodology in Damage Survivability

Chadi Khaddaj-Mallat, Jean-Marc Rousset, Bertrand Alessandrini,

G rard Delhommeau, and Pierre Ferrant

Laboratoire de M canique des Fluides (LMF-EHGO),  cole Centrale de Nantes, Nantes, France

## ABSTRACT

This study focuses on the fundamental nature of the flooding process, and attempts to determine the main contributing factors to its evolution. It is performed experimentally by measuring the forces and moments of interest, the water heights inside flooded compartments, and the air pressure inside the double bottoms of the PRR02 - ITTC/SiW passenger Ro-Ro ferry. The controllable factors are: initial draught, damage opening area, time of damage creation, dimensions and locations of flow obstructions inside a large compartment, cross-flooding, air ventilation, and external excitation. The applied Design of Experiments methodology manages to build a model of the transient flooding.

## KEYWORDS

Transient and progressive flooding; Ro-Ro passenger ferry; factors; model; Design of experiments.

## NOMENCLATURE

CD	Cross Duct
DBA	Double Bottom Aft
DBF	Double Bottom Forward
EB	Engine Block
ER	Engine Room
GM	Metacentric height
GR	Generator Room
IFS	Intermediate Flooding stages
OM	Opening Mechanism
SR	Storage Room
$T_\phi$	PRR02 natural period

## INTRODUCTION

Ro-Ro and Ro-Pax ferries have been growing in size for decades. Despite the global economic downturn, their industry continues to show positive signs. This is evident by the scheduled launch of some humongous new Ro-Pax vessels by 2012 (as the new Stena Line Superferries joining Hook of Holland – Harwich route in May 2010, etc.). The safety of such vessels remains of the utmost importance

in their design and operation stages, as accidents of a varying nature (collision, grounding, etc.) can occur. More investigations into these accidents need to be performed based on the available data, and substantial outcomes should be included in the relevant regulations to raise them beyond today's level hoping to prevent maritime accidents' occurrence in the future.

Commercially, Ro-Ro passenger ferries have proven to be successful. This is due to car decks stretching from board to board and from stem to stern, thus reducing the time required for operations onboard. However, it is well known that this characteristic is the main contributor to the sinking of these vessels, as the reserve of buoyancy above the bulkhead deck has completely vanished when the ship shell was damaged (Dand (1989), Spouge (1985)). On the other hand, the geometry of the spaces below the bulkhead deck is also of great importance indeed. When a maritime accident occurs, the geometry and the state of the spaces

below the bulkhead deck in such vessels contribute to determining the final state they will reach.

The effect of the intermediate flooding stages (IFS), i.e. transient and progressive, on ships' damaged survivability has been studied based on parametric investigations carried out both experimentally and computationally (Chang and Blume (1998), Chang (1999), Ikeda and Ma (2000)). Generally, these investigations have provided a better understanding of the basic fundamentals of the flooding physics, and have assisted in identifying some parameters which are significant for the assessed phenomena. Besides, when giving some recommendations to reliably assess the IFS, Khaddaj-Mallat et al. (2009) stressed on an actual need to identify the significant factors, their main effects, and the interactions linking them. Therefore, they proposed to apply Design of Experiments methodologies (DOE), in the hopes of meeting this need obviously unreachable by means of parametric investigations.

The paper under study chiefly aims at shedding lights on the DOE methodology applied in a particular Ocean-Engineering domain, the damage survivability. It also aims to better understand the IFS, determine the factors that govern them, and eventually build a model that could appropriately describe them. Thus, an experimental investigation was carried out in Sept/Oct 2009 using the midsection of the PRR02 - ITTC/SiW passenger Ro-Ro ferry. A detailed description of the experimental set up, as well as first findings relevant to one particular test (and not to any DOE plans) could be respectively found in Khaddaj-Mallat et al. (2010a, 2010b). Thus, this paper is devoted to presenting the guidelines of applying this methodology to perform tests, as well as the first findings, relevant to a DOE plan, the Fractional Factorial Design (FFD). A mathematical model that characterizes the IFS in Ro-Ro Passenger ferries is presented.

## EXPERIMENTAL METHODOLOGY

In this chapter, the guidelines for designing the experiment based on DOE approach and for analyzing the results are presented. The experimental quantities and results are presented in model scale.

### *Recognition of and statement of the problem*

Physically, the first phase of flooding that occurs after an abrupt damage creation, i.e. the transient phase, is dependent on the flooding process and the procedure of water accumulation inside internal compartments itself related to water ingress / egress through the damage hole. This phase is influenced by hosts of factors we aim to quantify their trends. Thus, two distinct tests in calm water using the ship midsection are performed as a first step:

- Flooding experiments in which the model is kept fixed. These tests are performed to a) assess the influence of the investigated factors on hydrodynamic efforts exerted on the model during the IFS, b) better understand the behavior of both implicated fluids, i.e. water and air.
- Forced oscillation tests performed for realistic combinations between the six degrees of freedom. These tests allow us to quantify the influence of external excitations on the measured quantities and sloshing.

### *A brief description of the experimental set up*

The tested body is a 1/38.25 scaled model of the PRR02 midsection. Its main dimensions and general arrangements are given in Table 1, and Figure 1, respectively.

**Table 1: Model main dimensions.**

Feature	Value
Length, L(m)	26.71
Beam, B(m)	25.00
Draft, T(m)	6.40
Car deck above baseline (m)	9.10
PRR02 Length, L <sub>pp</sub> (m)	174.80

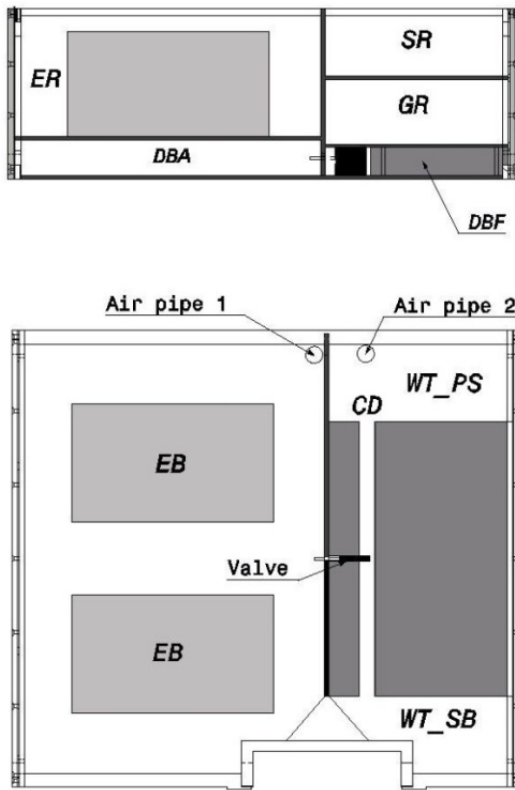


Figure 1: Model general arrangements.

In the DBF, a CD connects the two wings double bottom tanks. A valve is mounted at the midpart of the CD. It is either opened (On) or closed (Off) during the experiments. Moreover, two air pipes are included in the model, to reproduce air pressure fluctuations expected in full-scale ship.

The flooded compartments are chosen according to the worst SOLAS 90 damage scenario. The damage characteristics are as follows.

- A rectangular shape in side, reproducing the real bilge shape. Two damage areas pertaining to different types of accidents are tested. To do so, the vertical extent of the damages is varied while keeping its longitudinal one constant.
- Isosceles-triangles notches in all decks penetrating to the B/5 lines are performed, reproducing the damage that would be created by the striking

vessel's bow. Because of the hull bilge part and the opening door, the performed notch has the shape shown in Figure 1.

The damage OM comprises a vertical door that appropriately fits with the hull shape. An electrical motor, mounted on the deck along with a rope-pulley system, opens the door and lets it run on rails up alongside the hull and over the deck.

Thus, the experimental set up that we believe it appropriately enables meeting the drawn objectives, mainly relies on the use of a 6-DOF-motion platform "Hexapod" settled upside down, as well as a custom-made 6-DOF dynamometer attached to its movable plate. It is shown in Figure 2.

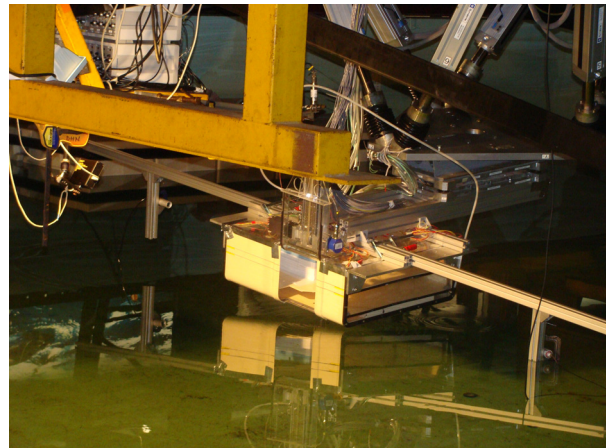


Figure 2: The experimental set up when drying the model.

The measured quantities are:

- The hydrodynamic efforts on the body kept fixed and under forced-oscillations.
- The water heights in several locations inside every flooded compartment.
- The air pressures in compartments of interest (the DBs).

In addition, a set of video cameras is used to visualize the physical conditions and both water and air behaviors. A sampling frequency of 1 kHz is used to capture expected peaks in the behaviors of all measured quantities.

**Why DOE Methodology?**

DOE offers several key advantages over the traditional one-variable-at-a-time approach. It allows for the evaluation of the statistical significance of individual process parameters, as well as the interaction between factors. Another major advantage of the DOE approach is that it requires only a small set of experiments and thus helps to reduce costs. It is hoped that DOE lets us develop a mathematical model able to predict how input variables interact to create output ones (responses and criteria) in the event of flooding. Detailed accounts of how to design DOE experiments can be found, for example, in Schimmerling et al. (1998) and Ryan (2006).

**Choice of factors, levels, and ranges**

IFS are dependent upon a fair number of factors related to the event of damage creation, the initial ship hydrostatic and the environmental conditions.

The selection of controllable factors and their levels is a demanding and intricate task, since the DOE plan performance is directly attached to the data used to train it. To do so, a number of discussions involving experienced individuals such as Mr. Paul Schimmerling of Renault, France, took place and valuable advice was provided on the reliability of the experimentation strategy.

Thus, we first screen initial heel and trim, as their influence on the IFS is relatively small. Besides, GM is not considered in the current experiment, as the experimental set up is conceived to measure hydrodynamic efforts. Thus, the design factors for this study, as well as their selected levels are determined and presented in Tables 2 and 3. It is worth to mention that this study deals with a large number of factors influencing the IFS; GM is the sole factor influencing these stages that is not taken into account.

**Table 2: List of the variables affecting the IFS.**

Variables of control	Symbol	Dimension
Initial draught	A	L [m]
Damage opening's area	B	L <sup>2</sup> [m <sup>2</sup> ]

Valve status	C	-
Air ventilation level	D	-
ER's permeability $\mu$	E	-
Transversal distance between the centerline and the EB	F	L [m]
Time of damage creation	G	T [s]
Motion amplitude of the midsection hull	H	L [m]

**Table 3: List of the controllable factors' levels.**

Factor	Level 1	Level 2
A	LC <sub>1</sub> A <sub>1</sub> = 0.167	LC <sub>2</sub> A <sub>2</sub> = 0.140
B	Small damage B <sub>1</sub> = 0.00946	Large damage B <sub>2</sub> = 0.04730
C	C <sub>1</sub> = 1; Opened valve C <sub>1</sub> = 0; Closed valve	C <sub>2</sub> = 0; Opened valve C <sub>2</sub> = 1; Closed valve
D	Fully ventilated D <sub>1</sub> = 0.146	Partially ventilated D <sub>2</sub> = 0.058
E	70% ER Permeability E <sub>1</sub> = 0.70	85% ER Permeability E <sub>2</sub> = 0.85
F	EBs 21.8cm far from the centerline F <sub>1</sub> = 0.218	EBs at the centerline F <sub>2</sub> = 0
G	Instantaneous damage opening G <sub>1</sub> = 0	Damage created in 4T <sub>φ</sub> /3 G <sub>2</sub> = 3.45
H	No external excitation H <sub>1</sub> = 0	Combined Heave & Roll Forced-Oscillation H <sub>2</sub> = 0.0298

**Selection of the response variable**

After conducting tests to assess the repeatability and the reproducibility of our experiment, we find that the experimental uncertainty is relatively small (<3.5%) and that our measurement system is reliable. Therefore, based on the quantities we measured, we have determined the following response variables.

- For F<sub>x</sub>, F<sub>y</sub>, M<sub>x</sub>, F<sub>z</sub>, and M<sub>y</sub>: The maximum amplitude, the time to reach

it with respect to the start of the damage creation, the amplitude after the IFS end, the amplitude when the door movement ceases, and the slope during the event of damage creation (only for  $F_z$  and  $M_y$ ).

- The flooding rates and the discharge coefficients through the damage opening.
- For air pressures in DBA and DBF: the peak and its correspondent time of occurrence, the values at the end of the door movement and after the IFS end.
- For water heights measured by means of twenty probes: the peak, time to reach it, and the slope during the water accumulation.

These quantities (89 outputs) are evaluated for each test providing a thorough account of data to analyze. The analysis will determine the response variables and the design factors that best characterize the IFS.

**Choice of experimental design**

A fractional factorial design (FFD) is used to design the experiments to minimize the runs. With eight factors, the quarter-fractional two-level factorial design ( $2^{8-2}$ ) requires a combination of 64 experimental tests. The 64 run combinations for the  $2^{8-2}$  design are shown in Table 4. The design is a Resolution IV design following  $Q_2$  strategy, which means that all main effects and two-factor interactions can be estimated without ambiguity (Schimmerling et al. (1998)).

**Table 4: FFD data sheet.**

Std. order	A	B	C	D	E	F	G	H
1	1	1	1	1	1	1	2	2
2	2	1	1	1	1	1	1	1
3	1	2	1	1	1	1	1	1
4	2	2	1	1	1	1	2	2
5	1	1	2	1	1	1	1	2
6	2	1	2	1	1	1	2	1
7	1	2	2	1	1	1	2	1
8	2	2	2	1	1	1	1	2
9	1	1	1	2	1	1	1	2
10	2	1	1	2	1	1	2	1
11	1	2	1	2	1	1	2	1
12	2	2	1	2	1	1	1	2
13	1	1	2	2	1	1	2	2
14	2	1	2	2	1	1	1	1

15	1	2	2	2	1	1	1	1
16	2	2	2	2	1	1	2	2
17	1	1	1	1	2	1	2	1
18	2	1	1	1	2	1	1	2
19	1	2	1	1	2	1	1	2
20	2	2	1	1	2	1	2	1
21	1	1	2	1	2	1	1	1
22	2	1	2	1	2	1	2	2
23	1	2	2	1	2	1	2	2
24	2	2	2	1	2	1	1	1
25	1	1	1	2	2	1	1	1
26	2	1	1	2	2	1	2	2
27	1	2	1	2	2	1	2	2
28	2	2	1	2	2	1	1	1
29	1	1	2	2	2	1	2	1
30	2	1	2	2	2	1	1	2
31	1	2	2	2	2	1	1	2
32	2	2	2	2	2	1	2	1
33	1	1	1	1	1	2	2	1
34	2	1	1	1	1	2	1	2
35	1	2	1	1	1	2	1	2
36	2	2	1	1	1	2	2	1
37	1	1	2	1	1	2	1	1
38	2	1	2	1	1	2	2	2
39	1	2	2	1	1	2	2	2
40	2	2	2	1	1	2	1	1
41	1	1	1	2	1	2	1	1
42	2	1	1	2	1	2	2	2
43	1	2	1	2	1	2	2	2
44	2	2	1	2	1	2	1	1
45	1	1	2	2	1	2	2	1
46	2	1	2	2	1	2	1	2
47	1	2	2	2	1	2	1	2
48	2	2	2	2	1	2	2	1
49	1	1	1	1	2	2	2	2
50	2	1	1	1	2	2	1	1
51	1	2	1	1	2	2	1	1
52	2	2	1	1	2	2	2	2
53	1	1	2	1	2	2	1	2
54	2	1	2	1	2	2	2	1
55	1	2	2	1	2	2	2	1
56	2	2	2	1	2	2	1	2
57	1	1	1	2	2	2	1	2
58	2	1	1	2	2	2	2	1
59	1	2	1	2	2	2	2	1
60	2	2	1	2	2	2	1	2
61	1	1	2	2	2	2	2	2
62	2	1	2	2	2	2	1	1
63	1	2	2	2	2	2	1	1
64	2	2	2	2	2	2	2	2

**Statistical analysis of the data**

After performing the FFD experimental runs, the obtainable data is analyzed to build a model for every output. Each of the 89 responses (Y) can be written as the summation of its mean effect, that of all the 8 controllable factors (each factor is considered individually), and those of second-order interactions (see Eq. (1)). Relevant coefficients are to be evaluated according to Schimmerling et al. (1998).

$$Y = I + [a_1 a_2].A + [b_1 b_2].B + [c_1 c_2].C + [d_1 d_2].D + [e_1 e_2].E + [f_1 f_2].F + [g_1 g_2].G + [h_1 h_2].H +$$

$$\begin{aligned}
 & B^T M_{BAA} + C^T M_{CAA} + D^T M_{DAA} + \\
 & E^T M_{EAA} + F^T M_{FAA} + G^T M_{GAA} + \\
 & H^T M_{HAA} + \\
 & C^T M_{CB B} + D^T M_{DB B} + E^T M_{EB B} + \\
 & F^T M_{FB B} + G^T M_{GB B} + H^T M_{HB B} + \\
 & D^T M_{DC C} + E^T M_{EC C} + F^T M_{FC C} + \\
 & G^T M_{GC C} + H^T M_{HC C} + \\
 & E^T M_{ED D} + F^T M_{FD D} + G^T M_{GD D} + \\
 & H^T M_{HD D} + \\
 & F^T M_{FE E} + G^T M_{GE E} + H^T M_{HE E} + \\
 & G^T M_{GF F} + H^T M_{HF F} + \\
 & H^T M_{HG G}
 \end{aligned} \tag{1}$$

Where:

- $X^T$  designates X transpose matrix,
- $A = [A_1 A_2]^T \dots H = [H_1 H_2]^T$  represent the input variables (see Table 3),
- I represents the response's mean effect,
- $[a_1 a_2] \dots [h_1 h_2]$  are the coefficients to evaluate that represent the individual effect of each factor, and
- $M_{BA} = [(ba)_{11} (ba)_{12}; (ba)_{21} (ba)_{22}] \dots M_{HG} = [(hg)_{11} (hg)_{12}; (hg)_{21} (hg)_{22}]$  are the coefficients to evaluate that represent second-order interactions.

Eq. (1) helps determine to which extent each of the input factors affects any selected response. Thus, with fixing a criterion, we are able to determine which factors are significant for the selected responses, and; therefore, for the physical phenomenon.

Determining Eq. (1)'s coefficients  $(I, (a_1, a_2) \dots (h_1, h_2), (ba)_{11} \dots (hg)_{11})$  is useful to evaluate Eq. (2)'s coefficients  $(\alpha_0, \alpha_1 \dots \alpha_8, \alpha_{12} \dots \alpha_{78})$ .

$$Y = \alpha_0$$

$$+ \alpha_1 X_1 + \alpha_2 X_2 + \alpha_3 X_3 + \alpha_4 X_4 + \alpha_5 X_5 + \alpha_6 X_6 + \alpha_7 X_7 + \alpha_8 X_8$$

$$+ \alpha_{12} X_1 X_2 + \alpha_{13} X_1 X_3 + \alpha_{14} X_1 X_4 + \alpha_{15} X_1 X_5 + \alpha_{16} X_1 X_6 + \alpha_{17} X_1 X_7 + \alpha_{18} X_1 X_8$$

$$+ \alpha_{23} X_2 X_3 + \alpha_{24} X_2 X_4 + \alpha_{25} X_2 X_5 + \alpha_{26} X_2 X_6 + \alpha_{27} X_2 X_7 + \alpha_{28} X_2 X_8$$

$$+ \alpha_{34} X_3 X_4 + \alpha_{35} X_3 X_5 + \alpha_{36} X_3 X_6 + \alpha_{37} X_3 X_7 +$$

(2)

$$\alpha_{38} X_3 X_8$$

$$+ \alpha_{45} X_4 X_5 + \alpha_{46} X_4 X_6 + \alpha_{47} X_4 X_7 + \alpha_{48} X_4 X_8$$

$$+ \alpha_{56} X_5 X_6 + \alpha_{57} X_5 X_7 + \alpha_{58} X_5 X_8$$

$$+ \alpha_{67} X_6 X_7 + \alpha_{68} X_6 X_8$$

$$+ \alpha_{78} X_7 X_8$$

Eq. (2) provides a general modeling of the output variables, as it enables evaluating any response (Y) for any values  $(x_1 \dots x_8)$  of any input variables (selected within their ranges of variations).

The evaluation of Eq. (1)'s coefficients for all the responses provides insight into the responses that best affect the physical phenomenon, i.e. the ship behavior during the IFS. Thus, among the 89 outputs, the following responses are found significant: the maximal amplitude of the Vertical Force Fz ( $Y_7$ ), the time to reach  $Y_7$  ( $Y_{10}$ ), the slope of Fz during the door vertical movement ( $Y_{11}$ ), the maximal amplitude of the roll moment My ( $Y_{15}$ ), the time to reach  $Y_{15}$  ( $Y_{18}$ ), the slope of My during the door vertical movement ( $Y_{19}$ ), the time needed for each water height probe to reach its maximum for the first time, the maximum flow rate ( $Y_{88}$ ), and the time to reach  $Y_{88}$  ( $Y_{89}$ ).

Then, a general analysis based on FFD results is conducted to refine the model, i.e. determine the factors and interactions which effectively contribute to every response judged significant. It is found that (B, H, A, G) are the most affecting factors; then (E, F) come with a relatively less influence. C and D factors show a relatively very little influence that allows us neglect them, as well as their interactions from the model showed in Eq. (2). Moreover, the interactions between A and F, on one hand, and between B and E, on the other hand, could be neglected. Some out-of-FFD-plan tests are conducted and their results serve in validating the refined model.

Thus, the model characterizing the IFS can be written as follows.

$$Y = \alpha_0'$$

$$+ \alpha_1' \cdot x_1 + \alpha_2' \cdot x_2 + \alpha_5' \cdot x_5 + \alpha_6' \cdot x_6$$

$$+ \alpha_7' \cdot x_7 + \alpha_8' \cdot x_8$$

$$+ \alpha_{12}' \cdot x_1 x_2 + \alpha_{15}' \cdot x_1 x_5 + \alpha_{17}' \cdot x_1 x_7 +$$

$$\begin{aligned}
 & \alpha_{18}' \cdot X_1X_8 \\
 & + \alpha_{26}' \cdot X_2X_6 + \alpha_{27}' \cdot X_2X_7 + \alpha_{28}' \cdot X_2X_8 \\
 & + \alpha_{56}' \cdot X_5X_6 + \alpha_{57}' \cdot X_5X_7 + \alpha_{58}' \cdot X_5X_8 \\
 & + \alpha_{67}' \cdot X_6X_7 + \alpha_{68}' \cdot X_6X_8 \\
 & + \alpha_{78}' \cdot X_7X_8
 \end{aligned}
 \tag{3}$$

## CONCLUSIONS

An experimental study is conducted to assess the transient and progressive flooding phases in the PRR02 Ro-Ro Passenger Ferry. The Design of Experiments methodology serves to plan the tests, conduct the experiments, and analyze the data. A Fractional Factorial Design is used as it allows us to determine the significant factors, as well as their interactions without ambiguity. It is worth to mention that ensuring both water and air tightness, changing some factors' levels between tests, and selecting the factors' levels and their variations' ranges are the most challenging tasks in preparing the experiments, conducting the tests, and designing the DOE plan, respectively. It is found that the IFS are mainly affected by the damage opening area, the external excitation (due to the environment and the accident), the initial draught, and the time of damage creation. A model is first built then successfully refined. It must be noted that the main objective of presenting this paper in the ISSW is to investigate and demonstrate the applicability, weaknesses and strengths of using DOE approaches in developing design formulae in the damage survivability domain. However, the authors would indicate that this study treats one particular ship, the metacentric height is not considered, and the results are based on a campaign planned as a first step in the DOE approach. These particularities clarify the perspective for further research in this domain. At last and not least, more detailed, illustrated, and further findings would be presented in the workshop, in the hope that fruitful discussions take place aiming to improve our common understanding of the damage survivability.

## REFERENCES

- Chang, B.-C., 1999, "On the Damage Survivability of Ro-Ro Ships Investigated by Motion Simulation in a Seaway", Ship Technology Research - Schiffstechnik, Vol. 46 (4), pp. 192-207.
- Chang, B.-C. and Blume, P., 1998, "Survivability of Damaged Ro-Ro Passenger Vessels", Ship Technology Research - Schiffstechnik, Vol. 45 (3), pp. 105-112.
- Dand, I.W., 1989, "Hydrodynamic Aspects of the Sinking of the Ferry 'Herald of Free Enterprise'", Transactions of the Royal Institution of Naval Architects, Vol. 131, pp. 145-165.
- Ikedo, Y. and Ma, Y., 2000, "An experimental study on large roll motion in intermediate stage of flooding due to sudden ingress of water", STAB2000, February 7-12, 2000, Australia.
- Khaddaj-Mallat, C. et al., 2009, "On Factors Affecting the Transient and Progressive Flooding Stages of Damaged Ro-Ro Vessels", STAB2009, June 22-26, 2009, Saint-Petersburg, Russia.
- Khaddaj-Mallat, C. et al., 2010a, "Investigating the Transient Flooding and Sloshing in Internal Compartments of an ITTC Damaged Ro-Ro Ferry - Part I: Experimental Set up", OMAE2010, June 6-11, 2010, Shanghai, China.
- Khaddaj-Mallat, C. et al., 2010b, "Investigating the Transient Flooding and Sloshing in Internal Compartments of an ITTC Damaged Ro-Ro Ferry - Part II: Experimental Analysis", OMAE2010, June 6-11, 2010, Shanghai, China.
- Ryan, T.P., 2006. "Modern Experimental Design", Wiley, New York.
- Schimmerling, P. et al., 1998, "Pratique des Plans d'expériences". Lavoisier Edition, in French.
- Spouge, J.R., 1985, "The Technical Investigation of the Sinking of the Ro-Ro Ferry 'European Gateway'", Transactions of the Royal Institution of Naval Architects, Vol. 128, pp. 49-72.



## The Capsize Band Concept Revisited

Nikolaos Tsakalakis, Jakub Cichowicz and Dracos Vassalos

The Ship Stability Research Centre, Department of Naval Architecture and Marine Engineering,  
University of Strathclyde, Glasgow, UK

### ABSTRACT

A concept for analytical representation of the capsize rate, a measure directly related to damage ship survivability, has attracted attention ever since the first attempts were made to explain the behaviour of a damaged ship in waves. Attempts in the late 1990s helped to enhance understanding and facilitate characterisation of phenomena pertaining to capsize probability and time to capsize in given environments and loading conditions, but a consistent verifiable formulation is still lacking. In this respect, pursuing an analytical approach to express the capsize rate offers many advantages, time efficiency being amongst the most important. In an era when stability/survivability calculations are required to be carried out in real time, there is a need for a model combining accuracy close to that of time-domain simulations whilst relying on hydrostatic models, catering for uncertainty and capsize boundaries in the process. This study is an attempt to establish a new methodology for survivability assessment by means of a multivariable analytical model based on numerical simulations, validated against the results of physical model tests.

### KEYWORDS

Damage Stability; Capsize Band; Critical Wave Height; Ro-Pax;

### INTRODUCTION

The concepts of capsize boundary and capsize band lie at the core of damage survivability assessment of ships. The s-factor used to derive the Attained Index of subdivision corresponds to the 50% probability of survival in damaged condition and in a sea state characterised by what is called *critical significant wave height*.  $H_{s_{crit}}$  is nothing else than a capsize boundary – a wave height at which the capsize rate ( $P_f$ ) equals 0.5. The capsize band, in turn, reflects the marginal nature of the capsize phenomena and by analogy to statistics it can be interpreted as a confidence interval about  $H_{s_{crit}}$ . In fact, the capsize band is not a confidence interval in a strict sense<sup>1</sup> – it is rather a measure of

dispersion of capsizes, separating sea states in which the capsize rate (i.e. the conditional probability of capsize given  $H_S$ ) is very low from those in which the rate is very high. In other words, the capsize band emphasizes a well-known fact that there is no distinct boundary separating safe from unsafe sea states; instead there is rather a transition zone within which capsize is possible. The presence of the band also implies that although there must be sea states at which the vessel will never capsize and that there must be sea states

---

simply be a band of wave heights containing most of the area under the  $p(H_S|\text{capsize})$  probability density function curve. Instead, boundaries of the capsize band are expressed with the use of the following equalities:

$$(H_S)_{low} = H_S |_{P_f(H_S)=\alpha} \quad \text{and}$$

$$(H_S)_{high} = H_S |_{P_f(H_S)=1-\alpha}, \quad \text{where } \alpha \text{ is some (small) number.}$$

---

<sup>1</sup> With significant wave height at the instance of capsize being a random variable, the confidence interval would

at which she would inevitably capsize, due to limited resolution of physical or numerical experiments the lower and upper boundaries can only be expressed by means of limits. Such asymptotic nature requires the use of some threshold values of  $P_f$  outside of which occurrence of capsize will either be virtually impossible or practically certain. Making use of analogy to statistics again, such limiting sea states corresponding to threshold values of  $P_f$ , can be interpreted as confidence limits.

Although the capsize rate,  $P_f$ , is a function of many variables, such as sea state, loading condition and damage characteristics, it has been observed that in all cases it follows a clear and recurring trend. This has triggered the pursuit for its analytical representation that could be used in parametric studies on capsize phenomena in order to derive universal formulae for probability of capsize and corresponding time to capsize.

Understandably, such studies require a vast number of experiments to be performed, which sets particular limits on the achievable resolution and accuracy of the results. In this paper, the authors present a brief account of the current state-of-the-art, discuss advantages and shortcomings and propose an alternative approach, which can offer significant reduction of effort (normally expended in numerical simulations and model experiments) whilst retaining comparable accuracy of the outcome.

## APPROACH

### Software Tools

Numerical experiments supporting this work have been carried out with PROTEUS3, the in-house developed software that has been successfully employed over many years in a number of research and commercial projects. It has been referenced a number of times, benchmarked against experimental data and other numerical codes successfully and has aided greatly in our understanding of capsize phenomena in damage conditions. OriginPro8 – a powerful statistical package – was used for

processing of the results, parametric studies and development of the methodology.

### Ship Models

Two models of Ro-Pax vessels have been studied for the purpose of this paper, of 89 and 170 metres in length between perpendiculars. The first ship (EUGD01-R2) is being extensively tested numerically at the moment for the on-going EU Project GOALDS that aims to re-engineer the probabilistic rules formulation for damage survivability of passenger ships. Physical model experiments are scheduled for this ship later in the course of the project. The larger Ro-Pax has been used in previous research projects, including HARDER, the foundation of the current probabilistic regulatory framework for damage stability. Results of physical model experiments carried out on this vessel are being used for validation of the numerical code.

**Table 1: Main Particulars of Models**

Model	PRR01	EUGD01-R2	
Passengers	1420	622	
L <sub>OA</sub>	194.3	97.9	m
L <sub>BP</sub>	176	89	m
Breadth	25	16.4	m
Deepest subdivision loadline	6.55	4	m
Depth to bulkhead deck	9.1	6.3	m
Displacement	16,558	3,445	tn
Service speed	21.0	19.5	kn

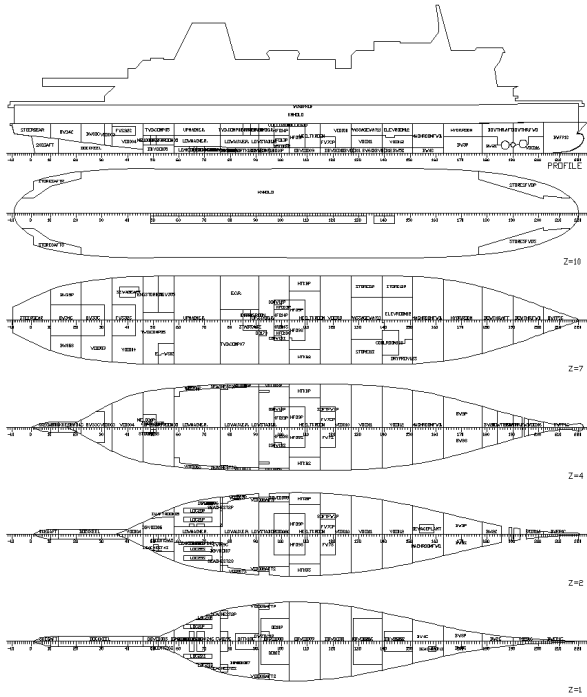


Fig. 1: Subdivision of PRR01 from NAPA

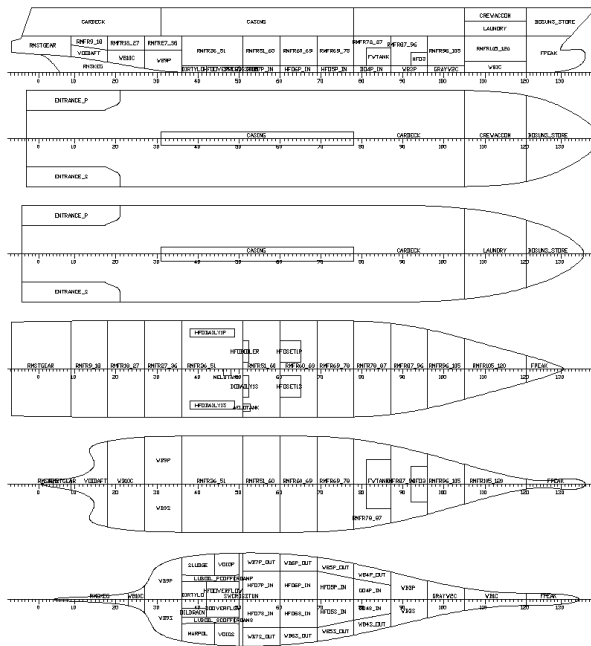


Fig. 2: Subdivision of EUGD01-R2 from NAPA

The two chosen ships cover different regions of the design space to ensure universal application of the results. The PRR01 was designed for transport of, primarily, vehicles across short routes such as the English Channel, actually converted to carry a number of passengers in addition to that during the

building stage. The second ship was designed for transport of a small number of both passengers and vehicles within an island archipelago in short-crested, choppy seas.

### Numerical Experiments

Accurate representation of the capsize rate characteristic across the entire capsize band, requires adequate resolution. Therefore, it was deemed necessary to use at least 10 measurements within the transition zone, performed by increasing  $H_s$  in small steps, varying from 0.1m to 0.25m depending on the width of the capsize band. For each wave height,  $P_f$  was determined on a basis of at least 20 wave realisations to maintain at least 5% resolution. The larger ship was tested in seven and the smaller in five different loading conditions, including variations of draught and KG. Additionally, the survivability of the smaller vessel was studied in two distinct damages and various wave spectra. Waves were modelled using JONSWAP spectrum of slope (height to length ratio) equal to 1/20 and 1/25, respectively. Each realisation was limited to 1,800 seconds, which is the maximum time currently required by regulations for evacuation of a vessel. Complete time history of the motions and water accumulation (including water on Ro-Ro deck) was measured and recorded. No wind effect was included in the experiments. All simulations started with the ship in the damage equilibrium position.

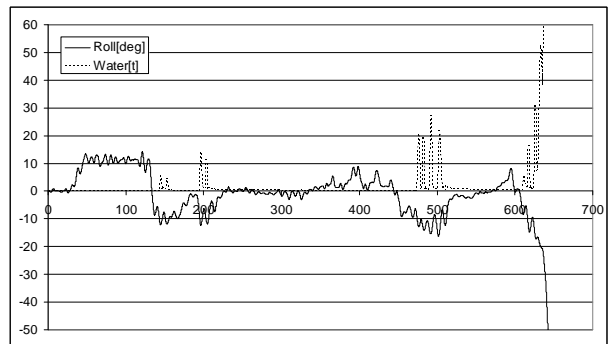


Fig. 3: Time history of Roll motion and water accumulation as recorded from PROTEUS3 for a capsizing case.

**Numerical code Validation**

Given the relative ease of use of numerical tools it is possible to carry out hundreds of simulations in a short period of time, given that results can be verified. Within the present study, the outcome of numerical software was benchmarked against available experimental data from project HARDER (availability of data was one of the reasons for selecting PRR01 as sample ship). Comparison between numerical and experimental results show satisfactory agreement (fig. 4).

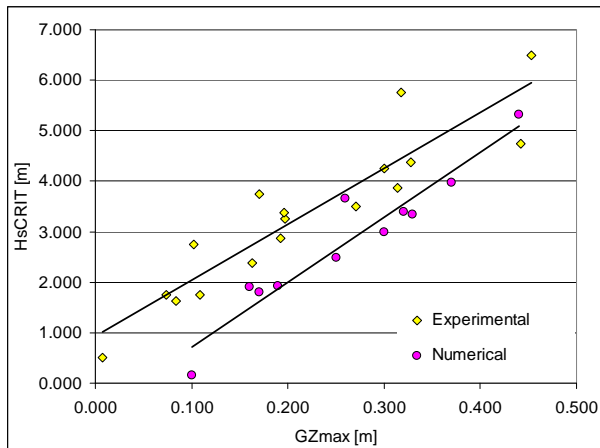


Fig. 4: Experimental versus numerical results for model PRR01

It should be noted here that the quantitative agreement between the results was considered of minor importance with emphasis being put on the observed trends. However large any discrepancies might be regarded, it is obvious that both sets of data bear large uncertainties.. Nevertheless, for the purpose of this work it was decided that as long as the differences are systematic an exact match is not required and no further numerical model calibration was performed, particularly as observations show that numerical results err on the side of safety.

**PROBABILITY OF CAPSIZE**

**Capsize rate**

The term capsize rate ( $P_f$ ) is used to denote the approximation<sup>2</sup> of the probability of capsize of

<sup>2</sup> This follows the classical definition of probability,

a damaged ship, given loading conditions and sea state. Predictably, for a given number of realisations<sup>3</sup>, capsize rate will vary from 0 for very small<sup>4</sup> to 1 for very large waves. Between minimum  $H_S$  for which  $P_f = 0$  and maximum  $H_S$  for which  $P_f = 1$ ,  $P_f$  can take any value ranging from 0 to 1. Following adopted convention (Vassalos et al, 1997), critical wave height corresponds to the significant wave height for which capsize rate is 0.5.

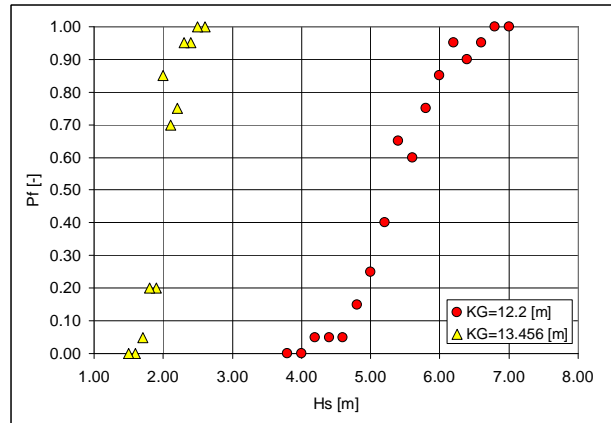


Fig.5: Capsize rate values for different loading conditions

Disregarding the experimental errors, it is obvious from figure 5 is that data follow a specific pattern throughout the range. The evident trend common for all the observations made across the entire  $H_S$  range led previous attempts to approach this characteristic by making use of its similarity to the integral of a normal Gaussian distribution – Cumulative Density Function (CDF) (Jasionowski et al, 2007). A major advantage of such approach is that the normal distribution is a well known function and statistical tools can be readily applied to the recorded data in order to find an interval around critical  $H_S$ , which could be interpreted as capsize band by use of standard deviation of the derivative of capsize rate. The biggest downside of this method is that it requires numerical differentiation of recorded

expressed as the ratio of favourable experiment outcomes over the total number of trials. It would become a probability of capsize (conditional on loading condition and wave parameters) if the number of trials approached infinity.

<sup>3</sup> A time series of seakeeping either by means of numerical simulations or physical model tests

<sup>4</sup> Relative to the critical significant wave height

data, i.e. it involves computation of the derivative of the capsize rate,  $P_f$ . As differentiation of infrequent data unequally distributed along the  $H_S$  range may introduce large uncertainties, the approach is practically limited to large<sup>5</sup> data sets.

**Non-Linear Regression**

Exhaustive pursuit for a more convenient functional representation of the capsize rate resulted in a parametrically defined sigmoid function that turned out to be an attractive alternative to the Gaussian distribution. Boltzmann’s sigmoid allows direct regression of measured rates, without the need for prior numerical differentiation. The resulting function can be differentiated easily afterwards to derive the requisite information on the capsize band. In its most general form the function is given by means of four parameters:  $A_1$ ,  $A_2$ ,  $x_0$  and  $d_x$ .

$$y(x) = \frac{A_2 + (A_1 - A_2) e^{-\frac{x-x_0}{d_x}}}{1 + e^{-\frac{x-x_0}{d_x}}} \quad (1)$$

Where:

- $A_1$  : asymptotic lower limit
- $A_2$  : asymptotic upper limit
- $x_0$  : ordinate of centre of symmetry
- $d_x$  : time constant<sup>6</sup>

By nature of the capsize rate observations, the first two parameters can be constrained to 0 and 1, respectively, which leaves just two parameters requiring estimation and allows for, after some basic manipulation, the expression of  $P_f$  as a function of  $H_S$ ,  $x_0$  and  $d_x$

(2). The derivative of  $P_f$  with respect to  $H_S$  is given as in (3)

$$P_f(H_S) = \frac{e^{\frac{H_S - x_0}{d_x}}}{1 + e^{\frac{H_S - x_0}{d_x}}} \quad (2)$$

$$\frac{dP_f}{dH_S} = \frac{e^{\frac{H_S - x_0}{d_x}}}{dx \left( 1 + e^{\frac{H_S - x_0}{d_x}} \right)^2} \quad (3)$$

Figures 6 and 7 depict an example of Boltzmann’s sigmoid fitted to the experimental data as well as residuals of fitting. Statistical data describing goodness of fit are presented in Tables 2 and 3.

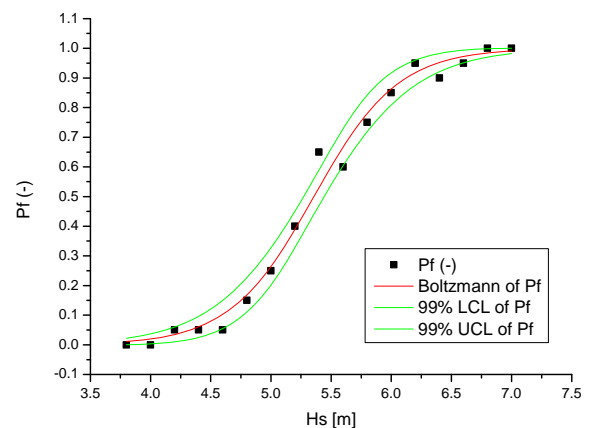


Fig. 6: Fitted sigmoid and 99% confidence boundaries

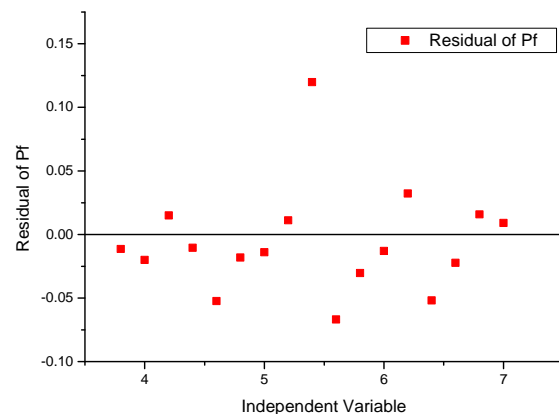


Fig. 7: Residuals of Pf sigmoid fitting

<sup>5</sup> Word *large* in this context refers rather to computational or experimental effort than actual, numerical size of the data.

<sup>6</sup> The parameter  $d_x$  is referred to by analogy to dynamic system response to step input. In context of current application is a span parameter (related to slope at inclusion point).

**Table 2: Parameters of sigmoid regression to  $P_f$  for  $T=6.25$  m,  $KG=12.200$  m, even keel.**

Parameters		
	Value	Standard Error
A1	0	0
A2	1	0
x0	5.35778	0.02832
dx	0.34893	0.02503

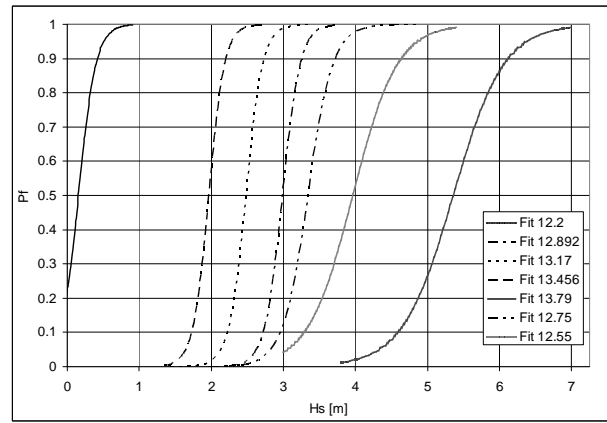


Fig. 8: Capsize rate for various critical significant wave heights

**Table 3: Statistics of sigmoid regression**

Statistics	
Number of Points	17
Degrees of Freedom	15
Reduced Chi-Sqr	0.00192
Residual Sum of Squares	0.02873
Adj. R-Square	0.98814

Results of employing this technique to data deriving from numerical simulations performed at different KGs are presented in figure 8. It can be readily seen that increasing KG causes a shift of  $P_f$  characteristics towards lower sea states with a more rapid transition from low to high capsize rates (probability distribution becoming narrower as KG increases). This implies that as survivability decreases the transition from the region considered safe to that considered as unsafe is faster. The performance of this particular probability distribution's parameters against other ship characteristics can be established in the same manner, with the scope to detect any dependencies between survivability and specific design variables.

### *Estimation of the capsize band*

The previous observation can be quantitatively confirmed by use of critical significant wave height and capsize band parameters. The first quantity is associated with  $x_0$  parameter of the regression's sigmoid function whereas the latter can be easily calculated using equation (1). By analogy to statistics the capsize band can be interpreted as the range of the probability distribution, spreading either side of the capsize boundary ( $P_f = 0.5$ ), symmetrically. In a more straightforward interpretation limits of the capsize band simply determine boundaries outside which capsize rate is either so high or so low that capsize in given  $H_s$  is either certain or unlikely, beyond upper and below lower limits, respectively. In order to determine such limits, it is convenient to take some small number  $\alpha$ , and find those values of  $H_s$ , which satisfy the following conditions:

$$(H_s)_{low} = H_s \Big|_{P_f(H_s)=\alpha} \quad (4)$$

And

$$(H_s)_{high} = H_s \Big|_{P_f(H_s)=1-\alpha} \quad (5)$$

The boundaries  $(H_S)_{low}$  and  $(H_S)_{high}$  can be calculated using the inverse  $P_f$  function, given as:

$$H_S(P_f) = x_0 + dx \cdot \ln\left(\frac{P_f}{1-P_f}\right) \quad (6)$$

Lower and higher limits of the capsize band, given as  $H_S(P_f = \alpha)$  and  $H_S(P_f = 1 - \alpha)$  are equal to:

$$H_S(P_f = \alpha) = x_0 + dx \cdot \ln\left(\frac{\alpha}{1-\alpha}\right) \quad (7)$$

And

$$H_S(P_f = 1 - \alpha) = x_0 + dx \cdot \ln\left(\frac{1-\alpha}{\alpha}\right) \quad (8)$$

The following figure demonstrates these limits, calculated with the parameter  $\alpha = 0.05$ .

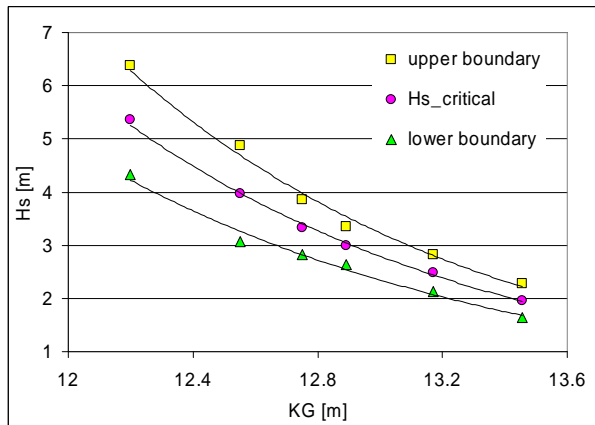


Fig. 9: Capsize band Vs KG

**Parameterisation**

Attempts to derive a simple analytical function to represent capsize boundaries and capsize band revealed new possibilities for parameterisation of the formula to populate a family of functions, which could be used as a universal tool for survivability assessment in both design and operational stages. In case of the sigmoid, the two defining parameters, i.e.  $x_0$  and  $dx$  can be expressed by means of wave

characteristics (other than  $H_S$ , which is explicitly present in the  $P_f$  formulae) or parameters related to loading condition, damage extent etc. Understandably, parametric studies require extensive and systematic simulation (testing) effort but some rough examples may be presented here. They may also shed some light on sensitivity problems associated with these studies. A single-variable parameterisation of the sigmoid's  $x_0$  and  $dx$  using KG as a parameter is presented in figure 10.

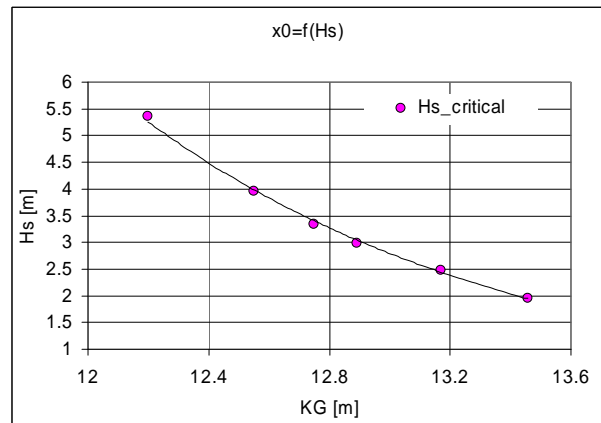


Fig. 10: Plot of critical significant wave height (capsize boundary) Vs KG (intact ship)

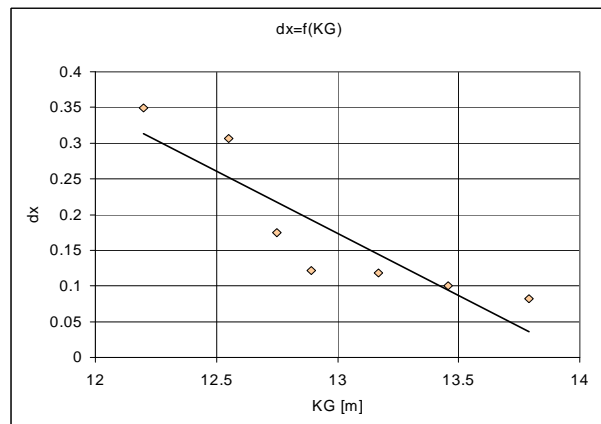


Fig. 11: Bandwidth parameter Vs KG (intact ship)

Obviously, the family of sigmoids describing the capsize rate should be populated with as many parameters as necessary, including also those specific to the damaged ship, e.g. residual freeboard, water head on a car deck etc. to enhance its functionality. For the purpose of this work, the parameters investigated are associated with the intact ship characteristics, leaving aside damage-related

quantities, until more research output is available. The following figure shows an example of decomposition of critical significant wave height with respect to (intact)  $GM$  and wave slope  $\lambda$ .

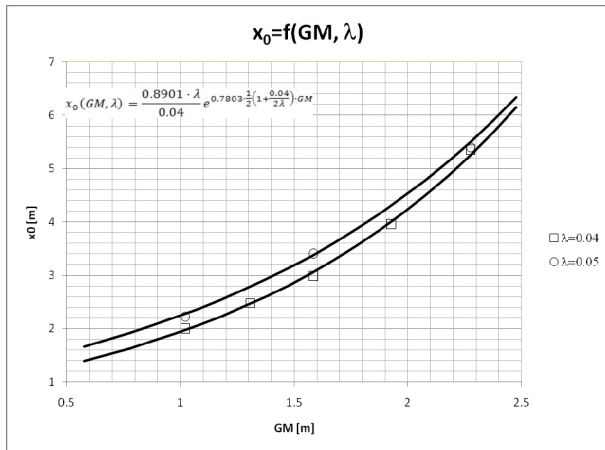


Fig. 12: Bi-variate parameterisation of critical significant wave height

**LINEAR APPROXIMATION**

However convenient the sigmoid regression is to use, it also comprises some significant drawbacks. To start with, something that is particularly evident in cases of very narrow capsizes band is that the goodness of fit depends strongly on the quality of data in the proximity of tail asymptotes. Unfortunately, due to limited resolution of experimental data, these regions bear the highest uncertainty.

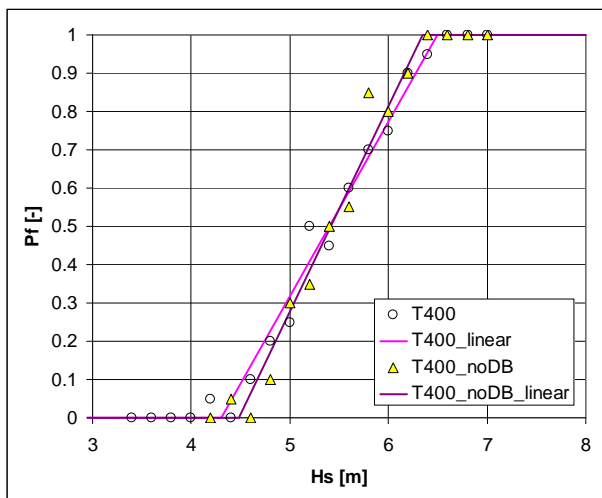


Fig. 13: Linear regression for different damage cases (EUGD01-R2)

Assuming that the data in proximity of the critical value, lying in the middle of the range of  $P_f$  should be the most reliable, an attempt has been made to simplify the approach and to use linear regression instead of non-linear, with encouraging results. It can be noticed that some cases demonstrate higher goodness of fit for linear regression than for a sigmoid. In order to achieve this, though, the tails of the series needed to be omitted as that is where the non-linear behaviour is dominant. However, it was observed that removing “tails” from the data set has no major impact on the result.

**Table 4: Sigmoidal Vs linear regression**

	Sigmoid	Linear
Number of Points	19	13
Degrees of Freedom	17	11
Reduced Chi-Squares	0.00211	
Residual Sum of Squares	0.03595	0.03247
Adj. R-Square	0.98703	0.97626

This, as demonstrated in table 4 by comparison of the residual sum of squares for one sample dataset, makes this approach really attractive. A major concern whilst using linear regression is related to the capsizes band and its analogy to the confidence interval. It is obvious that relying on statistical measures of goodness of fit may overshadow the fact that linear regression does not bring any information about the “tails” of the capsizes rate distribution and therefore any prediction of capsizes band based on this method should be approached carefully. However, closer examination of the linear regression and its affiliation with the sigmoid reveals some important virtues. Linear regression of the data close to  $x_0$  will actually result to the tangent of the sigmoid at the inclusion point  $(x_0, 0.5)$ . Therefore, for the linear regression parameters  $\alpha$  (slope) and  $\beta$  (intercept) the following relation holds:

$$\alpha = \left. \frac{dP_f}{dH_s} \right|_{H_s=x_0} = \frac{e^{-\frac{H_s-x_0}{dx}}}{dx \left( 1 + e^{-\frac{H_s-x_0}{dx}} \right)^2} = \frac{1}{4dx} \quad (9)$$

$$y(x_0) = \alpha x_0 + \beta = \frac{1}{2} \quad (10)$$

The parameters for the bandwidth and centre of symmetry of the sigmoid function can be derived directly from the linear regression formula:

$$dx = \frac{1}{4\alpha} \quad (11)$$

$$x_0 = \frac{0.5 - \beta}{\alpha} \quad (12)$$

Finally, since all the parameters required for the sigmoid representation can be evaluated on the basis of a linear fit, it is sufficient to apply linear regression to the observations and once  $x_0$  and  $dx$  are estimated, the capsizes band limits can be calculated with the use of equations 7 and 8, respectively.

**Table 5: Impact of slope estimate on capsizes band and  $H_s$  critical.**

	Fitted	Estimate 1	Estimate 2
0.05	1.28691	0.99266	1.16301
0.5 ( $H_{Scrit}$ )	1.68031	1.70087	1.68481
0.95	2.07372	2.40909	2.20661
band	0.78681	1.41643	1.0436

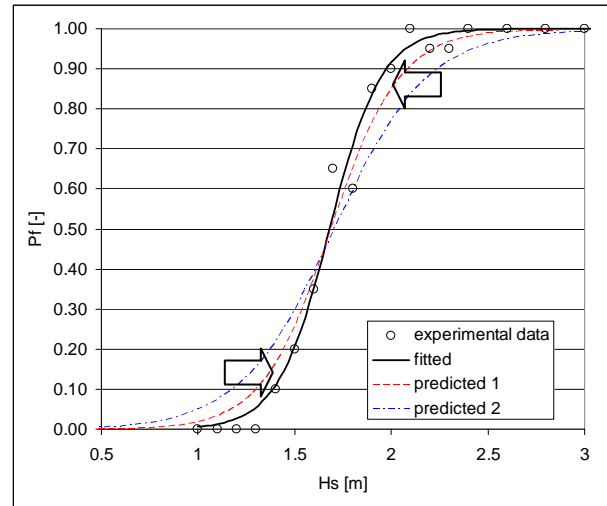


Fig. 14: Fit convergence - accurate estimate of slope at  $x_0$  results in closer match.

Such approach, based on linear regression, has some rather serious implications. First of all, it allows use of formulae derived for the sigmoid curve, well representing observed phenomena, but without the necessity of non-linear (least-squares) regression. Furthermore, as discussed earlier, experimental results in close proximity to 0 and 1 asymptotes are expected to suffer due to large uncertainties and in general, they require higher resolution. On the contrary, points corresponding to moderate capsizes rates are usually following the trend better. An approach based on linear regression makes it possible to disregard those regions entirely or just the parts that might be ambiguous. In the latter case (partial reduction) it is important that the remaining data preserve basic characteristics of the distribution, such as symmetry around  $x_0$ . Given that sufficient resolution is available around the  $x_0$  region, the resulting sigmoid function should be very accurate. The benefit of this approach is that one could derive an approximate capsizes band, having nothing more than 2 measurements of the capsizes rate, as long as they are different than 1 and 0 – ideally – and the smaller measurement corresponds to lower  $H_s$ . Of course, this should only be treated as an indication and a more accurate calculation of the slope of the probability distribution at its centre would have to be available for reliable results.

## CONCLUSIONS

This paper presents an alternative approach to the representation of the behaviour of a damaged ship in waves. The approach adopted for analytical approximation of the capsize band has both benefits (speed) and drawbacks (uncertainty) but some compromise is not only inevitable but also necessary in most engineering applications – particularly those that are exceptionally labour intensive and costly.

The characteristics of the probability distribution that describes the behaviour of Ro-Ro ships in boundary conditions have been identified and an analytical model describing the capsize band has been developed.

Furthermore, the way to utilise the outcome to predict the critical wave height has been demonstrated. In addition, the capability to facilitate these characteristics in the design process as constrains and/or objectives has been discussed.

Lastly, the merits of having an analytical approach to describe such a complex phenomenon are indisputable. The amount of realisation performed numerically for this work is counted in thousands, so the amount of work saved by such an approach is massive.

The presented analytical approach offers the necessary flexibility to integrate this with more complex models for prediction of time to capsize, which in turn can be associated with number of people to successfully evacuate and finally risk from flooding etc.

## REFERENCES

- HARDER (1999-2003). “Harmonization of Rules and Design Rational”. Project funded by the European Commission, DG XII-BRITE, 2000-2003.
- Jasionowski, A., Vassalos, D., Guarin, L., “Time-Based Survival Criteria for Passenger Ro-Ro Vessels”, 6<sup>th</sup> International Ship Stability Workshop, Webb Institute, 2002
- Jasionowski, A., Vassalos, D., Scott, A., Ship Vulnerability to flooding, 3<sup>rd</sup> international conference for maritime safety, Berkeley, California, 2007
- Vassalos, D., Turan, O. and Pawlowski, M.: “Dynamic Stability Assessment of Damaged Ships and Proposal of Rational Survival Criteria”, Journal of Marine Technology, Vol. 34, No. 4, pp 241-269, October 1997.

## A Critical Assessment of Ship Parametric Roll Analysis

Hisham Moideen,

Texas A&M University

Jeffrey Falzarano,

Texas A&M University

### ABSTRACT

Analysis of ship parametric rolling has generally been restricted to simple analytical models and sophisticated time domain simulations. However, simple analytical models do not capture all the critical dynamics while time-domain simulations are time consuming to implement. Our model captures the essential dynamics of the system without over simplification. This work incorporates important aspects of the system and assesses the significance of including or ignoring these aspects. Many of the previous works on parametric rolling make the assumption of linearized and harmonic behaviour of the time-varying restoring arm or metacentric height. This assumption enables modelling the roll as a Mathieu equation.

### KEYWORDS

Parametric Rolling; Mathieu Equation, Hills Equation

### INTRODUCTION

Analysis of ship parametric roll has generally been restricted to simple analytical models and sophisticated time domain simulations. Simple analytical models do not capture the all the critical dynamics while time-domain simulations are often time consuming to implement. Our model captures the essential dynamics of the system without over simplification. This work incorporates various important aspects of the system and assesses the significance of including or ignoring these aspects. Many of the previous works on parametric roll make the assumption of linearized and harmonic behavior of the time-varying restoring arm or metacentric height. This assumption enables modeling the roll motion as a Mathieu equation.

It is well known that most hull forms especially container ships, Ro-Ro ships and fishing trawlers are found to be prone to parametric roll instability are asymmetric about

the design water line. Hence the variation in the metacentric height will be asymmetric as well. This asymmetry invalidates the harmonic approximation. Studies by other researchers (ABS, 2004; Spyrou, 2000) have shown that the harmonic assumption is very crude.

Many of the past research on ship parametric roll have been to predict the occurrence of parametric roll. Fewer analytical methods have been developed to predict the resulting roll amplitude. Some studies were done by (Bulian, 2003). In his study a harmonic form was assumed for the response with a slowly varying amplitude and phase. However this required a complicated calculation and statistical linearization. Due to the large amplitude of motion resulting from the parametric instability the effects of non-linear damping also become important. Non-linear damping controls the bounded roll motion amplitude. So far there have been very few attempts to incorporate the effects of non-linear damping into analytical model to predict

roll motion amplitude. Many researchers have attempted to evaluate the effects of non-linear damping using time simulations which is very time consuming and does not help in understanding the behavior of the non-linearity throughout the entire domain.

Ships typically have varying forward speeds and hence varying encounter or exciting frequency. This property of ships makes them susceptible to both sub and super harmonic parametric resonance and possible instability as compared to offshore structures. Perturbation methods and harmonic assumption greatly affect the domain under which boundaries between the stable and unstable regions are valid. Extending the model to higher harmonics will enable accurate prediction over the entire range of operation. Such simple yet more accurate models can be used as benchmarks to predict parametric instability as well as bounded roll motion amplitude which in-turn can be utilized in the preliminary design stage so as to avoid hull forms prone to parametric rolling.

## BACKGROUND

Ship rolling motions is perhaps the most studied of the ship motions considering the disastrous consequences of failure. Large amplitude ship rolling motions can lead to progressive flooding and may eventually lead to the capsizing or foundering of a ship. Roll motion for ships is more complicated as compared to the other ship motions due to the presence of a non-linear restoring moment and small linear radiation damping. The presence of light damping leads to large amplitude motion when forced at the resonant frequency. As a consequence of the large amplitude roll motion the non-linear viscous damping becomes important and this further adds to the complexity of the analysis. Hence many studies have been carried out to predict ship roll motion in regular seas. The beam sea condition is believed to produce maximum rolling and hence has been extensively analyzed, see e.g (Nayfeh, 1986). Falzarano, (1990) analyzed the

complicated dynamics involved in roll motion leading to capsize using the Melnikov method. The beam seas rolling can be controlled with additional dampening such as that provided by bilge keels, roll tanks, stabilizing fins, etc. Apart from the beam sea capsizing condition, capsizing in the astern or following seas has also been analyzed (Hamamoto et al., 1996; Paulling, 1961; Umeda et al., 1995).

Parametric rolling is a form of parametric vibration due to time varying stiffness. Studies have shown that for some ships this phenomenon can lead to larger amplitude rolling motion in comparison to the beam seas condition. The change in the underwater hull form and hence the variation of the righting lever in waves leads to a time varying stiffness. If the variation in stiffness is large enough, it can result in large amplitude motion and eventual capsize. Numerical modeling of parametric rolling of ships in regular waves has been studied (Bulian et al., 2004; Munif and Umeda, 2006; Umeda et al., 2004). The Mathieu instability criterion is the most common method used to determine the onset of parametric roll. Most of the studies have been done with stability charts that do not indicate the effects of damping. Damping dramatically affects the boundaries between the stable and unstable region. Among container ships the post-Panamax container ship (C11 class) is the most studied vessel as a result of the cargo damage it suffered in 1998. The effect of parametric roll on the failure of container lashing system was studied by the SNAME ad-hoc panel #13 on Parametric Rolling (France et al., 2001). Spyrou (Spyrou et al., 2008) also studied the prediction potential of the parametric rolling for the post Pana-max container ships. This current paper discusses the methods commonly used to study parametric roll. One of the most common methods is to use simple Ince-Strutt stability diagram for Mathieu's equation in predicting the onset of parametric roll. A major drawback of the method is that the Ince-Strutt diagram for Mathieu's equation is generic and does not

depend on the ship characteristics. A stability chart which depends on the ship parameters would be a more accurate approach.

Since parametric excitation can lead to large amplitude roll motion, the effects of non-linear damping cannot be neglected. Nonlinear roll damping may lead to bounded motion. Hence incorporating the effects of non-linear damping into stability charts would give a more realistic prospect of predicting roll behavior. Hence without getting into complicated analyses, we can analyze the occurrence of parametric roll and also predict the roll motion amplitude using these charts at an early design stage.

### PARAMETRIC ROLL EQUATION

The roll equation of motion in general for linear uncoupled motion is given by

$$(I + A(\omega_D))\ddot{\phi} + B(\omega_D)\dot{\phi} + C\phi = M \cos(\omega t) \quad (1)$$

Where,

$\Phi$  – Roll Amplitude

$I$  – Moment of Inertia about Roll Axis

$A(\omega)$  – Added Inertia

$B(\omega)$  – Roll radiation wave damping

$C$  – Restoring moment in roll =  $\Delta \cdot GM$

$M$  – External roll moment

$\omega$  – Forcing Frequency

For the case of head/astern sea there would be no direct roll excitation. One would expect no motion considering (1). But as discussed, (1) only represents linear damping and stiffness. This is one of the assumptions in linear strip theory where the wave profile is approximated by a flat surface at the design draft. If one considers the actual wave profile then the underwater hull form of the vessel changes as the wave passes by the vessel. This leads to a time varying restoring moment and hence a time varying stiffness.

The parametric roll equation of motion in roll considering time varying hydrostatics is given by

$$(I + A(\omega_D))\ddot{\phi} + B(\omega_D)\dot{\phi} + C(t)\phi = 0 \quad (2)$$

Where,

$$C(t) = \Delta g \cdot GZ(t)$$

$GZ(t)$  – Time varying roll restoring arm

$$\omega_D = \omega_n \sqrt{1 - \zeta^2} \text{ - Damped natural frequency}$$

$\omega_n$  -natural frequency

$\zeta$  - Damping ratio

Note that in (2) the nonlinear viscous damping is not yet explicitly considered in the roll equation of motion.

The righting arm of a vessel is generally approximated by a polynomial function of the roll angle.

$$GZ = C_1\phi + C_3\phi^3 + C_5\phi^5 \dots \quad (3)$$

Here  $GM$  (metacentric height) of the vessel is given by slope of the  $GZ$  curve at origin, If we linearize and neglect higher order terms (since they are important only for large amplitudes of roll), then (2) becomes,

$$(I + A(\omega_D))\ddot{\phi} + B(\omega_D)\dot{\phi} + \Delta GM(t)\phi = 0 \quad (4)$$

If the time varying  $GM$  is modelled as

$$GM(t) = GM_0 + \delta GM \cos(\omega t) \quad (5)$$

Where,  $GM_0$ -still water  $GM$

Using the following transformation, Eq. (3) is converted into a non-dimensional form,

$$\tau = \omega t, \quad \omega_D = \sqrt{\frac{g\Delta GM_0}{(I + A(\omega_D))}}, \quad ( )' = \frac{d}{d\tau} \quad (6)$$

$$\alpha = \left(\frac{\omega_D}{\omega}\right)^2, \quad \gamma = \frac{\delta GM}{GM_0}, \quad \mu = \frac{B(\omega_D)}{(I + A(\omega_D))\omega}$$

$$\frac{d^2}{d\tau^2} \phi + \mu \frac{d}{d\tau} \phi + (\alpha + \gamma \cos(\tau)) \phi = 0 \quad (7)$$

With  $\mu=0$ , Eq. (6) represents a typical Mathieu Type equation (undamped). The Ince-Strutt diagram/Mathieu stability charts help determine the occurrence of parametric vibration.

Hence by determining the GM variation in waves one can predict the occurrence of parametric roll using the Ince-Strutt diagram. The method for developing Mathieu Charts and effects of Damping are discussed in the next section.

### MATHIEU EQUATION AND STABILITY CHARTS

Mathieu equation is extensively studied in the field of parametric vibration. Several approaches are used to develop the stability charts. Hayashi, (1960) used the perturbation method to obtain his charts. The range of validity of these charts as expected is limited. Another method is called the Hill's infinite determinant method can also be used to develop stability charts. These charts are very accurate in the region where they are defined.

The standard Mathieu Equation with damping is given by

$$x'' + \mu x' + (\alpha + \gamma \cos(\tau)) x = 0 \quad (8)$$

In order to develop the Mathieu charts the solution ( $2\pi$  &  $4\pi$ ) of the equation is expressed as Fourier series,

$$x_{2\pi}(t) = a_0 + \sum_{n=1}^{\infty} (a_n \cos(n\tau) + b_n \sin(n\tau)) \quad (9)$$

$$x_{4\pi}(t) = a_0 + \sum_{n=1}^{\infty} \left( a_n \cos\left(\frac{n\tau}{2}\right) + b_n \sin\left(\frac{n\tau}{2}\right) \right) \quad (10)$$

Substituting Eq. (8) & Eq. (9) into Eq. (7) and setting the secular terms to zero we get two matrices for each solution as given below.

Neglecting the trivial case of  $a_0=a_1=b_1\dots=0$ , the determinant of the parametric matrix (matrix containing  $\alpha$  &  $\gamma$ ) should be zero. This gives the relationship between the parameters  $\alpha$  and  $\gamma$ . The instability boundaries for various damping ratios are shown in fig 1.

$$\begin{bmatrix} \alpha & \frac{\gamma}{2} & 0 & 0 & 0 & \dots & 0 \\ \gamma & \alpha-1 & \mu & \frac{\gamma}{2} & 0 & \dots & 0 \\ 0 & -\mu & \alpha-1 & 0 & \frac{\gamma}{2} & \dots & 0 \\ 0 & \frac{\gamma}{2} & 0 & \alpha-4 & 2\mu & \frac{\gamma}{2} & 0 \\ \dots & & & & & & \end{bmatrix} \begin{bmatrix} a_0 \\ b_0 \\ a_1 \\ b_1 \\ a_2 \\ b_2 \\ \dots \\ \dots \end{bmatrix} = 0 \quad (11)$$

$$\begin{bmatrix} \alpha - \frac{1}{4} + \frac{\gamma}{2} & \frac{\mu}{2} & \frac{\gamma}{2} & 0 & \dots & 0 \\ \frac{\mu}{2} & \alpha - \frac{1}{4} - \frac{\gamma}{2} & 0 & \frac{\gamma}{2} & \dots & 0 \\ \frac{\gamma}{2} & 0 & \alpha - \frac{9}{4} & \frac{3\mu}{2} & \frac{\gamma}{2} & 0 \\ 0 & \frac{\gamma}{2} & -\frac{3\mu}{2} & \alpha - \frac{9}{4} & 0 & \frac{\gamma}{2} \\ \dots & & & & & \end{bmatrix} \begin{bmatrix} a_1 \\ b_1 \\ a_2 \\ b_2 \\ a_3 \\ b_3 \\ \dots \\ \dots \end{bmatrix} = 0 \quad (12)$$

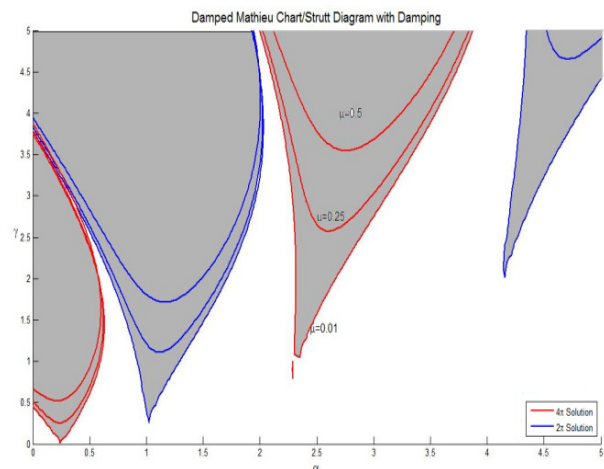


Fig1. Ince-Strutt diagram for Mathieu's Equation with constant damping. The shaded region indicates the unstable zone.

As evident from the charts, the effect of damping is to elevate the curves from the  $\alpha$  axis, thereby reducing the unstable region. In terms of energy one can imagine damping tending to drain the energy from the excitation until the threshold energy is reached to instigate parametric vibration. Hence one method of avoiding parametric roll in ships would be to increase the damping.

The advantage of the chart above is that it can be used to study the parametric instability of any dynamical system whose equation of motion can be modeled as a Mathieu equation. This is so because the charts are not affected by the parameters of the system under study. Depending on where the  $(\alpha, \gamma)$  pair falls in the chart, it becomes trivial to predict parametric instability.

If the stiffness variation is not single frequency harmonic and sinusoidal the system cannot be represented by a Mathieu equation. In such a case we can always represent the time varying coefficient (stiffness for ships) as a Fourier expansion. The resulting equation is called Hills Equation. Since the formulation of the Hills equation depends on ship parameters, these charts give a better prediction model. Our current and future work has concentrated on studying the details of Hills equation and developing the corresponding stability charts.

## GM VARIATION

### Ship Details

As discussed in the previous sections modern container ships seem to be more prone to parametric excitation. In order to develop realistic charts for prediction it is necessary to use a model which has parametric instability. It has been shown that post-Panamax C11 hull form exhibit parametric rolling(France et al., 2001). Here a modified C11 hull form is analyzed. The stern of the hull is modified to have fuller form, this model is named Pram aft body (MARIN Report No 17701-2-SMB,

2005). The main particulars of the vessel are shown in the Table 1.

**Table 1. Main Particulars of C11 Hull Form (pram aft body)**

$L_{PP}$ (m)	262.00
B (m)	40.00
D (m)	24.45
Mean Draught (m)	11.50
Displacement (tones)	69128.00
KG (m)	18.37
$GM_t$ (m)	1.96
Natural Roll Period, $T_\phi$ (sec)	25.14

The body plan of the modified C11 hull form is shown in Fig2. A 3D-wire mesh model of the vessel is shown in Fig3. The fine underwater hull form and wide flare above design draft is clearly evident from the wire mesh model. Such hull characteristics are one of the main reason for drastic variation of the submerged hull form and hence metacentric height. Hence ship stability in waves is a lot different from static stability.

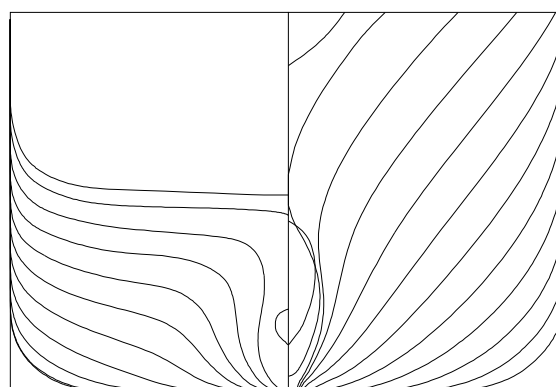


Fig 2. Body Plan of modified C11 Hull Form (not to scale)

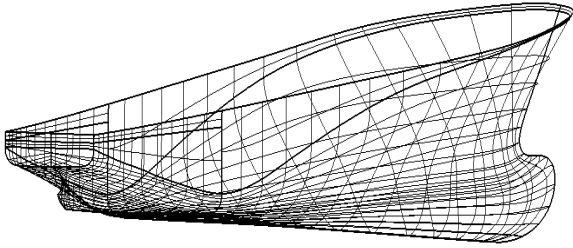


Fig3. Wire mesh model of modified C11 Hull

Fig4 shows the variation of the submerged hull with wave crest at midship and wave trough at midship.

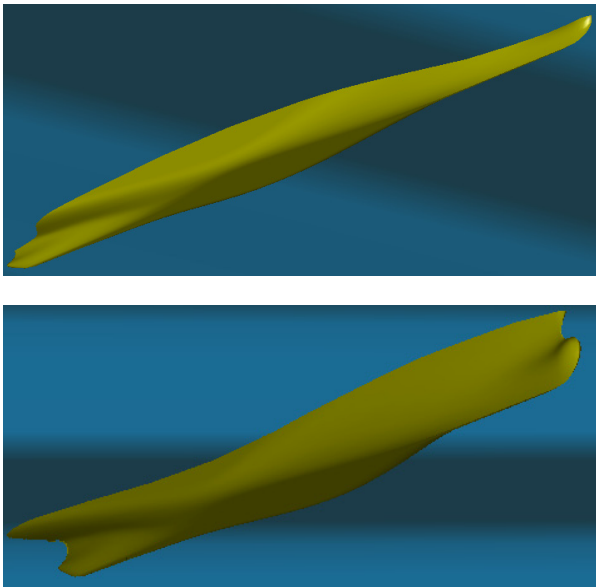


Fig4. Change in Underwater Hull form in waves of modified C11 Hull form. Top -Wave Crest Midship, Bottom -Wave Trough Midship. Wave Length=Ship LPP

**GM in regular waves**

In order to estimate the GM variation in regular waves, the roll restoring curve (GZ) for 10 different wave crest positions along the ship are calculated. The slope of the GZ curve at origin gives the GM. Standard hydrostatic software is used to obtain the GM for different wave crest position. Calculations are done for zero forward speed and free trim condition (hydrostatic balance). The details of the regular wave used for estimation is given below,

Wavelength  $\lambda = L_{PP} = 262\text{m}$

$$\text{Wave Number } = k = \frac{2\pi}{\lambda} = 0.024$$

For deep water the wave frequency is given by

$$\omega^2 = gk, \omega = 0.485 \text{ rad/s}$$

The ship's natural frequency of roll is given by

$$\omega_n = \frac{2\pi}{T_\phi} = 0.25 \text{ rad/sec}$$

$$\text{The damping ratio } \zeta = \frac{B(\omega_n)}{2(I + A(\omega_n))\omega_n} \sim 0.003$$

Hence  $\omega_D \sim \omega_n$

$$\text{Hence the parameter } \alpha = \left(\frac{\omega_n}{\omega}\right)^2 = 0.265$$

Looking at the Mathieu Chart (Fig.1) this value is very close to principal parametric resonance zone ( $\alpha = 0.25$ ). The value of metacentric height (GM) for the wave crest at different position along the ship length is shown in Fig. 5.

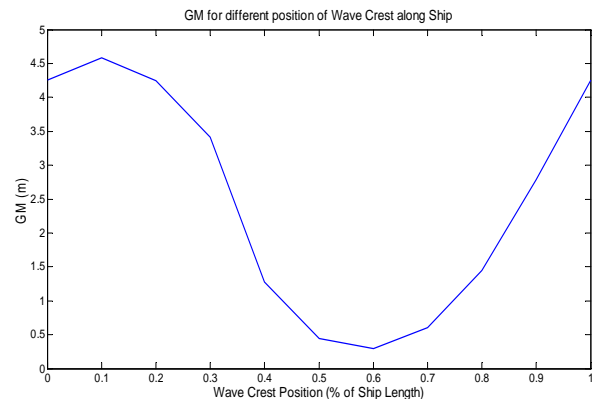


Fig5. GM for different position of wave crest

A wave height equal to 1/40 of wave length is used to estimate GM,  $H_w = 6.55\text{m}$ . The non-linear coupling effects of pitch and heave on the hydrostatics of the vessel is neglected.

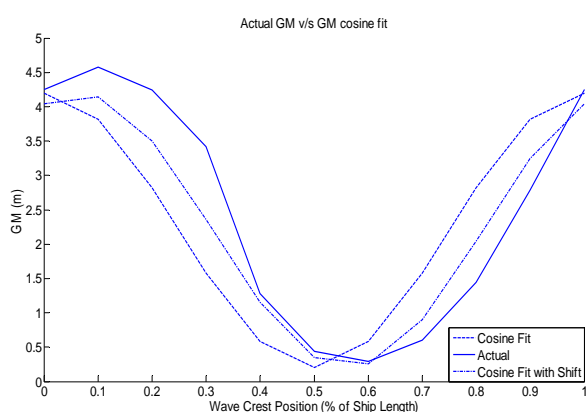


Fig6. Comparison of Cosine Fit of GM with Actual GM. (--- Cosine Fit and -.- Cosine Fit with Shift of  $\pi/8$ )

Fig. 5 depicts a form for the GM variation and hence can be approximated into Mathieu's equation. The comparison between the Mathieu fit and actual GM is shown in Fig. 6. As shown by (Spyrou et al., 2008) a case of cosine fit of GM with a phase shift (Fig6) has a better fit. The phase shift used here is  $\pi/8$ . The poor fit of the Mathieu approximation (even phase shifted) to the actual GM variation is clearly evident. Hence, there is a need to use a method with which we can approximate the GM variation more accurately. The Hill's equation and the corresponding stability charts could be a solution to this problem.

## CONCLUSIONS

The abrupt changes in the underwater hull of the vessel are one of the primary reasons for the drastic change in stiffness of the vessel. The analysis carried out in the paper clearly exhibits the usefulness of simple Ince-Strutt diagrams or instability chart in predicting parametric roll of ships. The chart also demonstrates the implicit dependence of the phenomenon on damping.

The ability of the charts to predict the bounded roll motion amplitude is perhaps a feature so far not discussed. The effects of non-linear damping (which is important due to large amplitude motion due to parametric roll) which is to bound the motion can be explained using

these stability charts. Being able to estimate the bounded roll motion amplitude can be very helpful in the initial design stage to study the implications of parametric roll on the stability of the vessel.

The Hill equation tend to consider the time varying stiffness better in comparison to a Mathieu and hence the use of a stability diagram for Hill's equations would give a much more accurate prediction of the occurrence of parametric roll especially in higher instability zones. The charts can also be used to calculate the critical frequency and the threshold wavelength which would initiate large amplitude rolling motion.

The parametric stability of the vessel for different forward speeds can also be predicted using these charts. The charts also enable the study of parametric stabilization. For example by merely increasing or decreasing the speed of the vessel we might be able to avoid parametric roll or worsen the situation by moving into a more unstable region. These instability charts can act as a guide for crew onboard a ship experiencing large amplitude motion in head/following sea in deciding whether to increase or decrease the vessel speed and to what extent.

Hence apart from serving the purpose of a simple and practical tool for parametric roll study during the initial design stage the Mathieu or Hill stability charts can also be helpful during the operation of the vessel in a seaway.

## ACKNOWLEDGEMENTS

The authors would like to thank Dr. Frans van Walree of MARIN for making available to us the hull form description for our analysis.

## REFERENCES

- ABS, 2004. ABS Guide for the assessment of parametric roll resonance in the design of container carriers. American Bureau of Shipping.

- Bulian, G., 2003. Development of analytical nonlinear models for parametric roll and hydrostatic restoring variations in regular and irregular waves, Department of Naval Architecture, Ocean and Environmental Engineering (DINMA). University of Trieste.
- Bulian, G., Francescutto, A., Lugni, C., 2004. On The Non Linear Modeling Of Parametric Rolling in Regular and Irregular Waves. *International Shipbuilding Progress* 51 (2/3), 173-203.
- S. Das and J. Falzarano “Transit Draft Roll Motion Stability Analysis of The Mobile Offshore Base (MOB) Using Time Varying Coefficients,” Eleventh International Offshore and Polar Engineering Conference, June 2001, Stavanger, Norway
- Falzarano, J.M., 1990. Predicting complicated dynamics leading to vessel capsizing, Naval Architecture and Marine Engineering. The University of Michigan, Michigan.
- France, W.N., MarcLevadou, Treakle, T.W., Paulling, J.R., 2001. An Investigation of Head-Sea Parametric Rolling and its Influence on Container Lashing Systems. SNAME Annual Meeting.
- Hamamoto, M., Enomoto, T., Sera, W., 1996. Model experiment of ship capsizing in astern seas-second report. *Journal of Society of Naval Architects of Japan* 179, 77-87.
- Munif, A., Umeda, N., 2006. Numerical prediction on parametric roll resonance for a ship having no significant wave-induced change in hydrostatically-obtained metacentric height. *International Shipbuilding Progress* 53, 183-203.
- Nayfeh, A.H., 1986. Nonlinear rolling of ships in regular beam seas. *International Shipbuilding Progress* 33 (40-49).
- Paulling, J.R., 1961. The Transverse Stability of a Ship in a Longitudinal Seaway. *Journal of Ship Research* 4 (1), 37-49.
- Spyrou, K.J., Thompson, J.M.T, 2000. The nonlinear dynamics of ship motions: a field overview and some recent developments. *Philosophical Transactions of Royal Society*, 1735-1760.
- Spyrou, K.J., Tigkas, I., Scanferla, G., Pallikaropoulos, N., Themelis, N., 2008. Prediction potential of the parametric rolling behaviour of a post-panamax containership. *Ocean Engineering* 35, 1235-1244.
- Umeda, N., Hamamoto, M., Takaishi, Y., 1995. Model experiments of ship vapsize in astern seas. *Journla of Society of Naval Architects of Japan* 177, 207-217.
- Umeda, N., Hashimoto, H., Vassalos, D., Urano, S., Okou, K., 2004. Nonlinear Dynamics on Parametric Roll Resonance with Realistic Numerical Modelling. *International Shipbuilding Progress* 51 (2/3), 205-220.

## On the prediction of parametric roll

Michiel Gusing

MARIN Wageningen

Reint Dallinga

MARIN Wageningen

### ABSTRACT

The numerical assessment of parametric rolling by means of time domain simulations is troublesome. This is due to a number of practical and conceptual problems. Therefore, simple transparent methods that give immediate insight in the characteristics of a particular design are still of interest. The present paper describes a method in which the results of linear calculations on the ship motions are used to estimate hydrostatic stability variations. Following Dunwoody (1989a) the stability variations are translated in a reduction of the roll damping and the safe operational limits of the ship. Numerical results are compared with experimental data.

### KEYWORDS

Seakeeping, Parametric Rolling, Stability Variations in Waves, Risk Assessment

### INTRODUCTION

Over the past years the assessment of the risk on parametric roll for new ships has received considerable attention. Despite these efforts the question how to perform a practical and reliable analysis has not been fully resolved.

In general, tests with a scale model are considered as the most reliable way to obtain data since most of the underlying physical phenomena are included. Think of relevant details like the natural speed variations in irregular waves (France et al. (2001)), the effect of large roll angles on the added resistance, the propulsive characteristics (including propeller ventilation), loss of rudder and stabilizer efficiency and the natural non-linearity's in the wave profile.

However, the design of an experiment with a scale model is not entirely straightforward. First of all there are a host of practical issues regarding the representation of the wind and waves (spectral shape, directional spread), the target mean speed (governed by the added

resistance and prudent seamanship), the modelling of active roll stabilisation, the steering and the modelling of the model propulsion (including the reaction of the main engines on the encountered propeller load variations). Secondly, and perhaps even more demanding, is the question what test duration will give a reliable assessment of the risk of encountering dangerous ship behaviour.

Numerical simulations offer a flexible alternative for tests with a scale model. On one hand in the spectrum of available tools one might consider CFD (Umeda et al(2008)), which incorporates potentially some (but not all) details of the nonlinear ship behaviour in waves if it covers details like appendages, moving rudders, fins and the steering. On the other end of the spectrum of tools are one degree of freedom (1-DOF) time domain models and methods based on statistical approaches (Archer et al. (2009)).

The commonly used time domain, “non-linear” potential flow calculations (see for example

France et al. (2001)) are in the midst of this spectrum of tools. They do account for 6-DOF ship behaviour and the weak non-linear effects related to rapid changes in hull geometry around the waterline. However, they neglect the non-linear diffraction and the non-wave making aspects of the roll damping. The latter omission requires correction on basis of empiricism. Furthermore, the added resistance is not covered correctly because of the neglect of the non-linear diffraction, the sustained speed and speed variations are not covered adequately.

Because of the fact that the efforts of going through time domain simulations do not necessarily bring the expected accuracy, there is an interest in simpler transparent methods. The approach adopted in the present paper is a combination of a new method to obtain the variations in stability ( $\delta GM$ ) and an existing formulation Dunwoody (1989a) to translate these variations in a decrease in effective roll damping.

The first step in this method uses linear frequency domain potential flow calculations to calculate the motion response and relative wave elevation along the waterline (accounting for reflected and radiated wave components). These results are used to calculate the hydrostatic stability variations, accounting for the hull form variations above and below the calm water line.

In a second step this (non-linear) transfer function of the stability variations is used in a formulation developed by Dunwoody (1989a) to estimate the apparent reduction in roll damping in irregular seas.

In a last step this result, which depends on significant wave height and mean wave period, is compared with the roll damping of the hull (estimated by means of an empirical method or existing model test data) to estimate the wave conditions in which the effective roll damping is negative. It is shown that the results of these computations show a fair agreement the results from tests with a scale model. A number of practical issues will be mentioned and an outlook to future developments will be given.

## STABILITY VARIATIONS AS THE CAUSE OF PARAMETRIC ROLL

To illustrate the physics of parametric rolling, a simple 1-DOF model with a time dependant spring term  $c(\tilde{t})$  is analysed.

$$a. \ddot{\phi}(t) + b. \dot{\phi}(t) + (c + c(\tilde{t})). \phi(t) = 0 \quad (1)$$

Where  $a$  represents the total of structural and hydrodynamic inertia,  $b$  the damping and  $c$  the restoring term. To understand why and how stability variations  $\tilde{c}(t)$  lead to large roll angles we will assume a harmonic roll oscillation with the associated roll velocity.

$$\phi(t) = \phi_a \sin(\omega_\phi t) \quad (2)$$

$$\dot{\phi}(t) = \phi_a \omega_\phi \cos(\omega_\phi t) \quad (3)$$

We will also assume a harmonic stability variation  $\tilde{g}\tilde{m}$  of the transverse metacentric height GM with a different frequency and phase angle given by Equation (4)

$$\tilde{c}(t) = \tilde{g}\tilde{m}. \rho g \nabla = \rho g \nabla GM_a \sin(\omega_{gm} t + \varepsilon_{gm}) \quad (4)$$

The roll moment exerted on the ship equals the product of the stability moment and the heel angle:

$$M(t) = -\tilde{c}(t) \sin(\phi(t)) \quad (5)$$

The mean of the product of the roll moment and the roll velocity, the work, over a longer period of time ( $T$ ) is given by:

$$P_{\bar{g}\bar{m}} = \frac{\int_0^T M(t)\dot{\phi}(t)dt}{T} \quad (6)$$

It can be shown that if  $\omega_{gm} \neq 2 \cdot \omega_{\phi}$  that  $P_{\bar{g}\bar{m}} = 0$ . Only if  $\omega_{gm} = 2 \cdot \omega_{\phi}$  the work performed by the stability variations affects the energy contained in the roll motion. The phase shift ( $\varepsilon_{gm}$ ) between the change in  $GM$  and the roll motion determines whether energy is added to or removed from the system. In Fig. 1 the roll angle, roll velocity and moment are shown for  $\varepsilon_{gm} = 180 \text{ deg}$ . In this case the moment due to the stability variations and the roll velocity always have the same sign. The related positive work implies that energy is added to the roll motion. Fig. 2 shows the energy added during one roll cycle.

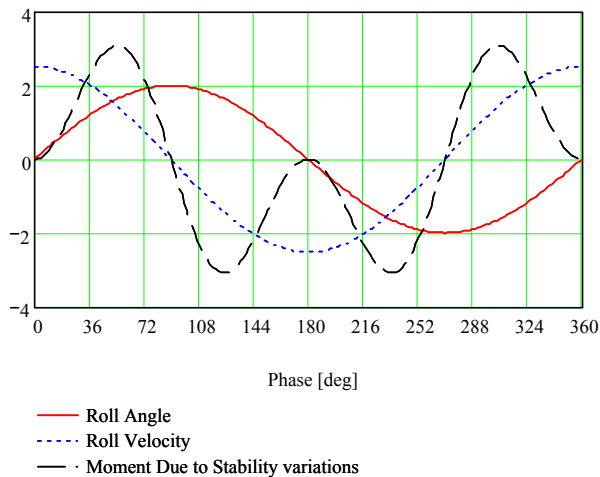


Fig. 1: The roll angle, roll velocity and righting moment during one roll period of roll, when roll and waves are in phase

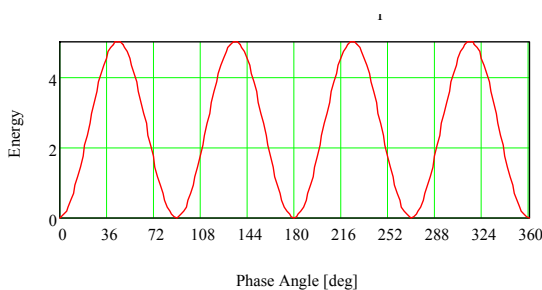


Fig. 2: Energy added during 1 roll cycle (phase shift 180 deg)

Fig. 3 and 4 show the same results, but now for a phase shift of for  $\varepsilon_{gm} = 90 \text{ deg}$ . Fig. 4 shows that on the average no energy is added over one roll cycle.

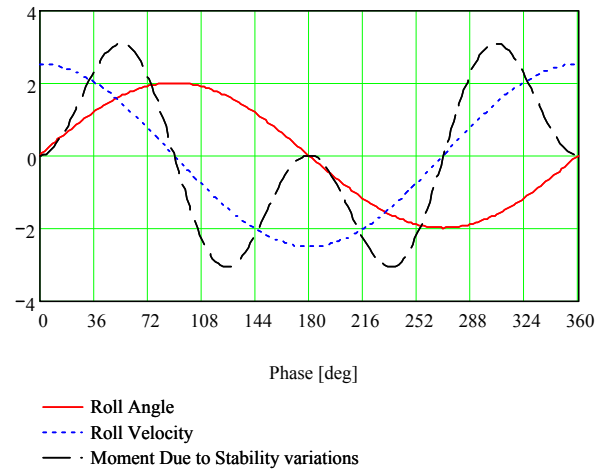


Fig. 3: The roll angle, roll velocity and righting moment during one roll period of roll, when roll and wave show a 90 degree phase shift.

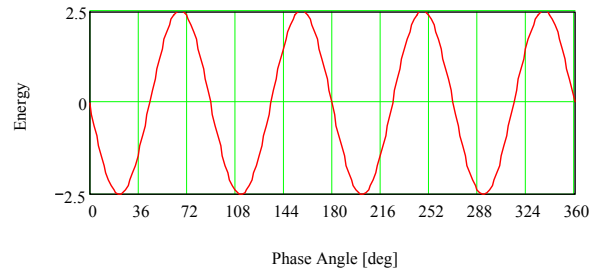


Fig. 4: Energy build up during 1 roll cycle (phase shift 90 deg)

Assuming small roll angles Equation (5) can be linearised in  $\phi$ . In this case the average amount of energy added in roll given by Equation (6) can be rewritten as:

$$P_{\bar{g}\bar{m}} = -\frac{\rho g \nabla GM_a \phi_a^2 \omega_{\phi}}{4} \cos(\varepsilon_{gm}) \quad (7)$$

Where  $\rho g \nabla$  is the ship displacement,  $GM_a$  the amplitude of the stability variation and  $\omega_{\phi}$  the natural frequency of roll.

Whether or not the above increase in energy materialises in an increased roll angle depends on the average (per roll cycle) amount of energy dissipated by the equivalent linear roll damping  $b_E$ , which is given by Equation (8).

$$P_b = \frac{1}{2} b_E \phi_a^2 \omega_{\phi}^2 \quad (8)$$

Equating Equations (7) and (8) yields a criterion in terms of roll damping. Parametric roll can start to develop when:

$$b_E < -\frac{\rho g \nabla GM_a \omega_\phi \cos \varepsilon}{2} \quad (9)$$

## IRREGULAR WAVES

As shown foregoing, the change in metacentric height due to the changing water height along the ship is driving parametric roll. It is also shown that the increase and decrease in roll amplitude can be written as a (negative) contribution to the roll damping.

In irregular waves the random phases of the wave components yield slow variations in the contribution of the stability variations in the total damping. Dunwoody(1989a) gives an expression for the reduction in irregular waves.

Assuming a broad band spectrum for  $S_{\bar{g}m}$  - the spectral density of stability fluctuations - and taking its value at the encounter frequency that matches twice the roll frequency he arrives at the following expression for the expected value for the reduction of the non-dimensional damping.

$$E[\delta b_E^*] = \frac{\pi g^2 S_{\bar{g}m}(\omega_e = 2\omega_\phi)}{4\omega_e \omega_\phi^2 k_{xx}^4} \quad (10)$$

Where  $\omega_e$  is the encounter frequency. In a dimensional format this result is given by:

$$E[\delta b_E] = \frac{\rho g \nabla \cdot \pi S_{\bar{g}m}(\omega_e = 2\omega_\phi)}{4 \cdot GM} \quad (11)$$

Noteworthy is the fact that the expected value for the damping reduction increases with the

spectral density of the stability variations. This implies it increases with the wave height squared.

The practical implication of the above result in terms of the risk of encountering parametric roll in a given time frame is an issue that requires further work.

Fig. 5 shows the character of the non-dimensional sum of the roll damping of hull and appendages and the expected value for the reduction due to the stability variations for a range of combinations of significant wave height and peak period. It is clear that a large negative damping is to be expected in the higher sea states in combination with a peak period of 16.5s, which is half the roll period of the subject vessel.

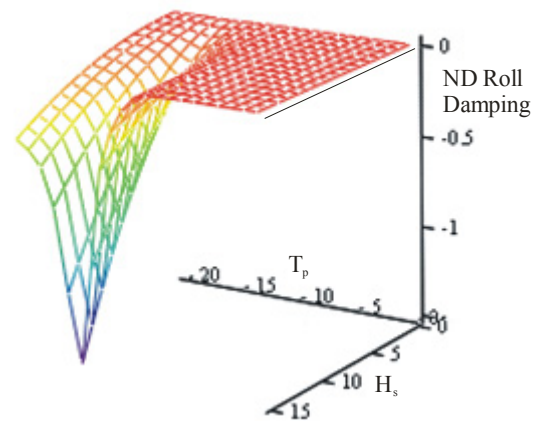


Fig. 5: Typical non-dimensional roll damping ratio as function of significant wave height  $H_s$  and wave peak period  $T_p$ .

## ROLL DAMPING

Obviously the roll damping of a vessel is an important parameter in the assessment of parametric roll. A relevant characteristic is the fact that it decreases with decreasing speed. In the lower speed range it is dominated by the non-linear eddy and bilge keel damping components. At moderate and higher speeds the linear lift damping of the hull becomes a dominant factor (Ikeda et al.(1978), Dallinga et al. (1998)). In other words: the risk on parametric roll decreases with increasing speed. Other means that increase the ships roll damping also decrease the risk on parametric rolling. For example an anti roll tank is a very effective way to increase the damping at low

speed. Fin stabilizers are effective as well, but only at some forward speed.

### MAGNITUDE OF THE STABILITY VARIATIONS

With the foregoing establishing the risk of parametric roll has reduced to estimating  $S_{\bar{g}m}$ . Assuming linearity this quantity is obtained from a multiplying the square of the transfer function  $GM_a/\zeta_a$  with the wave spectrum  $S_\zeta$ .

$$S_{\bar{g}m} = \left( \frac{GM_a}{\zeta_a} \right)^2 S_\zeta \quad (12)$$

A correction for forward speed yields the spectral density at the right encounter frequency. Regarding the evaluation of the stability variations experienced by the hull Dunwoody(1989b) uses a method that omits the diffracted and radiated waves. In Umeda et al(2008) a CFD approach was followed to obtain the roll moment, but they also showed that this was heavily overestimated by their method. This is probably due to the grid size. Very fine grids are needed capture all relevant details but this leads to unacceptable time consuming calculations.

In the present paper, the transfer function of the stability variation  $GM_a/\zeta_a$  is obtained by means of hydrostatic considerations from the relative wave elevations along the ship. The latter calculated by means of a linear three-dimensional frequency domain potential flow code PRECAL. This code calculates the wave induced excitation and the motion induced reaction forces using zero speed Greens functions. The calculated relative wave elevation accounts for the radiated and diffracted waves.

At low to moderate speeds, this method gives a good representation of the wave elevation along the ship, offering a fair and efficient estimate of the stability variations.

The above calculation yields the transfer function of the relative wave elevations (phase

and amplitude) at every waterline panel. From the surface elevation the vertical position of the buoyancy point above the baseline ( $KB$ ) is calculated by integrating over the underwater volume (Equation (13)) over the actual hull form. The actual waterline width and hull form are also used to calculate the vertical distance from the buoyancy point to the transverse metacentre ( $BM$ ).

$$KB = \frac{\iiint z dV}{\nabla} \quad (13)$$

$$BM_{xx} = \frac{I_{xx}}{\nabla} = \frac{\iint y^2 dA}{\nabla} \quad (14)$$

The overall values are obtained by integrating over the length of the ship.

The above evaluation is repeated for the full range of phase angles phase between 0 to  $2\pi$ , each resulting in different waterlines. For the amplitude  $GM_a$  the half of the dynamic range between the maximum value  $GM_{max}$  and the minimum value  $GM_{min}$  was taken.

$$GM_a = 1/2 [GM_{max} + |GM_{min}|] \quad (15)$$

### Sample results

A typical result for different wave amplitudes is given in Fig. 6. Since these data are given in a non-dimensional form, the data can be used for a range of ships with a comparable hull shape.

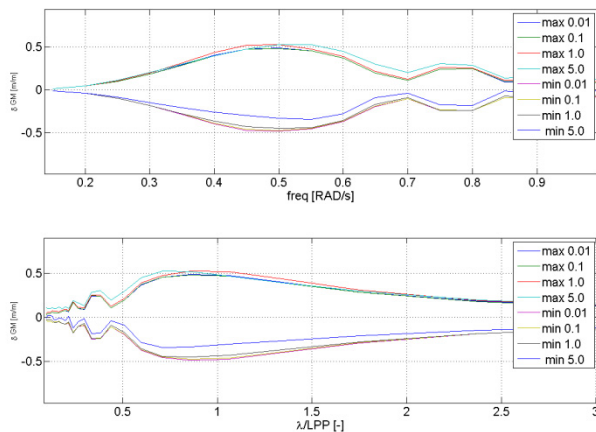


Fig. 6: Typical transfer function for the  $\delta GM$  as function of frequency(top) and as function of wave length  $\lambda/L_{pp}$ (bottom) for wave amplitudes between 0.01 and 5m.

Fig. 6. shows that the transfer function  $GM_a/\zeta_a$  reaches its maximum value at a wave length of about 80% of the ship length.

A second observation is that the peak value is relatively insensitive to wave height variations. The remark that the linear contribution to the stability variations is small compared to contribution of the hull shape is therefore not justified. If it would hold, this non-linearity would have been more pronounced in Fig. 6.

### Sectional contribution

In the calculation of the stability variations the sectional contribution of KB and BM became available. Fig. 7 shows typical distribution of sectional amplitude of KB and BM over the ship's length. The graph clearly shows that those parts of the ship that have a small draught, have large BM variations and contribute significantly more to the change in GM than those sections that have a large draft.

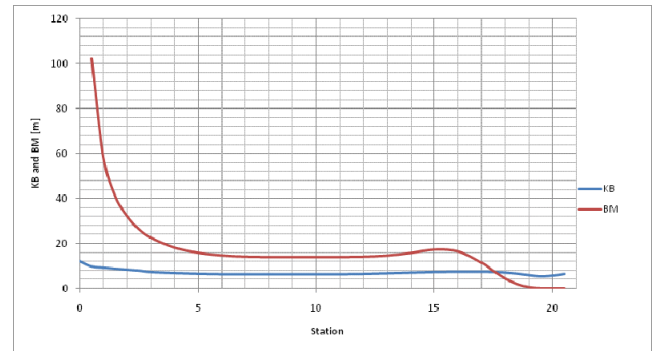


Fig. 7: Amplitude the sectional data on BM and KB

This is in line with theory. If one assumes a half submerged rectangle (draught= $T$  m), the buoyancy point is located half way the baseline and the waterline, at  $0.5 T$ . If the relative wave elevation increases the local draft by  $\Delta T$ , the height of the centre of buoyancy changes by  $0.5\Delta T$ . Because the waterline width is constant in this example BM changes only due to the change in displacement. The total change in GM for this example is given by Equation (16)

$$\Delta GM = \frac{\Delta T}{2} - \frac{B^2 \Delta T}{12 \cdot T^2} \quad (16)$$

It is clear from this equation that if  $T$  is small, a given  $\Delta T$  has a large impact on the GM. This is in line with observations that ships with a flat pram type stern have a higher risk on parametric rolling (Levadou et al. (2006) )

### Note on the method to calculate the relative wave elevation

Because of the use of zero-speed Greens functions in PRECAL, the prediction of the relative wave elevations becomes less accurate at higher speeds. Because the mis-prediction are particularly large in the diverging flow at the bow and the converging flow at the stern, they have a relatively large effect on the derived stability variations. At increasing speed a more accurate description of the dispersion of the waves should be considered (e.g. Bunnik (1999)).

## ESTIMATED OPERATIONAL LIMITS

Fig. 8 shows a typical result from a computation. The lines show the calculated results. The markers indicate experimental data. It can be seen that the numerical method predicts a threshold wave height of 2.5 to 3 m significant wave height at a wave peak period of around 16.5 seconds.

The markers in Fig. 8 show test results for a 290m container ship. Green triangles indicate tests that showed (within the adopted test duration) no parametric rolling; blue squares mark the position where large roll angles were found.

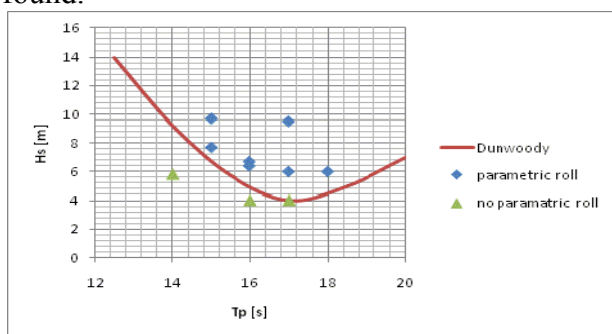


Fig. 8: Comparison of test results to calculated using the broadband approach.

Comparable result has been reproduced in a number of similar projects for different ship types. The calculated trends show a fair agreement with the character of the test results, indicating that the Dunwoody's approach, combined with the present way of evaluating the stability variations, offers a practical estimate of the operational limits.

## OUTLOOK/CONCLUSIONS

The method that has been presented in this paper, shows promising results, but the final objective of the developments is to enable an accurate and more transparent prediction of the risk of unacceptable ship behaviour in a particular time frame.

To achieve this there are two intertwined problems to overcome. The first problem is to establish what are the essential physical aspects

of the problem. The second problem concerns the statistical aspects.

In the near future we will address the statistical aspects first. The first step will investigate the relation between Dunwoody's estimate of the maximum excitation level with results of simple 1-DOF time domain calculations on the variations in the roll damping. A second step will investigate the related onset of parametric roll (limiting ourselves to the growth up to moderate roll angles), including the effects of non-linear roll damping. Efforts will be made to relate the frequency of critical events to the decrease in roll damping and spectral estimates of this quantity.

Depending on the outcome of the foregoing it may be of interest to improve aspects of full blown numerical simulations. The adequate modelling of the natural speed variations in high waves as well as the effects on non-linear diffraction in the parametric excitation come to mind.

## References

- ABS, Guide for the Assessment of parametric roll resonance in the design of container carriers, ABS, 2004(updated 2008)
- Archer, C. , van Daalen, E. , Dobberschutz, S., Godeau, M-F., Grasman, J. , Gusing, M., Muskulus, M., Pischanskyy, A., Wakker, M., Proceedings of the Sixty-Seventh European Study Group Mathematics with Industry, Dynamic Models of Extreme Rolling of vessel in head Waves, 2009
- Bunnik, T, PhD-Thesis TU-Delft, Seakeeping Calculations for Ships, taking into Account the Non-linear Steady Waves, 1999
- Dallinga, R.P., Blok, J.J and Luth, H.R., RINA International Conference on Ship Motions & Maneuverability, London, Excessive rolling of cruise ships in head and following waves 1998
- Dunwoody, Journal of Ship Research, Roll of a Ship in Astern Seas – Response to GM Fluctuations, 1989a, Vol 33 No. 4

Dunwoody, Journal of Ship Research, Roll of a Ship in Astern Seas – Metacentric Height Spectra, 1989b, Vol 33 No. 3

France, W.N., Levadou, M, Treacle, T.W., Paulling, J.R., Michel, R.K. and Moore C., SNAME Annual Meeting 2001, An investigation of head-sea parametric rolling and its influence on container lashing systems, 2001

Ikeda, Y and Himeno Y, Report of the Department of Naval Architecture University of Osaka Prefecture, A Prediction Method for ship Roll Damping, report number 00405, 1978

ITTC, Recommended procedures and guidelines – testing and extrapolation methods loads and responses, stability Predicting the occurrence and magnitude of parametric rolling, ITTC, 7.5-02, 2006

Levadou and van 't Veer, Proceedings of 9<sup>th</sup> International Symposium on Stability of Ships and Ocean Vessels, parametric roll and ship design, 2006

Umeda et al., Proceedings of 27<sup>th</sup> Symposium on naval hydrodynamics, Comparison Study on Numerical Prediction Techniques for parametric roll, 2008

## Integrity Diagrams of the Ship/U-Tank System Undergoing Parametric Rolling

Marcelo A. S. Neves\*, Claudio A. Rodríguez\*, Jerver E. M. Vivanco\*\*, José C. Villagómez Rosales\*\*, Radhesh Agarwal\*\*\*

\* LabOceano – COPPE/UFRJ; \*\* COPPE/UFRJ; \*\*\* IIT-Karagpur, India

### ABSTRACT

Unstable rolling motions in regular head seas are investigated in the case of a ship stabilized with an U-type anti-rolling tank (ART). A transom stern small vessel, well-known for her tendency to develop strong parametric excitation is investigated. Nonlinear equations are employed to describe the liquid motion inside the tank, the forces and moments generated by the tank on the ship and the coupled ship motions (heave, roll and pitch). These are numerically solved for different initial conditions. Nonlinear dynamics techniques are applied to the coupled ship/tank system. In particular, it is verified that the nonlinear system, despite the fact that the ship is stabilized with a tuned ART, as wave amplitude is increased there exists a process of erosion of the safe basin which is not smooth. Similarly to the case of the unstabilized ship, the integrity diagrams show a clear *cliff* tendency at some critical wave amplitudes. The implication of this aspect is relevant to the design of ART's against parametric rolling, in the sense that it allows for the definition and quantification of a critical wave amplitude for distinct tank designs in the context of an analysis that takes into account all the relevant nonlinearities of the coupled ship and tank motions under the influence of a whole set of initial conditions.

### KEYWORDS

Anti-rolling tanks; Parametric rolling; Nonlinear dynamics; Safe basins; Integrity diagram.

### INTRODUCTION

The phenomenon of parametric rolling of ships is a nonlinear dynamical instabilization process that has attracted much attention recently. Recent examples can be found in Neves and Belenky (2008).

By means of systematic variations of encounter frequency and wave amplitude Neves and Rodríguez (2007) numerically obtained Parametric Amplification Domains (PADs), based on coupled nonlinear equations. These new numerical diagrams display information not only on the boundaries of stability, but additionally they provide information on the nonlinear roll amplitudes in the whole domain inside the boundaries. A rich

picture is obtained, including the appearance of upper boundaries, a general tendency of the system to get stiffer due to coupling, abrupt decrease in the upper boundaries with fractal geometry.

Safe basin analysis has been performed in Neves et al. (2009a) having wave amplitude as the control parameter. It was shown that for relatively small wave amplitudes the appearance of fractal boundaries was counter-balanced by an increase in other areas of the safe basin, what resulted in an overall increase of the safe area. Yet, for higher waves, erosion of safe basin came up very rapidly. Finally, the integrity curve for the ship at the *exact* tuning  $w_e/w_{n4} = 2.0$  was obtained. It was observed that as erosion of the safe basin starts, a sharp

decline of the safe basin area defines a critical wave amplitude for the safety of the vessel in terms of the area of the safe basins.

In this paper the nonlinear ship/tank problem under parametric excitation as modeled in Neves et al. (2009b) is revisited. That paper presented a comprehensive analysis of PADs corresponding to the coupling of nonlinear ship motions with a nonlinear model of the motion of the internal fluid. One main conclusion was that for the range of parameters simulated, an Anti-Rolling Tank (ART) may eliminate parametric rolling at some conditions but these may persist (or appear) at some other conditions.

Nonlinear dynamics techniques previously employed by the authors are now applied to the problem of the ship with tank. In particular, it is verified that despite the fact that the ship is now stabilized with a tuned ART, there exists a process of erosion of safe basin which is not smooth. Similarly to the case of the unstabilized ship, the integrity diagrams show a clear *cliff* tendency at some critical wave amplitudes. The implications of this aspect are relevant to the design of ART's against parametric rolling, in the sense that it allows for the definition and quantification of a critical wave amplitude for distinct tank designs in the context of an analysis that takes into account all the relevant nonlinearities of the coupled ship and tank motions under the influence of a whole set of initial conditions. This methodology has clear advantages when compared with the less consistent maps of numerical domains of parametric amplification.

### MATHEMATICAL MODEL

Geometric characteristics of the U-tank are shown in Fig. 1. Two vertical reservoirs are connected by a transversal duct, with all elements having rectangular constant cross sections. A partial obstruction situated at the mid position of the horizontal duct allows the consideration of variable damping actions. Fluid motion, assumed to be unidirectional, is

described by fluid displacement  $Z(t)$ , defined in Fig. 1.

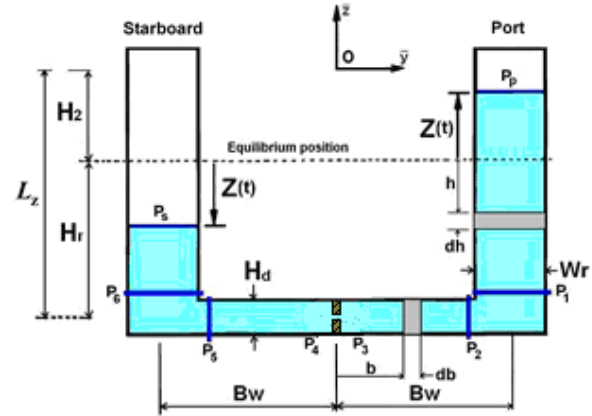


Fig. 1 Tank geometry

Nonlinear equations of ship motions may be represented as:

$$(\tilde{M} + \tilde{A})\ddot{\vec{S}} + \tilde{B}(\dot{\phi})\dot{\vec{S}} + \vec{C}_r(\vec{S}, \zeta) = \vec{C}_{ext}(\zeta, \dot{\zeta}, \ddot{\zeta}) + \vec{C}_t(Z, \dot{Z}, \ddot{Z}, \vec{S}, \dot{\vec{S}}, \ddot{\vec{S}}) \quad (1)$$

where vector  $\vec{S}(t) = [z(t), \phi(t), \theta(t)]^T$  represents rigid body motions in the heave, roll and pitch motions, respectively. In Equation (1),  $\tilde{M}$  is a 3x3 inertia matrix,  $\tilde{A}$  is a 3x3 added mass matrix. Matrix  $\tilde{B}$  is the damping matrix which may incorporate non-linear terms in the roll equation.  $\vec{C}_r$  is a 3x1 vector which describes non-linear restoring force and moments dependent on the relative motions between ship hull and wave elevation  $\zeta(t)$ . On the right hand side of equation (1), the generalized vector  $\vec{C}_{ext}$  represents wave external excitation, dependent on wave heading  $\chi$ , encounter frequency  $\omega_e$ , wave amplitude  $A_w$  and time  $t$ . Finally, the generalized vector  $\vec{C}_t$  represents nonlinear forces and moments acting on the ship due to the fluid motion inside the tank. For a ship without tank, Equation (1) reproduces the system of non-linear equations introduced in Neves and Rodríguez (2004). Due to space limitations, the detailed expressions of the components of equation (1) are not repeated here, see Neves et al. (2009b) for details. From

the theoretical point of view it is important to consider the internal fluid motion as nonlinear, interacting with the nonlinear ship motions. Therefore, the ship/tank problem may be investigated as a strongly coupled heave-roll-pitch-tank problem, resulting in a four degrees of freedom nonlinear problem. The 4th equation, describing the nonlinear internal fluid motion  $Z(t)$ , has also been derived in Neves et al. (2009b).

### SHIP AND TANK PARTICULARS

Ship TS hull forms are shown in Fig. 2; main characteristics are defined in Table 1. Dimensions and main characteristics of the ART employed in the present simulations are (see Fig. 1 for definitions):  $B_w=3.00$  m,  $W_r=1.5$  m,  $H_r=1.5$  m,  $H_d=0.381$  m,  $m\%=3.00$  is the percentage of mass of water relative to the mass of the ship,  $\omega_t / \omega_{n4}=1$  is the tuning of the tank with the ship, where  $\omega_t$  is the natural frequency of the tank and  $\omega_{n4}$  is the roll natural frequency of the ship. Non-dimensional damping is  $\eta_t = 0.3$ .

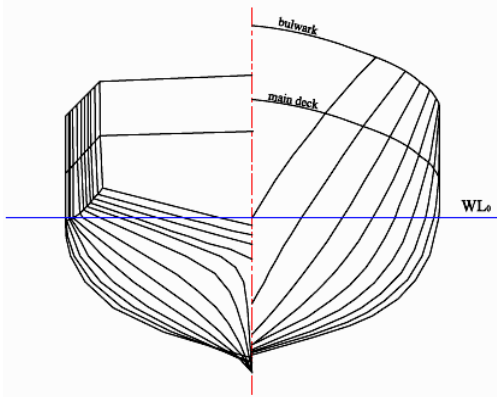


Fig. 2 Ship hull form, Transom Stern (TS).

Internal dissipative effects may be determined by means of decay tests in which an initial condition is applied to the internal fluid. The resulting oscillatory motion of the fluid inside the static tank is modeled as:

$$\ddot{Z} + p_1\dot{Z} + p_2|Z|\dot{Z} + \omega_t^2 Z = 0 \quad (2)$$

For reduced obstructions, the damping action is essentially linear ( $p_2 \approx 0$ ). The tank natural frequency is defined by geometrical characteristics of the tank (see Fig. 1 for definitions) and  $g$ , the gravitational acceleration:

$$\omega_t = \sqrt{\frac{g}{W_r \left( \frac{B_w}{H_d} + \frac{H_r}{W_r} \right)}} \quad (3)$$

Table 1: Ship main characteristics

Denomination	TS
Length overall	25.91 m
Length between perpend.	22.09 m
Breadth	6.86 m
Depth	3.35 m
Draft	2.48 m
Displacement	170.3 ton
Longit. radius of gyration	5.52 m
Metacentric height	0.37 m

### DOMAINS OF AMPLIFICATION

In the following, parametric rolling amplification is analyzed with respect to both wave amplitude and frequency. For a global analysis of these parameters, diagrams of  $\omega_e / \omega_{n4}$  vs  $A_w$  are developed in which roll amplitude is represented in a scale of colors. Fig. 3 shows the PADs for ship without and with ART considering  $F_n=0.3$ ,  $\chi = 180^\circ$ ,  $\eta_t = p_1/2\omega_t = 0.3$ ,  $p_2 = 0$  and  $\phi_0 = 0.8^\circ$ .

In particular, three aspects are relevant in the present context: i) existence of upper

boundaries of stability are observed; ii) areas of parametric amplification corresponding to  $\omega_e / \omega_{n4} \cong 2$  are bent to the right, as discussed in Neves and Rodríguez (2004, 2007) in the case of a ship without tank; iii) a tuned tank, in spite of being beneficial at most of the unstable domain, is not sufficient to avoid strong ship motions and capsize in the concave upper part of the PAD.

Therefore, contradictory to some arguments encountered in the literature stating that ARTs can in general cope well with parametric amplifications, the above results indicate that the situation may not be that simple.

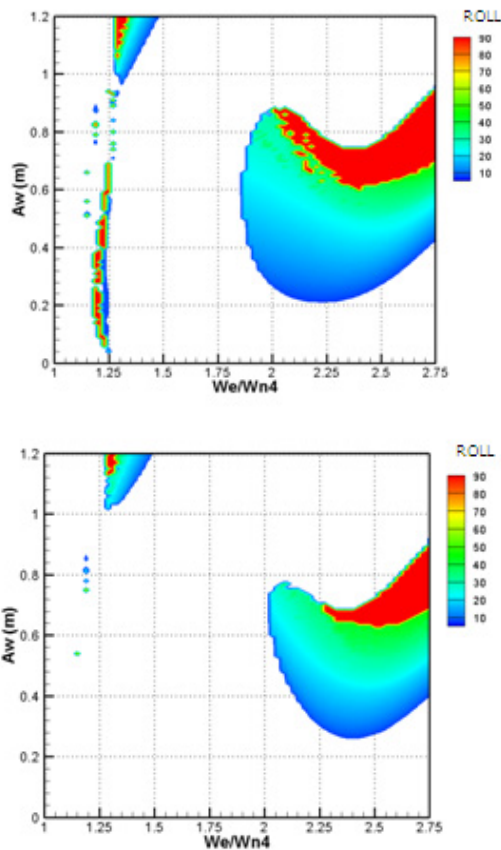


Fig. 3. PAD for ship without ART (upper); with ART (lower)

However, it is important to notice that these domains are numerically established for a single set of initial conditions (in this case,  $\phi_0 = 0.8^0$ ). Since parametric rolling is strictly a nonlinear phenomenon, it is sensitive to initial conditions of the system, Neves and Rodríguez

(2007). This aspect throws a certain level of uncertainties on the use of these domains as a practical tool for assessing the safe qualities of a ship design. Therefore, it becomes necessary to advance towards a more exhaustive and systematic analysis on the influence of initial conditions on parametric roll developments of the system.

### SAFE BASINS

Safe basins are used to perform analysis based on varying systematically initial conditions, Belenky and Sevastianov (2007). These are defined here as regions from which trajectories reach a determined set of maximum roll amplitudes within a time interval of 600 seconds. A resolution of 120x80 initial conditions separated regularly by steps of 1° (one degree) both in roll amplitude and velocity is employed. A comparison of safe basins for ship without (upper row) and with tank (lower row) is shown in Fig. 4, for  $\omega_e / \omega_{n4} = 2.08$  for low wave amplitudes ( $A_w = 0.2$  m, 0.4 m, 0.6 m).

It is noticed that for this range of low wave amplitudes the safe basin increases continuously. This is thought to be due to the increased rigidity (dependent on wave amplitude squared) introduced by the nonlinear coupling, as discussed in Neves and Rodríguez (2007). Up to  $A_w = 0.66$  m there is no noticeable fractal erosion of the safe basin. But, as the wave amplitude is increased beyond a threshold value (around  $A_w = 0.67$  m) the safe basin area undergoes a progressive level of erosion in the proximity of the saddle points. This may be observed in Fig. 5, which shows the safe basins for the ship/tank system for a given tuning ( $\omega_e / \omega_{n4} = 2.154$ ) and for wave amplitudes in the range  $A_w = 0.68$  m ~ 0.82 m.

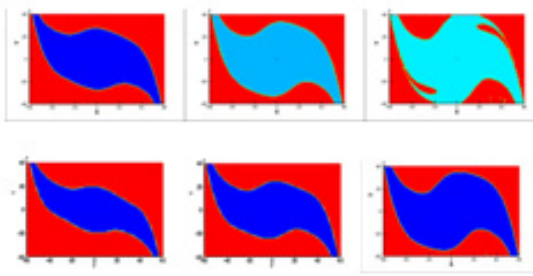


Fig. 4 Comparison of safe basins for ship without (upper row) and with tank (lower row)

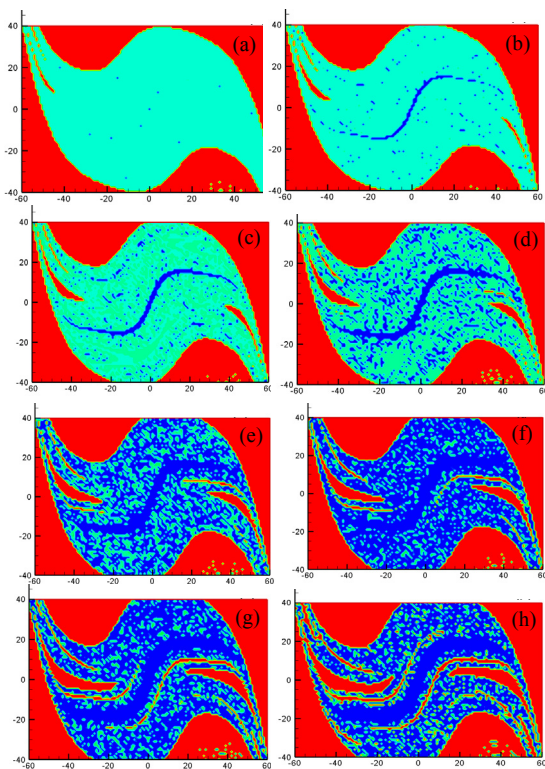


Fig. 5 Safe basins for the ship/tank system, higher range of wave amplitudes,  $\omega_e / \omega_{n4} = 2,154$ , a)  $A_w=0.68$  m, b)  $A_w=0.70$  m, c)  $A_w=0.72$  m, d)  $A_w=0.74$  m, e)  $A_w=0.76$  m, f)  $A_w=0.78$  m, g)  $A_w=0.80$  m and h)  $A_w=0.82$  m.

## INTEGRITY DIAGRAMS

Soliman and Thompson (1989) proposed and investigated the use of several different integrity measures. In the present study a definition will be considered which is particularly revealing of some important characteristics of coupled parametric resonance. Integrity diagrams – curves of integrity for a

determined range of wave amplitudes – for the ship with and without tank are drawn in Fig. 6 for the same tuning  $\omega_e / \omega_{n4} = 2.154$ . All these areas are non-dimensionalized with respect to the safe basin area of roll decay of ship without tank:  $\bar{A}(A_w) = A_s(A_w) / A_0$  where  $A_s(A_w)$  defines the safe basins areas for different wave amplitudes and  $A_0$  defines the safe basin area for  $A_w=0.0$  m (for the ship without tank). It is possible to appreciate in Fig. 6 the differences between their trends and the fact that for both curves the non-dimensionalized area starts to diminish dramatically – due to the fractal erosion - for higher wave amplitudes. The two-sided phenomenon of increased fractal erosion together with enlargement in other areas of the same basin persists in the case of ship without tank, however the area starts to be eroded for lower wave amplitudes than in the case of the ship with tank. When the U-tank is implemented, a shift of its integrity curve towards the right is observed, corresponding to the beneficial effect of the anti-rolling tank, since it represents the increase of wave amplitude after which the safe basin is dominated by fractal erosion. But it becomes clear that the integrity diagram is not smooth. Analogous to the case of the ship without tank, there is a clear change of tendency at certain *critical wave amplitude*, reflecting a sharp reduction of engineering integrity of safe motions, Thompson et al. (1990). This dynamical aspect of the ship/tank system enables the consideration of a quantitative safety measure of a given ART design.

## INTEGRITY SURFACES

A more general view of the trends of the areas of safe basin is obtained when surfaces of integrity are computed, resulting from the computation of integrity diagrams for a range of tunings. Integrity surfaces for the ship are shown in the upper part of Fig. 7, whereas the surface for the ship/tank system is shown in the lower figure; the range of tunings ( $\omega_e / \omega_{n4}$ ) is from 1.6 to 3.2.

An interesting characteristic to highlight in the surfaces of integrity is the fact that, like with the ship without tank, for the ship/tank system the non-dimensionalized areas starts to fall dramatically for all frequencies – due to fractal erosion - retaining the *cliff* tendency when the anti-rolling tank is on. The consideration of a critical wave amplitude may be associated to this characteristic tendency of the surfaces of integrity, common to the dynamics of the ship with or without an U-tank. It is possible to observe in the surface of integrity of the ship with tank that the *cliff* appears after a wave amplitude of about  $A_w=0.63$  m.

Fig. 8 shows, for the range of tunings  $\omega_e / \omega_{n4}$  from 1.6 to 2.7, the curves of critical wave amplitudes for the ship with/without tank. It is observed that a positive variation of critical amplitudes occurs, with respect to the values reached for the ship without tank, for a range of tunings. It is also observed that for the higher tunings no gain in increase of critical wave amplitude is obtained. Clearly, the general increase of critical amplitude for the ship with tank is considered beneficial, since it reflects its greater resistance to capsizing, keeping the ship stable for higher wave amplitudes.

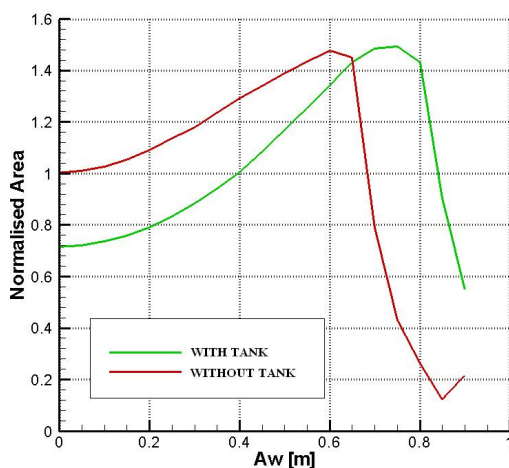


Fig. 6 Integrity diagrams for  $\omega_e / \omega_{n4}=2.154$

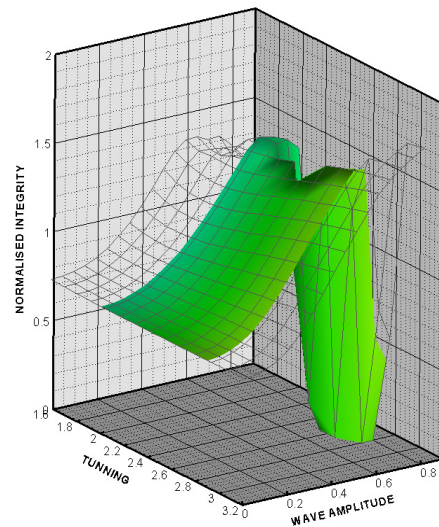
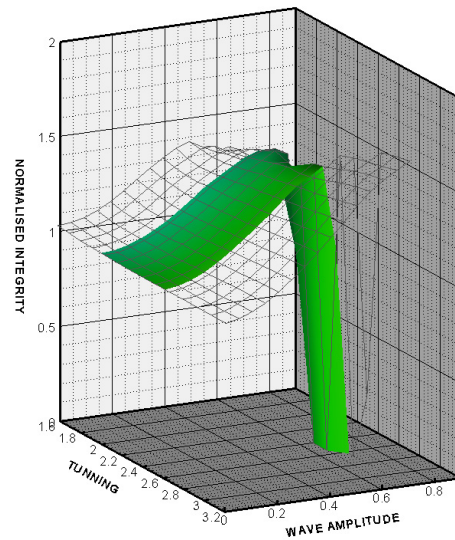


Fig. 7 Integrity surfaces for the ship and ship/tank system.

## CONCLUSIONS

A methodology to quantitatively analyze nonlinear responses of the unstable movements of the ship coupled with the water inside the tank in head seas for a broad set of roll initial conditions has been introduced. For the ship with tank the PAD is smaller and there is a general tendency to less intense roll amplifications but, equally important, areas adjacent to the upper boundaries still register ship capsize.

Analysis of integrity diagram and surface has shown that for the ship with tank, despite the

fact that the ship is stabilized with a tuned tank, there exists a process of erosion of the safe basin which is not smooth; as in the case of the unstabilized ship, the integrity surface shows a clear cliff tendency at critical wave amplitudes. It has also been shown that the resulting critical amplitudes are higher when the U-tank is activated, particularly at low frequencies. Based on that, it is concluded that there is an overall positive effect of the anti-rolling tank on the control of parametric roll, but safety from capsizing remains as a necessary design target.

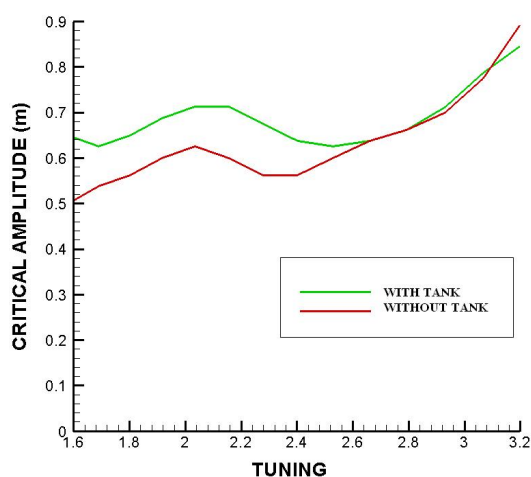


Fig. 8 Critical wave amplitude, ship with/without tank.

The present analysis incorporates sensitivity of the coupled nonlinear system ship/tank to a large set of initial conditions and allows quantification, in terms of increase of critical amplitude and reduction of safe basin, of the net effect of the anti-roll tank on the control of parametric rolling. Considering that as a result of the present analysis a measure of the safety of the ship at sea is obtained, now independent of initial conditions, the methodology could be of practical interest to the development of ship/tank designs. These aspects must be studied in more detail in the future, as well as their relation with irregular seas and introduction of active control to the systems.

## ACKNOWLEDGEMENTS

The present investigation is supported by CNPq within the STAB project (Nonlinear Stability of Ships). The authors also acknowledge support from CAPES, FAPERJ and LabOceano.

## REFERENCES

- Belenky, Sevastianov, *Stability and Safety of Ships, Risk of Capsizing*. 2<sup>nd</sup> ed., SNAME, USA, 2007.
- Neves, Belenky, Review of 9th International Conference on Stability of Ships and Ocean Vehicles (STAB 2006). *Marine Technology* Vol 45, No. 3, 2008, pp. 147-156.
- Neves, Merino, Rodríguez, A Nonlinear Model of Parametric Rolling Stabilization by Anti-roll Tanks, *Ocean Engineering*, doi: 10.1016/j.oceaneng.2009.07.005, 2009b.
- Neves, Rodríguez, Limits of Stability of Ships Subjected to Strong Parametric Excitation in Longitudinal Waves. *Proceedings, 2nd International Maritime Conference on Design for Safety*, Sakay, Japan, 2004, pp. 139-145.
- Neves, Rodríguez, An investigation on Roll Parametric Resonance in Regular Waves. *International Shipbuilding Progress*, Vol 54, 2007, pp. 207-225.
- Neves, Rodríguez, Vivanco, On the Limits of Stability of Ships Rolling in Head Seas. *Journal of Engineering for the Maritime Environment*, *Proceedings of the Institution of Mechanical Engineers*, Part M, U.K., doi: 10.1243/14750902JEME144, 2009a.
- Soliman, Thomson, Integrity Measures Quantifying the Erosion of Smooth and Fractal Basins of Attraction. *Journal of Sound and Vibration*, 135(3), 1989, pp.453-475.
- Thomson, Rainey, Soliman, Ship Stability Criteria Based on Chaotic Transients from Incurative Fractals. *Phil. Trans. R. Soc. London*, A 332, 1990, pp 149-167.



## **A study on Quantitative Prediction of Parametric Roll in Regular Waves**

Hirotsada Hashimoto and Naoya Umeda

Department of Naval Architecture and Ocean Engineering  
Graduate School of Engineering, Osaka University

### **ABSTRACT**

To investigate the influence of roll damping estimation methods on parametric roll prediction, a forced roll test was conducted to measure roll damping for large roll amplitude up to 30 degrees. Then, the 3DOF (degrees of freedom) numerical model based on a nonlinear strip theory was developed and numerical simulations in the time domain with roll damping estimated by a forced roll model test, a roll decay model test and the Ikeda's semi-empirical prediction method were conducted. By comparing these numerical results with an experimental result, the influence of different estimation methods for roll damping on parametric roll prediction was examined for developing reliable performance-based new Intact Stability criteria.

### **KEYWORDS**

Parametric Roll; Roll Damping; Forced Roll Test; Roll Decay Test; Ikeda's Prediction Method.

### **INTRODUCTION**

Since parametric roll is well known as one of the most dangerous phenomena which could lead to serious accidents due to significant roll, a new Intact Stability code, which is under development at IMO (International Maritime Organization), is required to cover this phenomenon. Although a lot of numerical models for parametric roll prediction have been proposed so far, roll damping for large amplitude and influence of roll damping estimation methods on parametric roll prediction have not been investigated enough.

Based on this situation, a forced roll model test for a containership was conducted for measuring roll damping up to 30 degrees of roll amplitude where the nonlinearity could appear remarkably. Then roll damping obtained by the forced roll model test was compared with those by a conventional roll decay model test and the Ikeda's semi-empirical prediction method

[Ikeda, 2004] to discuss the accuracy of each method for roll damping estimation.

For a numerical study on the influence of estimation methods for roll damping on parametric roll prediction, it is preferable to utilize a reliable numerical simulation model which can quantitatively predict large amplitude of parametric roll. For this purpose, we developed a coupled 3DOF (degrees of freedom) of heave-roll-pitch model based on a nonlinear strip theory, which considers time-dependent hydrodynamic forces for instantaneous submerged hull at each time step. To validate this numerical model, we conducted a model experiment to measure roll restoring variation, which is a major cause of parametric roll, with constant heel angles up to 30 degrees.

Finally a model experiment was conducted to measure occurrence region and roll amplitude of parametric roll in regular head seas. By comparing this experimental result with

numerical results with roll damping estimated from the forced roll model test, the roll decay model test and the Ikeda's prediction method, we examined the influence of roll damping estimation methods on parametric roll prediction.

## MATHEMATICAL MODEL

The coupled 3DOF mathematical model based on a nonlinear strip theory was developed for quantitative prediction of parametric roll. In this model, the nonlinear Froude-Krylov forces are calculated by integrating wave pressure up to wave surface. Dynamic components, i.e. radiation and diffraction forces are calculated for an instantaneous submerged hull by considering a time-dependent roll angle. Two-dimensional hydrodynamic forces are calculated by solving the boundary integral equation for the velocity potential. Diffraction forces are calculated by the STF method [Salvesen et al., 1970]. Hydrodynamic forces for heave and diffraction modes are calculated with encounter frequency and those for sway and roll modes are done with half the encounter frequency assuming principal parametric rolling. In a calculation of the radiation forces, so called the end term effect is included because a hydrodynamic lift effect on roll moment cannot be neglected when a ship has advance speed. Mathematical model of the 3DOF coupled ship motion is shown in Eqs.(1)-(3).

$$\begin{aligned} & (m + A_{33}(\phi))\ddot{\zeta} + B_{33}(\phi)\dot{\zeta} + A_{34}(\phi)\ddot{\phi} \\ & + B_{34}(\phi)\dot{\phi} + A_{35}(\phi)\ddot{\theta} + B_{35}(\phi)\dot{\theta} \\ & = F_3^{FK+B}(\xi_G / \lambda, \zeta, \phi, \theta) + F_3^{DF}(\phi) \end{aligned} \quad (1)$$

$$\begin{aligned} & (I_{xx} + A_{44}(\phi))\ddot{\phi} + N(\dot{\phi}) + A_{43}(\phi)\ddot{\zeta} \\ & + B_{43}(\phi)\dot{\zeta} + A_{45}(\phi)\ddot{\theta} + B_{45}(\phi)\dot{\theta} \\ & = F_4^{FK+B}(\xi_G / \lambda, \zeta, \phi, \theta) + F_4^{DF}(\phi) \end{aligned} \quad (2)$$

$$\begin{aligned} & (I_{yy} + A_{55}(\phi))\ddot{\theta} + B_{55}(\phi)\dot{\theta} + A_{53}(\phi)\ddot{\zeta} \\ & + B_{53}(\phi)\dot{\zeta} + A_{54}(\phi)\ddot{\phi} + B_{54}(\phi)\dot{\phi} \\ & = F_5^{FK+B}(\xi_G / \lambda, \zeta, \phi, \theta) + F_5^{DF}(\phi) \end{aligned} \quad (3)$$

## FORCED/FIXED ROLL TEST

To accurately measure roll restoring variation and roll damping for large angle/amplitude, which are dominant factors of parametric roll prediction, a new measurement system for forced/fixe roll test was newly developed. Roll moment around centre of ship gravity can be directly added by an electric motor and measured by a load cell located on the roll axis. [Hirayama and Takezawa, 1982] In the forced oscillation test, heave and pitch motions are allowed. Guaranteed operational range of this measurement system is -30 to 30 degrees of roll angle/amplitude, and 0.1 to 2.0 Hz of rotational frequency. Schematic view of the experimental setup is shown in Fig.1. Subject ship is a 6600TEU post-Panamax containership and its 1/100 scaled ship model was used for the experiment. Principal particulars and body plan of this ship are shown in Table 1 and Fig.2, respectively.

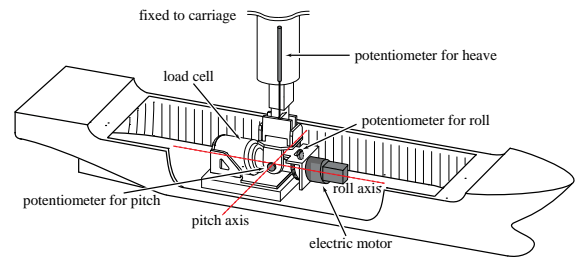


Fig.1 Schematic view of the experimental setup

Table 1 Principal particulars of the subject ship

Item	Value
Length between perpendiculars : $L$	283.8m
breadth : $B$	42.8m
depth : $D$	24.4m
mean draught : $T$	14.0m
block coefficient : $C_b$	0.629
metacentric height : $GM$	1.06m
natural roll period : $T_\phi$	30.3s

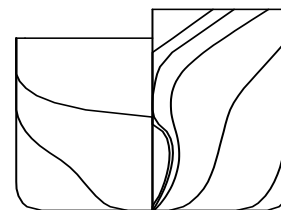


Fig.2 Body plan of the subject ship

**Roll Restoring Variation**

Although roll restoring variation is a most important factor for parametric roll prediction, the number of researches to investigate roll restoring variation in head waves is limited. As to experimental investigation on roll restoring variation for large roll angle with forward velocity, there have been only a few researches so far. Therefore, we conducted a model experiment for measuring roll restoring variation in regular head seas with large constant heel angle,  $\phi_c$ , up to 30 degrees for several Froude numbers. In the experiment, heave and pitch motions were in free and roll restoring moment around centre of ship gravity was measured by a load cell. Incident wave conditions are; wavelength to ship length ratio,  $\lambda/L$ , of 1.0 and wave steepness,  $H/\lambda$ , of 0.03.

The comparison of roll restoring variation between the model experiment and numerical calculations with the 1DOF of roll model [Hashimoto et al., 2006] and the developed 3DOF model are shown in Figs. 3-5. Here the relative position of the ship gravitational centre to a wave trough,  $\xi_G$ , is normalised with the wave length,  $\lambda$ ; so that  $\xi_G/\lambda=0.0$  and 1.0 means a wave trough,  $0<\xi_G/\lambda<0.5$  is a wave down-slope, 0.5 is a wave crest, and  $0.5<\xi_G/\lambda<1.0$  is a wave up-slope. The 1DOF model underestimates the amplitude of roll restoring variation particularly when a ship has forward velocity. On the other hand, the estimation accuracy of roll restoring variation is improved by the 3DOF model, in other words, becomes closer to the experimental result. It is concluded that the 3DOF model can estimate the roll restoring variation with practical accuracy for wide range of heel angle and ship advance speed relevant to parametric roll.

To investigate the major reason why the estimation accuracy is improved by the 3DOF model, the calculated heave and pitch motions with different heel angles were compared with the experimental result as shown in Fig.6. From the experimental result, the influence of heel angle on a heave motion is so large that it cannot be neglected for quantitative prediction. The 3DOF model can take account of this trend.

This result indicates that incorporating the effect of heel angle on a heave motion could improve the estimation accuracy of roll restoring variation.

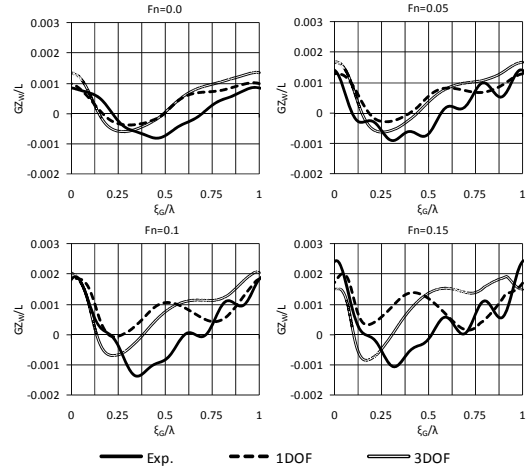


Fig.3 Comparison of roll restoring variation with  $\lambda/L=1.0$ ,  $H/\lambda=0.03$  and  $\phi_c=10$  degrees

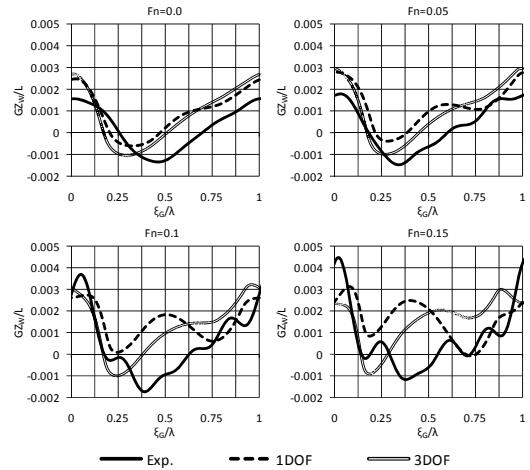


Fig.4 Comparison of roll restoring variation with  $\lambda/L=1.0$ ,  $H/\lambda=0.03$  and  $\phi_c=20$  degrees

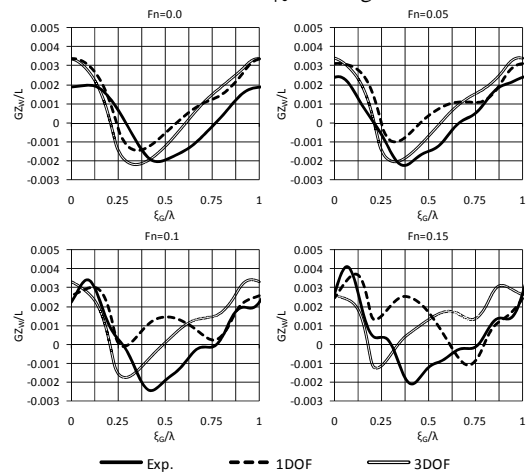


Fig.5 Comparison of roll restoring variation with  $\lambda/L=1.0$ ,  $H/\lambda=0.03$  and  $\phi_c=30$  degrees

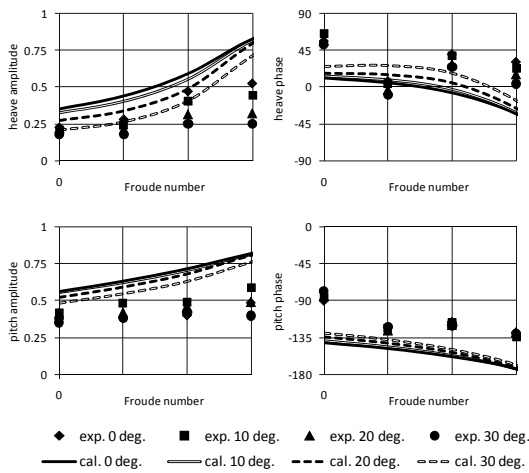


Fig.6 Comparison of heave and pitch motions at  $\phi_c=0, 10, 20, 30$  degrees

### Roll Damping

Since roll damping significantly affects on roll amplitude and occurrence region of parametric roll, accurate estimation of roll damping is crucial for quantitative prediction of parametric roll. In most researches of numerical prediction of parametric roll, a roll decay test or the Ikeda's semi-empirical prediction method are used for roll damping estimation. However their accuracy and applicability to the prediction of large amplitude of parametric roll has not been investigated sufficiently. Therefore we conducted a forced roll model test to measure roll damping with large roll amplitude up to 30 degrees with/without forward velocity. In the current experiment, heave and pitch motions were allowed because vertical motion could affect on measured roll damping particularly for large roll amplitude test, which Hirayama and Takezawa (1982) were not.

Normalised roll damping coefficients estimated by means of a forced roll test, a roll decay test and the Ikeda's prediction method are shown in Fig.7. Roll damping estimated from the roll decay test is significantly overestimated for small roll angle and is slightly underestimated for large roll angle. Furthermore, its accuracy becomes worse when the Froude number becomes large. This might be because the roll damping with the roll decay test is determined not for a steady rolling but also for transiently

decaying rolling. Estimated roll damping by the Ikeda's prediction method is significantly overestimated as compared to the result of forced roll test in all roll amplitudes and Froude numbers nevertheless the Ikeda's prediction method was developed for a steady roll motion. Further discussion on the Ikeda's prediction method is described in the latter chapter.

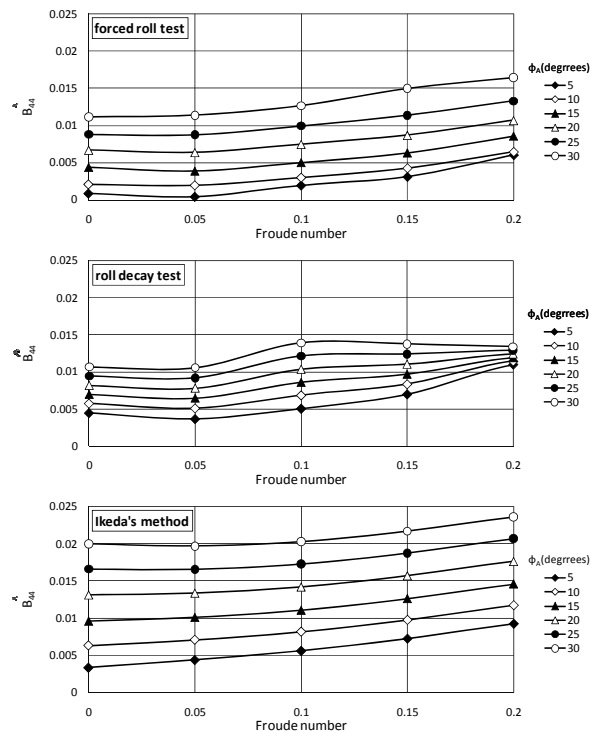


Fig.7 Roll damping coefficients estimated by a forced roll motion test, a roll decay test and the Ikeda's method

### PARAMETRIC ROLL PREDICTION

Model experiment was conducted to obtain the validation data for the numerical simulation model and discussion on the influence of estimation accuracy of roll damping on parametric roll prediction. Model experiment was done for  $\lambda/L=0.6, 0.8, 1.0, 1.2$  and  $1.4$ , constant wave height  $H=0.085\text{m}$  and  $F_n=0.0, 0.05, 0.1, 0.15$  and  $0.2$ . Numerical results with the 3DOF model utilizing the roll damping estimated from a forced roll test, a roll decay test and the Ikeda's prediction method were compared with the experimental result as shown in Fig.8. Since instantaneous roll amplitude is required for estimating roll

damping in the time-domain simulation, temporal roll amplitude,  $\phi_a$ , is approximated with roll angle and roll angular velocity as shown in the Eq.(4).

$$\phi_a = \sqrt{\phi^2 + (2\dot{\phi} / \omega_e)^2} \quad (4)$$

Numerical result with the roll damping estimated from a forced roll model test agrees well with experimental result of parametric roll for wide range of wave length and Froude number. The comparison demonstrates that using the roll damping estimated from a roll decay model test significantly overestimates parametric roll in certain conditions and it underestimates parametric roll if the Ikeda's prediction method is applied for roll damping estimation.

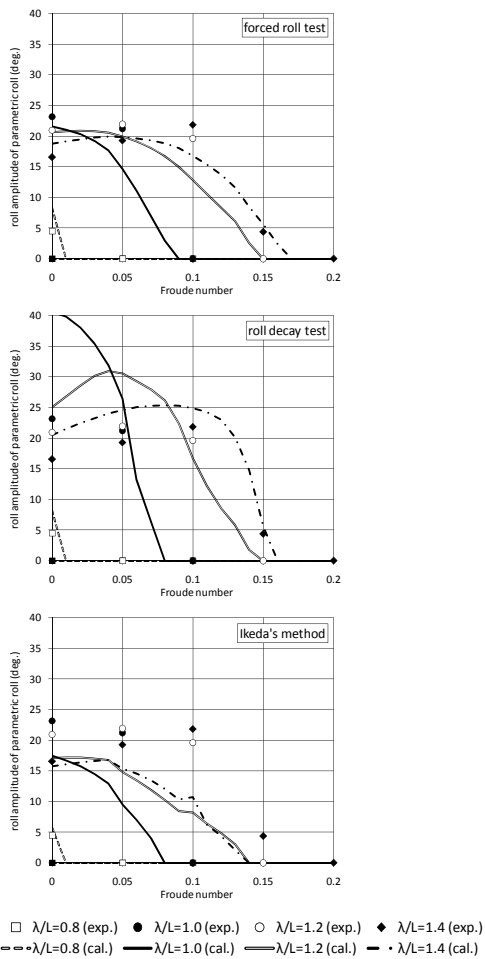


Fig.8 Numerical results of parametric roll with the roll damping estimated from a forced roll test, a roll decay test and the Ikeda's method with H=0.0851 m

### C11 CONTAINERSHIP

The similar investigation was executed for a C11 post-Panamax containership modified by MARIN. (Levadou and van't Veer, 2006) Principal particulars and body plan are shown in Fig.9 and Table 2, respectively.

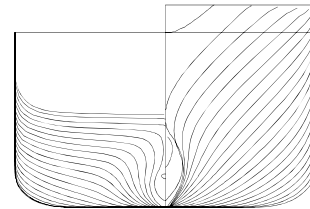


Fig.9 Body plan of the C11 containership

Table 2 Principal particulars of the C11 containership

Item	Value
Length between perpendiculars : $L$	262.0m
breadth : $B$	40.0m
depth : $D$	24.45m
mean draught : $T$	11.5m
block coefficient : $C_b$	0.56
metacentric height : $GM$	1.965m
natural roll period : $T_\phi$	25.1s

### Roll Damping

Estimated roll damping for the C11 containership by a roll decay test and the Ikeda's semi-empirical prediction method are shown in Fig.10. There are significant differences between the two estimation methods, and the trend of the differences is the same as the 6600 TEU containership.

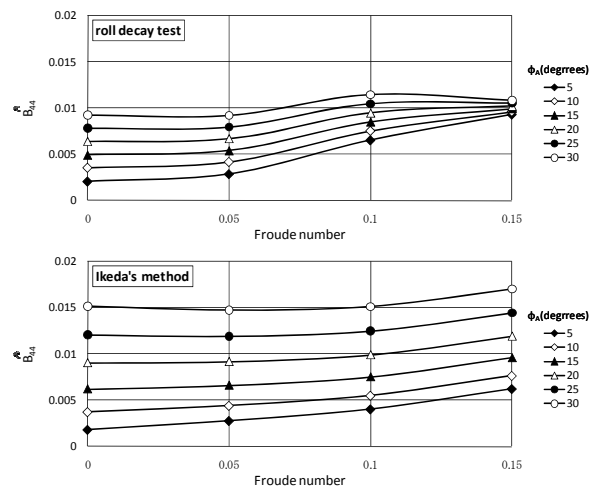


Fig.10 Roll damping coefficients estimated by a roll decay test and the Ikeda's method for the C11 containership

**Parametric Roll Prediction**

Comparisons of roll amplitude of parametric roll in regular head seas between the model experiment [Sogawa et al., 2010] and the numerical simulations with the roll damping estimated by the roll decay test and the Ikeda's prediction method are shown in Fig.11. Numerical result with the roll damping by the roll decay test almost agrees with the model experiment for all wave steepness and Froude numbers. By contrast, the numerical result with the roll damping by the Ikeda's semi-empirical prediction method significantly underestimates the model experiment because of its overestimation of roll damping as shown in Fig.10. Since the amplitude of roll restoring variation increases its nonlinearity with a roll angle, the difference of estimation methods of roll damping could significantly affect on parametric roll prediction and could result in completely different amplitude. Therefore more attention to the estimation methods of roll damping should be paid for quantitative validation of numerical simulation of parametric roll.

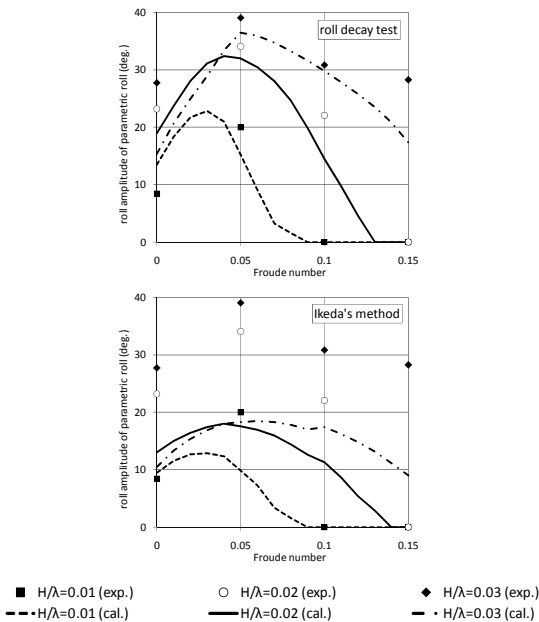


Fig.11 Numerical results of parametric roll with the roll damping estimated from a roll decay test and the Ikeda's method for the C11 containership with  $\lambda/L=1.0$

**DISCUSSION ON IKEDA'S METHOD**

For the estimation of roll damping by the Ikeda's semi-empirical prediction method, commercial software was used in this study. Since approximation of the each transverse section is performed automatically in the software, estimation accuracy of roll damping could depend on this approximation accuracy itself. Therefore we recalculated the roll damping coefficient both for the 6600 TEU and C11 containerships by imputing the exact position of the bilge keels for every transverse section by hand. As shown in Fig.12, the calculated result of roll damping for the 6600 TEU containership drastically changes and almost agrees with the experimental result of a forced roll model test except for small roll amplitude. On the other hand, the result for the C11 containership does not change very much even if the exact position of the bilge keels in each section is given, and the significant difference still remains between the roll damping estimated by a roll decay test and that by the Ikeda's prediction method. Further investigation, such as a forced roll motion test for the C11 containership and the similar examination for other types of ships, is required for further discussion.

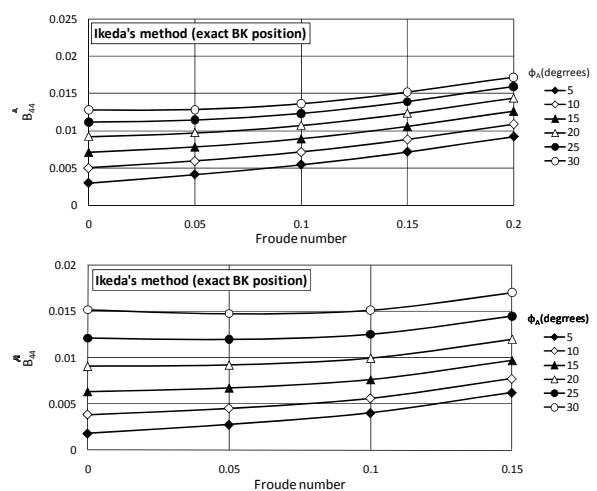


Fig.12 Estimated roll damping by the Ikeda's method with exact bilge keel position for the 6600TEU containership (upper) and the C11 containership (lower)

## CONCLUSIONS

Numerical investigation on the influence of roll damping estimation methods on parametric roll prediction was conducted. As a result, the estimation methods of roll damping significantly affect on the numerical prediction of parametric roll for the two containerships used here. Further investigations and discussions on roll damping matters are desirable to develop reasonable performance-based intact stability criteria on parametric rolling.

## ACKNOWLEDGEMENTS

This research was partly supported by a Grant-in Aid for Scientific Research of the Japan Society for Promotion of Science (No. 21360427). It was carried out in part as a research activity of Stability Project of Japan Ship Technology Research Association in the fiscal year of 2009, funded by the Nippon Foundation. The authors thank the ITTC (International Towing Tank), as well as MARIN, for providing geometric data of the modified C11 class containership for the work on new generation intact stability criteria development. The authors also thank Dr. Toru Katayama from Osaka Prefecture University for his useful discussion on the Ikeda's prediction method.

## REFERENCES

Hashimoto, H., Umeda, N. and Sakamoto, G., (2007), Head-Sea Parametric Rolling of a Car Carrier, Proceedings of the 9th International Ship Stability Workshop, CD

Hirayama, T. and Takezawa, S., (1982), Transient and Irregular Experiments for Predicting the Large Rolling in Beam Irregular Waves, Proceedings of the 2nd International Conference on Stability of Ships and Ocean Vehicles, pp.379-397.

Ikeda, Y., (2004), Prediction Methods of Roll Damping of Ships and Their Application to Determine Optimum Stabilization Devices, Marine Technology, Vol.41, No.2, PP.89-93.

Levadou, M. and van't Veer, R., (2006), Parametric Roll and Ship Design, Proceedings of the 9th International Conference of Ships and Ocean Vehicles, Vol.1, pp.191-206.

Salvesen, N., Tuck E.O. and Faltinsen, O., (1970), Ship Motions and Sea Load, TSNAME, Vol.78.

Sogawa, Y., Umeda, N., Hashimoto, H., (2010), Parametric Roll of a Post Panamax Containership in Regular Waves: Experiment, Analytical Method and Simulation", Proceedings of the 5th APHydro, in press.

## NOMENCLATURE

$A_{ij}$	Added mass/added moment of inertia
$B_{ij}$	Damping coefficient
$F_i^{DF}$	Diffraction force
$F_i^{FK+B}$	Froude-Krylov force and buoyancy
$F_n$	Froude number
$H$	Wave height
$I_{xx}$	Moment of inertia in roll
$m$	Ship mass
$N$	Roll damping coefficient
$\phi$	Roll angle
$\phi_a$	Roll amplitude
$\lambda$	Wave length
$\theta$	Pitch angle
$\omega_e$	Encounter frequency
$\zeta$	Heave displacement



## Damage Stability Making Sense

George Mermiris and Dracos Vassalos

*The Ship Stability Research Centre, Department of Naval Architecture and Marine Engineering,  
University of Strathclyde*

### ABSTRACT

Although aviation, nuclear, processing, etc. industries have long ago adopted and established preventative frameworks and procedures to safeguard against unwanted outcomes of daily operations, maritime industry still places the emphasis on the mitigation of consequences following an accident. Despite the widely expressed opinion that prevention is the way forward, curing occupies a central position not only in every day practice but in the underlying regulatory framework as well. Contrary to this approach, the work presented here aims to create the necessary momentum towards rationalisation of the fundamental choices made during the design process, thus attracting attention to areas where prevention strategies can find fertile ground and be fruitful and cost-effective. The methodology addresses the occurrence of a collision event and the crashworthiness capacity of a ship as prerequisites for its survivability assessment, with promising results to encourage further development.

### KEYWORDS

Accident prevention; Collision; Crashworthiness

### INTRODUCTORY INFORMATION FOR AUTHORS

#### *George Mermiris*

George Mermiris has graduated with MEng (2003) and PhD (2010) from the Department of Naval Architecture and Marine Engineering, University of Strathclyde. Currently he is a Research Fellow in the Ship Stability Research Centre (SSRC). The core of his work is on Risk-Based Design methodology and implementation with main emphasis on structural analysis and collision dynamics, advanced mathematical modelling and risk analysis. He has authored 10 journal and conference papers in this area.

#### *Dracos Vassalos*

Dracos Vassalos is Professor of Maritime Safety in the Department of Naval Architecture and Marine Engineering of the University of

Strathclyde and the Director of the Ship Stability Research Centre (SSRC), a world-leading centre of excellence on ship stability and safety. His motto is “safety enhancement through innovation”, an idea he has pursued single-mindedly in a career that spans over 30 years in industry and academia, promoting the use of scientific approaches in dealing with maritime safety. He has been instrumental in helping to create a critical mass in the research community on safety, through a series of initiatives that made SSRC the focus of active international collaboration. He travels the world over promoting maritime safety, lectures and publishes widely, with some 400 technical publications, 4 patents and 7 books/Conference proceedings to his credit and a string of prizes and awards, including some 100+ major research contracts amounting to over £20M. He served as Head of Department (1997-2007), Chair of the STAB Conferences and Workshops (1996-2006), Chair of the ITTC

Stability Committee in Waves (1996-2002), Chair of WEGEMT (the European Association of Universities in Marine Technology 1999-2001). Currently, Professor Vassalos is Chairman of the International Standing Committee of the “Design for Safety” Conference, a theme instigated and promulgated by SSRC. He is also a long-standing member of the UK delegation to IMO for ship stability and safety.

### INTRODUCTION

Traditionally, the damage stability and survivability performance of a ship are treated under the assumption that the hull is breached following a collision event. This approach has received considerable attention and significant effort has been spent in collating the required information for dimensioning the damage opening (SOLAS Ch.II-1).

Even though the probability of pertinent events that can compromise the watertightness of the hull, like collision and grounding, are consistently accounted for in quantitative risk analyses, the compulsory use of the Attained Index of subdivision, Eq. (1), discourages any focus on the associated causal factors and, in the particular case of collisions, on crashworthiness. As a result, accidents still happen, much more frequently than they should, and ships are lost with significant price for human life and the environment.

One key reason for this state of affairs relates to the fact that rule making in our industry focuses on damage limitation (cure) rather than damage prevention. Hence, the industry is pursuing happily a very ineffective means of sorting bad image and reputation. This being the case, the time for diverting attention towards an approach that makes sense of damage stability is long overdue but, fortuitously, ripe. More specifically, the emergence of the design for safety philosophy and the development of risk-based design methodology allows due attention on the risk pertinent to each vessel category in a scientific

and all-embracing way, capable of balancing risk reduction and mitigation with other design objectives cost-effectively.

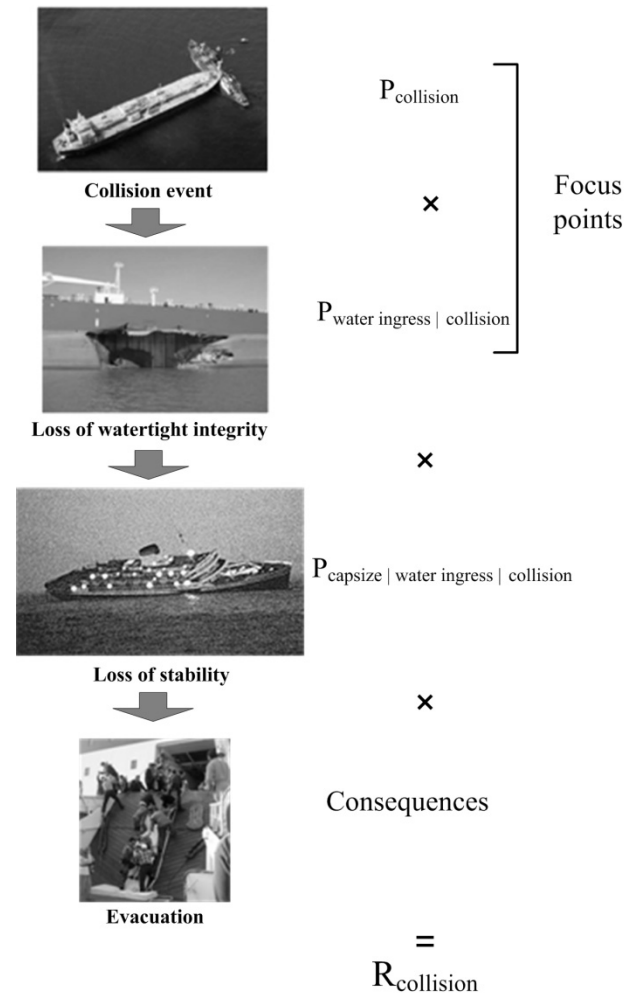


Fig. 1: Sequence of events in flooding scenario with the corresponding probability elements for the collision risk assessment.

The work presented here demonstrates that in order to integrate safety against collision in the design process, it is necessary to rationalise the survivability assessment as it is presented by Vassalos, (2004). This can be achieved by addressing the probability of collision occurrence, the probability of water ingress due to collision, the probability of capsize due to the ensuing water ingress and the consequential loss (Figure 1). Such an integrated approach has been the focus in SSRC over the past 5 years, reaching the stage where potential benefits from trying to make sense of damage stability are demonstrable. This offers new inroads for the integration of safety against

collision in the design process by drawing information from and feeding knowledge to the ship operation in an unprecedented way.

### THE REGULATORY FRAMEWORK

The assessment of the risk level following a ship collision event is presently performed according to Wendel's, (1960), probabilistic approach, which is practically implemented with the Attained Index of subdivision A, (IMO, 2009):

$$A = \sum_{j=1}^J \sum_{i=1}^I w_j P_i S_{ij} \quad (1)$$

Where

j: the counter for loading conditions;

i: the counter for damaged compartments or groups of adjacent compartments;

J: the number of loading conditions;

I: the number of damaged cases (single of groups of adjacent compartments) for each loading condition;

w<sub>j</sub>: probability mass function of the loading conditions;

p<sub>i</sub>: probability mass function of flooding extent of a compartment or group of compartments for loading condition j ( $\sum_i P_i = 1$ );

s<sub>ij</sub>: the average probability of surviving the flooding of a compartment (or group of compartments), for loading condition j.

Index A is the weighted average of the probability of survival, i.e. its expected value E(s), of all damage cases for a ship. As long as the value of A is greater than a prescribed threshold value (index R), the safety level of the ship is considered satisfactory, at least from a regulatory point of view.

### *A critique on the current approach*

The philosophy of this regulation is attractive (due to its scientific foundation on probability theory) and special (as few precedent frameworks, if any, have ever adopted a similar approach). However, the framework is based on statistical analysis of past accidents and unavoidably builds on the fact that a collision has occurred and the watertightness is lost (otherwise the accident would not be considered). Instead of using statistical information for rationalising the choices of the damage scenarios and benchmarking the results of structural analyses, the regulation puts emphasis on the identification of all damage cases that would compromise survivability. That is, irrespective of how improbable 5-compartment damage would be, this scenario will still be considered in the assessment. Hence, the process changes into a vulnerability analysis.

A closer look at the provisions of the framework will reveal determinism and inconsistency, as it is explained next:

- (i) The calculation of the probability of flooding is conditional on the collision occurrence, i.e. the probability of collision  $P_{\text{collision}} = 1.0$ . However, modern communication and IT developments in combination with improved training of the navigation officers contribute significantly towards the traffic management even in the most congested waters.
- (ii) The probability of flooding is also conditional on the probability of water ingress due to collision, i.e. the ship shell is breached and the penetration is of sufficient size to cause large scale flooding of one or more compartments instantly. Therefore,  $P_{\text{water ingress} | \text{collision}} = 1.0$ . Yet, a collision occurrence does not mean that the watertightness of the hull is lost. Statistical data and computer simulations clearly indicate that the overall damage can range between denting and breaching of the side shell, with large variation of the damage opening (Figure 2). In any case, instant flooding is expected to be very remote.

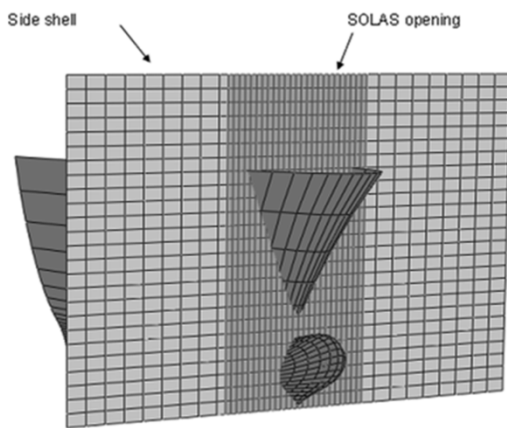


Fig. 2: Actual damage as opposed to SOLAS opening.

- (iii) The calculation of the p-factor is solely based on the location of transverse and longitudinal bulkheads. At the same time, the crashworthiness of the side panel of each compartment, i.e. its capacity to absorb impact energy, (Vredeveldt, 2005), is ignored.
- (iv) In the process of the above calculations, the operational profile of the struck ship should be taken into consideration for the following reasons: (i) in the case of  $P_{\text{collision}}$ , information on the traffic density and the geographical restrictions will indicate the level of congestion in a seaway, whereas (ii) in the case of  $P_{\text{water ingress | collision}}$  it will offer an estimation of the available kinetic energy and bow geometries (as it will be explained in the next section) that can compromise the side shell. This way, a ship, which operates in coastal waters and in open sea, will experience different collision risk levels but because the operational profile is not accounted for in the regulation, the p-factor will remain the same.

As a result, the level of assumptions in the calculation of the p-factor renders the value of A questionable. More importantly though, index R is derived on the basis of a sufficient number of A-values of ships that have survived the elements over their life-cycle and represents an acceptable level of safety standard, (HARDER, 2003). But if R is based on values of A, the value of which is fraught

with uncertainty, then R is also uncertain and the level of safety it represents is questionable.

### THE PROPOSED MODEL

Conventionally, the environment (in terms of wind, waves, etc.) in which a ship operates largely defines its design characteristics with respect to hydrodynamic and structural performance. In addition to the imposed loading on the hull girder, the operational environment also provides information concerning the accidental loading on the ship (congestion levels, speed and direction of the surrounding traffic, etc.), which until recently was of secondary or no importance during design. With this information readily available, the calculation of the p-factor can be rationalised as it is briefly described in the following two sections and in more detail in (Mermiris, 2010).

#### *Probability of collision*

The assessment of the probability of collision is based on the concept of *ship domain*, as it was introduced in the late 70's, (Goodwin, 1979), and treated in various contexts and studies, (Hansen et al., 2004), (Filipowicz, 2004), etc. It was initially defined as a circular area surrounding a ship and if an object entered this area then a collision was assumed.

In the proposed model, the shape of the domain is retained but its diameter varies as a function of operational and design parameters. When the domain diameter becomes equal to or less than the ship length then a collision occurs.

The elements of the model that define the ship domain are:

1. The ship length (L) is indicative of the size of the vessel in a seaway and it is inversely proportional to the diameter of the domain.
2. The response time (R) is the necessary time for the vessel to advance at 90 degrees and it defines how fast the ship will respond to a command for an evasive manoeuvre (ignoring any depth effects). R

is reciprocal to the size of the domain as well.

3. The speed of the vessel (V) is important from an operational point of view. Its value reflects the conditions (traffic density, visibility, time schedule, etc.) under which the vessel steams and its variation depends on the geography of the navigational area.
4. The traffic density ( $\rho$ ), i.e. the number of ships per unit area, in a seaway can impose further restrictions to the speed range. Evidently, speed and traffic density are inversely proportional to the domain size as well.
5. The transverse channel width (C) defines the topological boundaries of the course of the ship in a waterway. It varies proportionally to the domain size and, according to Kriastiansen, (2005), it is related to the traffic density:

$$\rho = \frac{N}{V' C} \quad (2)$$

Where N is the number of ship passages per unit time (e.g. annually), and V' is the speed of the surrounding traffic.

6. Over the years, authors like (Fujii et al., 1974) and accident investigators, e.g. (MAIB, 2005), have stressed that collision accidents (i) never occur instantaneously and without the right initial conditions (low visibility, early morning hours, etc.), and (ii) can be attributed to miscalculations, over-confidence, lack of communication, etc. When everything is orchestrated properly, then there is always a critical *point of no return*, which is measured consistently in the range of a few minutes, (Cahill, 2002)!

The fact that ship collisions always occur for a very specific set of initial conditions suggests that existing methodologies are fragmented (attributing the accident to human factors and adverse weather conditions or bad maintenance of hardware) and inadequate (the irreversibility of the situation is ignored).

In the proposed methodology the “softer” aspects of an accident are accounted for as disorder or uncertainty, i.e. in the form of entropy of a situation (H), (Williams, 1997), which is expressed as:

$$H = \sum_{j=1}^M \sum_{i=1}^{N_j} P_{ij} \log_2 \left( \frac{1}{P_{ij}} \right) \quad (3)$$

Where:

- i: counter for the number of states of each event,
- j: counter for the number of events,
- M: number of events,
- N<sub>j</sub>: number of states of event j,
- P<sub>ij</sub>: probability of occurrence of the state i and the event j, where  $\sum_i P_i = 1$ .

As the value of entropy increases, the more imminent a collision is. Examples of high and low entropy values are presented in Table 1.

**Table 1: Examples of high and low entropy situations**

High entropy	Low entropy	Remarks
Disorder, disorganisation, thorough mix-up	Order, high degree of organisation	Existence of a Vessel Traffic System (VTS) in the area of navigation
Great uncertainty	Near certainty, high reliability	Information about wind gusts, when close quarter manoeuvring is required.
Great surprise	Little or no surprise	The familiarity of the navigator with the area of operation and the dominant conditions

Establishment of threshold values for entropy is an ongoing development but this concept allows a broad range of critical information to be consolidated into a single number with widely accepted meaning.

In summary, the domain diameter is expressed as:

$$D = \frac{C}{V L R \rho} 10^{-H} = \frac{V' C^2}{V L R N} 10^{-H} \quad (4)$$

The probability of collision per unit time can be obtained with Monte Carlo sampling of the entailed parameters.

With Eq. (4) the point of no return is substantiated (due to its non-linear character) since the contribution to the entropy level of each of the participating events can be determined at successive instances and the escalation of a situation can be quantified, thus providing better decision support to the navigator, the port authorities, etc. An example of this is the comparison between navigation in open and closed waters for a ROPAX ship (Figure 3). In the former case a collision event is guaranteed for values of entropy approximately equal to 4.0, whereas in the latter case the entropy levels will have to be doubled. The fact that space availability allows longer decision-making times is reflected in the proposed model and justifies the choice of entropy as an aggregate measure for quantitative and qualitative information.

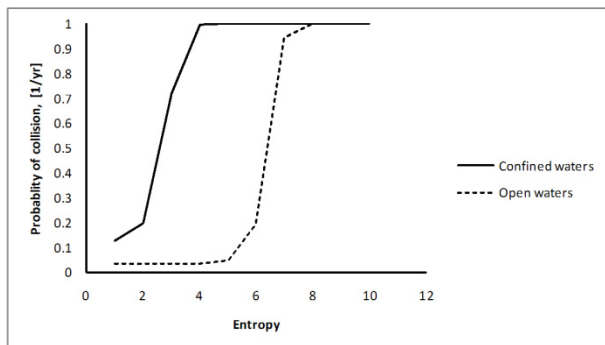


Fig. 3: Entropy variation for open, (Pedersen and Zhang, 1999), and confined waters, (Øresund, 2006).

It should be stressed that Eq. (4) is applicable when the ship is in sailing mode and when collision with other ships is considered; otherwise the element of speed of surrounding traffic ( $V'$ ) becomes meaningless.

#### **Probability of water ingress due to collision**

The extent of the structural damage following a collision event is tightly connected to the

crashworthiness of the side shell panels as it was stressed earlier. Although the highly non-linear failure of the structure intuitively calls for sophisticated analysis with the Finite Elements (FE) technique, the very nature of FE is prohibitive for early design application (where most of the main characteristics of a ship are decided) due to long modelling, processing and post-processing times, and because such results cannot be communicated easily to the rest of the design tools. This being the case, the designers can either consider a small number of selected damages (i.e. check the vulnerability of the hull) or ignore such input and resort to using damage openings as prescribed in SOLAS.

The proposed approach is founded on the absorption of the kinetic energy of the striking ship by a restricted portion of the structure of the struck ship. The phenomenon is governed by (i) the magnitude of the kinetic energy, (ii) the structural configuration of the struck panel, and (iii) the geometry of the striking bow (assumed rigid here). The first two aspects can be derived from the operational profile of the ship in terms of the surrounding traffic (i.e. the size and the speed of other vessels), and its structural configuration respectively. The latter complements the expectation of breach occurrence considering that the sharper the contact edge of the striking body is, the easier the panels of the side shell will rupture (i.e. with less expenditure of kinetic energy), as it is confirmed by numerical simulations and experiments.

The remaining factors, which affect the development of a collision event are related to the angle between the two ships (as the angle increases the sharpness of the striking bow is reduced), their inertia, i.e. their virtual (real plus added) mass before (striking ship) and after the contact (struck ship), and the friction during the penetration.

The link of the side structure deformation and the striking body geometry is the *principal radii of curvature* of the latter, which provides a measure of its sharpness at the contact points.

The radii of curvature of a three-dimensional surface can be obtained by its parametric definition:

$$x = x(p, t, w_0), \quad y = y(p, t, w_0), \quad z = z(p, t, w_0) \quad (5)$$

$$p, t \in [0, 1]$$

Where  $x$ ,  $y$  and  $z$  are real, continuous and at least twice differentiable functions (with respect to either of the two parameters) in a right-handed coordinate system and  $w_0$  is the indentation of the panel since in the current context interest lies in the necessary deformation to cause rupture. The geometry of the striking body is represented with a Bezier surface, whereas the struck surface deformation is modelled with the *Witch of Agnesi* function, which allows for explicit consideration of the deflection  $w_0$  as a function of radii of curvature of the striking body:

$$u(x, y, w_0) = C_x \frac{w_0}{\left(1 + \left(\frac{x}{r_1}\right)^2\right)},$$

$$v(x, y, w_0) = C_y \frac{w_0}{\left(1 + \left(\frac{y}{r_2}\right)^2\right)} \quad (6)$$

$$w(x, y, w_0) = C_{xy} \frac{w_0}{\left(1 + \left(\frac{x}{r_1}\right)^2 + \left(\frac{y}{r_2}\right)^2\right)}$$

Where:

- $u$ ,  $v$  and  $w$  are the deformation functions along  $x$  (longitudinal),  $y$  and  $z$  (vertical to its plane) directions of the stiffened panel.
- $C_x$ ,  $C_y$  and  $C_{xy}$  are constants accounting for the stiffening along the  $x$ ,  $y$  and the  $x$ - $y$  directions, respectively.
- $r_1$  and  $r_2$  are the radii of curvature of the striking bow at the point of contact.

Because of the substantial deformations experienced by the stiffened panel, the accumulated strain energy is dominated by membrane action and is expressed as:

$$V_{\text{mem}} = \frac{1}{2} \int_0^L \int_0^B (N_x \varepsilon_x + N_y \varepsilon_y + N_{xy} \gamma_{xy}) dy dx \quad (7)$$

Where  $N_x$ ,  $N_y$  and  $N_{xy}$  are forces per unit length of the plate edge and  $\varepsilon_x$ ,  $\varepsilon_y$  and  $\gamma_{xy}$  are the corresponding strains for large deflections, (Timoshenko and Woinowski-Kreiger, 1964).

The necessary energy for rupture initiation is obtained from the experimental work of Jones and Birch, (2006), where the diameter of the indenter is taken into account when measuring the responses of plates subjected to low speed (in the range of ships' speeds) collisions.

The above model is implemented in the CRASED (*CRashworthiness ASsessment for Early Design*) program. Its results are compared with the statistical data obtained in HARDER for the case of a ROPAX colliding with a similar ship. The length and breadth of the damage opening is presented in Figure 4 as a function of penetration.

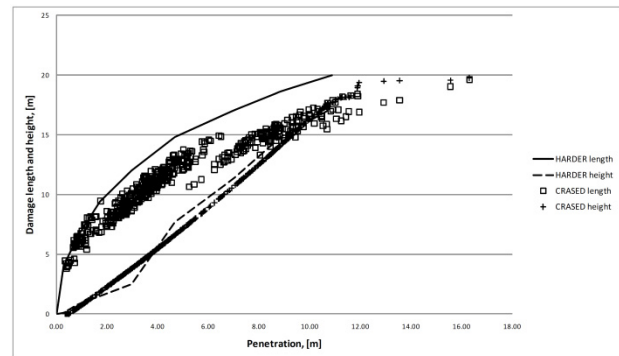


Fig. 4: Comparison between CRASED and statistical data

### The integrated model

Putting the two elements of probability together (for a particular waterway or a set of routes) will provide a concise picture of the flooding probability and its extent due to collision and will highlight potential deficiencies (e.g. in structural arrangement and watertight subdivision) that need to be addressed at design level. This way, the operational profile of a new ship and its physical properties are mutually contributing to the derivation of the ship collision risk levels.

## CONCLUSIONS

Although the probabilistic framework for damage stability is moving in the right direction for the quantification of safety levels of ships, its implementation is inconsistent as the weight is placed on the vulnerabilities of a ship. This way, any realistic treatment of the operational risks, and with it any serious attempt to build on prevention, is lost. The methodology proposed here aims to address this issue and, considering that accidents still happen despite the substantial effort spent for analysis and regulation, to create a momentum of thinking for rationalising the ship survivability assessment and the shipping operations in general.

## REFERENCES

- Cahill, R. A. (2002). "Collisions and their causes", The Nautical Institute, 3<sup>rd</sup> Edition
- Filipowicz, W. (2004). "Vessel traffic control problems", The Journal of Navigation, **57**, pp. 15-24
- Fujii, Y., Oshima, R., Yamanouchi, H., Mizuki, N. (1974). "Some factors affecting the frequency of accidents in marine traffic: I-The diameter of evasion for crossing encounters, II-The probability of stranding, III-The effect of darkness on the probability of collision and stranding, IV-Visual range and the degree of risk", The Journal of Navigation, **27**, 234-252
- Goodwin, E.M. (1979). "Determination of ship domain size", Published in "Mathematical aspects of marine traffic" based on the Proceedings of the "Conference on Mathematical Aspects of Marine Traffic" held at Chelsea College London in September, 1977, organized by the Institute of Mathematics and its Applications edited by S.H. Hollingdale, London Academic Press
- Hansen, P. F., Ravn, E. S., Hartman, J. P. and Sorensen, A. (2004) "FSA of the navigational safety in Baltic west", Proceedings of the 3<sup>rd</sup> International Conference on Collision and Grounding of Ships (ICCGS), Izu, Japan
- HARDER, (2003). "Final Technical Report", Det Norske Veritas, Harmonisation of Rules and Design Rationale (HARDER), GRD1-1999-10721
- IMO, (2009). "Adoption of amendments to the international convention of Safety Of Life At Sea, 1974, as amended", Resolution 216(82), Annex 2
- Jones, N. and Birch, R. S. (2006), "Low velocity perforation design of metal plates", Structures Under Shock and Impact IX, WIT Transactions on the Built Environment, Vol. 87, pp.179-186
- Kriastiansen, S. (2005). "Maritime Transportation: Safety Management and Risk Analysis", Elsevier Butterworth-Heinemann
- MAIB, (2005). "Report of the investigation of the collision between Cepheus J and Ileksa in the Kattegat, 22 November 2004", Marine Accident Investigation Branch, Report Number 12/2005
- Mermiris, G. (2010). "A Risk-Based Design Approach to Ship-Ship Collision", PhD Thesis, University of Strathclyde, Department of Naval Architecture and Marine Engineering, Glasgow
- Øresund, (2006). "Navigational safety in the sound between Denmark and Sweden (Øresund): Risk and Cost-benefit analysis", The Royal Danish Administration of Navigation and Hydrography, The Danish Maritime Authority, The Swedish Maritime Administration
- Pedersen, P. T. and Zhang, S. (1999). Collision analysis for MS Dextra. SAFEREURORO Spring Meeting, Paper No.2, Nantes, France
- Ravn, E., Hansen, P. F., Leva, C., Cernusco, A. and Lepsoe, A. (2006). "Modelling the causation factor for ship under power", SAFEDOR Project (IP-516278), Deliverable D2.4.3
- Timoshenko, S. P. & Woinowski-Kreiger, S. (1964). "Theory of plates and shells", McGraw-Hill Publishing Co
- Vassalos, D. (2004). "A Risk-based Approach to Probabilistic Damage Stability", Proceedings of the 7<sup>th</sup> International Ship Stability Workshop, Shanghai
- Vredeveltdt, A. (2005). "Crashworthiness", Training Course on Risk-Based Ship Design, Universities of Glasgow and Strathclyde, Glasgow, UK, 7-8 June, 2005
- Wendel, K. (1960), "Die Wahrscheinlichkeit des Uberstehens von Verletzungen", Schiffstechnik, Vol. 7, No. 36, pp.47-61
- Williams, G. P. (1997). "Chaos Theory Tamed", Joseph Henry Press

# Uncertainty Assessment in Experiments on a Floating Body in Forced Roll Motion in Calm Water

Jakub Cichowicz, Andrzej Jasionowski and Dracos Vassalos

*The Ship Stability Research Centre, Department of Naval Architecture and Marine Engineering, University of Strathclyde, Glasgow*

Accurate prediction of a ship response in roll motion is one of the fundamental problems in fluid dynamics. It has inspired numerous research activities, many of them involving physical tests. The tank experiments, although seemingly the most convenient for handling such complex problems, have proven to be very challenging, both technically and conceptually. This is due to the very convoluted nature of roll motion hydrodynamics as well as the small magnitude of dissipation forces compared to inertia and hydrostatic forces. When discussing the impact of roll damping prediction on damage ship stability and survivability, before migrating from simplified theories or semi-empirical models towards more complicated and time-demanding tools, the question whether accuracy of available alternatives is sufficient to justify such transition must first be addressed. Similarly, when experimental data is provided for validating CFD codes, it is sensible to do so only if the uncertainty limits of the former are evaluated. This makes uncertainty assessment a central problem in the pursuit for high-accuracy prediction of roll damping characteristics. It may also reveal the potential limit of applicability of the adopted approach.

This paper presents uncertainty assessment of forced roll measurements performed on a floating body in calm water and discusses the main sources of errors and impact on the final prediction.

## Introduction

An accurate prediction of hydrodynamic forces in roll motion is a problem of central importance in studies on ship stability and as such it has attracted numerous research studies addressing the issue both analytically and experimentally with works of Frank (Frank, 1967) and Vugts (Vugts, 1968) being among the finest examples. From the very beginning it has been clear, however, that methodologies based on linear theory and potential flow (inviscid fluid) is practically limited to small amplitude motions and does not represent well the dynamics of a dissipative system oscillating with finite amplitude. The semi-empirical method of Himeno and Ikeda (Himeno, 1981) employed for correcting damping coefficient has proven to be very useful but its applicability is limited to “standard” shapes and it generally suffers from drawbacks of regression-based techniques. On the other hand a more sophisticated approach, based on RANSE (CFD) codes, might help understand-

ing the problem better but in order to provide high quality data CFD findings have to be verified with experimental results – and here is where the real problem seems to start because hydrodynamic reaction in roll is small, much smaller than the dominant inertia and restoring moments. Indeed it can be readily shown that damping moment has a magnitude comparable to uncertainty in restoring and inertia moments (for the tested body the maximum ratio of damping moment to total inertia, external excitation and restoring moment does not exceed 6%, 12% and 0.5%, respectively). Furthermore, a ship in roll motion is a non-conservative system and although dissipation forces (in calm water) can be generally decomposed into wave radiation (potential damping), friction and vortex shedding (viscous effects), it is very difficult to measure (or assess) accurately individual components, with the last two being strongly dependent on motion amplitude and all three on frequency. Going down this route, one can quickly realise that a seemingly simple problem becomes a

real “beast” with more and more difficulties appearing whenever a new state variable is added to the equation (to mention only wave diffraction of a ship rolling in waves, Pawlowski, 1999). Finally, there is also the question of the experimental technique adopted, with measurements in-waves being one of the least controllable experimental environments, practically leaving room for calm water measurements only. These are traditionally being performed as either forced oscillations about fixed axis of rotation or roll decay tests. In case of the former, the experimental setup involves constrained motions, which deviate from realistic conditions whereas applicability of the latter is limited to single frequency estimates, which is of little, if any, use for numerical tools.

Measurements performed on a freely floating body forced to roll by an internal device seem to be an attractive alternative, retaining the virtues of calm-water techniques. Furthermore, the fact that model motions can be unconstrained and the forcing moment controllable, allow for investigating roll dynamics of a ship in damaged condition in an experimental environment accounting for transient phenomena.

Understandably, the technique adopted has certain limitations and it is the intention in this paper to discuss some of the key issues related to uncertainty assessment associated with the method and, to some extent, with measurements of hydrodynamic reaction in general. Detailed discussion is confined here to uncertainty of the mathematical model, which allows for comparison of experimental data with analytical and other experimental predictions, and on phase lag assessment – a factor thought to have the highest impact on the quality of the measured data. Some sources of errors are discussed briefly-mainly to demonstrate expected sensitivities of the results.

### Experiment Set-up

Experiments discussed in this paper have been carried out at the *Kelvin Hydrodynamics Laboratory*, a testing facility of the University of Strathclyde (UoS) in autumn 2009. These experiments are part of research activities aiming to address the hydrodynamic properties of ships in damaged condition and the results presented here are meant to validate the technique adopted.



**Figure 1** *Cylindrical section of a RO-PAX vessel subjected to forced roll in calm water.*

The tested model is a 1:40 scale cylindrical section of a RO-PAX vessel of length 60 m, draught 6.287 m, beam 27.8 m and vertical position of centre of gravity (KG) equal 8.337 m (GM = 5.509 m). An internal forcing device consists of set of coupled gyros of maximum 7000 rpm spin velocities and precession rates<sup>1</sup> limited to 1.7 Hz. Gyros are supported by common frame, pivoted alongside of the model centre-plane and with rotation about pivoting axis constrained by the strain gauge load cell measuring force component of the generated moment.

Motions of the body are recorded with use of optical motion capture system based on high-speed infrared cameras and set of reflective (passive) markers fitted to the body. Additionally there are two devices – single axis accelerometer and solid-state gyro for reference measurements of the phase lag of response.

### Uncertainty Assessment

#### *Uncertainties associated with the mathematical model*

For the purpose of this paper it is assumed that motions of a body rolling in calm water can be described by a set of linear ordinary differential equations. In such model, hydrodynamic reaction can be conveniently expressed by means of orthogonal components given as added inertia and damping coefficients. It should be noted here that the assumption of orthogonality of the hydrodynamic moment components holds only for purely

<sup>1</sup> This is equal to maximum roll frequency of the body

harmonic excitation - this assumption shall be discussed further in the following. Furthermore, it is assumed that the flow around the body can be considered two-dimensional and hence the problem can be reduced to vertical motions only, involving three degrees of freedom (DOF): sway ( $Y$ ), heave ( $Z$ ) and roll ( $\varphi$ ). In order to describe motions of the body in space two right-handed coordinate systems are employed. The global, fixed in space, reference system is described by a set of three orthogonal axes  $OXYZ$ . The second coordinate system is body-fixed, with origin at the intersection of the body centre-plane and midship-section ( $o$ ). The axes are denoted by  $x$ ,  $y$  and  $z$  with axes  $ox$  and  $oz$  at the centre-plane, the latter positive upward. Sway and heave motions are understood as rectilinear displacements of the origin  $o$  along the global axes  $OY$  and  $OZ$  respectively, and roll as rotation about the body-fixed axis  $ox$ . If the centre of gravity ( $G$ ) coincides with the origin of body-fixed system the equations of motion will take the following form

$$\begin{aligned} & \begin{bmatrix} m + a_{yy} & a_{yz} & a_{y\varphi} \\ a_{zy} & m + a_{zz} & a_{z\varphi} \\ a_{\varphi y} & a_{\varphi z} & I_{\varphi} + a_{\varphi\varphi} \end{bmatrix} \begin{bmatrix} \ddot{y} \\ \ddot{z} \\ \ddot{\varphi} \end{bmatrix} + \\ & + \begin{bmatrix} b_{yy} & b_{yz} & b_{y\varphi} \\ b_{zy} & b_{zz} & b_{z\varphi} \\ b_{\varphi y} & b_{\varphi z} & b_{\varphi\varphi} \end{bmatrix} \begin{bmatrix} \dot{y} \\ \dot{z} \\ \dot{\varphi} \end{bmatrix} + \\ & + \begin{bmatrix} c_{yy} & c_{yz} & c_{y\varphi} \\ c_{zy} & c_{zz} & c_{z\varphi} \\ c_{\varphi y} & c_{\varphi z} & c_{\varphi\varphi} \end{bmatrix} \begin{bmatrix} y \\ z \\ \varphi \end{bmatrix} = \begin{bmatrix} F_y \\ F_z \\ M_{\varphi} \end{bmatrix} \end{aligned} \quad (1)$$

Where

$m$  – mass of the body

$I_{\varphi}$  – mass moment of inertia

$a_{ii}$  – added mass or added moment of inertia coefficient in  $i$ -mode of motion

$a_{ij}$  – added mass coupling coefficient of  $j$ - into  $i$ -mode of motion

$b_{ii}$  – damping coefficient in  $i$ - mode of motion

$b_{ij}$  – damping coupling coefficient of  $j$ - into  $i$ -mode of motion

$c_{ii}$  – hydrostatic restoring coefficient in  $i$ -mode of motion

$c_{ij}$  – hydrostatic restoring coupling coefficient of  $j$ - into  $i$ -mode of motion

$F_y, F_z, M_{\varphi}$  – external forces/moment in  $OY, OZ$  and (about)  $ox$  axes, respectively

As the heave motion is symmetrical with respect to  $OZ$  axis, it alone cannot induce any lateral or angular motions and hence  $a_{iz}=b_{iz}=c_{iz}=0$ . Furthermore,  $c_{iy}=c_{yj}=0$ . Moreover, as the internal roll motion generator produces a pure moment, force components  $F_y$  and  $F_z$  are both equal to zero and the simplified equation (1) can be expressed in scalar form as follows:

$$\begin{aligned} & (m + a_{yy})\ddot{y} + a_{y\varphi}\ddot{\varphi} + b_{yy}\dot{y} + b_{y\varphi}\dot{\varphi} = 0 \\ & a_{zy}\ddot{y} + (m + a_{zz})\ddot{z} + a_{z\varphi}\ddot{\varphi} + b_{zy}\dot{y} + \\ & + b_{zz}\dot{z} + b_{z\varphi}\dot{\varphi} + c_{zz}z + c_{z\varphi}\varphi = 0 \quad (2) \\ & a_{\varphi y}\ddot{y} + (I_{\varphi} + a_{\varphi\varphi})\ddot{\varphi} + b_{\varphi y}\dot{y} + b_{\varphi\varphi}\dot{\varphi} + \\ & + c_{\varphi\varphi}\varphi = M_{\varphi} \end{aligned}$$

It can be readily seen from equation (2) that with focus on roll motion and with neither sway nor roll being coupled with heave, the heave equation can be excluded. Furthermore, although external forces in horizontal and vertical directions have been dropped from the equation, hydrodynamic coefficients remain, which is the consequence of the vertical position of axis of rotation (centre of rotation) expected to lie at some point between the origin  $o$  and the centre of gravity. In fact, the centre of rotation of a freely floating body, by analogy to the coupled-mass system, will lie at the centre of coupled mass of the rigid body and the accompanying fluid (Balcer, 2004).

So far it has been assumed that the body oscillates about the axis passing through the origin  $o$  and in such case the rolling body will become a single DOF system due to vanishing of the sway component ( $y=0$ ). In the general case however, roll about an axis not passing through  $o$  would result in sway motion given as

$$y = h \cdot \sin(\varphi) \quad (3)$$

Where,  $h$  is the vertical distance between the centre of rotation and origin  $o$  of the body fixed system (in upright position). On the other hand, in case of a floating body, the centre of rotation will not be fixed in space as due to instantaneous changes in submerged volume it will be subjected to vertical oscillations (roll-induced heave). This is a consequence of finite-amplitude angular displacement and would not be present if roll amplitude was infinitesimal or the body a circular cylinder. However, as figure (2) shows, for small and moderate roll angles roll-induced heave amplitude is expected to be small, constituting some 6% of  $\overline{oG}$  at 20 deg roll angle. Bearing this in mind, for the purpose of the initial uncertainty assessment it is assumed that vertical oscillations of the instantaneous axis of rotation can be neglected and therefore roll-induced sway motion can be expressed by means of equation (3).

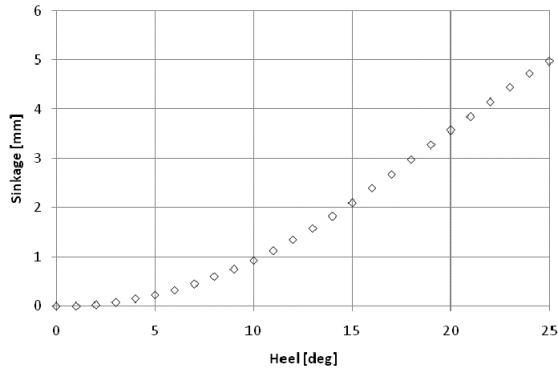


**Figure 2** Sinkage due to heel of the freely floating cylinder tested at UoS (model scale).

As equation (3) indicates, roll-induced sway is implicit function of time thus its time derivatives can be expressed as follows

$$\begin{aligned} \dot{y} &= h\dot{\varphi} \cos \varphi \\ \ddot{y} &= h(\ddot{\varphi} \cos \varphi - \dot{\varphi}^2 \sin \varphi) \end{aligned} \quad (4)$$

Assuming the external moment to be of the form:  $M_\varphi = M_A \sin(\omega t - \varepsilon)$ , where  $M_A$ ,  $\omega$  and  $\varepsilon$  stand for moment amplitude, circular frequency and phase lag respectively, the angular displacement and its time derivatives are given as

$$\begin{aligned} \varphi &= \varphi_A \sin(\omega t) \\ \dot{\varphi} &= \varphi_A \omega \cos(\omega t) \\ \ddot{\varphi} &= -\varphi_A \omega^2 \sin(\omega t) \end{aligned} \quad (5)$$

Where,  $\varphi_A$  stands for roll amplitude.

Making use of orthogonality of roll motion and its derivatives, equations (4) and (5) can be substituted into sway formulae (2), which after simple manipulation yields

$$\begin{aligned} a_{y\varphi} &= -(m + a_{yy})h \cos \varphi_A \\ b_{y\varphi} &= -h \cdot b_{yy} \end{aligned} \quad (6)$$

These equations express the relationship between coupling coefficients of roll into sway, sway coefficient and distance from centre of rotation to the origin  $o$  of body-fixed coordinate system. They can be combined with roll equation and after some rearrangement, roll added inertia and damping coefficients for oscillations about the natural axis of rotation can be expressed as follows<sup>2</sup>

$$\begin{aligned} a_{\varphi\varphi} &= \frac{c_{\varphi\varphi}}{\omega^2} - \frac{M_A \cos \varepsilon}{\varphi_A \omega^2} - I_{\varphi_o} + \\ &+ h^2 (m(1 - \cos^2 \varphi_A) + a_{yy} \cos^2 \varphi_A) \\ b_{\varphi\varphi} &= -\frac{M_A \sin \varepsilon}{\varphi_A \omega} + h^2 \cdot b_{yy} \end{aligned} \quad (7)$$

Where  $I_{\varphi_o}$  is mass moment of inertia of the body about the axis passing through the origin  $o$ .

The above equations form the basis for uncertainty assessment and sensitivity analysis. In the case of the experimental technique being discussed, sway coefficients are not assessed experimentally, so they can either be ignored or assessed by means of theoretical prediction. It is understood that if the body's centre of gravity lies close to the waterplane the last terms of equation (7) can be neglected (with  $h^2$  being second-order) but in the general case their contribution to the results is expected to

<sup>2</sup> These equations have been derived following an assumption that coupling coefficients are symmetrical, i.e. relations  $a_{\varphi y} = a_{y\varphi}$  and  $b_{\varphi y} = b_{y\varphi}$  hold.

be significant. For the purpose of the analysis presented here theoretical predictions of the sway added inertia and damping coefficients were taken into account. On the upside it can be said that, as previous experimental works indicate, predictions of added mass and damping coefficients in sway demonstrate good conformity with physical model tests.

Given that variables present in equation (7) are not correlated (i.e. there are no underlying functional relationships between measured variables), the systematic (bias) part of uncertainty can be expressed in a form based on second-order total differential (Coleman and Steele, 1999):

$$u_s(f)^2 = \sum_{i=1}^n \left( \frac{\partial f}{\partial x_i} u_s(x_i) \right)^2 \quad (8)$$

Where,  $f$  is a functional relation between measured variables  $x_i$ ,  $u_s(\cdot)$  denote systematic errors in derived quantities and measured variables;  $n$  stands for number of variables. Partial derivatives in the above formula are referred to as sensitivity coefficients. In principle, function  $f$  should be decomposed to the level of directly measured variables, i.e. mass, distance, force, motions and time as the remaining quantities are derived from them, e.g.:

1. Hull mass, moment of inertia in air and vertical coordinate of centre of gravity are measured prior to testing and the two quantities - force due to generated moment and motions of the body – are directly measured during the experiments.
2. Circular frequency and phase lag of the response are derived from the time history of force and motion recordings and, as such, they are subjected to uncertainties associated with the former. Similarly, moment of inertia in air will be affected by uncertainties in measured mass and period of oscillations in air.

For the purpose of illustrating the process of uncertainty assessment, only errors in moment, force and response lag will be discussed in detail in the following paragraphs whereas for

other terms, only sensitivity of the results will be briefly presented, based on estimates.

The following figures show comparison of experimental data with potential flow predictions obtained for the actual body shape and a rectangular cylinder of B/T ratio equal 4. Error bars correspond to the systematic part of uncertainties estimated for all variables present in the LHS of equation (7).

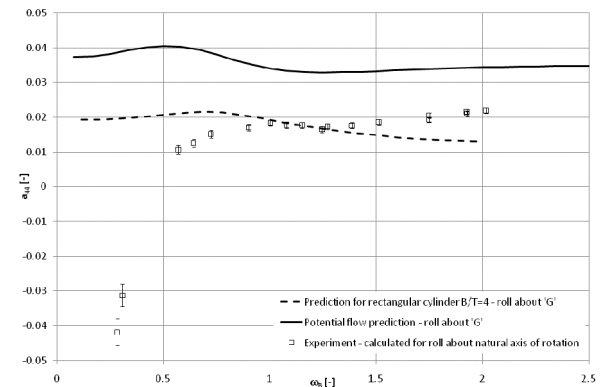


**Figure 3** Roll added moment of inertia coefficient – comparison with potential-flow prediction for the actual body shape (solid) and rectangular cylinder of B/T=4 (dashed).

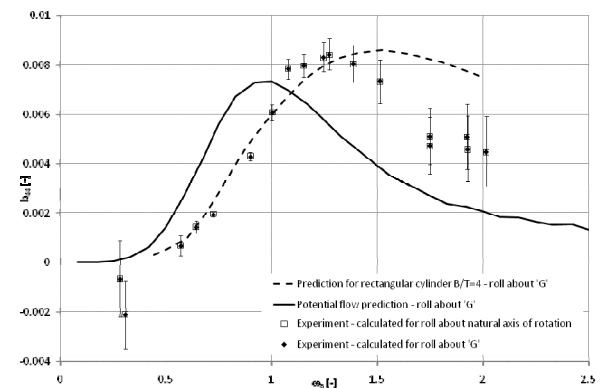


**Figure 4** Roll damping coefficient – comparison with potential-flow prediction for the actual body shape (solid) and rectangular cylinder of B/T=4 (dashed).

As can be seen from figures (3) and (4), experimental data follow an obvious trend but special attention should be paid to the two points corresponding to the lowest frequencies of oscillation, at which both added inertia and damping coefficients take negative values. Undoubtedly, these results are wrong but serve as good indication of difficulties in measurements at low frequencies where damping is small and phase angle approaches zero asymptotically. This behaviour is also confirmed by large systematic uncertainties. It is also worth

noting that damping prediction suffers from large biases not only at low- but also at high-frequency oscillations, caused by phase lag approaching -180 degrees<sup>3</sup>.

In order to present contributions of the individual components to the total bias, the following ratio is used

$$\frac{\left(\frac{\partial f}{\partial x_i} u_s(x_i)\right)^2}{u_s(f)^2} = \frac{\left(\frac{\partial f}{\partial x_i} u_s(x_i)\right)^2}{\sum_{i=1}^n \left(\frac{\partial f}{\partial x_i} u_s(x_i)\right)^2} \quad (9)$$

Individual contributions, expressed in terms of percentage, are presented in the following figures.

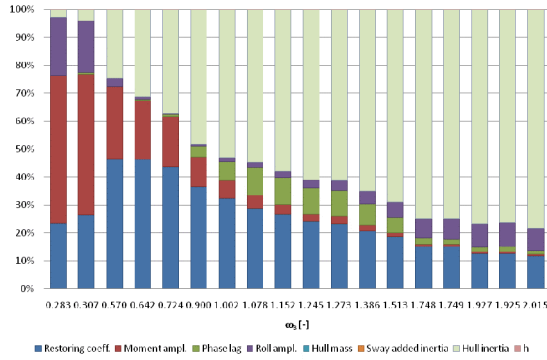


**Figure 5** Contributions of individual components in total bias error estimated for roll added inertia coefficient.

In case of added inertia coefficient it can be seen that there are five significant contributors: errors in amplitudes of external moment and response, restoring coefficient, hull inertia and response phase lag (in the middle- and high-frequency ranges). Comparison of this characteristic with that given by figure (3) may suggest that bias in moment amplitude causes the lowest frequency values to suffer larger uncertainties than the remaining values.

<sup>3</sup> According to the sign convention adopted phase angles are negative.

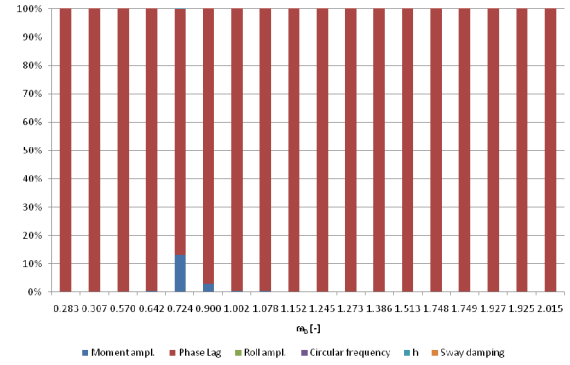


**Figure 6** Contributions of individual components in total bias error estimated for roll damping coefficient.

In case of damping coefficient it is clear that, practically, the sole contributor to the total bias is response phase angle with the exception at mid-range frequencies where there is some bias associated with moment measurements. In any case, systematic errors in roll and moment amplitudes as well as phase lag estimation are dominant. This being the case, the last two will be discussed in some detail. Before this, it might be useful to have a closer look at equations describing the rolling moment produced by the gyroscopic generator in order to justify the aforementioned assumption of orthogonality of hydrodynamic moment components.

#### Uncertainties associated with moment generation and measurement

In the most general form the equation of motion of the single gyro fitted to the hull is given as

$$\begin{aligned} & \ddot{\varphi} \left( J_z \cos^2 \theta_G + J_x \sin^2 \theta_G + J_z^o \right) + \\ & - \dot{\theta}_G h_G \cos(\theta_G) + \\ & + 2(J_x - J_z) \dot{\varphi} \dot{\theta}_G \sin \theta_G \cos \theta_G = \\ & = M_c \end{aligned} \quad (10)$$

Where,  $\varphi$  is the roll angle,  $\theta_G$  gyro precession angle,  $J_x$ ,  $J_z$  gyro moments of inertia with respect to local coordinate system,  $J_z^o$  is the system inertia with respect to roll axis and  $M_c$  is external moment about roll axis.

Without going into detail - this can be found in (Cichowicz, Vassalos, & Jasionowski, 2009) - it can be assumed that the moment  $M_c$  taken with minus sign can represent damping and restoring components (i.e.:  $M_c = -b_{\varphi\varphi} \dot{\varphi} - c_{\varphi\varphi} \varphi$ )

and therefore the equation (10) can be rewritten as

$$\begin{aligned} & \ddot{\phi}(J_z \cos^2 \theta_G + J_x \sin^2 \theta_G + J_z^o) + \\ & + 2(J_x - J_z)\dot{\phi}\dot{\theta}_G \sin \theta_G \cos \theta_G + \\ & + b_{\phi\phi}\dot{\phi} + c_{\phi\phi}\phi = \\ & = \dot{\theta}h_G \cos(\theta_G) \end{aligned} \quad (11)$$

The above equation shows clearly that the motions produced by the gyroscopic roll generator are not, in the general case, purely harmonic as there are quadratic and double-frequency terms present. However, it is so unless moments of inertia of the gyro and its gimbal ( $J_x$  and  $J_z$ ) about local axes are equal, in case of which, the quadratic and double-frequency components vanish:

$$\begin{aligned} & \ddot{\phi}(J_G + J_z^o) + b_{\phi\phi}\dot{\phi} + c_{\phi\phi}\phi = \\ & = \dot{\theta}h_G \cos(\theta_G) \end{aligned} \quad (12)$$

Where,  $J_G$  is a substitute gyro moment of inertia following that  $J_z \cong J_x \cong J_G$

Assessment of the gyro inertia properties has shown that indeed, differences in the moments are small and can be ignored – this can also be verified by observing the response power spectrum in figure 7, where there is no double-frequency component present<sup>4</sup>

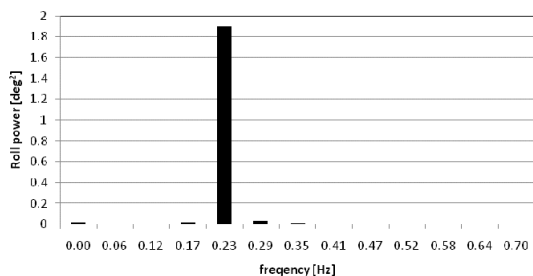


**Figure 7** Example of roll power spectrum for low frequency case ( $\omega=1.5$  rad/s).

Moment (force) measurement is thought to be very reliable, mainly due to use of simple strain gauge and pivoting gyro frame to eliminate (or minimize) impact of lateral inertia forces that might cause bending of the trans-

ducer. The load cell itself has low inertia and therefore short response time as well as linear characteristics with very low hysteresis in a broad range of loads. All this is particularly important for accurate prediction of the body response lag as discussed in the next section.

### *Uncertainties associated with response lag estimation*

It is a well known fact that accurate phase lag estimation is the most difficult task in measurements to determine hydrodynamic reaction. In the case of oscillations about the natural axis, the body motions can be recorded only by using non-contact techniques, based either on measurement of acceleration (velocity) components performed using an internal device or by an optical motion capture system. The former method can be referred to as “classical” approach and in principle such devices are widely used even as independent wireless units (La Gala, Gammaldi, 2009). In case of electromechanical devices, however, their response characteristics (i.e. internal damping and inertia) may be a serious issue and accurate dynamic calibration can be very difficult. Additionally, multi-mode (multi-axis) devices may suffer inaccuracies due to cross-coupled response. Optical motion capture systems are affected neither by mechanical factors like inertia nor by cross-coupling but, as it has been found in the course of experiments carried out at UoS, their real-time output may suffer time shift due to data processing. As a matter of fact the time shift itself would not be considered as a major issue but the real problem lies in its randomness, which makes correcting for the time lag practically impossible.

Electronic (solid state) devices, in turn, are compact, easy to use and calibrate but their accuracy might be questionable and hence readings should be approached cautiously.

During the present measurements the response phase angle has been estimated on the basis of three devices: single axis accelerometer, single axis solid-state (electronic) gyro and optical motion capture system. The last device proved to be unreliable for the aforementioned reasons whereas the first two devices have performed much better. However, as the comparison of damping prediction shows, there are significant discrepancies at super-critical frequencies

<sup>4</sup> This also implies that the following relation holds:

$$J_z \cos^2 \theta_G + J_x \sin^2 \theta_G \cong J_G .$$

(see figure below), for which a consistent explanation has not been found yet.

Comparison of the results shows clearly that low frequency predictions match well but high-frequency characteristics are completely different. In principle, it would be expected that mechanical devices performed worse at higher frequencies but accelerometer based characteristics follow the theoretical prediction better. Bearing this in mind it should be said that the problem has to be investigated in detail as to avoid speculative and somehow counter-intuitive judgment. For the time being it is assumed that accelerometer readings should be used as a basis for further analysis until the question of solid-state gyro accuracy is resolved.

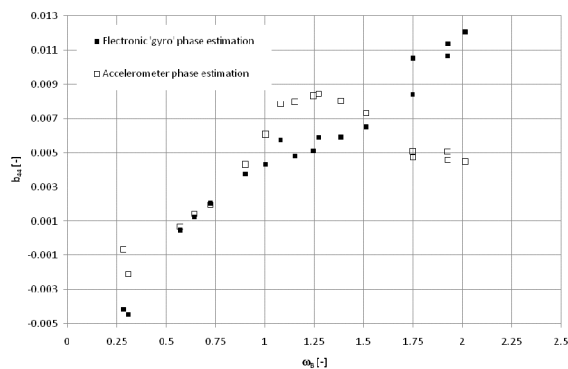


**Figure 8** Comparison of damping prediction based on solid-state gyro and single-axis accelerometer-based phase prediction.

Independently on the measurement method, there is also a question of assessing phases of the time histories of excitation moment and roll motion. Estimates presented in this paper are based on least-squares fit to the steady-state part of the raw data with standard deviations from the analysis constituting the basis for the bias error. Such approach is relatively easy to apply and provides instant information on errors but it is semi-manual and might be considered as not particularly systematic. Spectral techniques may be better alternative but there is some concern associated with them and related to the resolution of harmonic decomposition, particularly for low frequency oscillations and large phase velocity of the radiated waves, which if not damped suffi-

ciently may have difficult to assess impact on the results<sup>5</sup>.

Regarding the formal uncertainty assessment, there are certain points requiring attention. Firstly, there is strong dependency of phase angle estimate on circular frequency. This dependency is not clearly exposed in the state equation but consequences of its propagation into the results are apparent. In short, although expected variations in frequency estimates across the measured variables are small, even these negligible discrepancies introduce significant variations in the phase angle estimates. For this reason, in the least-squares fit, frequency is estimated on the basis of force recordings (considered to be most reliable) and passed as a constrained parameter to the estimates of the remaining signals. Although such approach is formally correct it is thought that harmonic analysis might be more suitable as it automatically averages frequency and, which is perhaps even more important, it makes phase angle formulae easy to process for purpose of uncertainty assessment.

From the formal point of view, uncertainties associated with curve fitting (or harmonic decomposition) are considered to be systematic errors. However, unlike “ordinary” biases, curve fitting errors can be reduced by increasing the length of the sample and in this respect they behave more like precision errors. This is very important as low and high frequency errors in damping could be further reduced by means of detailed investigation of all the motion components and more systematic selection of the data sample, i.e. by making sure that within the selected time the model was not subjected to transient motions, e.g. yaw caused by imperfections in gyros’ ramp velocity characteristics.

<sup>5</sup> In simpler terms there is certain concern that the radiated wave can be reflected from the wavemaker and add energy to the system. This, given the relatively high phase velocity of the low-frequency radiated waves, combined with the long transient period of the forced motions in consideration, constitutes a serious problem and may serve as an explanation for the large uncertainty in both added inertia and damping at very low frequencies, as well as for their negative magnitude.

### Additional considerations

Although the results do not exhibit sensitivity with respect to sway there is some indication that its contribution might be somehow underestimated. The figure below shows the vertical distance from origin of body-fixed coordinate system  $o$  to the predicted mean position of the natural axis of rotation (parameter  $h$ ) as derived on the basis of equation (3).

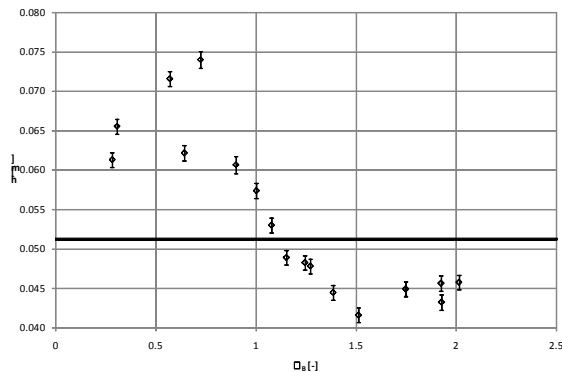


**Figure 9** Predicted mean vertical position of the instantaneous axis of rotation. The solid line corresponds to the vertical position of the centre of gravity ( $oG$ ).

As the figure indicates the predicted value of  $h$  varies with frequency, which can be explained by analogy to coupled-mass system with the axis of rotation passing through the centre of mass of the system. However, for lower frequencies the estimated  $h$  is larger than  $oG$ , which suggests negative added inertia. As by default added mass and inertia of mono-hulls must be non-negative the only reasonable explanation is, assuming correctly estimated centre of gravity, that the body “slides” due to asymmetric pressure distribution leading to sway amplitudes larger than the expected maximum, i.e.  $(y_A)_{\max} = oG \cdot \sin(\varphi_A)$ . Should this proved to be the case a mathematical model might have been revised to accommodate for such behaviour.

### Conclusions

The results presented in this paper demonstrate the outcome of the preliminary stage of uncertainty assessment and they clearly do not provide answers to many important questions. Nevertheless, even such rough estimates of errors allow narrowing down the broad spectrum of problems associated with the measurements and these can be addressed in detail in a more efficient way. Discussion on preci-

sion errors has been omitted entirely but, as it was shown, some of the systematic errors associated with the measurements are “precision” in their very nature with the only difference stemming from the way they are handled.

It should also be emphasised that the conclusions, as far as sway contribution is concerned, are valid for the particular case tested but their generalisation should be approached carefully. It is possible that for a more realistic, in terms of GM, example the sway damping and added mass might have more significant impact on the roll motion hydrodynamics. This is even more important as the present error estimates do not explain the divergence of the experimentally derived coefficients from the theoretical prediction for the very low frequencies and therefore prove only that such discrepancies cannot be solely justified by inaccuracy of measurements.

### Acknowledgments

The authors would like to thank all staff at the Kelvin Hydrodynamics Laboratory for their support and advice in undertaking this research. Special thanks are due to Professor Maciej Pawlowski for his valuable comments and discussion on the subject.

The work had originated within and been initially funded by the EU SAFEDOR Project (IP-516278) with additional support from the Kelvin Hydrodynamics Laboratory.

### References

- Balcer, L. (2004). Location of Ship Rolling Axis. *Polish Maritime Research*, 11.
- Cichowicz, J., Vassalos, D., Jasionowski, A. (2009). *Hydrodynamics of damaged ship in roll mode of motion – an experimental approach*. Proceeding of the 1st International Conference on Advanced Model Measurement Technology for the EU Maritime Industry, (pp. 68-82). Nantes, France.
- La Gala, F., Gammaldi, M. (2009). *A Wireless Inertial Motion Unit (WIMU) for Motion Analysis*. Proceeding of the 1st International Conference on Advanced Model Measurement Technology for the EU Maritime Industry, (pp. 43-54). Nantes, France.

Frank, W. (1967). *Oscillation of Cylinders in or below Free Surface of Deep Fluids*. Washington D.C.: Naval Ship Research and Development Center.

Himeno, Y. (1981). *Prediction of ship Rolling Damping. A State of the Art*. Michigan University.

Hugh W. Coleman, W. Glenn Steele. (1999). *Experimentation and Uncertainty Analysis for Engineers*. John Wiley & Sons, Inc.

Pawlowski, M. (1999). *Nonlinear Model of Ship Rolling in Irregular Waves*. Gdansk: Polish Register of Shipping.

Cannon, R. H. (1967). *Dynamics of Physical Systems*. McGraw-Hill Book Company.

Vugts, J. H. (1968). *The hydrodynamic coefficients For Swaying, Heaving and Rolling Cylinders in a Free Surface*. Netherlands Ship Research Centre TNO.